



THE MODELLING OF INTERNAL COMBUSTION ENGINE THERMAL SYSTEMS AND BEHAVIOUR

Tessa Joanne Morgan, M. Eng.

Thesis submitted to the University of Nottingham

for the degree of Doctor of Philosophy

June 2003

Contents

Abstract	iv
Acknowledgements	vi
Nomenclature	vii
Chapter 1 Introduction.....	1
1.1 Background.....	1
1.2 Model Overview	3
1.3 Thesis Overview	6
Chapter 2 Literature Review	9
2.1 Introduction	9
2.2 Engine Thermal Systems Modelling	9
2.2.1 Friction.....	9
2.2.2 Fuelling	12
2.2.3 Gas-side Heat Transfer.....	13
2.2.4 Coolant Heat Transfer	14
2.2.5 Engine Thermal Models.....	16
2.3 Engine Thermal Management	17
2.3.1 Faster Warm-up.....	17
2.3.2 Cooling System Developments	19
2.4 Discussion.....	23
2.4.1 Concluding Remarks	24
Chapter 3 The Theory of PROMETS	25
3.1 Introduction	25
3.2 Engine Structure	25
3.2.1 Boundaries of the Modelled System	25
3.2.2 Engine Structure Definition Using PROGEN.....	26
3.2.3 Lumped Capacity Analysis	28
3.2.4 Stability and Accuracy Criteria for the Structure	30
3.2.5 Boundary Conditions of the Engine Structure.....	33
3.3 Friction.....	34
3.3.1 Friction during Warm-up	37
3.4 Fuel Flow Prediction	39
3.5 Gas-side Heat Transfer	41
3.5.1 In-cylinder and Exhaust Port Gas-side Heat Transfer.....	41
3.5.2 Coolant Passage Heat Transfer	45
3.5.3 Correction for Coolant Composition.....	46
3.5.4 Corrections for Spark and Injection Timing.....	50
3.5.5 Correction for EGR.....	51
3.6 Coolant System.....	52

3.7	Oil System	54
3.8	Exhaust Gas Temperature.....	56
3.9	Turbocharger and Intercooler Models	58
3.9.1	Turbocharger.....	59
3.9.2	Intercooler	60
3.10	Heat Transfer to Ambient.....	60
3.11	Discussion	60
3.11.1	Concluding Remarks.....	63
Chapter 4 Simulink and the Structure of PROMETS.....		64
4.1	Introduction.....	64
4.2	MATLAB and Simulink.....	64
4.3	Model Conversion	65
4.4	Model Structure	66
4.4.1	Graphical User Interface (GUI).....	66
4.4.2	PROGEN	67
4.4.3	PROMETS	67
4.4.4	Inputs and Outputs	68
4.4.5	Operating Conditions of Interest.....	70
4.5	Sensitivity of the Model to User Inputs.....	70
4.5.1	Key engine dimensions	71
4.5.2	Scaling Factors	72
4.5.3	Ambient Temperature	73
4.5.4	Oil Circuits.....	74
4.5.5	Coolant Circuits	74
4.6	PROMETS Applications.....	75
4.5	Discussion.....	76
4.5.1	Concluding Remarks.....	78
Chapter 5 Sensitivity and Performance		79
5.1	Introduction	79
5.2	Sensitivity To Model Assumptions	80
5.2.1	Friction Index.....	81
5.2.2	Proportion of Frictional Dissipation Retained in Oil	83
5.2.3	Values of Gas-side Heat Transfer Constants, C1 & C2	84
5.2.4	Fixed Heat Transfer Coefficients	86
5.2.5	Ambient Temperature	90
5.3	Sensitivity to Simulink Parameters.....	91
5.4	Evaluating Model Performance	92
5.4.1	Experimental Data Collection	93
5.5	Performance Evaluations	94
5.6	Discussion	95
5.6.1	Concluding Remarks.....	97
Chapter 6 PROMETS Development – External Coolant Circuit.....		98
6.1	Introduction	98
6.2	Coolant Transport Delays.....	99
6.3	Thermostats	99
6.4	Cooling Fans.....	104
6.5	Radiators.....	104
6.5.1	Basic Theory	106
6.5.2	Effectiveness-NTU Theory	107

6.5.3	Evaluating the Overall Heat Transfer Coefficient, U	108
6.5.4	Comparison with Experimental Data	112
6.7	Model Exploitation	113
6.7.1	Comparison with Experimental Data	115
6.8	Discussion.....	116
6.8.1	Concluding Remarks.....	116
Chapter 7 Towards Rapid Warm-up		117
7.1	Introduction	117
7.2	Reduced Thermal Capacity	118
7.2.1	Alternative Materials.....	118
7.2.2	Mass and Volume Reductions.....	120
7.3	Oil Coolers.....	122
7.4	Sump Oil Heater	123
7.5	Oil-Exhaust Gas Heat Exchanger	125
7.6	Discussion.....	126
7.6.1	Concluding Remarks.....	129
Chapter 8 Discussion.....		130
8.1	Suggestions for Further Work	132
Chapter 9 Conclusions.....		135
9.1	PROMETS.....	135
9.2	Engine Thermal Behaviour.....	136
References		138
Tables.....		155
Figures.....		195

ABSTRACT

“The Modelling of Internal Combustion Engine Thermal Systems and Behaviour”

Tessa J. Morgan, 2003

The work described in this thesis concerns the continued development and application of a computational model to simulate the thermal behaviour of internal combustion engines. The model provides information on temperature and heat flow distributions within the engine structure, and on temperatures of oil, coolant and engine-out exhaust gas. Sub-models calculate friction levels, fuel flow rates and gas-side heat transfer, including the effects of exhaust gas recirculation (EGR), spark advance and turbocharging. The effects of auxiliary components such as a cabin heater, oil cooler, intercooler, supplementary heater and EGR cooler can also be simulated.

Model developments are aligned towards improving the accessibility of the model and the scope of engine systems that can be simulated. Early versions of the model have been converted from ‘C’ into the current MATLAB/Simulink versions. The model structure and conversion process are described. New developments undertaken have focused on the external coolant circuit and include the modelling of the thermostat and radiator. A semi-empirical thermostat model is presented. A radiator model based on the effectiveness-NTU method is described. Simulations using the developed model, including the thermostat and radiator sub-models, investigate the effect of thermostat position on engine thermal behaviour. Positioning the thermostat on the inlet to the engine reduces thermal shock.

Applications of the model to investigations of sensitivity and performance illustrate the accuracy of and confidence in model predictions. Assessments demonstrate that the model is relatively insensitive to variations of 10% in user

inputs and is very sensitive to model assumptions if simulation conditions, implied in the model assumptions, are not matched to test conditions. A process for evaluating model performance is described. Evaluation exercises applied to three different engines demonstrate that values predicted by the model are to within 5 to 10% of experimental values.

Investigations using the model of methods to improve warm-up times and fuel consumption prior to fully warm conditions show the benefits or otherwise of reduced thermal capacity, an oil cooler, a sump oil heater and an oil-exhaust gas heat exchanger. Each method is assessed over the New European Drive Cycle (NEDC) from a -10°C start. Of these methods, a combined reduction in coolant volume and engine structural mass is most beneficial for reducing coolant warm-up times. An oil-exhaust gas heat exchanger produces the greatest reduction in fuel consumption.

ACKNOWLEDGEMENTS

Firstly, I would like to thank my supervisor Paul Shayler for his help and support throughout the writing of this thesis and the research that preceded it.

I would also like to thank John McGhee, Chief Technician of the Engines Research Group, whose excellent tea and crossword answers have provided much needed sustenance and light relief. I am also grateful to my friends and colleagues of the Engines Research Group whose humour and assistance have been invaluable.

My gratitude also extends to Ford Motor Company, in particular Messrs Derek Eade, Andrew Durrant and Marcus Davies, who have provided financial and informative support for this project.

Last, but not least, I am grateful to my family for their continual support and encouragement throughout my life; to my mother, Clare, for her understanding, to my father, Rick, for his enthusiasm, to my brother, Tom, for long-distance motivation and to my sister, Pippa, for her cheer and perspective. Finally, I would like to thank Richard Gambrill for his support, encouragement and understanding.

This thesis is dedicated to the pursuit of knowledge and development of self.

NOMENCLATURE

A	Area	[m ²]
a, b	Equation Constants	[-]
B	Bore	[m]
C_1, C_2, C_3	Equation Constants	[-]
C_i	Heat Capacity of Element i	[J/K s]
c_p	Specific Heat Capacity	[J/kg K]
D	Diameter	[m]
D_h	Hydraulic Diameter	[m]
d	Characteristic Dimension	[m]
E	Energy	[J]
G	Mass Flow Velocity	[kg/m ² s]
g	Acceleration Due to Gravity	[m/s ²]
\dot{H}	Enthalpy	[J/kg]
h	Heat Transfer Coefficient	[W/m ² K]
Δh	Latent Heat of Vaporisation	[J]
k	Thermal Conductivity	[J/kg K]
L	Length	[m]
L_b	Length of Bearing	[m]
L_v	Length of Valve	[m]
l	Length of Passage	[m]
m	Mass	[kg]
\dot{m}	Mass flow rate	[kg/s]
N	Engine Speed	[rpm]
n_b	Number of Bearings	[-]
n_c	Number of Cylinders	[-]
n_v	Number of Valves	[-]
P	Perimeter	[m]
p	Pressure	[kPa]
\dot{q}''	Specific Heat Flux Density	[J/s m ²]
\dot{q}	Specific Heat Transfer Rate	[W/m ²]

Q	Heat	[J]
Q_{LHV}	Lower Heating Value of Fuel	[MJ/kg]
\dot{Q}	Heat Transfer Rate	[W]
r_c	Compression ratio	[-]
S	Stroke	[m]
S_p	Mean Piston Speed	[m/s]
ΔS	Degree of Superheat	[°C]
T	Temperature	[K] or [°C]
T_i	Temperature of Gas at Intake Port	[K]
t	Time	[s]
Δt	Time Step	[s]
U	Overall Heat Transfer Coefficient	[W/m ² K]
u	Fluid Speed	[m/s]
V	Volume	[m ³]
V_c	Clearance Volume	[m ³]
V_s	Swept Volume	[m ³]
\dot{V}	Volume Flow Rate	[l/s]
\dot{W}	Power	[W]
x	Distance	[m]
Δx	Conduction Path Length	[m]
x	Distance	[m]

SUBSCRIPTS

a	Air
act	Actual Value
amb	Ambient
$blockave$	Block Average
br	Brake
c	Of the Crankshaft
$comb$	Combustion
$comp$	Of the Compressor
$conv$	Convective
$cool$	Of the Coolant
$corr$	Corrected
cyl	Of the Cylinder

<i>eff</i>	Effective
<i>EGR</i>	Exhaust Gas Recirculation
<i>ex</i>	Exhaust
<i>f</i>	Fuel
<i>fin</i>	Of the Fins of the Heat Exchanger
<i>fric</i>	Friction
<i>fw</i>	Fully Warm Value
<i>g</i>	Gas Value
<i>g, a</i>	Effective Average Gas Value
<i>gr</i>	Gross
<i>head</i>	Of the Oil Gallery in the Head
<i>i</i>	Of Element <i>i</i>
<i>ic</i>	Of the Inner Coolant Circuit
<i>in</i>	Property of the Variable When Entering the Heat Exchanger
<i>ind</i>	Indicated
<i>l</i>	Liquid Value
<i>LHV</i>	Lower Heating Value
<i>liner</i>	Of the Piston Liner
<i>m</i>	Of the Coolant Mixture
<i>man</i>	For the Manifold
<i>max</i>	Maximum Value
<i>min</i>	Minimum Value
<i>misc</i>	For Miscellaneous
<i>mist</i>	Of the Oil Mist
<i>nucl, boiling</i>	Nucleate Boiling
<i>oc</i>	Of the Oil Cooler
<i>oil</i>	Oil
<i>out</i>	Property of Variable When Exiting the Heat Exchanger
<i>Patton</i>	Developed by Patton <i>et al</i> [1.7]
<i>pc</i>	Of the Piston Crown
<i>psg</i>	Of the Coolant Passage
<i>pt</i>	Of the Exhaust Port
<i>ref</i>	Reference Value
<i>rel</i>	Released from the Combustion Gases
<i>rings</i>	Of the Piston Rings
<i>s</i>	Of the Surface of Coolant Passage

<i>sat</i>	Saturation
<i>spark</i>	Spark Advance
<i>sump</i>	Of the Oil Sump
<i>T</i>	Taylor
<i>tube</i>	Of the Tube
<i>w</i>	Of the Wall or Plate
<i>wax</i>	Of the Wax
<i>wu</i>	During Warm Up
∞	Bulk Average Value

ACRONYMS AND ABBREVIATIONS

1-D	One Dimensional
AFR	Air Fuel Ratio
AMEP	Auxiliaries Mean Effective Pressure
BDC	Bottom Dead Centre
BMEP	Brake Mean Effective Pressure
CA	Crank Angle
CAD	Computer Aided Design
CAE	Computer Aided Engineering
CFD	Computational Fluid Dynamics
CGI	Compacted Graphite Iron
CHF	Critical Heat Flux
CI	Compression Ignition
CO	Carbon Monoxide
CR	Compression Ratio
DI	Direct Injection
DISI	Direct Injection Spark Ignition
DOHC	Double Over Head Cam
EC	European Community
EG	Ethylene Glycol
EGR	Exhaust Gas Recirculation
FMEP	Friction Mean Effective Pressure
FTO	Friction To Oil (the percentage of friction retained in the oil)
FTP	Federal Test Procedure (USA)
GDI	Gasoline Direct Injection

GUI	Graphical User Interface
HC	HydroCarbon
HTC	Heat Transfer Coefficient
IDI	InDirect Injection
IMechE	Institute of Mechanical Engineers (UK)
IMEP	Indicated Mean Effective Pressure
ISFC	Indicated Specific Fuel Consumption
Mb	Megabyte
MBT	Minimum advance for Best Torque
NEDC	New European Drive Cycle
NO _x	Nitrous Oxides
NTU	Number of Transfer Units
NUSim	Nottingham University Simulation
OBD	On Board Diagnostics
OC	Oil Cooler
ode	Ordinary Differential Equation
PC	Personal Computer
PMEP	Pumping Mean Effective Pressure
PROCESS	PROgram for
PROGEN	PROgram for creating GENeric engine representations
PROMETS	PROgram for Modelling Engine Thermal Systems
RAM	Random Access Memory
SAE	Society of Automotive Engineers
SI	Spark Ignition
SOHC	Single Over Head Cam
TDC	Top Dead Centre
TDi	Turbo Diesel Injection
VTMS	Vehicle Thermal Management Systems
WCR	Worldwide Customer Requirements (Ford)
WOT	Wide Open Throttle

GREEK SYMBOLS

α	Ratio of Total Area Available for Heat Transfer to Volume (heat exchangers)	[-]
γ	Ratio of specific heat capacities (c_p/c_v)	[-]

δ	Plate Thickness	[m]
ε	Effectiveness	[-]
η	Efficiency	[-]
θ	Spark Timing	[CA °]
λ	Latent Heat of Fusion of Thermostat	[J]
v	Characteristic Velocity of Fluid	[m/s]
μ	Dynamic Viscosity	[kg/m s]
ν	Kinematic Viscosity ($=\mu/\rho$)	[m ² /s]
π	Pi	[-]
ρ	Density	[kg/m ³]
σ	Ratio of Minimum Cross Sectional Area to Frontal area (Heat Exchangers)	[-]
τ	Delay	[s]
ϕ	Equivalence Ratio	[-]

DIMENSIONLESS GROUPS

Gr	Grashof Number	$Gr = gB \frac{(T_w - T_\infty)}{\nu^2} l^3$
Nu	Nusselt Number	$Nu = \frac{hD}{k}$
Pr	Prandtl Number	$Pr = \frac{c_p \mu}{k}$
Re	Reynolds Number	$Re = \frac{\rho v D}{\mu} = \frac{4 \dot{m}}{\pi D \mu}$

CHAPTER 1

INTRODUCTION

1.1 BACKGROUND

Historically, engine and vehicle development passed through a series of stages in which prototypes were tested and design modifications made based on the information obtained from the tests. The use of prototypes is both time-consuming and expensive and there is pressure from increasing competition between rival manufacturers to make more use of computer aided engineering (CAE) tools. These tools facilitate understanding of the complex phenomena and interactions that occur during engine operation and that cannot be easily observed through experimentation.

This thesis is concerned with the continuing development of a model of engine thermal behaviour, PROMETS (PROgram for Modelling Engine Thermal Systems), which has been developed to facilitate engine design decisions early in the design process. More specifically, PROMETS is used for investigating engine thermal behaviour and how it can be best managed. The engines of interest are internal combustion engines, both spark ignition and compression ignition, for light passenger vehicles. Generally, these have a total swept volume of between one and four litres, typically producing 40 kW/litre of brake power output at full load. Power output is generated from heat released by combustion in a conversion process involving high gas temperatures and brake thermal efficiencies of less than 40%. The study of thermal behaviour and thermal systems management is concerned with protecting the engine from overheating, engine design for high brake thermal efficiency, the promotion of fast warm-up and the utilisation of heat rejection in passenger compartment heating. Thermal behaviour influences friction, fuel consumption, the emission of pollutants and the efficiency of emission control measures. Thermal systems management is an area of continuing development in automotive engineering

and thermal behaviour influences engine control needs more generally. These various requirements and basic interests in understanding thermal behaviour drove the original work on PROMETS. The complexity of the task and the subject have driven the continuation, firstly to draw together the various elements of theory developed, secondly to advance the structure and utility of the model and thirdly to advance the understanding of thermal behaviour. The last of these forms a major part of the thesis.

At full load, fully warm operating conditions, the relative proportions of work output, heat rejected to coolant, exhaust enthalpy and heat rejected to ambient are typically 25-28%, 17-26%, 34-35% and 3-10% for gasoline engines and 34-38%, 16-35%, 22-35% and 2-6% for diesel engines [1.1][1.2][1.3][1.4]. A Sankey diagram for energy flow under these conditions is reproduced in Figure 1.1 (from [1.1]). A modified version for energy flows during warm-up operation of an engine is shown in Figure 1.2 (from [1.5]). These proportions and diagrammatic representations of energy flows point to the importance of heat rejection from the gas side into the engine structure through the walls of the cylinder and exhaust ports. The engine coolant system acts as the main heat sink for this and as the regulator of engine mean temperature. Details of geometric design, material and coolant properties, coolant path and coolant flow rate all influence temperature distribution around the mean.

The complexity of thermal behaviour is typified by the interaction between rubbing friction and thermal state of the engine during warm-up. The former reduces the work output from the engine by dissipation in crankshaft bearings, at piston ring and cylinder wall contact points, in the valve train, and so on. The dissipated work adds to the heat sources within the engine, increasing warm-up rate. Since friction depends on oil viscosity, which in turn depends upon temperatures, a fall in friction is promoted by faster warm-up. Describing this interaction quantitatively is a difficult task, and is typical of the problems that PROMETS has been developed to attack.

1.2 MODEL OVERVIEW

The PROMETS package is comprised of two MATLAB/Simulink programs run in series, as illustrated in Figure 1.3. These are PROGEN (PROgram for Generic ENgine representation) and PROMETS. The package can be used as a standalone model or as an integral component of other Simulink-based or Simulink-compatible packages. These include packages developed at The University of Nottingham, such as NUSim, PROCESS and PROMEX, and commercial software packages developed elsewhere, such as FLOWMASTER and WAVE.

PROGEN was developed to generate representations of an engine design from a small number of critical engine dimensions, specifications of valve-train type and layout, lubrication and coolant circuit features, and bearing numbers and positions. A number of generic engine templates are used to assist model building and matching, with a main division made between in-line and V-type cylinder layouts. Sub-divisions of the templates allow modelling of single and double overhead cam types of valve trains, and U-flow (with the intake and exhaust ports on the same side) and cross-flow (with the intake and exhaust ports on opposite sides) head types. PROGEN generates all the engine-build information that is required by PROMETS, including details of the lumped capacity elements that are used to represent the engine structure and the thermal connections between these.

PROMETS is comprised of seven main sections. These represent the engine structure, fuel flow prediction, gas-side heat transfer, frictional power losses, engine-out exhaust gas temperature, heat transfer to and from the cooling system and heat transfer to and from the oil. Further sub-sections model the effects of turbocharging and the impact of auxiliary components such as a cabin heater, oil cooler, intercooler, supplementary heater and exhaust gas recirculation (EGR) cooler. Transient heat flow and temperature patterns within the engine structure are modelled using the lumped capacity approach. The elements and thermal connections generated within PROGEN provide a set of governing equations that are solved by explicit time-marching methods. Heat transfer and temperatures at internal and external surfaces of the engine structure are the boundary conditions that link the sub-model of the structure

with the other sub-models. Fuel flow rate predictions are calculated from details of engine operating conditions. Gas-side heat transfer is described using a modified version of Taylor and Toong's [1.6] correlation, with corrections for coolant composition, EGR and spark-timing. Frictional power losses, during warm-up and at steady-state, are predicted using a modified version of the model developed by Patton, Nitschke and Heywood [1.7]. The influence of oil temperature on oil viscosity, and hence friction, is accounted for in the modification. Heat transferred from the structure to the coolant is used to predict coolant temperatures. Oil temperature is predicted using oil heat transfer from the structure and frictional dissipation. These sub-models are described in detail in Chapter 3. The coolant circuit is considered in three sections as illustrated in Figure 1.4: the circuit of coolant passages internal to the engine structure; the inner circuit that is comprised of auxiliary components such as the cabin heater, oil cooler, EGR cooler, intercooler and supplementary heater; the external circuit comprising of the thermostat, cooling fan and radiator, through which coolant flows after the thermostat has opened.

For computational efficiency, the thermal analysis of the engine structure can be based on either one representative cylinder or on all four (or six or eight) cylinders. Versions of the model that contain one representative cylinder are known as 'single cylinder' models. Versions representing all cylinders are 'multi-cylinder' models. Often the single cylinder model is sufficiently accurate and no serious errors arise when the gas-side heat transfer is scaled by the number of cylinders to give values for the whole engine. However, if specific data relating to individual cylinders is required for a multi-cylinder engine, the effects of thermal interactions between the cylinders and the impact of the coolant circuit can be examined. For a multi-cylinder simulation, the boundary conditions for each cylinder will differ; the inboard cylinders are treated as having adiabatic interfaces on both sides and the outboard cylinders are treated as having adiabatic inner surfaces and outer surfaces exposed to ambient conditions. The difference in predicted structural element temperatures and coolant temperatures for the single representative cylinder model and the multi-cylinder model is illustrated in Figure 1.5. In practice, the difference in predicted temperatures is not great (up to 10 K at the condition illustrated) and

the single cylinder model, which is quicker to load and run, can be used for most thermal analyses.

PROMETS meets a variety of needs for thermal analysis. Applications of the model by previous researchers have included investigations into a modified oil sump, the effect of valve train configuration on friction power losses and a novel cooling system [1.8], the effects of valve geometry and operating conditions on valve temperatures [1.9], designing towards rapid warm-up [1.10] and assessments of heater performance [1.11]. External users have applied the model to the analysis of heat flows, engine warm-up and coolant passage dimensions [1.12]. Applications of the model described in this thesis investigate the dynamics of the external coolant circuit and further methods for improving engine warm-up times and fuel consumption.

The work reported in the thesis has been carried out on or using three versions of PROMETS covering the basic family of internal combustion engine designs, namely in-line gasoline engines (PROMETSI4), in-line diesel engines (PROMETSD) and V-type gasoline engines (PROMETSV). The current features of each model are summarised in Table 1.1. The in-line diesel version has been developed to cover the features of a relatively complex thermal management system with a heater matrix, oil cooler (in either the inner circuit or the external circuit), EGR cooler and supplementary heater, placed in any order around the inner circuit. Details of components are described in Chapter 3 of the thesis. The gasoline in-line and V-type versions contain a heater matrix, oil cooler and supplementary heater in a fixed order. Figure 1.6 illustrates the typical positions of these auxiliary components for all versions of PROMETS. The development of the in-line and V-type gasoline versions to allow greater flexibility in defining the inner circuit is in prospect. Reflecting current technological applications, the in-line diesel version is also the only version that currently features a turbocharger and intercooler model. These may be added to the gasoline versions in the future if required.

1.3 THESIS OVERVIEW

The thesis describes PROMETS, its development and its application to investigations of engine thermal behaviour. The aims of the work are:

- Provide a thorough and complete description of the model theory.
- Develop and implement an alternative to the iterative calculation that corrects gas-side heat transfer values for coolant composition. Evaluate the impact of the alternative calculation on model predictions.
- Identify any model weaknesses or assumptions and areas of PROMETS that require further development.
- Convert PROMETS from 'C' into Simulink: convert the in-line gasoline, in-line diesel and V-type gasoline versions in multi-cylinder and equivalent representative single-cylinder forms.
- Develop a user interface for use with the Simulink versions of the model.
- Assess the sensitivity of PROMETS to user inputs and assumptions within the model.
- Develop a method for evaluating the performance of new engine data files or model versions in order to direct the collection of useful experimental data and enable rapid identification of discrepancies in model predictions.
- Evaluate the performance of Simulink versions of the model.
- Develop sub-models to simulate the thermostat and radiator in the external coolant circuit.
- Apply these sub-models to investigations of the impact of the external circuit on engine thermal behaviour.
- Apply PROMETS to investigations of methods for improving coolant warm-up times and reducing fuel consumption through faster engine warm-up.

The previous sections of this Chapter have presented a background to engine thermal behaviour and management, and an overview of PROMETS. A breakdown of the work presented in the body of the thesis is as follows.

Chapter 2 presents a review of literature relating to the modelling of engine thermal systems and current developments in the field of engine thermal management. Subjects include the modelling of friction, fuel flow rates, gas-side heat transfer and coolant heat transfer. Papers relating to engine thermal

management, including methods for improving engine/coolant warm-up rates and recent cooling system developments, are also reviewed.

This is followed in Chapter 3 by a thorough description of the current state of PROMETS, including details of the sub-models and calculations in the model. The Chapter is concluded with a discussion of the assumptions and weaknesses of the model.

The process undertaken to convert the model from 'C' into Simulink and the current structure of the model is described in Chapter 4. This includes details of the difficulties encountered in converting the model. A description of the inputs to and outputs from PROMETS is given. The sensitivity of the model to user inputs is examined. Finally, an illustration of applications of the model is presented.

In Chapter 5, the sensitivity of PROMETS to empirically defined constants and model assumptions is explored. A process for evaluating the performance of new engines or model versions is described. The performance of current Simulink versions is evaluated through comparisons with recent experimental data.

One area of particular interest that is highlighted in the literature review in Chapter 2 is the effect of the external coolant circuit on the thermal management of the engine once thermostat opening conditions are reached. In earlier work, details of the external circuit were not defined, but were assumed to satisfy the heat rejection requirements. The implied heat rejection rate is equated to the calculated heat transfer to the coolant. Chapter 6 presents formulations for the prediction of heat rejected from the radiator and behaviour of the thermostat with changes in coolant temperature. The radiator sub-model is based on an effectiveness-number of transfer units (NTU) description of performance. Comparisons of predicted effectiveness values with data supplied by the Ford Motor Company are well matched. The thermostat model presented is based on a physical analysis of heat transfer through the thermostat housing, but relies upon empirical data for a description of the behaviour of the wax. The sub-model developed from these components is applied to investigations of the impact of the external coolant circuit on engine thermal behaviour and

demonstrates that thermal shock is reduced when the thermostat is located at the inlet to the engine.

Applications of PROMETS are described in Chapter 7. These include an assessment of the relative merits of reductions in engine thermal capacity and the use of oil coolers, sump oil heaters and oil-exhaust gas heat exchangers as the means of improving engine warm-up. Each investigation is conducted at an ambient temperature of $-10\text{ }^{\circ}\text{C}$ and at operating conditions designed to simulate the New European Drive Cycle (NEDC). This permits a direct comparison of warm-up times and fuel consumption for each method and demonstrates that, of the methods tested, an oil-exhaust gas heat exchanger produces the greatest reduction in fuel consumption. Combined reductions of 10% in engine mass and 10% in coolant volume produce the greatest improvement in coolant warm-up times.

The main findings from Chapters 3 to 7 are brought together and discussed in Chapter 8, followed by an explicit statement of the conclusions drawn from this work in Chapter 9.

CHAPTER 2

LITERATURE REVIEW

2.1 INTRODUCTION

Heat flow and temperature distributions within the engine structure, frictional dissipation, heat transfer and heat rejection characteristics and thermal systems performance all figure in the analysis of engine thermal behaviour. Knowledge relating to these subject areas can be found throughout the literature. In particular, the Vehicle Thermal Management Systems (VTMS) biannual series of conferences, first held in 1993 jointly by the SAE and IMechE, has provided a platform for the dissemination of information in this field [2.1][2.2][2.3].

The following review covers elements of the literature relevant to the present study. Included are discussions on methods of determining engine friction values, fuel flow rates and heat transfer rates from the combustion gases to the cylinder and exhaust port. The mechanisms of heat transfer from the engine structure to the coolant are discussed. Current engine thermal models, reported in the literature, are also discussed. This is followed by an examination of developments in the area of engine thermal management, including published advances in accelerating engine warm-up rates and improvements in cooling system design.

2.2 ENGINE THERMAL SYSTEMS MODELLING

2.2.1 Friction

Rubbing friction losses account for approximately 10% of the net indicated power at full-load and (together with the power consumed driving engine auxiliaries) 100% at idle under fully warm conditions [2.4][2.5]. During urban driving, friction accounts for between 20 and 30% of the total engine output

[2.6]. These losses have a significant effect on the minimum brake specific fuel consumption and on the maximum brake torque. The total frictional losses are comprised of the losses from several components, notably the crankshaft, piston assembly, valve train, pumping losses and friction due to auxiliary components such as the water pump and alternator. Of these components, the piston assembly contributes most significantly to the total frictional loss [2.7][2.8][2.9][2.10][2.11]. Figure 2.1, reproduced from Ball [2.8], illustrates the relative proportions of the major categories of friction losses at different loads and speeds for 1.6l spark ignition and compression ignition engines.

The frictional losses are dissipated as heat transferred to the engine structure and as heat in the oil. The proportion of frictional dissipation that is retained as heat in the oil for gasoline engines generally lies between 10 and 15% of the total value [2.12]. For diesel engines, this increases to 20% due to differences in the conditions of contact between the oil and the structure [2.13].

The obvious benefit of a reduction in friction is an accompanying reduction in fuel consumption. According to Auiler et al [2.14], a 10% reduction in friction would reduce fuel consumption by up to 5% for a spark ignition engine and by as much as 7% for a compression ignition engine. However, as a proportion of the engine rubbing friction is dissipated as heat in the coolant and oil, a reduction in friction can also adversely affect warm-up times.

Engine friction dissipates work into heat through three basic mechanisms [2.4]. The first two occur at the interface of surfaces in relative motion with a lubricant in between. Boundary friction occurs when the layer of lubricant between the two surfaces is not sufficiently thick as to prevent metal-to-metal contact. Under these conditions, the friction is independent of engine speed. Hydrodynamic friction occurs when the layer of lubricant is such that the two surfaces are completely separated. Under hydrodynamic conditions, friction varies linearly with engine speed. The third type of friction is turbulent dissipation. As the cylinder gases, coolant and oil are pumped through engine restrictions, turbulence occurs and the energy of the fluid is dissipated. The work done in pumping each fluid is a function of the pressure drop across each circuit. Since the pressure drop across each circuit is calculated as a function of

the fluid velocity, the friction dissipated is a function of the engine speed, for coolant and oil, or the piston speed, for the in-cylinder gases.

The total friction losses of an engine are sometimes described by an equation of the form [2.5][2.15][2.16][2.17][2.18],

$$FMEP = C_1 + C_2N + C_3N^2 \quad (2.1)$$

In some cases, variants of Equation (2.1) have been proposed. Yagi *et al* [2.18], for example, proposed the form,

$$FMEP = (C_1N^2 + C_2)\sqrt{\frac{SD_c}{B}} \quad (2.2)$$

Where friction mean effective pressure, $FMEP$, is measured in MPa, C_1 and C_2 are empirical constants, S and B are the stroke and bore in metres and D_c is the crankshaft diameter.

Bishop [2.19] and Patton *et al* [2.7] developed cycle-averaged models that predict values for the friction of individual components. A modified version of the model developed by Patton *et al* is used in PROMETS and is described in Chapter 3. This separates frictional losses into contributions associated with the piston, valve train, main bearings and auxiliary components. Each contribution is described by equations based on empirical data and in a form consistent with lubrication theory.

A number of crank-angle resolved, or instantaneous models are also described in the literature [2.6][2.20][2.21][2.22][2.23]. As with the cycle-averaged models, these are broken down into individual components, divided into either piston ring assembly, bearing, valve train and auxiliary friction [2.20][2.22][2.23] or piston-ring assembly and crankcase assembly friction [2.21]. The model by Rezeki *et al* [2.21], which calculates friction based upon the instantaneous angular velocity of the crankshaft, has been compared to experimental data by several authors [2.24][2.25][2.26] with disappointing results. Kouremenos *et al* [2.25] concluded that the reason for this was that the initial constants derived for the Rezeki model were engine-specific and had been derived and tested at idle conditions. Development of the model by first

Kouremenos *et al* [2.25] and then Rakopoulos *et al* [2.26] improved predictions.

2.2.2 Fuelling

Information on the fuel consumption of production engines is often presented as a mapped function of speed and brake mean effective pressure. Figure 2.2 shows a fuel consumption map for a Ford 1.8L IDI (indirect injection) diesel engine. Since volumetric and mechanical efficiencies may differ, these maps are specific to a particular engine. During the initial stages of engine design and development, any kind of fuel consumption information is often unavailable. Thus, it is necessary to be able to model the fuel required by the engine to maintain a particular operating condition.

Several approaches for modelling fuel consumption have been described in the literature. Ross and An [2.27] developed a correlation for spark ignition engines and demonstrated that fuel consumption per revolution was approximately a linear function of work output per revolution. Although this gave good agreement over a large range of spark ignition (SI) engines, no account was taken of combustion timing, air-fuel ratio (AFR), compression ratio (which affects combustion and thermal efficiency) or differences between the friction values for different engines. Wu and Ross [2.28] developed a more detailed model for direct injection diesel engines, which takes account of friction and indicated thermal efficiency. Again, although good agreement with experimental data was achieved, their estimates of friction do not account for pumping losses; for turbocharged engines, these losses can have a significant effect on fuel consumption. Chick [2.29] and Baylis [2.13] describe a method, currently used within PROMETS, which enables fuel consumption to be predicted from generic information on engine behaviour. The method develops from the premiss that the rate at which fuel is consumed to produce a specified gross indicated power can be expressed as a function of fuel mass flow rate and gross indicated power. Described in detail in Chapter 3, the method takes account of pumping and auxiliary losses in addition to engine friction.

2.2.3 Gas-side Heat Transfer

Accurate prediction and measurement of heat transfer rates, both to the cylinder and to the exhaust port, are difficult. Heat transfer rates vary over the engine cycle and with location in the engine cylinder and port. These depend upon design detail, rendering the derivation and application of a detailed formulation for predicting local heat transfer rates extremely difficult, as many of the influencing factors in the calculation would be partly unknown [2.30]. It is generally agreed, however, that the dominant mechanism of heat transfer from the combustion chamber is turbulent forced convection. Radiation accounts for around 5% of the heat transfer in spark ignition engines and is generally ignored, but can account for as much as 50% of the heat transfer in compression ignition engines ([2.31] quoted in [2.32]). Measurement of in-cylinder heat transfer is further complicated by frictional dissipation to heat, most notably at the contact point between the piston rings and the cylinder liner.

Approaches to modelling the gas-side heat transfer vary from cycle-averaged correlations [2.33][2.34][2.35] to instantaneous, crank-angle resolved models [2.30][2.36][2.37][2.38][2.39][2.40] and also to spatially resolved formulations [2.41]. Since turbulent forced convection is assumed to be the dominant mechanism of heat transfer, the calculations are usually based on correlations between dimensionless parameters, such as Nusselt-Reynolds correlations. These usually take the form,

$$Nu = a Re^b \quad (2.3)$$

Generally, differences between the models lie in the definition of the Reynolds number, which may be based on piston speed or gas velocity, and on the exact value of the constant, a , and exponent, b . Some models require additional inputs, for example the models described by Woschni [2.38] and Suzuki *et al* [2.40] require the instantaneous in-cylinder pressure.

Other models that use spatially resolved formulations to predict the instantaneous variation of heat transfer from the cylinder gases to the cylinder walls by means of Fourier analysis [2.42][2.43], electrical analogy or numerical

methods [2.44][2.45] are also described in the literature. These models often utilise the thermodynamic results of two-zone combustion models, which account for turbulence in both the burned and unburned portions of the in-cylinder gas, to determine spatially resolved temperatures throughout the cylinder.

Nusselt-Reynolds number relationships are also widely used to determine the heat transfer rate to the exhaust port walls. Several authors [2.46][2.47] [2.48] developed correlations to determine the time-averaged heat transfer rate in the exhaust port. Experiments undertaken by Malchow *et al* [2.47] demonstrated that the standard Dittus-Boelter [2.49] correlation for fully developed turbulent flow conditions in pipes under predicted actual heat flux by up to 50%. Wendland [2.50], who assessed the steady-state correlations of four others [2.47][2.48][2.51][2.52], reported reasonable agreement with experimental results taken from six production and prototype exhaust systems, with the correlations by Meisner *et al* [2.48] and Huber *et al* [2.52] giving the closest predictions for the takedown pipe and exhaust pipe respectively. Caton and Heywood [2.53] refined the analysis by using a set of four Nusselt-Reynolds number correlations to represent the change in heat transfer conditions during different periods of the engine cycle. These instantaneous heat transfer correlations require accurate knowledge of the valve lifts. However, the authors report good correlation with experimental data. Table 2.1 gives a summary of the published correlations, by the above authors, for time-averaged exhaust port heat transfer.

2.2.4 Coolant Heat Transfer

Some form of engine cooling system is required to avoid component failure and to prevent degradation of the lubricating oil. The burning cylinder charge can reach peak temperatures of 2500K [2.4], which is much higher than the safe operating temperature of metals. Oil temperatures are limited to a maximum of around 425K. However, low cylinder wall temperatures are to be avoided, as this heat transfer raises losses from the combustion gases, reducing thermal efficiency [2.54]. Typical maximum temperatures in a conventional water-

cooled SI engine are listed in Table 2.2. For satisfactory thermal strength, upper limits of 380°C and 350°C are suggested for cast iron and aluminium respectively [2.55]. However, in many cases thermal strength is not the limiting factor. High surface temperatures can cause knock and valve seat distortion [2.56], piston scuffing can be induced when thermal expansion of the piston skirt is restrained by the cylinder liner [2.57] and cylinder liner temperatures should be kept below about 180 °C to maintain an adequate oil film [2.55].

The layout of a typical internal coolant circuit (within the engine structure) is illustrated in Figure 1.4. Coolant enters the block and circulates through the block and head before exiting from the head. The engine internal cooling passages occupy the remaining space enclosed between the upper and lower decks and the side walls that is not used for other features such as cylinders, bolt columns and fuel injector or spark plug housings. In these passages, heat transfer to the coolant occurs primarily through forced convection, although nucleate boiling may occur in some areas. There is considerable interest in exploiting nucleate boiling more effectively in precision cooling systems. The principle boiling regimes are shown in Figure 2.3 [2.58]. In regions of low heat flux, heat transfer occurs by forced convection and is governed by coolant composition, velocity and temperature. In regions of high heat flux, nucleate boiling arises; small bubbles of vapour form on the surface of the metal structure, grow and, when they reach a certain size, break away and dissipate, transporting additional heat into the body of the coolant, as illustrated in Figure 2.4a. This phenomenon is also partially regulated by system pressure [2.59]. Nucleate boiling produces a marked increase in the coolant passage heat transfer coefficient, but if the heat flux exceeds a critical heat flux (CHF) value, film boiling can occur, as illustrated in Figure 2.4b, and this can lead to engine damage [2.60]. Under film boiling, metal temperatures rise significantly due to the insulating layer of vapour that is formed between the coolant passage surface and the coolant.

Commonly, the engine coolant-side heat transfer coefficient is estimated using the Chen correlation for two phase, forced convection [2.61]. This assumes that convective and nucleate boiling contributions to a heat transfer coefficient can be calculated separately and then added. Collier [2.62] adapted the Chen

correlation for the case when the mass flow of vapour is very small; this has been used to good effect by Finlay *et al* [2.63][2.64][2.65]. The Chen formulation has also been adopted by Campbell *et al* [2.59][2.66][2.67][2.68] in studies aimed at improving cooling system design.

2.2.5 Engine Thermal Models

Several models of engine thermal systems are described in the literature. Applications include thermal analysis, engine design, cooling circuit design and optimisation, and engine cooling system diagnosis for on board diagnosis (OBD) [2.69]. Several papers describe the application of the 1-dimensional (1-D) commercial fluids model, FLOWMASTER [2.70] to [2.78]. In general, good estimates of flow rates, pressures and temperatures are reported. Network flow theory is applied in the models COOL [2.79][2.80] and KULI [2.70][2.81][2.82][2.83] to construct 1-D modular simulations of cooling systems. GT-Cool [2.84] is a 1-D fluid dynamics model for engine cooling systems analysis. Heat rejection, engine performance and fuel consumption are determined as a function of speed and load using engine maps. Da Silva *et al* [2.85] describe a multi-port approach to modelling a coolant system. In this method, each hydraulic junction is modelled using a friction orifice and central node, which dynamically represent the temperature and pressure of the fluid at that point. Libraries, containing basic components, can be used to construct individual models. A 3-D computational fluid dynamics (CFD) model is described by Seider *et al* [2.86], although the run-time of two and a half days, using 8 processors, restricts use of the model to later stages in the design process. In general, these cooling system models use empirical data or engine maps to determine the heat input to the coolant.

For investigations of engine thermal performance early in the design process, a lumped capacity approach has been adopted by a number of authors [2.87] to [2.94]. Kaplan and Heywood [2.87] use seven elements to represent the engine; one for the head, block, oil reservoir, coolant in the head, coolant in the block, coolant in the radiator and one for each of the pistons. They combine the thermal inertia of the crankshaft with the oil reservoir and that of the valve train

and camshafts with the head element. The conservation of energy and heat transfer at element boundaries are used to derive equations for each element that can be solved simultaneously to determine element temperatures. The model was used to investigate piston warm-up rate and the effect of this on hydrocarbon storage in the piston and liner crevice regions, deducing that this contributes substantially to unburned hydrocarbons during cold start. Veshagh and Chen [2.88] used 24 hexahedral elements to construct a single cylinder representation. Seven temperatures were calculated for each element; at the centre and at each of the six surfaces. The model was used to investigate the effects on the thermal response of the engine to variations in running condition, combustion chamber wall thickness, coolant and lubricant mass. A separate simulation program was used to determine the in-cylinder cycle-averaged gas temperatures and heat transfer coefficients between the gas and the structure. The model developed by Bohac *et al* [2.91] made use of either an instantaneous two-zone thermodynamic combustion model or the established Taylor and Toong [2.34] model to determine the gas-side heat transfer. The Vehicle Engine Cooling System Simulation [2.92][2.93][2.94] uses six volumes to represent the liner, head, piston, block coolant, head coolant and piston cooling oil. The conservation of mass and energy through each volume is used to determine time dependant differential equations, which are solved to obtain the temperatures of the block coolant, head coolant and piston cooling oil. The model uses Watson's [2.95] single zone combustion model, the results from which are averaged to give values over the engine cycle. The model was developed to facilitate the design of cooling systems for diesel truck engines.

2.3 ENGINE THERMAL MANAGEMENT

2.3.1 Faster Warm-up

Improving engine efficiency through, for example, advances in technology, improved combustion characteristics and friction reduction techniques can have the disadvantage of extending warm-up times. The penalties of increased fuel consumption and emissions, and poor cabin heater performance have raised interest in finding ways to promote fast warm-up. It has proved difficult to find

improvements that yield benefits in each area of performance, however. For example, measures employed to improve the rate of coolant temperature rise often increase fuel consumption. A number of approaches to improving warm-up times are described in the literature. Generally, the methods used fall into three categories; base engine design optimisation, the use of additional heat sources or heat recovery measures, and the manipulation of control strategies and operating conditions.

Base engine design optimisation revolves around the reduction of the engine thermal capacity through the reduction of structural masses and coolant and oil volumes, and around the redistribution of thermal energy to best effect. Both of these techniques can be effective in achieving improved fuel economy and heater performance benefits. Mandrusiak and Alkidas [2.90] note that the redistribution of fuel energy that occurs when a 50% lighter head is employed enables the whole engine to warm up more quickly. Shayler *et al* [2.96] report both fuel economy and heater performance benefits from using such techniques. Section 2.3.2 discusses the benefits that can be achieved through the optimisation of the engine cooling system and the effect that this has on warm-up.

The use of additional heat sources (either external or internal) or heat recovery measures is explored in a number of papers in the literature. Stecki *et al* [2.97], examining heating systems for cold starting, describe an internal electrical pre-heating system, with heating coils placed in the oil, coolant, air intake and fuel systems, and an external fuel-burning pre-heating system, which uses thermal energy from the combustion process to directly warm the engine. They conclude that the electrical system is more efficient as it enables the energy to be directed to areas of need, and is cheaper to install and run. However, the fuel burner raises the temperature of the engine to an appropriate level for starting much more rapidly. Several researchers [2.98] to [2.103] explore the use of internal heat batteries or heat storage devices, including Hellman [2.103], who reports a reduction in fuel consumption of up to 20% over the cold portion of the US Federal Test Procedure (FTP) drive cycle. Similarly, heat recovery measures such as exhaust-coolant heat exchangers have exhibited benefits for both fuel consumption and heater performance. Goettler *et al* [2.104] report a

fuel consumption reduction of 2.8% for a laboratory-based Buick V6 engine over a 7-minute warm-up period and Davies [2.105] found that an exhaust-coolant heat exchanger reduced fuel consumption by 0.54% in a simulation of a 1.6 Sigma engine in a Ford Focus over the New European Drive Cycle (NEDC). External heat sources, such as the fuel burning pre-heater described by Lindbert and Andersson [2.106], can also improve warm-up times. However, there is a fuel consumption penalty as the amount of fuel consumed to pre-warm the car is greater than the amount saved over a defined cycle.

Strategic control of engine parameters can also improve warm-up. Kern and Ambros [2.107] measured a saving of 1.8% of fuel consumption by controlling the supply of mass and heat flows around the engine. The use of higher gearing during warm-up has also been shown to improve fuel economy and heater performance [2.29][2.90].

2.3.2 Cooling System Developments

Alternatives to the traditional circuits described previously are being explored as a way to improve engine thermal management. Dual cooling circuits, smart systems and precision cooling concepts are under development or are beginning to emerge in production vehicles.

- **Dual Cooling Circuits**

In dual cooling circuits, such as that illustrated in Figure 2.5, separate circuits are employed for the head and block of the engine, enabling the head to be appropriately cooled whilst the block undergoes minimal or zero cooling to improve friction. This is particularly useful during cold and part load running. More generally, benefits include reduced fuel consumption, improved knock limits and higher compression ratios in SI engines, and an increase in engine power output. Kobayashi *et al* [2.108] attained an increase in compression ratio from 9:1 to 12:1 for a 1.3l SI engine using a dual circuit. This resulted in a 10% increase in power output and a 5% decrease in fuel consumption at part load. A disadvantage of the system is its higher cost than conventional designs due to additional components and more complex control requirements.

- **Smart Cooling Systems**

Smart cooling systems employ an electrically driven water pump and radiator fan to decouple these from engine speed. This has become possible in recent years due to the development of a 42V electrical system, instead of the conventional 12V system, which is capable of supplying a greater number of electrical components [2.109]. Electric water pumps have several advantages over mechanical pumps, as coolant flow rates are easier to control. Mechanical pumps, which are driven directly by the engine, have no minimum or zero cooling capacity and cold start or part load conditions are often overcooled. Cortona and Onder [2.110] demonstrated that an electrical coolant pump capable of reduced cooling strategies at cold start and part load conditions reduces coolant pump energy requirements by 16%, improving both coolant and oil warm-up times. Additional benefits of the electrical pump become apparent when the engine is shutdown, as cooling can continue after the engine has ceased operation, if necessary. When combined with an electrical thermostat or valve, the pump enables fast warm-up and smaller temperature overshoots at thermostat opening. Cortona *et al* [2.111] demonstrated savings of up to 4.5% of fuel over the NEDC for this set-up, and Choukroun and Chanfreau [2.112], who also used an electrical fan, found that warm-up times were reduced by 50%, using between 2 and 3% less fuel over the NEDC. Clearly, the control of coolant flow and therefore temperature that is obtained by using a smart system can deliver significant benefits.

- **Precision Cooling Circuits**

The poor control of coolant flow through, and positioning of, coolant passages, can result in under-cooling of areas of high heat flux, such as the exhaust ports, and over-cooling of areas of low heat flux. The philosophy of precision cooling is to achieve an optimised temperature distribution using the minimum cooling necessary. Several authors have shown that coolant pump flow rates and required pump power output may be reduced by precision cooling [2.113] to [2.115].

Other potential advantages include lower friction, faster warm-up, improved knock resistance and less cylinder-to-cylinder variability, all of which

contribute to lowering fuel consumption and emissions. The reduction of cylinder-to-cylinder variability is of greatest benefit in aluminium heads as fatigue properties are poorer than cast iron [2.116]. In principle, the benefits of precision cooling are greater for gasoline engines than for diesel engines due to the improvement in knock behaviour and wider use of aluminium heads [2.116].

Priede and Anderton [2.113], describing one of the earliest precision cooling experiments, designed small local passages to provide direct cooling with fully controllable coolant flow rates to thermally critical areas. Uncritical regions were not directly cooled. They reported that the precision cooling regime, applied to a 3.9l naturally aspirated diesel engine, reduced full load heat rejection to the coolant by 18%, resulting in a more even temperature distribution. Thus, the size of the radiator could be reduced, as could the fan power required, resulting in a reduction in fan noise. The areas that were not directly cooled experienced higher temperatures than with the standard cooling circuit but were within safe limits. Similar experiments performed on a 2.0l gasoline engine reduced the heat rejected to coolant by 14.5%.

Subsequent work has considered in some detail the method of heat transfer that occurs within the engine and the effect that this has on the amount of heat rejected to the coolant. Finlay *et al* [2.64] conducted a study of nucleate and film boiling in a uniformly heated duct of small cross section. The study revealed that, as nucleate boiling starts to occur, the resistance to flow in the coolant passage alters considerably due to the formation of vapour bubbles at the surface. This changes the characteristics of the coolant flow through that region. They also noted that the influence of nucleate boiling varied with coolant velocity. At high liquid velocities of around 5.5 m/s, nucleate boiling appeared to be suppressed. At flow rates of less than 1 m/s, nucleate boiling was more prevalent and had a significant effect on the heat transfer. Further studies conducted by Finlay *et al* [2.65] examined the cast iron cylinder head of a small gasoline engine. Comparing the base head design with a precision cooled head, they noted that the sensitivity to coolant pressure, which alters the coolant saturation temperature, was considerably reduced. This led them, supported by their previous work, to conclude that the high liquid velocities

employed in the precision cooled head suppressed nucleate boiling and that the heat transfer regime was purely convective. This was confirmed with further experiments to vary the pump flow. The performance of the engine, spatial heat flux variation and heat rejection to the coolant were similar for both engine builds.

Clough [2.114] conducted a precision cooling exercise on a 6-cylinder in-line SI engine. He re-designed the cooling passages by considering the estimated heat flux at several points. At each point, he then determined a desired local coolant velocity and designed the coolant passages accordingly. Comparing the base design and precision cooled design revealed a number of improvements. At 5000 rpm, wide open throttle (WOT), coolant warm-up time was 18% faster and peak head metal temperatures were reduced by 80°C for the precision cooled engine. This resulted in reduced temperature variability in both the head and the block. Additionally, the heat rejected to coolant was reduced from 41.5% of the input energy from the fuel to 37%. This would enable a reduction in the size of the radiator. The bulk coolant flow rate was also reduced to only 35% of the standard flow, enabling water pump power requirements to be reduced by 1.85kW at 5000 rpm. An increased resistance to coolant flow, due to nucleate boiling and bubble formation, resulted in an increased pressure drop across the engine. Additionally, Clough found that the reduction in temperature variation resulting from the precision cooling reduced friction and thereby improved fuel economy.

Both Campbell *et al* [2.67] and Porot *et al* [2.60] conclude that the most effective form of precision cooling is when stable general nucleate boiling occurs and the critical heat flux, at which the transition to film boiling begins to occur, is avoided. This involves careful coolant passage design, so that the passage diameter is not too small [2.64], when vapour blockages can cause problems, and not too big [2.66], when high flow rates can cause the suppression of nucleate boiling. Nucleate boiling does not appear to damage the engine structure [2.60]. However, the build up of deposits and contaminants over time in the coolant system does affect coolant passage heat transfer [2.59][2.68]. An increase in the roughness of the coolant passage surface results

in a higher heat flux [2.59][2.68]. This must be considered when designing to avoid the CHF.

2.4 DISCUSSION

Engine thermal management is still an innovative and developing area of engine design. The overview given here illustrates some of the issues, emerging technology and knowledge base of the subject. System modelling aids both the advancement of knowledge and its practical application. There are still uncertainties and room for improvement.

A comparison of the friction predicted for a four stroke, four cylinder, direct injection diesel engine by the models of ten different researchers is reproduced from Ciulli [2.20] in Figure 2.6. The original formulae were derived for different engines and conditions: diesel or gasoline engines, different numbers of cylinders, motored or firing engines, including or excluding pumping losses etc. Therefore the figure illustrates trends only, however, the substantial spread of the predictions indicates the difficulties that are encountered in trying to derive a comprehensive friction model. The process is further complicated by the difficulties in obtaining reliable friction test data, particularly since different friction levels can occur in nominally identical engines due to the tolerances that affect the bearing clearances between the relative moving parts of the engine.

Similarly, Figure 2.7 shows a comparison of the values predicted by five published correlations [2.35][2.46][2.53][2.117][2.118] for exhaust port heat rejection. Again, the spread of values illustrates the difficulties involved in accurate prediction of exhaust port heat transfer. According to Meisner and Sorenson [2.48], the relationships developed by Hires and Pochmara [2.46] and Caton and Heywood [2.53] tend to over-predict values, as the relationships were developed for the curved part of the exhaust port near to the valve where the heat transfer rate would be highest and are not representative of an average rate over the whole exhaust port.

2.4.1 Concluding Remarks

The comparisons of exhaust port heat transfer and friction correlations indicate the difficulties involved in thermal systems modelling. However, comparisons with experimental data presented later in the thesis show that the correlations used within PROMETS tend to predict to within a few percentage points.

This Chapter has highlighted that many thermal management investigations are currently centred on the coolant circuit. Investigations of precision cooling and dual cooling circuits are focused on changes to the internal engine cooling passages, both in the design and in the flow of coolant around the circuit. Smart cooling systems focus more specifically on the external coolant circuit and on the gains in fuel economy and warm-up times that can be achieved. PROMETS is well suited to these types of investigations as they often require the assessment of several engine set-ups, and systematic analysis can identify beneficial strategies from a number of different options. The development of PROMETS to facilitate the analysis of smart cooling systems and external coolant circuit strategies is discussed in Chapter 6.

CHAPTER 3

THE THEORY OF PROMETS

3.1 INTRODUCTION

In the following, the aim has been to present a description and analysis of the theoretical underpinning of the sub-models in PROMETS. The formulations are as currently used in 2003, and deal with the representation of the engine structure, fuel flow prediction, gas-side heat transfer, frictional power losses, engine-out exhaust gas temperature, coolant heat transfer and oil heat transfer. These formulations have been developed over a period of years by previous researchers and the author. Here, however, is the first attempt to draw together the various elements of the model to provide a coherent description. The majority of the code for each of these sections is the same for each version of PROMETS and where there are differences, these are noted in the text.

3.2 ENGINE STRUCTURE

3.2.1 Boundaries of the Modelled System

The engine structure as represented in PROMETS is the physical assembly of major components whose thermal states are of interest, and is illustrated in Figure 3.1. These are the engine block and cylinder head, the piston, intake and exhaust valves, coolant and oil masses, crankshafts, camshafts and balancer shafts (if used) and components in contact with the coolant or oil, such as pumps, oil cooler, hoses and the thermostat. Peripheral engine components such as the alternator, power steering pump, air conditioning pump, starter motor and fly wheel are sufficiently thermally detached from the engine to have negligible influence on thermal conditions within the engine boundary, although these do affect engine loading and can thereby influence operating conditions and fuel consumption. Intake and exhaust manifolds are not

modelled, although heat transfer from the exhaust manifold into the head is implicitly accounted for in the calculation of the gas-side heat transfer (see Section 3.5).

3.2.2 Engine Structure Definition Using PROGEN

The PROMETS package includes PROGEN (PROgram for creating GENeric engine representations) which is used to generate the lumped capacity elements (described in Section 3.2.3), thermal connections and other engine-build data required to fully characterize an engine.

The accurate prediction of engine thermal characteristics requires that engine mass and coolant volume are close to the true values (within a few percentage points) and that key engine dimensions are properly represented. In order to achieve this, generic engine templates are provided in PROGEN to assist model building and matching. The templates are based on an observation of design constraints and common dimensionless ratios. The shape and size of the engine is constructed from the key dimensions identified in Figures 3.2 to 3.4. The width of the block and head are determined from a consideration of the size of the bore, the thickness of the coolant passage surrounding the cylinder and the thickness of the walls. Similarly, the length of the block and head are calculated from the bore spacing, wall thickness, coolant passage thickness and bore dimensions. The thickness of walls is generally similar throughout the engine and a reference value of 7 mm is typical. The wall thickness required to meet material strength limits will be greater for aluminium than cast iron for a given material strength, thus increasing main engine dimensions. The height of the head is based on the length of the valves (a function of the bore dimension), radius of the cam and cam clearance dimensions. Thus, the choice of valve train affects the height and mass of the head. The depth of the block is determined from considerations of the stroke, depth of the piston and conrod length. Crankcase dimensions are a function of the clearance requirements of the big end assembly and are calculated from the piston depth, conrod length, wall thickness, bore and stroke dimensions. Bore spacing, wall thickness and coolant passage thickness dimensions are used to determine the coolant volume and

distribution in the head. Large bore spacing, giving an open water jacket, will increase the volume of coolant and mass of the head. Thus, the key dimensions for constructing the shape and size of the engine are the bore, bore spacing, wall thickness, coolant passage thickness, stroke, piston depth and conrod length. The configuration of the valve train is also a key variable. The sensitivity of predicted structural masses and coolant volumes to the key dimensions is examined in Chapter 4.

The generic templates can be adapted to match the geometric form of any engine whilst retaining a standardised description of each lumped capacity element and the thermal couplings between neighbouring elements. The ease with which minor or major changes can be made to an engine design is an additional advantage of the generic engine approach as it enables a family of similar engines to be assessed in a systematic way. Measured engine masses and coolant volumes can be used to verify that PROGEN is able to accurately represent the engine from the given data. Coolant volumes can be physically determined by filling the head, block and auxiliary components with water. The masses of the components can be weighed. Good correlation between measured and predicted values is essential. Figure 3.5a (based on data from [3.1]) illustrates the level of agreement between measured and predicted head and block masses for a number of V-type and in-line engines. Corresponding results for the total coolant volume in the engine are given in Figure 3.5b [3.1]. Agreement between the data is generally to within a few percentage points. In each case, the values were generated using a default set of scaling factors to generate initial values predicted by PROGEN. For each version of the model, up to ten scaling factors can be used to optimise the predictions of mass and coolant volume. The scaling factors are used to adjust the thickness of the coolant passage walls, crankshaft bearing housing, cylinder wall, portside outer wall and crankcase wall. They are also used to adjust the volume of additional coolant (in the auxiliaries and pipe work) and the volume of coolant in the block and the head. When optimised for specific engines, the scaling factors can improve default PROGEN predictions. This is illustrated in Figure 3.6 for the 1.25l Sigma and the 2.5l V6 engine. The sensitivity of PROGEN predictions to the scaling factors is examined in Chapter 4.

Two main templates were developed to represent in-line and V-type engines [3.1][3.2]. The in-line template is used as a base for both gasoline and diesel engines. Currently, the V-type template is used as a basis for gasoline engines only, although a V-type diesel version is undergoing development. Valve train configurations are selected from the five main types defined in the friction model (see Section 3.3). Similarly, either a flat or roller follower can be chosen. Both U-flow (intake and exhaust ports on the same side of the head) and cross-flow (intake and exhaust ports on opposite sides of the head) heads, illustrated in Figure 3.4, can be selected.

3.2.3 Lumped Capacity Analysis

The lumped capacity approximation used in PROMETS to describe the heat flow and temperature distributions requires the engine structure to be divided into a number of solid elements. Physical and thermal properties are defined for each element. The surface areas exposed to fluid or adjacent elements and the conduction path lengths between these are determined. The thermal coupling between adjacent elements or an element and the adjacent fluid enables the calculation of local conditions such as transient heat flows and temperatures within the engine structure. In areas of the engine where the thermal response is of particular interest, a greater number of smaller elements have been used to increase the resolution of the predicted temperature fields. The volumes and surface areas of individual elements can be specified accurately, although linear dimensions may be described less quantitatively.

The basis for decisions on the number of elements used to represent the engine structure is comparisons of predicted temperatures and heat flows with heat distributions predicted using a proprietary FE code (PAFEC) for identical boundary conditions [3.3]. Previous researchers have shown that, in general, the lumped capacity formulation gives reasonably accurate predictions of most thermal features that can be measured [3.2][3.3]. Stability criteria, described in the following Section, must also be met.

A general indication of how the engine structure is divided up into elements is shown for an in-line engine in Figure 3.7 and for a V-type engine in Figure 3.8. More detail is shown in the subsequent diagram (Figure 3.9), with explicit numbering of the elements shown for the head and the block of an in-line engine. In the current versions of PROMETS, the number of lumped capacity elements is 41 for the in-line models (both gasoline and diesel) and 54 for the V-type; the exact number will depend upon the number of valves per cylinder. The V-type model employs more elements than the in-line version in order to represent the cylinder block in more detail. For the V-type, the total number of elements is divided between 31 elements for the cylinder block, 7 elements for the head, 2 elements for the piston, 3 elements for each valve and a further 2 elements for miscellaneous items in the coolant and oil circuits. The in-line version uses 18 elements to describe the block.

Each element of the engine model is assumed to have a uniform temperature distribution and is thermally coupled to adjacent elements and/or adjacent fluid. For transient thermal analysis, the net energy transfer into an element must equal the increase in internal energy, ΔE , of that element [3.4]. The rate of change of internal energy of an element, i , is given by,

$$\frac{\Delta E}{\Delta t} = C_i \left(\frac{T_i^{p+1} - T_i^p}{\Delta t} \right) \quad (3.1)$$

Where

$$C_i = \rho_i c_i \Delta V_i \quad (3.2)$$

The superscript p is used to denote the time dependence of element temperature, Δt is the time step length, ρ_i is the element density, c_i is the specific heat capacity of the element, ΔV_i is the element volume, T_i^p is the element temperature at the current time step and T_i^{p+1} is the element temperature at the next time step. The energy balance for element i can therefore be written as,

$$\dot{Q}_i + \sum_j \frac{T_j^p - T_i^p}{R_{ij}} = C_i \left(\frac{T_i^{p+1} - T_i^p}{\Delta t} \right) \quad (3.3)$$

Where \dot{Q}_i is the internal heat generated, T_j^p is the temperature of an adjacent element or fluid at the current time step and R_{ij} is the thermal resistance between element i and an adjacent element or fluid.

An explicit forward difference method is employed in PROMETS to calculate the temperature of each element at time step $p+1$ from the knowledge of the temperatures of the same and adjacent element(s) at the preceding time step, p . The energy balance can be rearranged to give an expression for T_i^{p+1} ,

$$T_i^{p+1} = \frac{\Delta t}{C_i} \left[\dot{Q}_i + \sum_j \frac{T_j^p - T_i^p}{R_{ij}} \right] + T_i^p \quad (3.4)$$

3.2.4 Stability and Accuracy Criteria for the Structure

The validity of the lumped capacity assumption and number of elements used in PROMETS have been proven by comparisons with a proprietary FE code (PAFEC) for identical boundary conditions [3.3]. The validity of the assumptions is also supported if the following criteria are met, as these provide a necessary, if not comprehensive, assessment of the accuracy and stability of the model. These criteria demonstrate the minimum conditions that must be met to achieve accuracy and stability in the engine thermal structure.

- **Stability Criteria**

For the solution to Equation 3.4 to be numerically stable, the maximum size of the time step, Δt , must be fixed to avoid oscillation of the predicted temperature. The stability requirement can be examined by rearranging Equation 3.4 to give [3.3],

$$T_i^{p+1} = \frac{\Delta t}{C_i} \left[\dot{Q}_i + \sum_j \frac{T_j^p}{R_{ij}} \right] + \left[1 - \frac{\Delta t}{C_i} \sum_j \frac{1}{R_{ij}} \right] T_i^p \quad (3.5)$$

The value of \dot{Q}_i can influence stability, but it is possible to choose a safe limit by observing the behaviour of Equation 3.5 for the condition $\dot{Q}_i = 0$. If the coefficient of T_i^p becomes negative, a condition is then created which contradicts the second law of thermodynamics. To avoid this situation and achieve stability, the following Equation must be true,

$$1 - \frac{\Delta t}{C_i} \sum_j \frac{1}{R_{ij}} \geq 0 \quad (3.6)$$

This can be expressed in terms of the time step, Δt ,

$$\Delta t \leq \left[\frac{C_i}{\sum_j \frac{1}{R_{ij}}} \right]_{min} \quad (3.7)$$

The maximum allowable time step can be calculated for each element. The time step chosen for the whole model must be less than the smallest time step calculated using Equation 3.7. Generally, a time step larger than 0.3 seconds will not meet the convergence criteria. In the model, a time step of 0.1s is found suitable in most circumstances.

- **Accuracy Criteria**

A potential source of inaccuracy in the model solution results from the approximation of a uniform temperature distribution within each element. This is fundamental to the application of the lumped capacity technique. The heat transfer between connected elements 1 and 2, for example, is determined from,

$$\dot{Q}_{12} = A_{12} \frac{(T_1 - T_2)}{\frac{\Delta X_{1 \rightarrow 2}}{k_1} + \frac{\Delta X_{2 \rightarrow 1}}{k_2}} \quad (3.8)$$

Where A_{12} is the contact surface area and ΔX is the conduction path length. Figure 3.10 shows the definition of heat conduction path length for a pair of thermally coupled elements. In order for the assumption of a uniform temperature distribution to be true for elements in direct thermal contact, the

temperature difference between the two elements in contact must be as small as possible and both elements must contribute equally to the resistance to heat flow across the connecting surface. If there is a big temperature difference between elements 1 and 2, i.e. $T_1 \gg T_2$ or $T_1 \ll T_2$, there must be a large temperature gradient within one or both lumps, since not less than half the temperature change occurs in one lump. The largest temperature difference will occur in the lump with the greatest resistance element $\Delta X/k$.

It is assumed within PROMETS that temperatures are spatially uniform within each element that is adjacent to a fluid. In order to make this assumption, the resistance to convection from the element should be large compared to the resistance to conduction within the element. The Biot number (Bi) provides a measure of the temperature drop in the solid relative to the temperature difference between the surface and the surrounding fluid. This is actually defined for an element completely surrounded by fluid, but is applied to elements within PROMETS (which may only have one side in contact with the fluid and the rest in contact with other elements) as an assessment of the minimum conditions that must be met to ensure spatial uniformity of the temperature distribution. For conditions where $Bi \ll 1$, the resistance to conduction within the element is much less than the resistance to convection across the fluid boundary layer, and thus the assumption of a uniform temperature distribution across the element at any time during a transient is reasonable. The Biot number is defined as,

$$Bi = \frac{hV}{kA} \quad (3.9)$$

Where V is the element volume, A the element surface area, h the convective heat transfer coefficient and k is the element thermal conductivity. For $Bi \leq 0.1$, the error in the lumped capacity assumption is 5% or less [3.5].

Most modern internal combustion engines are manufactured from traditional engineering materials, such as cast irons and aluminium alloys. These materials have high thermal conductivities and satisfying the Biot number condition presents few problems. However, care must be taken with those parts of the engine structure that are in contact with engine coolant where the heat transfer

coefficient is high. If the model were to be extended to include engine designs employing modern engineering materials such as fibre reinforced polymers and ceramics, greater care would be needed in defining the elemental description of the engine, since these materials have thermal conductivities which are substantially lower than ferrous and aluminium alloys, as shown in Table 3.1.

3.2.5 Boundary Conditions of the Engine Structure

Although the lumped capacity model of the engine's metallic structure has been used as the core of the engine representation, various sub-models are required to calculate the boundary conditions at its internal and external surfaces. Energy is input to the engine structure by heat transfer from the combustion gases and by the dissipation of friction at the rubbing surfaces. Heat is transferred from the structure to the coolant at coolant passage surfaces and to the lubricating oil at the oil gallery surfaces and valve deck. Heat transfer also occurs to ambient from the external surfaces of the structure that are exposed to the surroundings. The main components of the sub-models used to define these heat transfer conditions are described in the following Sections (3.3 to 3.10). The head gasket is assumed to be thermally insulating and forms the boundary condition between the block and the head.

Generally, warm-up characteristics are least sensitive to details of features such as bearing support plates and the thermal coupling between the crank case wall and other structural parts. These can be modelled using relatively simple approximations. Of greatest importance are the boundary conditions for heat exchange between the structure and gas and oil film conditions. However, there is very little information on heat transfer coefficients that would allow this to be modelled in a fundamental way. The approach adopted during the development of PROMETS was to examine the sensitivities of predictions to the various uncertainties involved and show that predictions are well conditioned [3.3][3.6][3.7].

3.3 FRICTION

Frictional power dissipation in PROMETS is calculated using the Patton *et al* [3.8] model for fully warm friction. The fully warm case is considered here first before describing how corrections are made for the higher friction levels that pertain to warm-up conditions.

The Patton model calculates losses in terms of the friction mean effective pressure (FMEP) to enable the comparison of relative engine performance. Previous researchers [3.9][3.10] who examined the quality of predictions made by Patton's original model found that agreement between measured and predicted values of FMEP is poor for engines that lie outside the scope of the original work. Thus, a correction is applied to the FMEP calculated by the Patton model, $FMEP_{Patton}$. The correction takes the form outlined below:

$$FMEP_{corr} = (a + b\bar{S}_p)FMEP_{Patton} \quad (3.10)$$

The constants a and b change with engine type and are defined in Table 3.2. No correction is applied for diesel engines (the constants take the values 1 and 0), as the modified piston friction term, described below, eliminated any need. The inconsistency in correction term between the gasoline in-line and V-type engines is due to the calculation of the piston friction term in the original Patton model [3.2]. The values of a and b differ from the general V engine values for the Jaguar 4.0l V8 engine, as Hayden [3.11] found that the original V-type correction over-estimated friction by 50% at speeds in the region of 6000rpm. This was attributed to a low friction Nikasil coating on the cylinder liner; previous engines all had cast iron liners.

The calculation of fully warm friction is separated into four main components associated with reciprocating components, the valve train, the crankshaft and auxiliary components. The proportion of the total friction that is contributed by each component is indicated in Figure 2.1 for 1.6l gasoline and diesel engines. The frictional losses from each component group are broken down into sub-models based on lubrication theory (boundary, mixed or hydrodynamic); in other cases empirical correlations have been used. A description of each

component follows. The units for FMEP, mean piston speed, engine speed and engine dimensions are kPa, m/s, rev/min and m respectively.

- **Crankshaft Components**

Crankshaft friction is represented as the sum of three terms. The terms represent the main bearing seals and the main bearings operating under hydrodynamic friction and turbulent dissipation. The empirical constants for each term are listed in Table 3.3a [3.8].

$$FMEP_{crank} = C_{bl} \left(\frac{D_b}{B^2 S n_c} \right) + C_{hl} \left(\frac{N D_b^3 L_b n_b}{B^2 S n_c} \right) + C_{td} \left(\frac{D_b^2 N^2 n_b}{n_c} \right) \quad (3.11)$$

Where n_c is the number of cylinders, n_b is the number of bearings, D_b is the diameter of the bearings in m and L_b is the length of the bearings in m.

- **Reciprocating Components**

The reciprocating friction group is that defined by Patton *et al*, with the exception of the piston term, which for diesel engines was modified from the original term by Baylis [3.9]. Piston friction for gasoline engines is described according to the original Patton formulation.

Piston friction for gasoline engines,

$$FMEP_{piston} = C_{ps} \left(\frac{S_p}{B} \right) \quad (3.12)$$

Modified piston friction for diesel engines [3.9],

$$FMEP_{piston, mod} = 1.4 C_{ps} \left(\frac{S_p^{1.4}}{B} \right) \quad (3.13)$$

Where S_p is the mean piston speed in meters per second. The friction between the piston rings and liner is divided into two terms representing the predicted friction for the piston rings without gas pressure loading and with gas pressure loading. Both terms predict total values for all rings and the ring tension is assumed to be the same for all engines. The term for the effect of gas loading

on the piston rings is based on an empirical relationship developed by Bishop from firing friction data [3.12].

Piston rings, without gas loading,

$$FMEP_{piston\ ring,\ tension} = C_{pr,t} \left(\frac{1+1000}{N} \right) \frac{1}{B^2} \quad (3.14)$$

Piston rings, with gas loading,

$$FMEP_{piston\ ring,\ gas\ loading} = C_{pr,gl} \left(\frac{p_i}{p_a} \right) \left[0.088r_c + 0.182r_c^{(1.33-0.0238S_p)} \right] \quad (3.15)$$

Where p_i is the intake pressure and p_a the atmospheric pressure, r_c is the compression ratio and S_p the mean piston speed. The con rod bearings term takes the same form as the hydrodynamic term for the main bearings,

$$FMEP_{conrod} = C_{hl} \left(\frac{ND_b^3 L_b n_b}{B^2 S n_c} \right) \quad (3.16)$$

Where n_c is the number of cylinders, n_b is the number of bearings, D_b is the diameter of the bearings in m and L_b is the length of the bearings in m. The total friction due to reciprocating components is the sum of the above terms,

$$FMEP_{reciprocating} = (FMEP_{piston} \text{ or } FMEP_{piston, mod}) + FMEP_{piston\ ring,\ tension} + FMEP_{piston\ ring,\ gas\ loading} + FMEP_{conrod} \quad (3.17)$$

The constants for each term were determined using data from two motored open crank assemblies [3.8] and are shown in Table 3.3b.

• Valve Train

Patton *et al* [3.8] developed Equation 3.18 to describe the contribution of the valve train to the total FMEP. The different types of value train are illustrated in Figure 3.11. The values of the constants are given in Patton *et al* [3.8] and are tabulated in Table 3.3c.

$$\begin{aligned}
FMEP_{valvetrain} = C_{ind} + C_{cb} \left(\frac{Nn_b}{B^2 Sn_c} \right) + C_{rf} \left(\frac{Nn_v}{Sn_c} \right) + C_{ff} \left(1 + \frac{1000}{N} \right) \frac{n_v}{Sn_c} \\
+ C_{oh} \left(\frac{L_v^{1.5} N^{0.5} n_v}{BSn_c} \right) + C_{om} \left(1 + \frac{1000}{N} \right) \frac{L_v n_v}{Sn_c}
\end{aligned}
\tag{3.18}$$

Where n_v is the number of valves and L_v is the length of the valves. The first two terms of the expression represent the camshaft bearing hydrodynamic friction and the bearing seal friction. The third and fourth terms represent the friction generated by using a roller follower (third term) and a flat follower (fourth term); only one of these terms is used at any one time. The fifth and sixth terms represent the oscillating hydrodynamic and oscillating boundary friction respectively.

- **Auxiliary Components**

The components modelled consist of the oil and water pumps and non-charging alternator friction. Losses due to power steering and air conditioning pumps are not modelled. Patton *et al* [3.8] assumed that the modelled component power losses were proportional to engine displacement and therefore, that the FMEPs could be expressed as a function of engine speed only,

$$FMEP_{auxiliary} = C_{aux,1} + C_{aux,2}N + C_{aux,3}N^2 \tag{3.19}$$

The constants $C_{aux,1}$, $C_{aux,2}$ and $C_{aux,3}$ are shown in Table 3.3d. The individual terms of the expression have no physical significance.

3.3.1 Friction during Warm-up

Friction is higher during warm-up due to the effects of high oil viscosity at low temperatures. In the early seconds of engine operation, the rates of change in engine friction are high. This slows as quasi-steady thermal conditions are established in the engine. Under quasi-steady conditions, a viscosity dependent correction of the fully-warm value of friction power loss is applied and has been shown to give good agreement with experimental data [3.13].

$$FMEP_{wu} = \left(\frac{\mu_{oil}}{\mu_{oil, fw}} \right)^n FMEP_{fw} \quad (3.20)$$

Where μ_{oil} is the viscosity of the oil at the current temperature and $\mu_{oil, fw}$ is the reference oil viscosity at a temperature of 90°C. Christian [3.3] determined that the friction index, n , generally varies between 0.19 and 0.24, depending on engine type and is influenced by the non-linear dependence of viscosity on the temperature difference. For SAE 10W-30 and SAE 20W-50 oils, n was found to be 0.19 and 0.16 respectively [3.10]. The effect of values of n on predicted friction values is discussed in Chapter 5. Details of oil property calculations are given in Section 3.7.

During the initial seconds of engine operation, friction levels are significantly higher than predicted by Equation 3.20 alone. During the first minute or so of engine operation, friction levels depend on local thermal conditions at the rubbing surfaces, which can dictate the viscosity of the oil film. This can be more than double the oil-feed viscosity corrected value and is mostly dependant upon start temperature and on subsequent operating conditions [3.10][3.14]. Thus, a correction factor, C_{f0} is used to account for the higher friction levels on start up and is calculated using the following function [3.9],

$$C_{f0} = 1 + 0.55e^{-T_{oilfeed}/35} \quad (3.21)$$

Where $T_{oilfeed}$ is the initial oil temperature. The predicted friction at start up may then be adjusted by multiplying the result of Equation 3.20 by the factor C_f , where,

$$C_f = (C_{f0} - 1) e^{(-t/\tau)} + 1 \quad (3.22)$$

The rate of decay of the spike, defined by τ , was found to be independent of start temperature and a weak function of engine speed [3.9]. Using a value of $\tau = 50$ seconds provides a reasonable approximation that is adequate for modelling engine thermal behaviour. Figure 3.12 illustrates these components of friction prediction; initial start temperature, first 50 seconds and warm-up to steady state values.

3.4 FUEL FLOW PREDICTION

The prediction of fuel flow rates in the model is optional if experimental fuel flow rates are unavailable. Activation of the model is described in Chapter 4. The method described below enables fuel consumption to be predicted from generic information on engine behaviour [3.7][3.9]. It develops from the premiss that the rate at which fuel is consumed to produce a specified gross indicated power, the $ISFC_{gr}$, can be expressed as,

$$ISFC_{gr} = \frac{\dot{m}_f}{\dot{W}_{ind,gr}} \quad (3.23)$$

Where the gross indicated power, $\dot{W}_{ind,gr}$, is defined as,

$$\dot{W}_{ind,gr} = \frac{IMEP_{gr} V_s N}{2 * 60} \quad (3.24)$$

And where $IMEP_{gr}$ is an aggregate of brake, friction, auxiliary and pumping mean effective pressure,

$$IMEP_{gr} = BMEP + FMEP + FMEP_{auxiliary} + PMEP \quad (3.25)$$

BMEP is determined from the engine speed and load. FMEP is evaluated as described in Section 3.3. In the above equation, FMEP is taken as the fully warm value of friction. The $FMEP_{auxiliary}$ term is also described in Section 3.3. PMEP is calculated as the difference between exhaust and intake manifold pressures [3.9].

The $ISFC_{gr}$ can also be defined as,

$$ISFC_{gr} = \frac{1}{Q_{LHV} \eta_{comb} \eta_{ind,gr}} \quad (3.26)$$

For a diesel engine, the combustion efficiency, η_{comb} , is defined as [3.8],

$$\eta_{comb} = \min[0.98, 0.94 - 0.94 \ln(\phi)] \quad (3.27)$$

For a gasoline engine, the combustion efficiency, η_{comb} , is specified as [3.14],

$$\begin{aligned} \eta_{comb} &= 0.98 & \text{For } \phi < 1 \\ \eta_{comb} &= 2.662 - 2.26\phi + 0.577\phi^2 & \text{For } \phi \geq 1 \end{aligned} \quad (3.28)$$

Q_{LHV} , the lower heating value of the fuel, takes a value of 44.0 MJ/kg for gasoline and 41.5 MJ/kg for diesel fuels. The gross indicated thermal efficiency, $\eta_{ind,gr}$, is defined as,

$$\eta_{ind,gr} = \frac{\dot{W}_{ind,gr}}{\dot{m}_f Q_{LHV} \eta_{comb}} \quad (3.29)$$

In the diesel version of PROMETS, the gross indicated thermal efficiency is taken to be a fixed value of 0.41. In the gasoline versions of PROMETS this is represented by an empirical calculation as a function of compression ratio, r_c , and spark timing, θ , [3.7] where,

$$\eta_{ind,gr} = 0.86 \left(1 - \frac{1}{r_c^{\gamma-1}} \right) - 0.002\theta^2 \quad (3.30)$$

Equations 3.23, 3.24 and 3.26 can be combined to give an expression for the fuel flow rate,

$$\dot{m}_f = \frac{IMEP_{gr} V_s N}{Q_{LHV} \eta_{comb} \eta_{ind,gr} * 2 * 60} \quad (3.31)$$

In PROMETS, Equation 3.31 is solved using an iterative process. This is necessary as the exhaust manifold pressure, which is used to determine the pumping losses, is calculated as a function of air fuel ratio and fuel flow rate. Thus, an estimated value for the fuelling is required in order to determine the pumping losses. This is achieved by determining an initial estimate of the fuel mass flow rate, \dot{m}_f , based on zero pumping losses. This value can then be used to determine a more accurate value for PMEP (and therefore IMEP_{gr}) and hence enable a re-evaluation of \dot{m}_f . This process is repeated until convergence criteria are met. The algorithm for a gasoline engine is illustrated in Figure 3.13

[3.7]. Within PROMETS this method is used to calculate a fully warm fuelling value, based on fully warm FMEP.

The fully warm fuelling value can then be corrected for warm up using the following relationship,

$$\dot{m}_{f,wu} = \dot{m}_{f,fw} * \left[\frac{BMEP + FMEP_{wu}}{BMEP + FMEP_{fw}} \right] \quad (3.32)$$

Where $FMEP_{wu}$, the derivation of which is given in Section 3.3.1, is FMEP corrected for warm up.

3.5 GAS-SIDE HEAT TRANSFER

3.5.1 In-cylinder and Exhaust Port Gas-side Heat Transfer

The expression for gas-side heat transfer is derived from an energy balance of the heat transfer to and from the engine structure under fully-warm, steady-state conditions.

$$\dot{Q}_{cyl} + \dot{Q}_{pt} + \dot{Q}_{ex,man} + \dot{Q}_{fric} = \dot{Q}_{cool} + \dot{Q}_{amb} + \dot{Q}_{oc} \quad (3.33)$$

Terms on the left hand side of this energy balance represent the main sources of heat transfer while those on the right hand side represent the main heat sinks. Of the terms given, the cylinder and exhaust port heat transfer are the only contributions which are directly associated with gas-side heat transfer. However, for modelling purposes at most operating conditions it is possible to combine the term $\dot{Q}_{ex,man}$ with the exhaust port heat transfer term \dot{Q}_{pt} . Thus, the gas-side heat transfer rate, \dot{Q}_{clc2} can be defined as,

$$\dot{Q}_{cl,c2} = \dot{Q}_{cyl} + \dot{Q}_{pt} \quad (3.34)$$

This is expanded to include a weighted sum of the effective combustion chamber surface area and exhaust port area. Derivation of Equation 3.35 is given in Shayler *et al* [3.15].

$$\dot{Q}_{c1,c2} = C_1 \left(A_{cyl,eff} + C_2 A_{pt} \right) \frac{k_g}{B} (T_{g,a} - T_{cool}) Re_g^{0.7} \quad (3.35)$$

The effective cylinder area, $A_{cyl,eff}$, is defined in [3.13]. A_{pt} is the area of the exhaust port. k_g is the thermal conductivity of the combustion gases and $T_{g,a}$ is the effective gas average temperature. The constants C_1 and C_2 are defined in Table 3.4. The increase in the value of C_1 for diesel engines when compared to gasoline engines is attributed to the radiative component of the heat flux in the diesel engine. The difference between the values of C_1 for direct injection and indirect injection diesel engines is attributed to the improved thermal efficiency of the direct injection combustion chamber.

The weighted combustion chamber area accounts for the limited exposure of the lower liner when the piston is at BDC. The weighted exhaust port area accounts for differences between heat flux values in the cylinder and in the exhaust port.

The correlation can also be rearranged to give two separate expressions for the gas-side heat transfer rates in the cylinder and the exhaust port.

$$\dot{Q}_{cyl} = C_1 A_{cyl,eff} \frac{k_g}{B} (T_{g,a} - T_{cool}) Re_g^{0.7} \quad (3.36)$$

$$\dot{Q}_{pt} = C_1 C_2 A_{pt} \frac{k_g}{B} (T_{g,a} - T_{cool}) Re_g^{0.7} \quad (3.37)$$

For gasoline engines, the effective gas temperature, $T_{g,a}$, is expressed as a function of equivalence ratio,

$$T_{g,a} = \frac{1}{a - b\phi + c\phi^2 - d\phi^3} \quad (3.38)$$

The values for a , b , c and d are given in Table 3.5.

For diesel engines the effective gas temperature is also influenced by exhaust pressure [3.9], p_{ex} and can be described by,

$$T_{g,a} = a + bp_{ex} + (c + dp_{ex})\phi \quad (3.39)$$

The values for a , b , c and d are given in Table 3.6.

In addition to calculating the heat transfer rates to the cylinder and exhaust port, it is necessary to determine heat transfer rates to the liner, piston crown and cylinder head. These are calculated assuming that a reference surface flux density can be defined as [3.1],

$$\dot{q}'' = \frac{\dot{q}_{cyl}}{A_{pc} + A_{head} + \pi B \int_0^L F\left(\frac{x}{L}\right) dx} \quad (3.40)$$

Where A_{pc} is the area of the piston crown, A_{head} the area of the cylinder and,

$$F\left(\frac{x}{L}\right) = a_0 + a_1\left(\frac{x}{L}\right) + a_2\left(\frac{x}{L}\right)^2 + a_3\left(\frac{x}{L}\right)^3 + a_4\left(\frac{x}{L}\right)^4 + a_5\left(\frac{x}{L}\right)^5 \quad (3.41)$$

Values for the constants a_0 to a_5 are given in Table 3.7.

The heat transfer rate to the piston crown and cylinder head are determined by multiplying \dot{q}'' by the relevant areas, A_{pc} and A_{head} respectively.

The liner is heated by three different mechanisms; gas-to-surface heat transfer, frictional dissipation at the liner surface and by heat exchange with the piston rings. To determine the gas-to-surface heat transfer the function $F(x/L)$ is defined to relate the local heat flux at any point down the liner to the value at the top, which is always exposed to the cylinder gases. Hence, multiplying this function by the reference surface flux density gives a value for the gas-to-surface heat transfer of,

$$\dot{q}_{liner,C1C2} = \dot{q}'' \pi B \int_{x1}^{x2} F\left(\frac{x}{L}\right) \pi B dx \quad (3.42)$$

PROMETS models the frictional heating of the liner based on a constant friction force from each piston ring throughout a cycle. To determine the distribution of the frictional heating down the liner, the mean frictional force on the piston assembly is calculated using the Patton *et al* [3.8] model previously described in Section 3.3. The cycle-averaged distribution of the friction work is then

determined by considering the work done by friction during the movement of the piston through a distance, dx . If it is assumed that this dissipated energy is transferred to the liner, the energy transferred per unit area is then,

$$q'' = \frac{Fdx}{\pi B dx} = \frac{F}{\pi B} \quad (3.43)$$

Where F is the mean frictional force on the piston assembly.

Given that the piston will pass any one point in the liner four times during one cycle, the total heat flux per unit area at a given location is,

$$\dot{q}'' = \frac{4F}{\pi B} \cdot \frac{N}{120} \quad (3.44)$$

The liner receives heat from the piston rings over a section extending from the upper edge of the top piston ring at top dead centre (TDC) to the lower edge of the bottom piston ring at bottom dead centre (BDC). The heat transfer calculation is simplified by assuming that the heat flow through the rings is purely radial, and that there is no thermal contact resistance between the rings and the liner. The time averaged heat transfer rate through the piston rings can be written as [3.4],

$$\dot{q}_{rings} = Z \cdot \frac{2\pi k_{rings} w (T_{pc}^p - T_{liner}^p)}{\ln\left(\frac{B}{2} + \delta_c\right) - \ln\left(\frac{B}{2}\right)} \quad (3.45)$$

Where Z is the number of rings, k_{rings} is the average ring thermal conductivity, T_{pc}^p is the temperature of the piston crown at the current time step, p , and T_{liner}^p is the temperature of the liner. The ring dimensions, w and δ_c are illustrated in Figure 3.14. Since $\delta_c \ll (B/2)$, Equation 3.45 is approximated by,

$$\dot{q}_{rings} = Z \cdot \frac{2\pi k_{rings} w}{\delta_c} (T_{pc}^p - T_{liner}^p) \quad (3.46)$$

The variation of the total predicted heat flux distribution and of the individual components that contribute to the heating of the liner is shown in Figure 3.15.

3.5.2 Coolant Passage Heat Transfer

As described in Chapter 2, Section 2.2.4, two mechanisms of heat transfer operate in the cooling passages: forced convection and nucleate boiling [3.16]. The coolant passage heat transfer coefficient is calculated according to work by Chen [3.16] as a sum of the convective and nucleate boiling terms,

$$h = h_{conv} + h_{nucl,boiling} \left[\frac{(T_s - T_{sat})}{(T_s - T_{cool})} \right] \quad (3.47)$$

The convective term is represented by a modified Dittus-Boelter [3.17] equation,

$$h_{conv} = 0.023 Re^{0.8} Pr^{0.4} \frac{k}{D} \quad (3.48)$$

Where the Reynolds number, Re , the Prandtl number, Pr and the thermal conductivity, k , are values for the coolant. The nucleate boiling term is calculated as follows (the variables in Equation 3.49 are defined in the nomenclature),

$$h_{nucl,boiling} = 0.00122 \Delta T_{sat}^{0.24} \Delta p_{sat}^{0.75} S \left[\frac{k_l^{0.79} c_{p,l}^{0.45} \rho_l^{0.49}}{\sigma_l^{0.5} \mu_l^{0.29} (\Delta h_{lg} \rho_g)^{0.24}} \right] \quad (3.49)$$

Where S is a suppression factor defined by Chen [3.16], which takes a value near unity at low Reynolds numbers and decreases asymptotically as the Reynolds number increases.

The coolant passage heat transfer coefficient, h , as calculated above, does not yet account for variations in coolant and surface temperatures around the coolant circuit. To determine the corrected heat transfer coefficient, \bar{h} , the coolant passage heat transfer coefficient, h , is modified according to,

$$\bar{h} = \frac{1}{A} \int_0^A h F dA \quad (3.50)$$

Where,

$$F = \frac{(T_s - T_{cool})}{(T_s - T_{cool})_{ave}} \quad (3.51)$$

A typical distribution of F , for the 1.8l Zetec engine, is shown in Figure 3.16, and illustrates that F is reasonably uniform throughout the circuit except in the region of the exhaust port where F is typically doubled [3.7]. A simple approximation for F , based upon the total surface area of the coolant passage, A_{psg} and the passage area in the vicinity of the exhaust port, A_{pt} , can be defined such that,

$$F = \frac{A_{psg}}{A_{psg} + A_{pt}} \quad (3.52)$$

Except for the area around the exhaust port, A_{pt} , where,

$$F_{pt} = 2F \quad (3.53)$$

Integrating these values over the total area gives an average value of unity, consistent with Equation 3.47.

The determination of the corrected heat transfer coefficient facilitates the calculation of the heat transfer rate for each element, i , in contact with the coolant,

$$\dot{Q}_i = \bar{h}_i A_i (T_{cool} - T_s) \quad (3.54)$$

Where T_s is the surface temperature of the element. It is assumed that the surface temperature of the element can be approximated by the bulk element temperature.

3.5.3 Correction for Coolant Composition

Inspection of the equation for gas-side heat transfer (Equation 3.35) indicates that the predicted rate of heat transfer is independent of coolant composition. However, the composition of the coolant can have a significant effect on the heat rejected to the coolant and therefore on the gas-side heat transfer. Nucleate

boiling occurs when the coolant saturation temperature, which varies with composition as illustrated in Table 3.9, is reached and is accompanied by a marked increase in heat transfer to the coolant. Additionally, the other properties of the coolant change with composition, as illustrated in Figures 3.20 and 3.21 [3.18]. As a result, heat rejection to coolant decreases with an increasing proportion of ethylene glycol (EG) in the coolant, as EG has a higher saturation temperature than water. A change from a coolant composition of 50% water, 50% EG to 100% EG can result in as much as a 28% decrease in heat rejection [3.19]. Thus, nucleate boiling occurs at much higher temperatures in a water and EG mixture than in water alone, and for a given engine under the same operating conditions, less nucleate boiling will occur around the circuit containing the mixed coolant.

The expression for gas-side heat transfer, Q_{C1C2} , Equation 3.35, is derived for a coolant composition of 100% water [3.20], for which maximum heat rejection to coolant occurs. Thus, for compositions other than 100 % water it is necessary to correct the gas-side heat transfer to take account of the change in heat rejected to the coolant. This is achieved by defining a correction to the heat rejection to coolant based on the actual heat rejection rate and the reference heat rejection rate for 100% water [3.21]. This takes the form,

$$\frac{\dot{Q}_{act}}{\dot{Q}_{ref}} = \frac{\dot{Q}_m}{\dot{Q}_{water}} = [Correction] \quad (3.55)$$

Where \dot{Q}_m is the heat transfer rate to the coolant mixture. The correction is derived in Shayler *et al* [3.20] and is defined as,

$$[Correction] = \frac{\dot{Q}_m}{\dot{Q}_{water}} = \frac{1}{\left(\left(1 - \frac{\bar{h}_m}{\bar{h}_{ref}} \right) \frac{U^*}{h_m A} + 1 \right)} \quad (3.56)$$

Where,

$$U^* = 10.4k_g \left(\frac{\pi B}{4} \right) \text{Re}_g^{0.75} \quad (3.57)$$

\bar{h}_m is determined as described in Section 3.5.2.

Below coolant saturation temperature, coolant passage heat transfer is by convection only and can be calculated using Equation 3.48. Above this temperature nucleate boiling occurs. Solution of Equations 3.47 and 3.54 to determine the reference coolant passage heat transfer rate, \dot{Q}_{ref} , becomes more complicated when the heat transfer to coolant is by both convection and nucleate boiling, as a definition of the coolant passage surface temperature, T_s , is required. Previously implemented as an iterative set of equations in the 'C' version of PROMETS, the difficulty of implementing an iterative solution in the MATLAB/Simulink environment led the author to develop an alternative method of calculating the reference heat transfer coefficient. Simplifying Equation 3.47, the reference heat transfer coefficient can instead be expressed in terms of the degree of superheat, ΔS ,

$$h_{ref} = h_{conv,ref} + h_{nucl,boiling,ref} \left[\frac{\Delta S}{\Delta S + T_{sat,ref} - T_{cool}} \right] \quad (3.58)$$

Where,

$$\Delta S = (T_s - T_{sat,ref}) \quad (3.59)$$

This eliminates the need to determine a value for T_s and instead relies on the determination of a value for an effective degree of superheat, $\Delta \bar{S}$, that can be applied to all evaluations of the coolant passage heat transfer coefficient. The value of $\Delta \bar{S}$ should be such that for water, the mean corrected reference heat transfer coefficient is equal to the mean corrected actual heat transfer coefficient,

$$\bar{h}_{ref} = \bar{h}_m \quad (3.60)$$

In order to prevent the generation of negative or infinite values for Equation 3.55, the chosen value of ΔS should also be such that:

$$\Delta S + T_{sat,ref} - T_{cool} > 0 \quad (3.61)$$

An initial assessment, using a 1.6l Sigma engine, demonstrated that ΔS varies with brake power as shown in Table 3.8. A value of $\Delta S = 21^\circ\text{C}$ was chosen in

order to minimise errors across the speed-load range whilst meeting the criteria described above. In order to assess the impact of using this fixed value for ΔS , the locations at which nucleate boiling is predicted were determined for both low speed, low load (1000 rpm, 50 Nm) and high speed, high load conditions (6000 rpm, 120 Nm). In both cases, nucleate boiling only occurred in the coolant passages surrounding the exhaust port. Therefore, a fixed value of ΔS will only cause errors in the coolant passage heat transfer coefficients and structural temperatures around the exhaust port. Furthermore, any errors will only occur once nucleate boiling has commenced.

In order to determine the magnitude of the errors introduced, the coolant passage heat transfer coefficients, structural temperatures and bulk coolant and oil temperatures predicted using the fixed value of $\Delta S = 21^\circ\text{C}$ were compared with the results predicted using values of ΔS at which $\bar{h}_{ref} = \bar{h}_{act}$. Therefore, at the low speed, low load condition (1000 rpm, 50 Nm) results were compared for ΔS equal to 9.4°C and 21.0°C . For the high speed, high load condition (6000 rpm, 120 Nm) results were compared for ΔS equal to 21.0°C and 42.0°C . Comparisons were made for coolant mixture compositions of 50% water, 50% ethylene glycol (EG), as most simulations are performed under these conditions. Figures 3.19 and 3.20 illustrate the correlation between the results for both operating conditions. At steady state, low speed and load, an error of 1.6% is introduced into the calculation of the heat transfer coefficient. However, structural temperatures and bulk coolant and oil temperatures are unaffected. At steady state, high speed and load, a negligible error is introduced and again, structural temperatures and bulk coolant and oil temperatures are unaffected.

In order to confirm that the error introduced is negligible for any engine, predicted values of the steady-state reference heat transfer coefficient and the actual heat transfer coefficient are compared in Figure 3.19 for a coolant composition of 100% water, when the reference heat transfer coefficient should equal the actual heat transfer coefficient. This illustrates that the error introduced is much less than 5%.

Note that for a coolant composition of 100 % water the coolant correction term will approximately be one. For mixtures of water and EG the term will always be less than one. Nucleate boiling generally occurs, in a conventional coolant circuit, around the majority of the circuit under high load conditions and with a coolant composition of between 100% water and 50% ethylene glycol, 50% water. If 100% ethylene glycol is used as the cooling medium, nucleate boiling will only occur at the hottest parts in the circuit, such as around the exhaust ports. Figure 3.22 shows the predicted effect of the coolant composition on the heat rejected to coolant and coolant temperature during a low speed, high load warm-up.

3.5.4 Corrections for Spark and Injection Timing

The equation for gas-side heat transfer rate given in Section 3.5.1 applies for both SI and CI engines. For CI engines this is taken as the gas-side heat transfer rate for optimum injection timing and combustion. In practice, optimum injection timing is difficult to achieve and actual timing will vary depending on a number of parameters including engine speed, engine load, injection pressure and the properties of the fuel-air mixture. Given the complexity of these interactions, no correction for injection timing is currently made to the calculated gas-side heat transfer rate within PROMETSD.

For SI engines, Equation 3.35 is taken as the gas-side heat transfer rate at the Minimum advance for Best Torque (MBT); when spark timing is set at optimum. Although MBT calibrations are often used during warm-up and fully warm conditions, there are certain calibrations that may require alternative spark timing to be used, such as retardation of the spark to avoid knock and calibrations to control emissions. It is generally accepted, for example, that retarding spark timing reduces NO_x since the peak in-cylinder pressure, and hence temperature, are reduced. Additionally, some aftertreatment components, such as catalytic converters, require retardation of the spark to increase exhaust gas temperature and hence improve the performance of the component.

Since the in-cylinder temperatures are affected by spark timing, the heat transfer rate to coolant is also affected. Previous research [3.2] has found that the coolant heat transfer rate is proportional to the square of the retardation of the spark, relative to MBT in degrees. Thus, the gas-side heat transfer rate given by Equation 3.35 is corrected by a factor F_{spark} ,

$$\dot{Q}_{C1C2} = F_{spark} \dot{Q}_{C1C2} \quad (3.62)$$

Where

$$F_{spark} = 1 + 0.0002\theta^2 \quad (3.63)$$

3.5.5 Correction for EGR

The use of exhaust gas recirculation (EGR) has been introduced in both SI and CI engines as a method of reducing NO_x levels; increasingly stringent emissions legislation introduced in stages over the past three decades has lowered the level of NO_x permitted in the exhaust gas. All internal combustion engines have a degree of internal EGR due to residual gas dilution associated with clearance volumes and gas flow during the period of overlap when the intake and exhaust valves are open simultaneously. When external EGR is used, a proportion of the exhaust gas is recirculated to the intake system. By mixing the unburned cylinder charge with a proportion of exhaust gas, the heat capacity of the cylinder charge is increased due to the presence of additional dilutants from the exhaust gas.

The addition of EGR decreases the heat rejection rate to the coolant [3.2]. This effect is attributed to three mechanisms. The first is an increase in inlet charge temperature. Equation 3.64, which is based on experimental work by Povolny *et al* [3.19], takes account of the increase in charge temperature.

$$T_{g,a} = T_{g,a,298} + 0.35 \times (T_i - 298) \quad (3.64)$$

Where T_i is the gas temperature at the intake port and $T_{g,a,298}$ is the average effective gas temperature expressed as a function of equivalence ratio when the

intake temperature is 298 K, as previously described (see Equations 3.38 and 3.39).

The second mechanism is an increase in charge flow resulting from the introduction of EGR. This results in a change in the Reynolds number as defined below.

$$\text{Re} = \frac{4\dot{m}_f (1 + AFR / (1 - EGR))}{\pi B \mu_g} \quad (3.65)$$

Where the percentage EGR is defined as,

$$EGR = \left(\frac{m_{EGR}}{m_a + m_{EGR}} \right) \quad (3.66)$$

The third mechanism through which EGR affects gas-side heat transfer is an increase in the thermal capacity of the cylinder charge per unit mass of fuel burnt. This reduces the effective gas temperature. The net effect of these two changes can be accounted for using a simple correction F_{EGR} , applied to the basic correlation given in Equation 3.35. Details of the derivation of this empirical correction can be found in Hayden [3.2],

$$F_{EGR} = 1 - EGR \quad (3.67)$$

These three corrections can be easily applied to Equation 3.35 to account for EGR.

3.6 COOLANT SYSTEM

In the single representative cylinder version of PROMETS, details of the internal coolant circuit are not defined. The coolant volume, bulk temperature and representative flow velocity (to allow heat transfer coefficients to be calculated) are sufficient information to define behaviour. In the multi-cylinder version of PROMETS, two (or three, in PROMETSV) selectable designs of internal coolant circuit are available. These are illustrated in Figures 3.23, 3.24 and 3.25.

Temperatures around the circuits are calculated at the eleven defined points marked on the Figures.

Coolant flow rate through inner circuit components is calculated as a linear function of engine speed [3.6] and takes the form,

$$\dot{V}_{cool,ic} = aN + b \quad (3.68)$$

Where a and b are values that the user specifies. Alternatively, flow rates through the inner circuit as a whole can be similarly specified. In this case, the flow through each part of the inner circuit remains subject to the user-defined maximum flow rates that are imposed by flow restrictions in each component.

As previously mentioned, PROMETSD has been developed to cover the features of a relatively complex thermal management system with a heater matrix, oil cooler, EGR cooler and supplementary heater, that can be selected as required and placed in any order around the inner circuit. The oil cooler can be as part of the inner or the external coolant circuit. Examples of inner circuit configurations are shown in Figure 1.6. PROMETSI4 and PROMETSV contain a heater matrix, oil cooler and supplementary heater in the fixed order. The development of the in-line and V-type gasoline versions to allow greater flexibility in defining the inner circuit is in prospect.

The cabin heater, oil cooler and EGR cooler are all modelled using the effectiveness method of calculating heat transfer that is described by Kays and Crawford [3.22] and detailed in Chapter 6. For the cabin heater, values of effectiveness are determined from a 2-dimensional table as a function of air and coolant flow rates. Similarly, a 2-dimensional table of effectiveness values is used to determine oil cooler effectiveness in PROMETSD; this has yet to be implemented in the other versions of PROMETS (PROMETSI4 and PROMETSV) where a fixed effectiveness value of 0.4 is used. A fixed effectiveness value of 0.65 is used for the EGR cooler (an exhaust gas-air heat exchanger). The supplementary heater within PROMETS is modelled simply as an additional heat source to coolant where the rate of heat transfer is a function of coolant flow rate.

3.7 OIL SYSTEM

PROMETS has two oil circuit options based upon the oil circuits of two I4 engine designs. These are shown in Figures 3.26 and 3.27. The point at which a proportion of the oil is diverted to the head to lubricate the valve train and deck (point A) is different for each circuit. In V-engines, the oil flow at A is divided equally between the two heads. Since only one head is modelled, the heat transfer from the valve train and deck to the oil is calculated and then doubled. The ten different points around the oil circuit at which oil temperature is calculated are shown in Figure 3.28. Each of these points is also indicated on the two oil circuit diagrams, Figures 3.26 and 3.27.

Heat exchange with the structure enclosing the oil galleries occurs at the temperature points T_{U1} , T_{U4} , T_{C1} and T_{C2} . Temperature point T_{MI} models the temperature due to heat exchange between the crankcase walls and oil returning to the sump from the piston. Heat transfer between the piston underside and the oil cooling jets, the liner and oil mist (spray from the oil cooling jets) and the valve deck and oil is calculated using an empirically determined heat transfer coefficient of $50 \text{ W/m}^2 \text{ K}$ [3.3]. Heat transfer in the oil galleries depends upon local heat transfer coefficients and temperatures; these are directly related to the gas-side heat transfer to the cylinder and exhaust port walls. A laminar pipe flow correlation is used within PROMETS to represent heat exchange between the oil and the galleries. This assumption is supported by the calculated oil gallery Reynolds numbers that are given in Table 3.10 for different engines. The values were calculated from Ford-supplied mass flow rates and gallery dimensions and, since the transition from laminar to turbulent flow occurs at Reynolds numbers of between 2000 and 4000 [3.23], indicate that flow through the galleries is likely to be laminar. The temperature of the oil reaching the head, T_{U1} , for example, is defined as follows (the variables in Equations 3.69 – 3.71 are defined in the nomenclature),

$$T_{U1} = \frac{T_{blockave} + T_{C1} \left[\frac{\dot{m}_{oil} C_{p,oil}}{h \pi D_{head} l_{head}} \right] - 0.5}{\left[\frac{\dot{m}_{oil} C_{p,oil}}{h \pi D_{head} l_{head}} \right] + 0.5} \quad \text{For oil circuit 1} \quad (3.69)$$

$$T_{U1} = \frac{T_{blockave} + T_{B1} \left[\frac{\dot{m}_{oil} c_{p,oil}}{h \pi D_{head} l_{head}} \right] - 0.5}{\left[\frac{\dot{m}_{oil} c_{p,oil}}{h \pi D_{head} l_{head}} \right] + 0.5} \quad \text{For oil circuit 2} \quad (3.70)$$

Representative heat transfer coefficients are used to model heat transfer at boundaries where oil flow conditions are more complex, for example the temperature of oil reaching crankcase walls, T_{M1} ,

$$T_{M1} = T_{B1} + \frac{\dot{q}_{mist}}{\dot{m}_{oil} x c_{p,oil}} \quad (3.71)$$

Where \dot{q}_{mist} is the oil mist heat transfer rate to and from the oil and x is the proportion of oil flowing through the block.

Heating due to friction occurs at T_{P1} , T_{U2} , T_{U3} and T_{B1} where frictional losses occur from the piston, valve train, valve deck and crankshaft main bearings respectively. The value calculated for frictional loss (see Section 3.3) is dissipated both as heat in the oil and as heat transferred to the engine structure. The proportion of friction dissipated as heat in the oil for gasoline engines generally lies between 10 and 15 % of the total value [3.3]. A higher value of 20 % gives better agreement between predicted and experimental data for diesel engines [3.9]. This is attributed to differences in the conditions of contact between the oil and the structure.

The sump oil is assumed spatially uniform and the rate of change of sump oil temperature is determined from an energy balance [3.13].

$$M_{oil} c_{p,oil} \frac{dT_{oil}}{dt} = \dot{m}_{oil} c_{p,oil} (T_{U4} - T_{oil}) - h_{sump} A_{sump} (T_{oil} - T_{air}) \quad (3.72)$$

Where M_{oil} is the sump oil mass, T_{oil} is the sump oil temperature and T_{U4} the temperature of the oil returning to the sump. The sump heat transfer coefficient, h_{sump} , takes a value of 10 W/m² K [3.3]. The terms on the right hand side of the equation represent the energy of the oil returning to the sump and convective heat losses to ambient from the sump.

Oil viscosity in the gasoline versions of PROMETS is calculated using the Walther equation for kinematic viscosity, ν , in m^2/s [3.24],

$$\nu = \frac{\{ \exp [\exp (Walther1 + Walther2 * \log (T_{oil}))] - 0.6 \}}{10e06} \quad (3.73)$$

The constants Walther1 and Walther2 change with oil grade and are given in Table 3.11. In the diesel version, the Vogel equation [3.25] for dynamic viscosity, in kg/ms , is used as this was found to give better agreement with measured data [3.9],

$$\mu_0 = k_v * \left[\exp \left(\frac{\theta_1}{\theta_2 + T_{oil}} \right) \right] \quad (3.74)$$

The subscript, 0, refers to the low shear viscosity and the constants k_v , θ_1 and θ_2 depend on the oil grade used. Constants for SAE5W-30 and SAE10W-30 are given in Table 3.11. A comparison of the kinematic oil viscosity calculated using both Equations is given in Figure 3.29. Other oil properties are determined from a table of properties taken from Holman [3.4].

3.8 EXHAUST GAS TEMPERATURE

Prediction of the state of exhaust gas leaving the exhaust port of an engine is vital for the simulation of exhaust aftertreatment systems. The expression currently used within PROMETS is based on work by Allen and Baylis [3.26] and replaces the previous expression used in the original 'C' code version. Thus, at present, exhaust gas temperature within PROMETS is calculated using an energy balance across the engine, equating the energy input to the engine with the energy output from the engine, and is designed for use with both naturally aspirated and turbocharged engines. Naturally, the term \dot{H}_{EGR} is relevant only when EGR is being used.

$$\dot{H}_a + \dot{H}_f + \dot{H}_{egr} + \dot{H}_{rel} = \dot{P}_{br} + \dot{P}_{fric} + \dot{Q}_{cyl} + \dot{Q}_{pt} + \dot{Q}_{ex,man} + \dot{Q}_{amb} + \dot{H}_{ex} \quad (3.75)$$

The left hand side of the energy balance represents the enthalpies of the air and fuel at inlet to the engine and the heat released by the combustion of the fuel. The right hand side of the balance represents the combustion heat released to the major sources of energy dissipation; engine brake power, friction power, heat transfer to the cylinder, exhaust port, exhaust manifold and ambient, and the heat exiting the engine in the exhaust gas stream. The energy balance can be rearranged to give an expression for the exhaust gas energy,

$$\dot{H}_{ex} = (\dot{H}_a + \dot{H}_{egr} + \dot{H}_f + \dot{H}_{rel}) - (\dot{P}_{br} + \dot{P}_{fric} + \dot{Q}_{cyl} + \dot{Q}_{pt} + \dot{Q}_{ex,man} + \dot{Q}_{amb}) \quad (3.76)$$

Brake power, friction power, in-cylinder heat transfer, exhaust port heat transfer and ambient heat transfer are already calculated elsewhere in the model (see Sections 3.3, 3.5 and 3.10). The exhaust port heat transfer term includes heat transfer to the exhaust manifold.

The enthalpies of the fuel, air and EGR are calculated using equations of the form,

$$\dot{H}_x = \dot{m}_x c_{p_x} (T_x - T_{amb}) \quad (3.77)$$

Where the subscript x represents the fuel, air or EGR respectively.

These expressions account for the additional energy within the cylinder that arises from the increased temperature of the fluids above ambient. In a turbocharged engine, even when inter-cooled, the intake air will be at a temperature higher than ambient. On a naturally aspirated engine, the intake air temperature will be slightly greater than ambient due to heat transfer from the intake manifold to the intake air. Additionally, the temperature of EGR gas remains above ambient even after cooling.

The heat released by the combustion of the fuel is calculated from the following,

$$\dot{H}_{rel} = \dot{m}_f Q_{LHV} \eta_{comb} \quad (3.78)$$

The mass flow rate of fuel, \dot{m}_f , is calculated as described in Section 3.4. Q_{LHV} is the lower heating value of the fuel and takes a value of 44.0 MJ/kg for gasoline and 41.5 MJ/kg for diesel fuels. The efficiency of the combustion process, η_{comb} , is evaluated as in Equations 3.27 and 3.28.

Once \dot{H}_{ex} has been calculated using Equation 3.76, Equation 3.77 can be rearranged to give an expression for the temperature of the exhaust gas,

$$T_{ex} = \frac{\dot{H}_{ex}}{\dot{m}_{ex} c_{p,ex}} + T_{amb} \quad (3.79)$$

The mass flow rate of the exhaust, \dot{m}_{ex} , can be determined from a consideration of mass continuity across the engine.

3.9 TURBOCHARGER AND INTERCOOLER MODELS

Turbochargers are used to improve the specific power output of an engine by increasing the inducted air charge density. This allows a greater mass of fuel to be burnt within the cylinder at a given AFR. An exhaust gas turbocharger, consisting of a compressor impeller and a turbine on a single shaft, uses energy from the engine exhaust to drive the turbine. The impeller thus compresses the inducted air, increasing its density and temperature. Intercoolers are often used post-compressor to reduce the temperature of the charge entering the cylinder.

Estimates of intake temperatures and intake and exhaust pressures are required in order to evaluate the effect of turbocharging on heat rejection and pumping losses. Exhaust port pressures can reach 3 bar absolute for a turbocharged and intercooled engine compared to a maximum of 1.2 bar for a naturally aspirated diesel or SI engine at wide open throttle. Compressor outlet temperatures can be as high as 150 °C.

Reflecting current technological applications, the in-line diesel version is also the only version that currently features a turbocharger and intercooler model. These may be added to the gasoline versions in the future if required.

3.9.1 Turbocharger

Estimations of turbocharger performance in PROMETSD are based on static pressures and temperatures [3.9] in order to maintain consistency with manufacturers' definitions of temperatures and pressures. The analysis is also based upon adiabatic flow assumptions [3.27] as heat rejection to the turbine and impeller rotors is small in comparison to the energy flow through the system. At present, PROMETSD models a fixed geometry, wastegated turbocharger. The implementation of a variable geometry turbocharger sub-model, for engines such as the 2.0l Puma, is expected in the near future. Figure 3.30 illustrates the arrangement of a fixed geometry turbocharger. The subscripts 0, 1, 2, 3 and 4 are used for ambient, post compressor, post intercooler, pre turbine and post turbine positions around the engine. The temperature of the air exiting the compressor at a given exit pressure is given by [3.9],

$$T_1 = T_0 \left[1 + \frac{(p_1 / p_0)^{(\gamma-1)/\gamma} - 1}{\eta_{s,comp}} \right] \quad (3.80)$$

The temperature and pressure ratios are related through the perfect gas equation,

$$\left(\frac{p_1}{p_0} \right) \left(\frac{T_0}{T_1} \right) = \left(\frac{\rho_1}{\rho_0} \right) \quad (3.81)$$

The above Equations 3.80 and 3.81 can be solved for pressure ratio and temperature ratio for a given compressor isentropic efficiency and density ratio. In practice, it is difficult to determine a true value for compressor isentropic efficiency, as it is a function of several parameters. In PROMETS compressor isentropic efficiency is set at a value of 0.6. Previous research [3.9] has shown that this value is typical for the maximum measured efficiency. The density ratio is estimated from the following equation [3.9],

$$\frac{\rho_1}{\rho_0} \approx \frac{120\dot{m}_a}{\rho_0 V_d N \eta_v (1 - EGR)} \quad (3.82)$$

Where the engine speed, N , is in rev/min, V_d is the engine displacement in m^3 and η_v is the cylinder volumetric efficiency based on inlet manifold conditions. η_v is defined as a function of the mean piston speed, S_p [3.9],

$$\eta_v = 0.7 + 0.06S_p - 0.004S_p^2 \quad (3.83)$$

3.9.2 Intercooler

The intercooler is modelled as an ‘air to air’ cross-flow heat exchanger. The effectiveness-NTU method, described in detail in Chapter 6, is used to determine intercooler outlet temperatures.

3.10 HEAT TRANSFER TO AMBIENT

The heat transfer from the surface of a lumped capacity element that is exposed to ambient is determined from the following equation,

$$\dot{q}_{amb} = h_i A_i (T_i^p - T_{air}) \quad (3.84)$$

where h_i is the heat transfer coefficient of the surface of element i , A_i is the surface area of element i , T_i^p is the temperature of element i at the current time step, p , and T_{air} is the temperature of the surrounding air. The heat transfer coefficient takes an assumed value of $10 \text{ W/m}^2 \text{ K}$ [3.4] and it is assumed that the air temperature remains constant throughout the analysis.

3.11 DISCUSSION

The aim of the work presented in this Chapter is to provide a complete, thorough and up to date description of all versions of PROMETS. A summary of the fundamental differences between the versions is given in Table 3.12. There are several assumptions identified within the model that warrant the following observations:

At present, PROMETS assumes that the temperature of the air surrounding the engine remains constant throughout the analysis. This is generally representative of laboratory test conditions and of in-vehicle testing conditions at fully warm. The sensitivity of the model to the ambient air temperature, input by the user, is examined in Chapter 4. However, the air temperature in the compartment that surrounds the engine in-vehicle will change during warm-up as the compartment acts as an insulator, particularly in soundproofed diesel engines. The insulating effect of the compartment results in a gradual reduction in heat transfer to ambient as the under-bonnet temperature increases. The sensitivity of the model to this effect is examined in Chapter 5.

Oil mass flow rate is currently a user input to PROMETS. As fluid flow rates are often unknown and are seldom measured experimentally, a fixed bulk mass flow rate is used. In practice, oil mass flow rates are proportional to the rotational speed of the oil pump, subject to a limiting pressure controlled by the pressure regulation valve that is present on most engines. For oil pumps that are driven by connection to the crankshaft, this could be expressed as a linear function of engine speed, below a set maximum.

$$\dot{m}_{oil} = aN + b \quad \text{For} \quad p_{oil} < p_{max} \quad (3.85)$$

$$\dot{m}_{oil} = c \quad \text{For} \quad p_{oil} = p_{max} \quad (3.86)$$

Since the oil mass flow rate will have an effect on heat transfer rates and temperatures around the oil circuit, it would be appropriate to implement the above calculation, subject to sufficient available information from which to define the correlation.

The boundary condition between the head and the block was originally defined assuming that the head gasket is manufactured from cork and is thermally insulating. Most contemporary engines use pressed steel head gaskets. Experiments by Bohao *et al* [3.28] have demonstrated that a negligible amount of heat is conducted through such a gasket. However, if a dual cooling circuit, such as that shown in Figure 2.5 was in operation, the temperature difference between the head and the block could be greater, resulting in significant heat transfer across the boundary.

The Patton friction model calculates piston friction assuming that the combined ring tension from three rings (one oil control ring and two compression rings) remains the same for all engines. There is a general desire to move towards lower friction and in particular to reduce piston friction, as this contributes most significantly to overall engine friction [3.29]. Piston assembly friction is dominated by the ring friction, and thus the model would not cope with radical changes in design practice, such as a reduction in the number of compression rings or a removal of the oil control ring.

At present, the indicated thermal efficiency for diesel engines is set at a value of 0.41. Inspection of the equation for gasoline indicated thermal efficiency (Equation 3.30) and work by other researchers [3.7][3.9] shows that thermal efficiency varies with a number of factors, including compression ratio and equivalence ratio. Therefore, a fixed value is not representative for all engines and conditions and it would be appropriate to address this in the diesel model.

In Section 3.7 it was noted that the proportion of friction dissipated as heat in the oil for gasoline engines generally lies between 10 and 15 % of the total value [3.3] and that a higher value of 20 % gives better agreement between predicted and experimental data for diesel engines [3.9]. In order to determine the uncertainty that is introduced by this range of values, the sensitivity of PROMETS to the proportion of friction dissipated in the oil is explored in Chapter 5.

PROMETS uses five empirically determined heat transfer coefficients, for heat transfer between the structure and ambient, the sump and ambient, the piston underside and oil cooling jets, the liner and oil mist and the valve deck and oil. These were originally determined from comparisons between predicted and experimental oil warm-up data for an in-line gasoline engine over the full load and speed range. In general, PROMETS predictions compare well with experimental data, see Chapter 5, Section 5.4, however, the validity of these values for other engines has not been explicitly verified. The sensitivity of the model to these heat transfer coefficients is explored in Chapter 5.

In addition to the assumptions discussed above, there is also a discrepancy in the way that gas-side heat transfer constants, $C1$ and $C2$, were determined for

diesel engines. Normally, these are determined experimentally using an energy balance across the engine. In order for the coolant composition correction within the model to remain useable, these constants must be determined for a coolant composition of 100 % water. The values of C1 and C2 for diesel engines, which were determined by Baylis [3.9], were evaluated on engines using 50% water, 50% EG coolant mixtures. Therefore, for these values of C1 and C2 to be valid, the coolant composition correction must be deactivated when the model is run, to prevent the heat transfer rate from being further reduced. This also suggests that, had C1 and C2 been determined for 100% water, both values would have been higher than the current values for diesel engines listed in Table 3.4.

3.11.1 Concluding Remarks

Four key points can be drawn from this Chapter. Firstly, that PROMETS is a complex model comprising of several sub-models developed from physical and empirical correlations. Secondly, that the model requires user inputs to define the engine and operating conditions. Thirdly, that several sub-models utilise heat transfer coefficients and constants based on empirical data taken from specific engines and finally that the influence of current model assumptions must be considered when undertaking explorations of novel cooling circuits and engine designs.

Clearly, although the model is largely comprehensive, some of the assumptions made in the model need addressing. Chapter 4 examines the sensitivity of PROMETS to user inputs. The sensitivity of the model to assumptions made in the theory, where appropriate, is explored in Chapter 5. Areas that require or may require further development, such as the calculation of oil mass flow rates, are listed at the end of Chapter 9.

CHAPTER 4

SIMULINK AND THE STRUCTURE OF PROMETS

4.1 INTRODUCTION

At the outset of the author's investigations, PROMETS existed as a set of versions produced in 'C' code. The conversion of PROMETS into MATLAB/Simulink was undertaken by the author because MATLAB/Simulink was gaining rapid acceptance as the programming language of choice in the automotive industry. Considerations of compatibility with other CAE software, familiarity of users with Simulink and ease of software maintenance all suggested that conversion to Simulink would be a necessary and advantageous change.

In the previous Chapter, the main equation set and the theory behind each sub-model in PROMETS were outlined. This is followed here by an outline of the MATLAB/Simulink environment, details of the conversion of the model from 'C' to Simulink and a description of the structure and use of the model. Inputs to and outputs from the model are discussed, and the sensitivity of the model to user inputs is explored.

4.2 MATLAB AND SIMULINK

MATLAB is a suite of programs from Mathworks Inc. that includes dynamic system simulation software called Simulink. Simulink provides a graphical user interface (GUI) for building models in a block diagram format. Simulink models are hierarchical and can therefore be built using both top-down and bottom-up approaches. A hierarchical model structure simplifies understanding of complex systems, as the user can view the systems on the top level and then progress down through the levels to view more detail. This provides good

insight into the model structure and the interaction between its various parts. Simulink supports linear and non-linear systems modelled in continuous time, sampled time or a combination of both. Systems can also be sampled or updated at different rates if required. Models developed in existing code such as 'C' can be implemented using S-functions. The existing code is combined with the standard Simulink format of inputs and outputs and is then compiled into a dynamically linked library '.dll' file. The '.dll' file is then executed from the S-function block within the Simulink model.

4.3 MODEL CONVERSION

There is no automated process in MATLAB for converting programs from 'C' into Simulink. Eleven versions of the model were created during the conversion process from the original 3 'C' versions, as the practicality of loading and running each model placed restrictions on the size of each model. PROMETSV, for example, therefore includes 7 versions of the model: a single cylinder version, V6 multi-cylinder models for coolant circuits 1, 2 and 3, and V8 multi-cylinder models for coolant circuits 1, 2 and 3. A list of all versions and their sizes in Megabytes (Mb) is given in Table 4.1. The gasoline and diesel in-line multi-cylinder models contain descriptions of coolant circuits 1 and 2 (see Chapter 3, Section 3.6) The PROMETS package, comprising of the models, interface and help documentation, requires 40Mb of memory for the in-line gasoline and diesel versions and 130Mb of memory for the gasoline V-type.

The main difficulty encountered during conversion was in implementing iterative calculations. In the 'C' versions, fuel flow rates, the reference coolant passage heat transfer coefficient, the turbocharger (in the diesel version) and the distribution of heat flux down the liner were all calculated iteratively. Details of these calculations can be found in Chapter 3, Sections 3.4, 3.5.2, 3.9 and 3.5.1 respectively. In each case, the difficulty was overcome by implementing these calculations in Simulink as S-functions. However, without the original source files the user cannot access the compiled code, and so development of the model is underway to remove the S-functions, commencing with the non-

iterative solution to determining the reference coolant passage heat transfer coefficient that is described in Chapter 3, Section 3.5.3.

4.4 MODEL STRUCTURE

4.4.1 Graphical User Interface (GUI)

The graphical user interface (GUI), shown in Figure 4.1, is the main link between the user and PROMETS. Basic operations are performed through this Main Menu and subsequent menu systems by pressing ‘buttons’, removing the necessity for the user to learn commands in order to use the model. The GUI was developed by the author using the object orientated programming package available in MATLAB. In object oriented programming, basic objects, such as buttons, lists and text boxes, are arranged on a figure and can be programmed to specify an initial state and/or function when activated.

The Edit Menu, accessed from the main menu, is used to enter or edit engine geometry data and consists of several pages, as illustrated in Figure 4.2. The pages are divided into sections for head geometry data, block geometry data, details of cooling and oil circuits, details of auxiliary components and scaling factors (for optimisation of the masses and coolant volumes predicted by PROGEN, see Chapter 3, Section 3.2.2 and Section 4.5.2). Any changes made to the data on each page can be saved. In PROMETSD, two further pages containing details of the inner circuit and turbocharger are accessed from the main menu. Engine operating conditions and initial temperatures (see Section 4.4.4) are specified in the Operating Conditions Menu. The PROGEN Summary, as shown in Figure 4.3, displays the calculated masses for the block, head, crankshaft, piston, conrod, cam and valves, coolant auxiliaries, oil auxiliaries and the total engine mass. The volumes of coolant in the head, block, additional coolant (specified by the user in the scaling factors, see Section 4.4.4) and the total coolant in the engine are also displayed. PROGEN is run from the GUI and the PROMETS Simulink model, shown in Figure 4.4, is loaded. The GUI also contains a Results Plotter, developed by Gupta [4.1], designed to enable the

user to view basic variable plots. Data from previous sessions, which can be saved to a file through the Results Plotter, can also be loaded and reviewed.

The GUI is designed to minimise the possibility of user error. Pre-defined engine build files cannot accidentally be overwritten, values input to the engine geometry data file are subject, where appropriate, to geometrically imposed limits and the PROMETS model cannot be loaded if PROGEN has not been run.

4.4.2 PROGEN

At present, PROGEN comprises a number of files of MATLAB textual code, m-files, that are compiled to create a dynamic link library, '.dll', file. The structure of the files is shown in Figure 4.5 and the calculations undertaken in each file are described in Table 4.2. Although users cannot read the compiled file, this is not a problem as changes to the code are rarely required. The executable file is run from the PROGEN/PROMETS GUI. On a PC with an AMD Athlon 1.0 GHz processor and 1.0 Gb RAM, PROGEN takes about 4 seconds to run.

Data such as constants and engine geometry information that are used and generated by PROGEN is stored in MATLAB '.mat' files. These are loaded into the MATLAB workspace through the GUI as appropriate, so that the required variables are available to PROGEN or PROMETS. A list of the mat files used by PROGEN and PROMETS, and descriptions of the information they contain, are given in Tables 4.3 and 4.4 respectively.

4.4.3 PROMETS

The structure of PROMETS is hierarchical and is shown in Figure 4.6. Each block on the diagram represents a subsystem in Simulink. Lower systems are viewed either by clicking down through system blocks on the level above or through the Simulink model browser, which is accessed from the Simulink 'View' menu and displays the structure of the model. PROMETS is structured by thermodynamic function rather than by engine component. For example,

friction is calculated in one subsystem rather than individually in a subsystem for each applicable engine component. This is largely a result of the incremental development of the model over time, as individual models were developed and implemented separately in PROMETS. The structure enhances the possibilities of linking PROMETS with other models and of using PROMETS sub-models, such as the friction or fuelling models, within other simulation packages.

To link the systems and subsystems, calculated values are passed around the model using labelled ‘goto’ and ‘from’ flags, as illustrated in Figure 4.7.

4.4.4 Inputs and Outputs

Engine geometry data, ambient conditions and engine operating conditions are required inputs to PROMETS. Engine geometry data is required to generate the descriptions of the elements, coolant passages, oil galleries and engine set up. The required data includes the key dimensions identified in Chapter 3, Section 3.2.2, details of engine materials, piston dimensions, bearings, intake and exhaust port dimensions, valve train configuration and details of the coolant circuit, oil circuit and auxiliaries. A full list and description of the required engine geometry data is given in Morgan [4.2]. Scaling factors, that are used to optimise the masses and volumes predicted by PROGEN, as described in Section 4.5.2, also form part of the engine geometry data. These are used to adjust the thickness of the coolant passage walls, crankshaft bearing housing, cylinder wall, portside outer wall, crankcase wall and, for U-flow diesel engines, the wall thickness in the head on the injector side. They are also used to adjust the volume of additional coolant (in the auxiliaries and pipe work) and the volume of coolant in the block and the head. The sensitivity of PROGEN and PROMETS to the key engine dimensions and to the scaling factors is explored in Section 4.5.

Initial metal, oil and coolant temperatures are required to define the initial state of the engine. Ambient air temperature must also be defined and the sensitivity of PROMETS to this value is examined in Section 4.5.3. Operating conditions are necessary to define the drivecycle, steady state or warm-up conditions that are

to be simulated. Operating conditions that are used in thermal analysis simulations are discussed in the following Section. The minimum operating conditions required to define a simulation are engine speed, N (rpm), applied engine load, T (Nm), air-fuel ratio, AFR , and heater air flow rate, $\dot{m}_{a,hm}$ (l/s), spark advance ($^{\circ}$) or EGR percentage where applicable. When only a minimum set of operating conditions are specified, PROMETS predicts values for fuel flow rate, coolant flow rate (bulk and through the heater matrix) and engine out exhaust gas temperature. Alternatively, these variables can be specified if known. An example of an operating conditions input file for a gasoline engine is given in Table 4.5. For diesel engines, the spark advance column is removed and is replaced by columns for road speed and supplementary heat input to the coolant. Generally, operating conditions are specified at 1-second intervals and must commence at time 0 seconds, as in Table 4.5. However, they can be specified as any multiple of the basic time step of 0.1s, which is determined in Chapter 3, Section 3.2.4. It should be noted that the length of the simulation is controlled by the start and stop times specified in the simulation parameters in Simulink and not by the length of the operating conditions file. If the stop time specified in Simulink is after the end of the operating conditions specified, the conditions detailed in the last line of the file are used until the end of the simulation.

The most commonly required variables have been chosen as default outputs from PROMETS. Since temperatures do not generally change rapidly, all structural, coolant and oil temperatures are measured at 1-second intervals to reduce the amount of measured data. Heat transfer rates to or from the oil, coolant, piston underside, piston crown, piston rings, liner, head, intake and exhaust valves, exhaust port and ambient are measured at 0.1-second intervals, as are values for friction, indicated and brake power. Further outputs can be added to record any variable in the model if desired. The inputs to and outputs from PROMETS are illustrated in Figure 4.8.

4.4.5 Operating Conditions of Interest

PROMETS is capable of simulating engine thermal performance under a variety of operating conditions. Of particular interest are defined operating conditions such as Ford's Worldwide Customer Requirements (WCR) and the New European Drive Cycle (NEDC).

The WCR is designed to assess the performance of the cabin heater under the least favourable conditions; at low speed and light load conditions for an extended period with sub-zero initial and ambient conditions. The WCR specifies a minimum volume flow rate of air through the heater core for which the minimum acceptable air temperatures are then defined.

The NEDC is used to determine the quantities of CO, HC and NO_x produced by new vehicles over the cycle. The cycle itself, illustrated in Figure 4.9, consists of various idle and load conditions and is designed to be representative of typical driving patterns in Europe. The standard drive cycle is cold started at a temperature of 20 °C from 'key-on'. Guidelines for the NEDC cycle are set out in the EC Directive 91/441/EEC [4.3]. Using PROMETS, a simulation of the twenty-minute NEDC will take 3 minutes on a PC with an AMD Athlon 1.0 GHz processor and 1.0 Gb of RAM.

4.5 SENSITIVITY OF THE MODEL TO USER INPUTS

Required user inputs were discussed in Section 4.4.4. The aim of this sensitivity analysis is to indicate the level of confidence the user must have in input values. The sensitivity of the model to uncertainties in model assumptions, such as heat transfer coefficients, is dealt with in Chapter 5. The analyses described in the following Sections were carried out for a 1.6l Sigma engine. Since PROGEN and PROMETS are largely identical for all engine types, excepting the small differences identified in Chapter 3, the results derived for the Sigma engine will also apply more generally for other engine types such as diesels and V-type gasolines. The analyses described in Sections 4.5.3 to 4.5.5 were carried out at speed and load conditions of 1000 rpm, 120Nm and 3000 rpm, 5 Nm.

These conditions are designed to exaggerate the effects on friction and gas-side heat transfer respectively (as discussed in Chapter 5, Section 5.4). The simulations were conducted with zero EGR, zero spark advance, zero heater matrix air flow (effectively no cabin heater) and with an oil cooler in the inner circuit.

4.5.1 Key engine dimensions

The key dimensions for constructing the shape and size of the engine were identified in Chapter 3, Section 3.2.2 and in Figures 3.2 to 3.4 as the bore, bore spacing, wall thickness, coolant passage thickness, stroke, piston depth and conrod length. The configuration of the valve train was also identified as a key variable. Major engine dimensions such as the bore, bore spacing and stroke form part of the base specification of an engine and are usually well defined and readily available. As a result, there are not large uncertainties involved in specifying these dimensions. Details of the piston and valve train configuration are not always readily available during the earlier stages of engine design. Smaller dimensions, which are more difficult to measure, involve larger uncertainties, particularly for dimensions such as the wall thickness and coolant passage thickness, which vary around the engine. For these dimensions, PROGEN relies on the specification of an average value. This analysis examines the effect of a $\pm 10\%$ variation in the input values for wall thickness, coolant passage height, coolant passage width, piston depth and conrod length on the masses and coolant volumes predicted by PROGEN. The effect of the different valve train configurations is also explored. All tests were conducted with the scaling factors set to default, inactive values.

The results of the tests can be seen in Table 4.6, which shows the variation in percentages from the base engine predicted values for variations in the wall thickness, coolant passage height, coolant passage width, piston depth and conrod length. The masses of the head, block and piston, and the total mass of the engine, are most sensitive to changes in the wall thickness. For a 10% variation in wall thickness, the head mass changes by 2.5%, the block mass by

5.4%, the mass of the piston by 9.1% and the overall mass by 1.4%. The mass of the block is also sensitive to the conrod length and the piston depth, which affect the predicted values by 2.6 and 2.1% respectively. The piston mass is also sensitive to the piston depth, resulting in a variation of 7.5%.

The volumes of coolant in the head and the block are most sensitive to the coolant passage dimensions. A 10% variation in the coolant passage height affects the block coolant volume by 10%, and the total coolant volume by 2.9%. Similarly, a $\pm 10\%$ variation in the coolant passage width affects the block coolant volume by 10%, the head coolant volume by 1.7% and the overall coolant volume by 4.2%. The coolant volumes are also sensitive to the wall thickness, which affects the predicted values by 1.5% in the block and 1.4% in the head.

The effect of different valve train configurations on predicted head masses is shown in Table 4.7. As can be seen, the only valve train configuration to affect the head mass is that of the single overhead cam (SOHC) with a rocker arm (RA), which increases the mass of the head by 14.3%.

Although each of the key dimensions identified has an effect on either the total engine mass or the total coolant volume, it is clear from this analysis that the most significant dimension for determining engine mass is the wall thickness and that predicted coolant volumes are most sensitive to coolant passage dimensions. Conversely, the only valve train configuration to which the model is sensitive (in terms of predicted masses), is the SOHC with a rocker arm.

4.5.2 Scaling Factors

PROGEN uses up to ten scaling factors to enable the user to optimise the correlation between experimental and predicted masses and coolant volumes. This analysis examines the effect of a $\pm 10\%$ variation in each factor. The results of the investigation can be seen in Table 4.8, which shows the percentage variation from the base value for the masses of the head, block, piston, total engine mass, head coolant volume, block coolant volume,

additional coolant volume and total coolant volume. The other components listed on the PROGEN Summary - the masses of the crankshaft, conrod, cams and valves, coolant auxiliary components and oil auxiliary components - were not affected by changes in the scaling factors and have not been included in the Table.

The mass of the head is most sensitive to the scaling factor that alters the thickness of the portside outer wall, and shows a variation of 3.1% for the 10% change in scaling factor. This also has the greatest effect on the total engine mass at 0.5%. The mass of the block is most sensitive to the factor that alters the thickness of the crankcase walls, changing by 1.1%. The mass of the piston varies by 2.1% for the 10% change in the factor that alters the thickness of the piston crown.

The three factors that influence coolant volumes are direct acting; additional coolant specified is added directly to the total coolant volume, a ten percent increase in either scaling factor for the volume of coolant in the head or block results in a direct 10% increase in the coolant in the head or block respectively.

For the scaling factors that affect engine mass, this analysis shows that the model is well conditioned; the 10% variations in scaling factor value do not result in large changes for any of the masses predicted. Therefore, the scaling factors can reasonably be used for small adjustments only.

4.5.3 Ambient Temperature

It was noted in the Discussion in Chapter 3 that PROMETS assumes that the temperature of the air surrounding the engine remains constant throughout the analysis. This sensitivity analysis examines the effect of a $\pm 10\%$ variation in the ambient air temperature. The base case considered is for an ambient temperature of 20°C, thus the analysis examines the effect of ambient temperatures of 18°C and 22°C.

The effect of these temperature variations on the heat transfer to ambient is shown in Figure 4.10. The variations are similar for both operating conditions

tested and show a 2.4W change in the steady state heat transfer rate, 2% of the base heat transfer rate, for a 2°C change in ambient temperature. The variation in ambient temperature does not result in changes to engine external structural temperatures or in bulk coolant and oil temperatures.

Overall, this demonstrates that the model is not significantly sensitive to small variations in ambient air temperature.

4.5.4 Oil Circuits

Two oil circuits are modelled in PROMETS, as discussed in Chapter 3, Section 3.7 and shown in Figures 3.26 and 3.27. The work reported here examines the sensitivity of the model to the circuit chosen.

The net heat transfer rates to the oil, comprising of the heat transferred from the structure, frictional heat retained in the oil and heat transferred to or from the coolant, are shown in Figure 4.11 for both operating conditions. The figure shows that the choice of circuit has no effect at the low speed, high load condition, and that a small but negligible effect is seen at the high speed, low load condition. At this condition, at fully warm, the heat transfer rate to the oil is 974.1 W for circuit 1 and 979.1 W for circuit 2. This difference is a 0.5% change in heat transfer rate and has no effect on bulk oil temperature.

4.5.5 Coolant Circuits

Three coolant circuits are modelled in PROMETS, as discussed in Chapter 3, Section 3.6. Only two of these circuits, shown in Figures 3.23 and 3.24 are available in all three versions of the model and so only the influence of these two circuits is illustrated here.

Tests conducted using the single cylinder model showed no difference in the heat transfer to coolant or in bulk coolant temperatures between the two coolant circuits, as these are not explicitly modelled in the single cylinder version. Tests conducted using the multi-cylinder model, which calculates the

temperature of the coolant at points around the internal coolant circuit, are shown in Figures 4.12 and 4.13. The results show a negligible effect at the high speed, low load condition but a noticeable effect on heat transfer to coolant, and bulk coolant and oil temperatures at the low speed, high load condition. At fully warm, the heat transfer rate to coolant for circuit 1 was 7.3 kW and for circuit 2 was 7.2kW, which represents a 1.4% change in heat transfer rate. Fully warm bulk coolant and oil temperatures are identical, but a noticeable difference occurs for approximately 200 seconds after thermostat opening. At high load, the heat transferred from the combustion gases to the cylinder and hence to the coolant is much greater, and so the effect of the different coolant circuit is exaggerated.

4.6 PROMETS APPLICATIONS

PROMETS meets a variety of applications needs for thermal analysis. These range from more basic applications and engine design optimisation tasks to the limited addition to or alteration of the original model in order to examine a particular component or design change. PROMETS is also constantly being developed as the model is updated to reflect new research or as new functionality is added to meet industry research needs.

Basic applications of PROMETS usually involve little user interaction with the model. The pre-defined engine build files are used to generate the engine geometry data, through PROGEN, and PROMETS generates warm-up or steady-state coolant, friction, fuelling or exhaust gas temperature profile predictions. The most basic application of the model is illustrated in the flow diagram in Figure 4.14. A typical simulation using the single cylinder version of PROMETS will take 3 minutes on a PC with an AMD Athlon 1.0 GHz processor and 1.0 Gb RAM. The same simulation using the multi-cylinder version takes 7 minutes.

Engine design optimisation involves the assessment of a family of engine designs in order to determine which is most fit for purpose. Often, the user needs to generate a new base engine build file. Existing files can be used as the

base for new engine build files by altering the data and saving the file with a new name. Once engine geometry data has been entered into the engine build file through the GUI, an iterative process takes place to optimise PROGEN-predicted masses and coolant volumes by using the scaling factors described in Chapter 3, Section 3.2.2 and Section 4.5.2. The optimisation process is illustrated in the flow diagram in Figure 4.15 and is conducted through the GUI as before. Once the engine geometry data has been collected, entering the data into a build file and using the scaling factors to optimise the masses and coolant volumes predicted by PROGEN takes approximately 30 minutes.

4.5 DISCUSSION

The aim of the work presented in this Chapter is to empower the reader to use PROMETS. The general structure and function of the model has been described. Required inputs and default outputs have been detailed. Studies of the sensitivity of the model to user inputs have highlighted areas where caution is required in determining input values and those where values do not need to be as accurate.

PROGEN currently offers a choice of cast iron and aluminium for engine materials. However, demands for weight reduction, to improve thermal performance and fuel economy, have forced manufacturers to investigate other materials. Most recently, compacted graphite iron (CGI) has been adopted as an alternative to conventional grey iron. CGI has significant advantages over traditional materials and offers opportunities for reduction in engine weight and size, improvement in long-term dimensional stability, wear resistance and noise vibration harshness (NVH) [4.4][4.5][4.6]. Several production engines now use CGI [4.7][4.8] and it is expected that CGI will be used for the next generation of diesel engines as peak in-cylinder pressures continue to increase [4.8]. The development of PROGEN to allow user inputs for material properties or to widen the selection of engine materials available would be appropriate to meet the expected desire to model CGI components. However, since the conductivity of CGI is much lower than that for aluminium alloy or cast iron (see Table 3.1), it

would also be necessary to confirm that the Biot number condition for model accuracy is still met (see Chapter 3, Section 3.2.4).

The examination of the sensitivity of predicted masses and coolant volumes to the key engine dimensions showed that the wall thickness is the most important variable for determining the mass of the engine. Similarly, the coolant passage dimensions are most significant for calculating the volume of coolant in the head and block. It is imperative, therefore, that the user takes great care in specifying these variables. The difficulty lies both in measuring these and subsequently in determining an average value that represents the variation of these dimensions around the engine. Ideally, these dimensions should be specified from CAD (computer aided design) drawings or other documents, to reduce measurement errors. However, these are often unavailable, and instead the wall thickness and coolant passage dimensions should be measured at as many points around the engine as possible. In this case, the average value should be determined by considering the median, rather than the mean value, to avoid taking too great an account of very small or very large values.

All other sensitivity analyses were conducted with no EGR, spark advance or cabin heater air flow rate. This does not affect the results presented in this Chapter. The operating conditions that were chosen for these investigations were selected in order to exaggerate the effects on friction and gas-side heat transfer respectively (as discussed in Chapter 5, Section 5.4). Additionally, a study of driving behaviour [4.9] found that 91% of a vehicle trip is carried out at engine speeds of less than 3000 rpm. This indicates that the two speeds chosen for this study (1000 rpm and 3000 rpm) are also representative of vehicle engine speeds and that the results determined from the sensitivity analyses apply more generally.

The choice of oil circuit has little effect on heat transfer to oil, bulk oil and coolant temperatures or FMEP at the lower speed condition tested. A small difference in the net heat transfer rate to the oil was seen at 3000 rpm, although the effect on bulk oil and coolant temperatures and FMEP was negligible. Given the dependence of friction on speed, it is likely that the difference in heat

transfer rate between the two oil circuits would be greater at speeds higher than those tested. However, the difference is unlikely to be significant.

The internal coolant circuit chosen is not significant for simulations conducted using the single cylinder model. However, multi-cylinder simulations are responsive to the internal coolant circuit, particularly at high load.

4.5.1 Concluding Remarks

Two key points can be drawn from this Chapter. Firstly, the hierarchical structure of PROMETS is well suited to several types of application of the model, enabling different levels of understanding and access as required. Secondly, the relative insensitivity of the model to user inputs demonstrates that the model is well conditioned to the small inaccuracies imposed by systematic measurement errors and, in general, absolute precision measurements are not required. However, the model is sensitive to user inputs of coolant passage and wall thickness dimensions, which must be specified as accurately as possible.

The following Chapter explores the effect of model assumptions on output values.

CHAPTER 5

SENSITIVITY AND PERFORMANCE

5.1 INTRODUCTION

Assessments of model fidelity are usually based on evaluations of the performance and stability of the model, sensitivity analyses and user judgement. It is important that the user has faith in the model predictions and also comprehends the level of accuracy that can be expected in comparisons between experimental and predicted data. Generally, this is achieved through the comparison of predictions with experimental data at a few operating conditions that represent the operating range of the engine. Previous 'C' versions of PROMETS have been evaluated over a range of operating conditions for a range of engine types. This has included evaluations of individual sub-models and of global model variables. Test data have included temperature distributions along the liner, see Figure 5.1 [5.1], full and part load heat rejection rates to coolant under steady-state conditions for various cases, see Figure 5.2 [5.2] and local metal temperatures for the cylinder head combustion surfaces, and coolant and oil heat rejection, see Figure 5.3 [5.3].

One formulation for determining the maximum usable time step has been examined in Chapter 3. Using the criteria described, the maximum time step for stability was determined to be 0.3s, and a time step of 0.1s is currently used in the model. However, PROMETS has many interacting components and it is possible that either individually or as a result of the interactions that the actual limits may be tighter. Consideration of the time scales over which variables experience significant change provides one qualitative assessment of the suitability of the chosen time step. For example, as illustrated in Figure 5.4, the response of liner temperatures to a step change in operating condition, from idle to maximum speed and load, demonstrates the shortest time scales over which engine structural temperatures change. The change in input results in a

maximum temperature gradient of 5 °C per second. In the 0.1s between time steps, the maximum temperature change experienced will therefore be 0.5 °C. It is possible to use a smaller time step in the model. However, this will increase run times without significantly increasing the resolution of calculated variables.

An indication of model self-consistency can be obtained by performing an energy balance on the engine structure to verify that energy is conserved within PROMETS. In the model, the energy source to the engine structure is the sum of in-cylinder heat flux, exhaust port heat transfer rate and the generated friction power losses. The energy sink is the sum of the increase in internal energy of the structure, the heat rejected to coolant, the heat transferred to the oil and ambient heat losses. Figure 5.5 shows a typical energy balance during warm-up on a 2.5l V6 engine model at 3000 rpm, 120 Nm. The difference between the accumulated energy source and energy sink is 2.4% at steady-state conditions, approximately 600 seconds from the engine start in this case. When the run-time is extremely long, for example 6000 seconds, the difference is approximately 0.6%, illustrating that the model is consistent to within acceptable limits.

Part of the previous Chapter explored the sensitivity of the model to user input values. In this Chapter, the effect of model assumptions on output values is explored. An approach to evaluating model performance is also described, including examples of evaluations carried out following the conversion of PROMETS into Simulink. The evaluation of structural temperatures is not directly addressed, as these are not routinely measured.

5.2 SENSITIVITY TO MODEL ASSUMPTIONS

In order to indicate the level of confidence the user can have in the assumptions within the model, it is relevant to assess the sensitivity of PROMETS to the values of empirically determined constants used in various sub-models. The sensitivity of PROMETS to the assumed degree of superheat, ΔS , has already been explored in Section 3.5.3 of Chapter 3.

The analyses described in the following Sections were carried out for a 1.6l Sigma engine. Since PROGEN and PROMETS are largely identical for all engine types, excepting the small differences identified in Chapter 3, the results derived for the Sigma engine will also apply more generally for other engine types such as diesels and V-type gasolines. The analyses described in the following Sections were carried out at speed and load conditions of 1000 rpm, 120Nm and 3000 rpm, 5 Nm. These conditions are designed to exaggerate the effects on friction and gas-side heat transfer respectively (as discussed in Section 5.3). The simulations were conducted without EGR or heater matrix air flow (effectively no cabin heater) and at MBT spark timing. The Sigma engine also uses an oil cooler in the inner coolant circuit. Throughout the analyses, comparisons of warm-up rates are based upon coolant and oil half-rise times. These are defined as the time taken for the temperature of the coolant to rise by 60 degrees and the time taken for the temperature of the oil to rise by 40 degrees. Each test was carried out over 1200 seconds to ensure that fully warm conditions were reached for each operating condition.

5.2.1 Friction Index

The value of the friction index, n , used in Equation (3.12) to calculate the level of friction during warm-up was found by Christian [5.4] to vary between 0.19 and 0.24 depending on engine type and is influenced by the non-linear dependence of viscosity on the temperature difference. For SAE 10W-30 and SAE 20W-50 oils, n was found to be 0.19 and 0.16 respectively [5.5]. Recent work by Baylis [5.6] on a 1.9 TDi engine found that n is a function of engine speed for speeds between 0 and 1000 rpm:

$$n = (1 + 0.006N)^{-0.9} \quad (5.1)$$

At 1000 rpm, this gives a value of 0.17. Presently, the value of n used in PROMETS is dependant upon the oil grade and takes the values listed above as appropriate. In this analysis, the effect of n at values of 0.16, 0.20 and 0.24 is assessed to evaluate the sensitivity of the model.

The analysis shows that the value of the friction index affects a number of engine variables. Figures 5.6a and 5.6b show the variation of FMEP with friction index at both operating conditions. As the friction index, n , is used to correct values of friction during warm-up, fully warm FMEP values are unaffected by the variations in n . However, initial FMEP values, at both operating conditions, are significantly affected, with a change from n at 0.16 to 0.20 resulting in a 9.4% rise in initial FMEP value. Similarly, a change in n from 0.20 to 0.24 results in a further 10.4% rise. The rises in FMEP during warm-up affect net heat transfer rates to the oil (comprising of the heat transferred from the structure, frictional heat retained in the oil and heat transferred to or from the coolant) prior to fully warm as shown in Figure 5.7. The increases in n from 0.16 to 0.20 to 0.24 result in 9.4% and 10.4% increases in the initial net heat transfer rate to the oil. This gives rise to an increase in the heat rejected to the coolant, shown in Figure 5.8, as heat is transferred from the oil to the coolant via the oil cooler. As with the heat transfer rate to the oil, the effect levels off as fully warm values are approached.

The effect of the changes in heat transfer rates to the oil and coolant can be seen in the bulk coolant and oil temperature profiles shown in Figure 5.9. Both coolant and oil half rise times decrease as the friction index increases, as shown in Table 5.1. The effect is significant; the coolant half rise time is reduced by 20 seconds when the friction index is increased from 0.16 to 0.24 at a speed of 3000 rpm. Coolant half rise time for a friction index of 0.16 is 205 seconds, so this represents a 10% reduction in the half rise time. Similarly, the oil half rise time is reduced by 16 seconds when the friction index is increased from 0.16 to 0.24 at 3000 rpm. This represents a 9% reduction in the half rise time. The difference in fully warm oil and coolant temperatures is negligible.

It is clear from this analysis that, at the conditions tested, the friction index has an effect of up to 10% on predictions of initial friction values and friction during warm-up. This translates directly to predictions of the heat transferred to the oil during warm-up and to the heat rejected to coolant, resulting in changes of up to 10% in the bulk coolant and oil half rise times. The effects are greater at higher speeds. Fully warm predictions are unaffected.

5.2.2 Proportion of Frictional Dissipation Retained in Oil

Previous research [5.4][5.6] has indicated that the proportion of frictional heat retained in the oil (rather than conducted locally into the engine structure) varies between 10 and 20%, depending upon the engine examined. In this analysis, the effect of varying the proportion from 10 to 15 to 20% is examined to determine the sensitivity of the model to the value used.

The percentage retained in the oil (Friction To Oil – FTO) was found to have an effect on a number of different variables. Figure 5.10 shows the variation of the net heat transferred to the oil (comprising of the heat transferred from the structure, frictional heat retained in the oil and heat transferred to or from the coolant) for different percentages of friction retained. It is evident that the different FTOs have a significant effect on initial heat transfer rates. The initial net heat transfer rate to the oil is 33% higher for an FTO of 15% than for 10%, and again 33% higher for an FTO of 20% than for 15%. Once the thermostat has opened, the heat transfer rate to the oil is the same for all FTOs as excess heat is transferred to the coolant through the oil cooler.

The percentage FTO also affects the heat transfer rate to the coolant. Steady state heat transfer rates at 3000 rpm, 5 Nm decrease by 0.8% for each increase in FTO. The effect at 1000 rpm, 120 Nm is negligible, a 0.1% decrease in heat transfer rate, as the contribution of heat from the combustion gases to the heat transfer rate to the coolant is much greater than that from the oil. This effect is because as the percentage of frictional heat dissipation retained in the oil increases, less heat is transferred to the structure and thus directly to the coolant. The rate of heat transfer to the coolant from the oil via the oil cooler is subject to the effectiveness of the oil cooler (see Chapter 7, Section 7.3).

The overall effects of the changes in heat transfer rates to the oil and coolant can be seen in the bulk coolant and oil temperature profiles shown in Figure 5.11. Coolant warm-up is not greatly affected at either operating condition, although the warm-up slows marginally with increasing FTO. However, oil warm-up times, particularly at the high speed condition, decrease noticeably with the increase in FTO, as indicated by the oil half rise times shown in Table

5.2b. Fully warm oil temperatures at the high speed condition increase by 2 °C for each increase in FTO. The higher oil temperatures also have implications for the overall FMEP, as oil viscosity decreases with increasing oil temperature. There is very little difference in FMEP at the low speed condition, but at the high speed condition each increase in FTO results in a 1.5% decrease in FMEP, as shown in Figure 5.12a. This results in a 1.1% and 2.0% decrease in the total fuel consumed over the 1200 seconds of the simulation when the FTO is increased from 10% to 15% and from 10% to 20% respectively, as shown in Figure 5.12b. This is summarised in Table 5.2c.

5.2.3 Values of Gas-side Heat Transfer Constants, C1 & C2

The model to determine heat transfer from the combustion gases to the cylinder liner and exhaust port that is described in Section 3.5 of Chapter 3 uses empirically derived constants C1 and C2 to determine the distribution of the heat between the cylinder and the port. The total gas-side heat transfer is calculated using the following formulation,

$$\dot{Q}_{c1,c2} = C_1 (A_{cyl,eff} + C_2 A_{pt}) \frac{k_g}{B} (T_{g,a} - T_c) Re_g^{0.7} \quad (5.2)$$

In this analysis, the effect on engine variables of varying C1 and C2 and thus the distribution of heat is explored. In order to maintain the same overall gas-side heat transfer, C1 and C2 are adjusted using the following relationship:

$$C_{1,new} A_{cyl,eff} + C_{1,new} C_{2,new} A_{pt} = C_{1,old} A_{cyl,eff} + C_{1,old} C_{2,old} A_{pt} \quad (5.3)$$

The analysis was conducted by varying C1 by $\pm 10\%$ and calculating C2 from Equation (5.3). A 10% increase in the value of C1 results in an 18.7% decrease in the value of C2. A 10% decrease in the value of C1 results in a 22.7 % increase in the value of C2. The values of C1 and C2 used are given in Table 5.3a. Since the percentage change in C2 is so much greater than the 10% change in C1, it is clear that if C2 were altered by 10% the change in the value of C1, calculated from Equation (5.3), would be much less than 10%. Thus, the

overall change in the distribution of the gas-side heat would be less than that described above and any variations in engine variables would be smaller.

The proportions of the gas-side heat transferred to the cylinder and to the exhaust port for each case are shown in Table 5.3b. A 10% increase in the value of C1 corresponds to a 5.2% increase in the proportion of heat transferred to the cylinder and a 5.2% decrease in the proportion of heat transferred to the exhaust port. The inverse is true for a 10% reduction in the value of C1. Figures 5.13 and 5.14 show heat transfer rates to the cylinder and exhaust port for both operating conditions. The 10% change in C1 results in a constant 10.5% change in the actual heat transfer rates to the cylinder and the exhaust port at both operating conditions.

The effect on liner and exhaust port temperatures is illustrated in Figures 5.15 and 5.16, which show temperatures for liner elements 1 (top of the liner) and 6 (bottom of the liner) and the exhaust port element. The effect of the change in the distribution of heat is marginally greater at the low speed, high load condition as the gas-side heat transfer is a larger proportion of the heat transferred to the structure than friction at this condition. Fully warm liner and exhaust port temperatures are only affected by 1 or 2 °C, as shown in Tables 5.4a, b and c. Prior to thermostat opening, however, exhaust port temperatures are affected by up to 7 °C, as shown in Table 5.5a.

At neither condition does the variation in C1 and C2 have a significant effect on coolant and oil heat transfer rates, although at the low speed, high load condition, the onset of nucleate boiling occurs sooner and the heat transfer rate to the coolant responds, as shown in Figure 5.17a. This translates into a small improvement in coolant half rise times, as is evident in Figure 5.17b and listed in Table 5.5b. Predictions of FMEP are unaffected.

Overall, although the distribution of the gas-side heat between the cylinder and the exhaust port is sensitive to the changes in the values of C1 and C2, the change in the distribution does not translate into significant changes in steady state liner or exhaust port temperatures, coolant or oil heat transfer rates or bulk coolant and oil temperatures. However, exhaust port temperatures prior to thermostat opening are sensitive.

5.2.4 Fixed Heat Transfer Coefficients

Chapter 3 identified four empirically determined heat transfer coefficients that are used in PROMETS. In this Section, the sensitivity of the model to variations in the values used is examined.

Several cases of interest are examined for the ambient and sump heat transfer coefficients. Standard correlations for free convection are used to estimate heat transfer coefficients for the 1.6l Sigma engine in the laboratory or a stationary vehicle and correlations for forced convection are used to estimate heat transfer coefficients for the engine in a moving vehicle. The heat transfer coefficient for free convection from an isothermal surface can be calculated using the following Nusselt-Grashof correlation [5.7],

$$Nu_f = C(Gr Pr)^m \quad (5.4)$$

C and m vary with application and are listed in Table 5.6.

$$Gr = gB \frac{(T_w - T_\infty)}{\nu^2} l^3 \quad (5.5)$$

$$\text{Where, } B = \frac{1}{T_{film}}, l = \frac{A}{P}, T_{film} = \frac{(T_w + T_\infty)}{2}$$

T_w is the temperature of the plate, T_∞ is the temperature of the air, T_{film} is the film temperature, A is the area of the plate in m^2 , P is the perimeter of the plate in m, ν is the kinematic viscosity in m^2/s and g is the acceleration due to gravity in m/s^2 .

Heat transfer coefficients for forced convection from the sump are estimated from flat plate analyses that assume the surface is isothermal. For laminar flow, where the Reynolds number, $Re < 5 \times 10^5$, the heat transfer coefficient can be determined from the following Nusselt-Reynolds correlation [5.7],

$$Nu = 0.664 Re^{\frac{1}{2}} Pr^{\frac{1}{3}} \quad (5.6)$$

For turbulent flow, where $Re \geq 5 \times 10^5$, the following correlation applies [5.7],

$$Nu = Pr^{\frac{1}{3}}(0.037 Re^{0.8} - 871) \quad (5.7)$$

Figure 5.18 illustrates the variation of Nu with Re determined using the correlations in Equations 5.6 and 5.7. Heat transfer coefficients for forced convection from the surface of the engine to ambient are estimated using the flat plate analyses above and by considering a bluff body. For a bluff body, the average heat transfer coefficient can be determined from the following correlation [5.7],

$$\frac{hd}{k} = C \left(\frac{u_{\infty} d}{\nu_f} \right)^n Pr^{\frac{1}{3}} \quad (5.8)$$

Where C and n are constants and are given in Table 5.7 for a range of shapes. u is the air speed in m/s, ν_f is the kinematic viscosity of the air in m^2/s and d is the characteristic dimension in m, indicated for each shape in Table 5.7.

The oil heat transfer coefficient is used to calculate heat transfer between the valve deck and the oil and between the oil mist (created by the piston cooling jets) and the liner. The piston underside heat transfer coefficient is used to calculate the heat transfer between the piston cooling oil jets and the piston underside. Figure 5.19 illustrates the locations for which the oil and piston underside heat transfer coefficients are defined. Oil and piston underside heat transfer coefficients are varied by $\pm 10\%$. The magnitude of this change is relatively small. Typically, the uncertainty in the value of heat transfer coefficients that are internal to the engine (and that are therefore difficult to determine experimentally) might be $\pm 100\%$. Therefore, the variation examined here is intended as an indication of the response of the model.

- **Sump Heat Transfer Coefficient**

At present, the sump heat transfer coefficient in PROMETS takes a value of $10 \text{ W/m}^2 \text{ K}$. Using the correlation for free convection, Equation 5.4, a heat transfer coefficient of $7 \text{ W/m}^2 \text{ K}$ was determined. At a vehicle speed of 70 mph (112 kph) and air speed of 31 m/s, flow over the engine sump is laminar and a heat transfer coefficient of $50 \text{ W/m}^2 \text{ K}$ was calculated using the correlation for

laminar forced convection, Equation 5.6. Both values were determined for a fully warm engine in an ambient air temperature of 20°C. These two values are used in conjunction with the current value to illustrate the sensitivity of the model to the value of the heat transfer coefficient.

The heat transfer rate to ambient through the sump is illustrated in Figure 5.20 for heat transfer coefficients of 7, 10 and 50 W/m² K at both operating conditions. At fully warm, there is an increase of 675% between the heat transfer rates from the sump to ambient for heat transfer coefficients of 7 and 50 W/m² K. The increase in the heat transfer rate to ambient affects oil temperatures, reducing the fully warm oil temperature by up to 4°C at both operating conditions, as shown in Table 5.8a. This results in an increase in FMEP and consequential increase in fuel consumption of up to 1.3% at the high speed condition. Fuel consumption details are given in Table 5.8b. Although, through the oil cooler, the reduction in oil temperature also affects the heat transfer rate to the coolant, the change in coolant temperatures is negligible.

For laboratory testing, the heat transfer coefficient is sufficiently close to that determined above for the effect on oil temperatures and fuel consumption to be negligible. However, for comparisons against data for the engine in a moving vehicle, the change in heat transfer coefficient and its effect on oil temperatures and fuel consumption must be taken into account.

- **Ambient Heat Transfer Coefficient**

At present, the ambient heat transfer coefficient in PROMETS takes a value of 10 W/m² K. Using the correlation for free convection, Equation 5.4, a heat transfer coefficient of 5 W/m² K was determined. Considering an under-bonnet air flow rate of 5 m/s, heat transfer coefficients of 17 W/m² K and 21 W/m² K were determined when considering a square bluff body and flat plate respectively. All values were determined for a fully warm engine in an ambient air temperature of 20°C. The sensitivity of the model to the value of the heat transfer coefficient is assessed by comparing heat transfer coefficients of 5 and 20 W/m² K with the current value of 10 W/m² K.

The heat transfer rate to ambient is illustrated in Figure 5.21 for the heat transfer coefficients at both operating conditions. There is a marked difference in the heat transfer rates, which are listed in Table 5.9a. In general, the temperatures of elements exposed to ambient on the external surface of the engine are not affected, although crankcase temperatures vary by up to 4°C from the temperatures predicted for the current heat transfer coefficient of 10 W/m² K as shown in Table 5.9b. The temperature variations have a small effect on oil temperatures, resulting in changes in the heat transfer rate to coolant and thus coolant temperatures. However, steady state oil temperatures vary by less than 1°C and coolant and oil half rise times vary by a few seconds, as shown in Tables 5.9c and d.

The effect on predicted variables is small for the range of heat transfer coefficients considered in this analysis, demonstrating that assumption of a fixed heat transfer coefficient of 10 W/m² K is adequate for the range of conditions experienced by the engine.

- **Oil Heat Transfer Coefficient**

The oil heat transfer coefficient currently used in PROMETS takes a value of 50 W/m² K. Values of 45 and 55 W/m² K are used to assess the sensitivity of the model to the value used. The variations of the heat transfer rates between the valve deck and oil, and liner and oil mist are seen in Figures 5.22 and 5.23. At the point of maximum difference, changes of up to 9.9% and 9.7% are seen in the heat transfer rates to the valve deck and oil mist respectively when varying the heat transfer coefficient from the base value of 50 W/m² K. The percentage difference in the heat transfer rate to the valve deck remains constant during warm-up and until steady state is reached. However, the heat transfer rate to the oil mist is slightly less under steady state conditions at 9.0%. The effect on liner and valve deck temperatures is negligible, as these two heat transfer rates are much smaller than other heat transfer rates to and from the valve deck and liner respectively, as shown in the energy balances in Figure 5.24 and 5.25.

This analysis suggests that larger variations of ±100% in the heat transfer coefficients would not have a large effect on liner or valve deck temperatures.

- **Piston Underside Heat Transfer Coefficient**

The piston underside heat transfer coefficient currently used in PROMETS takes a value of $50 \text{ W/m}^2 \text{ K}$. This analysis examines heat transfer coefficients of 45, 50 and $55 \text{ W/m}^2 \text{ K}$ to assess the sensitivity of the model.

It can be seen in Figure 5.26 that the variation in the heat transfer coefficient has a significant affect on the heat transfer rate between the piston underside and the oil. A change of up to $\pm 9\%$ is seen in the heat transfer rate when varying the heat transfer coefficient from the base value of $50 \text{ W/m}^2 \text{ K}$. However, the effect on piston temperatures is negligible, as the heat transfer rate from the piston underside to the oil is much less than either the heat transfer rate from the combustion gases to the piston crown or the heat transfer rate from the piston through the rings to the liner. This is shown in the energy balance in Figure 5.27. Thus, the variation in piston underside heat transfer rate has little effect on the overall energy balance and piston temperatures. As a result, no other variables are affected.

This analysis suggests that larger variations of $\pm 100\%$ in the heat transfer coefficients would not have a large effect on piston temperatures.

5.2.5 Ambient Temperature

PROMETS assumes that the temperature of the air surrounding the engine remains constant throughout any analysis. Whilst this is generally representative of laboratory test conditions and of in-vehicle testing conditions at fully warm, the insulating effect of the engine compartment during warm-up is not accounted for. Modelling the effect of the engine compartment on the ambient air temperature would require the development of a new sub-model. However, an appreciation of the effect can be gained by considering a warm-up from 20°C to fully warm with an insulated engine structure. This represents the case where the ambient air temperature is the same as the temperature of the structure and thus no heat transfer occurs.

The simulated compartment has a negligible effect on the external surfaces of the engine in the head and the portion of the block down to BDC, with steady state temperatures affected by less than 1 °C. However, crankcase temperatures are affected by up to 5°C at steady state, as shown in Table 5.10a. This has an effect on the net heat transfer rate to the oil (comprising of the heat transferred from the structure, frictional heat retained in the oil and heat transferred to or from the coolant), as shown in Figure 5.28, and on the heat transfer to the coolant, through the oil cooler, as shown in Figure 5.29. The effect on the net heat transfer rate to the oil is only visible prior to thermostat opening, as after this excess heat is rejected to ambient through the coolant and radiator. Fully warm heat rejection rates to the coolant are increased by 3.2% and 4.9% with the addition of the compartment at the high speed and low speed conditions respectively. The additional heat transferred to the oil and coolant affects oil and coolant half rise times, although the effect is small, with oil and coolant half rise times reduced by 3 seconds or fewer, as shown in Tables 5.10b and c.

This analysis clearly shows that fully insulating the engine has a significant effect on crankcase temperatures, oil and coolant heat transfer rates and oil and coolant temperatures. Whilst the effects seen would be reduced in an engine compartment, since some heat transfer to ambient occurs, it is evident that the effect of the compartment must be taken into consideration when predicting variables for an engine in-vehicle.

5.3 SENSITIVITY TO SIMULINK PARAMETERS

Of the number of solvers available in Simulink, the ordinary differential equation (ode), ode1 (Euler), is currently used for PROMETS. The other solvers available are ode2 (Heun), ode3 (Bogacki-Shampine), ode4 (Runge-Kutta), ode5 (Dormand-Prince) and discrete (no continuous states). Tests were carried out at a single mid-speed, mid-load condition (2500 rpm, 50 Nm) with other conditions remaining as for previous tests. Oil temperature, coolant temperature, FMEP, gas-side heat transfer, and heat transfer rates to the oil and coolant are not sensitive to the solver used: identical traces were produced for each variable.

5.4 EVALUATING MODEL PERFORMANCE

A method of indicating the level of confidence the user can have in the performance of a model is the evaluation of model versions and new engine build files through the comparison of predicted and experimental data. Evaluations can be used to assess the performance of a new model at operating conditions that represent the operating range of the engine. Constant speed and load conditions that exaggerate the most common errors can be used to provide an overall indication of the performance of the model, whilst highlighting any discrepancies in the prediction of friction, fuelling, gas-side heat transfer, heat rejection to coolant or warm-up times. Discrepancies in the prediction of these variables most commonly arise due to the application of new technologies or operational techniques not accounted for in the model. The following three operating points give a broad indication of the model performance:

- Low speed, high load
- High speed, low load
- Mid-speed, mid-load

An example of appropriate speed and load points, based on maximum speed and load conditions, is given in Table 5.11 for the 1.6l Sigma engine. At each of these operating conditions at least the following experimental and predicted variables should be compared over a period of time sufficient for the engine to reach fully warm operation.

- Coolant temperature (K) or (°C)
- Oil temperature (K) or (°C)
- Friction mean effective pressure (bar)
- Fuel flow rate (kg/s)

Under low speed, high load conditions, heat transferred from the combustion gases to the structure is the most significant source of heat to the structure. Therefore, errors in the prediction of fuel flow rates or the gas-side heat transfer (evident in the coolant temperature) are exaggerated. Under high speed, low load conditions, friction is a much more significant source of heat to the

structure and to the oil, and errors in the prediction of friction values are exaggerated. The relative proportions of heat transferred from the gases to the structure and friction dissipated as heat in the structure are illustrated in Figure 5.30 for the 1.6l Sigma engine at each of these conditions. The mid-speed, mid-load condition is used in conjunction with the other test points to identify problems that are visible across the operating range of the engine. Discrepancies in the oil-coolant coupling through the oil cooler, heater matrix operation or heat rejected to coolant can be identified by consistent discrepancies across the engine operating range.

Initial evaluations can be simplified by performing comparisons without EGR, spark advance (if possible), a heater matrix or oil cooler. Subsequent simulations can demonstrate if the addition of, for example, EGR or a heater matrix has the expected effect, as shown in Figure 5.31. Experimental values for fuel flow rates fed into PROMETS also eliminate the possibility of errors arising from incorrect fuelling predictions. Subsequent predictions of fuel flow rates can be verified against the measured fuel flow data.

5.4.1 Experimental Data Collection

Figure 5.32 illustrates the preferred location around the engine of thermocouples required for the validation of PROMETS. With two exceptions, these points mirror the locations at which temperatures are calculated. These discrepancies exist due to the nature of PROMETS and limitations in obtaining experimental temperature measurements. The bulk oil temperature, as calculated in PROMETS, cannot be measured experimentally, and experimental sump oil temperature is usually assumed comparable. However, (as seen in Figures 5.36, 5.37 and 5.38) the experimental sump oil temperature experiences a delay in warming up, due to the thermal inertia and slow mixing of the oil, which results in an initial period of steady or slightly decreasing oil temperature. Measurements of oil sump temperature will also vary between experimental rigs, depending upon the exact location of the thermocouple within the sump. Similarly, the bulk coolant temperature, as calculated in

PROMETS, cannot be measured experimentally, and the experimental temperature of the coolant at the inlet to the engine is usually assumed comparable¹.

5.5 PERFORMANCE EVALUATIONS

Much of the original data used to evaluate the 'C' versions of PROMETS has been lost and a direct comparison of 'C' and Simulink predictions was used to assess the performance of the Simulink version. These evaluations were also used to diagnose and correct any discrepancies arising from coding or data entry errors that occurred during the model conversion. Once variable traces predicted by the 'C' and Simulink models were matched, evaluations of each version were supplemented by comparisons with experimental data.

For the in-line gasoline version, comparisons with new engine data from a Mitsubishi 1.9 Direct Injection SI (DISI, or Gasoline Direct Injection, GDI) were performed, details of which can be found in Jones [5.8]. Figures 5.33 to 5.35 show coolant, oil and friction profiles for three warm-up conditions. Predicted and experimental values compare well at all conditions, although friction is slightly over-predicted. This might be improved by the modified piston friction calculation noted in Chapter 3, Section 3.3, which has not yet been implemented in the in-line gasoline version. At each operating condition, the kink seen in the friction profiles (at 155, 115 and 60 seconds for Figures 5.33b, 5.34b and 5.35b respectively) is due to the initiation of charge stratification [5.8].

Experimental data from 1.8 l IDI and 2.0 l PUMA diesel engines were used to evaluate the performance of the in-line diesel version. Details of the experimental rigs used to generate the data can be found in Baylis [5.6] and Clark [5.9]. Examples of these comparisons can be seen in Figures 5.36 to 5.38. In these Figures coolant temperatures compare well, whereas the comparison of oil temperatures is not as favourable. The predicted oil temperature is based on

¹ When using the multi-cylinder version of PROMETS, it is possible to make a direct comparison between the experimental and predicted coolant inlet temperatures.

a bulk oil temperature. However, experimental oil temperature is measured from a thermocouple in the sump. The exact profile recorded depends on the location of the thermocouple.

5.6 DISCUSSION

The aim of the work presented in this Chapter is to demonstrate the fidelity of PROMETS. This is achieved through an assessment of the appropriateness of the current time-step length, an example of the consistency of the model, examinations of the sensitivity of the model to assumed constants and by demonstrations of the performance of the model when compared to experimental data.

Assessments of the sensitivity of the model to assumed constants were conducted at operating conditions of 3000 rpm, 5 Nm and 1000 rpm, 120 Nm. These conditions are designed to emphasise the effects of variations in the assumptions on friction and gas-side heat transfer respectively. These two speeds are also representative of typical vehicle engine speeds, according to one study of engine driving behaviour [5.10]. The study found that 91% of all vehicle trips is carried out at speeds of less than 3000 rpm. The sensitivity analyses were conducted with no EGR, spark advance or cabin heater air flow rate. The impact of these variables on results is discussed in the following paragraphs as appropriate.

Changes in the friction index, n , were shown to significantly affect initial FMEP values at a speed of 3000 rpm. Since the model predicts initial FMEP values based on the initial start temperature, the model will be even more sensitive at colder temperatures. Whilst the model is less sensitive to this value at lower speeds, this is clearly an area where further work to determine a more precise strategy for allocating the value of n could be beneficial. Fully warm FMEP predictions are, however, unaffected by the friction index.

Improvements in coolant half rise times resulting from changes to the friction index will be reduced if there is air flow through the cabin heater. Similarly, if

the tests are conducted without an oil-cooler, the improvement in coolant rise times will be reduced. Instead, higher oil temperatures will result in a lower FMEP and a greater fuel economy benefit.

The difference in the percentage of friction retained in the oil (Friction to Oil - FTO) between gasoline and diesel engines is attributed to differences in the conditions of contact between the oil and the structure [5.6]. It has been demonstrated that a higher FTO results in a fuel consumption benefit. A further study conducted at the 3000 rpm, 5 Nm condition illustrated that if the contact between the oil and the structure was reduced so that the FTO increased to 50%, fuel savings of 6.9% (compared to a FTO of 10%) could be achieved. Figure 5.39 illustrates the fuel consumed over 1200s at 3000 rpm for different FTOs.

The size of the effective cylinder area, $A_{cyl,eff}$, and exhaust port area, A_{pt} , vary from engine to engine. Thus, the changes to the distribution of heat demonstrated by varying C1 and C2 will vary with engine. In general, a larger effective cylinder area, for the same exhaust port area and 10% increase in the value of C1, will result in a lower value for C2, when calculated from Equation 5.3. This will result in a larger change in exhaust port temperatures. A larger exhaust port area, for the same effective cylinder area and 10% increase in the value of C1, will result in a higher value for C2, resulting in a smaller change in exhaust port temperatures.

Section 5.4 demonstrated the performance of PROMETS for three engines against experimental data. The performance of the model in predicting data for these three engines is summarised in Figure 5.40, which illustrates the correlation between predicted and experimental values for coolant half rise time, oil half rise time and FMEP at a variety of operating conditions. Accuracy of the predictions is generally to within 10% of experimental values. Discrepancies between experimental and predicted coolant and oil half rise times arise due to the difference in the measurement of experimental and predicted variables. Some error is also introduced by the estimation of rig coolant and oil volumes.

A direct comparison of the effect of model assumptions upon predicted variables of interest is difficult to make, as the ranges used in the sensitivity

analyses vary. However, it is possible to make statements regarding the sensitivity of PROMETS to the uncertainty introduced by each model assumption and reflected by the range of values assessed. Table 5.12 shows a summary of the percentage changes in predicted variables for each model assumption examined. From this it is clear that predictions of friction during warm-up are most sensitive to the uncertainty in the value of the friction index, n . The sensitivity of the model is greater at higher engine speeds and lower start temperatures. Predictions of friction at steady state are most sensitive to the uncertainty in the percentage of frictional dissipation retained in the oil. This uncertainty also has the greatest effect on predictions of fuel flow rates. Predictions of the heat rejected to the coolant are most sensitive to the effect of the engine compartment. Liner temperatures are most sensitive to uncertainty in the values of C1 and C2.

5.6.1 Concluding Remarks

Three main points can be drawn from this Chapter. Firstly, that the accuracy of PROMETS predictions is generally to within $\pm 10\%$ of experimental values. Secondly, that further work should be undertaken to clarify the dependence of the friction index, n , on engine speed and the value(s) appropriate for different engine types, and finally, that fuel consumption could be improved if contact between the oil and structure was reduced. However, this would increase coolant warm-up times.

Overall, this Chapter has demonstrated that PROMETS performs well when compared to experimental data. However, if PROMETS predictions are compared to experimental data taken under conditions not currently represented by the model assumptions, such as in-vehicle engine data at high vehicle speeds, large errors will be introduced into the prediction of some variables.

CHAPTER 6

PROMETS DEVELOPMENT – EXTERNAL COOLANT CIRCUIT

6.1 INTRODUCTION

The external circuit provides a flow path to and return from the radiator. The main components of the simplest circuit design are a thermostat, the radiator and a cooling fan. The circuit becomes operational once the coolant has reached thermostat opening temperature at around 88°C. The thermostat opens from fully closed to fully open over a range of about 5°C, allowing coolant flow through the radiator, which rejects heat from the coolant to ambient. Upon initial opening, the coolant that has been static in the radiator is released into the cooling system. This influx of cold fluid reduces the coolant temperature and the thermostat begins to close. Once sufficient heat has been rejected to the coolant to raise the bulk temperature, the thermostat begins to open again. This effect continues until equilibrium is reached, causing coolant temperature excursions such as those seen in Figure 5.38. If the load on the engine increases or the speed of the vehicle decreases and the heat rejected to ambient through the radiator is no longer sufficient to maintain the target temperature, the cooling fan will activate. The increase in air flow enables additional heat to be rejected to ambient. Generally, predictions of external circuit behaviour rely heavily on empirical correlations or maps of the heat rejected to coolant and do not model the engine explicitly [6.1][6.2][6.3][6.4]. The addition of an external coolant circuit model would open up new applications for PROMETS in this area.

This Chapter presents formulations for models of the thermostat and radiator to facilitate predictions of external circuit behaviour. Initially, the prediction of the delays introduced by the transport of coolant around the circuit is addressed. Subsequent sections explore the thermostat, cooling fan and radiator in turn. Finally, the model is applied to assess the impact of the position of the thermostat in the circuit (engine inlet or outlet).

6.2 COOLANT TRANSPORT DELAYS

Delays in the coolant circuit due to the transport of the coolant around each section have an effect on the behaviour of the engine before steady-state is reached. The time taken for the coolant to travel around the whole coolant circuit can be calculated by considering the total coolant volume, V , in litres and the volume flow rate, \dot{V} , in litres per second,

$$\tau = \frac{V}{\dot{V}} \quad (6.1)$$

More specifically, the time delay associated with coolant travelling between different parts of the coolant circuit, τ_{delay} , depends upon the coolant mass flow rate, \dot{m}_{cool} (kg/s), the density of the coolant, ρ , the distance between the points at which temperatures are calculated, x (m), and the diameter of the hose through which the coolant flows, D (m),

$$\tau_{delay} = \frac{\pi D^2 x \rho}{4 \dot{m}_{cool}} \quad (6.2)$$

The coolant circuit for the 1.6l Sigma engine is illustrated in Figure 6.1. Time delays for the circuit are given as a function of coolant mass flow rate (dependant upon engine speed) in Table 6.1.

6.3 THERMOSTATS

Currently, both mechanical wax thermostats and electronic thermostats are used in automotive applications to control coolant temperature through adjustments to flow resistance. Electronic thermostats are often multi-port valves, allowing full control of coolant flow through the engine bypass, inner circuit and radiator simultaneously. Additionally, the thermostat opening temperature can be varied according to the engine operating condition.

Mechanical thermostats contain a pellet consisting of a mixture of paraffin wax and copper flakes. The copper is used as a filler and to conduct heat to achieve

an even temperature distribution throughout the wax. When the wax reaches a certain temperature, typically between 60 and 70°C depending upon the exact chemical composition of the wax, the wax begins to expand. The expansion is the result of the wax changing phase from solid to liquid. A typical wax thermostat is illustrated in Figure 6.2, which shows the opened and closed positions of the thermostat. As the wax expands, it compresses the spring and opens the valve to the radiator, allowing coolant to flow through the external circuit. Although control over this traditional type of thermostat is limited, partial control can be achieved by using a small electric heater in the wax. Using this method, which enables the engine to run at 100 °C at part load and 85 °C at full load, fuel benefits of up to 3% can be achieved [6.5].

The methods for modelling mechanical thermostats reported in the literature include the use of ordinary differential equations [6.6][6.7][6.8][6.9], fluid dynamics analysis [6.10], physical heat transfer modelling [6.11] and the assumption of a linear relationship between coolant flow and temperature [6.12][6.13]. The main difficulty in all of these approaches is in modelling the expansion properties of the wax within the thermostat. Figure 6.3 shows a curve fit through data [6.14] for the position of the thermostat as a function of wax temperature. It is clear from the diagram that the thermostat exhibits hysteretic behaviour: the way in which the thermostat opens differs from the way in which it closes. The reason for this is unclear, although Nelson *et al* [6.9] and Sidders *et al* [6.10] suggest it is due to a combination of the effects of friction within the thermostat and the phase change of the wax.

The following paragraphs describe a model that utilises a physical heat transfer description of the thermostat. Since the dynamic behaviour is complex, the model uses the data shown in Figure 6.3 to characterise the hysteretic behaviour of the wax.

Heat exchange between the engine coolant and thermostat wax is by convection from the coolant to the brass capsule, by conduction through the wall of the brass capsule and by conduction from the brass capsule to the wax pellet as indicated in Figure 6.2. These processes are modelled here on one-dimensional heat flows. The wax is assumed to be homogeneous and isotropic at all times.

Referring to Figure 6.2, the instantaneous heat transfer rate from the coolant to the wax pellet, $\dot{q}_{cool-wax}$, is described as follows,

$$\dot{q}_{cool-wax} = -UA(T_{wax} - T_{cool}) \quad (6.3)$$

Where

$$\frac{1}{U} = \frac{1}{\alpha_{conv,cool}} + \frac{x_{brass}}{k_{brass}} \quad (6.4)$$

U represents the overall heat transfer coefficient between the coolant and the wax, A is the contact area between the coolant and the brass sleeve of the thermostat housing, x_{brass} is the thickness of the brass sleeve and $\alpha_{conv,cool}$ the convection heat transfer coefficient. An estimate of the convection heat transfer coefficient can be derived by considering an analysis of a cylinder in cross flow, where ([6.15] cited in [6.16] pp 299),

$$\frac{hd}{k} = C \left(\frac{u_{\infty} d}{\nu_f} \right)^n Pr^{\frac{1}{3}} \quad (6.5)$$

For the cylinder, C takes a value of 0.683 and n takes a value of 0.466 for Reynolds numbers between 40 and 4000. For higher Reynolds numbers (4000 – 40 000), C is 0.193 and n is 0.618. u_{∞} is the coolant flow rate per unit cross-sectional area in m/s, ν_f is the kinematic viscosity of the coolant and d is the diameter of the thermostat. The variation of the heat transfer coefficient with coolant flow rate at a coolant temperature of 20°C is shown in Figure 6.4.

For transient thermal analysis, the net energy transfer into the wax must equal the increase in internal energy of the wax, plus the latent heat required for the phase change from solid to liquid and the energy required to compress the thermostat spring,

$$\dot{q}_{cool,wax} = \left\{ m_{wax} c_{v,wax} + \left[m_{wax} \lambda_{wax} + kg^2 \left(\frac{y_1}{g} + x \right) \right] \left(\frac{dx}{dT_{wax}} \right)^p \right\} \frac{dT_{wax}}{dt} \quad (6.6)$$

Where,

$$\frac{dT_{wax}}{dt} = (T_{wax}^{p+1} - T_{wax}^p) \quad (6.7)$$

λ_{wax} is the specific latent heat of fusion of the wax, and takes a value of 200 kJ/kg [6.7][6.17]. The stiffness of the thermostat spring, k , is estimated from experimental data (see Section 6.7) to take a value of 30 N/mm. g is the constant of proportionality between the proportion of wax that is liquid, x , and linear distance, y , in millimetres, by which the spring is compressed, such that,

$$\frac{dy}{dx} = g \quad (6.8)$$

For a typical thermostat with a travel of 8mm from closed to fully open [6.9], $g = 8$. y_I is the initial linear compression of the spring when the thermostat is closed, thus, kgy_I represents the pre-load force on the thermostat spring in Newtons. T_{wax}^p is the temperature of the wax at the current time step and T_{wax}^{p+1} is the temperature of the wax at the next time step.

If it is assumed that the pre-load force on the spring is light and can be neglected, Equation 6.6 simplifies to,

$$\dot{q}_{cool-wax} = \left\{ m_{wax} c_{v_{wax}} + \left[m_{wax} \lambda_{wax} + kg^2 x \left(\frac{dx}{dT_{wax}} \right)^p \right] \right\} \frac{dT_{wax}}{dt} \quad (6.9)$$

Equating 6.3 and 6.6 gives the following expression,

$$\left\{ m_{wax} c_{v_{wax}} + \left[m_{wax} \lambda_{wax} + kg^2 x \left(\frac{dx}{dT_{wax}} \right)^p \right] \right\} \frac{dT_{wax}}{dt} = -UA(T_{wax}^p - T_{cool}) \quad (6.10)$$

This can be rearranged to give an expression for the temperature of the wax at the next time step,

$$T_{wax}^{p+1} = T_{wax}^p - \frac{UA(T_{wax}^p - T_{cool})dt}{m_{wax} c_{v_{wax}} + \left[m_{wax} \lambda_{wax} + kg^2 x \left(\frac{dx}{dT_{wax}} \right)^p \right]} \quad (6.11)$$

The proportion of liquid wax, x , is assumed to be proportional to the thermostat opening position. When the thermostat is fully closed, all the wax is solid ($x = 0$) and when it is fully open, all the wax is liquid ($x = 1$). Figure 6.3 shows a curve fit through experimental data from [6.14] illustrating the position of the thermostat (pos) as a function of wax temperature, T_{wax} . The function is defined as follows,

$$x(\%) = pos(\%) = \begin{cases} 0 & \text{for } T_{wax} < T_1 \\ f(T_{wax})_1 & \text{for } T_1 < T_{wax} < T_2, T_{wax}^{p+1} > T_{wax}^p \\ f(T_{wax})_2 & \text{for } T_1 < T_{wax} < T_2, T_{wax}^{p+1} < T_{wax}^p \\ 1 & \text{for } T_{wax} \geq T_2 \end{cases} \quad (6.12)$$

Where

$$f(T_{wax})_1 = aT_{wax}^5 + bT_{wax}^4 + cT_{wax}^3 + dT_{wax}^2 + eT_{wax} + f \quad (6.13)$$

$$f(T_{wax})_2 = gT_{wax}^5 + hT_{wax}^4 + iT_{wax}^3 + jT_{wax}^2 + kT_{wax} + l \quad (6.14)$$

T_1 is the temperature at which the thermostat starts to open and T_2 is the temperature at which the thermostat is fully open. The values of the constants are given in Table 6.2. Equation 6.10 requires the derivative of the function defined in Equation 6.11, which is,

$$\frac{dx}{dT_{wax}} = \frac{d(pos)}{dT_{wax}} = \begin{cases} 0 & \text{for } T_{wax} < T_1 \text{ and } T_{wax} \geq T_2 \\ f'(T_{wax})_1 & \text{for } T_1 < T_{wax} < T_2, T_{wax}^{p+1} > T_{wax}^p \\ f'(T_{wax})_2 & \text{for } T_1 < T_{wax} < T_2, T_{wax}^{p+1} < T_{wax}^p \end{cases} \quad (6.15)$$

Where,

$$f'(T_{wax})_1 = 5aT_{wax}^4 + 4bT_{wax}^3 + 3cT_{wax}^2 + 2dT_{wax} + e \quad (6.16)$$

$$f'(T_{wax})_2 = 5gT_{wax}^4 + 4hT_{wax}^3 + 3iT_{wax}^2 + 2jT_{wax} + k \quad (6.17)$$

Thus, Equation 6.11 can be solved to determine the temperature of the wax, and the position of the thermostat can then be calculated using the expressions in Equation 6.12.

6.4 COOLING FANS

Cooling fans are used to increase air flow through the radiator, and thus the heat transfer from the coolant to the air, in situations where the ram air flow rate through the radiator is not sufficient to maintain the target coolant temperature at the thermostat. Fans are typically driven by an electric motor at one or two speeds. When the coolant reaches an unacceptably high temperature, usually around 95 °C, a thermostatic switch activates the fan. Once the coolant temperature has dropped to 5 degrees below the thermostatic switch cut-in temperature, the fan cuts out. Several methods of modelling fans are described in the literature, including the use of CFD [6.18][6.19], Finite Volume methods [6.20] or physical models based on the conservation of momentum and energy [6.11][6.21]. Within the constraints of this study it is assumed that the radiator installation is matched to the required air flow for heat rejection. However, the minimum air mass flow rates required to limit the rise in air temperature across the radiator to a specified value can be made by equating the enthalpy flux change to the heat rejection rate. The relationship is shown in Figure 6.5 for several values of air temperature rise. For situations in which the ram air flow rate does not meet the required level, it can be assumed that the fan will provide the remaining required air flow.

6.5 RADIATORS

The radiator is a significant component in the thermal management of the engine, as the amount of heat that can be rejected from the coolant is controlled by the size and configuration of the radiator. If the radiator is too small, it is not possible to reject sufficient heat from the coolant and the engine can over-heat. If the radiator is too large, too much heat will be rejected from the coolant and the temperature of the coolant will fluctuate as the thermostat opens and closes. Usually, the radiator is sized to reject sufficient heat from the coolant under towing conditions.

The heat rejected by the radiator is dependent on the flow rates of the coolant and air, the temperatures and properties of both fluids and the configuration of the radiator. The air flow rate is dependent upon the vehicle speed, the size of the front grill and under-bonnet factors such as available space and bonnet contours. The coolant flow rate through the radiator is a function of engine speed when the thermostat is fully open, but prior to this is controlled by both the engine speed and the thermostat position. The configuration of the radiator is influenced by space constraints and heat rejection requirements, however, radiators are typically cross-flow, tube-fin compact heat exchangers mounted directly in front of the engine behind the front grill. The basic configuration is illustrated in Figure 6.6. In general the fluid makes a single pass from one side of the radiator to the other. Multi-pass configurations, where the fluid path may be a two-pass U, with the coolant entering and exiting on the same side, or a three-pass S, with the coolant entering and exiting on different sides, are more common in heater matrices, which are similar in configuration to radiators but smaller. If the space available for the radiator is limited, the rate of heat transfer can be increased by using tubes with internal fins [6.22], ribs, dimples or internal offset strip fins [6.23] or interrupted surfaces on the air side such as offset strip fins [6.24] or wavy plates. These techniques can increase the heat transfer coefficient by between 50 and 150% [6.25].

Radiators are modelled in the literature using CFD techniques [6.26-6.28], the log-mean temperature difference (LMTD) approach [6.29] or the effectiveness-number of transfer units (NTU) approach [6.30][6.31]. For PROMETS, the effectiveness-NTU method described by Kays and London [6.30] is most appropriate as it enables fluid outlet temperatures and heat transfer rates to be determined from a set of basic dimensions. The formulation of the model given in the following Section provides an insight to the nature of compact heat exchanger performance, what influences this and the type of information required to define the heat exchanger. The formulation describes a circular tube, flat plate heat exchanger. This type of design is sometimes used for the cabin heater matrix, oil coolers and intercoolers. It is not representative of many of the engine radiator designs currently used. This is an important limitation and should be the subject of future work (this is noted in Chapter 8).

6.5.1 Basic Theory

The heat transfer effectiveness, ε , is defined as the ratio of the actual heat transfer to the theoretical maximum heat transfer possible,

$$\varepsilon = \frac{\dot{q}_{act}}{\dot{q}_{max}} \quad (6.18)$$

Where \dot{q}_{act} and \dot{q}_{max} are the actual and theoretical maximum possible heat rejection rates through the heat exchanger for given flow rates. Assuming a quasi-steady state, the actual heat transfer between two fluids is obtained by considering an energy balance for the radiator, where the energy lost from the hot fluid is equal to the energy gained by the cold fluid. Assuming air is a perfect gas and that the coolant is undergoing a constant pressure process,

$$\dot{q}_{actual} = C_{air}(T_{air,out} - T_{air,in}) = C_{cool}(T_{cool,in} - T_{cool,out}) \quad (6.19)$$

The subscripts *air* and *cool* indicate the properties of the air and coolant respectively. C_{air} and C_{cool} represent the heat capacity rates for the air and coolant,

$$C_{air} = (\dot{m}c_p)_{air} \quad (6.20)$$

$$C_{cool} = (\dot{m}c_p)_{cool} \quad (6.21)$$

The maximum heat transfer in the heat exchanger, \dot{q}_{max} , is given by,

$$\dot{q}_{max} = C_{min}(T_{cool,in} - T_{air,in}) \quad (6.22)$$

Where C_{min} is the minimum capacity rate, the lowest of either C_{air} or C_{cool} . Thus, the effectiveness, ε , of the heat exchanger can be determined by substituting Equations 6.19 and 6.22 into Equation 6.18,

$$\varepsilon = \frac{C_{air}(T_{air,out} - T_{air,in})}{C_{min}(T_{cool,in} - T_{air,in})} = \frac{C_{cool}(T_{cool,in} - T_{cool,out})}{C_{min}(T_{cool,in} - T_{air,in})} \quad (6.23)$$

Once the effectiveness of the heat exchanger has been determined, Equation 6.23 can be rearranged to determine the output temperature of either fluid,

$$T_{air,out} = \frac{\varepsilon C_{min} (T_{cool,in} - T_{air,in})}{C_{air}} + T_{air,in} \quad (6.24)$$

$$T_{cool,out} = \frac{\varepsilon C_{min} (T_{cool,in} - T_{air,in})}{C_{cool}} + T_{cool,in} \quad (6.25)$$

6.5.2 Effectiveness-NTU Theory

The effectiveness of a heat exchanger is expressed as a function of the flow arrangement and two non-dimensional parameters, the number of transfer units (NTU) and the capacity rate ratio C ,

$$\varepsilon = f(NTU, C, flow\ arrangement) \quad (6.26)$$

Where

$$C = \left(\frac{C_{min}}{C_{max}} \right) \quad (6.27)$$

The number of transfer units is defined as,

$$NTU = \frac{AU}{C_{min}} \quad (6.28)$$

Where U is the overall heat transfer coefficient for heat transfer from the hot to the cold fluid and A is the heat transfer surface area upon which U is based. C_{min} is defined as before and C_{max} is defined as maximum capacity rate, the highest of either C_{air} or C_{cool} . Automotive radiators commonly have a single pass, cross-flow configuration with both fluids unmixed. For these, the effectiveness is calculated using the following correlation (obtained by numerical solution [6.30, pp 432]),

$$\varepsilon = 1 - e^{\left[\frac{e^{(-NTU^{0.78}C)} - 1}{NTU^{-0.22}C} \right]} \quad (6.29)$$

The variation of effectiveness with the number of transfer units (NTU) is shown in Figure 6.7 for different capacity rate ratios.

For multi-pass heat exchangers, such as cabin heaters, effectiveness is determined by calculating the effectiveness of a single pass, using the above Equations, for an equivalent heat exchanger of double the width and half the thickness. The effectiveness value calculated in Equation 6.29 is then used in Equation 6.30 (developed from energy balances [6.30, pp 434]) to calculate the multi-pass effectiveness,

$$\varepsilon_0 = \frac{\left(\frac{1 - \varepsilon_p C}{1 - \varepsilon_p} \right)^n - 1}{\left(\frac{1 - \varepsilon_p C}{1 - \varepsilon_p} \right)^n - C} \quad (6.30)$$

Where ε_p is the effectiveness of each identical pass and n is the number of passes.

6.5.3 Evaluating the Overall Heat Transfer Coefficient, U

A value for U can be determined by considering a small section of the wall separating the two fluids. U is calculated using the two heat transfer coefficients on either side of the wall and the conduction resistance of the wall material. For the general case of a heat exchanger with fins and unequal heat transfer surface areas,

$$\frac{1}{U_{cool}} = \frac{1}{\eta_{o,cool} h_{cool}} + \frac{a}{(A_w / A_{cool})k} + \frac{1}{(A_{air} / A_{cool})\eta_{o,air} h_{air}} \quad (6.31)$$

Where $\eta_{o,cool}$ and $\eta_{o,air}$ represent the effectiveness of the heat transfer surface for the coolant and air sides and are equal to 1 when the surface is not extended (i.e. no fins are used) [6.30, pp15]. A_{cool} , A_{air} and A_w represent the total heat

transfer areas on the coolant, air sides and the wall respectively, a is the thickness of the wall and h_{cool} and h_{air} are the convective heat transfer coefficients for the coolant and air respectively. In this case, the wall thermal resistance component may be neglected, as the fluid side resistances are much greater [6.30, pp 14],

$$\frac{1}{U_{cool}} = \frac{1}{\eta_{o,cool} h_{cool}} + \frac{1}{(A_{air} / A_{cool}) \eta_{o,air} h_{air}} \quad (6.32)$$

- **Air heat transfer coefficient**

The heat transfer coefficient for air, h_{air} , is a function of the Stanton number, St , and mass velocity, G in $\text{kg/m}^2 \text{ s}$ (It is perhaps more appropriate to describe G as the mass flow rate through the minimum cross sectional area, however, the phrase ‘mass velocity’ is standard terminology.).

$$h_{air} = St G c_{p,air} \quad (6.33)$$

Where,

$$G = \frac{\dot{m}}{A_c} \quad (6.34)$$

A_c is the minimum flow cross sectional area on the air side and is defined as,

$$A_c = \sigma A_{fr} \quad (6.35)$$

The frontal area on the air side, A_{fr} is product of the height and width of the heat exchanger. The ratio of the minimum flow cross sectional area to the frontal area, σ , is defined in Equation 6.39.

The Stanton number is defined below for fully developed turbulent flow in circular pipes [6.32]. This is not truly representative of air flow through fins in an automotive radiator but has been used here for simplicity and gives heat transfer coefficients of similar magnitude.

$$St = \frac{0.023 Re^{-0.2}}{Pr^{2/3}} \quad (6.36)$$

Where,

$$Re = \frac{D_h G}{\mu} \quad (6.37)$$

The definitions of the Stanton number and Reynolds number use the mass velocity, G , because the velocity of the fluid varies across the radiator. This is due to the changes in density as the fluid temperature changes along the length of the radiator.

The hydraulic diameter, D_h , is defined as 4 times the minimum cross sectional area divided by the wetted perimeter,

$$D_h = 4r_h = 4 \frac{A_c L}{A} = \sigma \alpha \quad (6.38)$$

Where σ is the ratio of the minimum flow cross sectional area, A_c , to the frontal area, A_{fr} , and α is the ratio of the total area available for heat transfer, A , to the volume, V , of the radiator. Estimates of σ and α can be calculated from considerations of the geometry of one section of the radiator. The variables x , y , z , D and δ are defined for the radiator in Figure 6.6,

$$\sigma = \frac{A_c}{A_{fr}} = \left(\frac{A_c}{A_{fr}} \right)_{section} \approx \frac{y(z - \delta) - D(z - \delta)}{yz} \quad (6.39)$$

$$\alpha = \frac{A}{V} \approx \frac{2xy + \pi D(z - \delta) - \frac{\pi D^2}{2}}{xyz} \quad (6.40)$$

The dimensions x and y are calculated by assuming that the tubes are equally spaced in the radiator matrix. A typical value of 0.006m is used for the spacing of the fins, z . The ratios σ and α can then be used to calculate overall values of the minimum flow cross sectional area and total heat transfer area: the frontal area and volume of the radiator are easily determined from overall radiator dimensions.

- **Coolant heat transfer coefficient**

The heat transfer coefficient for the coolant is a function of the Nusselt number, Nu , the hydraulic diameter of the tubes, D_h , and conductivity of the coolant, k_{cool} ,

$$h_{cool} = \frac{Nu k_{cool}}{D_h} \quad (6.41)$$

Where, for laminar flow in a smooth tube ($Re < 2300$) ([6.33] cited in [6.16]),

$$Nu = 4.364 \quad (6.42)$$

For turbulent fluid flow ($Re \geq 2300$) in a smooth tube where the fluid is being cooled [6.34],

$$Nu = 0.023 Re^{0.8} Pr^{0.3} \quad (6.43)$$

For a circular tube, the hydraulic diameter is the tube diameter,

$$D_h = D_{tube} \quad (6.44)$$

For a rectangular tube,

$$D_h = \frac{\text{tube width} * \text{tube height}}{2(\text{tube width} + \text{tube height})} \quad (6.45)$$

The variation of the coolant and air heat transfer coefficients with Reynolds number is shown in Figure 6.8 for the radiator characterised in Table 6.3.

- **Air-side and coolant-side surface effectiveness**

Since the surface on the coolant side is not extended it is assumed that the overall surface effectiveness for the coolant side, $\eta_{o,cool}$, is equal to 1, as above. For the gas side of the heat exchanger, the overall surface effectiveness, $\eta_{o,air}$, is a function of the ratio of fin surface area to total area, A_{fin}/A , and the fin effectiveness, η_{fin} ,

$$\eta_{o,air} = 1 - \frac{A_{fin}}{A} (1 - \eta_{fin}) \quad (6.46)$$

Where,

$$\eta_{fin} = \frac{\tanh(ml)}{ml} \quad (6.47)$$

For thin sheet fins,

$$m = \sqrt{\frac{2h_{air}}{k\delta}} \quad (6.48)$$

In the above equations, l represents the effective fin length and takes a value of half the fin spacing, 0.003m. The heat transfer coefficient for air, h_{air} , was determined previously. The thermal conductivity of the fin, k , depends upon the material used. Fins are usually manufactured from aluminium; the thermal conductivities of several engineering materials are listed in Table 3.1. The thickness of the fins, δ , is typically 0.001m. The ratio of fin surface area to total area, A_{fin}/A , is often unavailable, although values for similar heat exchangers can be found in Kays and London [6.30]. However, a value of 0.7, an average of the values listed in Kays and London for appropriate heat exchanger configurations, is proposed where data is otherwise unavailable.

The variation of $\mu_{o,air}$ with the air-side heat transfer coefficient is shown in Figure 6.9 for the variable values suggested above.

6.5.4 Comparison with Experimental Data

The results of calculations performed using the heat exchanger model described in the previous Section are compared with effectiveness data supplied by Ford Motor Company [6.35] in Figure 6.10. The supplied effectiveness data was generated using a Ford in-house CFD code. Two heater matrices, designed for use in the Mondeo/IDI TCi combination, were simulated. In each case, the coolant mass flow rate was varied from 0.06 to 0.6 kilograms/second, and the air mass flow rate was varied from 0.0075 to 0.1378 kilograms/second. The agreement between the supplied data and predicted values is good, to within $\pm 5\%$, and illustrates that the effectiveness-NTU method works reasonably well.

6.7 MODEL EXPLOITATION

Using the radiator and thermostat models described above, an external coolant circuit model has been constructed, based on the circuit for the 1.6l Sigma engine shown in Figure 6.1.

Increasingly, engine manufacturers position the thermostat on the inlet to the engine rather than on the outlet from the engine, as this reduces thermal shock. However, the reason why thermal shock is reduced by positioning the thermostat on the inlet is not well documented. The two thermostat positions are illustrated in Figure 6.1. Simulations were performed in which the thermostat was positioned at the inlet and outlet for a range of engine speeds. In each case, the same thermostat model (and thermostat opening temperature) was used. Predictions of coolant temperature were calculated at the same place, on the outlet from the engine, as marked on Figure 6.1.

Figure 6.11 shows a comparison between coolant and oil temperature profiles for the two thermostat positions at an engine speed of 2500 rpm. Four observations can be made,

1. Peak coolant temperature is greater when the thermostat is on the inlet and occurs four seconds later.

This is due to the transport delay between the point at which the temperature is measured and the position of the thermostat. (If the temperature were calculated at the inlet to the engine, the reverse would be seen.)

2. The magnitude of the first and all subsequent temperature excursions is smaller when the thermostat is on the inlet.
3. The frequency of the coolant temperature oscillations is greater when the thermostat is on the inlet.

Since the thermostat is operating based on the temperature of the coolant directly after the radiator, it responds more rapidly to the effect of flow through the radiator on the coolant temperature. As a result, the magnitude of the temperature excursions is smaller and the frequency of them greater. When the

thermostat is on the outlet from the engine, it cannot respond to changes in flow through the radiator, and thus changes in coolant temperature, until the coolant has travelled to its position on the engine outlet. Furthermore, the magnitude and frequency of the coolant temperature excursions are controlled by the delay in transporting the coolant to the thermostat position.

4. Coolant and oil temperatures are higher when the thermostat is on the inlet.

Coolant and oil temperatures are higher when the thermostat is on the inlet to the engine as the thermostat is regulating the temperature of the coolant based on the lowest temperature in the circuit (after the radiator and at the inlet to the engine).

Figures 6.12a and b summarise simulations of the frequency and magnitude of coolant temperature excursions at several coolant flow rates and with the thermostat positioned on the inlet to and outlet from the engine. When the thermostat is on the outlet, the frequency of the coolant temperature excursions is lowest at idle and increases until it reaches a maximum value of 0.083Hz at flow rates in excess of 1.2l/s. This suggests that at lower coolant flow rates the response of the thermostat is controlled by the transport delays in the coolant circuit. At flow rates in excess of 1.2l/s, the frequency of the coolant temperature excursions is controlled by the inherent response time of the thermostat. When the thermostat is on the inlet to the engine, the frequency of the coolant temperature excursions remains constant at 0.083Hz. This supports the above statement, as the response of the thermostat on the inlet to the engine is subject only to the inherent thermostat response time and not coolant transport delays.

For both thermostat positions, the magnitude of the temperature excursions increases with coolant flow rate. This is because the higher the flow rate, the greater the change in temperature during the time required for the thermostat to respond.

Overall, it is clear from this analysis that placing the thermostat on the inlet to the engine results in a higher frequency and lower magnitude of coolant

temperature excursions. This reduces the thermal shock to the engine after thermostat opening.

6.7.1 Comparison with Experimental Data

The measured frequency and magnitude of coolant temperature oscillations for several engines are shown in Figure 6.12. Values for the Valencia and 2.0l DOHC (two sets) were measured from thesis figures in Christian [6.36], Yuen [6.37] and Chick [6.38] respectively. Points for the remaining engines were taken directly from experimental data; some of the oscillations measured for the 1.8l IDI and Puma engines can be seen in Figures 5.36 to 5.38.

For all the engines except the Lion DV6, the thermostat is on the outlet from the engine. The magnitudes of the temperature excursions range from 0.5 to 11°C. It is likely that the range of magnitudes is due to the age range of the engines tested; the Valencia and 2.0l DOHC engines are older designs than the 2.0l Puma, 2.7l Lion DV6 and 1.8l IDI engines. The frequencies of the oscillations vary from 0.01 to 0.09 Hz. In agreement with the predictions discussed in the previous Section, the frequency of oscillations is generally higher and the magnitude of oscillations generally lower for the Lion DV6, which has the thermostat on the inlet to the engine.

Comparing the predicted and experimental data, it is clear that the trends predicted by PROMETS for the thermostat on the outlet are the same as those seen experimentally. The frequency of oscillations increases with coolant flow rate until a constant value is reached at flow rates in excess of 1.2 l/s – this is seen most clearly for the 2.0l DOHC although the data for the 2.0l Puma also follows the same trend. The magnitudes of the oscillations also show a similar upward trend with increasing coolant flow rate. Overall, the predicted magnitudes and oscillations for the thermostat on the outlet fall within the ranges measured experimentally.

6.8 DISCUSSION

This Chapter has presented formulations for modelling the thermostat and radiator and has applied the resulting external circuit model to investigations of the impact of the external circuit on the thermal management of the engine.

The model of the radiator relies on the specification of default values for the dimensions, z , the distance between the fin surfaces, δ , the thickness of the fins and A_{fin}/A , the ratio of fin surface area to total heat transfer area. The sensitivity of the model to $\pm 10\%$ variations in these values is shown in Table 6.4. It is clear that the model is not sensitive to variations in the values of A_{fin}/A and δ . However, variations of $\pm 10\%$ in the value of the plate spacing, z , produce variations of $\pm 8\%$ in the calculated value of effectiveness. This will clearly have an effect on the heat transfer rate and so, where possible, this dimension should be measured for the radiator to be modelled.

Assessments of the impact of thermostat position on coolant temperature were carried out for the 1.6l Sigma coolant circuit. The results presented here will change for different coolant circuits, although the trends will remain the same. For smaller coolant circuits with shorter pipe work, the thermostat response frequency will be reached at coolant flow rates lower than those seen here. Conversely, the frequency of coolant temperature excursions for circuits containing longer pipe work will reach the thermostat response frequency at higher flow rates.

6.8.1 Concluding Remarks

Two key points can be drawn from the work in this Chapter. Firstly, that positioning the thermostat on the inlet to rather than the outlet from the engine reduces the thermal shock experienced by the engine. This is important to reduce engine and component wear and to facilitate consistent cabin heating. Secondly, that thermostat opening temperature must be reduced if the thermostat is placed on the inlet to the engine, in order to keep bulk coolant temperature at the desired value.

CHAPTER 7

TOWARDS RAPID WARM-UP

7.1 INTRODUCTION

The advantages of rapid warm-up and methods for achieving it were discussed in Chapter 2, Section 2.3.1. The main aims of promoting fast warm-up are to reduce cold-starting fuel consumption and emissions over the warm-up period, and to improve passenger comfort through rapidly achieved cabin heater temperatures. In this Chapter, the effectiveness of four ways of achieving improvements is investigated. In the first instance, the benefits of reducing thermal capacity are examined. Secondly, work is presented that examines the use of oil-coolant heat exchangers and how the redistribution of thermal energy, which occurs when such heat exchangers are used, affects warm-up times. Thirdly, the effect of using a sump oil heater driven by the engine alternator is investigated. Finally, an oil-exhaust gas heat exchanger to recover energy from the exhaust gases is evaluated.

The study is based on modelling the behaviour of a 1.6l Sigma engine in a Ford Focus. The simulations are for the conditions of the NEDC, with a -10°C cold start for each technique examined. Except where stated, no oil cooler is used. It is also assumed that the engine is operating at stoichiometric AFR, MBT spark advance and with zero EGR. This enables a direct comparison of warm-up rates and fuel consumption to be made for all of the techniques assessed. Comparisons of warm-up rates are based upon coolant and oil half-rise times. These are defined as the time taken for the temperature of the coolant to rise by 60°C and the time taken for the temperature of the oil to rise by 40°C .

7.2 REDUCED THERMAL CAPACITY

During warm-up, the rates of rise of temperature in the engine depend on the net heat transfer rates and the thermal capacity of engine to store internal energy. The larger the thermal capacity of the engine, the slower the rates of temperature rise. Thermal capacity, in this context, is the sum of values for the engine structure, coolant in the internal and inner coolant circuits (see Figure 1.4) and the oil. The total can be decreased by reducing the thermal capacity of any or all of these, subject to maintaining the structural integrity of the engine, lubrication function and cooling function, particularly under high load and speed conditions. Thermal capacity is the product of density, volume and specific heat capacity of a solid or liquid,

$$C = \rho V c_v \tag{7.1}$$

Table 7.1 lists the properties, including the thermal capacity of one cubic metre, of common engine materials.

7.2.1 Alternative Materials

A reduction in the thermal capacity of the engine can be achieved either through a direct reduction in the engine mass, as in the following Section, or by reducing engine mass through the use of different engine materials. The following example illustrates the effect of using different materials for the block and head of a 1.6l Sigma engine, both components of which are usually manufactured from aluminium. Throughout the example, the volume of material in the head and block remains the same. The masses of the components change with the densities of the different materials, as shown in Table 7.2. A comparison of the coolant and oil warm-up profiles for aluminium and cast iron head and block combinations is shown in Figure 7.1.

The coolant and oil half rise times for each combination are summarised in Figure 7.2a. The shortest half rise times for both the block and head arise from the all aluminium engine, demonstrating that the lower thermal capacity of

aluminium results in faster warm-up times. The longest half rise times arise from the all cast iron engine. Of the two remaining tests, the oil half rise time is shortest for the aluminium block (and cast iron head) and the coolant half rise time is shortest for the aluminium head (and cast iron block). This suggests that the coolant half rise time is influenced by the thermal capacity of the head and that the oil half rise time is influenced by the thermal capacity of the block. This is supported by the following extreme example, in which the thermal capacity of the head or block is reduced by 80% when compared to the equivalent thermal capacity for an aluminium component. Figure 7.2b shows coolant and oil half rise times for an all cast iron engine and engines with a combination of cast iron and the example material with extremely low thermal capacity. Clearly, the thermal capacity of the head has a strong influence on the coolant half rise time. The oil half rise time is also strongly affected by the thermal capacity of the block, although the effect is not as extreme as the effect of the head thermal capacity on the coolant.

The longer warm-up times associated with using the cast-iron components result in increased fuel consumption over the NEDC. Table 7.3 shows the percentage increase in fuel consumed over the NEDC for each case when compared to an aluminium head and block combination. Fuel consumption increases by almost 0.8% for the cast iron/aluminium combinations and almost 1.6% for the all cast-iron engine. These increases are not great, but illustrate that, for the same volume of material, the all-aluminium engine has an advantage over a part- or all-cast iron configuration.

In practice, few contemporary engines use cast-iron heads. Most diesel engines have a cast iron block, as the material strength is greater and cylinder walls can be thinner whilst withstanding higher compression ratios. If the Sigma engine had a cast-iron block, the volume of material required to meet material strength needs would be smaller and the differences in warm-up times and fuel consumption given in the above example would be reduced. Recent developments in the machinability of compacted graphite iron (CGI), as discussed in Chapter 4, Section 4.5 and presented in Dawson [7.1] have led to an increased use of CGI as an engine block material, particularly in diesel engines due to better material strength. The properties of CGI given in Table

7.1 illustrate that the thermal capacity of 1 m³ of CGI is greater than that of aluminium but less than cast iron, suggesting that a CGI block would also benefit from a faster warm up than the traditional grey cast iron. However, warm-up times are also affected by the thermal conductivity of the material, values of which are given in Table 3.1. This is lower for CGI than cast iron and will compromise the potential advantages arising from reduced thermal capacity.

7.2.2 Mass and Volume Reductions

The relative merits of reductions in the structural mass and volumes of the oil and coolant are examined here. In each case, the mass or volume currently specified for the Sigma engine is reduced by 10% and the effects recorded. For the oil, the volume input to the engine build file (see Chapter 4, Section 4.4.4) is altered. For the coolant, scaling factors (see Chapter 4, Sections 4.4.4 and 4.5.2) are used to alter the value. Reductions in engine mass are achieved by using scaling factors to reduce the thickness of the walls surrounding the crankshaft and the crankshaft bearing housing. The scenarios evaluated are individual reductions in engine mass, oil volume and coolant volume, and combinations of these to investigate interactions: oil and coolant volume; oil volume, coolant volume and engine mass; coolant volume and engine mass; oil volume and engine mass.

Figure 7.3a shows coolant and oil half rise times for each test. A noticeable difference is seen in the warm-up rates. Of the individual reductions, a reduction in coolant volume has the smallest effect on coolant and oil half rise times, although both are reduced. A reduction in structural mass also reduces both coolant and oil half rise times. The reduction of the volume of oil has the greatest effect on oil half rise times, which are reduced from 293 seconds for the base engine case to 278 seconds. However, the coolant half rise time is increased from the base engine case by 5 seconds. This is due to the higher oil temperature resulting from the reduction in oil volume, which reduces the viscosity of the oil and hence reduces friction. The reduction in friction results

in less heat transfer to the structure and hence less heat rejection to the coolant, resulting in the increased coolant warm-up time.

The effects of the combined reductions in oil volume, coolant volume and structural mass loosely reflect the sum of the individual reductions. Thus, the combination of all three reductions gives the shortest oil half rise time, but the shortest coolant half rise time occurs when only the coolant and structural mass are reduced, as the reduction in oil volume increases coolant half rise times as described previously. The reductions in oil half rise times result, through the reduction in friction, in a lower fuel consumption over the NEDC as shown in Figure 7.3b, with the shortest oil half rise times resulting in the lowest fuel consumption and visa versa. Compared to the fuel consumed by the base engine set-up for each test, the actual difference in fuel saved varies from 0.07% for a reduction in coolant volume to 1.04% for a simultaneous reduction in structural mass, oil volume and coolant volume. A 10% reduction in oil volume produces a fuel saving of 9 times that produced for a 10% reduction in coolant. Similarly, the oil volume reduction saves 2.75 times as much fuel as the reduction in structural mass.

In practice, reductions in engine mass, coolant volume and oil volume are subject to constraints and the 10% reductions investigated here might be difficult or impossible to achieve. A reduction in the volume of coolant can be achieved through a reduction of auxiliary pipe work. In the 1.6l Sigma engine set-up, fluid in auxiliary pipe work accounts for 17.4 % of the total 2.2 litres of coolant in the engine system. The alteration of coolant passage size can have a significant effect on warm-up rates, as the reduction in the passage diameter results in a decrease in the bulk coolant volume and an increase in the velocity of the coolant (for the same bulk coolant flow rate). The increase in velocity has been shown to increase heat transfer for both the convective and nucleate regimes [7.2][7.3][7.4]. However, when reducing coolant volume, it is necessary to ensure that there is adequate cooling in areas of high heat transfer, such as the exhaust ports, to prevent film boiling (see Chapter 2, Section 2.2.4). Reductions in the mass of oil by altering oil gallery dimensions are similarly constrained by required flow rates at rubbing surfaces. The total volume of oil must also be considered; the quantity of oil is chosen in order to prolong the life

of the oil so that it only requires changing at each service interval, usually every year or 10, 000 miles. Developments in oil properties are, however, improving the possibilities of reducing the total quantity of oil required to meet service interval changes.

7.3 OIL COOLERS

At temperatures in excess of about 160 - 180 °C, oil begins to degrade [7.5], reducing the lubrication properties and life of the oil. Most oil coolers are oil-to-coolant heat exchangers (rather than oil-to-air) used to limit peak oil temperatures. These are either constantly streamed or contain a thermostat and operate only when a certain oil or coolant temperature has been reached. Oil coolers have been used in engines for several years, however, there is little in the literature on their overall effect on internal engine heat transfer rates and performance. The use of an oil-water oil cooler creates a direct heat flow path between the oil and the coolant, in addition to that which already exists through the structure of the engine. The effect that this has on warm-up rates and fuel consumption is reported here.

Oil cooler performance is modelled in PROMETS using the effectiveness method of calculating heat transfer that is described by Kays and Crawford [7.6] and detailed in Chapter 6. The effectiveness is defined as the ratio of actual heat transfer to the maximum heat transfer possible,

$$\varepsilon = \frac{\dot{q}_{act}}{\dot{q}_{max}} \quad (7.2)$$

The effectiveness varies with the type and size of oil cooler and engine operating conditions, which determine oil and coolant flow rates. The variation of effectiveness with oil and coolant flow rates is shown in Table 7.4 for the oil cooler of a 2.4l Puma diesel engine [7.7]. The Table shows that effectiveness generally varies between 0.18, which occurs for the maximum oil flow rate and minimum coolant flow rate, and 0.4, which occurs for the minimum oil flow rate and maximum coolant flow rate. Generally, at low engine speeds the oil

cooler operates with an effectiveness of approximately 0.4 reducing to around 0.32 at high engine speeds.

This investigation assesses the effect of the oil cooler performance. The effectiveness has been varied between 0.0 (no oil cooler) and 1.0 (when the heat exchange rate is the maximum for the given stream inlet conditions) in steps of 0.2. Coolant and oil temperature profiles for each value of effectiveness are shown in Figure 7.4, illustrating that increasing the effectiveness of the oil cooler increases the coupling between the two fluids. The resulting coolant and oil half rise times are given in Table 7.5. During the first 900 seconds or so, heat is transferred from the coolant to the oil as shown in Figure 7.5. This initially lowers the temperature of the coolant and raises the temperature of the oil. Subsequently, when the coolant temperature is stable (after the radiator thermostat has opened) and the oil temperature has exceeded that of the coolant, heat is transferred from the oil to the coolant and the temperature of the oil is lowered. The final oil temperature recorded at the end of the NEDC reduces with increasing oil cooler effectiveness, as shown in Figure 7.6a, demonstrating that the aim of reducing peak oil temperatures using an oil cooler is achieved. The reductions in the oil half rise times result in a reduction in the fuel consumed over the NEDC of between 1.7 and 2.8%, as illustrated in Figure 7.6b. However, the lower oil temperatures over the latter half of the NEDC result in higher friction, which increases as the effectiveness of the oil cooler becomes greater as shown in Figure 7.7. Thus, although a fuel consumption benefit is shown over the 20 minutes of the NEDC, the oil cooler would increase fuel consumption over a longer journey due to the higher steady state friction value.

7.4 SUMP OIL HEATER

The use of additional heat sources (either external or internal) has been explored by others [7.8] to [7.15]. Although warm-up times can be improved the heat input is often at the cost of additional fuel use either before or during engine running. The aim of the work reported here is to determine if a fuel

consumption benefit is gained by using a sump oil heater that is driven using the engine alternator. For this analysis, the additional load on the alternator from the sump oil heater is modelled as additional load on the engine. Internal data shows that a 2kW rated alternator operates with an efficiency of between 65 and 50 % over the speed range of the NEDC, for a 1.6 Sigma engine in a Ford Focus. Thus, when operating at 65% efficiency, 0.5kW of heat added into the sump results on an increased load on the engine of 0.769kW (an additional 10.5 Nm at 700 rpm). The effect of adding different amounts of heat into the sump is examined for the highest alternator efficiency. Fuel flow rates are calculated from the following formulation as a function of IMEP (see Chapter 3, Section 3.4),

$$\dot{m}_f = \frac{IMEP_g V_s N}{Q_{LHV} \eta_{comb} \eta_{ind,gr} * 2 * 60} \quad (7.3)$$

Where,

$$IMEP_g = BMEP + FMEP + FMEP_{auxiliary} + PMEP \quad (7.4)$$

The combustion efficiency, η_{comb} , and gross indicated thermal efficiency, $\eta_{ind,gr}$, are calculated using Equations 3.28 and 3.30. In order for there to be a fuel consumption benefit from using a sump oil heater, the decrease in FMEP resulting from the heated oil must be greater than the increase in BMEP resulting from the extra load on the alternator. PMEP will also decrease with the increase in engine load. However, the effect will be much smaller than that on FMEP and BMEP and so is not considered here. Predicted fuel flow rates are not examined directly, as the formulation for calculating fuel flow rates during warm-up (see Chapter 3, Section 3.4) is an approximation and would introduce uncertainties into the results in this case.

The brake and friction work done without a sump oil heater and with heaters adding 0.5kW and 1.0kW into the sump are shown in Figure 7.8a and 7.8b respectively. It is clear from these diagrams that the reduction in friction work resulting from the heaters is much less than the increase in brake work done to compensate for the additional load on the alternator. The increase in work done

is shown in Figure 7.9 for each case. It is clear that there is no fuel consumption benefit in either case. The coolant and oil half rise times are shown for each additional heat input and the base engine in Table 7.6. Coolant warm-up times are increased by 11 and 14 seconds for an additional heat input of 0.5 and 1.0kW respectively. Oil half rise times are reduced by 75 and 126 seconds for an additional heat input of 0.5 and 1.0kW respectively.

7.5 OIL-EXHAUST GAS HEAT EXCHANGER

Coolant-exhaust gas heat exchangers have been examined previously by others [7.16][7.17] who have demonstrated that a reduction in fuel consumption can be achieved with such devices. Previous research [7.14] concluded that raising the temperature of the oil, rather than the coolant, is most advantageous for reducing fuel consumption as this reduces friction. The aim of this exercise is, therefore, to assess the benefits that may be obtained by using an oil-exhaust gas heat exchanger to recover heat from the exhaust. As with each of the previous investigations, this work is conducted using PROMETS to model the behaviour of a 1.6l Sigma in a Ford Focus over the NEDC. Values for the exhaust gas temperature were generated using NUSim and PROMEX. The measured value is taken as the temperature of the exhaust gas 1 metre down the tailpipe, just before the catalytic converter, as shown in Figure 7.10.

It is assumed that the oil-exhaust gas heat exchanger operates with an effectiveness of 0.4, as with the heater matrix and oil cooler modelled in PROMETS (see Chapter 3, Section 3.6). The effect that the heat recovered has upon the oil and coolant temperatures is shown in Figure 7.11a. As can be seen, the effect on the oil temperature is dramatic, and the oil half rise time reduces from 293 seconds to 179 seconds. The effect on the coolant temperature is smaller and coolant half rise time increases from 311 seconds to 330 seconds. The increased oil temperature reduces friction and thus fuel consumption by 5.4% over the NEDC, as shown in Figure 7.11b. It is clear in Figure 7.11a that the heat input into the oil has, however, increased the steady state oil temperature. The peak temperature recorded during the cycle is 405 K or

132°C. This value is close to the oil degradation limit of approximately 160 °C and is reached at a condition of 2500 rpm and 50 Nm. Evidently, the engine will be run at higher load and speed conditions than this, for example during motorway driving or when heavily loaded, and therefore the oil degradation limit would be exceeded.

One solution to this would be to fit an oil cooler. Figure 7.12 shows the combined effect of the oil cooler and the oil-exhaust gas exchanger on the oil and coolant temperatures. The peak oil temperature is noticeably reduced, accompanied by a small increase in oil half rise time. The coolant half rise time remains the same. The coolant and oil half rise times for all cases are summarised in Table 7.7. The addition of the oil cooler reduces the fuel consumption benefit by only 0.1%, giving a reduction of 5.3% in fuel consumed over the NEDC. An alternative solution would be to use a thermostat or valve on the exhaust gas side to divert the gas once the oil had reached a maximum temperature. Diverting the exhaust gas, rather than the oil, would avoid trapping residual oil still exposed to the high exhaust temperatures in the heat exchanger, thus preventing the re-circulation of carbonised oil and associated reduction in the efficiency of the lubrication.

7.6 DISCUSSION

This Chapter has assessed four different methods for improving warm-up rates and reducing fuel consumption. Assessments of these methods were conducted over the NEDC from a -10°C start. The NEDC is designed to be representative of typical driving patterns in Europe, but does not simulate motorway or long-distance driving. The implications of these other types of driving conditions are discussed in the following paragraphs as appropriate. A -10°C start temperature was chosen to exaggerate warm-up times and friction values during warm-up. For a higher start temperature, the reductions in fuel consumption and improvements in warm-up times over the NEDC that are reported here would be reduced. To maintain stable combustion at low temperatures excess fuel is required. Therefore, in practice, it would therefore not be possible to run at

stoichiometric with a start temperature of -10°C . However, this is unlikely to affect the fuel consumption trends identified in the work reported here.

The investigations were also conducted with no oil cooler (except where stated), EGR, spark advance or cabin heater air flow rate and at stoichiometric AFR. The addition of an oil cooler would reduce the fuel consumption benefits reported here. The reductions in oil warm-up times would be less significant as part of the heat causing the reductions in oil warm-up times would be transferred to the coolant through the oil cooler. The addition of EGR reduces in-cylinder temperatures and thus heat transfer from the combustion gases to the structure. Overall, the rates of rise of coolant and oil temperatures seen in these investigations would reduce with the addition of EGR. However, since the proportion of the total heat transfer to the structure that is accounted for by friction would increase, the reductions in oil half rise time and resulting fuel consumption benefits seen in these investigations would increase. Retarding spark timing from MBT will have a similar effect, and the reverse will be true for advancing spark timing. Activation of the cabin heater air flow rate results in heat transfer from the coolant to ambient air. The rate of rise of coolant temperature would therefore be slower and engine warm-up times would increase. The effect on engine warm-up times will be greatest for the oil cooler investigation, as the reduced coolant temperatures will reduce the oil temperature (with increasing effect as the effectiveness of the oil cooler increases). The reductions in oil temperature will therefore reduce the fuel consumption benefits reported here.

Of the engine thermal capacity reductions, the greatest reduction in fuel consumption is achieved through a simultaneous reduction of 10% in oil volume, coolant volume and structural mass. Under these conditions, fuel consumption is reduced by 1.04% when compared to the base engine case. The greatest reduction in coolant half rise time is achieved through a simultaneous reduction in coolant volume and structural mass. Under these conditions, coolant half rise time is reduced by 27 seconds. Overall, the 10% reductions in engine structural mass, coolant volume and oil volume and combinations of these produced reductions in fuel consumption of between 0.07 and 1.04%. These modifications were shown to have a small effect on coolant and oil

warm-up rates. It may be possible to design for greater mass or fluid volume reductions, and therefore to achieve further reductions in fuel consumption. However, these results suggest that any such design changes would have to be significant to produce large reductions in fuel consumption and warm-up times.

The addition of an oil cooler shows savings in fuel consumed over the NEDC of between 1.7% and 2.8%, depending upon the effectiveness of the oil cooler. At an effectiveness of 0.4, as currently modelled in PROMETS, a saving of 2.3% is seen. However, the coolant warm-up rate is reduced as heat is transferred from the coolant to the oil during warm-up. In addition to the heater performance penalty, increased steady-state friction values resulting from lower peak oil temperatures will increase fuel consumption over longer journeys. The fuel consumption and final friction values for increasing values of oil cooler effectiveness were shown in Figures 7.6b and 7.7, demonstrating that as the effectiveness increases, both the fuel consumption reduces and the final friction value increases. Given that the reduction in fuel consumption does not increase substantially for effectiveness values greater than 0.4, there is little to be gained through the development of a more effective oil cooler. Although the increased fuel saving over the NEDC arising from a higher oil cooler effectiveness is desirable, the benefit is outweighed by the increased steady-state friction at higher effectiveness values and the increased fuel consumption over longer journeys that this entails. It would be beneficial to fit an oil cooler to every engine, even where there is no need to reduce peak oil temperatures, in order to improve fuel consumption during warm-up. However, it would be necessary to deactivate the oil cooler during fully warm operation in order to prevent additional fuel use over longer journeys. The reduction in fuel consumption, and therefore emissions, must also be weighed against the increased coolant warm-up times and reduced passenger comfort.

The oil-exhaust gas heat exchanger produced the largest reduction in fuel consumption of 5.4%. With an oil cooler to reduce the peak oil temperature this reduced to 5.3%. Davies [7.12] investigated the use of a coolant-exhaust gas heat exchanger over the NEDC for the 1.6l Sigma in a Ford Focus for a 20°C start, and found that the exhaust cooler alone reduced fuel consumption by 0.54%. When an oil cooler was added this increased to 3.11%. Further

simulations by the author of the oil-exhaust gas heat exchanger for a 20°C start demonstrated fuel savings of 4.2% and 3.6% for the exhaust cooler alone and with an oil cooler respectively. The primary difference between the two heat recovery mechanisms is the effect on coolant half rise times. The oil-exhaust heat exchanger increases coolant half rise times, reducing passenger comfort, whereas the coolant-exhaust heat exchanger reduces coolant half rise times, increasing passenger comfort. Thus, the coolant-exhaust heat exchanger achieves both aims of a rapid warm-up where the oil-exhaust heat exchanger does not. This illustrates that although the reduction in fuel consumption is greater when the recovered heat is added directly into the oil, overall it is more beneficial to add the recovered heat directly into the coolant.

An additional concern of using an energy recovery system connected to the exhaust gas is the effect that the recovery of the heat will have on after-treatment systems. In the case of the oil-exhaust heat exchanger modelled, pre-catalyst exhaust temperatures were reduced by an average of 47 degrees. The temperature of the exhaust gas, with and without a heat exchanger, is illustrated in Figure 7.13. The temperature drop could significantly affect after-treatment systems. Further modelling would be required to determine the combined impact of the reduction in fuel consumption and reduced exhaust gas temperature on tail pipe emissions.

7.6.1 Concluding Remarks

The results of these investigations are summarised in Figures 7.14 and 7.15, which show coolant and oil half rise times for each case and the reduction in fuel consumed over the NEDC (as a percentage) compared to the base case. Not all of the methods investigated improve both fuel consumption and coolant warm-up rates. These analyses have shown that the redistribution of energy flows and heat recovery methods are beneficial for fuel economy. However, improvements in coolant warm-up times, directed towards improving cabin heater performance, are small. No fuel economy or warm-up benefits were found for the additional heat source of the oil sump heater.

CHAPTER 8

DISCUSSION

This thesis has presented a full description of the theory of the thermal analysis model, PROMETS. The current form and structure of the model has been described and a sensitivity analysis has demonstrated the appropriate care required in defining user inputs. The level of confidence a user can have in model predictions has been explored through an analysis of the sensitivity of PROMETS to model assumptions and by examples of the performance of the model when compared to experimental data. Formulations for the development of an explicitly modelled external coolant circuit have been presented and applied to determine the implications of thermostat position on engine thermal management. The application of PROMETS has also permitted investigations of methods for improving warm-up times. This Chapter draws together the results and conclusions from the previous Chapters and discusses the work reported in a wider context.

The work reported in this thesis shows that PROMETS is a well-conditioned model and useful tool for investigations of engine thermal behaviour. Throughout the thesis, different aspects of the model have been examined. The sensitivity analyses conducted in Chapters 4 and 5, the results of which are summarised in Table 8.1, explored the sensitivity of the model to user inputs and model assumptions. It was demonstrated that PROMETS is relatively insensitive to 10% variations in user input values. The analysis of the sensitivity of the model to assumptions illustrated that PROMETS is sensitive to certain assumptions. From Table 8.1, it appears that PROMETS is more sensitive to model assumptions than to user inputs. However, the uncertainties tested for the model assumptions were much greater and therefore a direct comparison is difficult to make.

The uncertainty introduced by the friction index, n , has a significant effect on initial friction and coolant warm-up times. The percentage of friction retained

in the oil similarly affects steady-state friction, fuel consumption, initial heat transfer rates to the oil and oil warm-up times. These uncertainties should be addressed, and this is discussed in Suggestions for Further Work (Section 8.1). The analysis also highlighted the necessity of matching simulation conditions with experimental conditions. For simulations of an engine in a laboratory environment (no engine compartment and little or no air flow) the current assumptions of coefficients for heat transfer from the external surfaces of the engine are reasonable. However, these must be adjusted for simulations of an engine in a vehicle, whether stationary or at speed.

The necessity of matching simulation conditions with test conditions was also discussed in Chapter 3, which highlighted current model assumptions regarding the head gasket and piston assembly. It was noted that for novel cooling circuits or piston designs, these assumptions would have to be addressed.

Comparisons of model predictions and experimental data were presented in Chapter 5, demonstrating the level of accuracy that can be expected from PROMETS. The fidelity shown in these comparisons, within $\pm 10\%$ of experimental values, is generally representative of the ability of PROMETS to predict global model variables such as coolant and oil temperatures, friction values, fuel flow rates and exhaust gas temperatures. Whilst the ability of PROMETS to predict local variables such as structural temperatures is not directly addressed in this thesis, previous work [8.1][8.2] has shown that predictions of these variables are also generally to within $\pm 10\%$ of experimental values. This level of accuracy is also the experience of PROMETS users worldwide [8.3].

The uncertainties discussed in the previous paragraphs have implications for the results of the thermal analysis investigations conducted in Chapter 7. For the 1.6l Sigma engine tested, the friction index is specified as 0.24. If a lower value had been used, the trends seen in the investigation, such as the percentage of fuel consumption penalty or improvement, or the number of seconds improvement in coolant warm-up time, would not change although the absolute values would alter. Similarly, a different percentage of friction retained in the oil would not alter the trends seen, although the absolute values would change.

Many of the implications of the faster warm-up investigations discussed in this thesis in relation to the gasoline 1.6l Sigma engine apply equally to other SI engines and to their CI counterparts as the principle of improving the efficiency of the heat distribution process applies for any engine, although the details of the process may change. Changes to the thermal capacity of the engine coolant, oil or structure should have a similar effect for any engine. Likewise, the use of an oil cooler to increase the oil-coolant coupling will lengthen coolant warm-up times and reduce oil warm-up times, with increased effect as the effectiveness of the oil cooler increases. The results presented and discussed for the exhaust gas-oil heat exchanger will have similar implications for V-type engines, however, since the exhaust gas temperature of a diesel engine at a given operating condition is lower than that of a gasoline engine, less heat will be transferred to the oil in a diesel engine and the reduction in fuel consumption seen will be smaller.

8.1 SUGGESTIONS FOR FURTHER WORK

At present, the level of description is not consistent for all PROMETS model versions and further work to bring all versions to the same level is suggested. The areas requiring work are listed in Table 8.2. This thesis describes the theory upon which versions for the in-line and V-type gasoline and in-line diesel models are based in Chapter 3. A further model version is required to complete the family of internal combustion engine models. PROMETSDV, a V-type diesel version of the model, is currently under development and is an amalgamation of the V-type gasoline and in-line diesel versions. It will have the features listed for the in-line diesel version in Table 1.1. The need for further model versions is not anticipated, although continued advances in ICE-electric hybrid vehicles may generate a need for the development of additional sub-models to represent electric motors and batteries.

Several suggestions for further developments of the model have arisen from the evaluations of PROMETS described in this thesis. Chapter 3 suggested the implementation of oil mass flow rates as a linear function of engine speed. The

current fixed flow rate does not reflect the changes in oil mass flow rate with engine speed and the consequential effect this has on heat transfer rates to and from the oil.

Chapter 4 highlighted a desire for the removal of the remaining S-functions from the Simulink versions of PROMETS. This would improve the transparency of the model to the user, reduce initialisation and run times, and make the model easier to maintain. The remaining S-functions calculate the heat flux and friction distribution down the liner (see Chapter 3, Section 3.5.1), fuel flow rates (see Chapter 3, Section 3.4) and turbocharger performance in the diesel version (see Chapter 3, Section 3.9). The calculation of the heat flux and friction distribution could be implemented as part of PROGEN, as the calculation only needs to be performed once. Non-iterative solutions must be developed to replace the other two S-functions.

Chapter 5 highlighted the uncertainty surrounding the specification of the friction index, n , and the implications of this uncertainty for model predictions. Since the friction index has a significant effect upon predicted friction values during warm-up, heat transfer rates to the oil, and coolant and oil warm-up times, it would be prudent to investigate further and clarify the dependence of the friction index upon speed and the value(s) used for different engine types. The percentage of friction retained in the oil was also highlighted as an uncertainty within the model. Similarly, since this has a significant effect on steady-state friction, fuel consumption, initial heat transfer rates to the oil and oil warm-up times, an improved understanding of the oil and structure contact conditions influencing this variable is desirable.

There is scope for improving the range of user inputs available. Chapter 4 highlighted an increasing need to be able to simulate CGI engine blocks. For this material it would be necessary to verify that stability requirements are met (see Chapter 5, Section 5.1) and to add the material properties to the choices available through the Graphical User Interface (see Chapter 4, Section 4.4.1) within PROGEN. Additionally, as highlighted by the sensitivity analysis in Chapter 5, it would be prudent to be able to select ambient and sump heat transfer coefficients based on the test conditions being simulated.

Feed back from users, particularly in the United States of America, has drawn attention to a need to be able to simulate the hot soak experienced by the engine after key off. This is necessary to fully simulate the conditions of the Federal Test Procedure (FTP75), which is used for emissions testing in the same way as the NEDC (see Chapter 4, Section 4.4.5). Further details of the FTP can be found in [8.4]. Development of PROMETS to allow this feature involves eliminating the origins of 'divide by zero' errors generated by zero fuel, oil and coolant flow rates and the development of sub-models for heat transfer to the oil and coolant to model conduction only. The simulation of heat transfer within the model structure should not be affected.

The formulation of the heat exchanger model given in Chapter 6 describes a circular tube, flat plate configuration and is not representative of all current radiator configurations. A more typical radiator configuration is a flattened tube-continuous fin configuration. The fins may be wavy and with or without louvers. For these types of configurations, calculation of the air side heat transfer coefficient is very difficult as the flow pattern and heat transfer mechanism around each fin is complex. Thus, experimental data must be relied upon to determine the air side heat transfer coefficient. Kays and London [8.5] give experimental data of Reynolds number vs. $(StPr^{1/3})$ for several different configurations.

Finally, although several methods to improve warm-up times have been investigated, there is still scope for investigation of a number of other methods. These include investigations into the effectiveness of dual coolant circuits and split coolant circuits.

CHAPTER 9

CONCLUSIONS

The work reported in this thesis covers the theory, structure, sensitivity, performance and development of PROMETS, and the application of the model to investigations of engine thermal behaviour. The conclusions of the thesis can be summarised as follows:

9.1 PROMETS

- PROMETS is a complex model comprising of several sub-models developed from physical and empirical correlations. The model has been converted from 'C' to Simulink. It is now easier to use, understand and modify than previous versions. A simulation of a twenty-minute drive cycle will take 3 minutes on a PC with an AMD Athlon 1.0GHz processor and 1.0Gb RAM.
- A non-iterative solution to the correction of the gas-side heat transfer for coolant composition has been developed. This has replaced the original S-function, improving understanding and modification of this part of the model. The degree of superheat, which is the difference between the surface temperature of the coolant passage and the saturation temperature of 100% water, is set to a value of 21°C, introducing a small but negligible error of 1.6% or less into the calculation of the coolant passage heat transfer coefficient.
- The influence of current model assumptions must be considered when undertaking simulations of novel cooling circuits, novel engine designs or of the engine in-vehicle, particularly at high vehicle speeds.
- PROMETS is generally insensitive to the uncertainties involved in specifying user inputs. However, coolant passage and wall thickness dimensions must

be specified carefully to enable accurate predictions of coolant volume and engine mass.

- Provided that simulations are matched to theoretical model assumptions, PROMETS is most sensitive to model assumptions of the value of the friction index and percentage of frictional heat dissipation retained in the oil.
- Evaluations of the performance of PROMETS are best carried out at a high speed, low load condition, a mid-speed, mid-load condition and a low speed, high load condition. The speeds and loads employed can be adapted for each engine, and are dependent upon individual maximum speed and load capabilities. These conditions emphasise the effects of friction and gas-side heat transfer on predicted variables, facilitating diagnosis of any discrepancies between predicted and experimental data.
- Evaluations of PROMETS, based on three different engines, have demonstrated that the model predicts values of friction mean effective pressure (bar), fuelling (kg/s), oil half rise times and coolant half rise times (seconds) to within $\pm 10\%$ of experimentally measured data.

9.2 ENGINE THERMAL BEHAVIOUR

- Simulations using the external circuit sub-model of PROMETS with the thermostat positioned at the inlet to and outlet from the engine have shown that thermal shock is reduced when the thermostat is positioned at the inlet.
- To maintain a desired bulk coolant temperature, thermostat opening temperature must be reduced when the thermostat is located at the inlet to the engine (rather than at the outlet).

Methods to improve engine warm-up times and fuel consumption have been compared for a 1.6l Sigma engine in a Ford Focus over the NEDC from a start temperature of -10°C . From the investigations described in Chapter 7, the following conclusions can be drawn:

- Reductions in coolant volume and structural mass are beneficial for both fuel consumption and coolant warm-up times. Reductions in oil volume are beneficial for fuel consumption, but increase coolant warm-up times.
- The use of an oil cooler reduces peak oil temperatures at fully warm and reduces fuel consumption during warm-up. Fully warm friction values and coolant half rise times are increased. An oil cooler of effectiveness 0.4 offers the best balance between these compromises, reducing fuel consumption by 1.4% over the NEDC and the peak oil temperature from 376 to 369K. The final friction value is increased from 0.95 bar to 0.98 bar and coolant half rise time increases by 53 seconds.
- It would be beneficial for fuel consumption to fit oil coolers in all engines provided they could be deactivated under fully warm conditions.
- The use of a sump oil heater is not beneficial for fuel consumption or coolant warm-up times.
- An oil-exhaust gas heat exchanger has been shown to reduce fuel consumption by 5.4% over the NEDC. Coolant half rise time is increased by 19 seconds. Oil half rise time is reduced by 114 seconds. However, the peak oil temperature over the NEDC reaches 132°C, approaching the oil degradation limit of $\approx 160^\circ\text{C}$.
- An oil-exhaust heat exchanger and oil cooler combination has been shown to reduce fuel consumption by 5.3% over the NEDC. Coolant half rise time is increased by 19 seconds. Oil half rise time is reduced by 102 seconds. Peak oil temperatures remain well below the degradation limit.
- A coolant-exhaust heat exchanger is more beneficial than an oil-exhaust heat exchanger as it reduces fuel consumption and improves coolant warm-up times.

REFERENCES

CHAPTER 1

- [1.1] Heywood, J.B., Internal Combustion Engine Fundamentals, International Edition, McGraw-Hill, 1988
- [1.2] Khovakh, M., The Design of High Speed Diesel Engines, Chap. 5, Constable, London, 1966
- [1.3] Sitkei, G., *Heat Transfer and Thermal Loading in Internal Combustion Engines*, Akademiai Kiado, Budapest 1974
- [1.4] Burke, J. and Haws, J., *Vehicle Thermal Systems Modelling using FLOWMASTER2™*, SAE Paper 2001-01-1696, 2001
- [1.5] Shayler, P.J., Baylis, W.S. and Chick, J.P., *Routes to Improving Heater and Engine Performance During Warm-up*, Proc. Instn. Mech. Engrs. Paper C543/061/99, 1999
- [1.6] Taylor, C.F. and Toong, T.Y., *Heat Transfer in Internal Combustion Engines*, ASME Paper 57-HT-17, 1957
- [1.7] Patton, K.J., Nitschke, R.G., Heywood, J.B., *Development and Evaluation of a Friction Model for Spark Ignition Engines*, SAE Paper 890836, 1989
- [1.8] Christian, S.J., *A Spark Ignition Engine Model for Heat Flow and Friction Characteristics*, PhD Thesis, University of Nottingham, 1992
- [1.9] Yuen, H.C.R., *An Investigation of Thermal Conditions In Spark Ignition Engines*, PhD Thesis, University of Nottingham, 1995
- [1.10] Chick, J.P., *The Modelling of Engine Thermal Systems*, PhD Thesis, University of Nottingham, 1998
- [1.11] Baylis, W.S., *An Investigation of Heat Transfer and Friction in Turbocharged Diesel Engines*, PhD Thesis, University of Nottingham, 1999
- [1.12] Dmitrieva, I., *Personal Communication*, Ford Motor Company, July 2001

CHAPTER 2

- [2.1] *Vehicle Thermal Management Systems*, Conference, Columbus, Ohio, USA, 29 March – 1 April 1993
- [2.2] *Vehicle Thermal Management Systems*, Conference, London, UK, 9 – 12 May 1995
- [2.3] *Vehicle Thermal Management Systems*, Conference, Indianapolis, Indiana, USA, 19 – 22 May, 1997
- [2.4] Heywood, J.B., *Internal Combustion Engine Fundamentals*, International Edition, McGraw-Hill, 1988
- [2.5] Winterbone, D.E. and Tennant, D.W.H., *The Variation of Friction and Combustion Rates During Diesel Engine Transients*, SAE Paper 810339, 1981
- [2.6] Uras, H.M. and Patterson, D.J., *Measurement of Piston and Ring Assembly Friction Instantaneous IMEP Method*, SAE Paper 830416, 1983
- [2.7] Patton, K.J Nitschke, R.G. and Heywood, J.B., *Development and Evaluation of a Friction Model for Spark Ignition Engines*, SAE Paper 890836, 1989
- [2.8] Ball, W.F. Jackson, N.S. Pilley, A.D. and Porter, B.C., *The Friction of a 1.6 litre Automotive Engine – Gasoline and Diesel*, SAE Paper 860418, 1986
- [2.9] Rosenberg, R.C., *General Friction Considerations for Engine Design*, SAE Paper 821576, 1982
- [2.10] Burrows, J.A., *An Investigation into the Cold Start Performance of Automotive Diesel Engines*, PhD Thesis, University of Nottingham, 1997
- [2.11] McGheean, J.A., *A Literature Review of the Effects of Piston and Ring Friction and Lubricating Oil Viscosity on Fuel Economy*, SAE Paper 780673, 1978
- [2.12] Christian, S.J., *A Spark Ignition Engine Model for Heat Flow and Friction Characteristics*, PhD Thesis, University of Nottingham, 1992
- [2.13] Baylis, W.S., *An Investigation of Heat Transfer and Friction in Turbocharged Diesel Engines*, PhD Thesis, University of Nottingham, 1999
- [2.14] Auiler, J.A., Zbrozek, J.D. and Blumberg, P.N., *Optimisation in Automotive Engine Calibration for Better Fuel Economy – Methods and Application*, SAE Paper 770076, 1977
- [2.15] Barnes-Moss, H.W., *A Designer's Viewpoint, in Passenger Car Engines*, Proc. Instn. Mech. Engrs., pp 133-147, 1975

- [2.16] Millington, B.W. and Hartles, E.R., *Frictional Losses in Diesel Engines*, SAE Paper 680590, 1968
- [2.17] Thiele, E., *Determination of Frictional Losses in Internal Combustion Engines*, Motortechnische Z, 43 (6), pp 253-258, 1982
- [2.18] Yagi, S., Fujiwara, K., Kurok, N. and Maeda, Y., *Estimate of Total Engine Loss and Engine Output in Four Stroke SI Engines*, SAE Paper 910347, 1991
- [2.19] Bishop, I.N., *Effect of Design Variables on Friction and Economy*, SAE Paper 812A, 1964
- [2.20] Ciulli, E., Rizzoni, G. and Dawson, J., *Numerical and Experimental Study of Friction on a Single Cylinder CFR Engine*, SAE Paper 960357, 1996
- [2.21] Rezek, S.F. and Henein, N.A., *A New Approach to Evaluate Instantaneous Friction and Its Components in Internal Combustion Engines*, SAE Paper 840179, 1984
- [2.22] Taraza, D., Henein, N. and Bryzin, W., *Friction Losses in Multi-Cylinder Diesel Engines*, SAE Paper 2000-01-092
- [2.23] Zweiri, Y.H., Whidborne, J.F. and Seneviratne, L.D., *Instantaneous Friction Components Model for Transient Engine Operation*, Proc. Instn. Mech. Engrs, Vol 214 Part D, pp 809 – 824, 2000
- [2.24] Arsie, I., C. Pianese, G Rizzo, R. Flora and G. Serra, *Development and Validation of a Model for Mechanical Efficiency in a Spark Ignition Engine*, SAE Paper 1999-01-090, 1999
- [2.25] Kouremenos, D.A., Rakopoulos, C.D., Hountalas, D.T. and Zannis, T.K., *Development of a Detailed Friction Model to Predict Mechanical Losses at Elevated Maximum Combustion Pressures*, SAE Paper 2001-01-0333, 2001
- [2.26] Rakopoulos, C.D., Hountalas, D.T., Koutroubousis, A.P. and Zannis, T.C., *Application and Evaluation of a Detailed Friction Model on a DI Diesel Engine with Extremely High Peak Combustion Pressures*, SAE Paper 2002-01-0068, 2002-10-01
- [2.27] Ross, M. and An, F., *The Use of Fuel by Spark Ignition Engines*, SAE Paper 930329, 1993
- [2.28] Wu, W. and Ross, M., *Modelling of Direct Injection Diesel Engine Fuel Consumption*, SAE Paper 971142, 1997
- [2.29] Chick, J.P., *The Modelling of Engine Thermal Systems*, PhD Thesis, University of Nottingham, 1998
- [2.30] Hohenberg, G.F., *Advanced Approaches for Heat Transfer Calculations*, SAE Paper 790825, 1979

- [2.31] Boulouchos, K. and Hannoschock, N., *Der Wärmetransport zwischen Arbeitsmedium und Brennraumwand*, Motortechnische Zeitschrift MTZ (47), 1986
- [2.32] Eiglemeier, C., Lettmann, H., Steisch, G. and Merker, G.P., *A Detailed Phenomenological Model for Wall Heat Transfer Prediction in Diesel Engines*, SAE Paper 2001-01-3265, 2001
- [2.33] Taylor, C.F. and Toong, T.Y., *Heat Transfer in Internal Combustion Engines*, ASME Paper 57-HT-17, 1957
- [2.34] Lundin, B.T., Polovny, J.H. and Chelko, L.J., *Correlation of Cylinder Head Temperatures and Coolant Heat Rejections of a Multicylinder, Liquid-Cooled Engine of 1710 Cubic Inch Displacement*, NACA Report 930, 1949
- [2.35] Shayler, P.J. and Chick, J.P., *Correlation of Engine Heat Transfer for Heat Rejection and Warm-Up Modelling*, SAE Paper 971851, 1997
- [2.36] Elser, K., *Der Instationaere Waermeuebergang in Diesel-Motoren*, Mitt. Inst. Thermodyn. Zurich, No. 15, 1954
- [2.37] Annand, W.J.D., *Heat Transfer in the Cylinders of Reciprocating Internal Combustion Engines*, Proc. Instn. Mech. Engrs. Vol 177, No. 36, 1963
- [2.38] Woschni, G., *A Universally Applicable Equation for the Instantaneous Heat Transfer Coefficient in the Internal Combustion Engine*, SAE Paper 670931, 1967
- [2.39] Bohao, S., Baker, D.M. and Assanis, D.N., *A Global Model for Steady State and Transient SI Engine Heat Transfer Studies*, SAE Paper 960073, 1996
- [2.40] Suzuki, T., Oguri, Y. and Yoshida, M., *Heat Transfer in the Internal Combustion Engine*, SAE Paper 2000-01-0300, 2000
- [2.41] Davis, G.C. and Borgnakke, C., *The Effect of In-Cylinder Flow Processes (Swirl, Squish and Turbulence) on Engine Efficiency – Model Predictions*, SAE Paper 820045, 1980
- [2.42] Han, S.B., Lee, N.H. and Lee, S., *Analysis of Thermal Loading in a Turbocharged Gasoline Engine*, SAE Paper 970205, 1997
- [2.43] Oude Nijeweme, D.J., Kok, J.B.W., Stone, C.R. and Wyszynski, L., *Unsteady In-cylinder Heat Transfer in a Spark Ignition Engine: Experiments and Modelling*, Proc. Instn. Mech. Engrs. Vol. 215, Part D, pp747 – 760, 2001
- [2.44] Borgnakke, C., Arpaci, V.S. and Tabaczynski, R.J., *A Model for the Instantaneous Heat Transfer and Turbulence in a Spark Ignition Engine*, SAE Paper 800287, 1980

- [2.45] Morel, T. and Keribar, R., *A Model for Predicting Spatially and Time Resolved Convective Heat Transfer in Bowl-in-Piston Combustion Chambers*, SAE Paper 850204, 1985
- [2.46] Hires, S.D. and Pochmara, G.L., *An Analytical Study of Exhaust Gas Heat Loss in a Piston Engine Exhaust Port*, SAE Paper 760767, 1976
- [2.47] Malchow, G.L., Sorenson, S.C. and Buckius, R.O., *Heat Transfer in the Straight Section of an Exhaust Port of a Spark Ignition Engine*, SAE Paper 790309, 1979
- [2.48] Meisner, S. and Sorenson, S.C., *Computer Simulation of Intake and Exhaust Manifold Flow and Heat Transfer*, SAE Paper 860242, 1986
- [2.49] Dittus, F.W. and Boelter, L.M.K., Univ. Calif. (Berkeley) Pub. Eng., Vol. 2, p. 443, 1930
- [2.50] Wendland, D.W., *Automobile Exhaust System Steady State Heat Transfer*, SAE Paper 931085, 1993
- [2.51] Seider, E.N. and Tate, C.E., *Heat Transfer and Pressure Drop of Liquids in Tubes*, Ind. Eng. Chem., Vol. 28, p 1429, 1936
- [2.52] Huber, E.W. and Koller, T., *Pipe Friction and Heat Transfer in the Exhaust Pipe of a Firing Combustion Engine*, 12th Int. Congress on Combustion Engines, Tokyo, Japan, 1977
- [2.53] Caton, J.A. and Heywood, J.B., *An Experimental and Analytical Study of Heat Transfer in an Engine Exhaust Port*, Int. Journal of Heat and Mass Transfer, Vol. 24, pp581-595, 1981M.
- [2.54] Pischinger, R., *The Importance of Heat Transfer to IC Engine Design and Operation*, in XIX International Symposium, International Centre for Heat and Mass Transfer in Gasoline and Diesel Engines, Dubrovnik, August 1987
- [2.55] French, C.C.J. and Atkins, K.A., *Thermal Loading of a Petrol Engine*, Proc. Instn. Mech. Engrs. Vol. 187, pp 561-573, 1973
- [2.56] Li, C.-H., *Thermal and Mechanical Behaviour of an L-4 Engine*, SAE Paper 881149, 1988
- [2.57] Hosakowa, T., Tsukada, H., Maeda, H., Nakakubo, Y. and Nakada, M., *Development of Computer Aided Engineering for Piston Design*, SAE Paper 890775, 1989
- [2.58] Farber, E.A. and Scorah, R.L. *Heat Transfer to Water Boiling under Pressure*, Transactions of the ASME, No. 79, pp 369-348, 1948
- [2.59] Campbell, N., Hawley, J., Tilley, D., Wong, L. and Horrocks, R., *Nucleate Boiling Investigations using Simulated Engine Cooling Passages*, Proc. Instn. Mech. Engrs., Paper C543/002/99, 1999

- [2.60] Porot, P., Menegaz, P. and Ag, N., *Understanding and Improving Evaporative Engine Cooling at High Load, High Speed by Engine Tests and 3D Calculations*, SAE Paper 971797, 1997
- [2.61] Chen, J.C., *Correlation for Boiling Heat Transfer to Saturated Fluids in Convective Flow*, I&EC Proc. Design and Development, Vol. 5, pp 332-329, 1963
- [2.62] Collier, J.G. and Thome, J.R., Convective Boiling and Condensation, Clarendon Press, London, 1994
- [2.63] Finlay, I.C, Harris, D., Boam, D.J. and Parks, B.I., *Factors Influencing Combustion Chamber Wall Temperatures in a Liquid-cooled, Automotive, Spark-ignition Engine*, Proc. Instn. Mech. Engrs., Vol. 99, pp 207-214, 1985
- [2.64] Finlay, I., R. Boyle, J. Pirault and T. Biddulph, *Nucleate and Film Boiling of Engine Coolants Flowing in a Uniformly Heated Duct of Small Cross Section*, SAE Paper 870032, 1987
- [2.65] Finlay, I., Gallacher, G., Biddulph, T. and Marshall, R., *The Application of Precision Cooling to the Cylinder Head of a Small, Automotive, Petrol Engine*, SAE Paper 880263, 1988
- [2.66] Campbell, N., Charlton, S. and Wong, L., *Designing Towards Nucleate Boiling in Combustion Engines*, Proc. Instn. Mech. Engrs., Paper C496/092/95, 1995
- [2.67] Campbell, N., Tilley, D., MacGregor, S. and Wong, L., *Incorporating Nucleate Boiling in a Precision Cooling Strategy for Combustion Engines*, SAE Paper 971791, 1997
- [2.68] Campbell, N., Hawley, J., Leathard, M., Horrocks, R. and Wong, L., *Nucleate Boiling Investigations and the Effects of Surface Roughness*, SAE Paper 1999-01-0577, 1999
- [2.69] Yoo, I.K., Simpson, K., Bell, M. and Majkowski, S., *An Engine Coolant Temperature Model and Application for Cooling System Diagnosis*, SAE Paper 2000-01-0939, 2000
- [2.70] Valaszka, L. and Jouannet, B., *Cooling System Optimisation for Euro4 – EPA/02 Heavy Duty Trucks*, SAE Paper 2000-01-0964, 2000
- [2.71] Berry, A., M. Blissett, J. Steiber, A.T. Tobin and S.T. McBroom, *A New Approach to Improving Fuel Economy and Performance Prediction through Coupled Thermal Systems Simulation*, SAE Paper 2002-01-1208, 2002
- [2.72] Austin, K. and Botte, V., *An integrated Air Conditioning (AC) Circuit and Cooling Circuit Simulation Model*, SAE Paper 2001-01-1691, 2001

- [2.73] Zoz, S., Strepek, S., Wiseman, M. and Qian, C., *Engine Lubrication System Model for Sump Oil Temperature Prediction*, SAE Paper 2001-01-1073, 2001
- [2.74] Perset, D. and Jouannet, B., *Simulation of a Cooling Loop for a Variable Speed Fan System*, SAE Paper 1999-01-0576, 1999
- [2.75] Burke, J. and Haws, J., *Vehicle Thermal Systems Modelling using FLOWMASTER2™*, SAE Paper 2001-01-1696, 2001
- [2.76] Blissett, M. and Austin, K., *Engine Thermal Management Comparison between Predicted and Measured Results*, Proc. Instn. Mech. Engrs. Paper C543/087/99, 1999
- [2.77] Etemad, S., Thorell, A., Barnard, P. and Stevens, S., *Integrating Modelling Techniques for Engine Thermal Analysis*, Proc. Instn. Mech. Engrs. Paper C543/059/99, 1999
- [2.78] Butler, D., Stevens, S. and Owen, N., *Modelling of Vehicle Thermal Systems*, Proc. Instn. Mech. Engrs. Paper C543/057/99, 1999
- [2.79] Koch, F., Maassen, F. and Haubner, F., *Cooling System Development and Optimisation with the Computer Code COOL*, SAE Paper 980425, 1998
- [2.80] Koch, F. and Haubner, F., *Cooling System Development and Optimisation for DI Engines*, SAE Paper 2000-01-0283, 2000
- [2.81] Eichlseder, W. and Raab, G., *Calculation and Design of Cooling Systems*, SAE Paper 931088, 1993
- [2.82] Sakai, T., Ishiguro, S. and Sudoh, Y., *The Optimum Design of Engine Cooling System by Computer Simulation*, SAE Paper 942270, 1994
- [2.83] Eichlseder, W., Raab, G., Hager, J. and Raup, M., *Use of Simulation Tools with Integrated Coolant Flow Analysis for the Cooling System Design*, SAE Paper 971815, 1997
- [2.84] Morel, T., Wahiduzzaman, S., Kasten, M. and Klug, M., *System Model of Engine Thermal Management*, Proc. Instn. Mech. Engrs. Paper C543/069/99, 1999
- [2.85] da Silva, A., M. Lebrun and S. Samuel, *Modelling and Simulation of a Cooling System using Multiport Approach*, SAE Paper 2000-01-0292, 2000
- [2.86] Seider, G., Bet, F., Heid, T., Hess, U., Klein, T. and Sauer, J., *A Numerical Simulation Strategy for Complex Automotive Cooling Systems*, SAE Paper 2001-010-1722, 2001
- [2.87] Kaplan, J.A. and Heywood, J.B., *Modelling the Spark Ignition Engine Warm-up Process to Predict Component Temperatures and Hydrocarbon Emissions*, SAE Paper 910302, 1991

- [2.88] Veshagh, A. and C. Chen, *A Computer Model for Thermofluid Analysis of Engine Warm-up Process*, SAE Paper 931157, 1993
- [2.89] Sidders, J. and Tilley, D., *Optimising Cooling System Performance Using Computer Simulation*, SAE Paper 971802, 1997
- [2.90] Mandrusiak, G. and Aklidas, A., *Impact of Engine Design on Vehicle Heating System Performance*, SAE Paper, 971839, 1997
- [2.91] Bohac, S., Baker, D. and Assanis, D., *A Global Model for Steady State and Transient SI Engine Heat Transfer Studies*, SAE Paper 960073, 1996
- [2.92] Mohan, K., Arici, O., Yang, S. and Johnson, J., *A Computer Simulation of the Turbocharged Diesel Engine as an Enhancement of the Vehicle Engine Cooling System Simulation*, SAE Paper 971804, 1997
- [2.93] Arici, O., Johnson, J. and Kulkarni, A., *The Vehicle Engine Cooling System Simulation Part 1 – Model Development*, SAE Paper 1999-01-0240, 1999
- [2.94] Arici, O., Johnson, J. and Kulkarni, A., *The Vehicle Engine Cooling System Simulation Part 2 – Model Validation Using Transient Data*, SAE Paper 1999-01-0241, 1999
- [2.95] Watson, N., Pilley, A.D. and Marzouk, M., *A Combustion Correlation for Diesel Engine Simulation*, SAE Paper 800029, 1980
- [2.96] Shayler, P.J., Baylis, W.S. and Chick, J.P., *Routes to Improving Heater and Engine Performance During Warm-up*, Proc. Instn. Mech. Engrs. Paper C543/061/99, 1999
- [2.97] Stecki, J.S., Cichocki, W., Garbacik, A. and Szewczyk, K., *Heating Systems for Cold Starting of IC Engines*, SAE Paper 920002, 1992
- [2.98] Woschni, V.G., *Use of Stored Heat During the Start and Warm-up Period of Automobile Engines*, MTZ Motortechnische Zeitschrift, Vol. 56, No. 6, pp 364 – 369, 1995
- [2.99] Heck, E., *Latent-heat Storage Battery for Reducing Engine Warm-up Time*, MTZ Motortechnische Zeitschrift, Vol. 55, No. 6, pp 334-340, 1994
- [2.100] Schatz, O., *Cold Start Improvements With a Heat Store*, SAE Paper 910305, 1991
- [2.101] Zobel, W. and Strahle, R., *Heat Storage Battery for Car Applications*, Proc. VTMS 1995, Paper C496/017/95, 1995
- [2.102] Marston, A.M., Armstrong, S. and Miaoulis, I.N., *A Novel Automobile Preheating System for Cold Starts*, SAE Paper 941995, 1994

- [2.103] Hellman, K.H., *Evaluation of Heat Storage Technology for Quick Engine Warm-up*, SAE Paper 922244, 1992
- [2.104] Goettler, H. J., Vidger, L.J. and Majkrzak, D.S., *The Effect of Exhaust-to-Coolant Heat Transfer on Warm-up Time and Fuel Consumption of Two Automobile Engines*, SAE Paper 860363, 1986
- [2.105] Davies, M., *Personal Communication*, Ford Motor Company, March 2002
- [2.106] Lindbert, L. and Andersson, M., *Thermal Power Booster*, SAE Paper 900222, 1990
- [2.107] Kern, J. and Ambros, P., *Concepts for a Controlled Optimised Vehicle Engine Cooling System*, SAE Paper 971816, 1997
- [2.108] Kobayashi, H., Yoshimura, K. and Hirayama, T., *A Study on Dual Circuit Cooling for Higher Compression Ratio*, Proc. Instn. Mech. Engrs. Paper C427/84, SAE Paper 841294, 1984
- [2.109] Chanfreau, M., Joseph, A., Butler, D. and Swiatek, R., *Advanced Engine Cooling Thermal Management System on a Dual Voltage 42V-14V Minivan*, SAE Paper 2001-01-1742, 2001
- [2.110] Cortona, E. and Onder, C., *Engine Thermal Management with Electric Cooling Pump*, SAE Paper 2000-01-0965, 2000
- [2.111] Cortona, E., Onder, C. and Guzzella, L., *Engine Thermomanagement with Electrical Components for Fuel Consumption Reduction*, Int. Journal of Engine Research, Vol. 3, No. 3, pp 157-170
- [2.112] Choukroun and M. Chanfreau, *Automatic Control of Electronic Actuators for an Optimised Engine Cooling Thermal Management*, SAE Paper 2001-01-1758, 2001
- [2.113] Priede, T. and Anderton, D., *Likely Advances in Mechanics, Cooling, Vibration and Noise of Automotive Engines*, Proc. Instn. Mech. Engrs., Vol. 198D, No. 7, 1984
- [2.114] Clough, M., *Precision Cooling of a Four Valve per Cylinder Engine*, SAE Paper 931123, 1993
- [2.115] Fisher, E., *Means of Improving the Efficiency of Automotive Cooling Systems*, Proc. Instn. Mech. Engrs., Paper C372/001, Apr. 1989
- [2.116] Robinson, K., Campbell, N., Hawley, J. and Tilley, D., *A Review of Precision Engine Cooling*, SAE Paper 1999-01-0578, 1999
- [2.117] Holman, J.P., Heat Transfer, McGraw-Hill Book Co., 1992
- [2.118] Sachdev, R., *An Investigation of Instantaneous Heat Transfer Rates in the Exhaust Port of an Internal Combustion Engine*, Master's Thesis, Department of Mechanical and Industrial Engineering, University of Illinois, Urbana, Illinois, 1981

- [2.119] Farber, E.A. and Scorah, R.L. *Heat Transfer to Water Boiling under Pressure*, Transactions of the ASME, No. 79, pp 369-348, 1948
- [2.120] McAulay, K.J., Wu, T., Chen, S.K., Borman, G.L., Myers, P.S. and Uyehara, O.A., *Development and Evaluation of the Simulation of the Compression –Ignition Engine*, SAE Paper 650451, 1965
- [2.121] Fujii, I., Yagi, S., Sono, H. and Kamiya, H., *Total Engine Friction in Four Stroke SI Motorcycle Engine*, SAE Paper 880268, 1988
- [2.122] Chen, S.K. and Flynn, T., *International Harvester-LABECO High BMEP Single Cylinder Research Engine*, SAE Paper 650733, 1965
- [2.123] Gish, R.E., McCulloch, J.D., Retzloff, J.B. and Mueller, H.T., *Determination of True Engine Friction*, SAE transactions, Vol. 66, 1958

CHAPTER 3

- [3.1] Shayler, P.J., Chick, J.P., Hayden, D.J. and Yuen, H.C.R., *Progress on Modelling Engine Thermal Behaviour for VTMS Applications*, SAE Paper 971852, 1997
- [3.2] Hayden, D.J., *Investigations and Modelling of Thermal Conditions in Spark Ignition Engines and Aftertreatment Systems*, PhD Thesis, University of Nottingham, 1999
- [3.3] Christian, S.J., *A Spark Ignition Engine Model for Heat Flow and Friction Characteristics*, PhD Thesis, University of Nottingham, 1992
- [3.4] Holman, J.P., *Heat Transfer*, 7th Edition, McGraw-Hill, 1992
- [3.5] Myres, G.E., *Analytical Methods in Heat Transfer*, McGraw-Hill, 1971
- [3.6] Yuen, H.C.R., *An investigation of thermal conditions in spark ignition engines*, PhD Thesis, University of Nottingham, 1995
- [3.7] Chick, J.P., *The Modelling of Engine Thermal Systems*, PhD Thesis, University of Nottingham, 1998
- [3.8] Patton, K.J., Nitschke, R.G. and Heywood, J.B., *Development and Evaluation of a Friction Model for Spark Ignition Engines*, SAE 860418, 1996
- [3.9] Baylis, W.S., *An Investigation of Heat Transfer and Friction in Turbocharged Diesel Engines*, PhD Thesis, University of Nottingham, 1999

- [3.10] Burrows, J.A., *An Investigation into the Cold Start Performance of Automotive Diesel Engines*, PhD Thesis, University of Nottingham, 1997
- [3.11] Hayden, D.J., *PROMETSV Jaguar 4.0l V8 Validation Progress Report 10b*, University of Nottingham Internal Report, June 1999
- [3.12] Bishop, I.N., *Effect of Design Variables on Friction and Economy*, SAE Paper 812A, 1964
- [3.13] Shayler, P.J. and Christian, S.J., *A Model for the Investigation of Temperature, Heat Flow and Friction Characteristics During Engine Warm-up*, SAE Paper 931153, 1993
- [3.14] Darnton, N.J., *Fuel Consumption and Pollutant Emissions of Spark Ignition Engines During Cold-Started Drive Cycles*, PhD Thesis, University of Nottingham, 1997
- [3.15] Shayler, P.J. and Chick, J.P., *Correlation of Engine Heat Transfer for Heat Rejection and Warm-up Modelling*, SAE Paper 971851, 1997
- [3.16] Chen, J.C., *Correlation for Boiling Heat Transfer to Saturated Fluids in Convective Flow*, I&EC Proc. Des. and Dev. 5(3), 322-329, 1963
- [3.17] Dittus, F.W. and Boelter, L.M.K., Univ. Calif. (Berkeley) Pub. Eng., Vol. 2, p. 443, 1930
- [3.18] Union Carbide, *Properties of Ethylene Glycol Mixtures*, Internal Report 1980
- [3.19] Polovny, J.H., Bogdan, L.J. and Chelco, L.J., *Cylinder Head Temperatures and Coolant Heat Rejection of a Multi Cylinder Liquid Cooled Engine of a 1650 Cubic Inch Displacement*, NACA TN 2069, 1950
- [3.20] Shayler, P.J. and Chick, J.P., *Effect of Coolant Mixture Composition on Engine Heat Rejection Rate*, SAE Paper 960275, 1996
- [3.21] Taylor, C.F and Toong, T.Y., *Heat Transfer in Internal Combustion Engines*, ASME Paper 57-HT-17, 1957
- [3.22] Kays, W.M. and Crawford, M.E., Convective Heat and Mass Transfer, McGraw-Hill, 3rd Edition, 1993
- [3.23] Massey, B.S., Mechanics of Fluids, 6th Edition, Chapman and Hall, 1992
- [3.24] Shilling, A., Motor Oils and Engine Lubrication, Scientific Publications (G.B.) Limited, 2nd Edition, 1968
- [3.25] Cameron, A., Basic Lubrication Theory, Ellis Horwood Limited, 3rd Edition, 1981

- [3.26] Allen, A.J. and Baylis, W.S., *Calculation of Exhaust Gas Temperature within NUSim-D*, University of Nottingham Internal Report, August 2001
- [3.27] Milton, B.E., Thermodynamics, Combustion and Engines, Chapman and Hall, 1995
- [3.28] Bohao, S., Baker, D.M. and Assanis, D.N., *A Global Model for Steady State and Transient SI Engine Heat Transfer Studies*, SAE Paper 960073, 1996
- [3.29] Heywood, J.B., Internal Combustion Engine Fundamentals, International Edition, McGraw-Hill, 1988

CHAPTER 4

- [4.1] Gupta, V., *The Development of a Plotter for NUSim and PROMETS*, Internal Report, March 2001
- [4.2] Morgan, T.J., *PROMETS14 Input Data*, University of Nottingham Internal Report, July 2002
- [4.3] Directive 91/441/EEC, *Motor Vehicle Emissions*, Appendix 1, 30th August 1991
- [4.4] Louckes, T.N., *A Practical Economic Solution to Weight Reduction and Increased Performance in Diesel Engines*, SAE Paper 912711, 1991
- [4.5] Dawson, S., *Compacted Graphite Iron: New Opportunities for Engine Design*, SAE Paper 952226, 1995
- [4.6] Tholl, M., Magata, A. and Dawson, S., *Practical Experience with Passenger Car Engine Blocks Produced in High Quality Compacted Graphite Iron*, SAE Paper 960297, 1996
- [4.7] Mortimer, J., *Audi Set to Follow Ford in Use of CGI for Diesels*, Auto Technology, Vol.2, p.32, 2002
- [4.8] Kimberly, W., *Winner of the Block Vote?*, Automotive Engineer, p. 62, July/August 2002
- [4.9] Andre, M., *In Actual Use Testing; 70 000 km and 10 000 Trips by 55 French Cars Under Real Conditions*, SAE Paper 910039

CHAPTER 5

- [5.1] Shayler, P.J. and Christian, S.J., *A Model for the Investigation of Temperature, Heat Flow and Friction Characteristics During Engine Warm-up*, SAE Paper 931153 (1993)

- [5.2] Shayler, P.J. and Chick, J.P., *Correlation of Engine Heat Transfer for Heat Rejection and Warm-up Modelling*, SAE Paper 971851 (1997)
- [5.3] Shayler, P.J., Chick, J.P., Hayden, D.J. and Yuen, H.C.R., *Progress on Modelling Engine Thermal Behaviour for VTMS Applications*, SAE Paper 971852, 1997
- [5.4] Christian, S.J., *A Spark Ignition Engine Model for Heat Flow and Friction Characteristics*, PhD Thesis, University of Nottingham, 1992
- [5.5] Burrows, J.A., *An Investigation into the Cold Start Performance of Automotive Diesel Engines*, PhD Thesis, University of Nottingham, 1997
- [5.6] Baylis, W.S., *An Investigation of Heat Transfer and Friction in Turbocharged Diesel Engines*, PhD Thesis, University of Nottingham, 1999
- [5.7] Holman, J.P., Heat Transfer, 7th Edition, pp 541, McGraw-Hill Inc., 1992
- [5.8] Jones, S., *Experimental Investigations, Modelling and Control of Direct Injection Gasoline Engines*, PhD Thesis, University of Nottingham, 2002
- [5.9] Clark, L., *Experimental Studies and Systems Modelling to Investigate the Behaviour of DI Diesel Engines*, PhD Thesis, University of Nottingham, 2002
- [5.10] Andre, M., *In Actual Use Car Testing: 70, 000 km and 10, 000 Trips by 55 French Cars Under Real Conditions*, SAE Paper 910039, 1991
- [5.11] Taylor, C.F. and Toong, T.Y., *Heat Transfer in Internal Combustion Engines*, ASME Paper 57-HT-17, 1957
- [5.12] Alkidas, A.C., *Effects of Operational Parameters on Structural Temperatures and Coolant Heat Rejection of a S.I. Engine*, SAE Paper 931124, 1993

CHAPTER 6

- [6.1] Morel, T., Wahiduzzaman, S., Kasten, M. and Klug, M., *System Model of Engine Thermal Management*, Proc. Instn. Mech. Engrs., Paper C543/069/99, 1999
- [6.2] Koch, F., Maassen, F. and Haubner, F., *Cooling System Development and Optimisation with the Computer Code COOL*, SAE Paper 980425, 1998
- [6.3] Butler, D.J., Stevens, S.P. and Owen, N.J., *Modelling of Vehicle Thermal Systems*, Proc. Instn. Mech. Engrs., Paper C543/057/99, 1999

- [6.4] Perset, D. and Jouannet, B., *Simulation of a Cooling Loop for a Variable Speed Fan System*, SAE Paper 1999-01-0576, 1999
- [6.5] Website address: http://www.indiacar.com/index2.asp?pagename=http://www.indiacar.com/infobank/ntech_fordengines.htm
- [6.6] Chipman, J.C., Hontz, W. and Shillor, M., *Simulations of a Thermostat Model I: Approach to Steady States*, Journal of Mathematical and Computer Modelling, Vol. 32, pp 765-790, 2000
- [6.7] Zou, X., Jordan, J.A. and Shillor, M., *A Dynamic Model for a Thermostat*, Journal of Engineering Mathematics, Vol. 36, pp 291-310, 1999
- [6.8] Arici, O., Johnson, J.H. and Kulkarni, A.J., *The Vehicle Engine Cooling System Simulation Part 1 – Model Development*, SAE Paper 1999-01-0240, 1999
- [6.9] Nelson, V.A. and Robinchaux, J.D., *A Model to Simulate the Behaviour of an Automotive Thermostat*, SAE Paper 971814, 1997
- [6.10] Sidders, J.A. and Tilley, D.G., *Optimising Cooling System Performance Using Computer Simulation*, SAE Paper 971802, 1997
- [6.11] Veshagh, A. and Moffatt, R., *Computer Aided Analysis of Heat Flows in Vehicle Cooling System*, SAE Paper 920010, 1992
- [6.12] Wagner, J.R., Ghone, M.C., Dawson, D.W. and Marotta, E.E., *Coolant Flow Control Strategies for Automotive Thermal Management Systems*, SAE Paper 2002-01-0713, 2002
- [6.13] Yoo, K., Simpson, K., Bell, M. and Majkowski, S., *An Engine Coolant Temperature Model and Application for Cooling System Diagnosis*, SAE Paper 2000-01-0939, 2000
- [6.14] Davies, M., *Personal Communication*, Ford Motor Company, August 2002
- [6.15] Knudsen, J.D. and Katz, D.L., Fluid Dynamics and Heat Transfer, McGraw-Hill, New York, 1958
- [6.16] Holman, J.P., Heat Transfer, 7th Edition, McGraw-Hill, London, 1992
- [6.17] Website address: http://www.rubitherm.com/english/pages/04b_glossary_02.htm
- [6.18] Greeley, D.S., Stairs, R.W. and Hickey, R.I., *Rapid On-System Cooling Fan Design and Analysis Using CFD and Lifting Surface Theory*, Proc. Instn. Mech. Engrs, Paper C543/051/99, 1999
- [6.19] Baude, P., Moreau, S., Haertig, J. and Johe, C., *Inlet and Outlet Flow Visualisation on Engine Cooling Fans*, Proc. Instn. Mech. Engrs, Paper C543/077/99, 1999

- [6.20] Spindler, T., Reister, H. and Stetter, H., *Numerical Simulation and Measurement of a Vehicle Cooling Fan at a Fan Test Rig*, Proc. Instn. Mech. Engrs., Paper C543/070/99, 1999
- [6.21] Capdevila, H., Elias, S., Martinuzzi, R. and Surry, D., *Development of Analytical Capabilities for the Design of Integrated Automotive Radiator-Fan Assemblies*, Proc. Instn. Mech. Engrs., Paper C543/095/99, 1999
- [6.22] Parrino, M., Dentis, L. and Parola, A., *Effects of Internally Spiral Finned Tubes on the Performance of Mechanically Assembled Heat Exchangers*, SAE Paper 954015, 1995
- [6.23] Olsson, C.O. *Hydraulic and Thermal Performance of Radiator Tubes*, SAE Paper 954055, 1995
- [6.24] DeJong, N. *et al*, *A Complementary Experimental and Numerical Study of the Flow and Heat Transfer in Offset Strip-Fin Heat Exchangers*, SAE Paper 954015, 1995
- [6.25] Kim, N., Yun, J-H. and Webb, R., *Heat Transfer and Friction Correlations for Wavy-Plate Fin and Tube Heat Exchangers*, ASME Journal of Heat Transfer, Vol. 119, pp 560, 1997
- [6.26] Karbach, T., *Determination of Air Side Fluid Flow and Heat Transfer Characteristics in Heat Exchangers Using CFD*, SAE Paper 971847, 1997
- [6.27] Woodcock, J. and Baxendale, A., *An Evaluation of the Use of CFD for Investigating the Performance of Intercooler Assemblies*, SAE Paper 971856, 1997
- [6.28] Thorne, N.J.A., Charlton, S.J. and MacGregor, S.A., *Computational and Experimental Investigation of Airflow Through a Vehicle Intercooler Duct*, SAE Paper 931079, 1993
- [6.29] Stevens, F., *Mean Temperature Difference in One, Two and Three Pass Cross-Flow Heat Exchangers*, ASME Journal of Heat Transfer, Vol. 79, pp 287-297, 1957
- [6.30] Kays, W. M and London, A.L., Compact Heat Exchangers, 3rd Edition, Krieger Publishing Company, 1998
- [6.31] Kern, J. and Eitel, J., *State of the Art and Future Developments of Aluminium Radiators for Cars and Trucks*, SAE Paper 931092, 1993
- [6.32] Kays, W.M. and Crawford, M.E., Convective Heat and Mass Transfer, 3rd Edition, McGraw-Hill, Inc., 1993
- [6.33] Sellars, J.R., Tribus, M. and Klein, J.W., *Heat Transfer to Laminar Flows in a Round Tube or Flat Conduit: The Graetz Problem Extended*, Trans. ASME, Vol. 787, p. 441, 1956

- [6.34] Dittus, F.W. and Boelter, L.M.K., Univ. Calif. (Berkeley) Pub. Eng., Vol. 2, p. 443, 1930
- [6.35] Fischer, D., *Personal Communication to J.P. Chick*, Ford Motor Company, March 1997
- [6.36] Christian, S. J., *A Spark Ignition Engine Model for Heat Flow and Friction Characteristics*, PhD Thesis, University of Nottingham, 1992
- [6.37] Yuen, H.C.R., *An Investigation of Thermal Conditions in Spark Ignition Engines*, PhD Thesis, University of Nottingham, 1995
- [6.38] Chick, J.P., *The Modelling of Engine Thermal Systems*, PhD Thesis, University of Nottingham, 1998

CHAPTER 7

- [7.1] Mortimer, J., *Audi Set to Follow Ford in Use of CGI for Diesels*, Auto Technology, Vol. 2, 2002
- [7.2] Finlay, I.C., Boyle, R.J., Pirault, J.P. and Biddulph, T., *Nucleate and Film Boiling of Engine Coolants Flowing in a Uniformly Heated Duct of Small Cross Section*, SAE Paper 870032, 1987
- [7.3] Campbell, N.A.F, Tilley, D.G., MacGregor, S.A. and Wong, L., *Incorporating Nucleate Boiling in a Precision Cooling Strategy for Combustion Engines*, SAE Paper 971791, 1997
- [7.4] Campbell, N.A.F., Hawley, J.G., Tilley, D.G., Wong, L. and Horrocks, R.W., *Nucleate Boiling Investigations Using Simulated Engine Cooling Passages*, Proc. Instn. Mech. Engrs. Paper C543/002/99, 1999
- [7.5] Shilling, A., Motor Oils and Engine Lubrication, Scientific Publications (GB) Ltd, 2nd Edition, 1968
- [7.6] Kays, W.M. and Crawford, M.E., Convective Heat and Mass Transfer, 3rd Edition, McGraw-Hill, Inc., 1993
- [7.7] Bell, P., *Personal Communication to J. Chick*, Ford Motor Company, 1997
- [7.8] Lindbert, L. and Andersson, M., *Thermal Power Booster*, SAE Paper 900222, 1990
- [7.9] Schatz, O., *Cold Start Improvements With a Heat Store*, SAE Paper 910305, 1991
- [7.10] Hellman, K.H., Piotrowski, G.K. and Schaefer, R.M., *Evaluation of Heat Storage Technology for Quick Engine Warm-up*, SAE Paper 922244, 1992

- [7.11] Zobel, W. and Strahle, R., *Heat Storage Battery for Car Applications*, SAE Paper 954047, 1995
- [7.12] Marston, A.M., Armstrong, S. and Miaoulis, I.N., *A Novel Automobile Preheating System for Cold Starts*, SAE Paper 941995, 1994
- [7.13] Boam, D.J., Finlay, I.C., Biddulph, T.W., Ma, T., Lee, R., Richardson, S.H., Bloomfield, J., Green, J.A., Wallace, S., Woods, W.A. and Brown, P., *The Sources of Unburnt Hydrocarbon Emissions From Spark Ignition Engines During Cold Starts and Warm-up*, IMechE Paper No. C44/064, 1992
- [7.14] Chick, J.P., *The Modelling of Engine Thermal Systems*, PhD Thesis, University of Nottingham, 1998
- [7.15] Goettler, H.J., Vidger, L.J. and Majkrzak, D.S., *The Effect of Exhaust-to-coolant Heat Transfer on Warm-up Time and Fuel Consumption of Two Automobile Engines*, SAE Paper 960363, 1986
- [7.16] Davies, M., *Personal Communication*, Ford Motor Company, March 2002

CHAPTER 8

- [8.1] Shayler, P.J. and Christian, S.J., *A Model for the Investigation of Temperature, Heat Flow and Friction Characteristics During Engine Warm-Up*, SAE Paper 931152, 1993
- [8.2] Shayler, P.J. and Chick, J.P., *Correlation of Engine Heat Transfer for Heat Rejection and Warm-up Modelling*, SAE Paper 971851, 1997
- [8.3] *PROMETS Correspondence*, Internal File, May 2000 – May 2003
- [8.4] Website address: [http:// www.epa.gov](http://www.epa.gov)

TABLES

PROMETSI4 : in-line gasoline	●	●	Single Representative Cylinder
PROMETSD : in-line diesel	●	●	Multiple Cylinders
PROMETSV : V-type gasoline	●	●	Friction Prediction
	●	●	Fuel Flow Rate Prediction
	●	●	Structural Temperatures
	●	●	Coolant Temperatures
	●	●	Oil Temperatures
	●	●	Exhaust Gas Temperature Prediction
	●	●	Effect of Heater Matrix
	●	●	Effect of Oil Cooler in Inner Circuit
		●	Effect of Oil Cooler in Outer Circuit
	●	●	Effect of Supplementary Heater
		●	Effect of EGR Cooler
		●	Effect of Turbocharger
		●	Effect of Intercooler

●	Feature included
	Feature not included

Table 1.1 The features of the current versions of PROMETS.

Correlation	Author(s)	Notes
$Nu=0.258Re^{0.8}$	Hires and Pochmara [2.47]	SI engine exhaust port
$Nu=0.0483Re^{0.783}$	Malchow, Sorenson and Buckius [2.48]	Straight section extension to SI exhaust port
$Nu=0.0774Re^{0.769}$	Meisner and Sorenson [2.49]	SI engine exhaust port
$Nu=0.35Re^{0.6}$	Caton and Heywood [2.53]	SI engine exhaust port
$Nu=0.023Re^{0.8}Pr^{0.3}$	Dittus and Boelter [2.119]	Steady turbulent pipe flow

Table 2.1 Steady state time averaged exhaust port heat transfer correlations.

Location	Maximum Temperature (°C)
Valve bridge	347
Exhaust valve seat	316
Inlet valve seat	206
Top of cylinder liner	132
Exhaust valve	830
Piston crown	295
Piston, behind top ring groove	242
Spark Plug	800

Table 2.2 Typical maximum metal temperatures in a water-cooled spark ignition engine [2.55].

Material	Thermal Conductivity (W/mK)
Aluminium Alloy 195 (Cast, 4.5% Cu)	168
Grey Cast Iron (GG-25)	58
Compacted Graphite Iron (10% nodularity)	36
Partially stabilised Zircona	22
Glass reinforced epoxy (30% w/w)	0.38

Table 3.1 Typical thermal conductivities of common and experimental engine materials.

Engine	a	b
In-line gasoline	1.34	0.000
In-line diesel	1.00	0.000
V-type gasoline	0.51	0.103
Jaguar 4.0l V8 gasoline	0.67	0.050

Table 3.2 Empirical constants for correction to the Patton *et al* [3.8] friction model.

a)

Crankshaft	
Constant	Value
C_{bl}	1.2×10^5
C_{hl}	3.03×10^{-4}
C_{td}	1.35×10^{-10}

b)

Reciprocating	
Constant	Value
C_{hl}	3.03×10^{-4}
C_{ps}	2.94×10^2
$C_{pr,t}$	4.06×10^4
$C_{pr,gl}$	6.89

c)

Valve-train	
Constant	Value
C_{ind}	4.12
C_{cb}	2.44×10^2

d)

Auxiliary	
Constant	Value
$C_{aux, 1}$	6.23
$C_{aux, 2}$	5.22×10^{-3}
$C_{aux, 3}$	-1.79×10^{-7}

Table 3.3 Empirical friction constants for **a)** crankshaft, **b)** reciprocating components, **c)** valve train and **d)** auxiliary components [3.8].

Engine	C1	C2
Gasoline	1.8	1.5
Direct Injection Diesel	2.2	1.5
Indirect Injection Diesel	2.3	1.5

Table 3.4 Values of the constants C1 and C2 for the calculation of gas-side heat transfer.

Constant	Value
<i>a</i>	0.002861351
<i>b</i>	0.0027456016
<i>c</i>	0.0015209422
<i>d</i>	0.00016374834

Table 3.5 Empirical constants for the calculation of effective gas temperature, $T_{g,a}$, for gasoline engines.

Constant	Value
a	340
b	0.12×10^{-3}
c	310
d	0.47×10^{-3}

Table 3.6 Empirical constants for the calculation of effective gas temperature, $T_{g,a}$, for diesel engines.

Constant	Value
a_0	0.903004882
a_1	-7.31935594
a_2	29.92304919
a_3	-58.8857809
a_4	54.09533405
a_5	-18.7220533

Table 3.7 Empirical constants for the calculation of heat flux down the liner.

Composition	Pressure (bar)	
	1.0	2.0
100% water	99.8	120.2
50% water, 50% EG	108.7	130.9
100% EG	197.3	222.2

Table 3.8 The variation of coolant saturation temperature, in °C, with the percentage of ethylene glycol (EG) in the coolant.

Brake Power (kW)	ΔS (°C)
5.24	9.4
20.94	15.0
32.73	19.2
47.12	21.2
75.40	42.0

Table 3.9 The variation of ΔS with brake power.

Engine	Gallery Diameter (m)	Flow Rate (kg/s)	Reynolds number
1.8l Zetec	0.025	0.072	3216
	0.005	0.072	1608
2.0l Mazda	0.0145	0.072	554
	0.016	0.072	502
2.0l Puma	0.016	0.087	607
	0.011	0.087	883
1.8l IDI	0.011	0.075	761
	0.011	0.075	761
2.5l V6	0.006	0.108	2010
	0.005	0.108	2412
4.6l V8	0.0065	0.144	2474
	0.005	0.144	3216

Table 3.10 Reynolds numbers in the oil galleries for different engines.

Oil Type	Walther		Vogel		
	1	2	k_v	θ_1	θ_2
SAE5W-30	17.9821	-2.8894	0.078	1180.3	1332.
SAE10W-30	19.0638	-3.0724	0.0568	1171.2	126.9

Table 3.11 Constants for the Walther and Vogel equations (Equations 3.73 and 3.74 respectively) for determining the viscosity of oil.

Differences	Engine		
	In-line gasoline	V-type gasoline	In-line diesel
Friction Correction Factor	1.34	(a + bS _p)	1.00
Number of Elements	41	54	41
Gas-side Heat Transfer Constants, C1/C2	1.8/1.5	1.8/1.5	2.2/1.5 ¹ 2.3/1.5 ²
Lower Heating Value of Fuel (MJ/kg)	44.0	44.0	41.5
Coolant Circuit Layouts	1, 2	1, 2, 3	1, 2
Effective Gas Temperature (K), T _{g,a}	a	a	b
Gross Indicated Thermal Efficiency, η _{ind,g}	c	c	0.41

¹ For indirect injection engines

a:
$$T_{g,a} = \frac{1}{a - b\phi + c\phi^2 - d\phi^3}$$

b:
$$T_{g,a} = a + bP_{ex} + (c + dP_{ex})\phi$$

c:
$$\eta_{ind,g} = 0.87\left(1 - \frac{1}{CR^3}\right) - 0.0002\theta^2$$

² For direct injection engines

Constants are defined in Table 3.4

Constants are defined in Table 3.5

Constants are defined in Table 3.6

Table 3.12 The differences between calculations in sub-models for versions of PROMETS

Fuel	Model Version	Model Size (Mb)
Gasoline in-line	Single cylinder	6.0
	Multi-cylinder	30.4
Diesel in-line	Single cylinder	6.8
	Multi-cylinder	17.3
Gasoline V-type	Single cylinder	5.2
Gasoline V6	Multi cylinder, Coolant Circuit 1	12.9
	Multi cylinder, Coolant Circuit 2	12.9
	Multi cylinder, Coolant Circuit 3	12.9
Gasoline V8	Multi cylinder, Coolant Circuit 1	13.6
	Multi cylinder, Coolant Circuit 2	13.6
	Multi cylinder, Coolant Circuit 3	13.6

Table 4.1 The versions of PROMETS models and their sizes in Megabytes (Mb)

File Name	Function of the File
auxcomp_calcs	Generates information regarding the auxiliary components
piston_defaults	Calculates default values for the piston if unknown
geometry	Calls the following 8 files, as shown in Figure 4.5
factor_check	Checks that scaling factor values are within acceptable limits
material_props	Sets element material properties and saves to props.mat
block_calcs	Performs general block geometry calculations, incl. block mass
uflow_/puma_head	Performs general head geometry calculations, incl. head mass
piston_calcs	Calculates volumes of piston elements and mass of piston
valve_calcs	Calculates geometry of the valves
engdimns_output	Configures and saves element volume data to volume.mat
summary_output	Saves PROGEN Summary information to file summary.mat
topology	Calculates element contact areas and conduction path lengths
in_circ	Saves inner circuit information to in_circ.mat
turbo	Saves turbocharger information to turbo.mat
energy	Saves selected engine variables to energy.mat
piston	Saves piston information to piston.mat
oil	Calculates the geometry of oil galleries and saves to oil.mat
friction	Sets friction correction constants and saves to friction.mat
time	Saves time related variables to time.mat

Table 4.2 PROGEN files and their functions. The file structure is illustrated in Figure 4.5.

‘.mat’ File Name	Description of Variables Stored in File
engine	A copy of the engine geometry variables selected by the user
in_circ_in	Inner circuit variables
initcond	Initial engine conditions (metal, oil, coolant and air temp)
progend_constants	Constants used by PROGEN
time_in	Time step details
turbo_in	Turbocharger and intercooler variables

Table 4.3 The contents of ‘.mat’ files generated through the GUI and used by PROGEN.

‘.mat’ File Name	Description of Variables Stored in File
amb_info	HTCs and contact areas for elements exposed to ambient
coolant	Properties of elements in contact with the coolant
deck	HTCs and contact areas of valve deck elements
energy	Selected engine variables including bore and stroke
exhaust	Properties of exhaust valve and port elements
flux	Contact areas and conduction path lengths for liner elements
friction	Friction model variables
head	Areas of head elements
in_circ	Inner circuit variables
intake	Properties of intake valve and port elements
oil	Oil circuit variables including oil gallery dimensions
oilmist	HTCs and contact areas between the liner and oil mist
piston	Piston variables
progen_constants	Constants used throughout PROGEN
props	Materials properties for each element
time	Time step details
topology	Contact areas and conduction path lengths between elements
turbo	Turbocharger and intercooler variables
piston	Piston variables
volume	Volumes of all elements

HTC: Heat transfer coefficient

Table 4.4 The contents of ‘.mat’ files created by PROGEN and used by PROMETS.

Time (S)	Engine Speed (rpm)	Engine Load (Nm)	AFR (-)	Fuel Flow Rate (kg/s)	Coolant Flow Rate (l/s)	Heater Coolant Flow Rate (l/s)	Heater Air Flow Rate (l/s)	Exhaust Gas Temp. (K)	Spark Advance (°)	EGR (%)
0	700	4.3	14.7	-1	-1	-1	0	-1	0	0
1	700	4.3	14.7	-1	-1	-1	0	-1	0	0
2	700	4.3	14.7	-1	-1	-1	0	-1	0	0
3	1200	32.0	14.7	-1	-1	-1	0	-1	0	0
4	1200	32.0	14.7	-1	-1	-1	0	-1	0	0
5	1200	32.0	14.7	-1	-1	-1	0	-1	0	0
6	1200	32.0	14.7	-1	-1	-1	0	-1	0	0

Table 4.5 Example of a portion of an operating conditions file, input to PROMETS. Entries of ‘-1’ indicate that variables are automatically calculated by PROMETS. The operating conditions are defined from 0 seconds in steps of 1-second intervals.

Engine Variable	Wall Thickness Height		Coolant Passage Height		Coolant Passage Width		Piston Depth		Conrod Length	
	-10%	+10%	-10%	+10%	-10%	+10%	-10%	+10%	-10%	+10%
Total mass of the head	-2.5	2.5	0.0	0.0	0.6	-0.6	0.0	0.0	0.0	0.0
Total mass of the block	-5.4	5.4	-0.7	0.7	-0.4	0.4	-2.1	2.1	-2.6	2.6
Crankshaft mass	0.0	0.0	0.0	0.0	0.0	0.0	0.0	0.0	0.0	0.0
Piston mass	-8.9	8.9	0.0	0.0	0.0	0.0	-7.5	7.5	0.0	0.0
Conrod mass	0.0	0.0	0.0	0.0	0.0	0.0	0.0	0.0	0.0	0.0
Cam and valve mass	0.0	0.0	0.0	0.0	0.0	0.0	0.0	0.0	0.0	0.0
Coolant auxiliaries mass	0.0	0.0	0.0	0.0	0.0	0.0	0.0	0.0	0.0	0.0
Oil auxiliaries mass	0.0	0.0	0.0	0.0	0.0	0.0	0.0	0.0	0.0	0.0
Total engine mass	-1.4	1.4	-0.1	0.1	0.0	0.0	-0.4	0.4	-0.4	0.4
Block coolant volume	1.7	-1.7	-10.0	10.0	-10.1	10.1	0.0	0.0	0.0	0.0
Head coolant volume	1.4	-1.4	0.0	0.0	-1.7	1.7	0.0	0.0	0.0	0.0
Total coolant volume	1.5	-1.5	-2.9	2.9	-4.2	4.2	0.0	0.0	0.0	0.0

Table 4.6 Percentage variation from base engine values for $\pm 10\%$ variation in engine geometry variable.

Engine Variable	Valve Train Configuration			
	1	2	3	4
Total mass of the head	0.0	+14.3	0.0	0.0
Total mass of the block	0.0	0.0	0.0	0.0
Crankshaft mass	0.0	0.0	0.0	0.0
Piston mass	0.0	0.0	0.0	0.0
Conrod mass	0.0	0.0	0.0	0.0
Cam and valve mass	0.0	0.0	0.0	0.0
Total engine mass	0.0	+2.3	0.0	0.0

Table 4.7 Percentage variation from base engine values for different valve train configurations.

Engine Variable	Horizontal coolant passage walls		Crankcase walls		Outer vertical wall of block coolant passage		Crankshaft bearing housing thickness		Head portside outer wall thickness	
	-10%	+10%	-10%	+10%	-10%	+10%	-10%	+10%	-10%	+10%
Total mass of the head	0.0	0.0	0.0	0.0	0.3	-0.3	0.0	0.0	-3.1	3.1
Total mass of the block	-0.4	0.4	-1.1	1.1	-0.9	0.9	-0.9	0.9	0.0	0.0
Crankshaft mass	0.0	0.0	0.0	0.0	0.0	0.0	0.0	0.0	0.0	0.0
Piston mass	0.0	0.0	0.0	0.0	0.0	0.0	0.0	0.0	0.0	0.0
Conrod mass	0.0	0.0	0.0	0.0	0.0	0.0	0.0	0.0	0.0	0.0
Cam and valve mass	0.0	0.0	0.0	0.0	0.0	0.0	0.0	0.0	0.0	0.0
Coolant auxiliaries mass	0.0	0.0	0.0	0.0	0.0	0.0	0.0	0.0	0.0	0.0
Oil auxiliaries mass	0.0	0.0	0.0	0.0	0.0	0.0	0.0	0.0	0.0	0.0
Total engine mass	-0.1	0.1	-0.2	0.2	-0.1	0.1	-0.1	0.1	-0.5	0.5
Block coolant volume	0.0	0.0	0.0	0.0	0.0	0.0	0.0	0.0	0.0	0.0
Head coolant volume	0.0	0.0	0.0	0.0	-0.9	0.9	0.0	0.0	3.7	-3.7
Extra coolant volume	0.0	0.0	0.0	0.0	0.0	0.0	0.0	0.0	0.0	0.0
Total coolant volume	0.0	0.0	0.0	0.0	-0.7	0.7	0.0	0.0	2.7	-2.7

Table 4.8 Percentage change in PROGEN calculated masses and volumes with $\pm 10\%$ changes in scaling factors.

Continued overleaf ...

Engine Variable	Piston crown or cylinder wall thickness		Additional Coolant		Coolant volume in the head		Coolant volume in the block	
	-10%	+10%	-10%	+10%	-10%	+10%	-10%	+10%
Total mass of the head	0.0	0.0	0.0	0.0	0.0	0.0	0.0	0.0
Total mass of the block	0.0	0.0	0.0	0.0	0.0	0.0	0.0	0.0
Crankshaft mass	0.0	0.0	0.0	0.0	0.0	0.0	0.0	0.0
Piston mass	-2.1	2.1	0.0	0.0	0.0	0.0	0.0	0.0
Conrod mass	0.0	0.0	0.0	0.0	0.0	0.0	0.0	0.0
Cam and valve mass	0.0	0.0	0.0	0.0	0.0	0.0	0.0	0.0
Coolant auxiliaries mass	0.0	0.0	0.0	0.0	0.0	0.0	0.0	0.0
Oil auxiliaries mass	0.0	0.0	0.0	0.0	0.0	0.0	0.0	0.0
Total engine mass	0.0	0.0	0.0	0.0	0.0	0.0	0.0	0.0
Block coolant volume	0.0	0.0	0.0	0.0	0.0	0.0	-10.0	10.0
Head coolant volume	0.0	0.0	-10.0	10.0	-10.0	10.0	0.0	0.0
Extra coolant volume	0.0	0.0	0.0	0.0	0.0	0.0	0.0	0.0
Total coolant volume	0.0	0.0	0.0	0.0	-7.3	7.3	-2.7	2.7

Table 4.8 **Cont.** Percentage change in PROGEN calculated masses and volumes with $\pm 10\%$ changes in scaling factors.

a)

Friction Index	Coolant Half Rise Time (s)	
	1000 rpm, 120 Nm	3000 rpm, 5 Nm
0.16	318	205
0.20	312	195
0.24	305	185

b)

Friction Index	Oil Half Rise Time (s)	
	1000 rpm, 120 Nm	3000 rpm, 5 Nm
0.16	287	177
0.20	281	169
0.24	275	161

Table 5.1 a) Coolant and b) oil half rise times for different values of friction index, *n* at the operating conditions tested. The half rise times are defined as the time taken for the coolant to rise by 60°C and for the oil to rise by 40°C.

a)

FTO (%)	Coolant Half Rise Time (s)	
	1000 rpm, 120 Nm	3000 rpm, 5 Nm
10	301	179
15	302	183
20	030	187

b)

FTO (%)	Oil Half Rise Time (s)	
	1000 rpm, 120 Nm	3000 rpm, 5 Nm
10	290	177
15	285	168
20	280	158

c)

FTO (%)	Fuel Consumed (kg)	Reduction in Fuel Consumption (%)
10	0.72675	0.00
15	0.71914	1.05
20	0.71201	2.03

Table 5.2 a) Coolant and b) oil half rise times for different values of the percentage of friction retained in the oil (FTO) at the operating conditions tested. c) Fuel consumed over 1200 seconds for different FTOs at 3000 rpm, 5 Nm. The reduction is calculated from the preceding value in the table.

a)

Variation	C1	C2
C1 – 10%	1.98	1.22
C1	1.80	1.50
C1 + 10%	1.62	1.84

b)

Variation	Proportion to Cylinder (%)	Proportion to Exhaust Port (%)
C1 – 10%	56.0	44.0
C1	50.8	49.2
C1 + 10%	45.7	54.3

Table 5.3 **a)** The values of C1 and C2 used in the sensitivity analysis and **b)** the proportions of heat transferred from the combustion gases to the cylinder and exhaust port with varying values of C1 and C2.

a)

Variation	Element 1 Temperature (°C)	
	1000 rpm, 120 Nm	3000 rpm, 5 Nm
C1 – 10%	104	100
C1	105	101
C1 + 10%	106	102

b)

Variation	Element 6 Temperature (°C)	
	1000 rpm, 120 Nm	3000 rpm, 5 Nm
C1 – 10%	106	119
C1	108	120
C1 + 10%	109	121

c)

Variation	Element 20 Temperature (°C)	
	1000 rpm, 120 Nm	3000 rpm, 5 Nm
C1 – 10%	145	139
C1	144	137
C1 + 10%	143	136

Table 5.4 Fully warm element temperatures for different values of C1 and C2 at the operating conditions tested, showing **a)** element 1, at the top of the liner, **b)** element 6, at the bottom of the liner and **c)** element 20, exhaust port element.

a)

Variation	Exhaust Port Temperatures (°C)	
	1000 rpm, 120 Nm	3000 rpm, 5 Nm
C1 – 10%	138	128
C1	132	122
C1 + 10%	124	115

b)

Variation	Coolant Half Rise Time (s)	
	1000 rpm, 120 Nm	3000 rpm, 5 Nm
C1 – 10%	310	185
C1	305	186
C1 + 10%	301	186

c)

Variation	Oil Half Rise Time (s)	
	1000 rpm, 120 Nm	3000 rpm, 5 Nm
C1 – 10%	275	161
C1	275	161
C1 + 10%	274	160

Table 5.5 a) Exhaust port temperatures after 100 seconds, prior to thermostat opening, b) coolant half rise times and c) oil half rise times for different values of C1 and C2 at the operating conditions tested.

Geometry	GrPr	C	m
Vertical Plane	$10^{-1} - 10^4$	-	-
	$10^4 - 10^9$	0.59	$\frac{1}{4}$
	$10^9 - 10^{13}$	0.021	0.4
Upper surface of heated plates or lower surface of cooled plates	$2 \cdot 10^4 - 8 \cdot 10^6$	0.54	$\frac{1}{4}$
	$8 \cdot 10^6 - 10^{11}$	0.15	$\frac{1}{3}$
Lower surface of heated plates or upper surface of cooled plates	$10^5 - 10^{11}$	0.27	$\frac{1}{4}$

Table 5.6 Constants for use with Equation 5.4 for isothermal surfaces to determine free convection heat transfer coefficients [5.7].


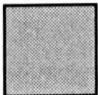

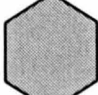

Geometry	GrPr	C	n
 d	$5 \cdot 10^3 - 10^5$	0.246	0.588
 d	$5 \cdot 10^3 - 10^5$	0.102	0.675
 d	$5 \cdot 10^3 - 1.95 \cdot 10^4$	0.160	0.638
	$1.95 \cdot 10^4 - 10^5$	0.0385	0.782
 d	$5 \cdot 10^3 - 10^5$	0.153	0.638
 d	$4 \cdot 10^3 - 1.5 \cdot 10^4$	0.228	0.731

Table 5.7 Constants for use with Equation 5.8 to determine heat transfer coefficients from bluff bodies [5.7]. The characteristic dimension is indicated by **d**.

a)

Sump HTC	Steady State Oil Temperature (°C)	
	1000 rpm, 120 Nm	3000 rpm, 5 Nm
7	94.7	102.9
10	94.4	102.6
50	90.3	101.1

b)

Sump HTC	Increase in Fuel Consumed (%)	
	1000 rpm, 120 Nm	3000 rpm, 5 Nm
7	-	-
10	0.1	-
50	1.3	0.2

Table 5.8 **a)** Steady state oil temperatures and **b)** percentage increase in fuel consumed (compared to the preceding value) over 1200s for different values of sump heat transfer coefficient (HTC).

a)

Ambient HTC	Heat Transfer Rate to Ambient (W)	
	1000 rpm, 120 Nm	3000 rpm, 5 Nm
5	48.1	50.2
10	95.2	99.5
20	186.6	195.5

b)

Ambient HTC	Steady State Crankcase Temperature (°C)	
	1000 rpm, 120 Nm	3000 rpm, 5 Nm
5	99.3	116.5
10	96.9	114.8
20	92.5	111.1

c)

Ambient HTC	Coolant Half Rise Time (s)	
	1000 rpm, 120 Nm	3000 rpm, 5 Nm
5	301	183
10	303	184
20	306	185

d)

Ambient HTC	Oil Half Rise Time (s)	
	1000 rpm, 120 Nm	3000 rpm, 5 Nm
5	272	159
10	273	160
20	276	161

Table 5.9 a) Heat transfer rate to ambient, b) crankcase temperatures c) coolant half rise time and d) oil half rise time for different values of ambient heat transfer coefficient (HTC).

a)

Engine Compartment?	Steady state Crankcase Temperature (°C)	
	1000 rpm, 120 Nm	3000 rpm, 5 Nm
No	114.9	96.8
Yes	119.7	100.8

b)

Engine Compartment?	Coolant Half Rise Time (s)	
	1000 rpm, 120 Nm	3000 rpm, 5 Nm
No	303	184
Yes	300	182

c)

Engine Compartment?	Oil Half Rise Time (s)	
	1000 rpm, 120 Nm	3000 rpm, 5 Nm
No	273	160
Yes	270	159

Table 5.10 **a)** Steady state crankcase temperatures, **b)** coolant half rise times in seconds and **c)** oil half rise times in seconds for simulations with and without an engine compartment.

Operating Condition	Specific Values
High speed, low load <ul style="list-style-type: none"> • Cold start 	6000 rpm, 5 Nm -18°C
Mid-speed, mid-load	3000 rpm, 60 Nm
Low speed, high load <ul style="list-style-type: none"> • Increasing EGR • Increasing heater air flow 	1000 rpm, 120 Nm From 0 to 30 % EGR From 0 to 20 l/s air flow rate

Table 5.11 Suggested speed and load conditions for evaluating the performance of PROMETS in predicting variables for the 1.6l Sigma engine.

Model Assumption		Initial friction	S.S. friction	Fuel consumption	Initial htr to oil	S.S. htr to coolant	Htr to ambient	Htr from sump	Coolant half rise time	Oil half rise time
		(%)	(%)	(%)	(%)	(%)	(%)	(%)	(s)	(s)
Friction index	0.16	-	-	-	-	-	-	-	-	-
	0.20	+9.4	-	+0.3	+9.4	-	-	-	-10	-8
	0.24	+10.4	-	+0.5	+10.4	-	-	-	-10	-8
FTO (%)	10	-	-	-	-	-	-	-	-	-
	15	-	-0.4	-	+33.0	-0.1	-	-	+0.3	-9
	20	-	-0.4	-	+33.0	-0.1	-	-	+0.3	-10
C1/C2	-10%	-	-	-	-	-	-	-	-	-
	-	-	-	-	-	-0.4	-	-	-5	-
	+10%	-	-	-	-	-0.7	-	-	-4	-1
Compartment	No	-	-	-	-	-	-	-	-	-
	Yes	-	-0.8	-	-	+4.9	-	-	-3	-3
Ambient HTC (W/m ² K)	5	-	-	-	-	-	-	-	-	-
	10	-	-	-	-	-2.3	+97.9	-	+2	+1
	20	-	+0.1	-	-	-4.8	+96.0	-	+3	+3
Sump HTC (W/m ² K)	7	-	-	-	-	-	-	-	-	-
	10	-	-	-	-	-0.3	-	+42.2	+1	+1
	50	-	+2.5	+0.2	-	-4.2	-	+372.5	+1	+10

S.S. Steady state

Htr Heat transfer rate

HTC Heat transfer coefficient

Table 5.12a Summary of the percentage change in predicted variables at 1000 rpm, 120 Nm for all model assumptions examined. Positive values represent an increase in the variable. Negative values represent a decrease in the value.

Model Assumption		Initial friction	S.S. friction	Fuel consumption	Initial htr to oil	S.S. htr to coolant	Htr to ambient	Htr from sump	Coolant half rise time	Oil half rise time
		(%)	(%)	(%)	(%)	(%)	(%)	(%)	(s)	(s)
Friction index	0.16	-	-	-	-	-	-	-	-	-
	0.20	+9.4	-	+0.6	+9.4	-0.8	-	-	-10	-8
	0.24	+10.4	-	+0.6	+10.4	-0.7	-	-	-10	-8
FTO (%)	10	-	-	-	-	-	-	-	-	-
	15	-	-1.5	-1.1	+33.0	-0.8	-	-	+4	-9
	20	-	-0.8	-0.9	+33.0	-0.8	-	-	+4	-10
C1/C2	-10%	-	-	-	-	-	-	-	-	-
	-	-	-	-	-	-0.1	-	-	+1	-
	+10%	-	-	-	-	-0.2	-	-	-	-1
Compartment	No	-	-	-	-	-	-	-	-	-
	Yes	-	-0.8	-0.2	-	+3.4	-	-	-2	-1
Ambient HTC (W/m ² K)	5	-	-	-	-	-	-	-	-	-
	10	-	-	-	-	-1.7	+98.2	-	-1	-1
	20	-	-	-	-	-3.2	+96.5	-	-1	-1
Sump HTC (W/m ² K)	7	-	-	-	-	-	-	-	-	-
	10	-	-	+0.1	-	-0.2	-	+42.4	+1	+1
	50	-	+2.3	+1.3	-	-2.2	-	+374.2	-	+5

S.S. Steady state

Htr Heat transfer rate

HTC Heat transfer coefficient

Table 5.12b Summary of the percentage change in predicted variables at 3000 rpm, 5 Nm for all model assumptions examined. Positive values represent an increase in the variable. Negative values represent a decrease in the value.

Pipe Position in Circuit	Pipe Diameter (m)	Pipe Length (m)	Time Delay (s)
Prior to heater matrix	0.016	0.50	$0.0533/\dot{m}_{cool}$
After heater matrix	0.016	0.50	$0.1067/\dot{m}_{cool}$
Engine bypass	0.019	1.23	$0.1805/\dot{m}_{cool}$
Prior to radiator	0.028	0.24	$0.0653/\dot{m}_{cool}$
After radiator	0.028	0.81	$0.3267/\dot{m}_{cool}$

Table 6.1 Time delays around the 1.6l Sigma coolant circuit (shown in Figure 6.1) as a function of coolant mass flow rate, \dot{m}_{cool} , determined using Equation 6.2.

a)

Opening	
Constant	Value
<i>a</i>	1.0×10^{-6}
<i>b</i>	-0.0018
<i>c</i>	1.2853
<i>d</i>	-453.6
<i>e</i>	79951
<i>f</i>	-6×10^6

b)

Closing	
Constant	Value
<i>g</i>	5×10^{-6}
<i>h</i>	-0.0094
<i>i</i>	6.8396
<i>j</i>	-2475.8
<i>k</i>	448029
<i>l</i>	-3×10^7

Table 6.2 Constants for the equations representing the variation of thermostat opening and closing with coolant temperature

Variable	Value
Width (m)	0.496
Height (m)	0.322
Thickness (m)	0.023
Number of tubes across face	17
Number of tubes deep	2
Number of passes	1
Tube diameter (m)	0.007

Table 6.3 Description of the radiator used in the external circuit model.

Variable	Change in Effectiveness (%)	
	-10%	+10%
z	+8.1	-7.8
δ	-0.5	+0.5
A_{fin}/A	0.0	0.0

Table 6.4 The sensitivity in percentage change of the calculated value of effectiveness to variations of the input values for the plate spacing, z , fin length, l , fin thickness, δ and ratio of fin area to total area, A_{fin}/A .

Material	Density (kg/m ³)	Specific Heat Capacity (J/kg K)	Thermal Capacity of 1 m ³ (kJ/K)
Aluminium alloy 195 (cast, 4.5% Cu)	2660	871	2317
Grey cast iron (GG-25)	7570	470	3558
Compacted Graphite Iron (CGI) (10% nodularity)	7000	450	3173

Table 7.1 Properties relating to thermal capacity of common engine materials

Material	Head Mass (kg)	Block Mass (kg)
Aluminium alloy	9.63	8.92
Grey cast iron	27.42	19.47

Table 7.2 Masses of the head and block in different materials for the same volume

Engine Set-up	Fuel consumed (kg)	Increase (%)
All aluminium	0.53427	-
Cast iron head, aluminium block	0.53836	0.77
Aluminium head, cast iron block	0.53848	0.79
All cast iron	0.54266	1.57

Table 7.3 Fuel consumed in kg and percentage increase in fuel consumption compared to an all aluminium engine for different combinations of head and block materials. Simulations were conducted for a 1.6l Sigma engine over the NEDC.

		Oil Flow Rate (l/s)						
		0.00	0.13	0.21	0.25	0.29	0.33	0.37
Coolant Flow Rate (l/s)	0.05	0.3998	0.3113	0.2491	0.2256	0.2059	0.1893	0.1751
	0.12	0.4000	0.3540	0.3050	0.2851	0.2664	0.2498	0.2350
	0.18	0.4000	0.3587	0.3299	0.3117	0.2948	0.2794	0.2653
	0.24	0.4000	0.3758	0.3428	0.3255	0.3112	0.2958	0.2835
	0.30	0.4000	0.3800	0.3508	0.3360	0.3218	0.3083	0.2958
	0.35	0.4000	0.3825	0.3552	0.3424	0.3291	0.3154	0.3044
	0.42	0.4000	0.3845	0.3600	0.3472	0.3346	0.3225	0.3110
	0.48	0.4000	0.3859	0.3630	0.3508	0.3388	0.3272	0.3150
	0.54	0.4000	0.3859	0.3663	0.3536	0.3421	0.3309	0.3201
	0.60	0.4000	0.3877	0.3671	0.3559	0.3448	0.3339	0.3234

Table 7.4 Table of oil cooler effectiveness for the 2.4l Puma engine [7.7]. Coolant and oil flow rates are given in l/s.

Oil cooler effectiveness	Coolant Half Rise Time (s)	Oil Half Rise Time (s)
0.0	311	293
0.2	328	266
0.4	335	254
0.6	338	245
0.8	340	238
1.0	341	234

Table 7.5 The effect of oil cooler effectiveness on coolant and oil half rise times in seconds. The half rise times are defined as the time taken for the coolant to rise by 60°C and for the oil to rise by 40°C.

Engine Set-up	Coolant Half Rise Time (s)	Oil Half Rise Time (s)
Base engine	311	293
0.5kW additional heat input	322	218
1.0kW additional heat input	325	167

Table 7.6 The effect of adding heat into the oil sump, using a heater driven by the engine alternator, on coolant and oil half rise times in seconds.

Engine Set-up	Coolant Half Rise Time (s)	Oil Half Rise Time (s)
Base engine	311	293
Oil-exhaust heat exchanger	330	179
Oil-exhaust heat exchanger + OC	330	191

Table 7.7 The effect of an oil-exhaust gas heat exchanger, and an oil-exhaust gas heat exchanger with an oil cooler (OC) on coolant and oil half rise times in seconds.

Model Assumption		Initial friction	S.S. friction	Fuel consumption	Initial htr to oil	S.S. htr to coolant	Htr to ambient	Htr from sump	Coolant half rise time	Oil half rise time
		(%)	(%)	(%)	(%)	(%)	(%)	(%)	(s)	(s)
Ambient Temperature (°C)	18	-	-	-	-	-	-	-	-	-
	20	-	-	-	+0.5 ¹	+0.4 ¹	-2.5 ¹	-	-1 ¹	-1 ¹
	22	-	-	-	+0.5 ¹	+0.4 ¹	-2.4 ¹	-	-1 ¹	-
Coolant circuit (multi)	1	-	-	-	-	-	-	-	-	-
	2	-	-	-	-	-1.2 ¹	-	-	-1 ^{1,2}	-1 ^{1,2}
Oil circuit	1	-	-	-	-	-	-	-	-	-
	2	-	-	-	+1.1 ²	-	-	-	-	-
Friction index	0.16	-	-	-	-	-	-	-	-	-
	0.20	+9.4 ^{1,2}	-	+0.6 ²	+9.4 ^{1,2}	-0.8 ²	-	-	-10 ²	-8 ²
	0.24	+10.4 ^{1,2}	-	+0.6 ²	+10.4 ^{1,2}	-0.7 ²	-	-	-10 ²	-8 ²
FTO (%)	10	-	-	-	-	-	-	-	-	-
	15	-	-1.5 ²	-1.1 ²	+33.0 ^{1,2}	-0.8 ²	-	-	+4 ²	-9 ²
	20	-	-0.8 ²	-0.9 ²	+33.0 ^{1,2}	-0.8 ²	-	-	+4 ²	-10 ²
C1/C2	-10%	-	-	-	-	-	-	-	-	-
	-	-	-	-	-	-0.4 ¹	-	-	-5 ¹	-
	+10%	-	-	-	-	-0.7 ¹	-	-	-4 ¹	-1 ¹
Compartment	No	-	-	-	-	-	-	-	-	-
	Yes	-	-0.8 ^{1,2}	-0.2 ²	-	+4.9 ¹	-	-	-3 ¹	-3 ¹
Ambient HTC (W/m ² K)	5	-	-	-	-	-	-	-	-	-
	10	-	-	-	-	-2.3 ¹	+98.2 ²	-	+2 ¹	+1 ¹
	20	-	+0.1 ¹	-	-	-4.8 ¹	+96.5 ²	-	+3 ¹	+3 ¹
Sump HTC (W/m ² K)	7	-	-	-	-	-	-	-	-	-
	10	-	-	+0.1 ²	-	-0.3 ¹	-	+42.4 ²	+1 ¹	+1 ¹
	50	-	+2.3 ²	+1.3 ²	-	-4.2 ¹	-	374.2 ²	+1 ¹	+10 ¹

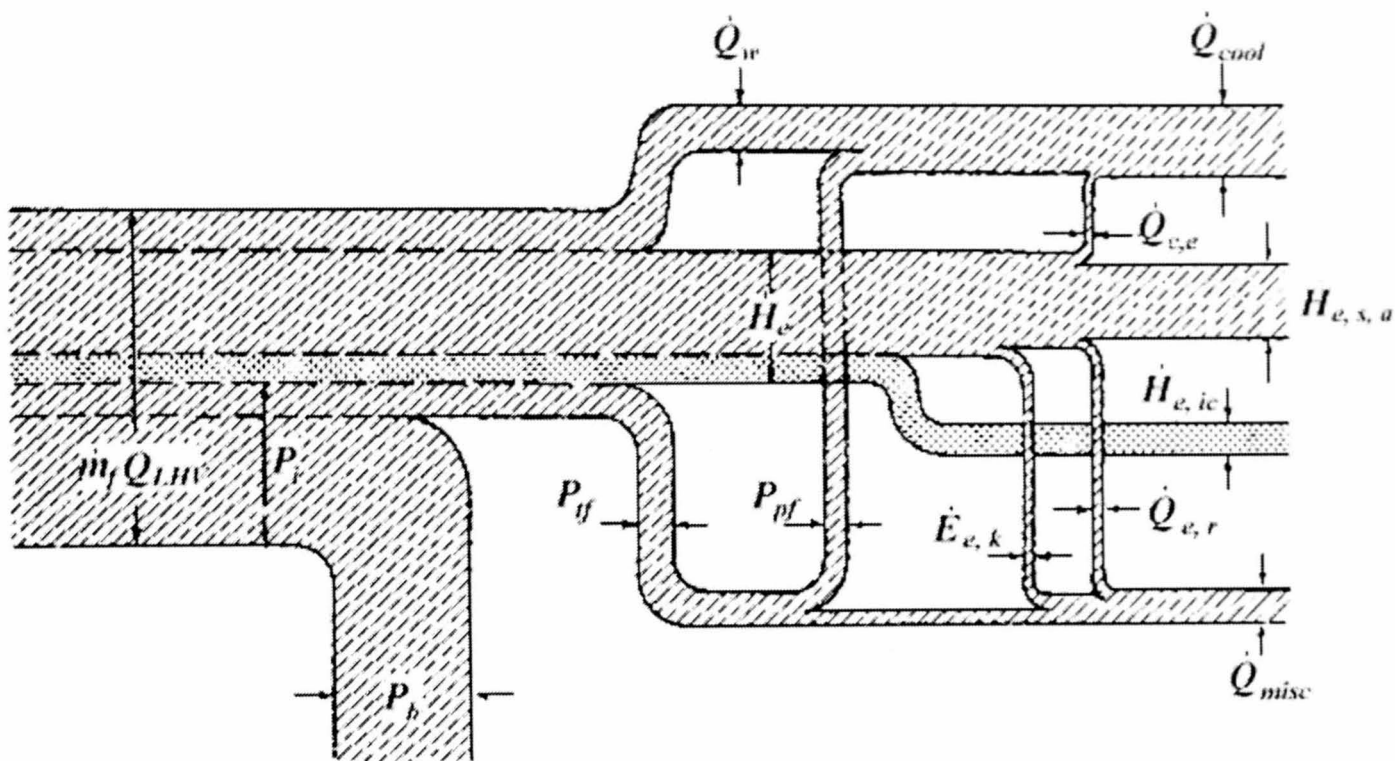
Table 8.1 Summary of the maximum effect of user inputs and model assumptions on predicted variables. Superscripts represent effect at 1) 1000 rpm, 120 Nm and 2) 3000 rpm, 5 Nm.

PROMETS Version	Calculation of gross indicated thermal efficiency	Flexible inner circuit description	Turbocharger model	Intercooler model	External circuit model	Coolant circuit 3
PROMETSI4 (in-line gasoline)		•	•	•		•
PROMETSD (in-line diesel)	•				•	•
PROMETSV (V-type gasoline)		•	•	•	•	

• Feature not available in current version

Table 8.2 Summary of the work required to bring all versions of PROMETS to the same level.

FIGURES



$(\dot{m}_f Q_{LHV})$	Fuel flow rate \times lower heating value
\dot{Q}_q	Heat transfer rate to the combustion chamber wall
\dot{H}_{ex}	Exhaust enthalpy flux
P_b	Brake power
P_{tf}	Total friction power
P_i	Indicated power
P_{pf}	Piston friction power
\dot{Q}_{cool}	Heat rejection rate to coolant
$\dot{Q}_{c,e}$	Heat transfer rate to coolant in the exhaust ports
$\dot{H}_{e,s,a}$	Exhaust sensible enthalpy flux entering atmosphere
$\dot{H}_{e,ic}$	Exhaust chemical enthalpy flux due to incomplete combustion
$\dot{Q}_{e,r}$	Heat flux radiated from the exhaust system
$\dot{E}_{e,k}$	Exhaust kinetic energy flux
\dot{Q}_{misc}	Sum of remaining energy fluxes and transfers

Figure 1.1 Sankey energy flow diagram for an internal combustion engine at full load, fully warm (reproduced from Heywood [1.1]).

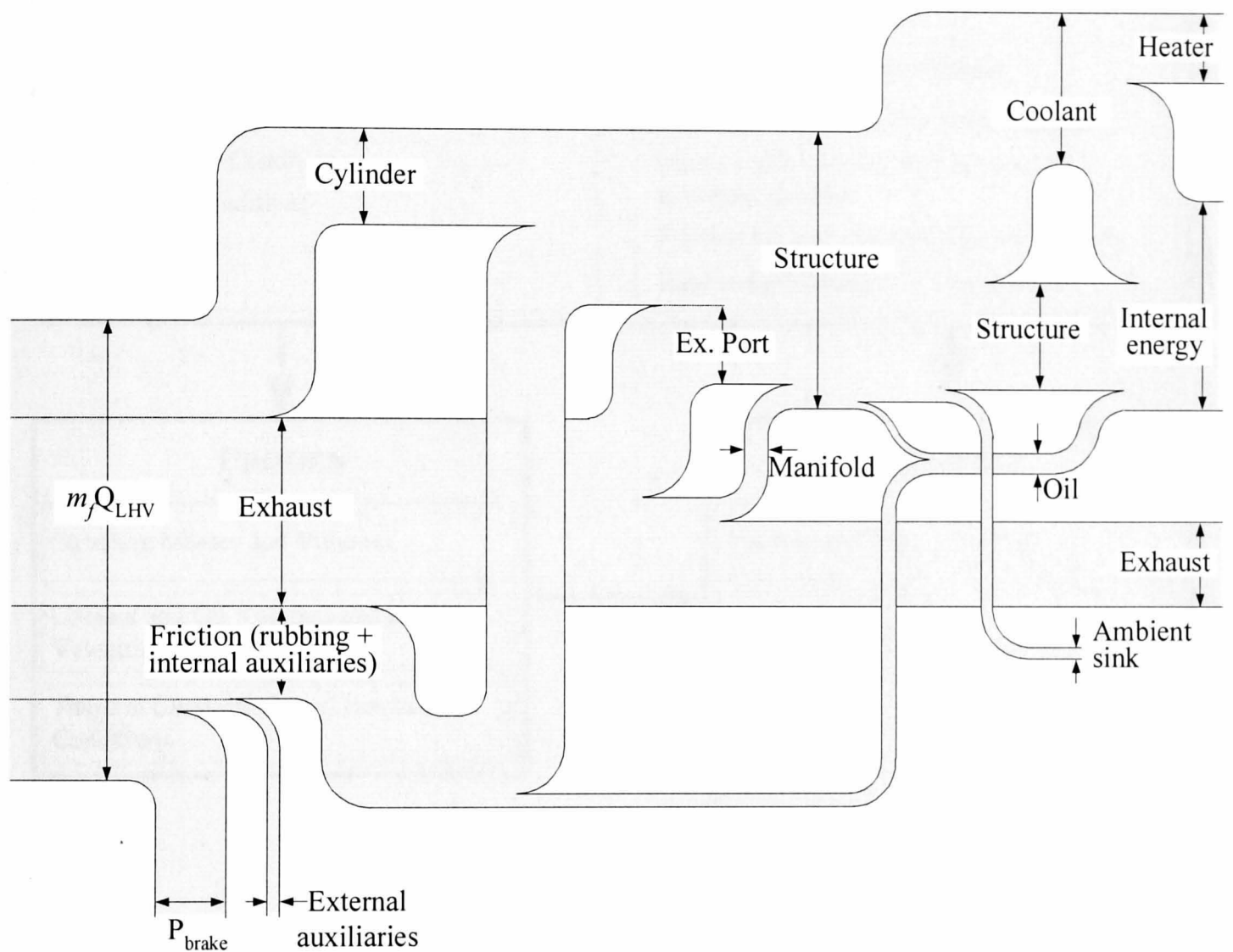


Figure 1.2 Engine heat flow diagram during warm-up (reproduced from [1.5] and originally adapted from Heywood [1.1]).

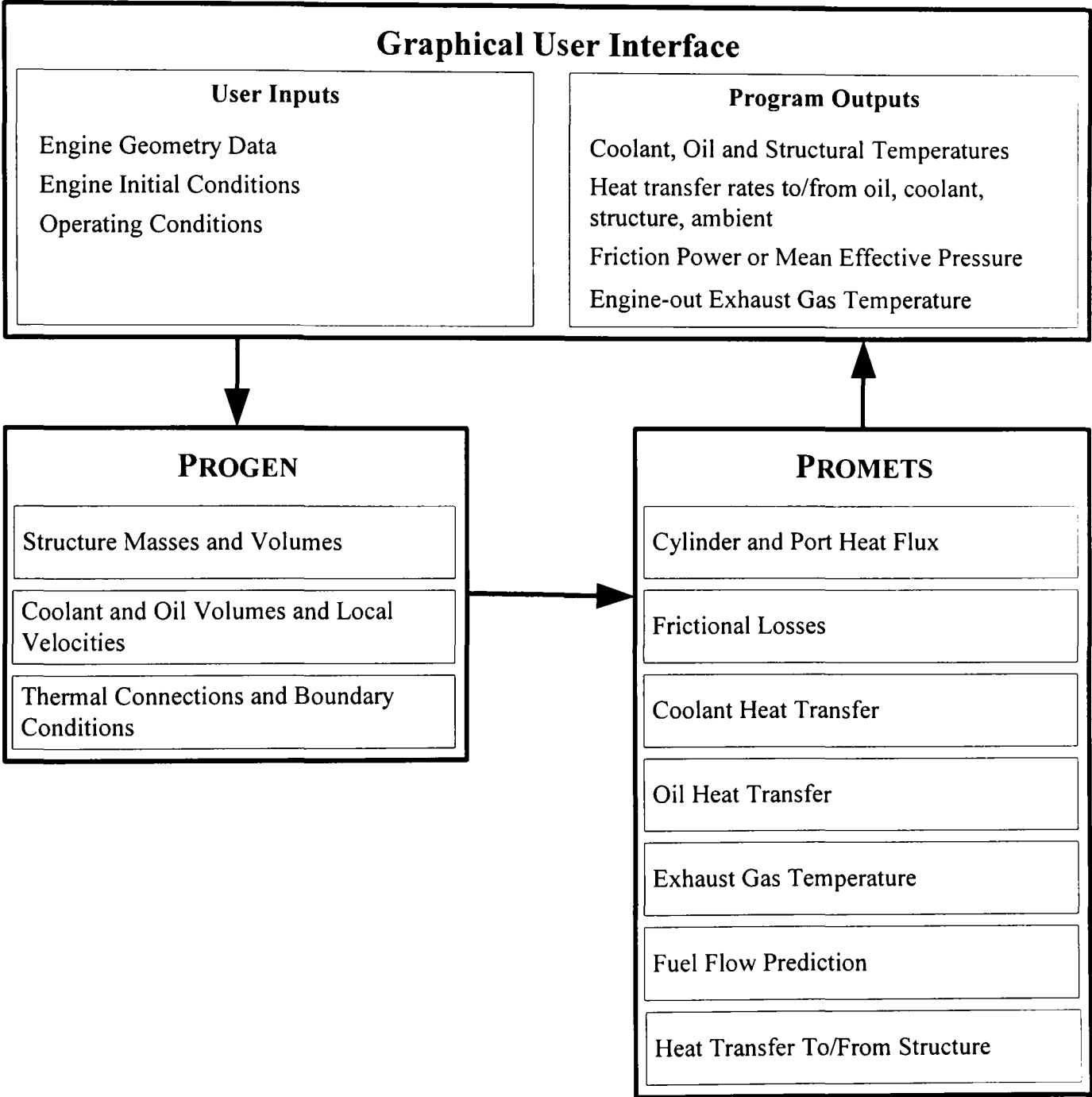


Figure 1.3 Illustration of the components and structure of PROMETS.

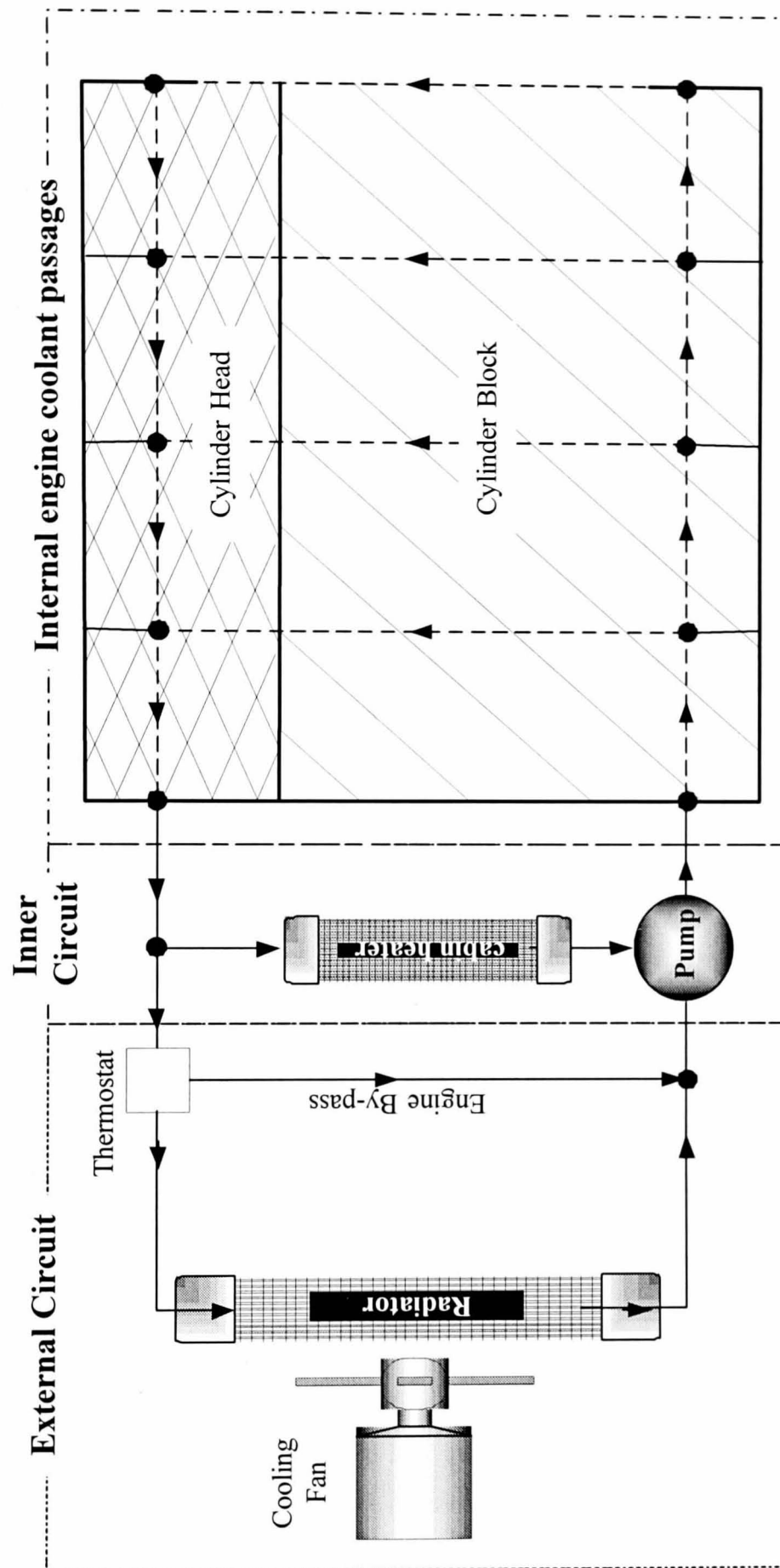


Figure 1.4 Illustration of a conventional engine cooling system: internal coolant passages, the inner circuit and the external circuit.

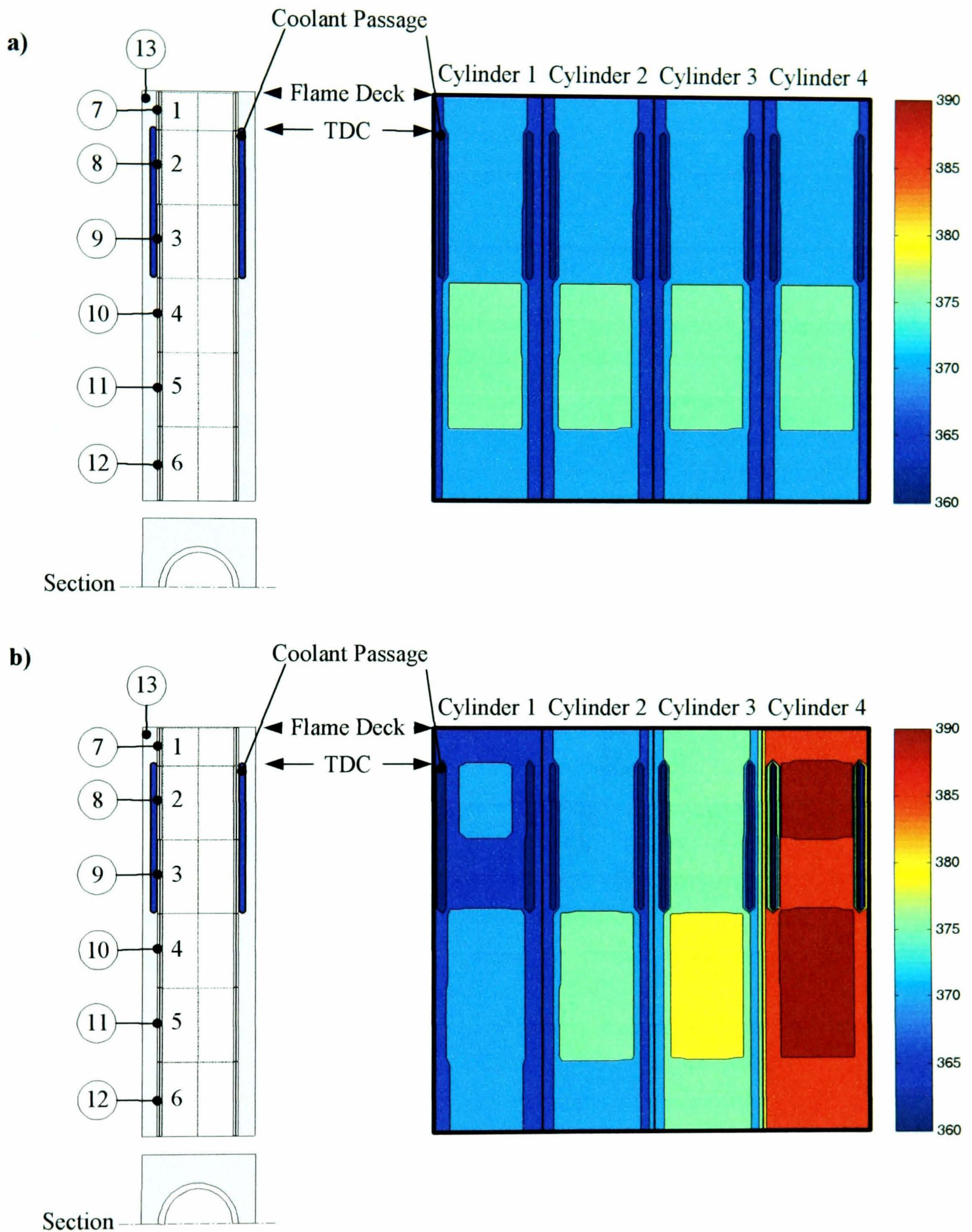


Figure 1.5 Illustration of the difference in predicted structural temperatures in K when using **a)** the single cylinder model and **b)** the multi-cylinder model for the 1.6l Sigma at 1500 rpm and 50 Nm after 1600 seconds. Initial and ambient temperatures were -18°C . Numbers on the left hand portions of the diagrams show element numbers (see Figure 3.9).

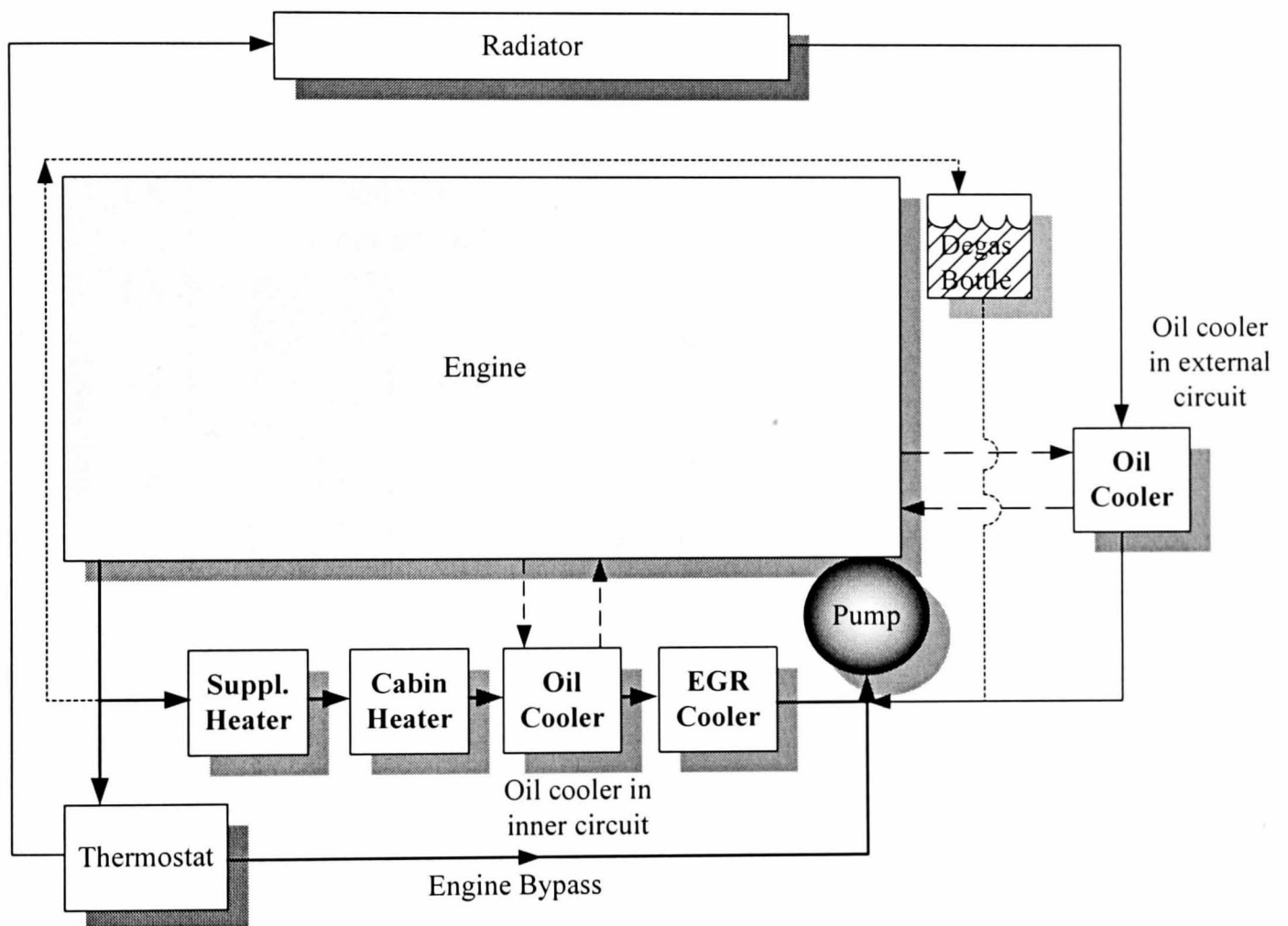


Figure 1.6 Typical inner circuit layout, illustrating the position of the auxiliary components for all versions of PROMETS. The supplementary heater (suppl. heater), cabin heater and oil cooler (in inner circuit) are in the fixed order modelled in the gasoline versions of PROMETS. The typical position of the EGR cooler (modelled in PROMETSD) is also shown.

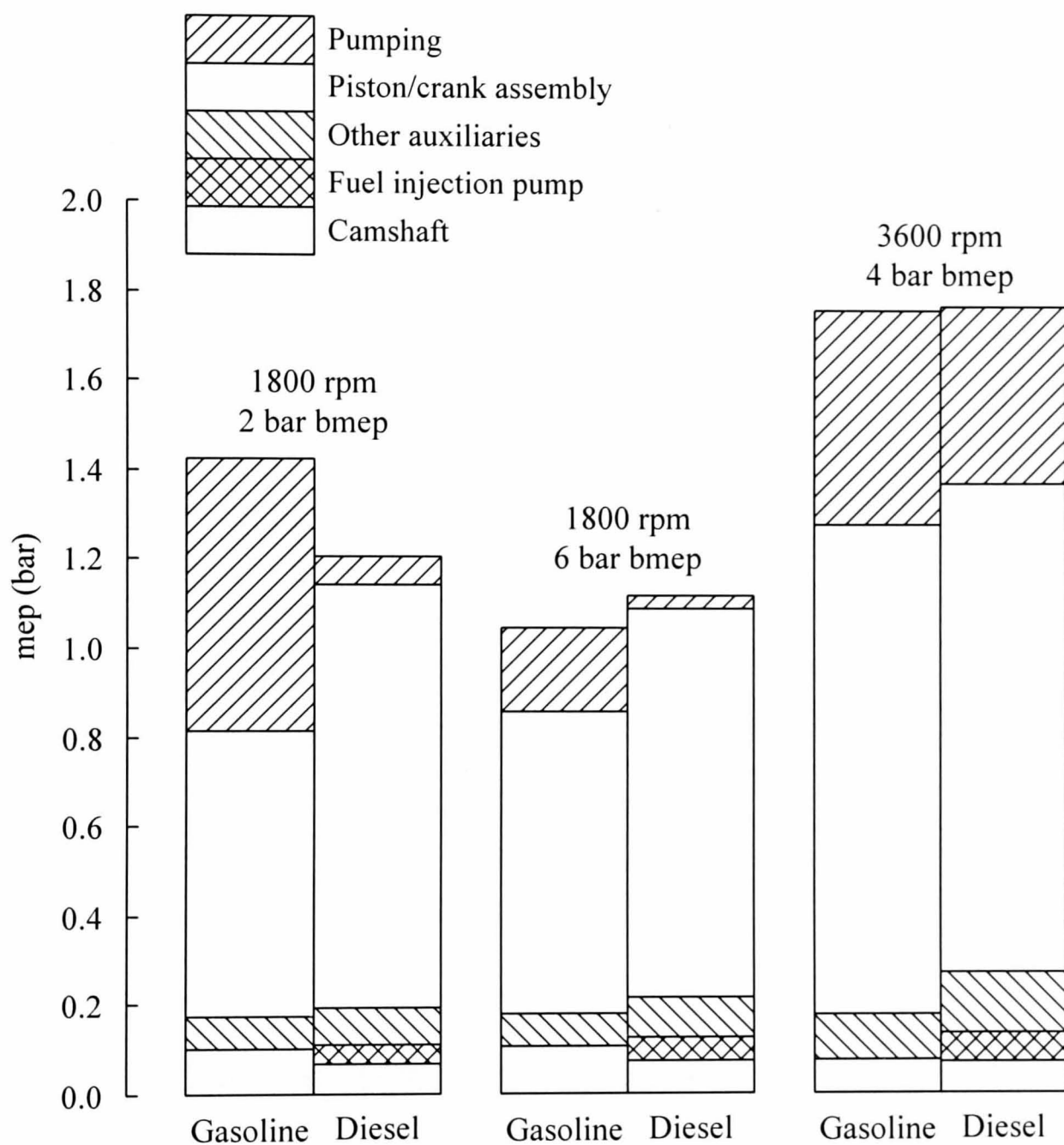


Figure 2.1 Comparison of pumping and mechanical friction losses for 1.6l spark ignition and compression ignition engines [2.8].

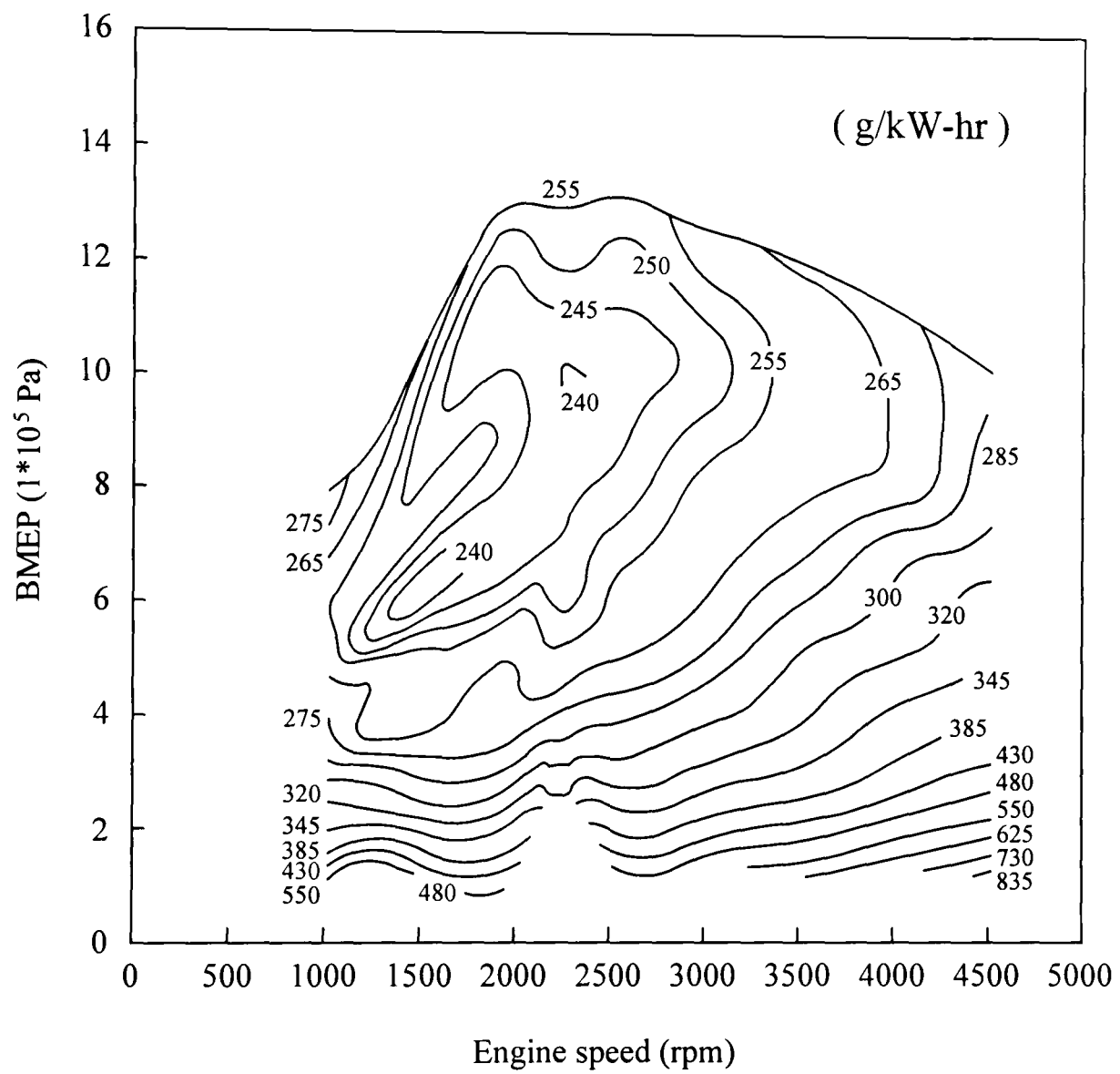


Figure 2.2 Fuel consumption map for a 1.8 IDI engine. The contours show lines of equal fuel consumption in g/kW hr.

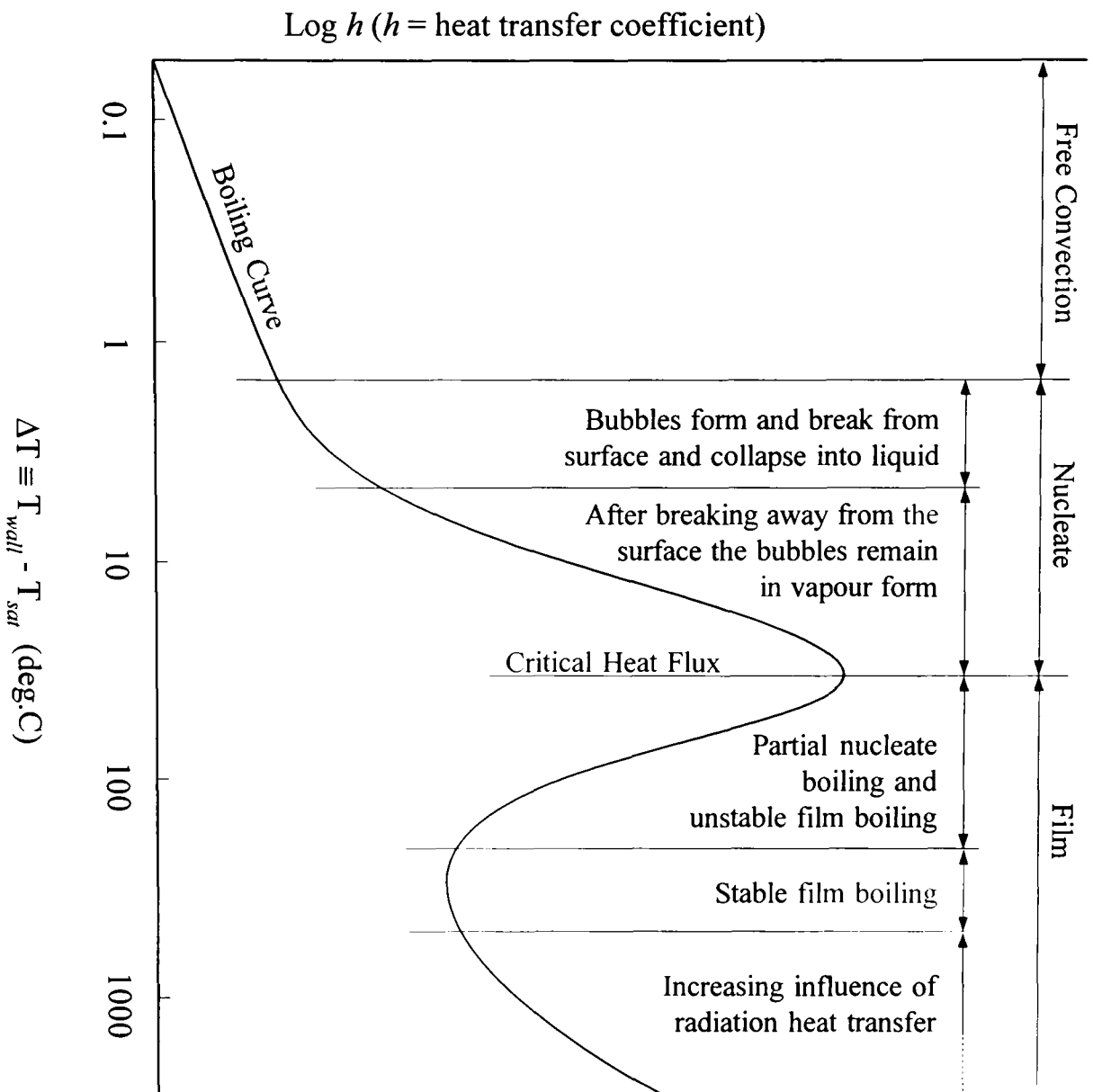
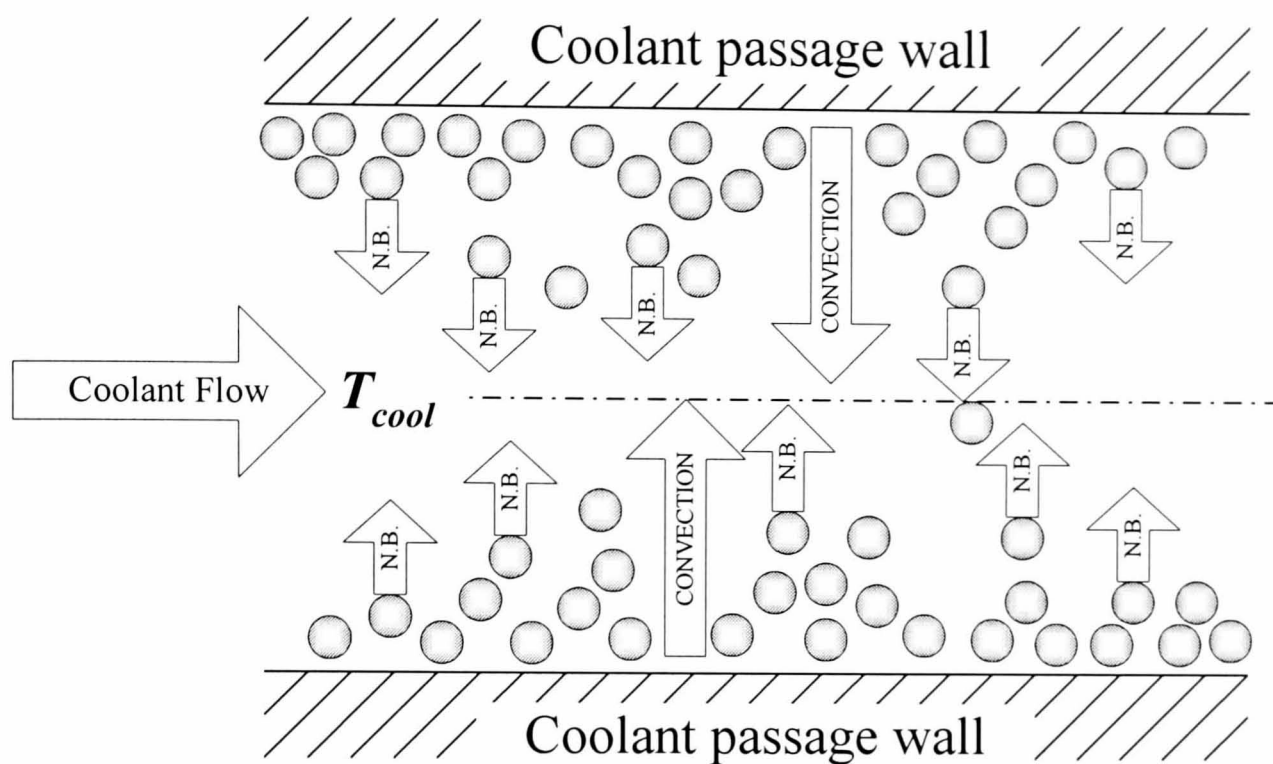


Figure 2.3 Principle boiling regimes in pool boiling of water at atmospheric pressure and saturation temperature T_{sat} [2.58].

a)



b)

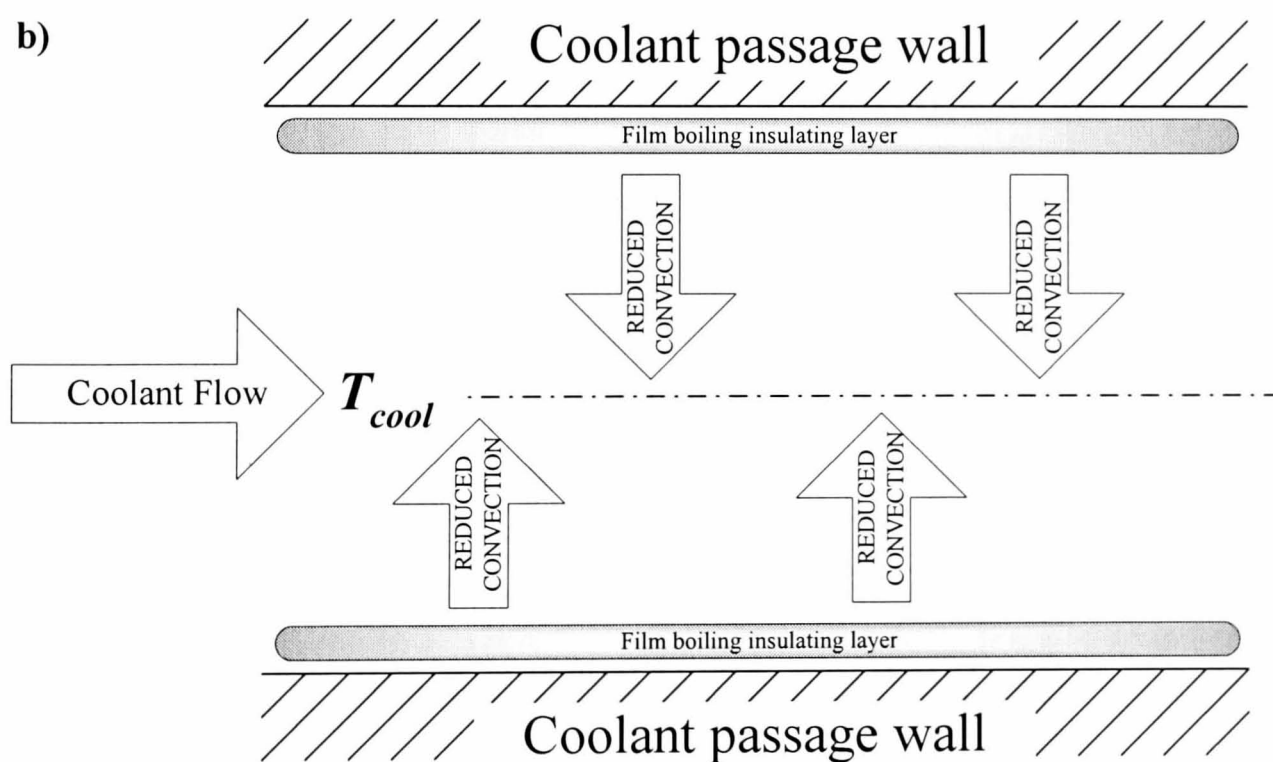


Figure 2.4 Illustrations of a) nucleate boiling (N.B.) and b) film boiling due to convective heat transfer from the coolant passage walls to the engine coolant.

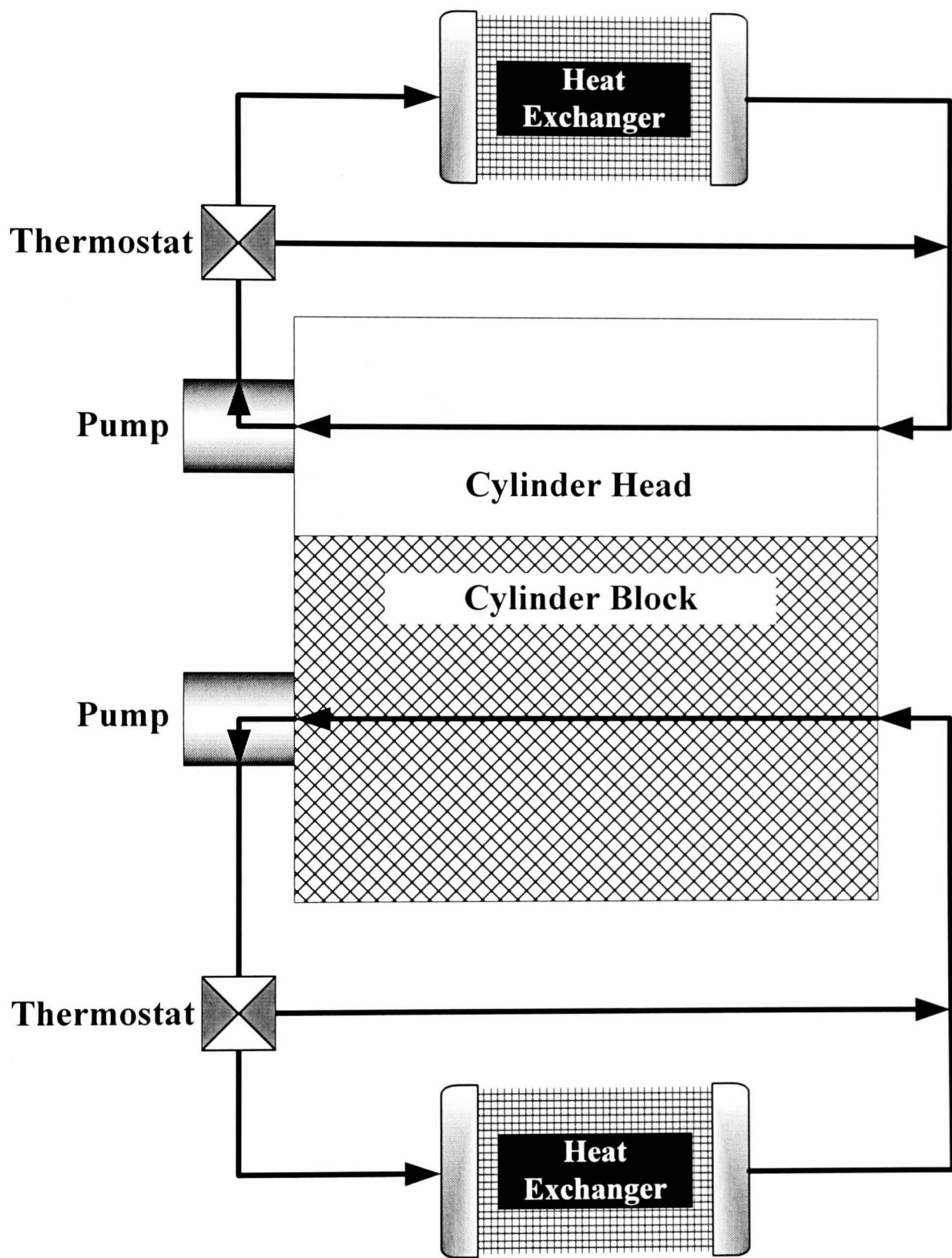
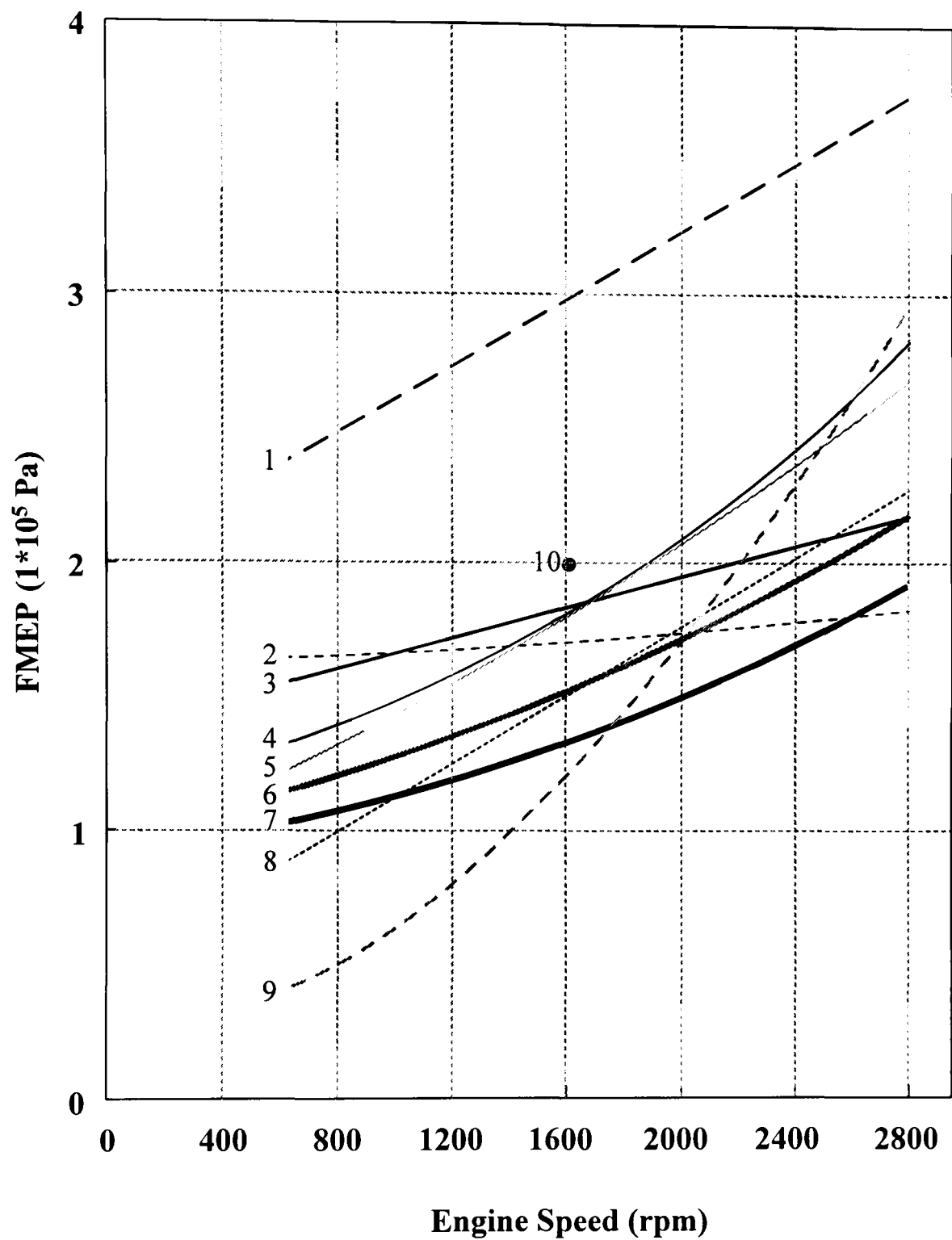
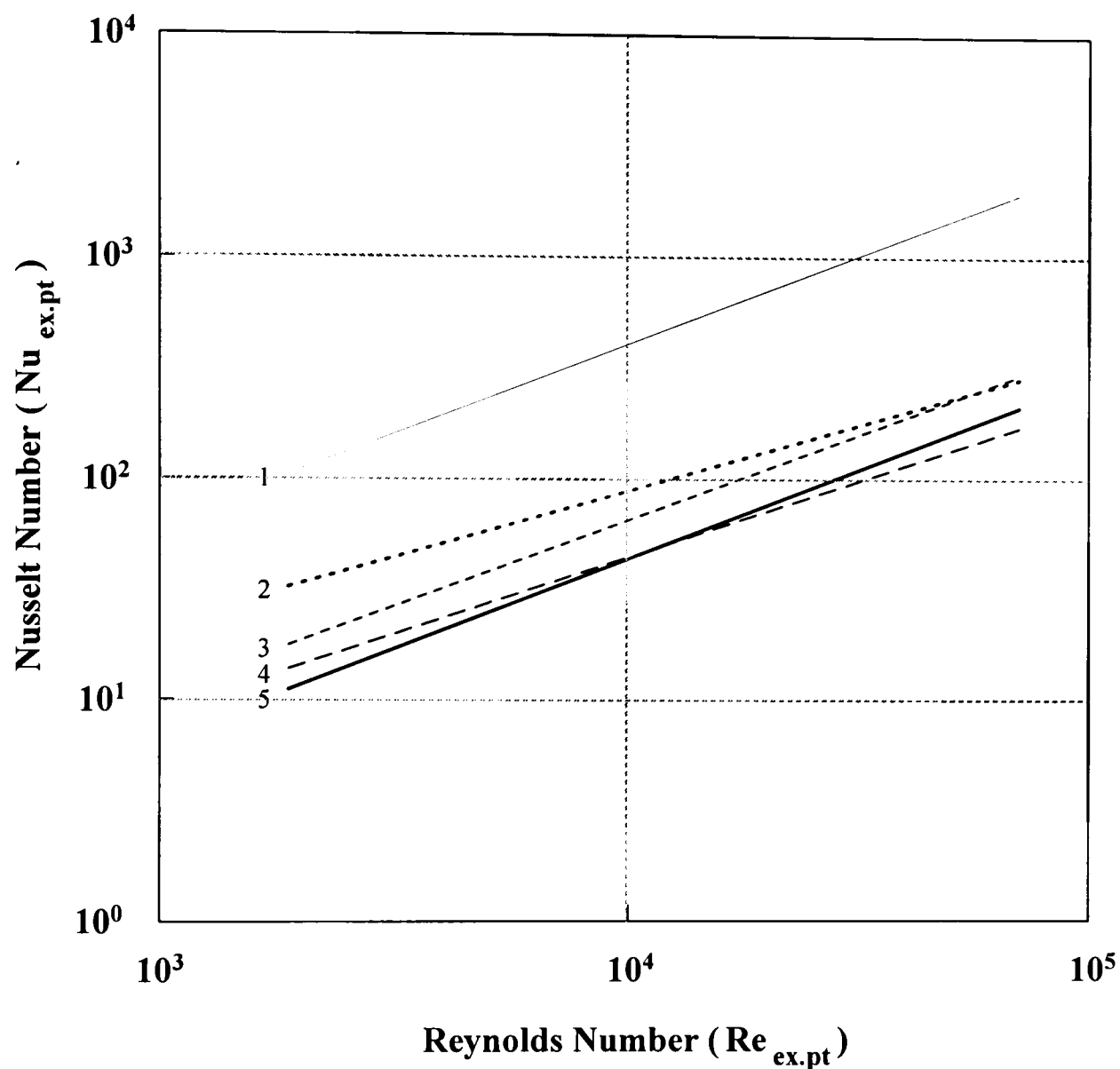


Figure 2.5 Illustration of a dual cooling circuit: coolant flow through the block and head is controlled separately.



1. McAulay	[2.120]	6. Bishop	[2.19]
2. Fujii	[2.121]	7. Patton	[2.7]
3. Winterbone	[2.5]	8. Chen	[2.122]
4. Yagi	[2.18]	9. Thiele	[2.17]
5. Millington	[2.16]	10. Gish	[2.123]

Figure 2.6 Trends of engine losses predicted using formulations derived by a number of researchers. The figure offers an indication of the trends only since the formulae were derived for different engines and conditions [2.20].



- | | |
|----------------------------------|--------|
| 1. Hires and Pochmara | [2.46] |
| 2. Caton and Heywood | [2.53] |
| 3. Malchow, Sorenson and Buckius | [2.47] |
| 4. Meisner and Sorenson | [2.48] |
| 5. Dittus and Boelter | [2.49] |

Figure 2.7 Comparison of the values predicted by five published correlations. The relationships developed by Hires and Pochmara [2.46] and Caton and Heywood [2.53] were developed for the curved part of the exhaust port near to the valve.

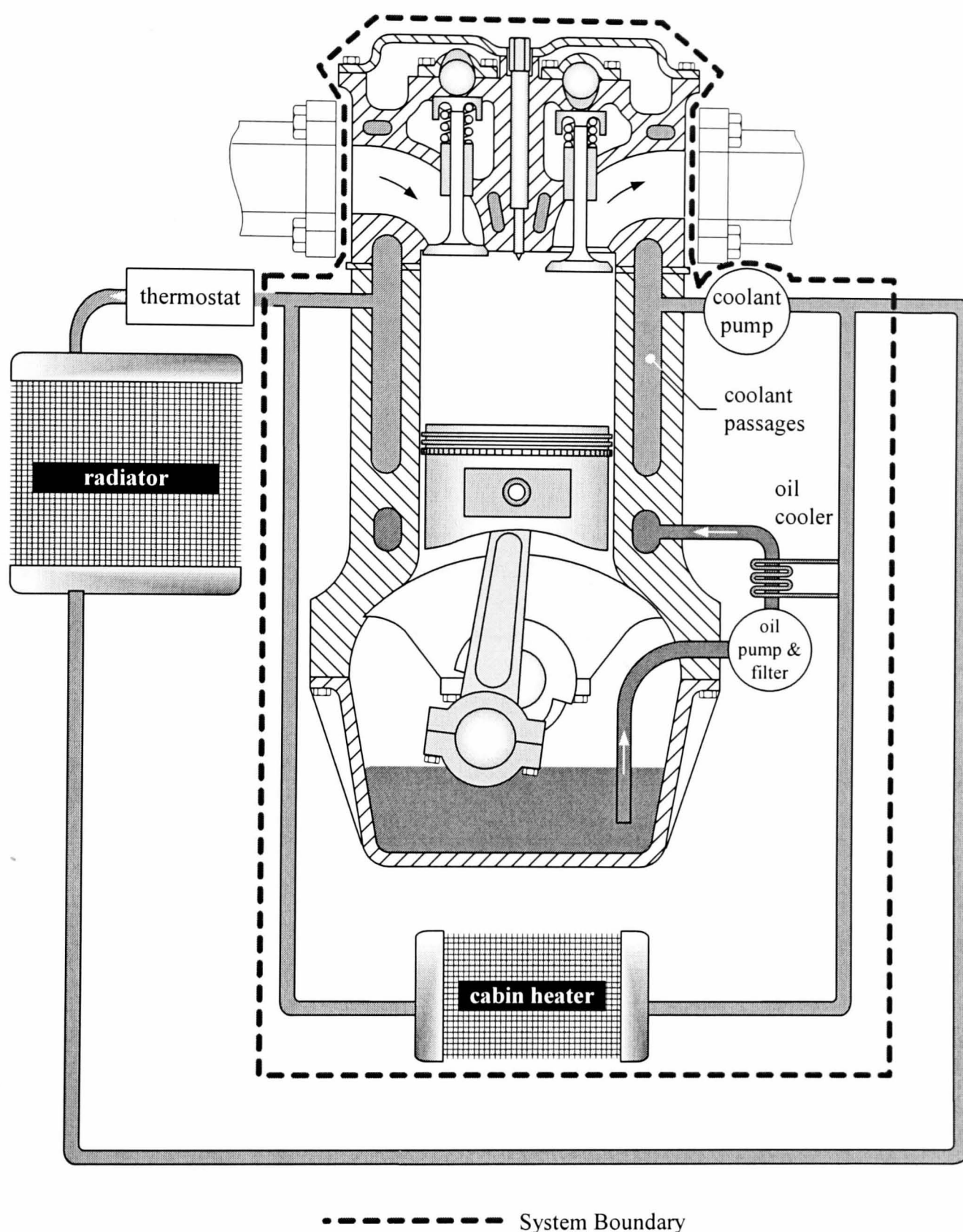


Figure 3.1 The boundaries of the system modelled in PROMETS. The alternator, power steering pump, air conditioning pump, starter motor and fly wheel are not included. It should be noted that the external circuit (radiator, thermostat and pipework) is implicitly, but not explicitly, modelled.

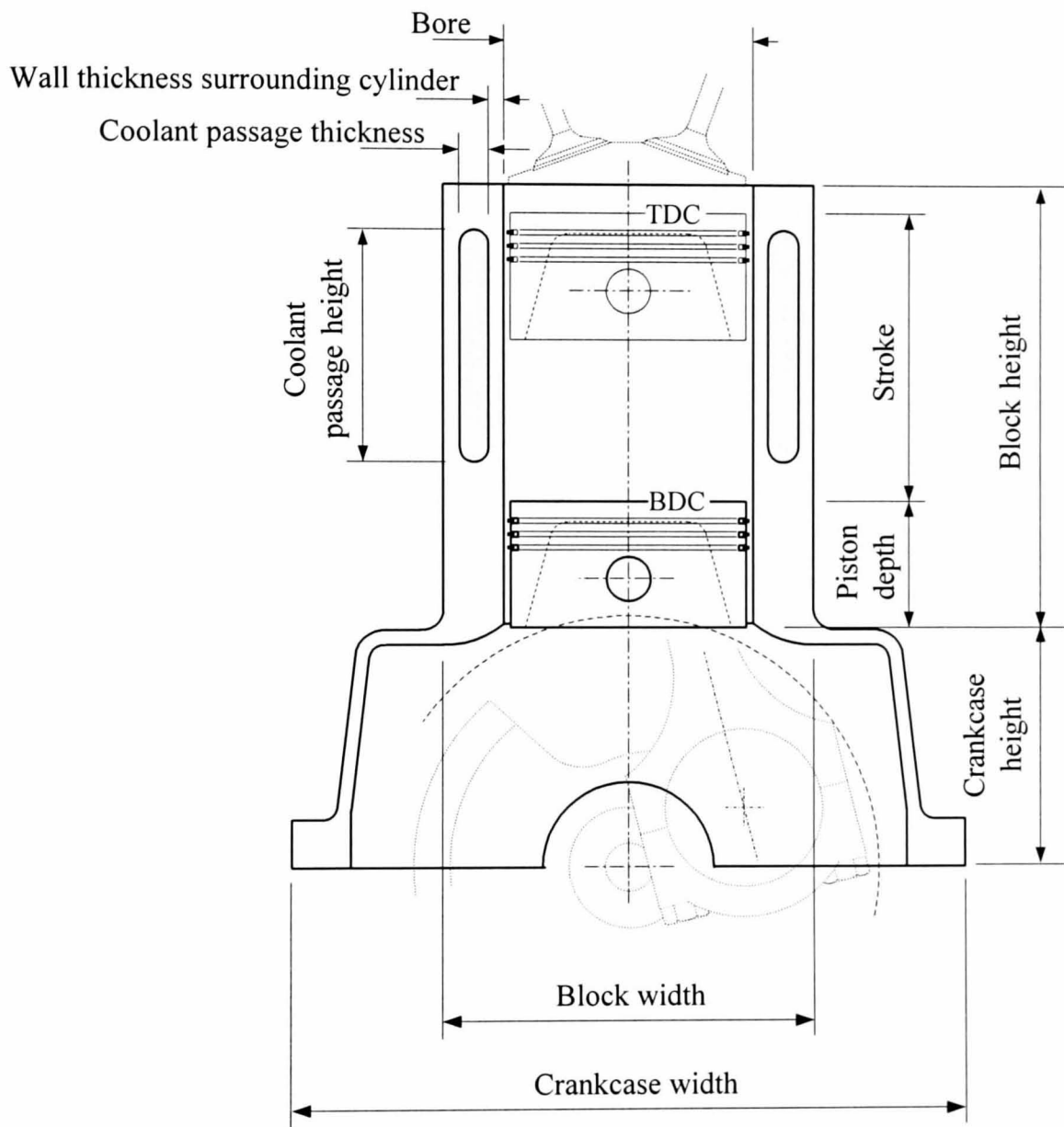


Figure 3.2 Section view through the block, showing some of the key dimensions in determining the block shape and size.

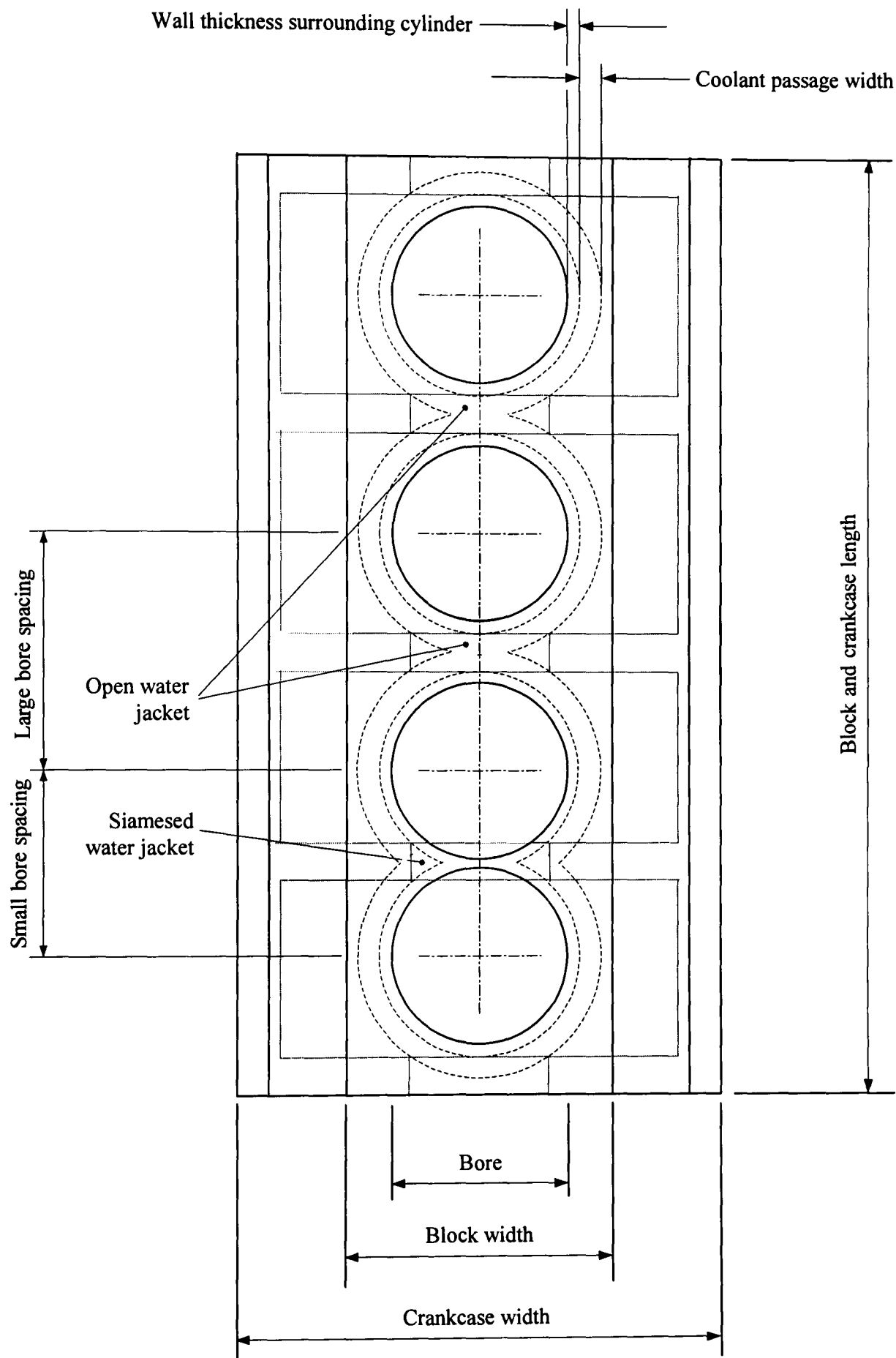


Figure 3.3 Plan view of the block, showing some of the key dimensions in determining the shape and size of the block. Both siamesed and open water jackets are shown, although only one configuration is used in any one engine.

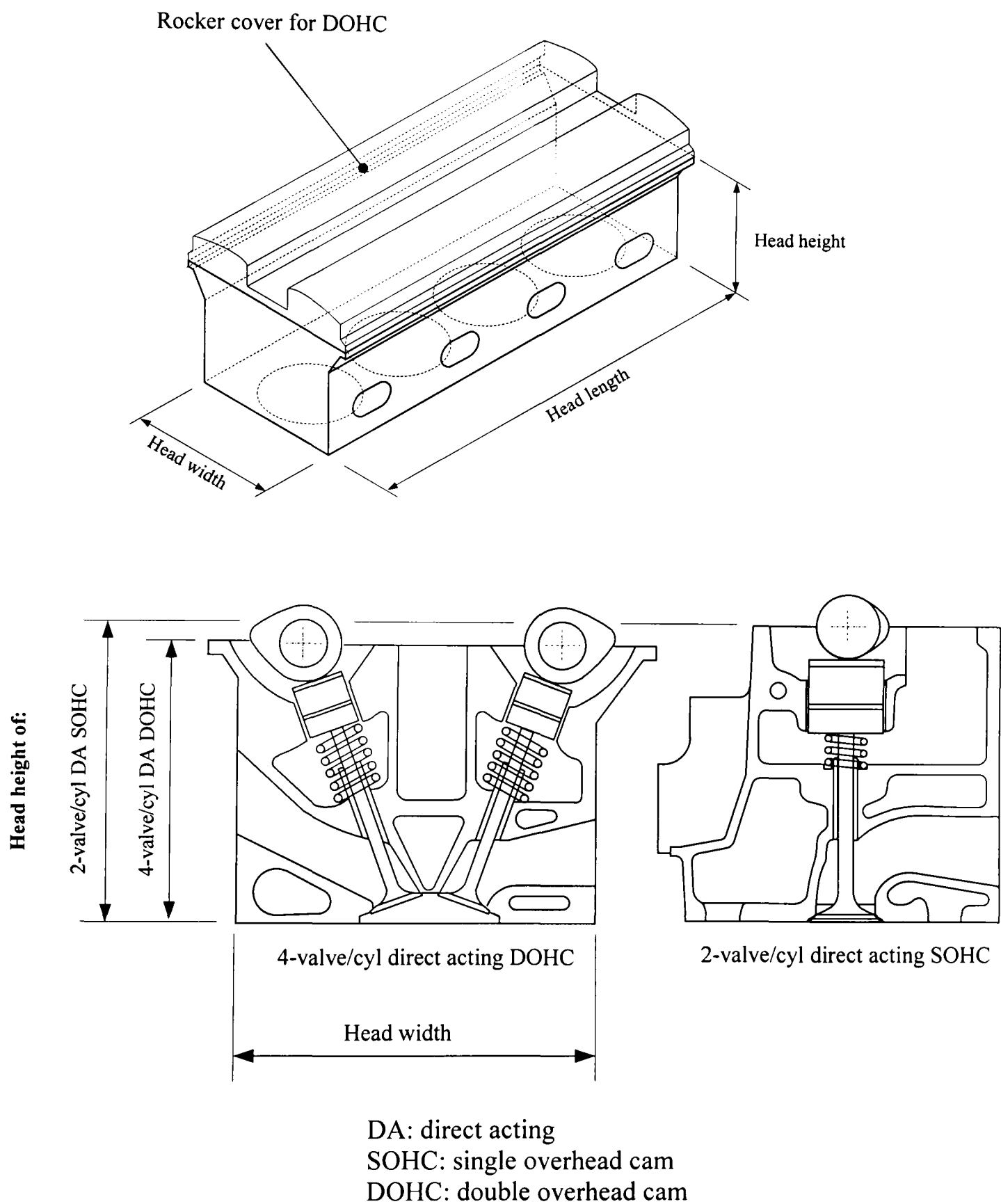


Figure 3.4 Section views through heads with two different valve train configurations. The left hand figure is based on a design used in diesel engines and illustrates a cross-flow head; the right hand figure is based on a spark ignition engine design and illustrates a U-flow head. The swept volume per cylinder is similar for both engines.

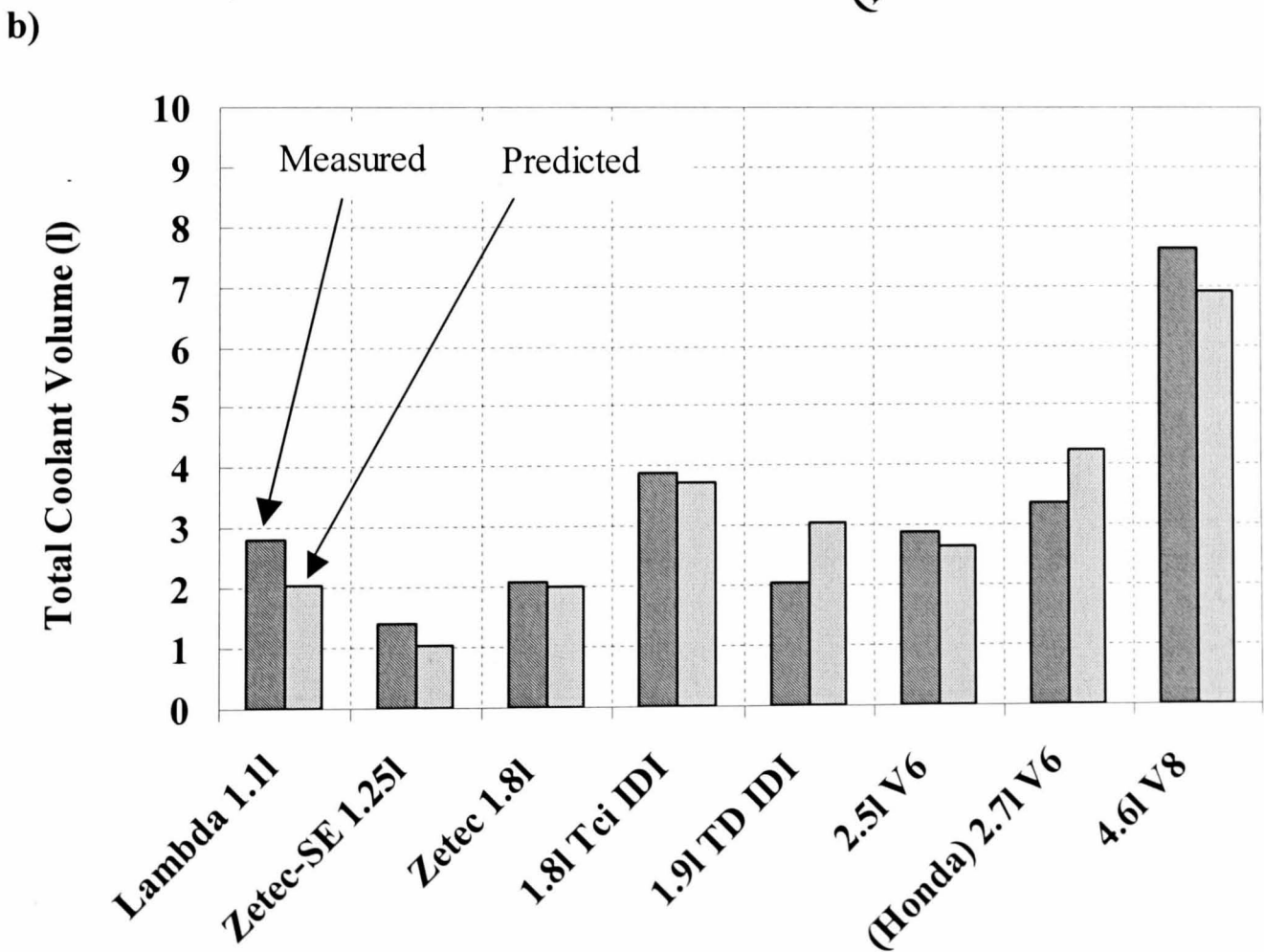
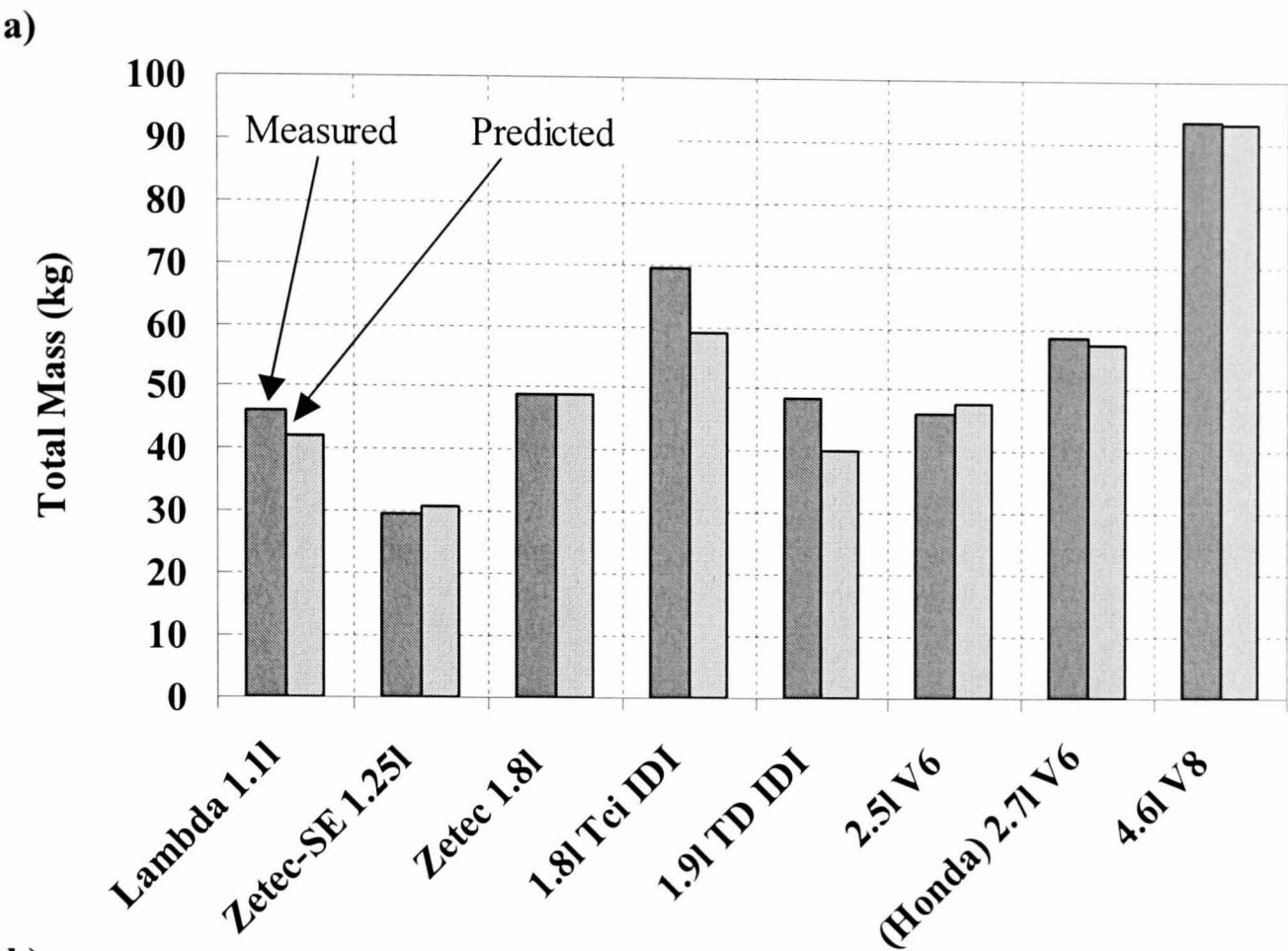


Figure 3.5 Illustration of the level of agreement between measured and predicted
a) engine masses b) coolant volumes [3.1].

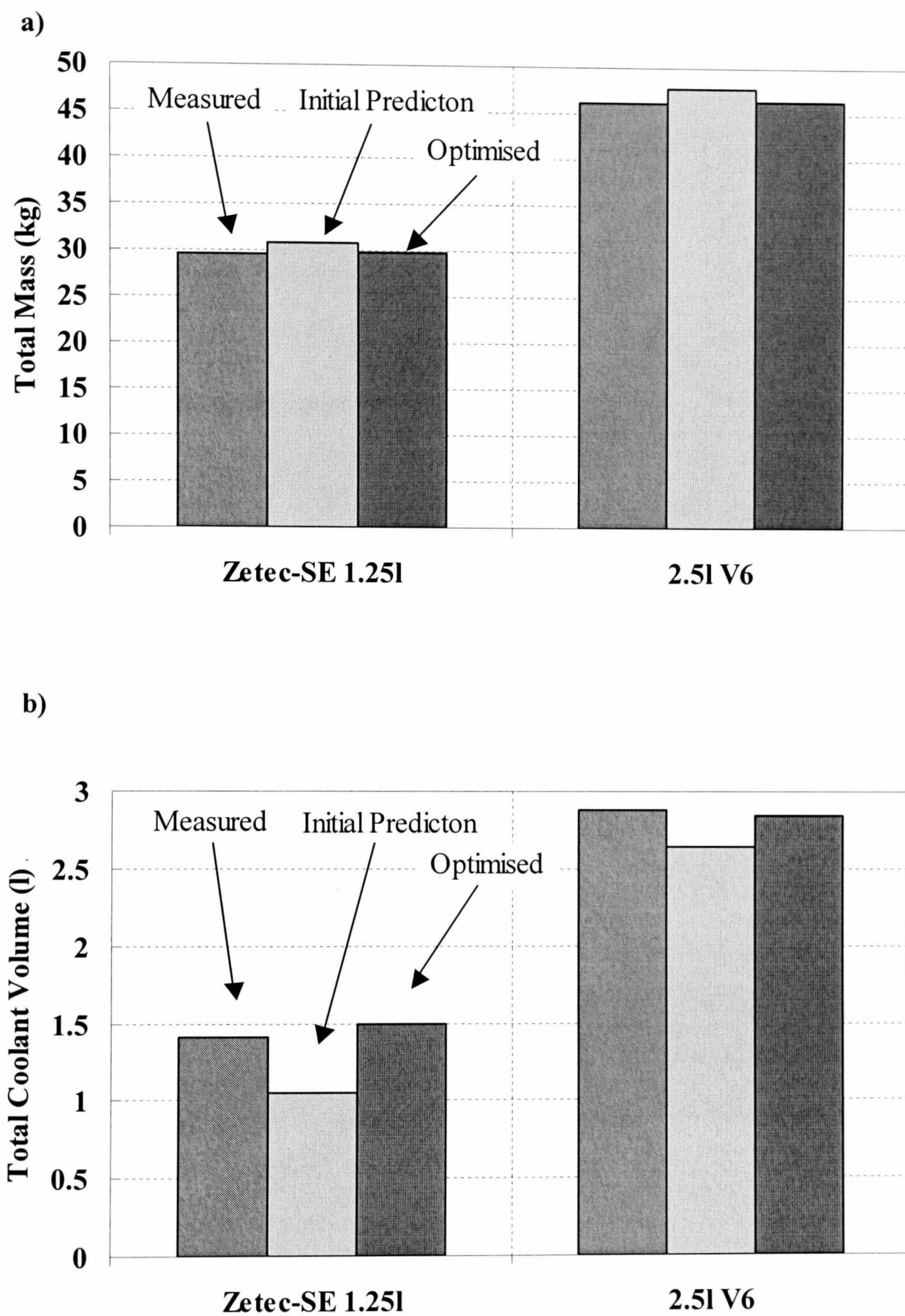


Figure 3.6 Examples of optimised predictions of a) structural masses and b) coolant volumes for the 1.25l Sigma engine and the 2.5l V6 engine.

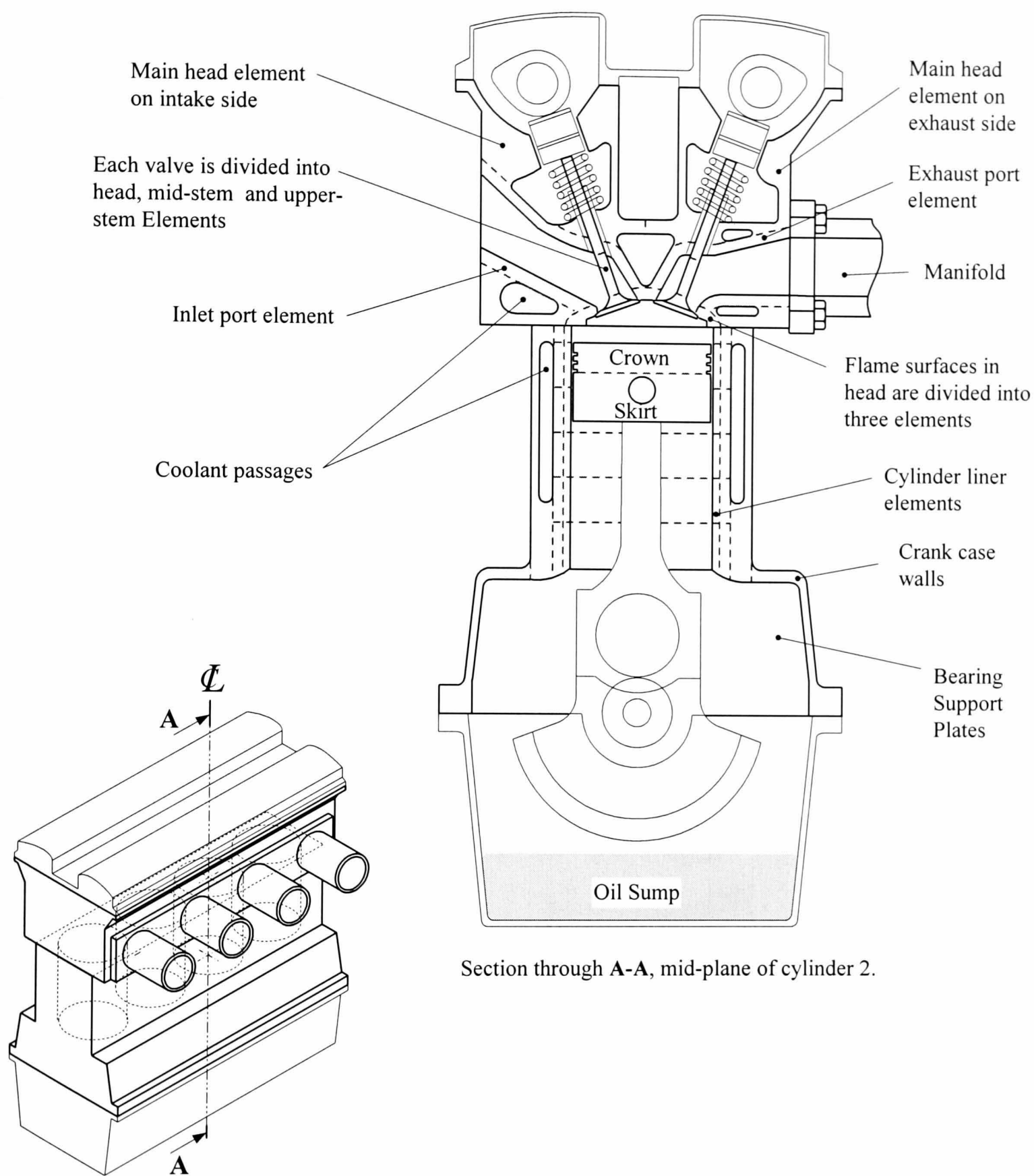
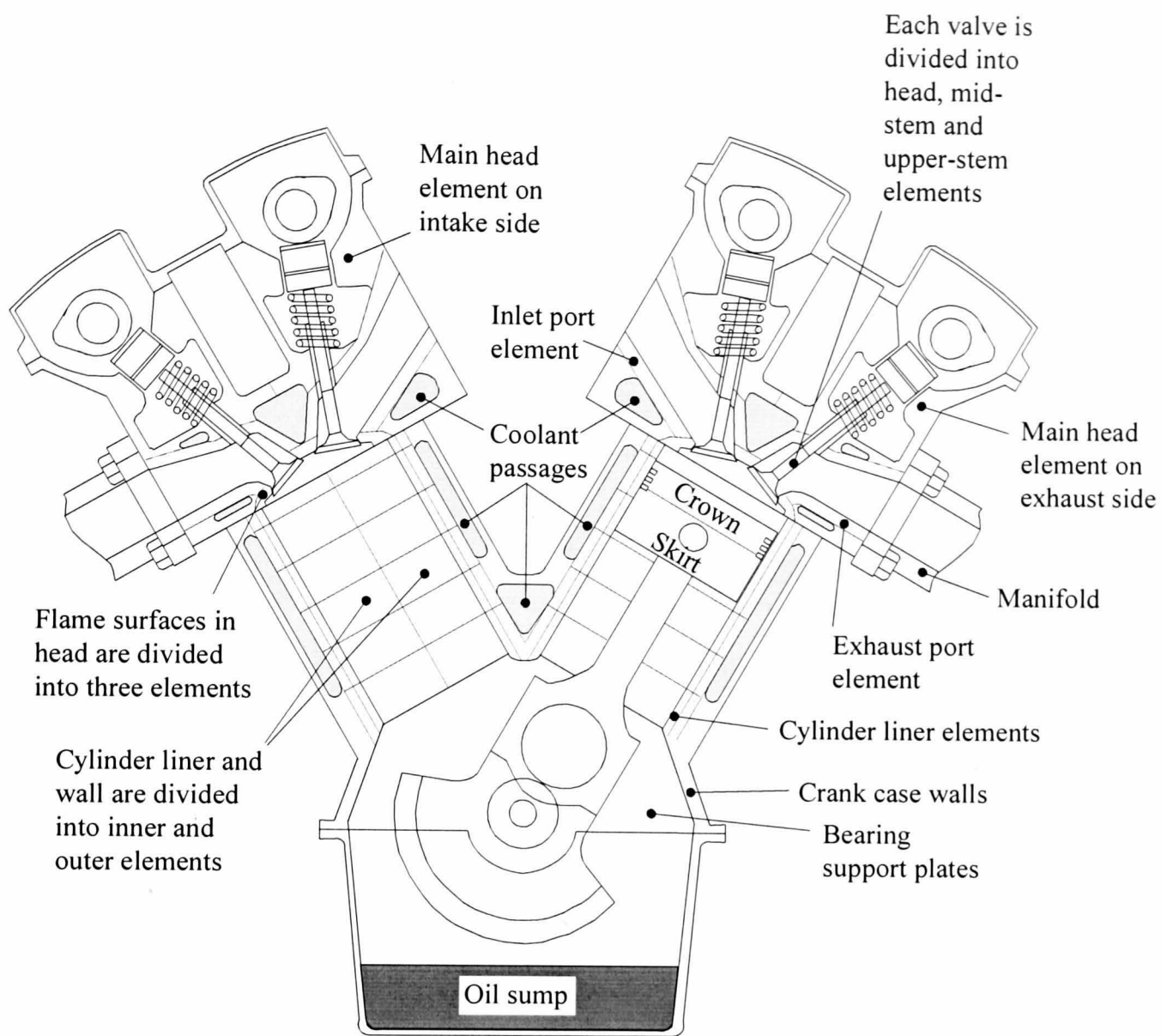


Figure 3.7 Illustration of the location of the main elements used by PROMETS to represent an in-line engine.



Section through A-A, mid-plane of cylinder 2.

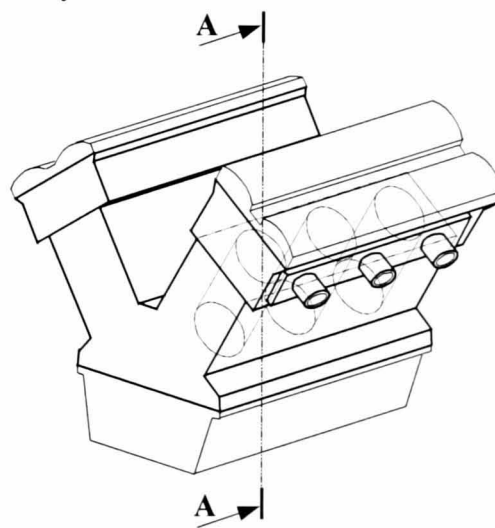


Figure 3.8 Illustration of the location of the main elements used by PROMETS to represent an V-type engine.

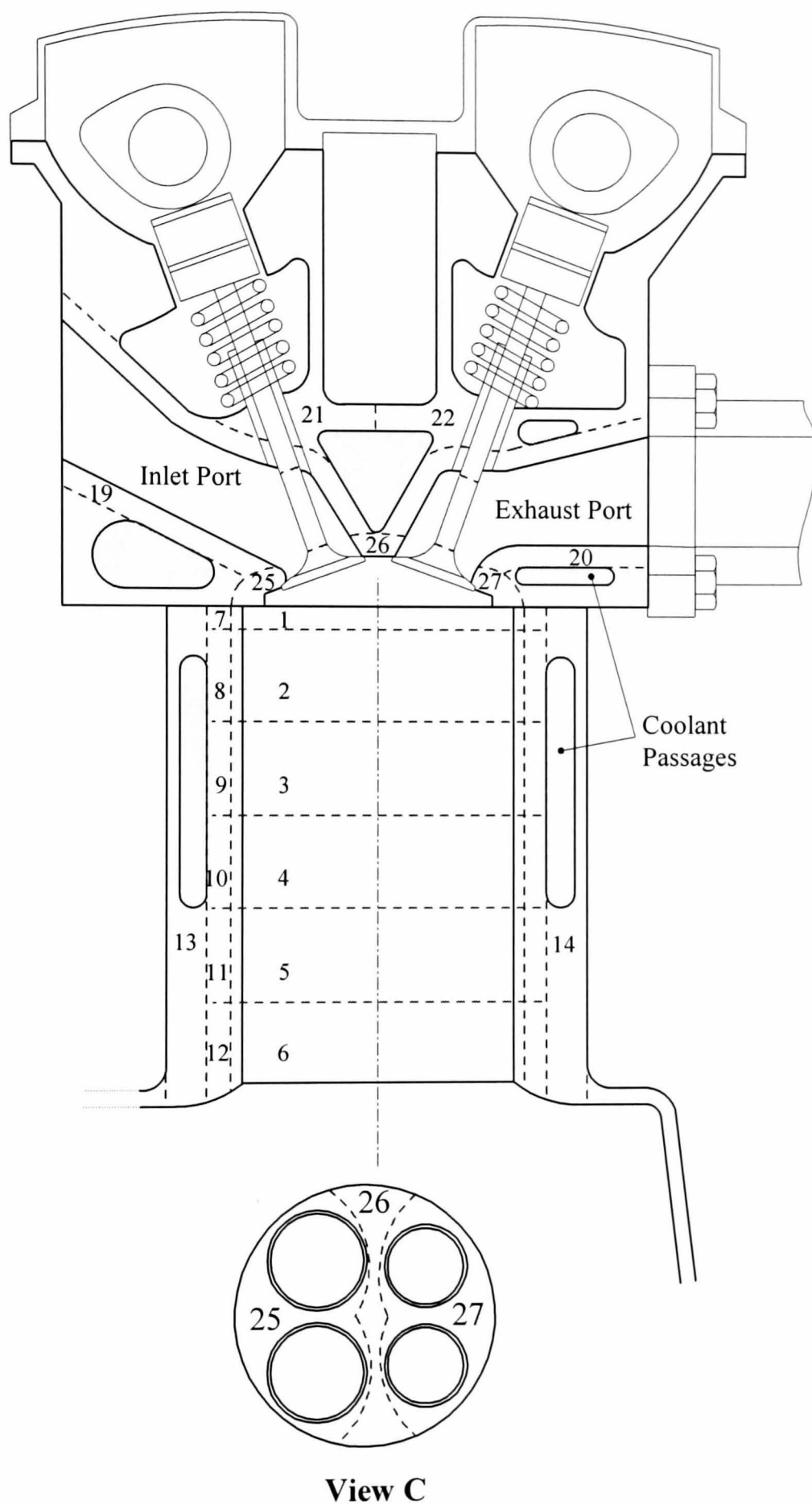
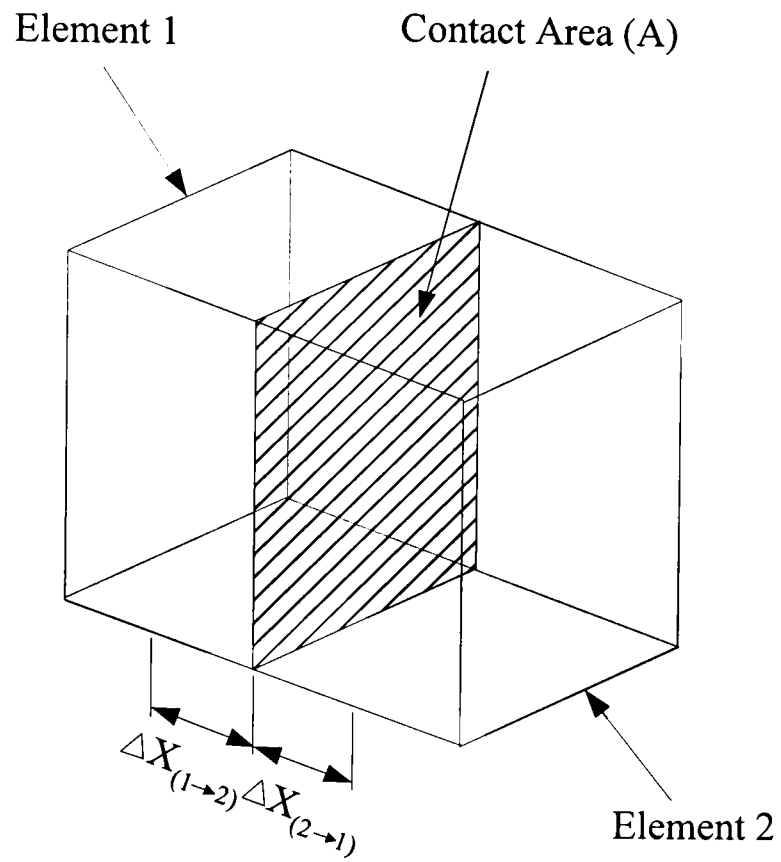


Figure 3.9 Cross section through the modelled cylinder head and block of an in-line engine, showing the position of structural elements.



Heat transfer from element 1 to element 2:

$$\dot{Q}_{12} = A_{12} \frac{(T_1 - T_2)}{\frac{\Delta X_{1 \rightarrow 2}}{k_1} + \frac{\Delta X_{2 \rightarrow 1}}{k_2}}$$

Where $\Delta X_{1 \rightarrow 2}$ = distance from contact area to centroid of element 1.

$\Delta X_{2 \rightarrow 1}$ = distance from contact area to centroid of element 2.

Figure 3.10 Definition of the heat conduction path length for a pair of thermally coupled elements.

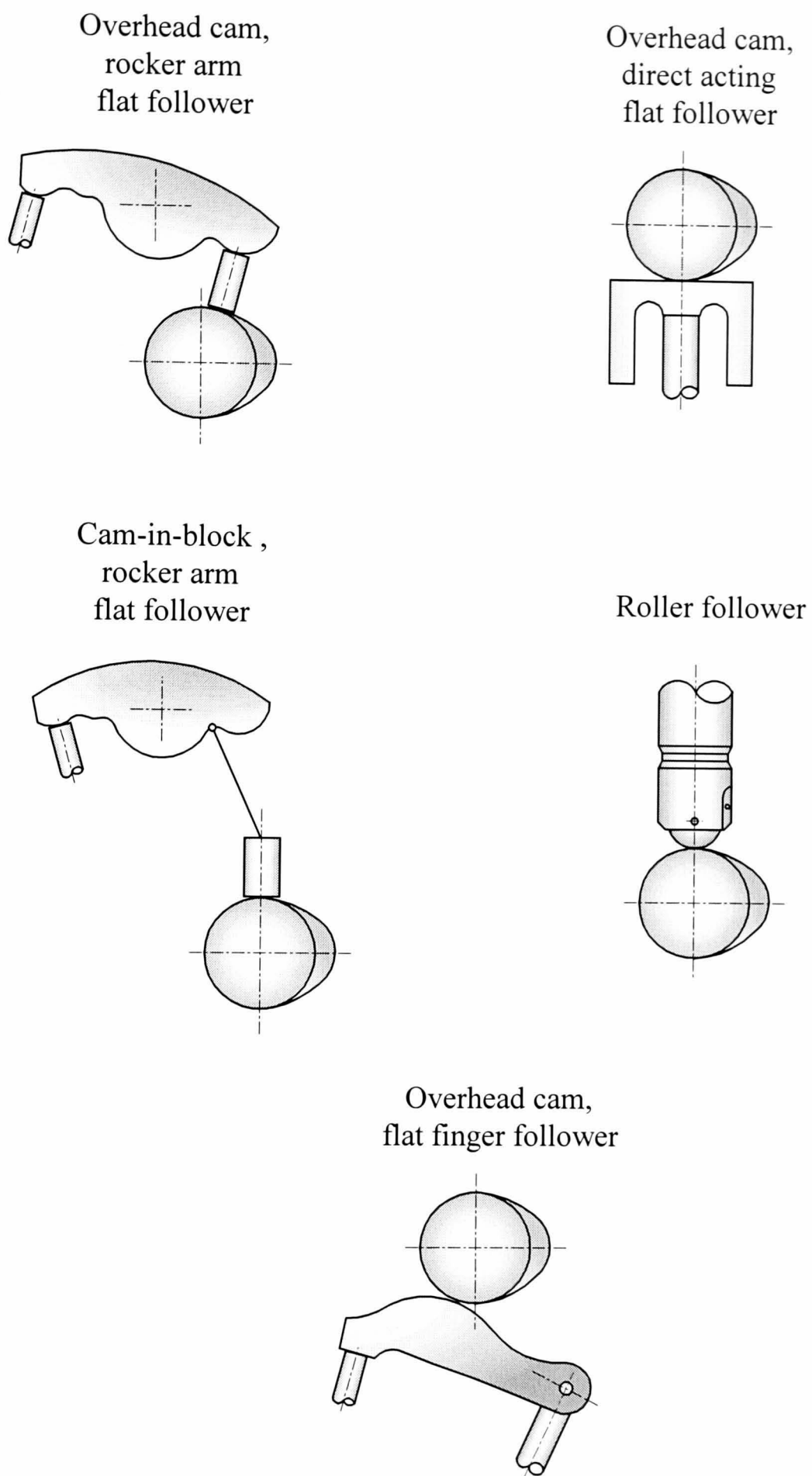


Figure 3.11 Available valve train configurations modelled by Patton, Nitschke and Heywood [3.8].

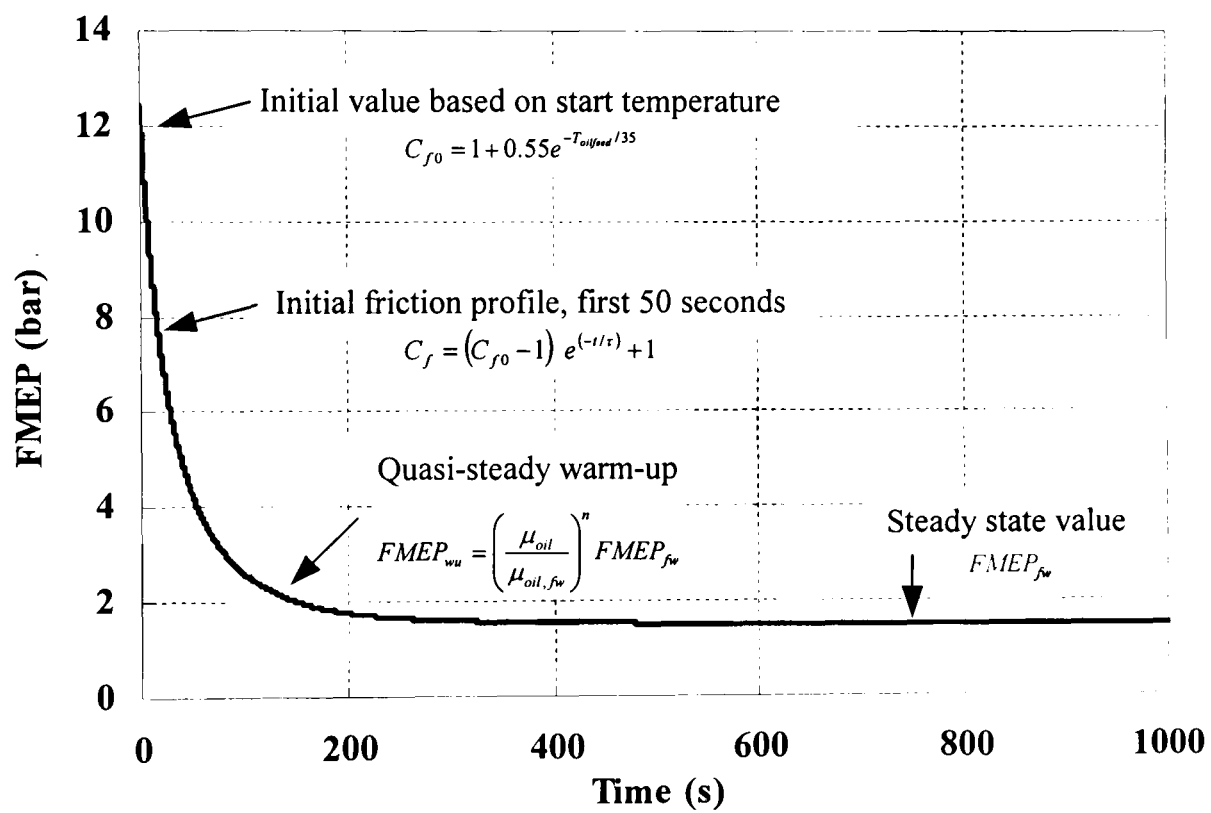


Figure 3.12 Illustration of friction prediction showing steady-state, quasi-steady warm-up and initial friction profile.

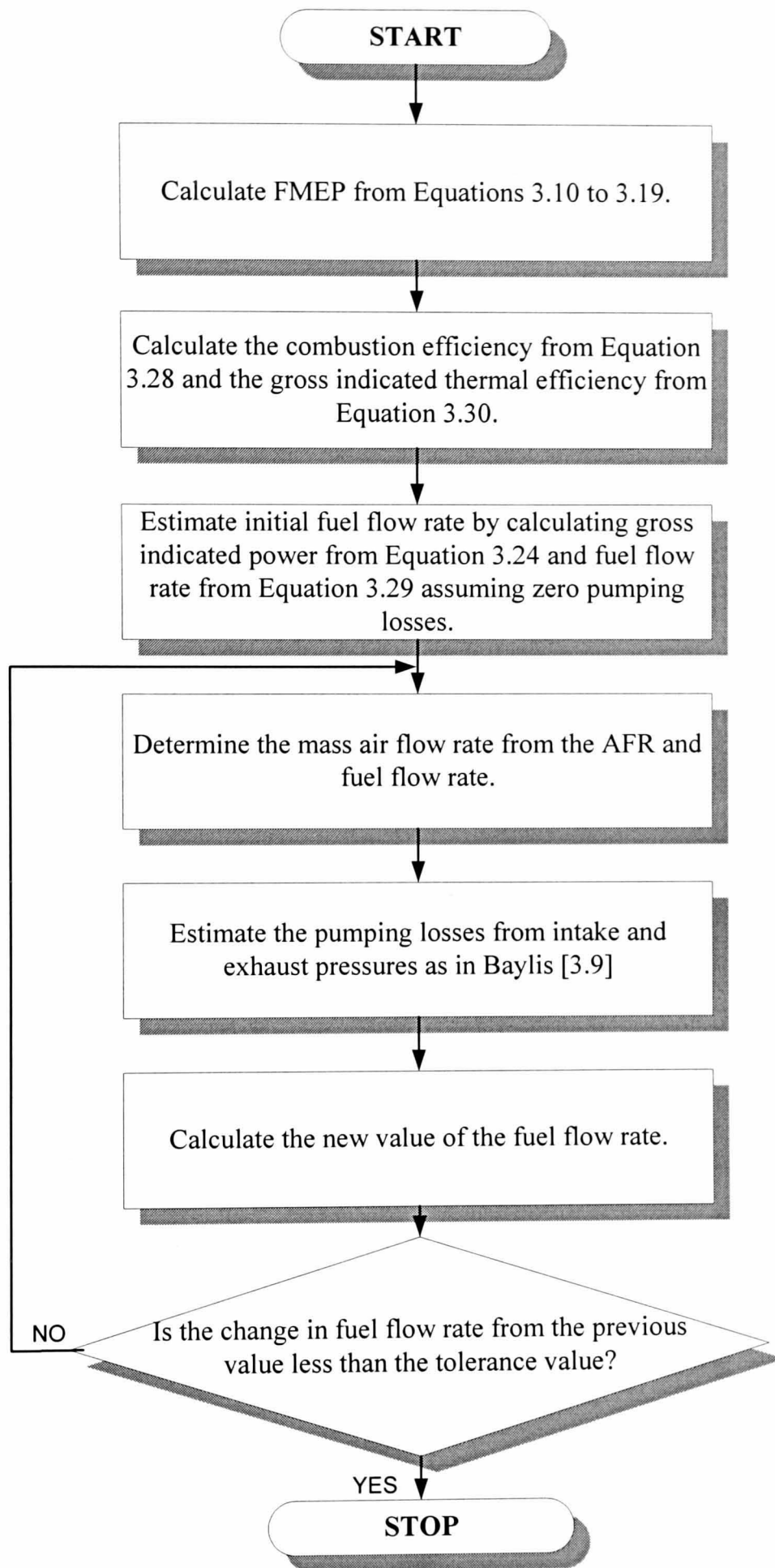


Figure 3.13 Flow diagram illustrating the algorithm for determining fuel flow rate for a gasoline engine [3.7].

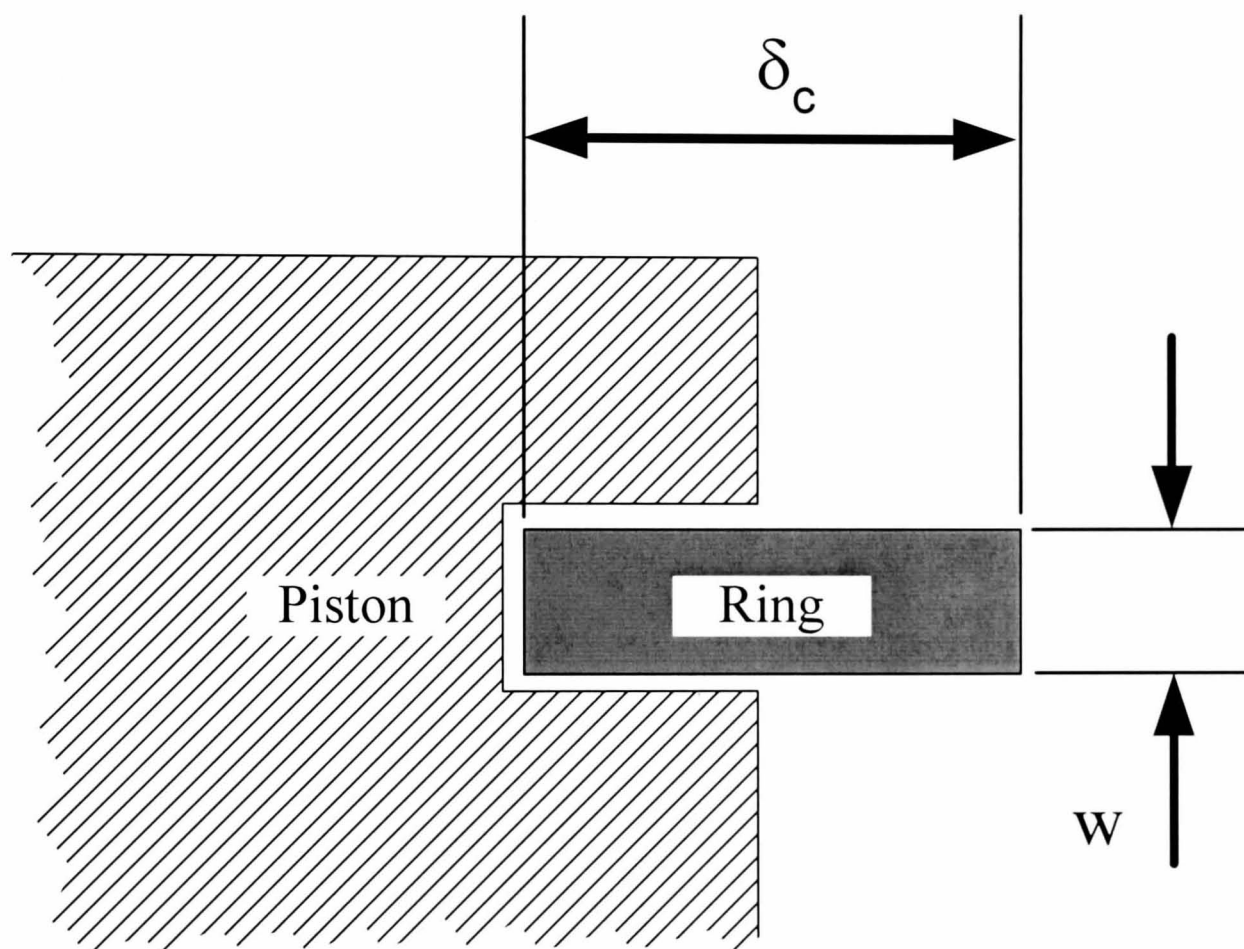


Figure 3.14 Piston ring dimensions, w and δ_c .

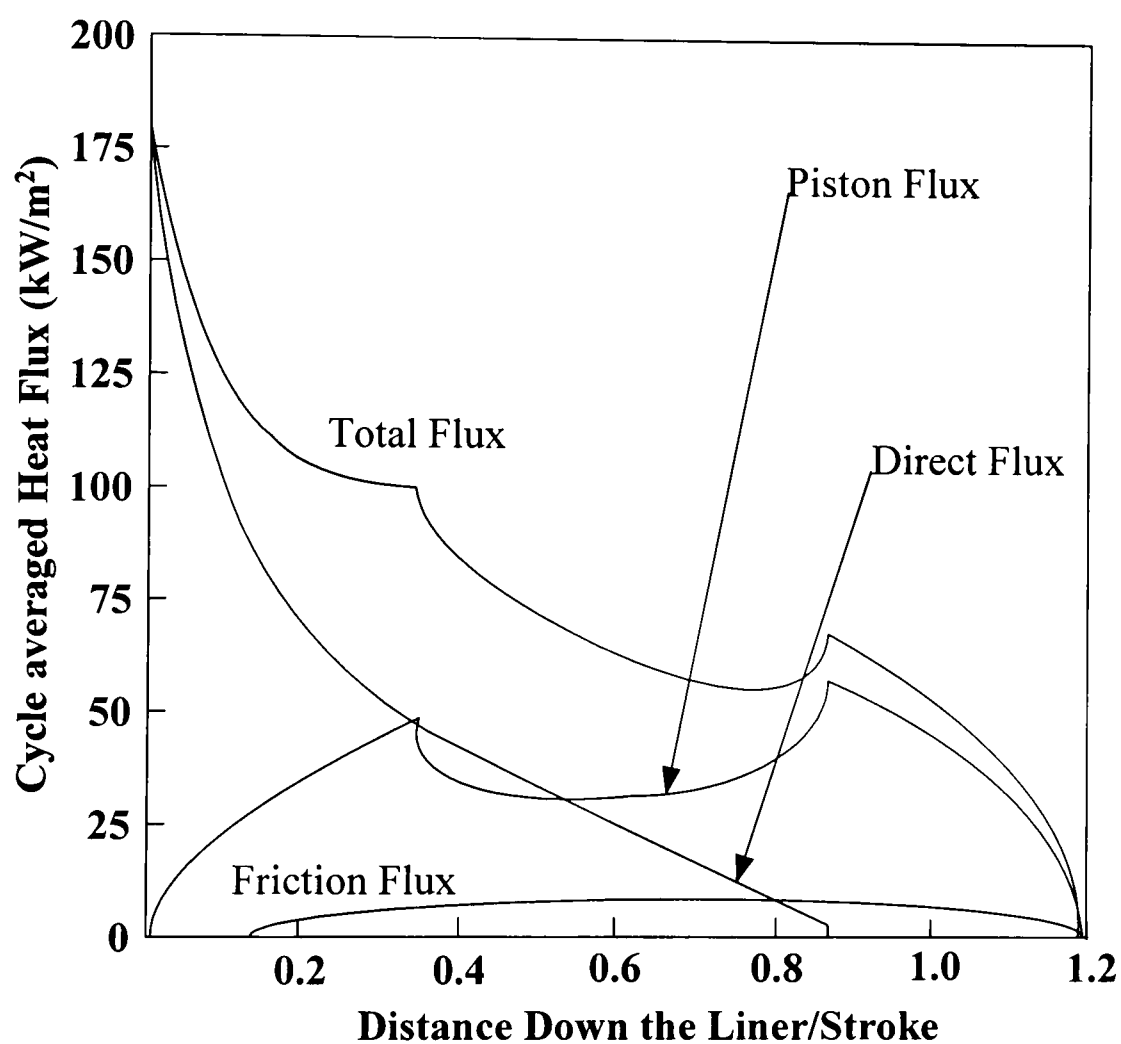


Figure 3.15 Typical heat flux distribution for the cylinder liner for a 1.6l CVH engine at 2500 rpm, 50Nm.

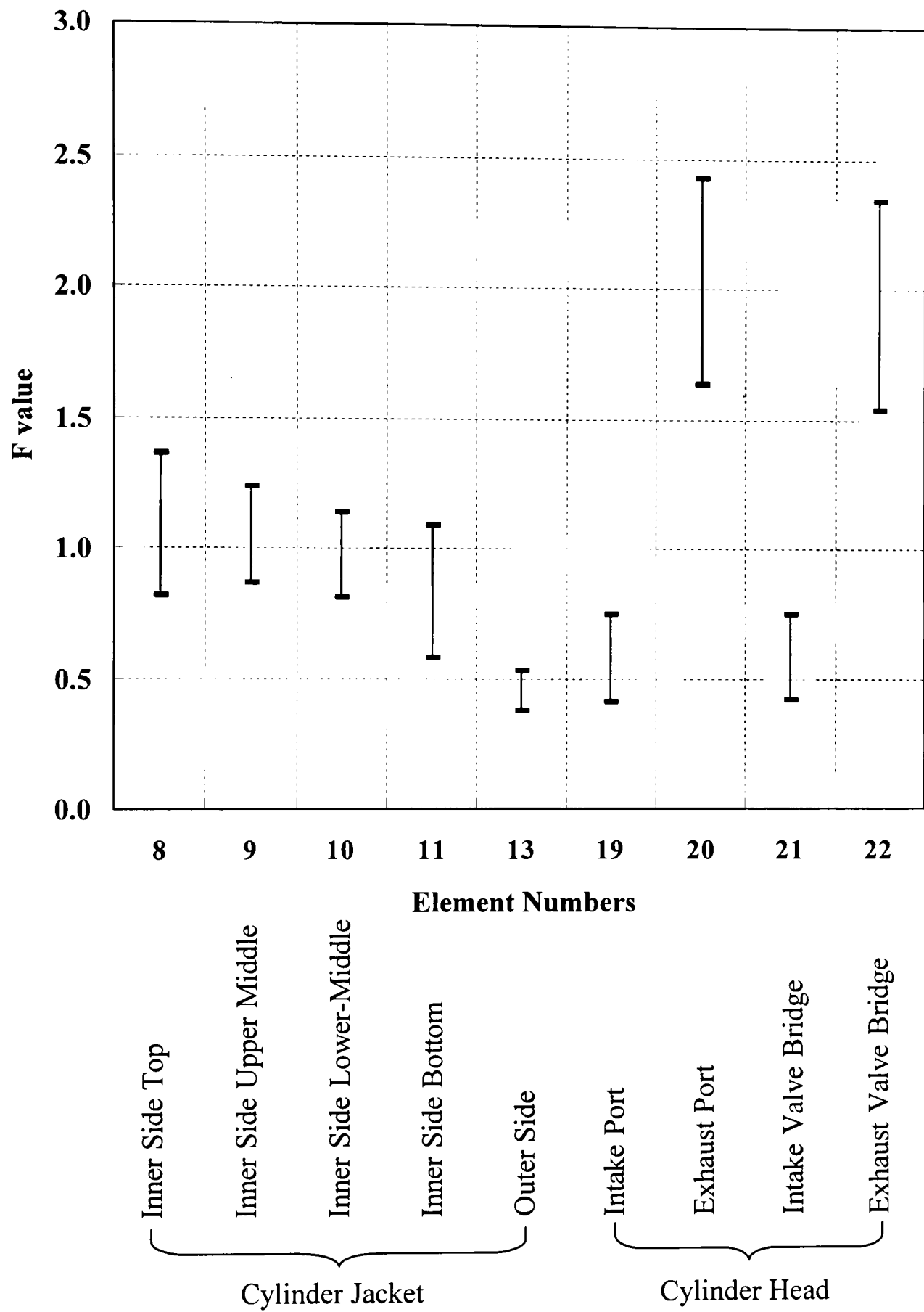


Figure 3.16 Mean values of $F \pm$ one standard deviation from the mean for the Ford Zetec 1.8l engine.

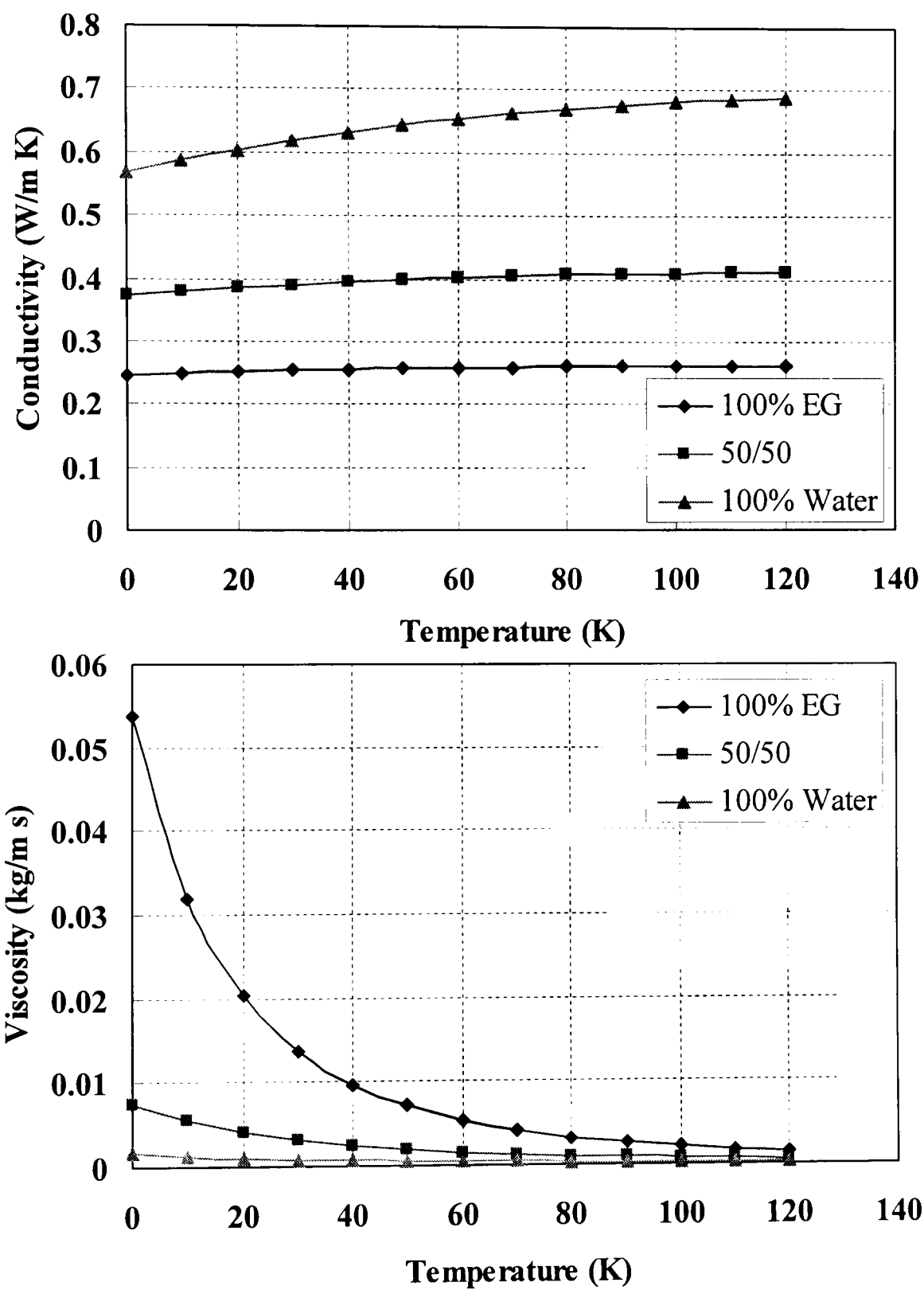


Figure 3.17 Coolant conductivity and viscosity properties for coolant compositions of 100% water, 50/50% water/ethylene glycol and 100% ethylene glycol.

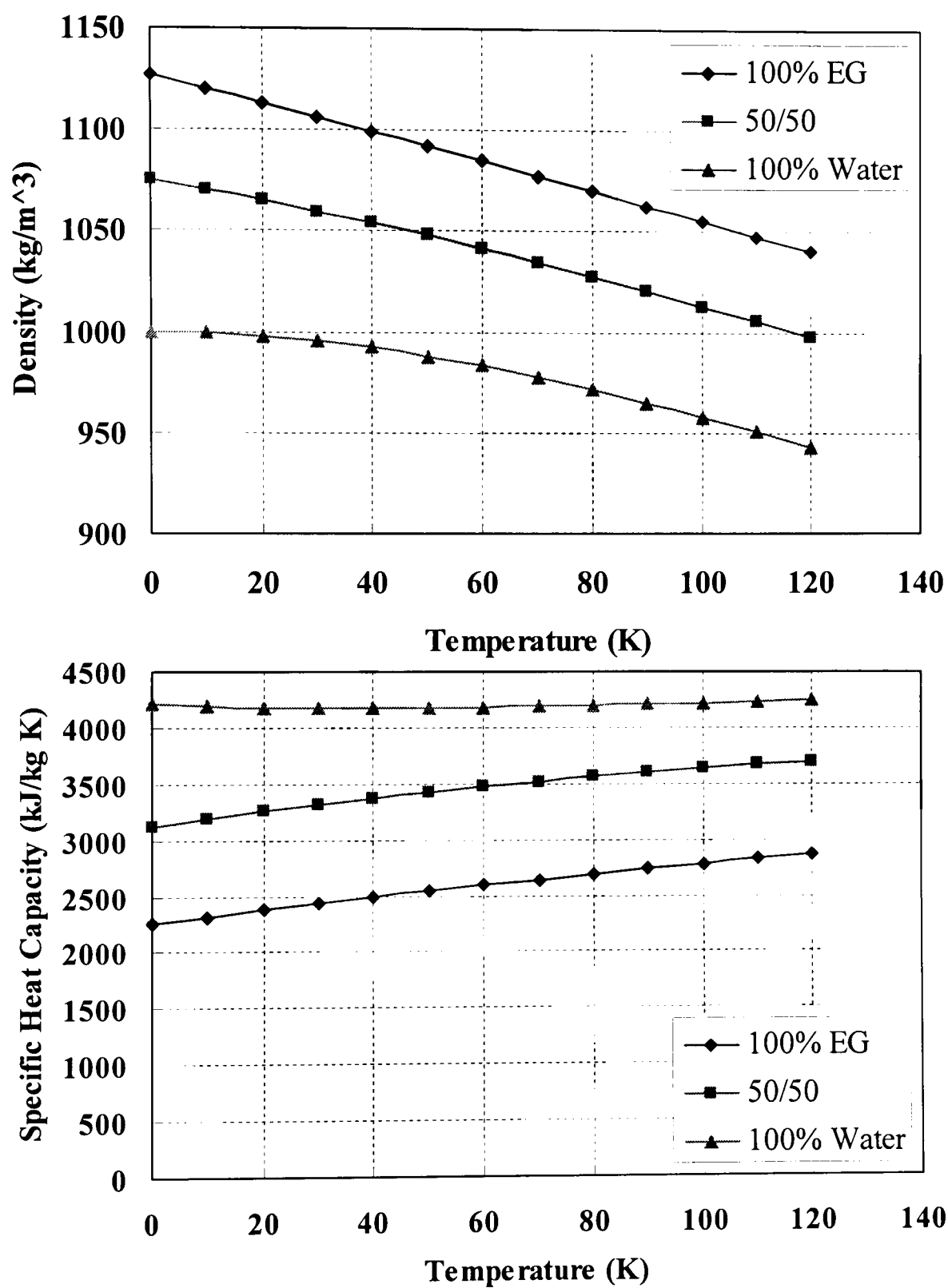


Figure 3.18 Coolant density and specific heat capacity properties for coolant compositions of 100% water, 50/50% water/ethylene glycol and 100% ethylene glycol.

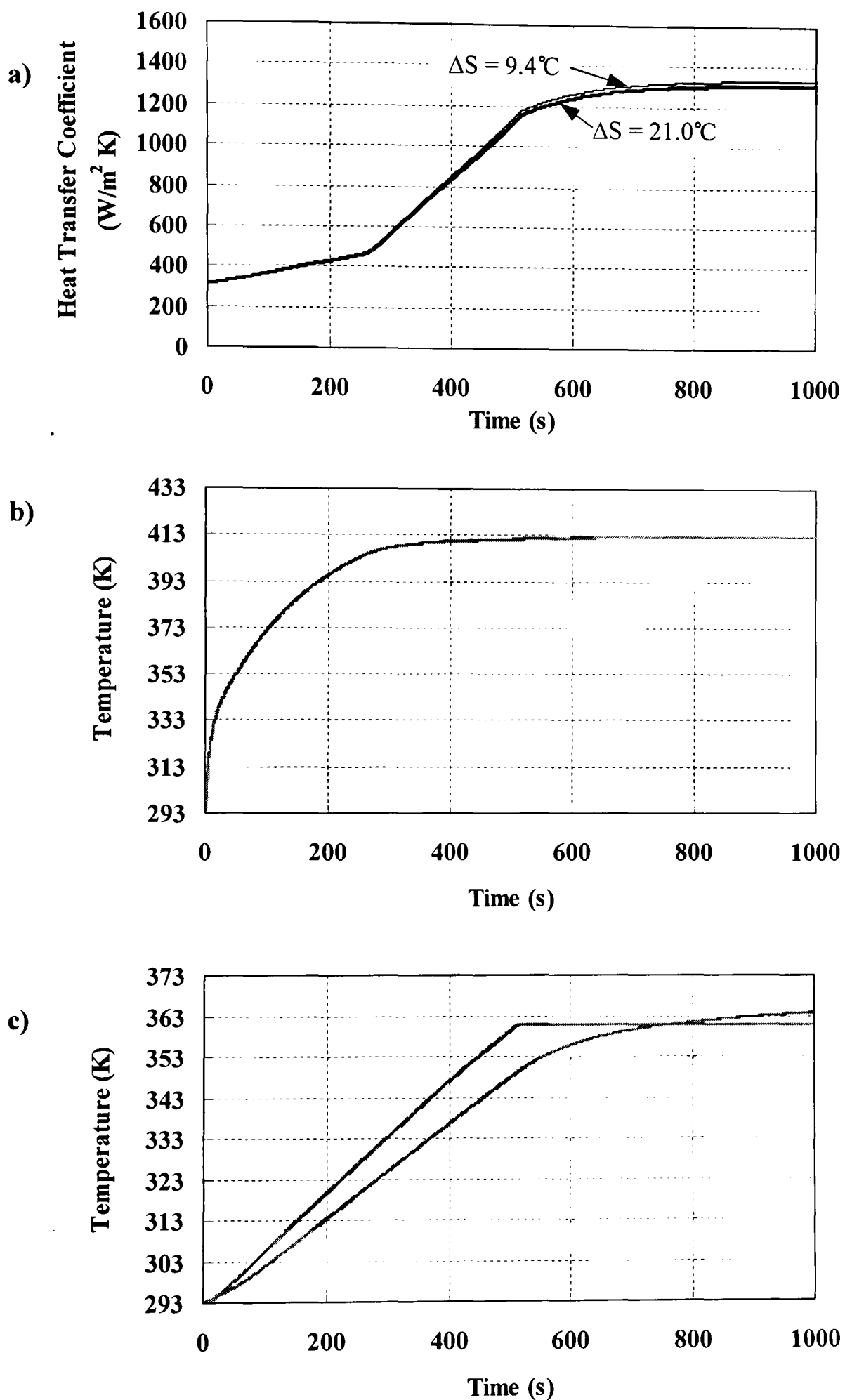


Figure 3.19 Effect of optimised and fixed values of ΔS on a) heat transfer coefficient at the exhaust port, b) temperature of metal around exhaust port and c) coolant and oil temperatures at 1000 rpm, 50 Nm for a 1.6l Sigma.

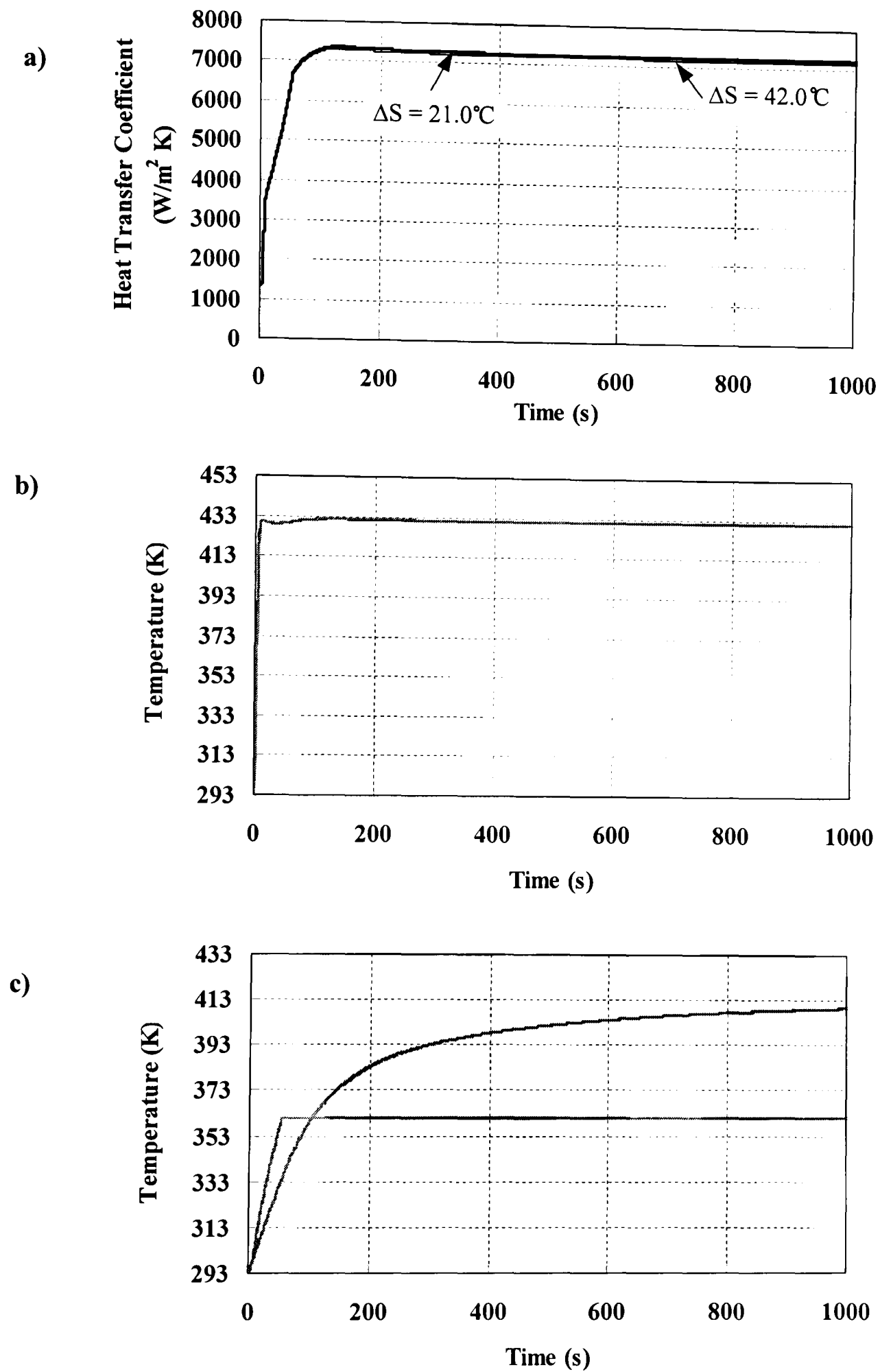


Figure 3.20 Effect of optimised and fixed values of ΔS on **a)** heat transfer coefficient at the exhaust port, **b)** temperature of metal around exhaust port and **c)** coolant and oil temperatures at 6000 rpm, 120 Nm for a 1.6l Sigma.

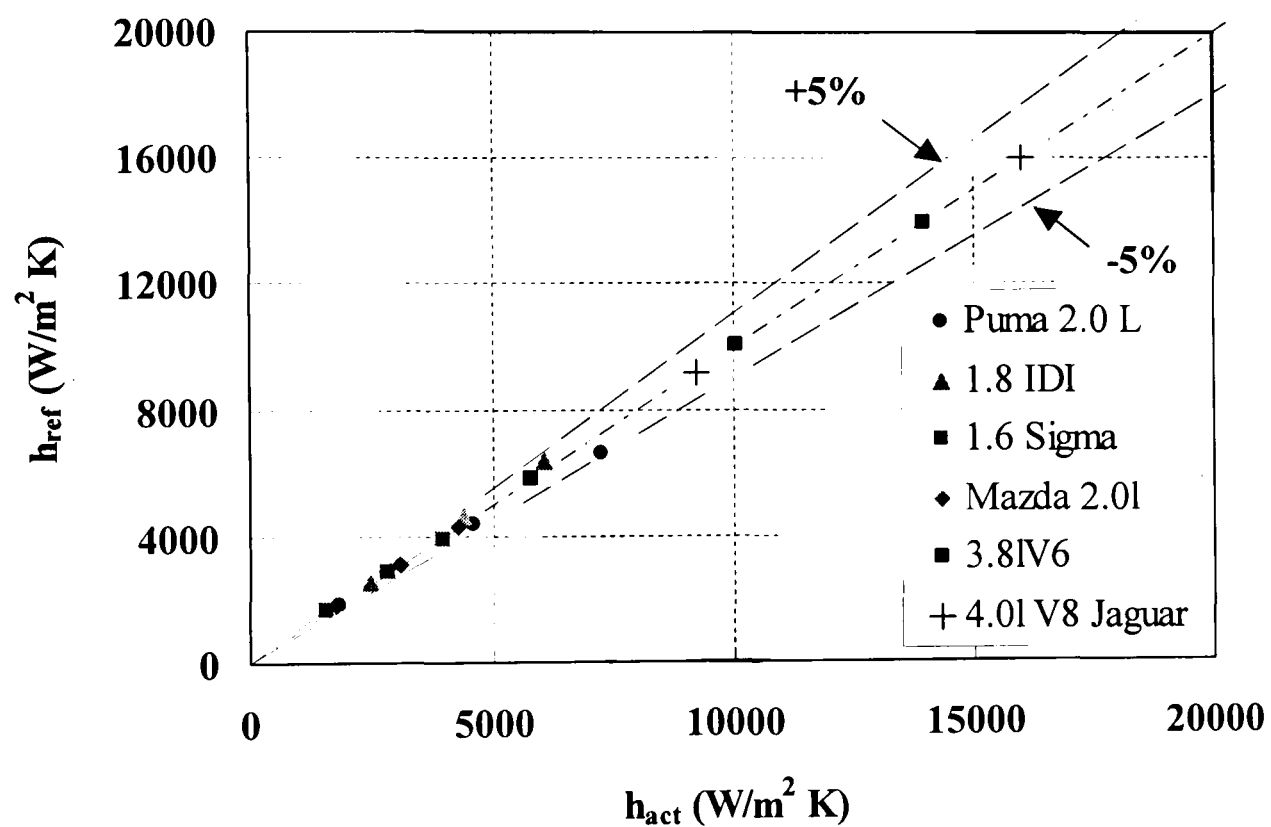
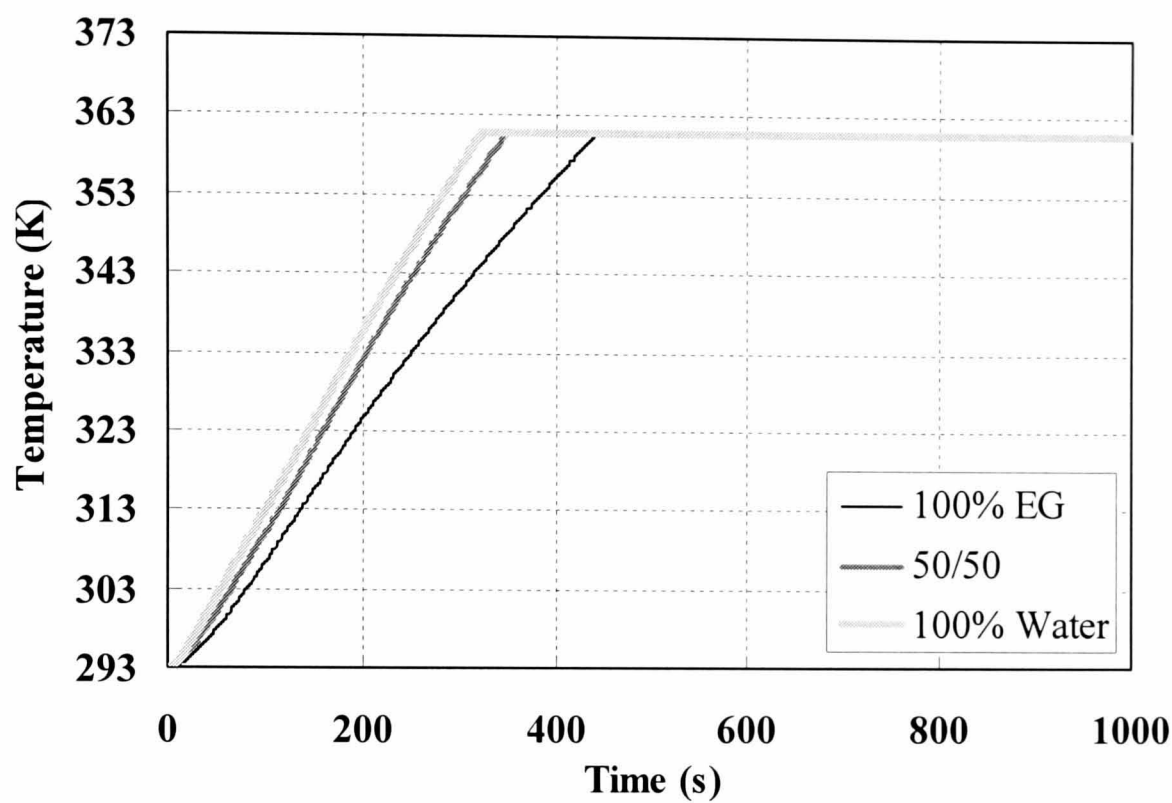


Figure 3.21 Comparison of reference and actual heat transfer coefficients calculated for a coolant composition of 100% water, when $\Delta S = 21^\circ C$.

a)



b)

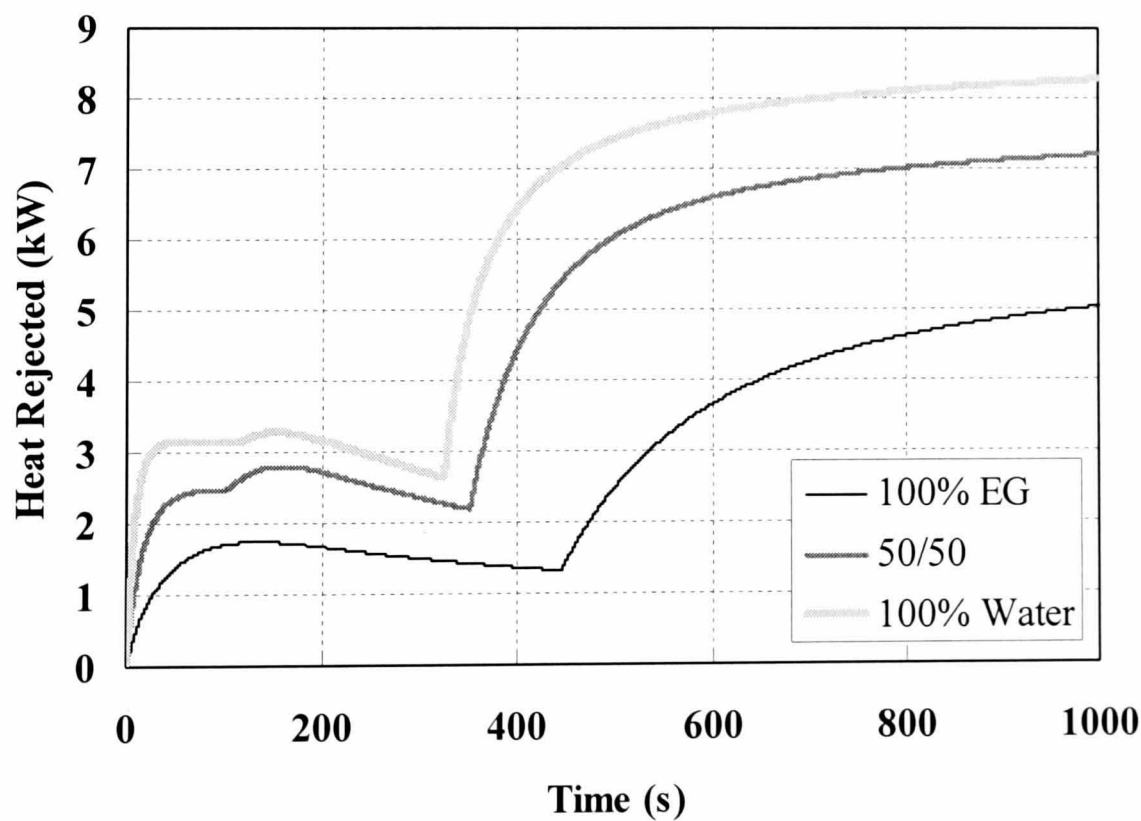
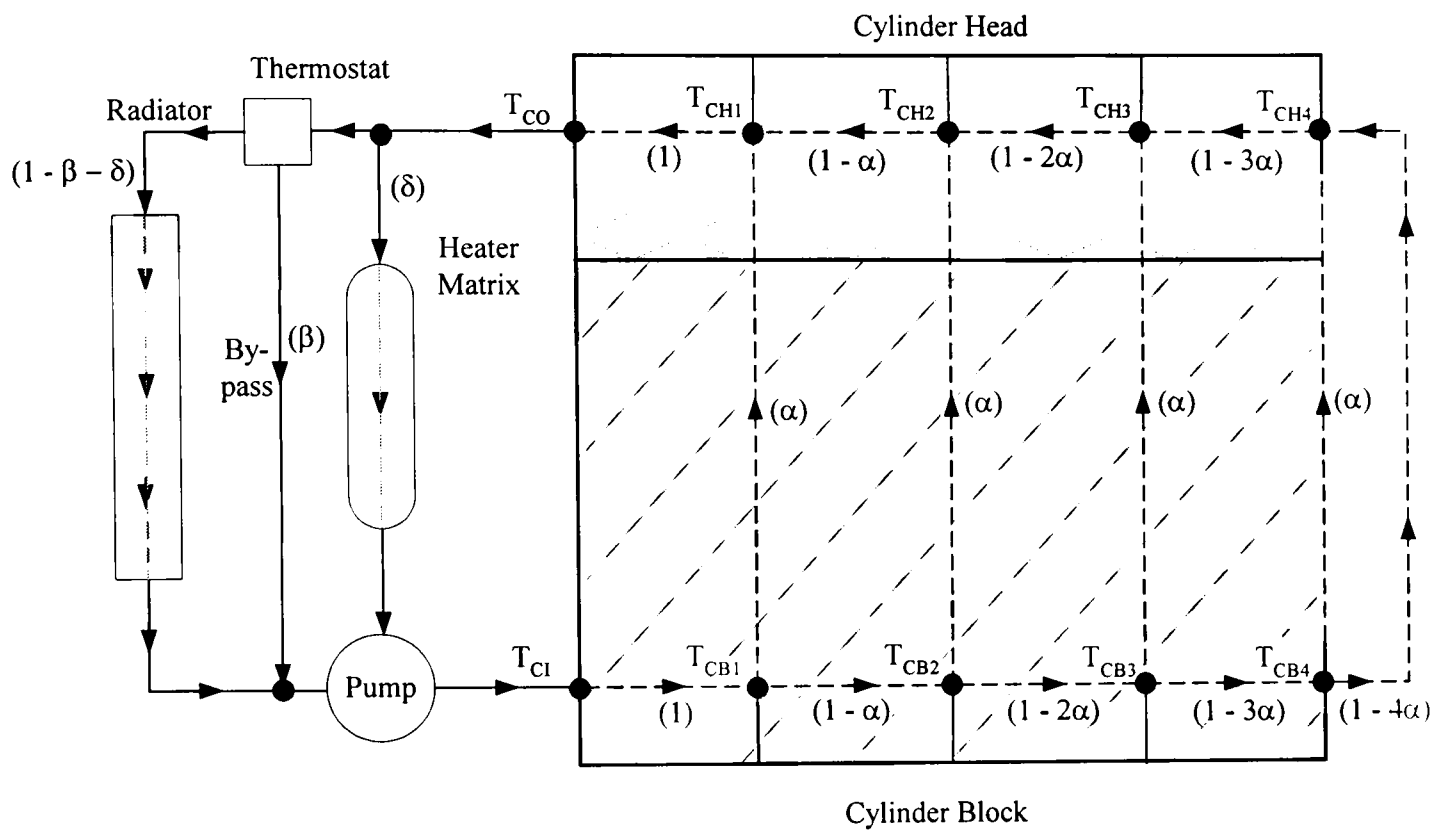


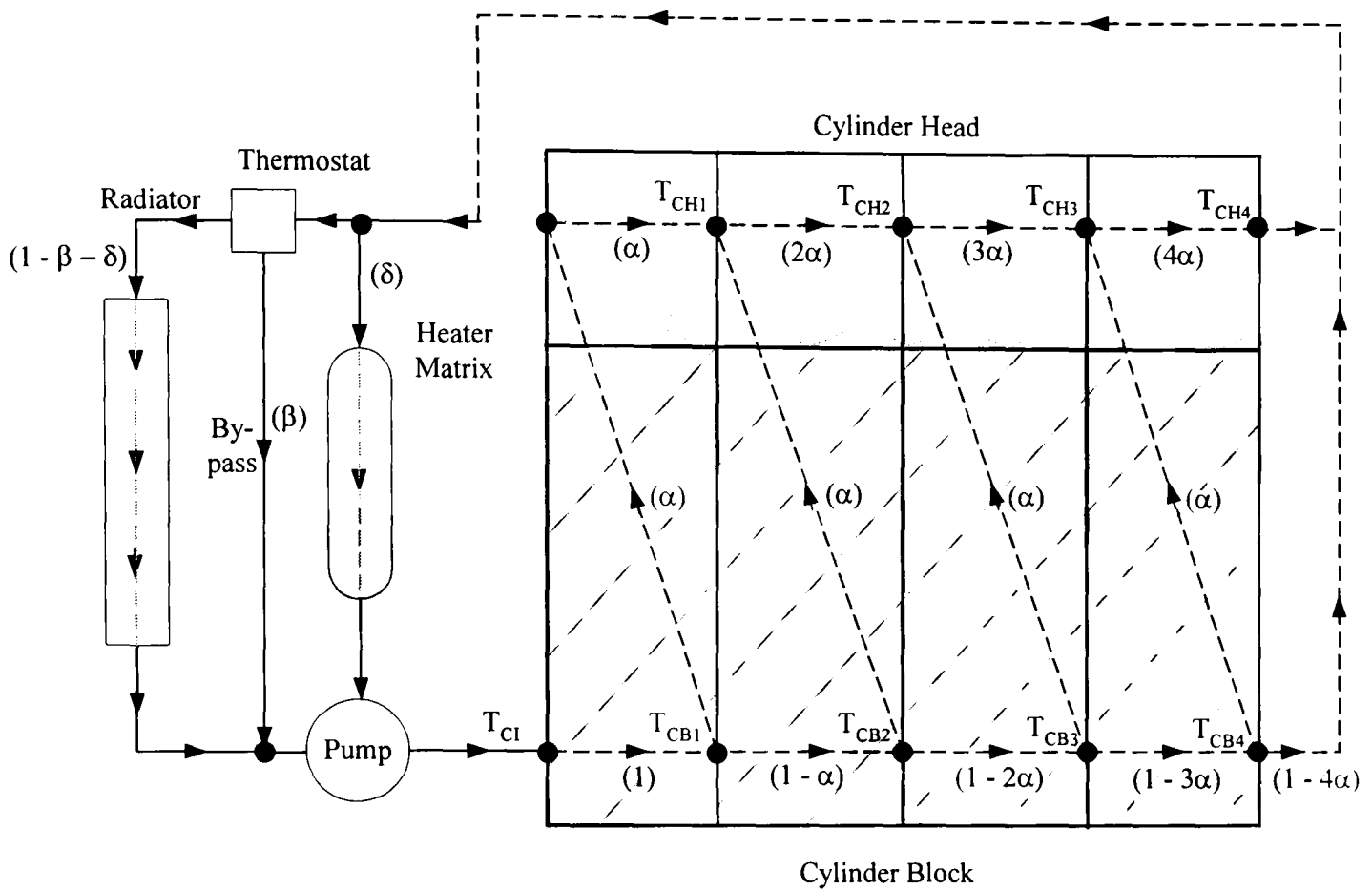
Figure 3.22 Effect of coolant composition on **a)** coolant temperature and **b)** heat rejected to coolant during warm-up at 1000 rpm, 120 Nm for a 1.6l Sigma engine. The kink which occurs at around 120 seconds in the 100% water and 50% ethylene glycol (EG) profiles is due to the onset of nucleate boiling.



Symbols :

- α Fraction of bulk coolant flow rate between cylinder head and block
- β Fraction of bulk coolant flow rate through the thermostat by-pass
- δ Fraction of bulk coolant flow rate through the heater circuit
- T_{CI} Coolant Inlet Temperature
- T_{CO} Coolant Outlet Temperature
- T_{CBi} Coolant Block Temperature for Cylinder i ($i = 1 - 4$)
- T_{CHi} Coolant Head Temperature for Cylinder i ($i = 1 - 4$)

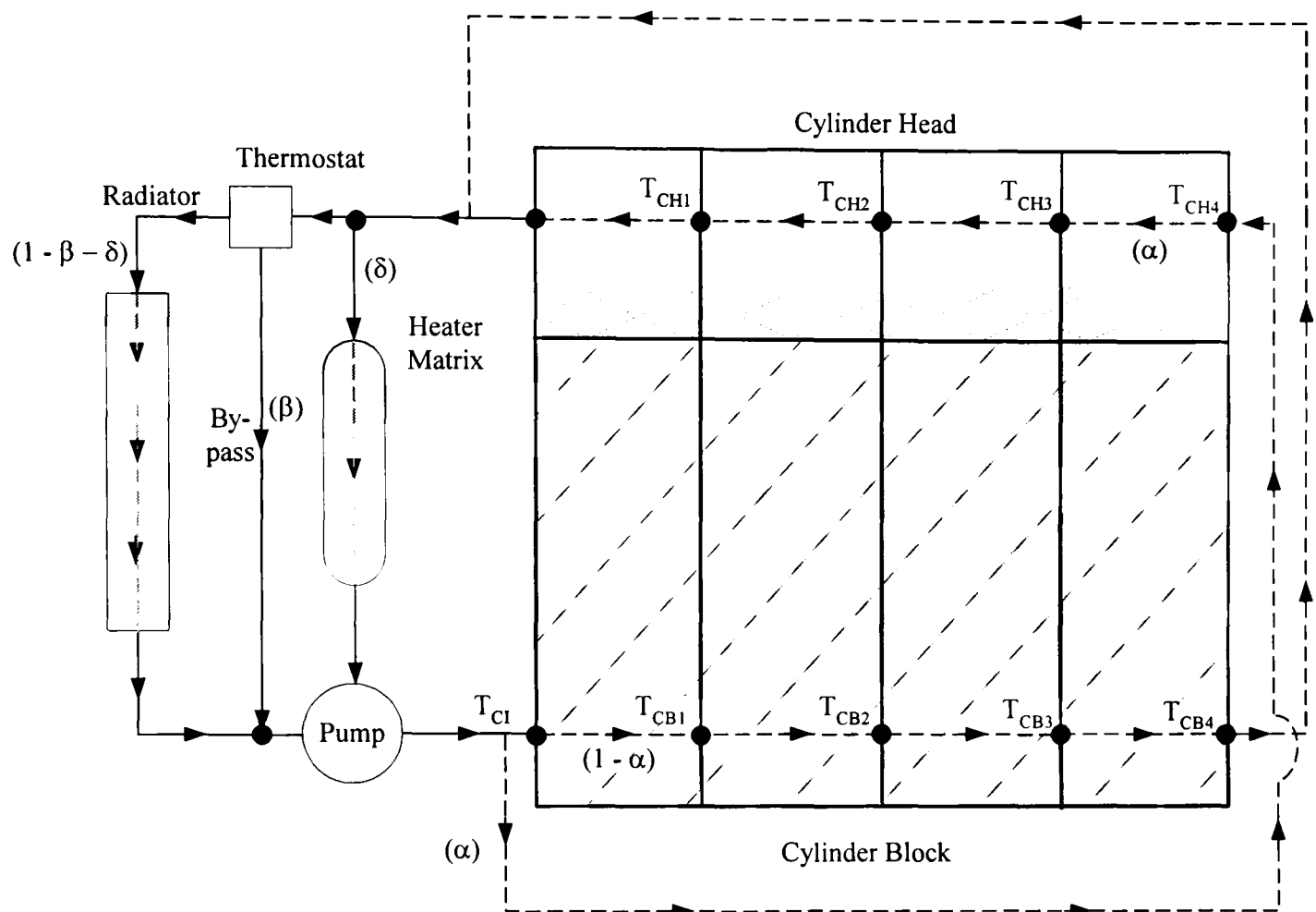
Figure 3.23 Coolant circuit 1: inlet and outlet on the same side of the engine.



Symbols :

- α Fraction of bulk coolant flow rate between cylinder head and block
- β Fraction of bulk coolant flow rate through the thermostat by-pass
- δ Fraction of bulk coolant flow rate through the heater circuit
- T_{CI} Coolant Inlet Temperature
- T_{CO} Coolant Outlet Temperature
- T_{CBi} Coolant Block Temperature for Cylinder i ($i = 1 - 4$)
- T_{CHi} Coolant Head Temperature for Cylinder i ($i = 1 - 4$)

Figure 3.24 Coolant circuit 2: inlet and outlet on opposite sides of the engine



Symbols :

α Fraction of bulk coolant flow rate between cylinder head and block

β Fraction of bulk coolant flow rate through the thermostat by-pass

δ Fraction of bulk coolant flow rate through the heater circuit

T_{Ci} Coolant Inlet Temperature

T_{Co} Coolant Outlet Temperature

T_{CBi} Coolant Block Temperature for Cylinder i ($i = 1 - 4$)

T_{CHi} Coolant Head Temperature for Cylinder i ($i = 1 - 4$)

Figure 3.25 Coolant circuit 3: separate block and head cooling.

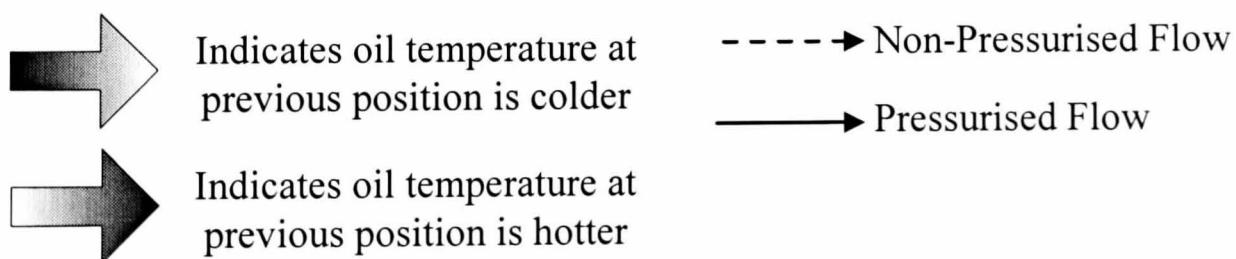
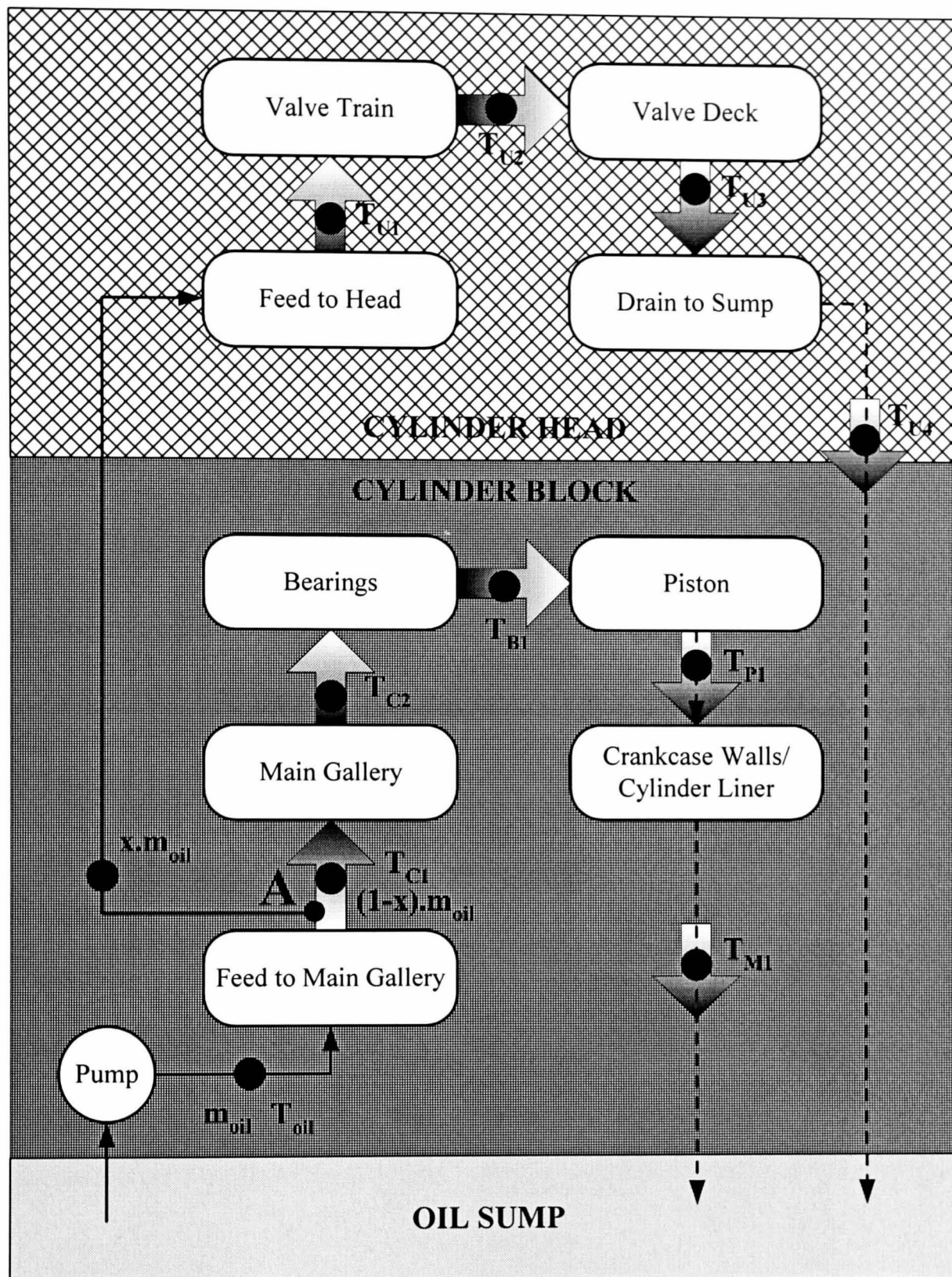
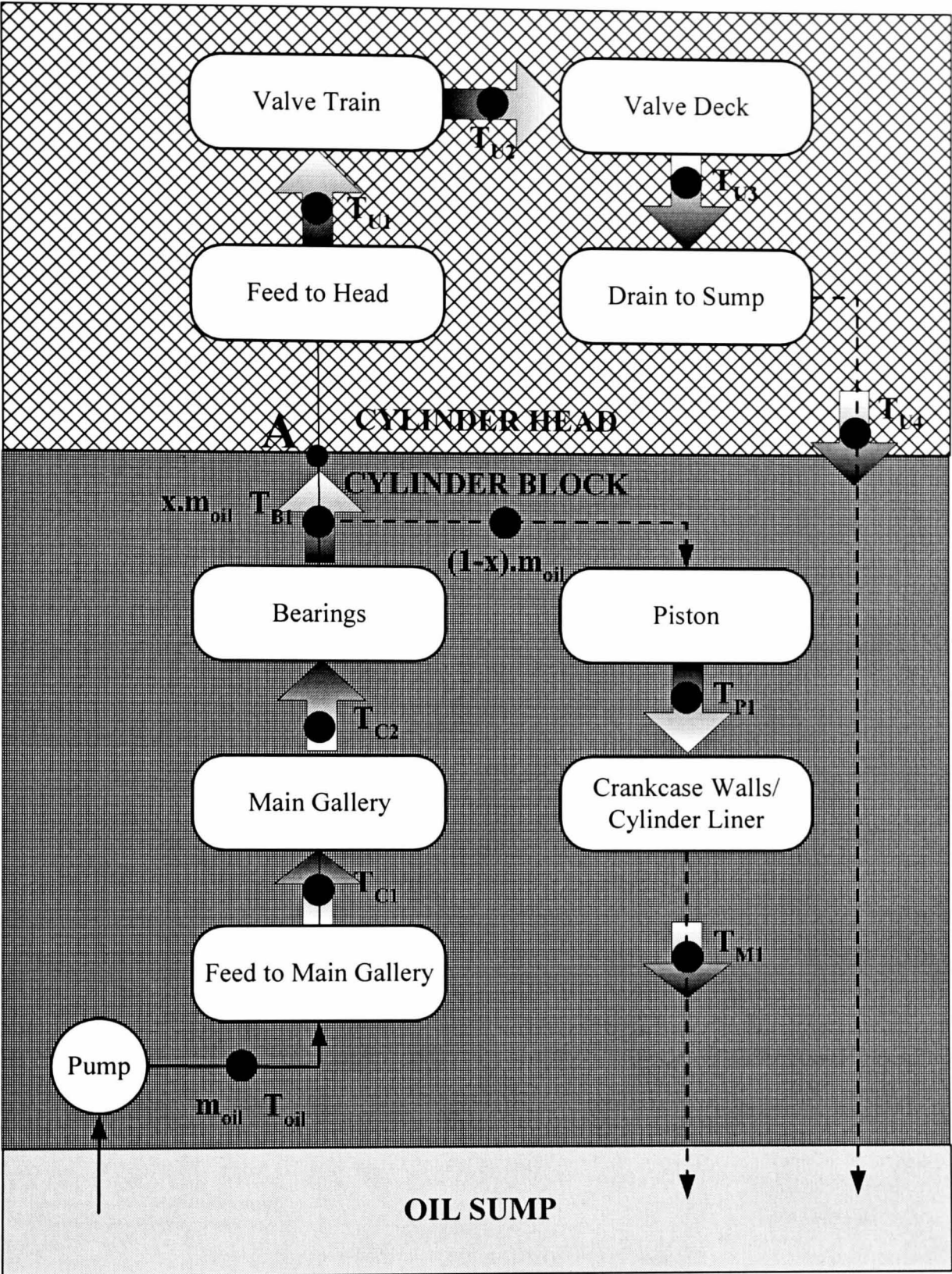


Figure 3.26 Diagrammatic representation of oil circuit 1 (as for CVH, DOHC and Zetec engines). In V-engines, the flow at A is equally divided between the two heads.



➡ Indicates oil temperature at previous position is colder
➡ Indicates oil temperature at previous position is hotter
- - - ➡ Non-Pressurised Flow
— ➡ Pressurised Flow

Figure 3.27 Diagrammatic representation of oil circuit 2 (as for Valencia engine). In V-engines, the flow at A is equally divided between the two heads.

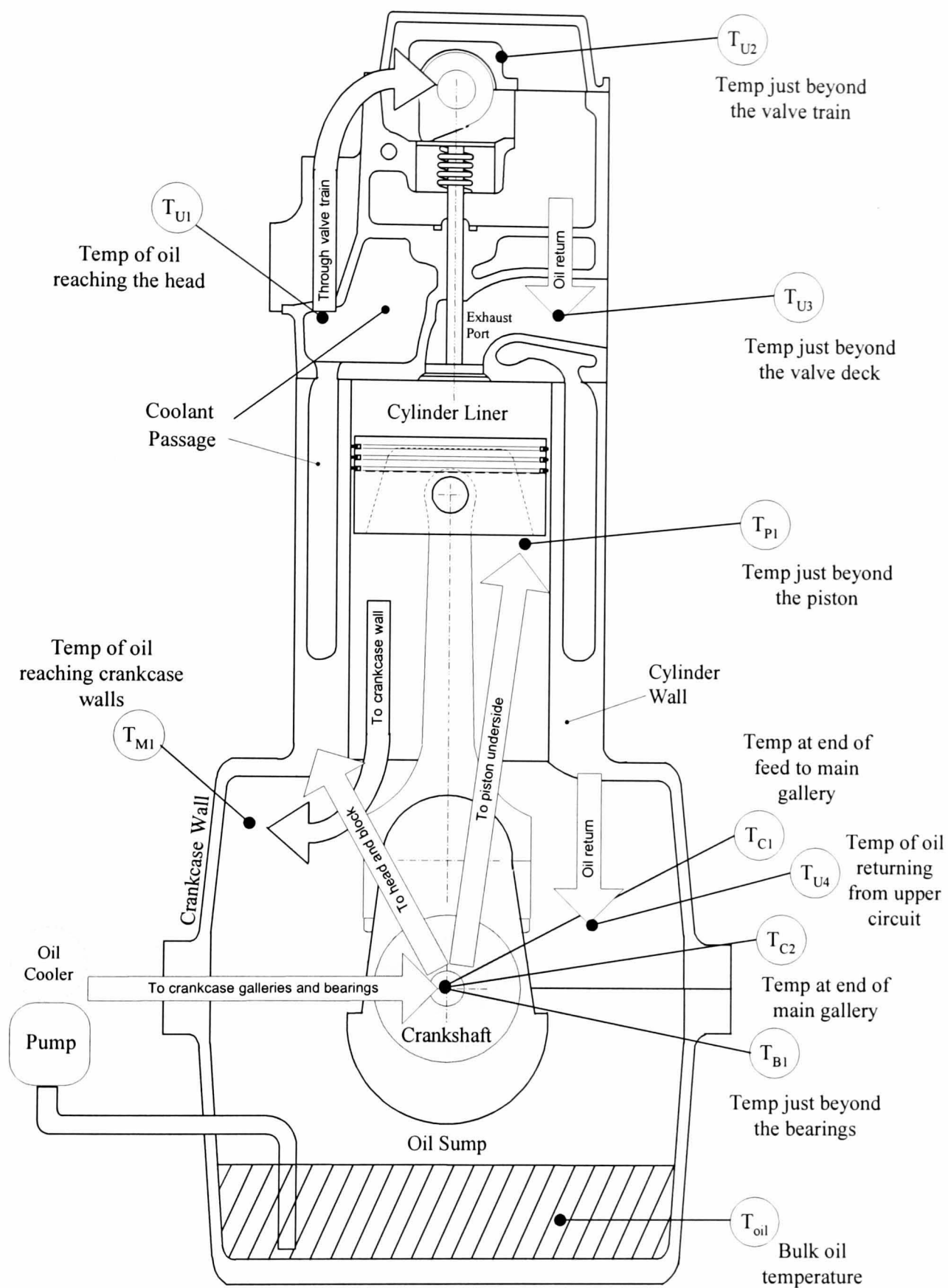


Figure 3.28 The points at which temperatures are calculated and the flow of oil around an engine.

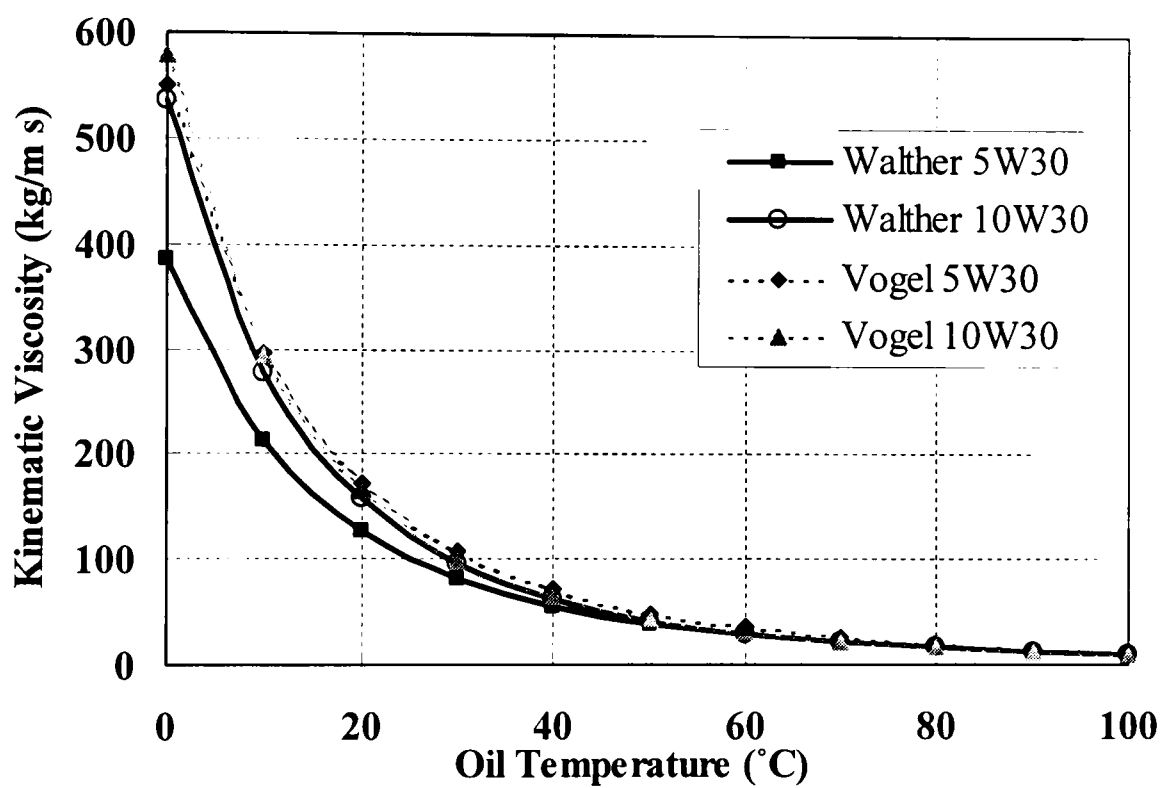


Figure 3.29 Kinematic oil viscosity as a function of oil temperature as calculated by the Vogel Equation [3.24] and the Walther Equation [3.23] for SAE5W30 and SAE10W30 oils.

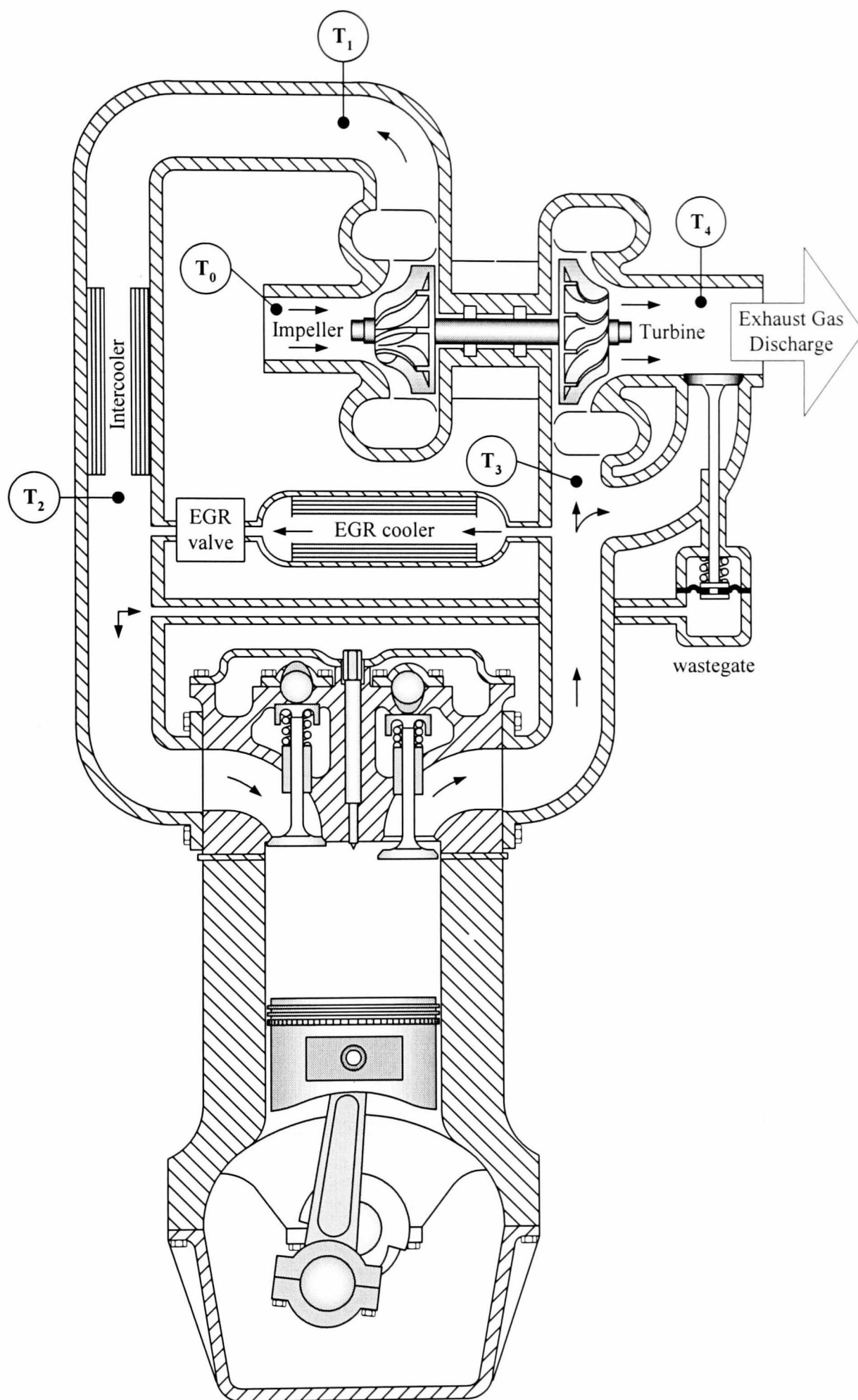


Figure 3.30 A typical set-up for a wastegated turbocharger, showing the position of calculated temperatures, T . The subscripts 0, 1, 2, 3 and 4 represent ambient, post-compressor, post-intercooler, pre-turbine and post-turbine positions respectively. [39]

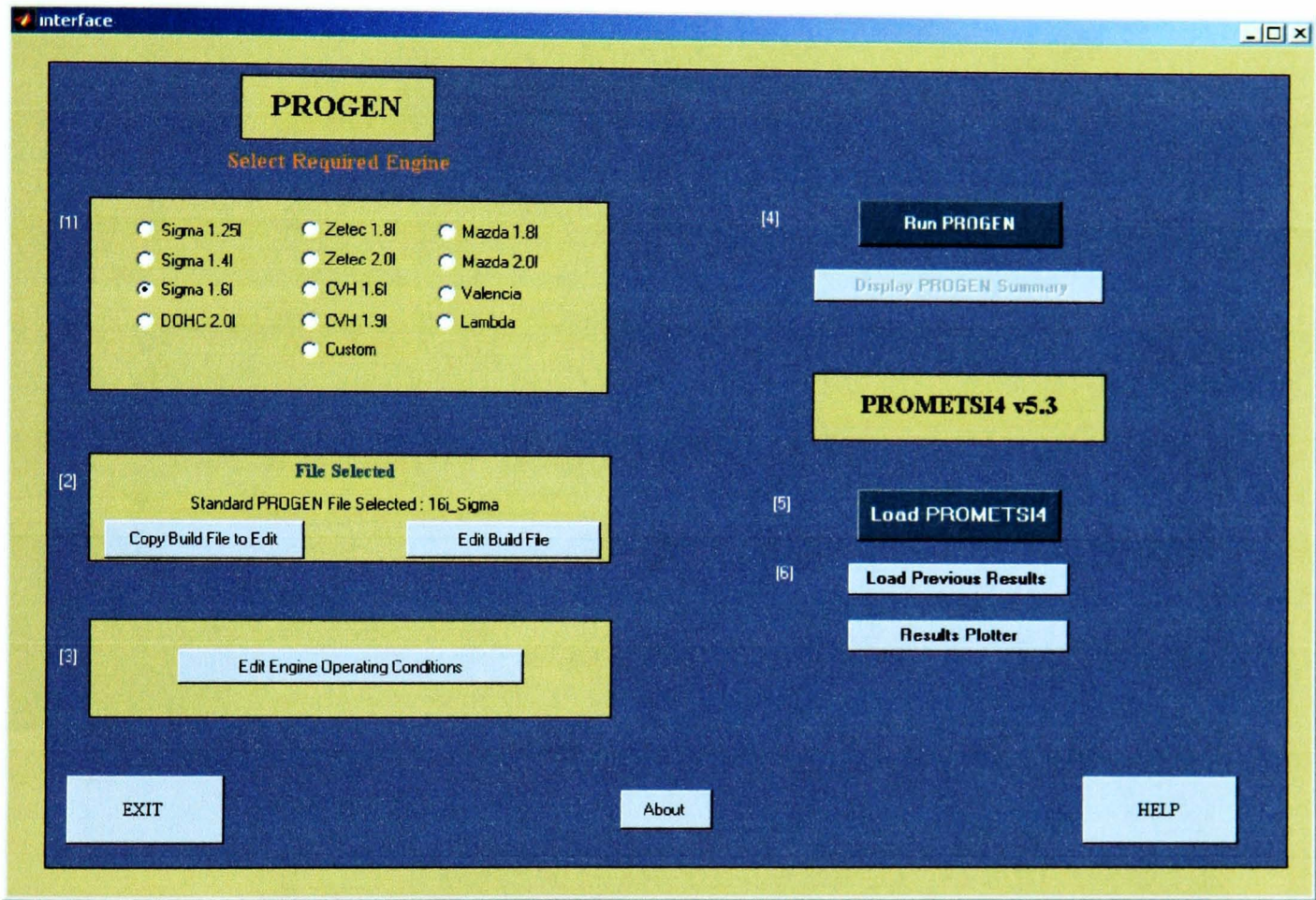


Figure 4.1 Simulink PROMETS Graphical User Interface (GUI) Menu for PROMETSI4 (gasoline in-line). The numbers in square brackets indicate progression (from [1] to [6]) from start to finish for a basic application of the model (see also Figure 4.15).

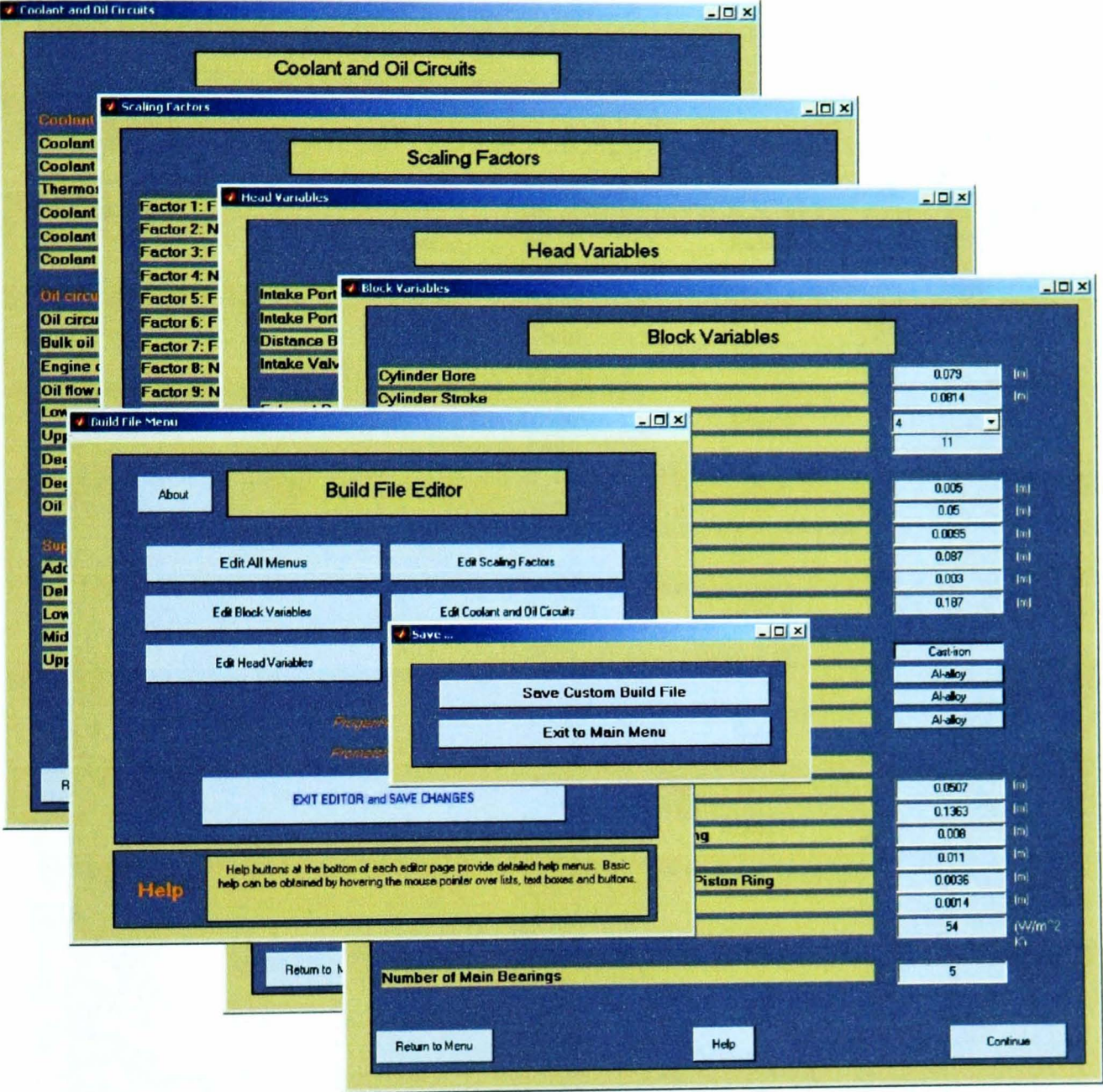


Figure 4.2 Pages from the Edit Menu for PROMETSI4 (gasoline in-line) used to enter engine geometry data into PROMETS.

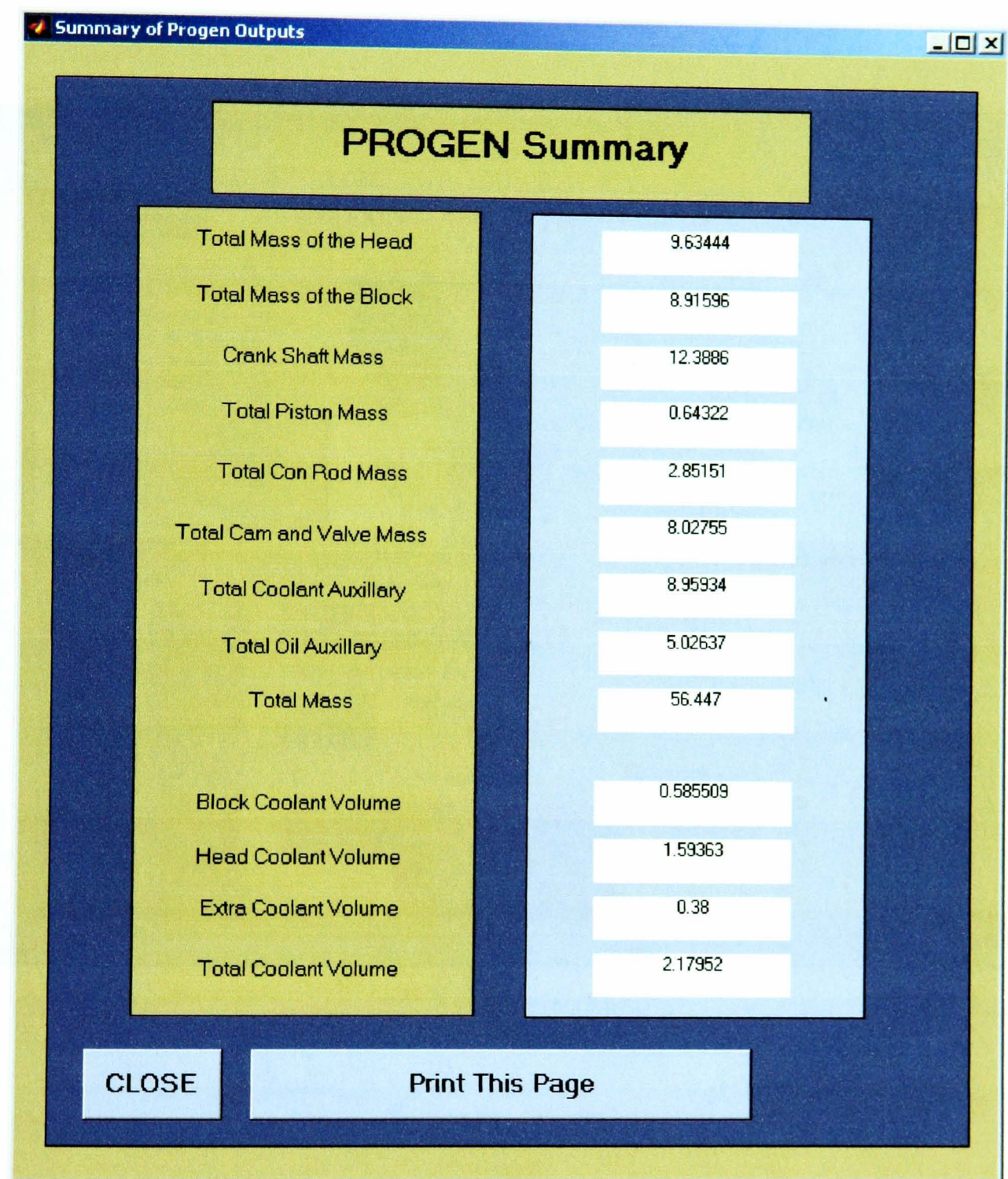


Figure 4.3 The PROGEN Summary page of the Graphical User Interface displays the predicted masses in kilograms and coolant volumes in litres for the selected engine. The details displayed here are for the gasoline 1.6l Sigma engine.

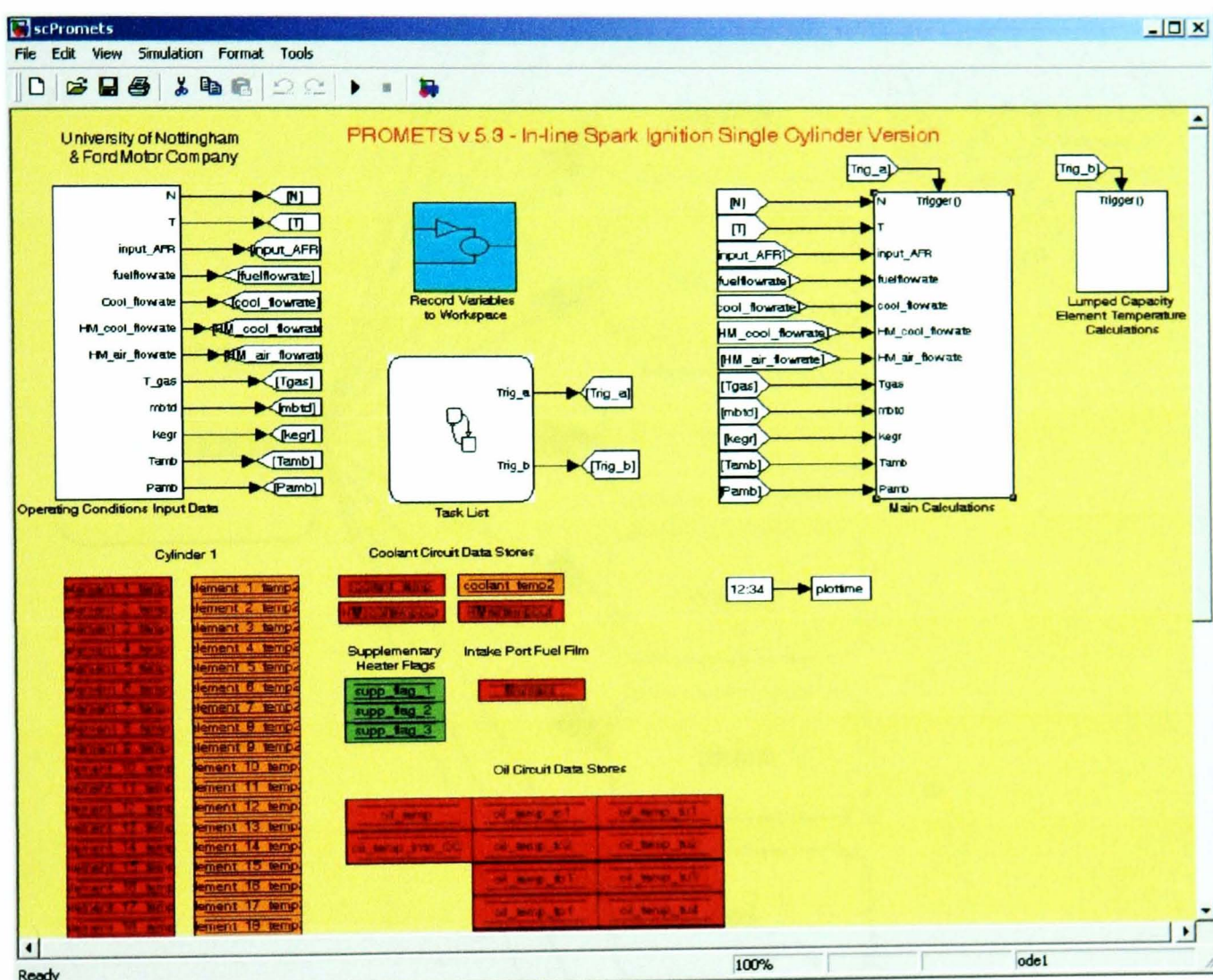


Figure 4.4 The PROMETS Simulink model. The model is activated by pressing the 'play' button, ►, in the top left hand corner of the screen.

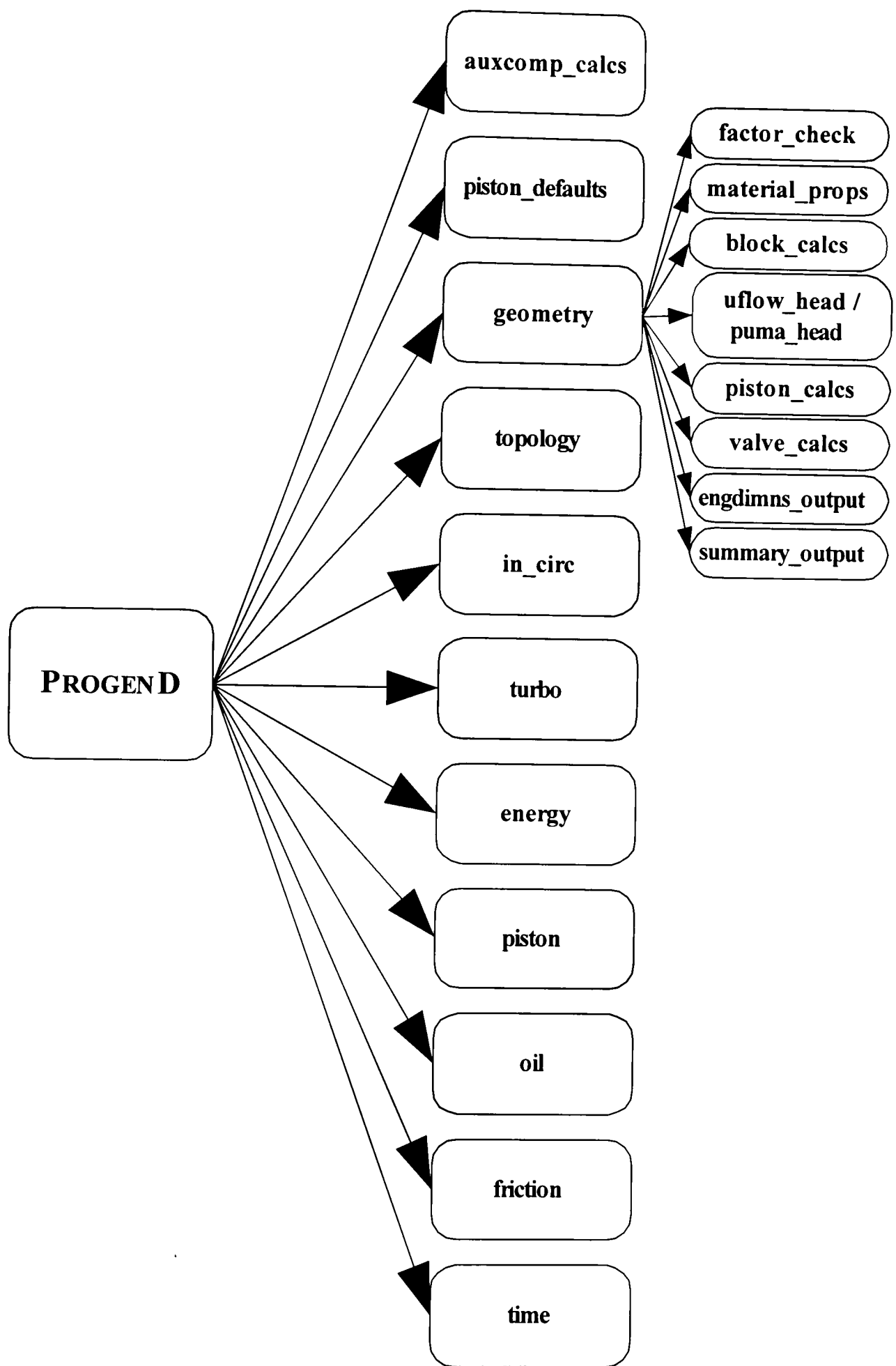


Figure 4.5 Illustration of the structure of the diesel in-line version of PROGEN. Each block shown represents a MATLAB m-file.

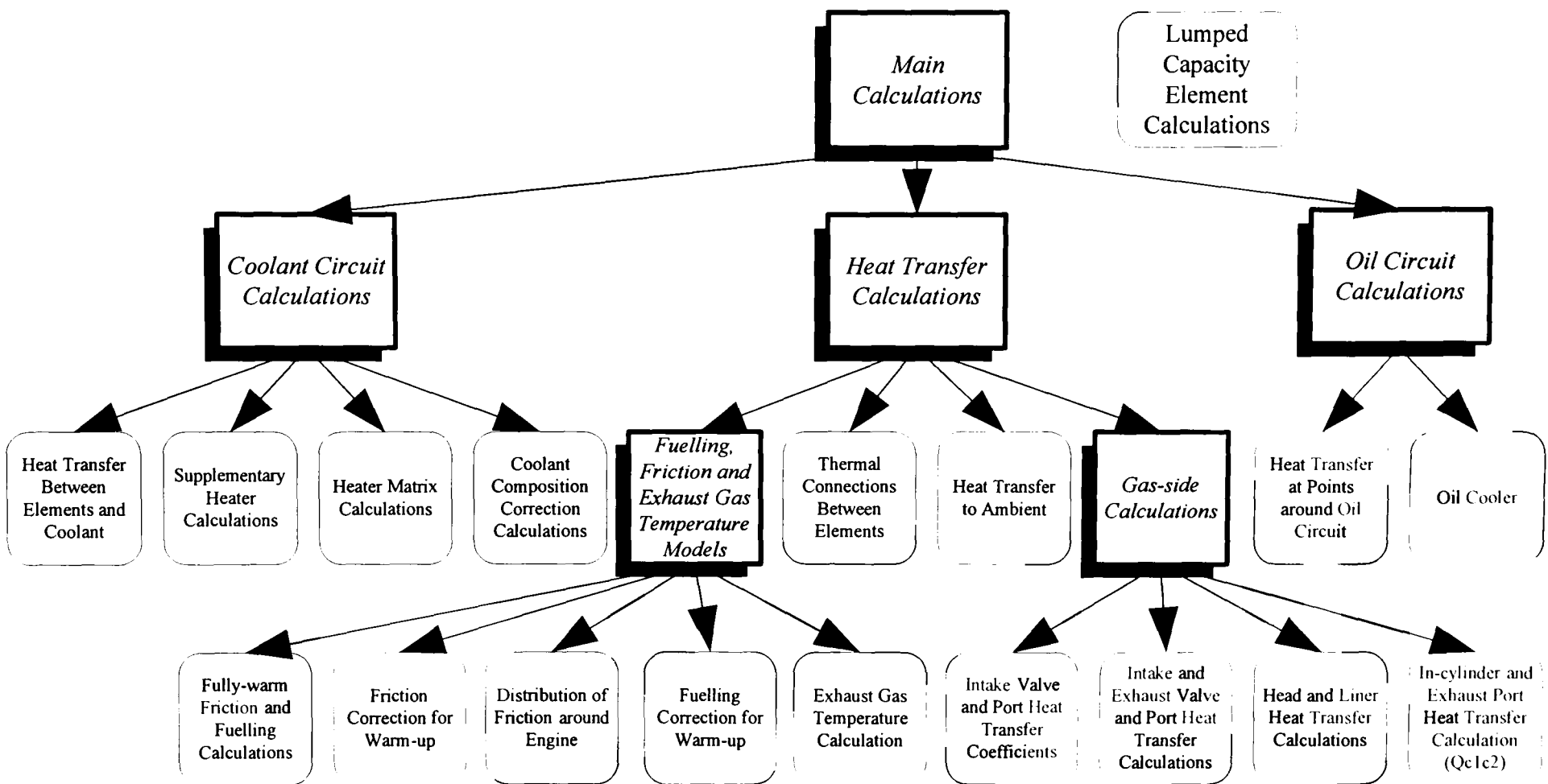


Figure 4.6 Illustration of the structure of the in-line gasoline version of PROMETS: there are four levels, with each subsystem reached through the route indicated by the arrows.

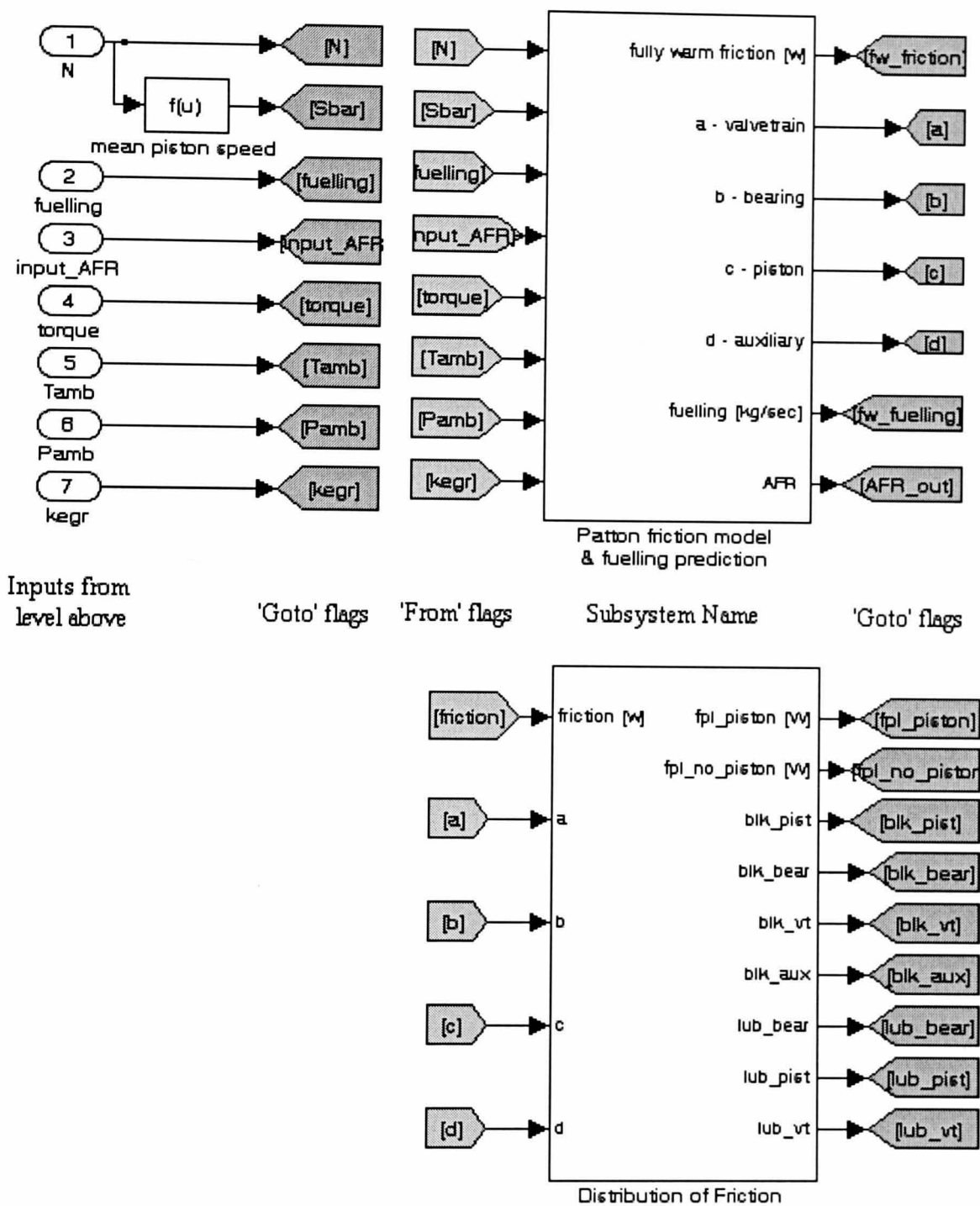


Figure 4.7 Illustration of the Simulink programming environment, showing a section of PROMETS, including subsystems, 'Goto' and 'From' flags, and inputs from the level above.

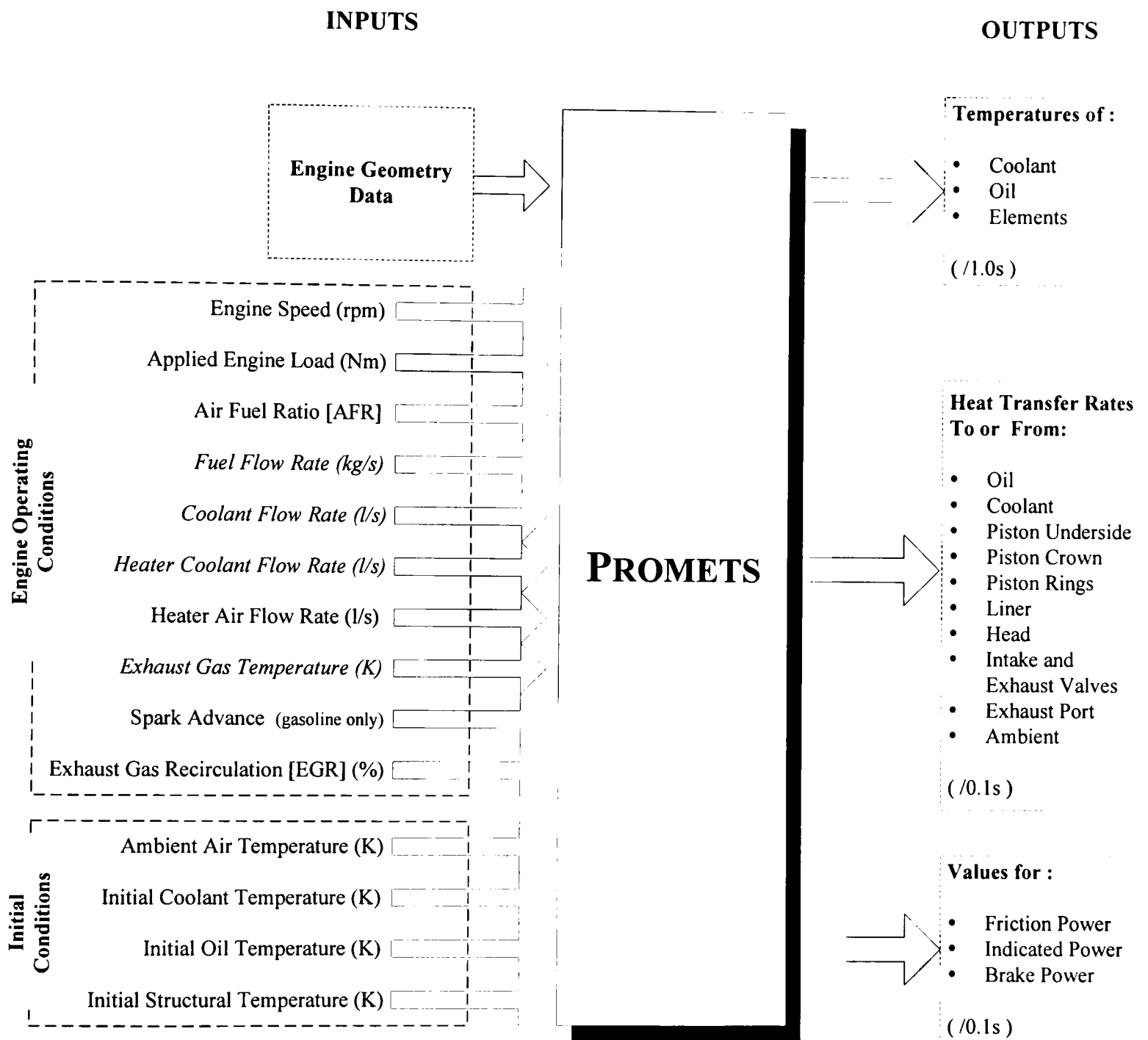


Figure 4.8 Illustration of the inputs to and outputs from PROMETS. Optional inputs are in italics – these variables can be automatically calculated by PROMETS by entering ‘-1’ in the operating conditions file.

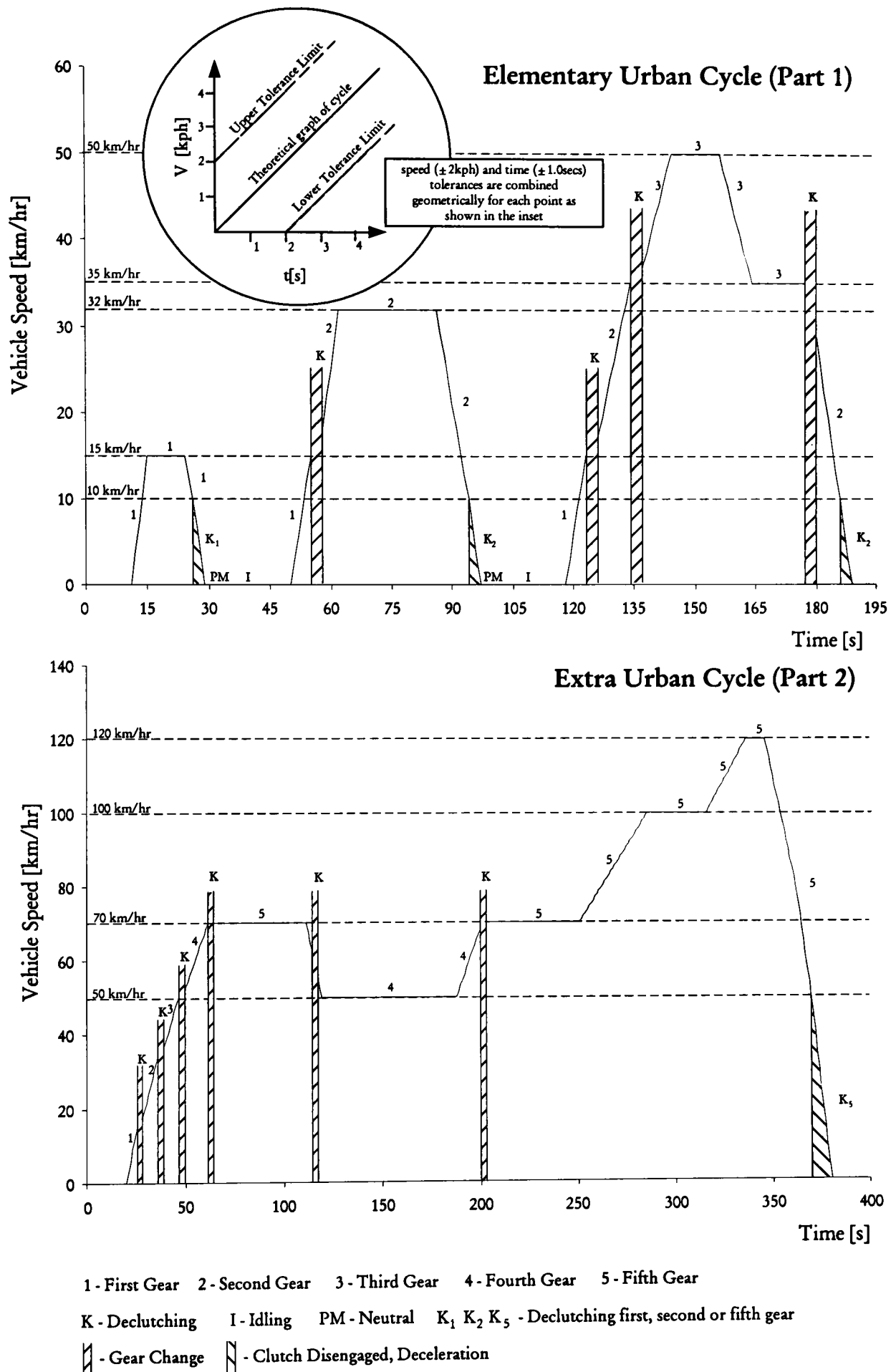
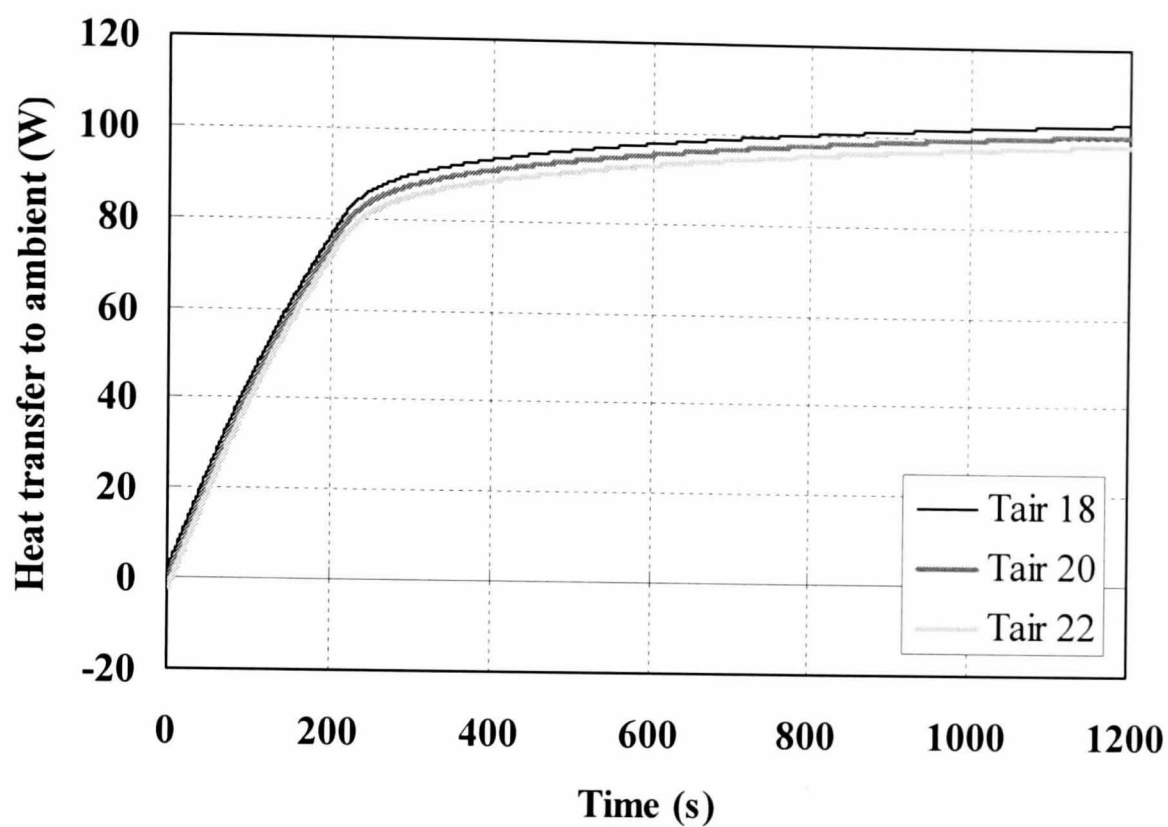


Figure 4.9 New European Drive Cycle (4 parts ECE and 1 part EUDC), cycle distance = 11.0 km, cycle duration = 1180s, average speed = 32.5 kph and maximum speed = 120.0kph [4.3].

a)



b)

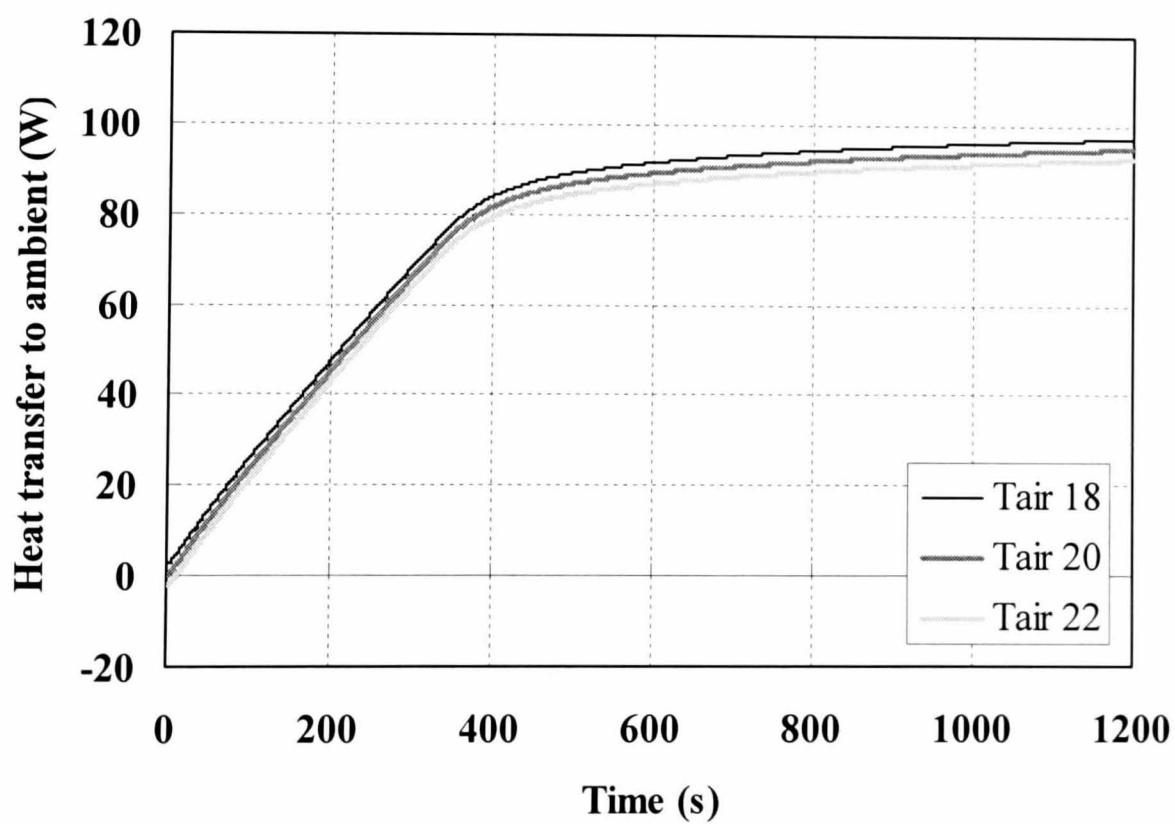
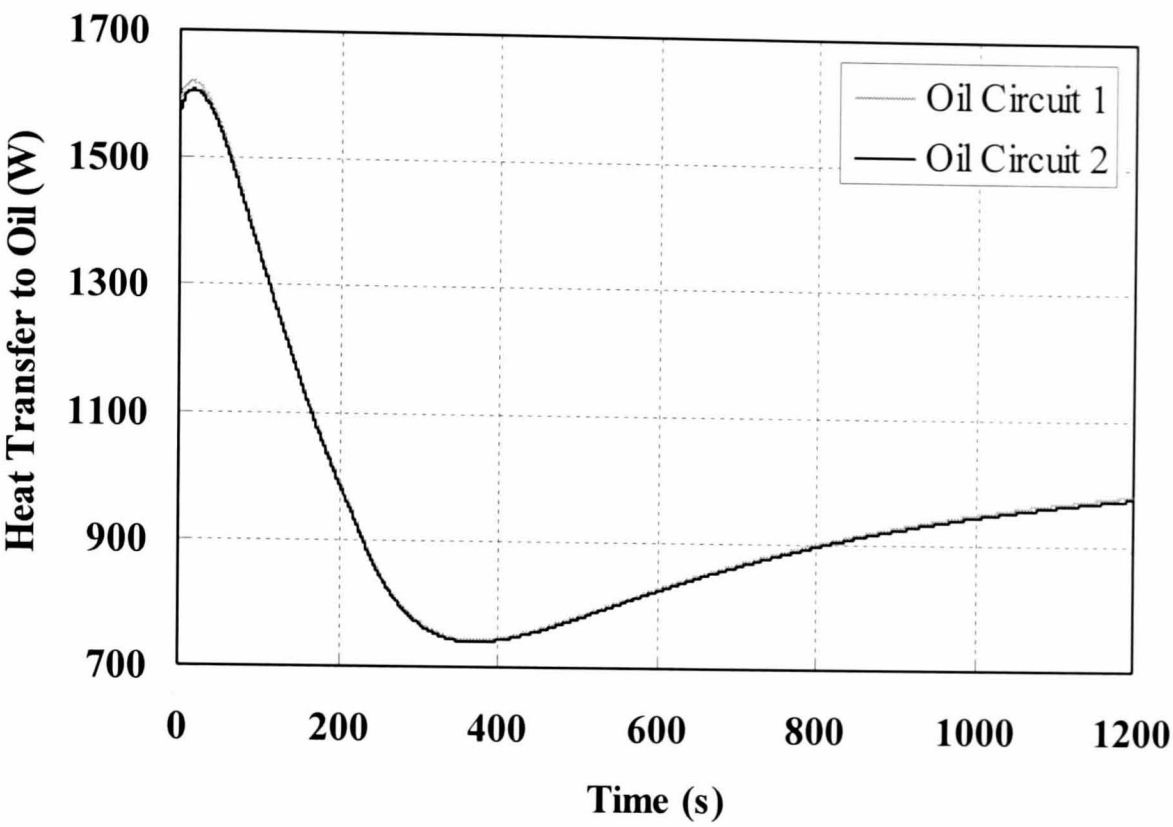


Figure 4.10 Heat transfer rates to ambient for different ambient air temperatures (Tair) in °C at a) 3000 rpm, 5 Nm and b) 1000 rpm, 120 Nm.

a)



b)

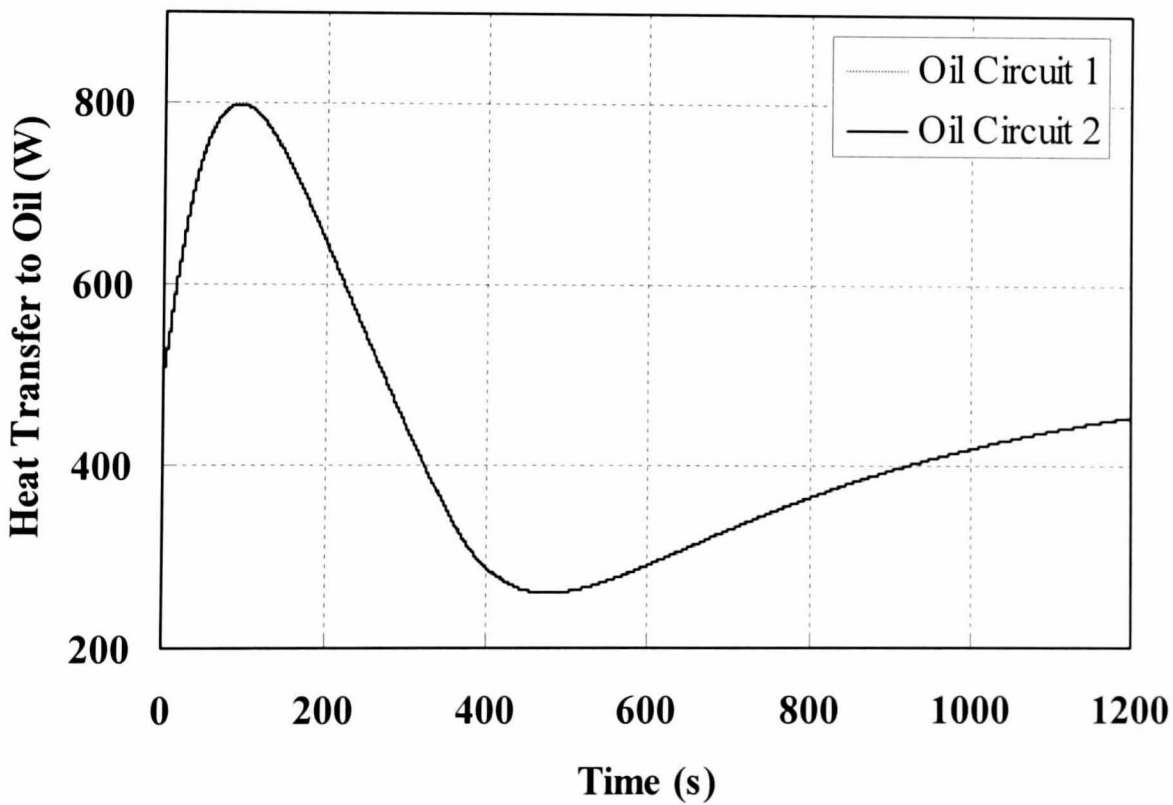
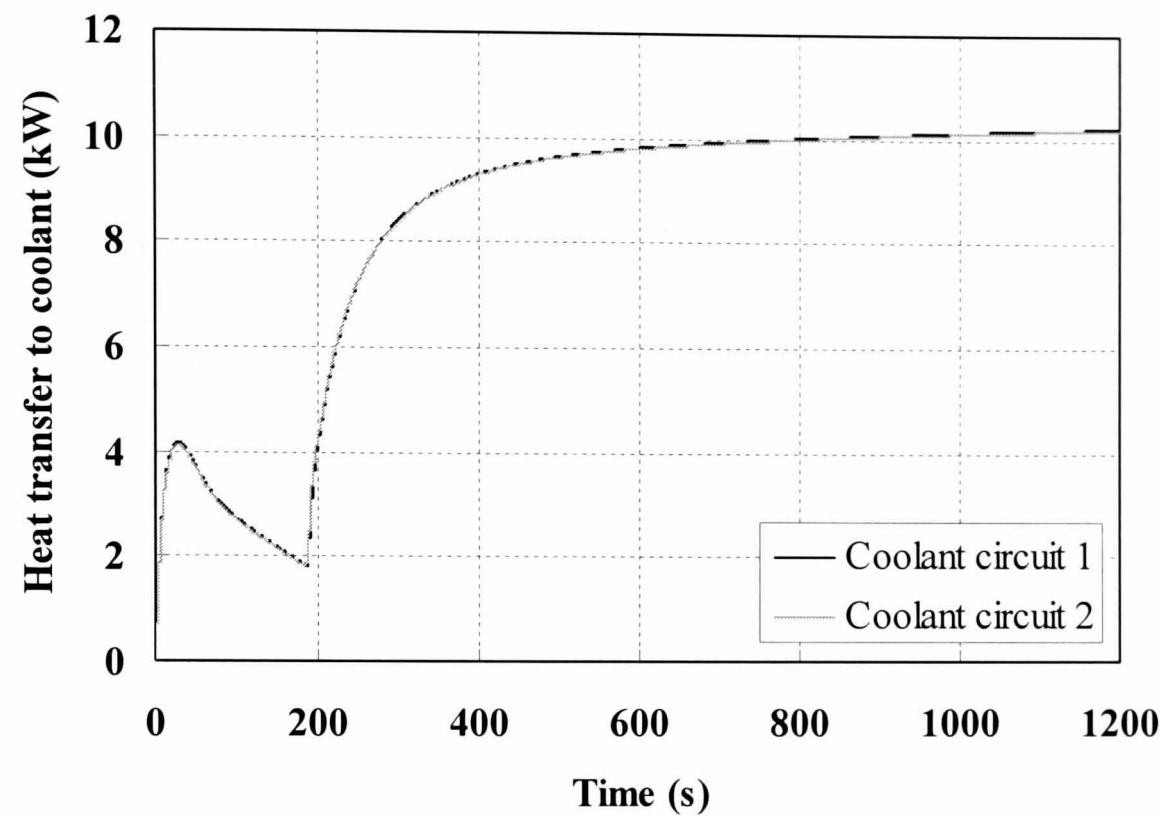


Figure 4.11 Net heat transfer rates to the oil, comprising of the heat transferred from the structure, frictional heat retained in the oil and heat transferred to or from the coolant, for oil circuits 1 and 2 at operating conditions of **a)** 3000 rpm, 5 Nm and **b)** 1000 rpm, 120 Nm. At 3000 rpm the difference in the steady state heat transfer rates is 5W.

a)



b)

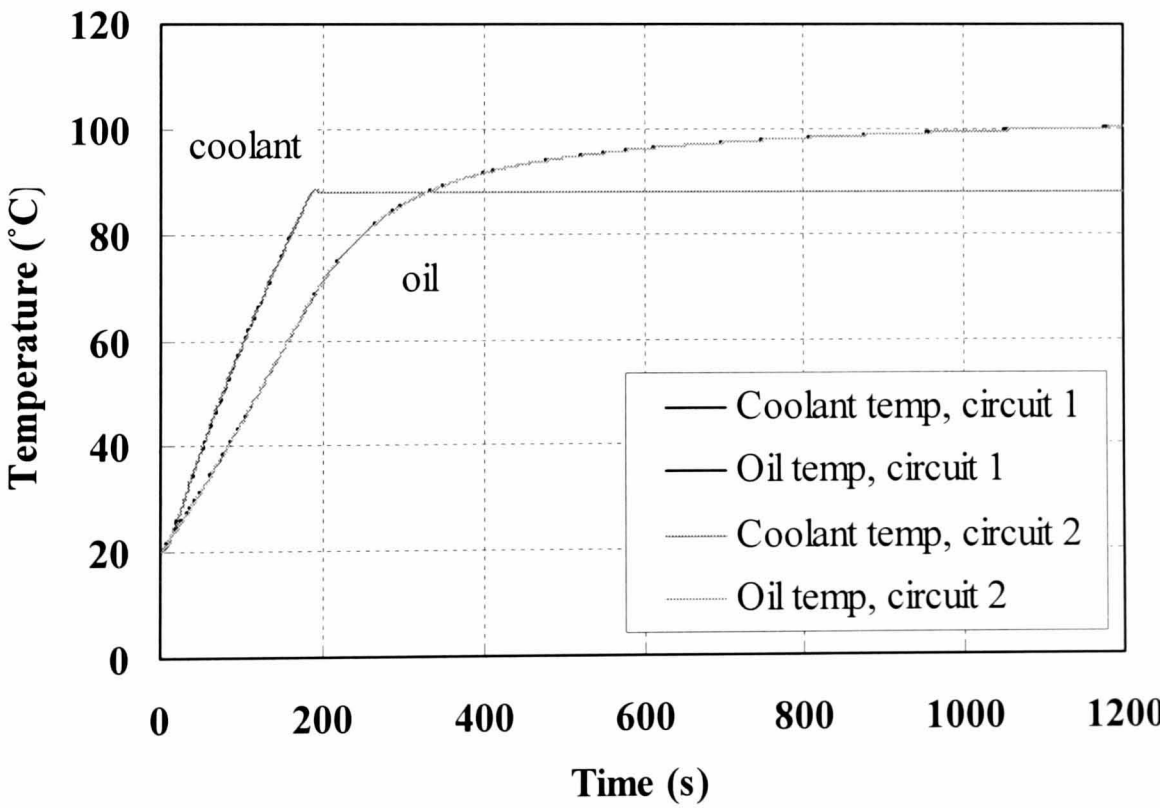
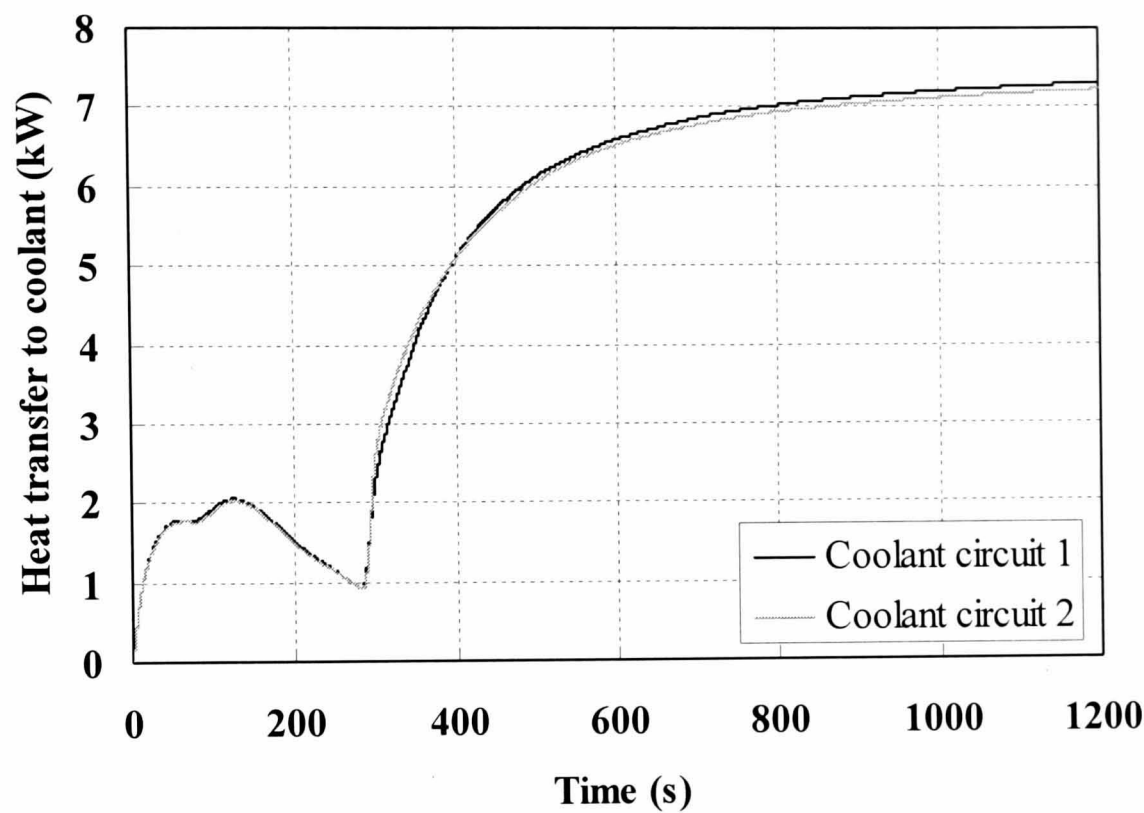


Figure 4.12 The effect of coolant circuit chosen for a multi-cylinder simulation at 3000 rpm, 5Nm on **a)** heat rejected to coolant and **b)** bulk coolant and oil temperatures.

a)



b)

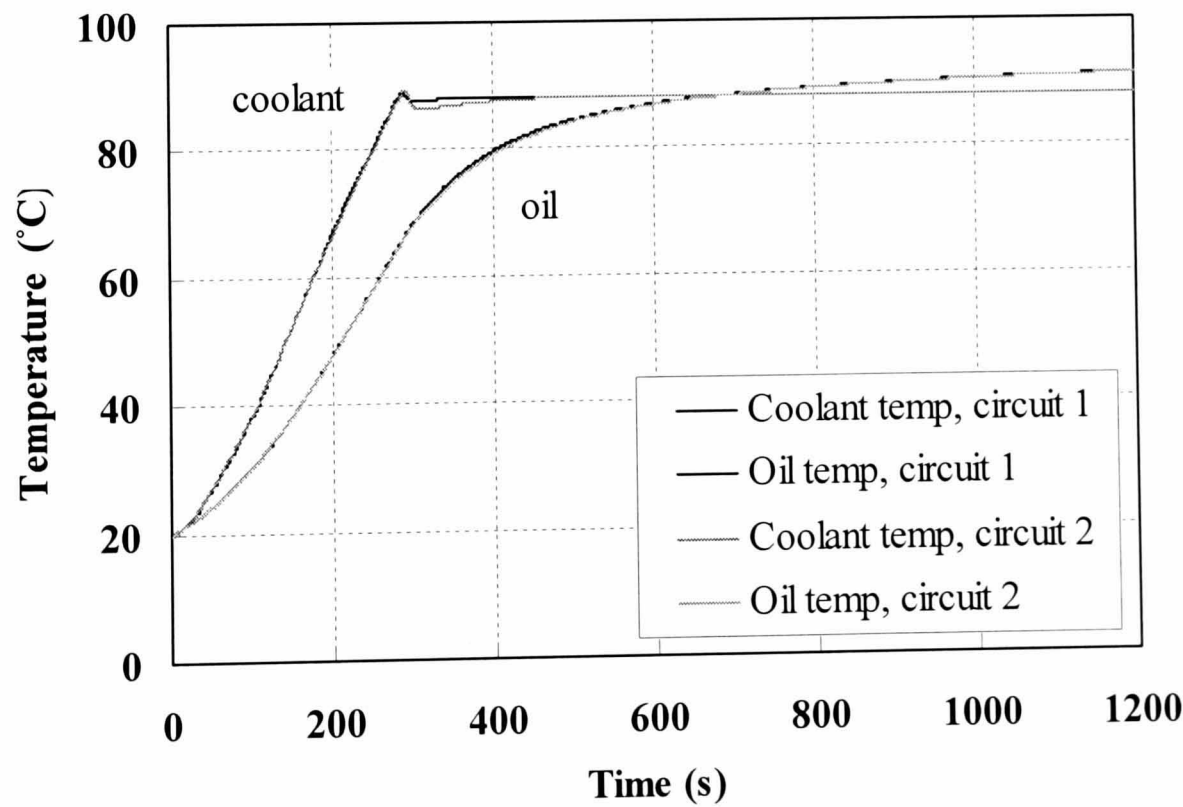


Figure 4.13 The effect of coolant circuit chosen for a multi-cylinder simulation at 1000 rpm, 120Nm on **a)** heat rejected to coolant and **b)** bulk coolant and oil temperatures.

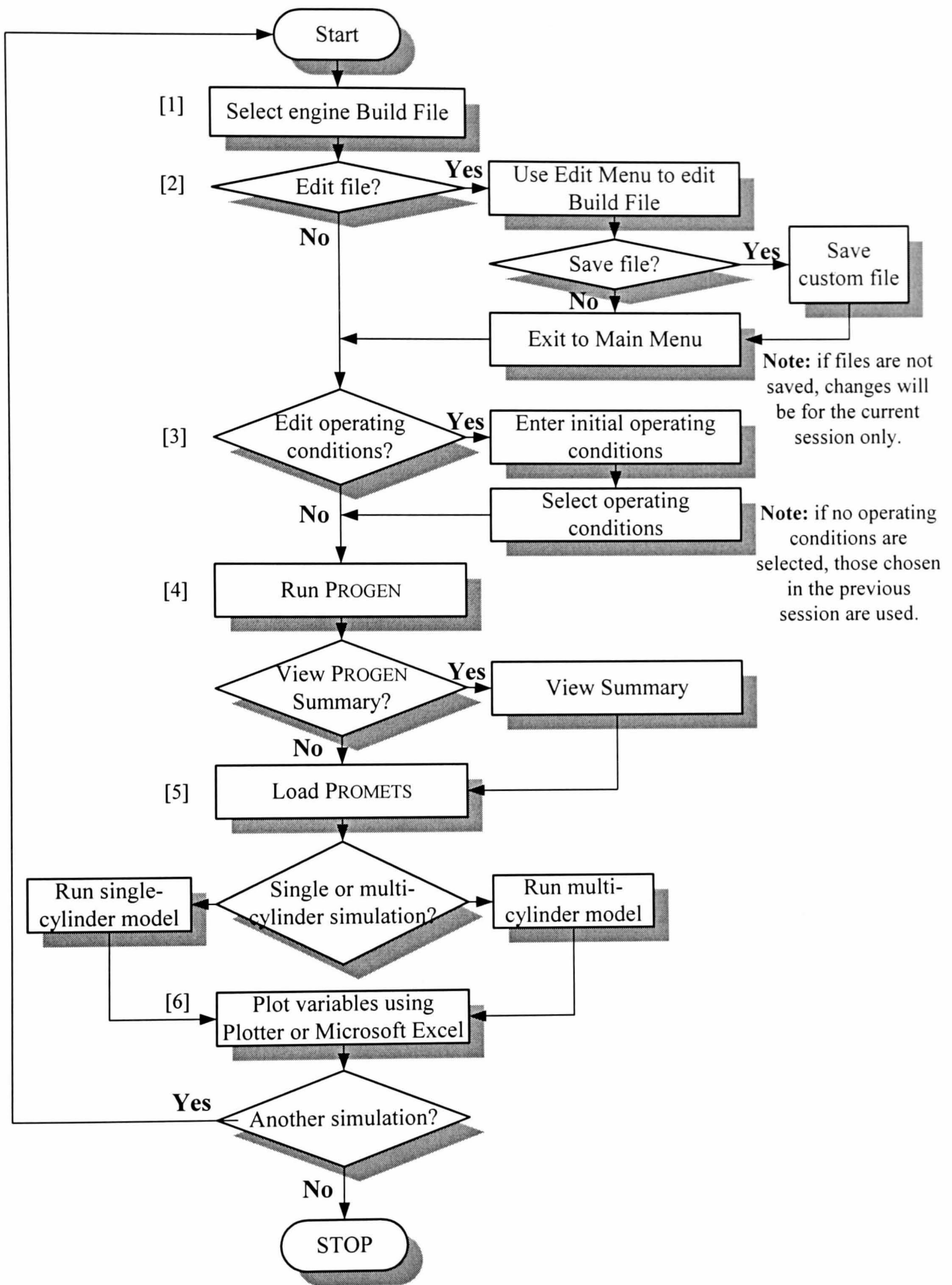


Figure 4.14 Flow diagram to illustrate a basic application of PROMETS. The numbers in square brackets indicate steps using the graphical user interface as shown in Figure 4.1.

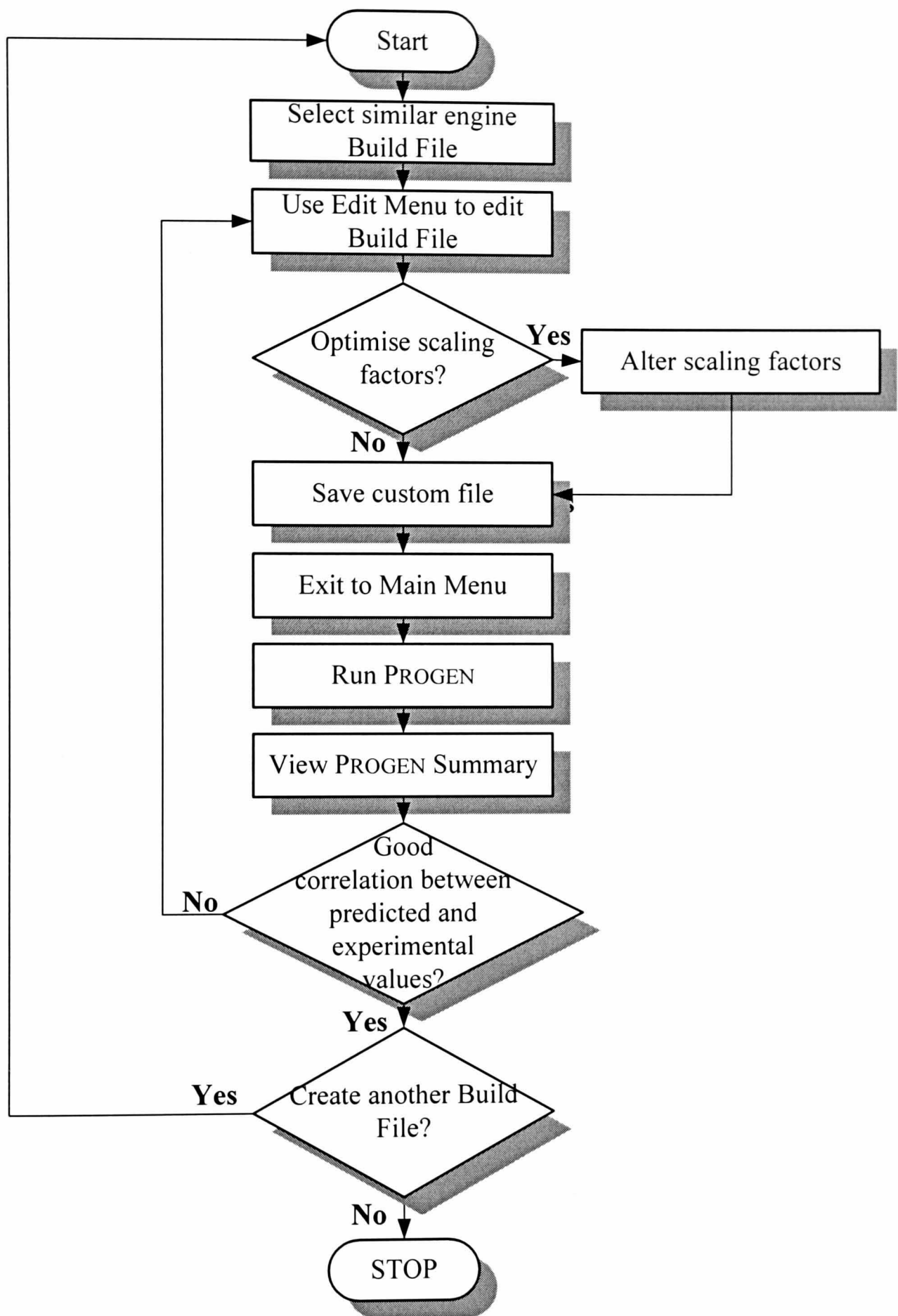


Figure 4.15 Flow diagram to illustrate the creation of a new engine build file in PROMETS.

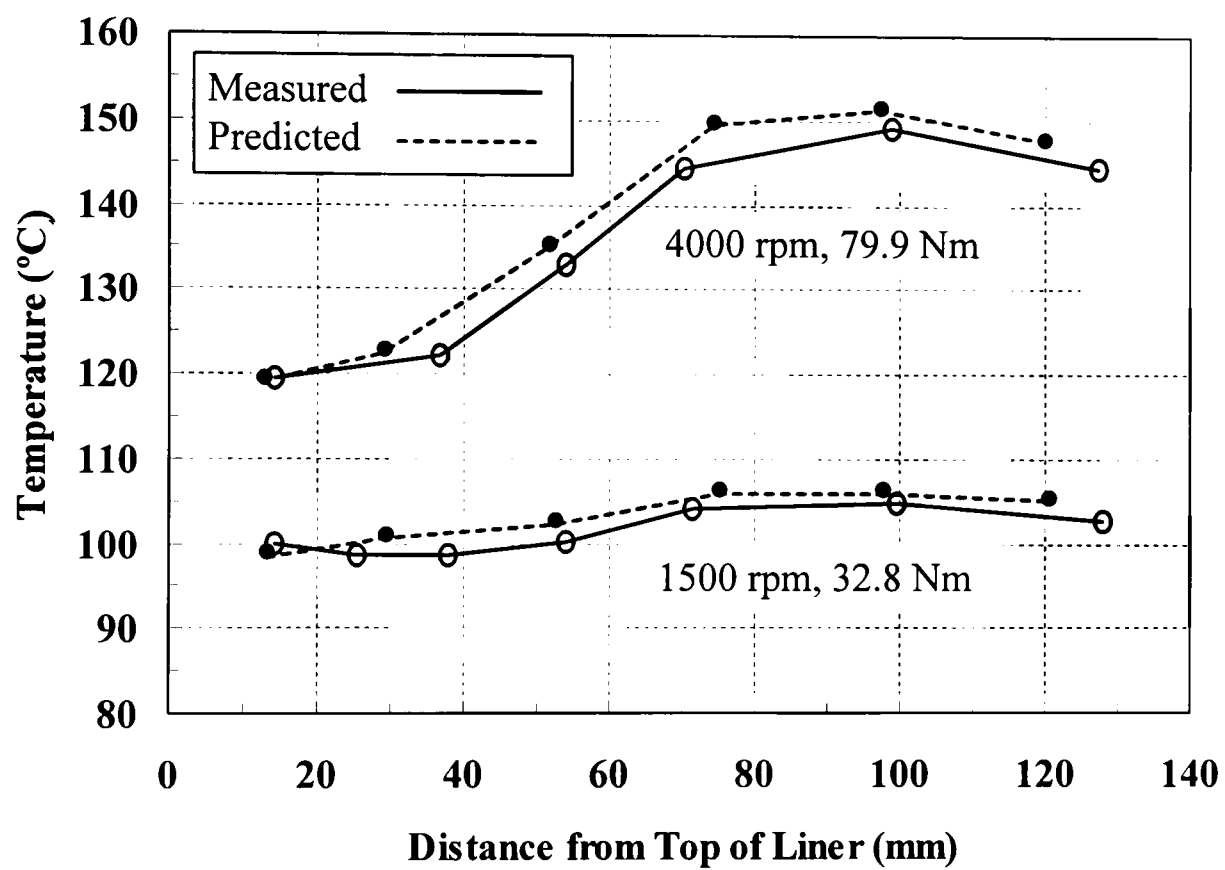


Figure 5.1 Temperature distributions along the liner, reproduced from [5.1].

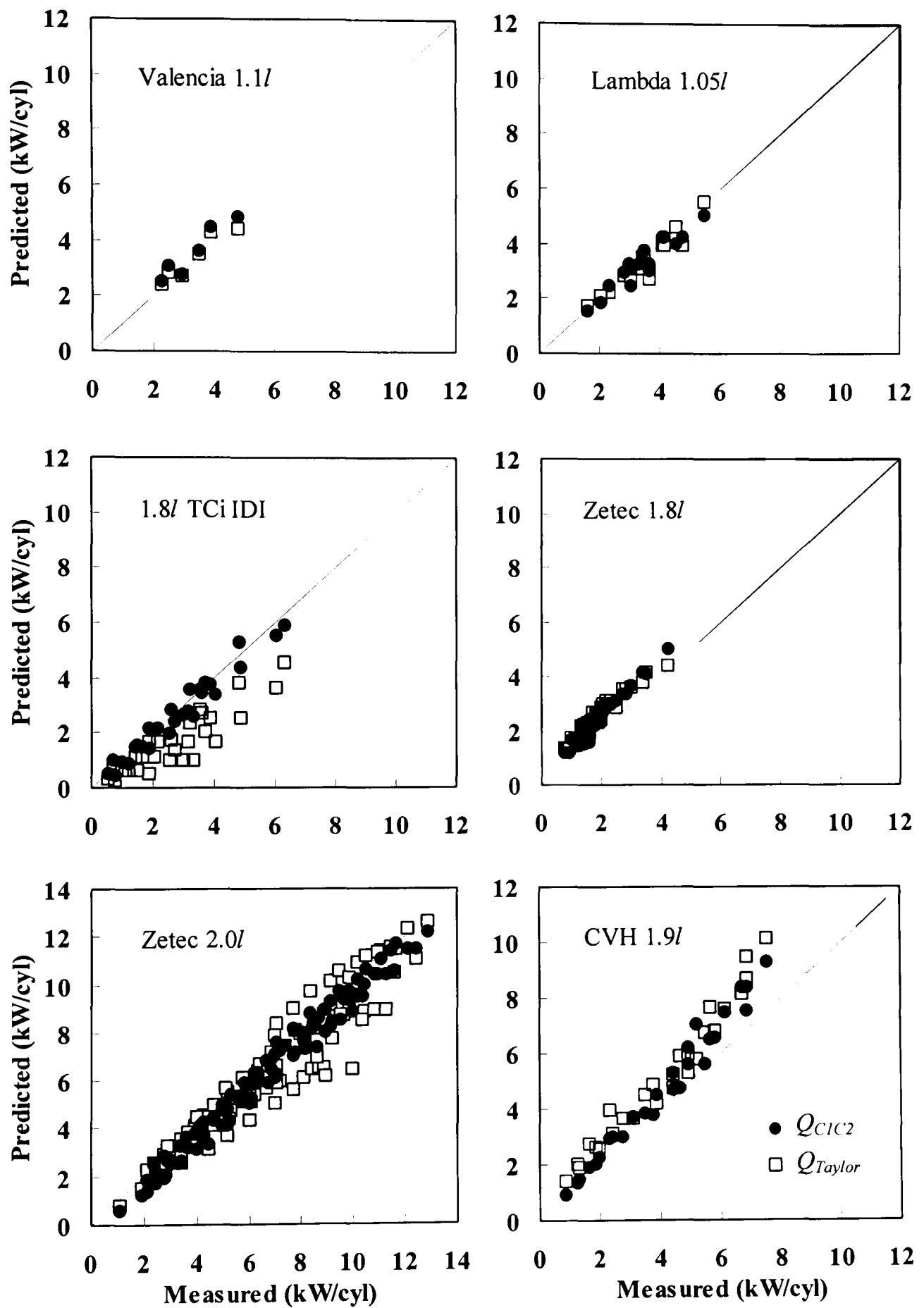


Figure 5.2 Comparison of measured and predicted values of heat rejection to coolant using Q_{CIC2} and Q_{Taylor} [5.11] for a range of engines and operating conditions, reproduced from [5.2].

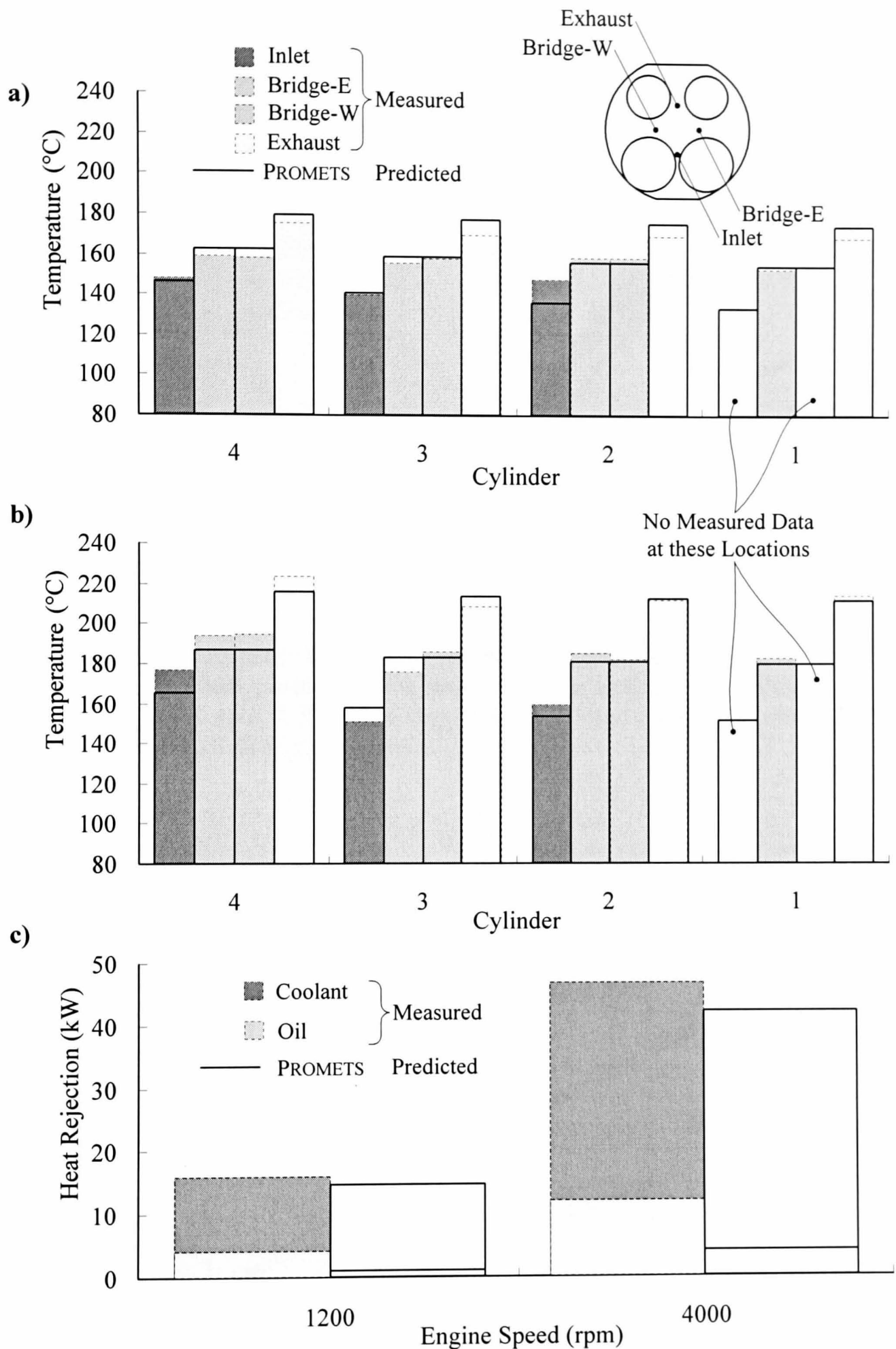


Figure 5.3 Measured (from a 2.26l gasoline engine [5.12]) and predicted local metal temperatures for the cylinder head combustion surfaces at **a)** 1200 rpm **b)** 4000 rpm **c)** measured and predicted oil and coolant heat rejection, reproduced from [5.3].

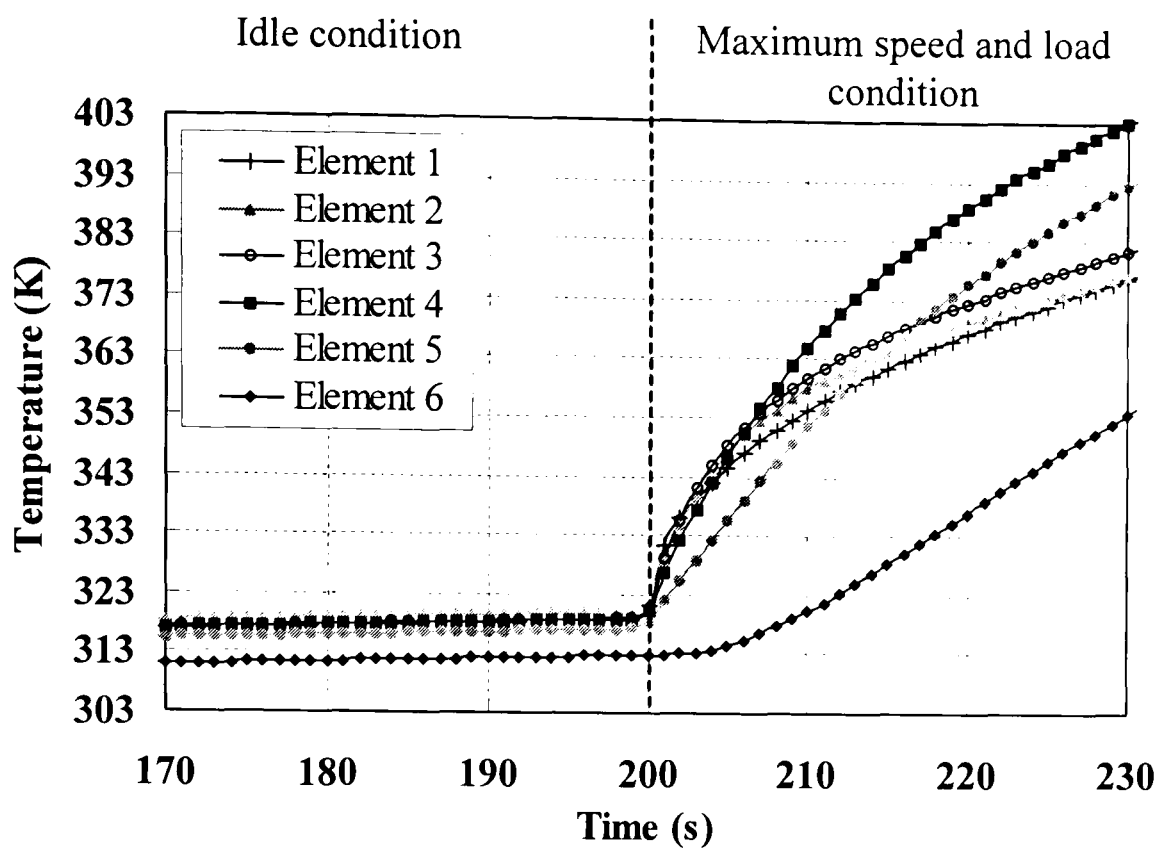


Figure 5.4 The response of element temperatures down the liner (see Figure 3.9 for element positions) to a step change in operating condition from idle (700 rpm, 4.3 Nm) to maximum speed and load (6000 rpm, 120 Nm) for a 1.6l Sigma engine.

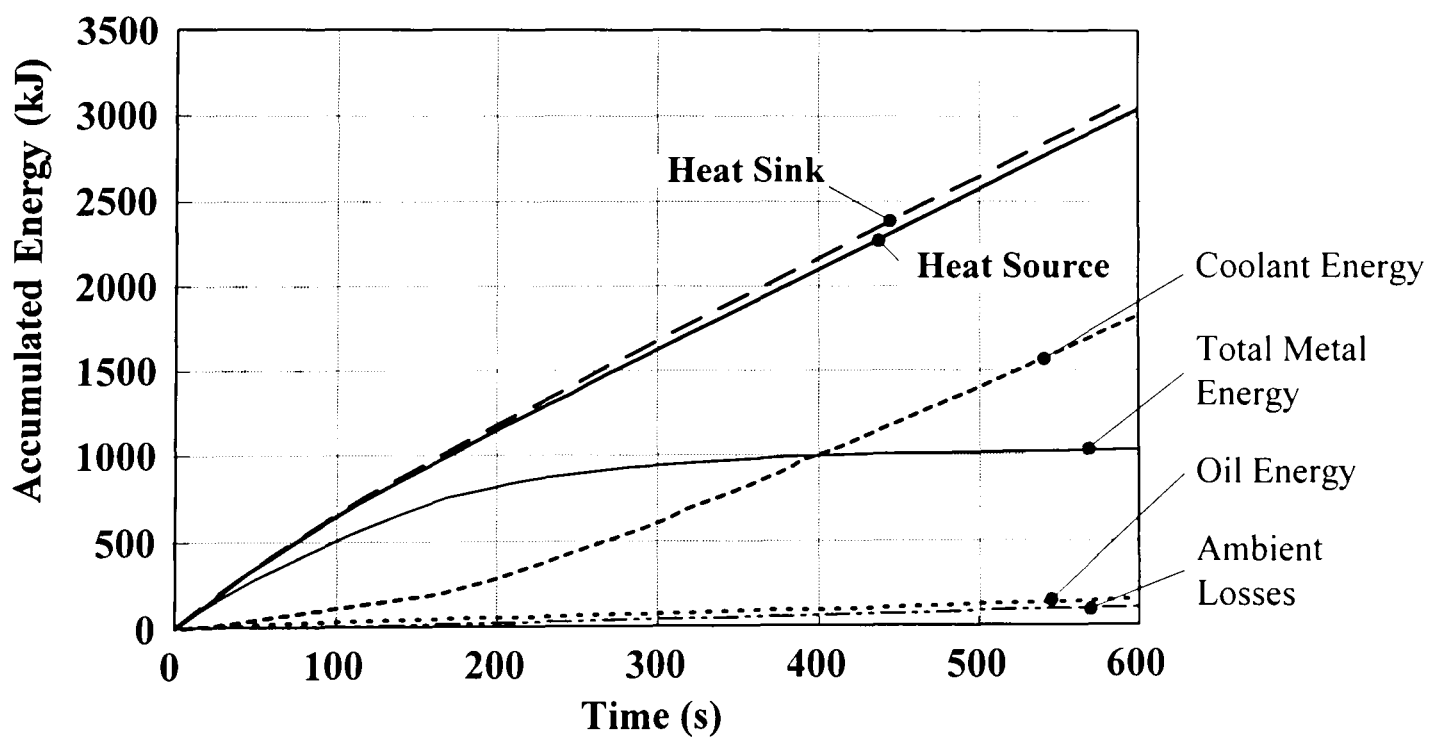


Figure 5.5 Model self-consistency test for PROMETS, for a 2.5l V6 engine at 3000 rpm, 120 Nm. The difference between the accumulated energy source and energy sink is 2.4% at 600 seconds.

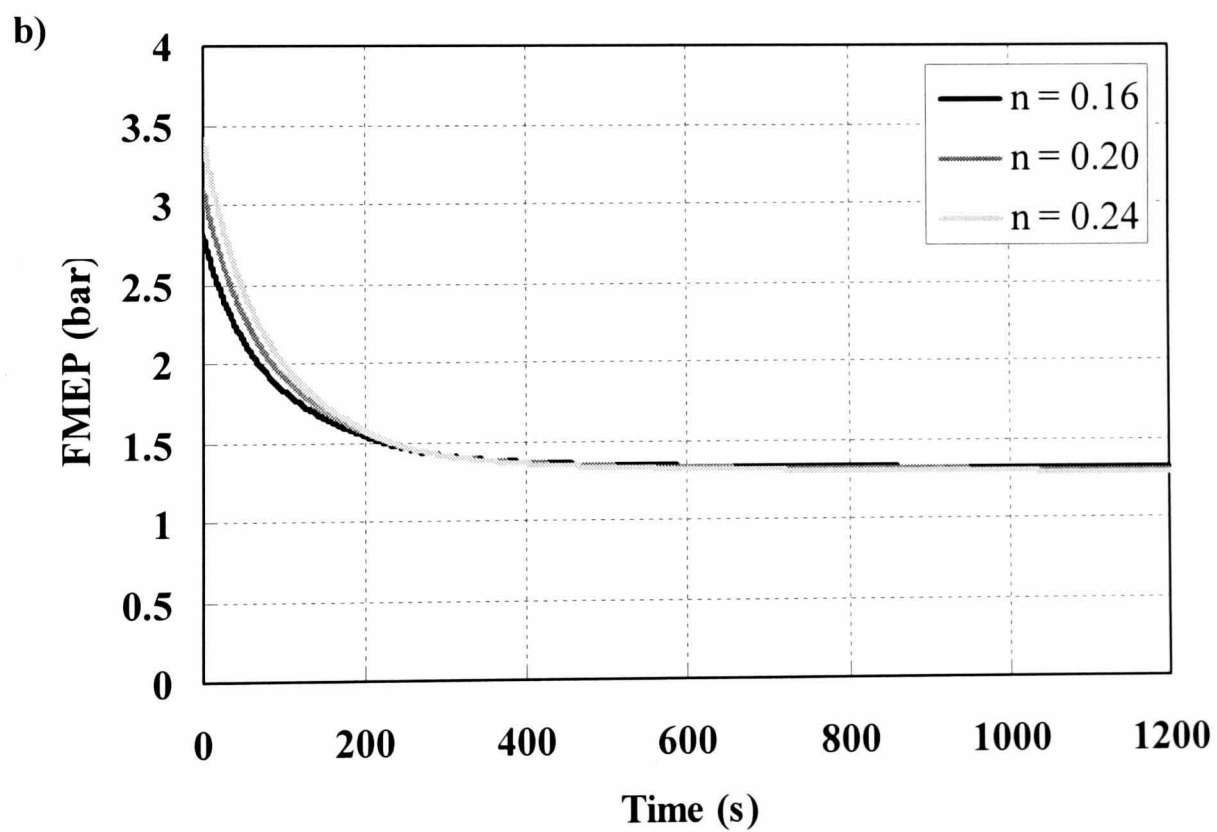
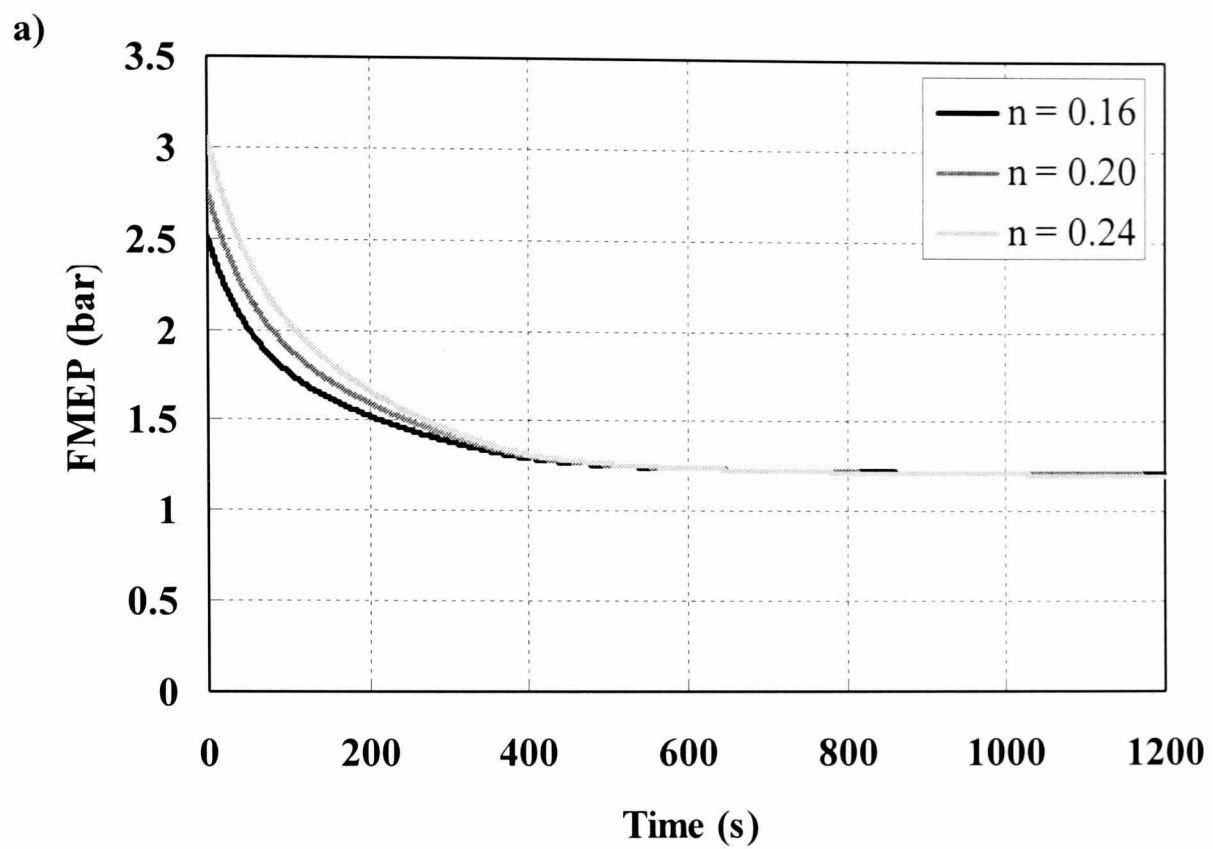


Figure 5.6 Effect of the friction index, n , on FMEP at a) 1000 rpm, 120 Nm, and b) 3000 rpm, 5 Nm.

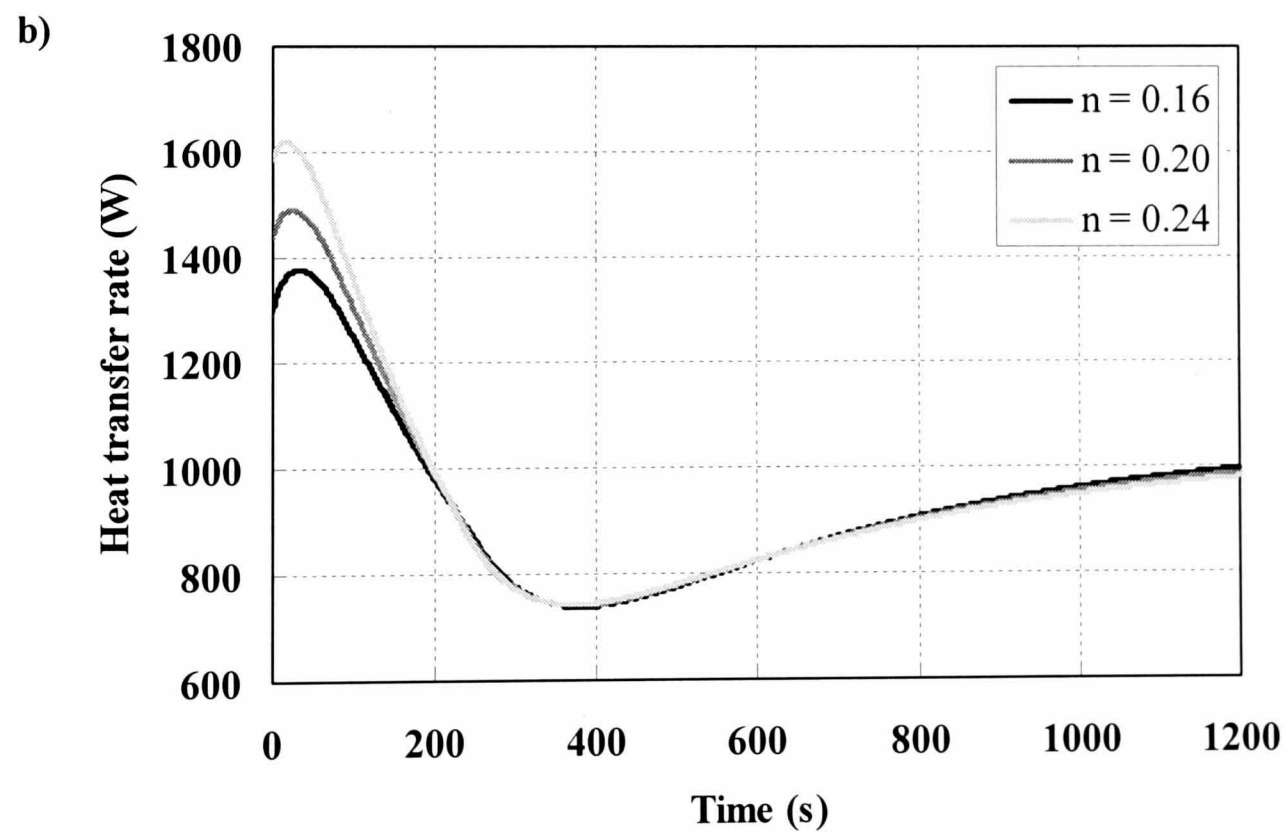
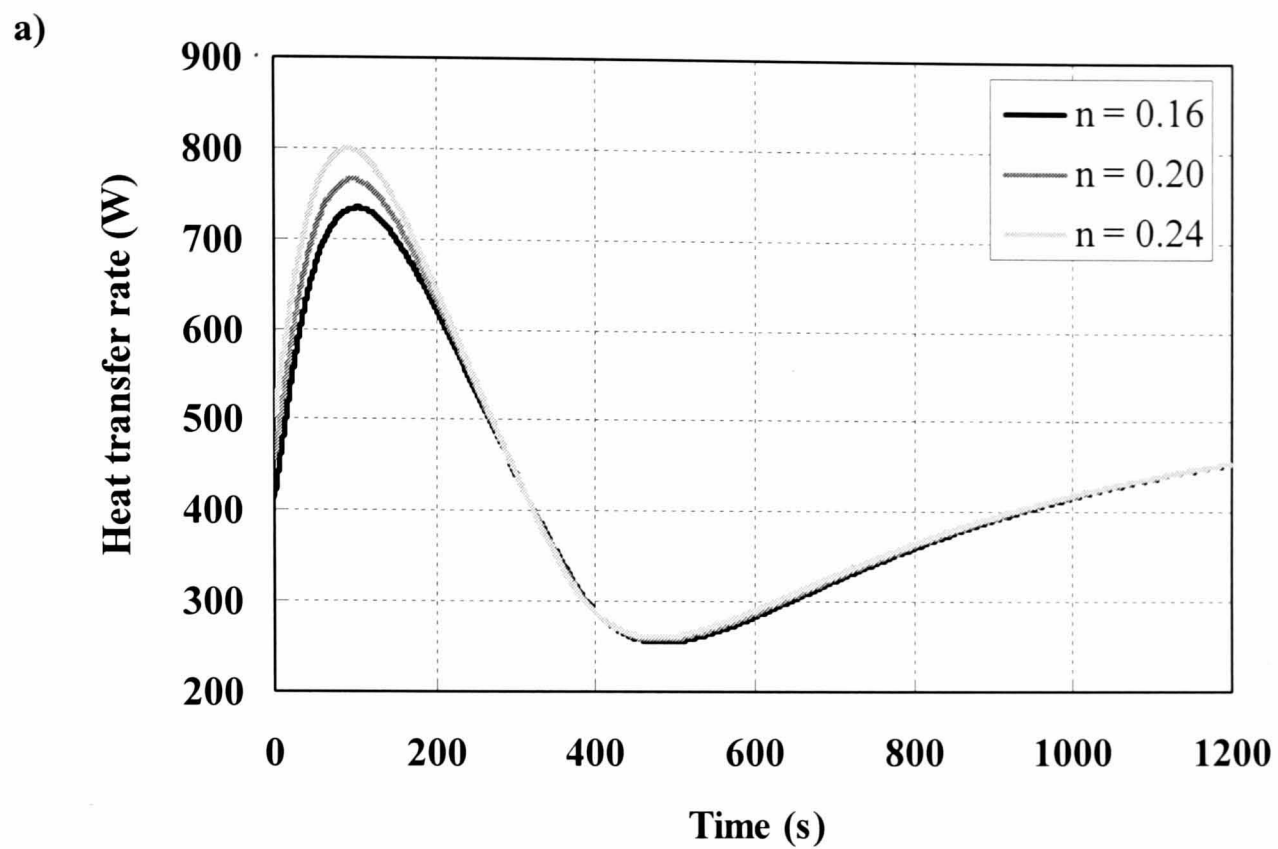
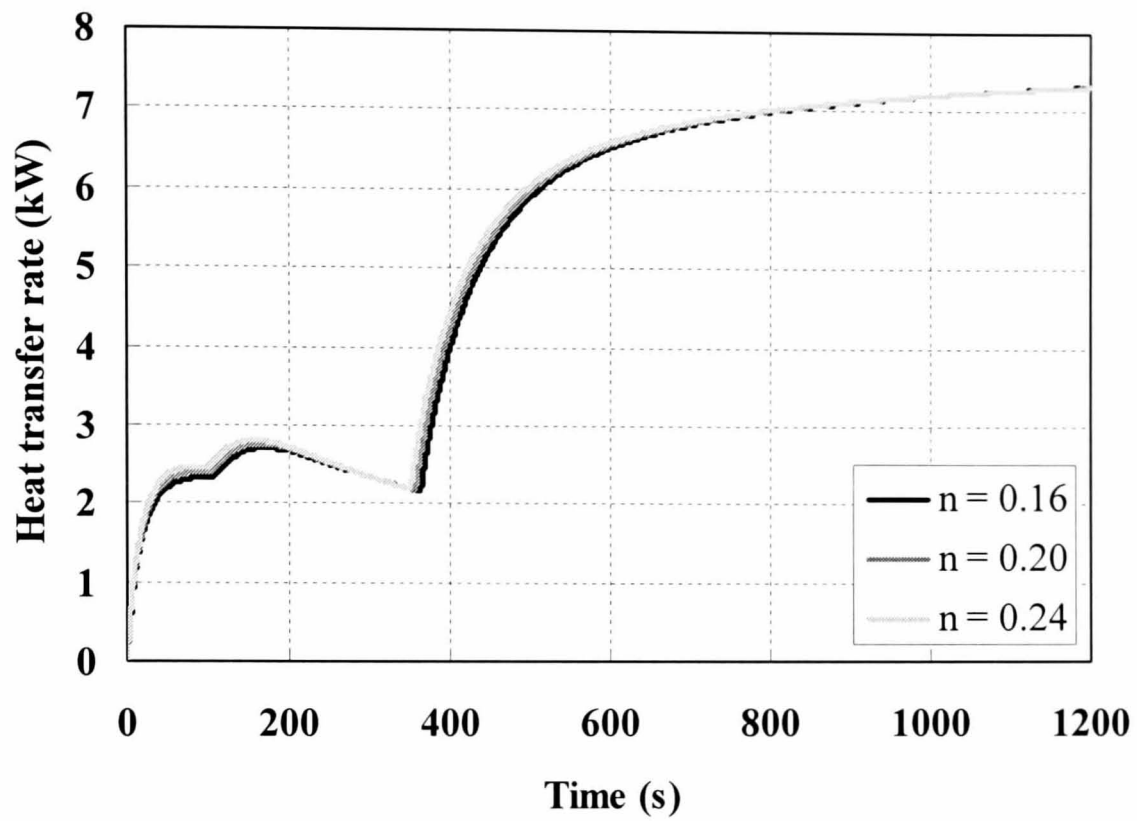


Figure 5.7 Effect of the friction index, n , on the net heat transfer rate to the oil, comprising of the heat transferred from the structure, frictional heat retained in the oil and heat transferred to or from the coolant, at **a)** 1000 rpm, 120, and **b)** 3000 rpm, 5 Nm.

a)



b)

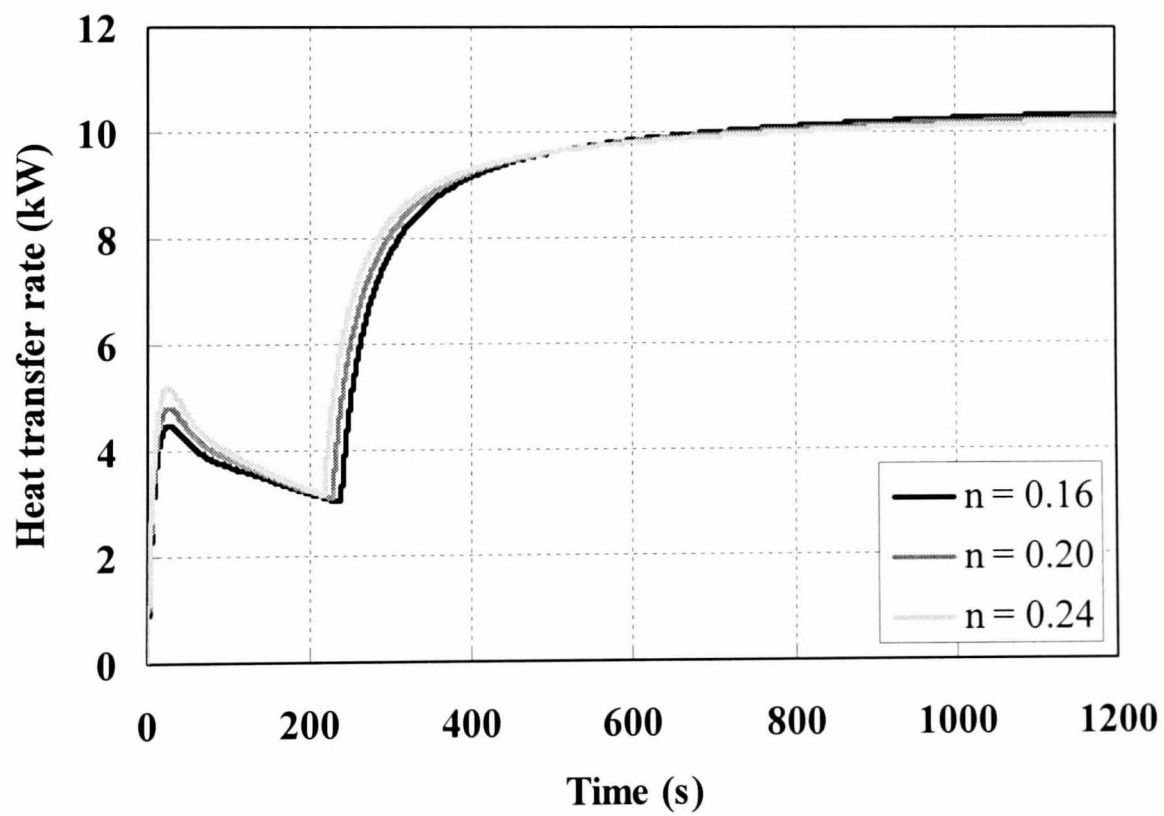


Figure 5.8 Effect of the friction index, n , on the total heat transfer rate to the coolant at a) 1000 rpm, 120, and b) 3000 rpm, 5 Nm.

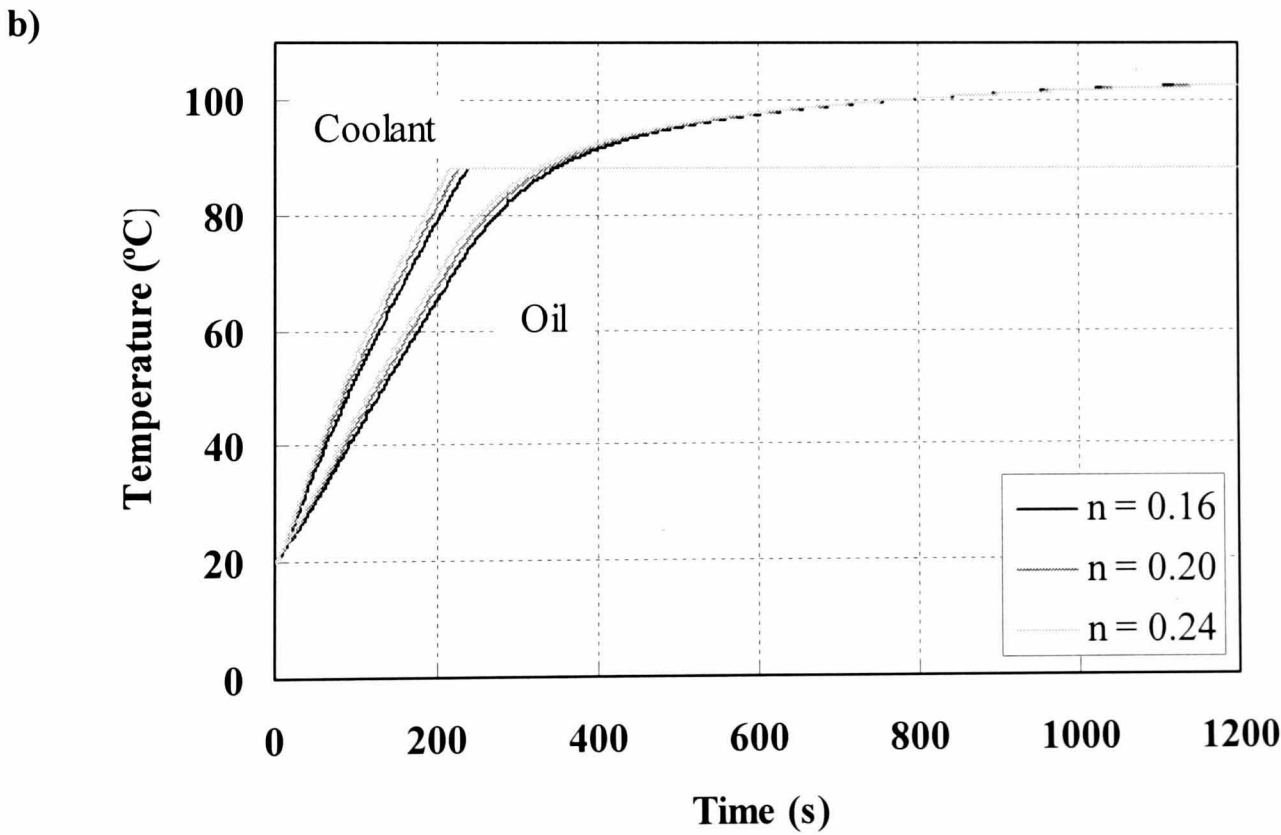
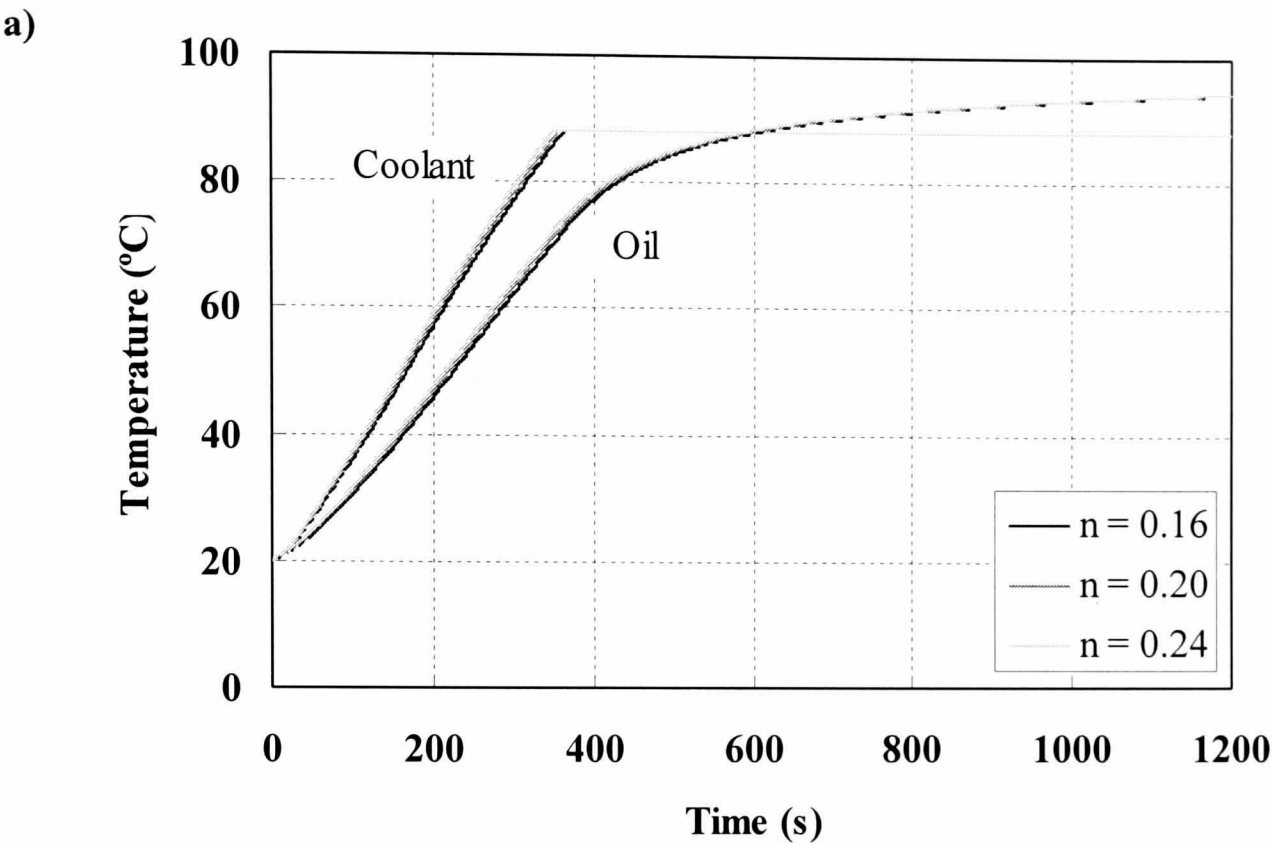


Figure 5.9 Effect of the friction index, n , on bulk coolant and oil temperatures at a) 1000 rpm, 120, and b) 3000 rpm, 5 Nm.

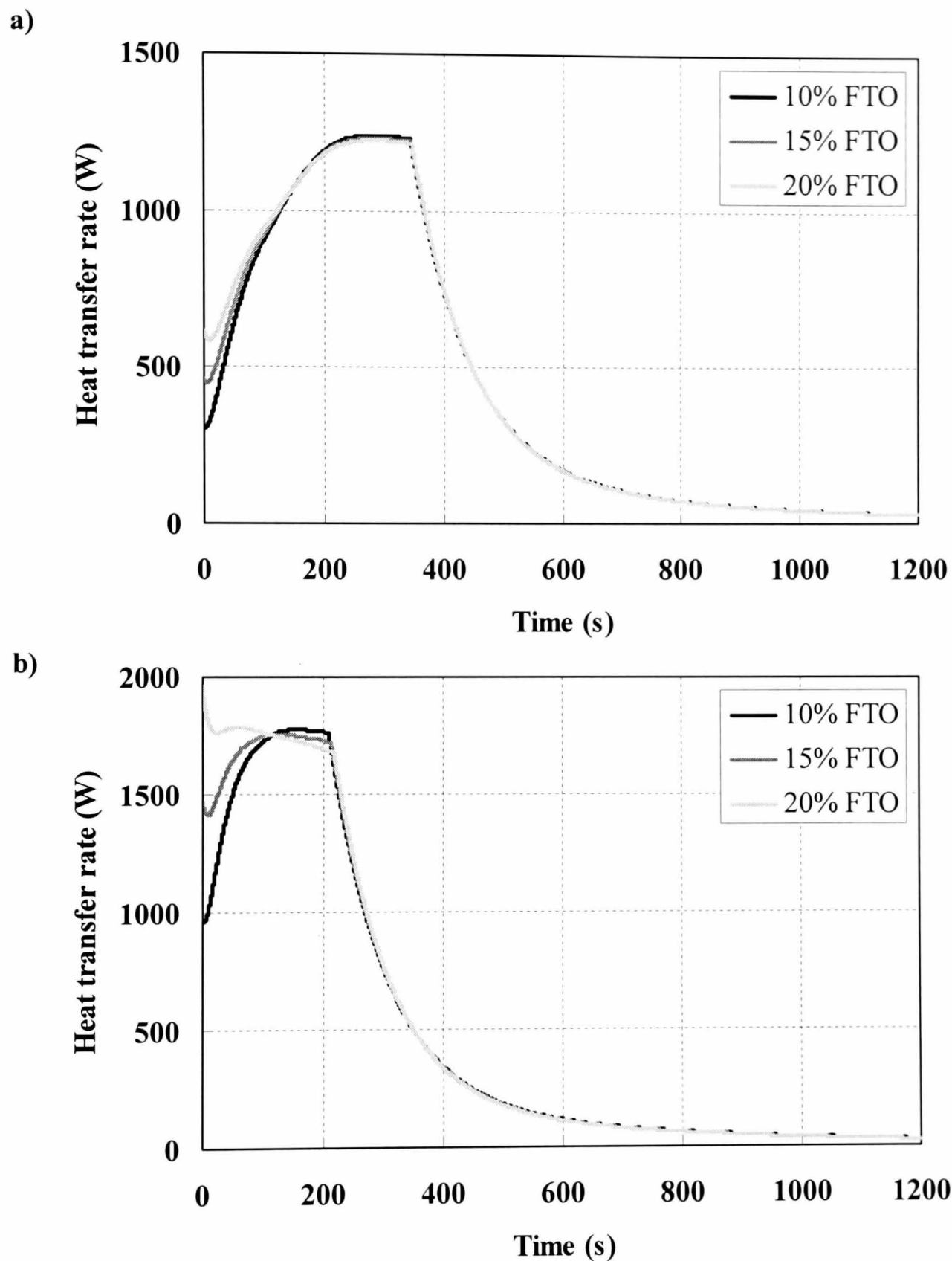


Figure 5.10 Effect of the percentage of friction dissipated in the oil (FTO) on the net heat transfer rate to the oil, comprising of the heat transferred from the structure, frictional heat retained in the oil and heat transferred to or from the coolant, at **a)** 1000 rpm, 120, and **b)** 3000 rpm, 5 Nm.

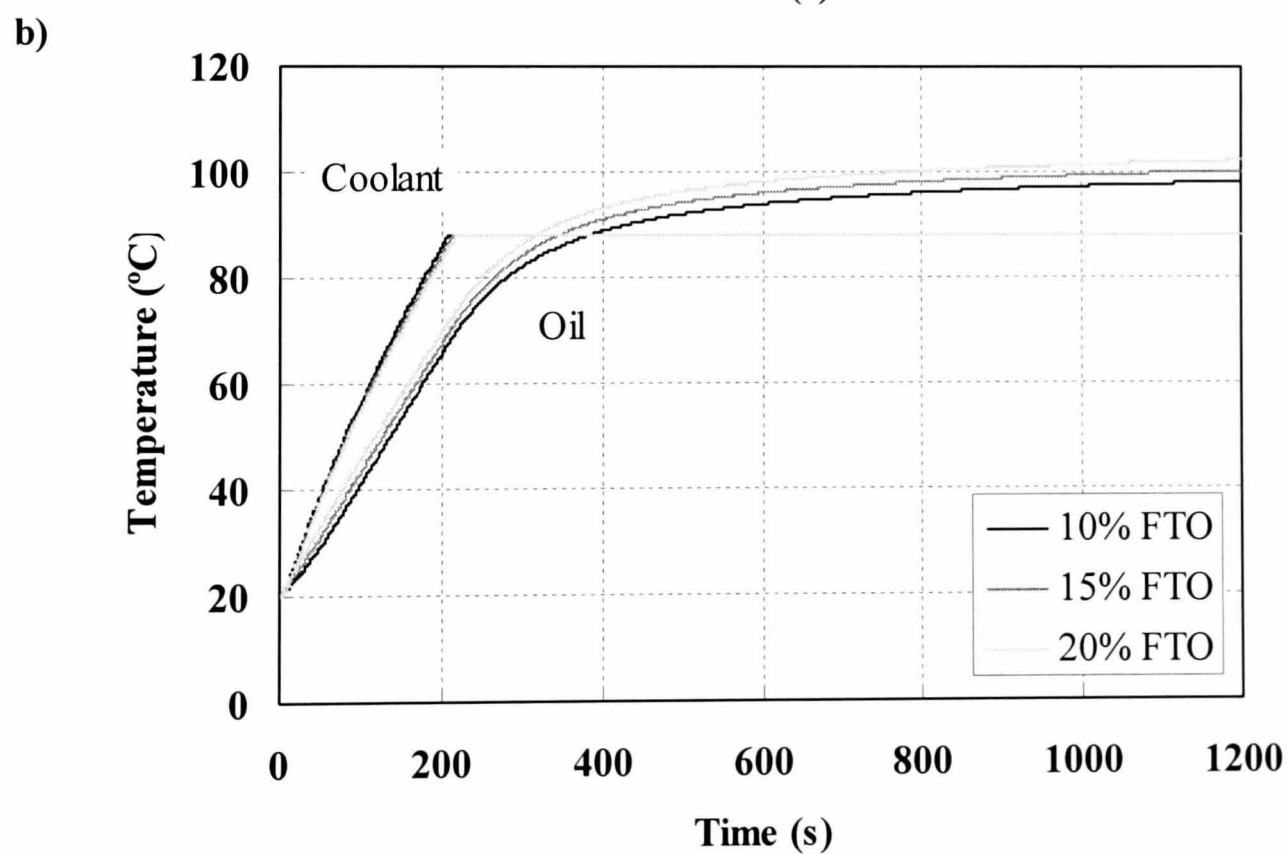
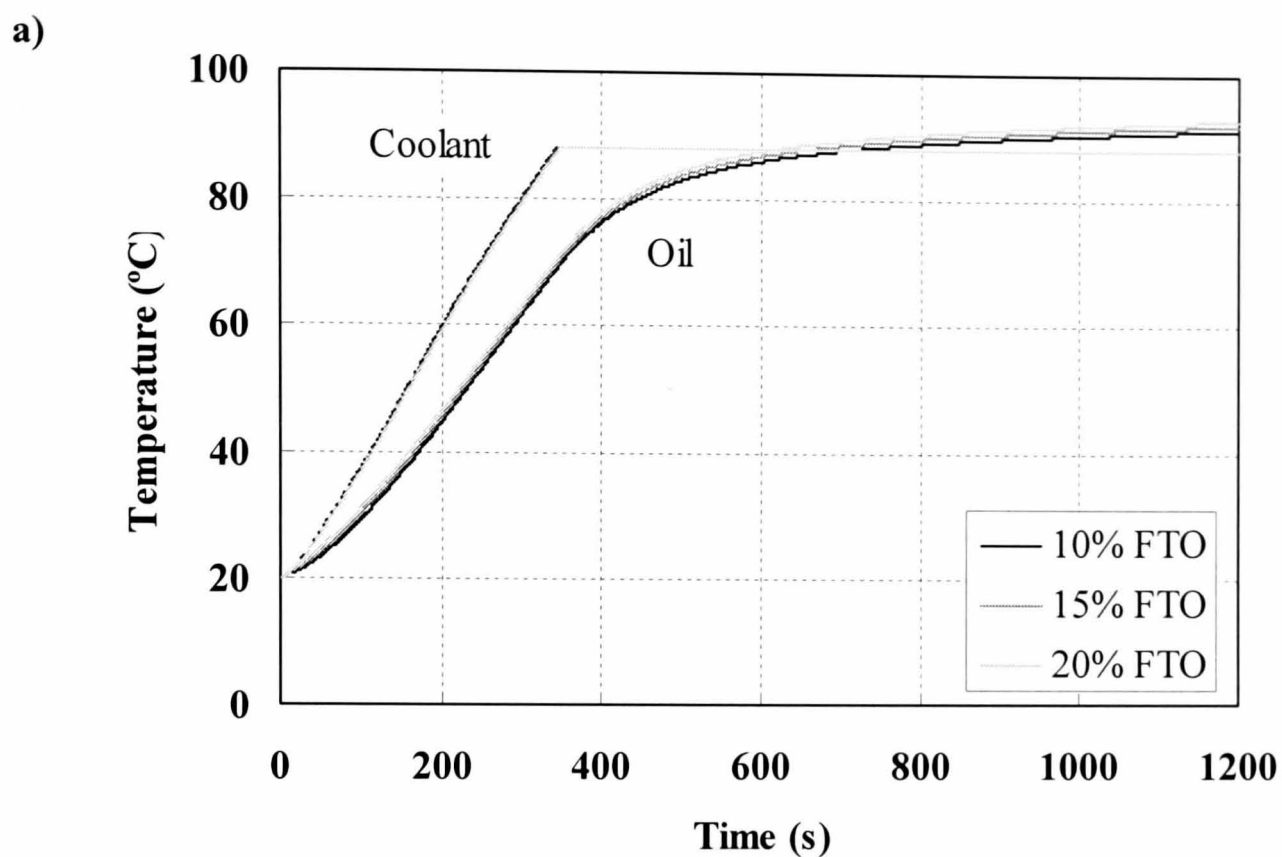


Figure 5.11 Effect of the percentage of friction dissipated in the oil (FTO) on the bulk coolant and oil temperatures at **a)** 1000 rpm, 120, and **b)** 3000 rpm, 5 Nm.

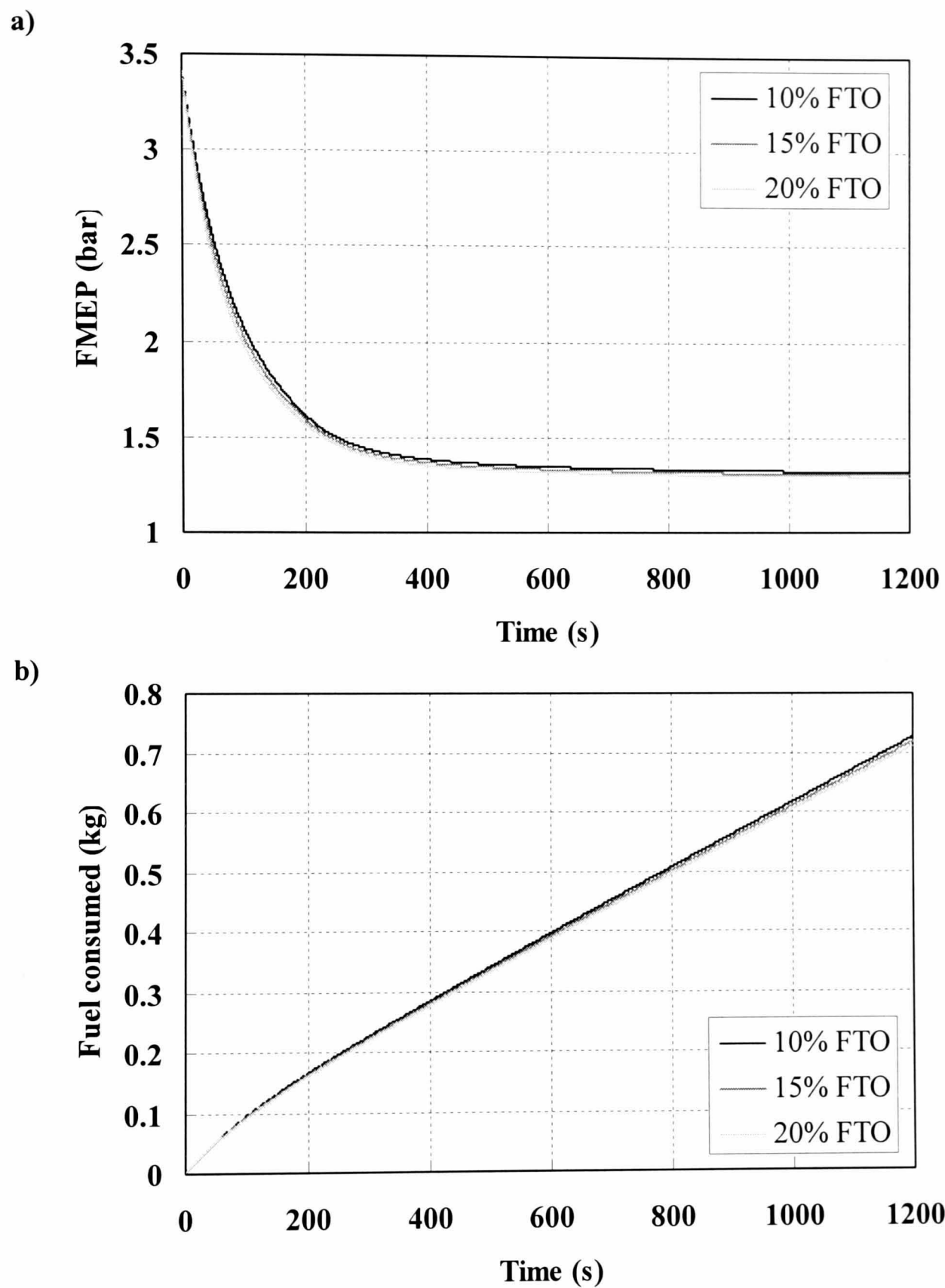


Figure 5.12 Effect of the percentage of friction dissipated in the oil on a) FMEP and b) fuel consumed over 1200 seconds at 3000 rpm, 5 Nm.

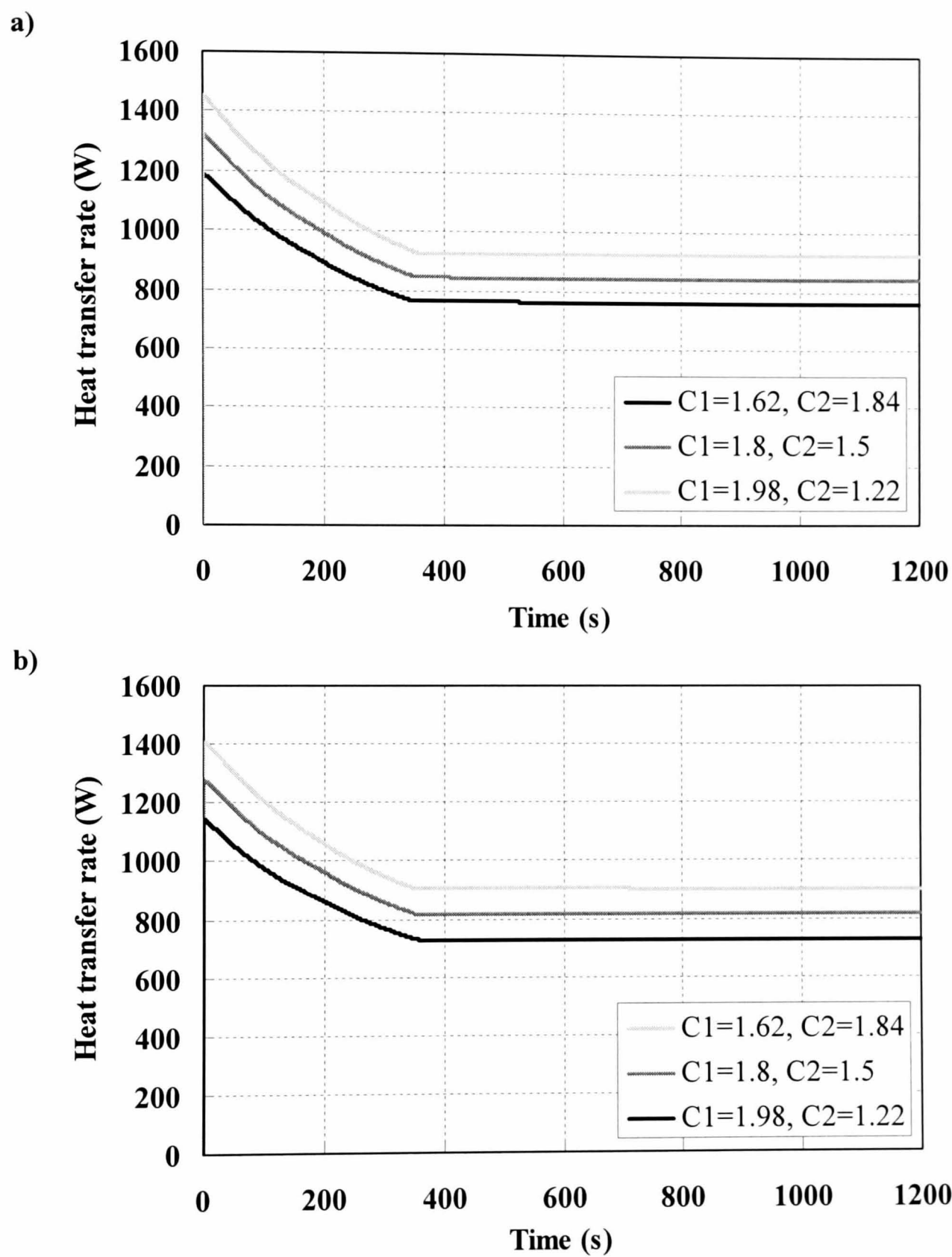


Figure 5.13 Effect of the values of the gas-side heat transfer coefficients, $C1$ and $C2$, on **a)** the heat transfer rate to the cylinder, and **b)** the heat transfer rate to the exhaust port at 1000 rpm, 120 Nm.

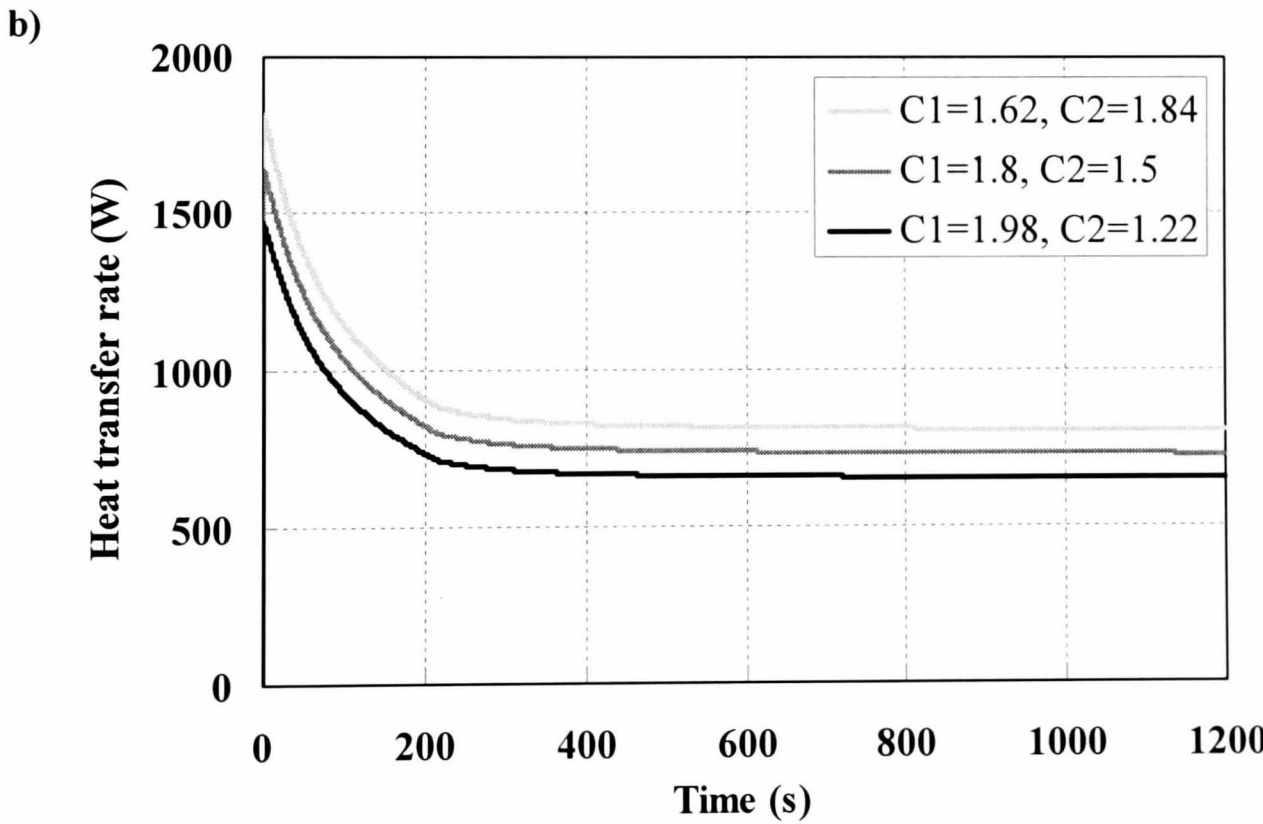
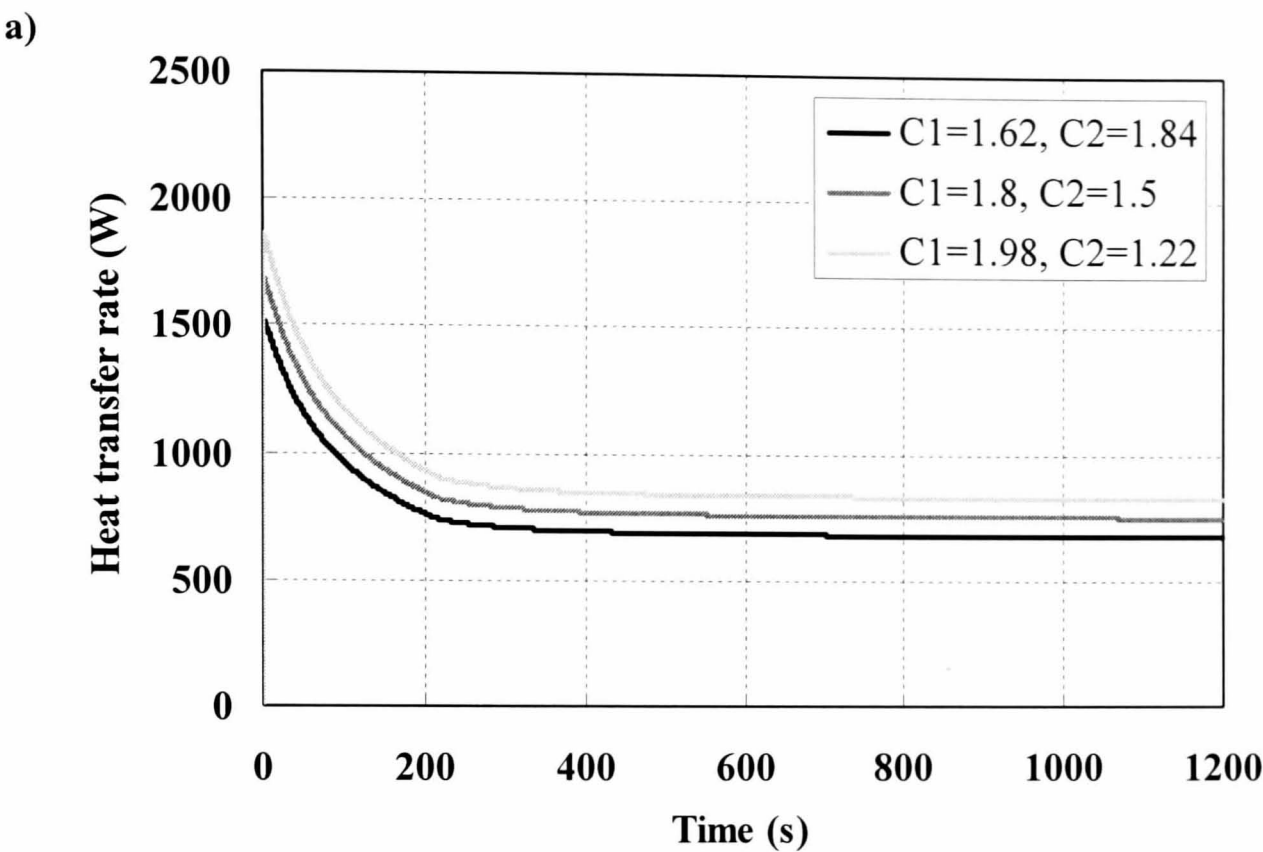


Figure 5.14 Effect of the values of the gas-side heat transfer coefficients, $C1$ and $C2$, on a) the heat transfer rate to the cylinder, and b) the heat transfer rate to the exhaust port at 3000 rpm, 5 Nm.

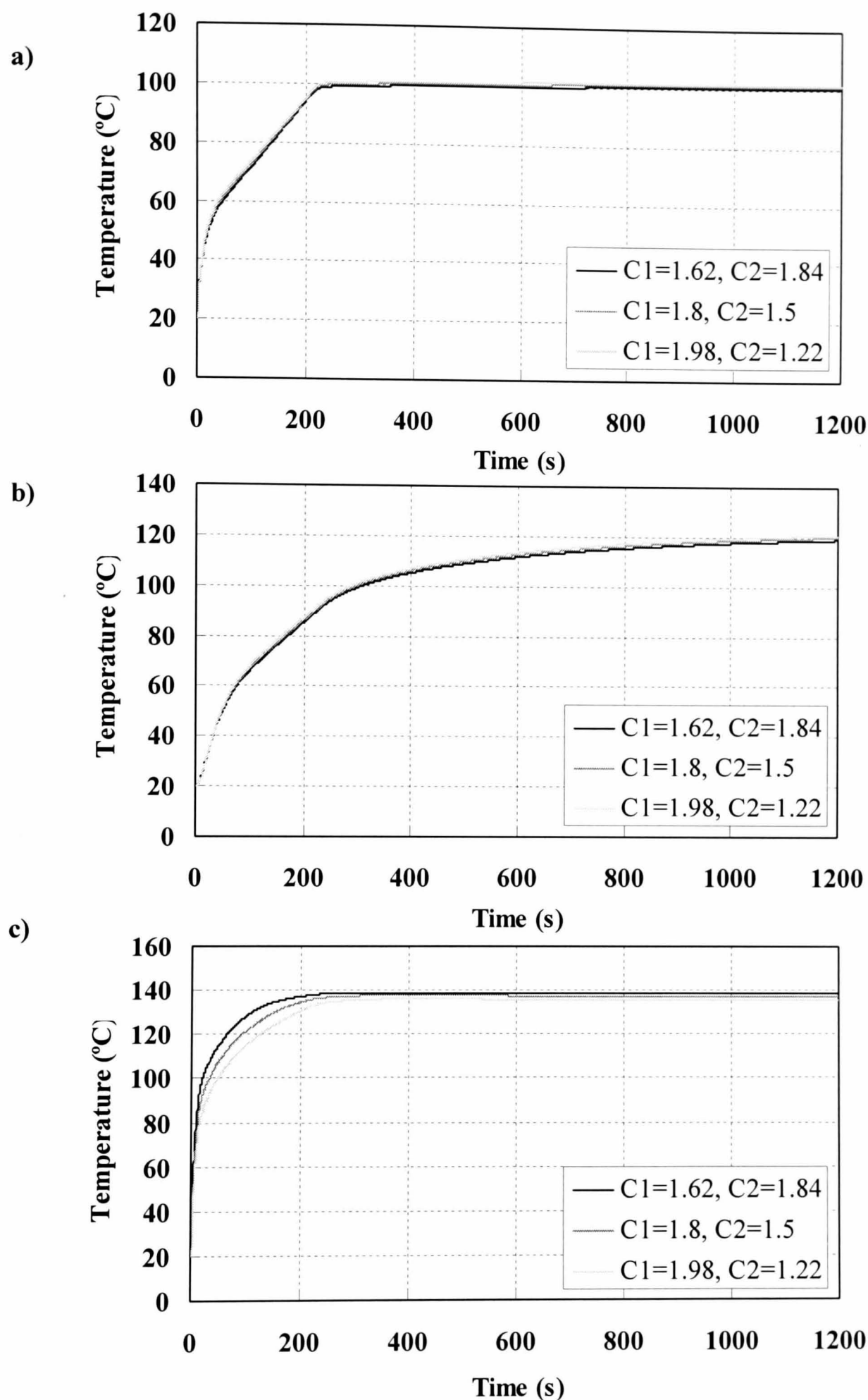


Figure 5.15 Effect of the values of the gas-side heat transfer coefficients, $C1$ and $C2$, on **a)** liner temperature, top of the liner (element 1), **b)** liner temperature, bottom of the liner (element 6) and **c)** exhaust port temperature (element 20) at 1000 rpm, 120 Nm.

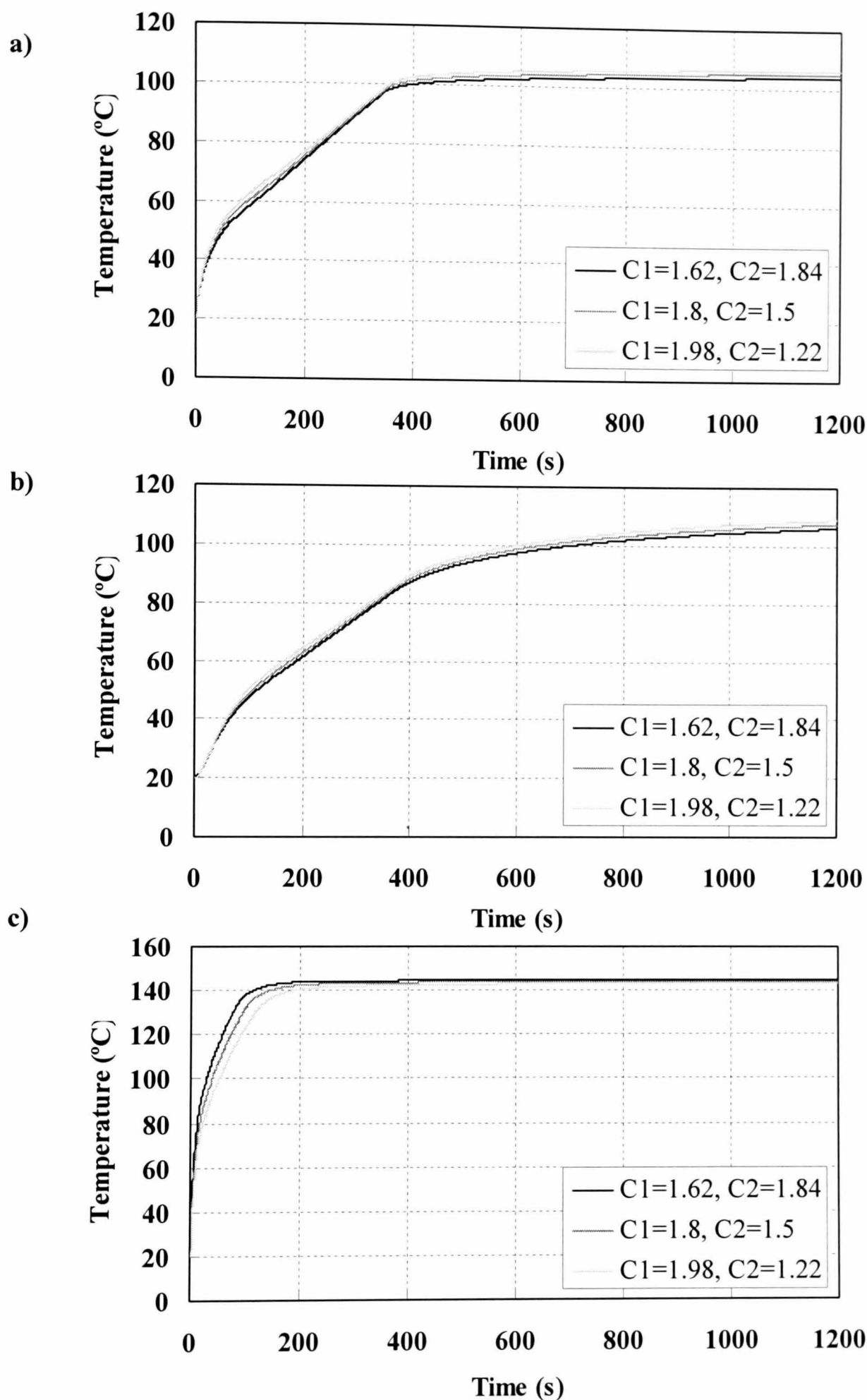
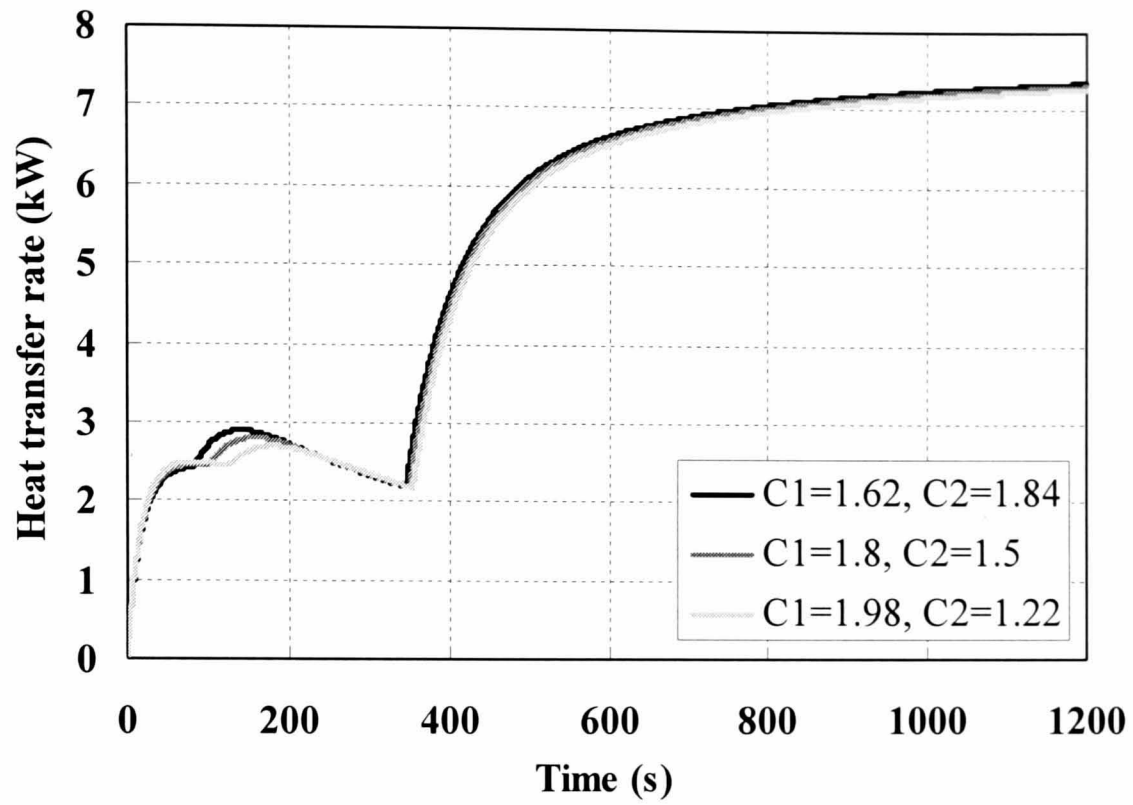


Figure 5.16 Effect of the values of the gas-side heat transfer coefficients, $C1$ and $C2$, on **a)** liner temperature, top of the liner (element 1), **b)** liner temperature, bottom of the liner (element 6) and **c)** exhaust port temperature (element 20) at 3000 rpm, 5 Nm.

a)



b)

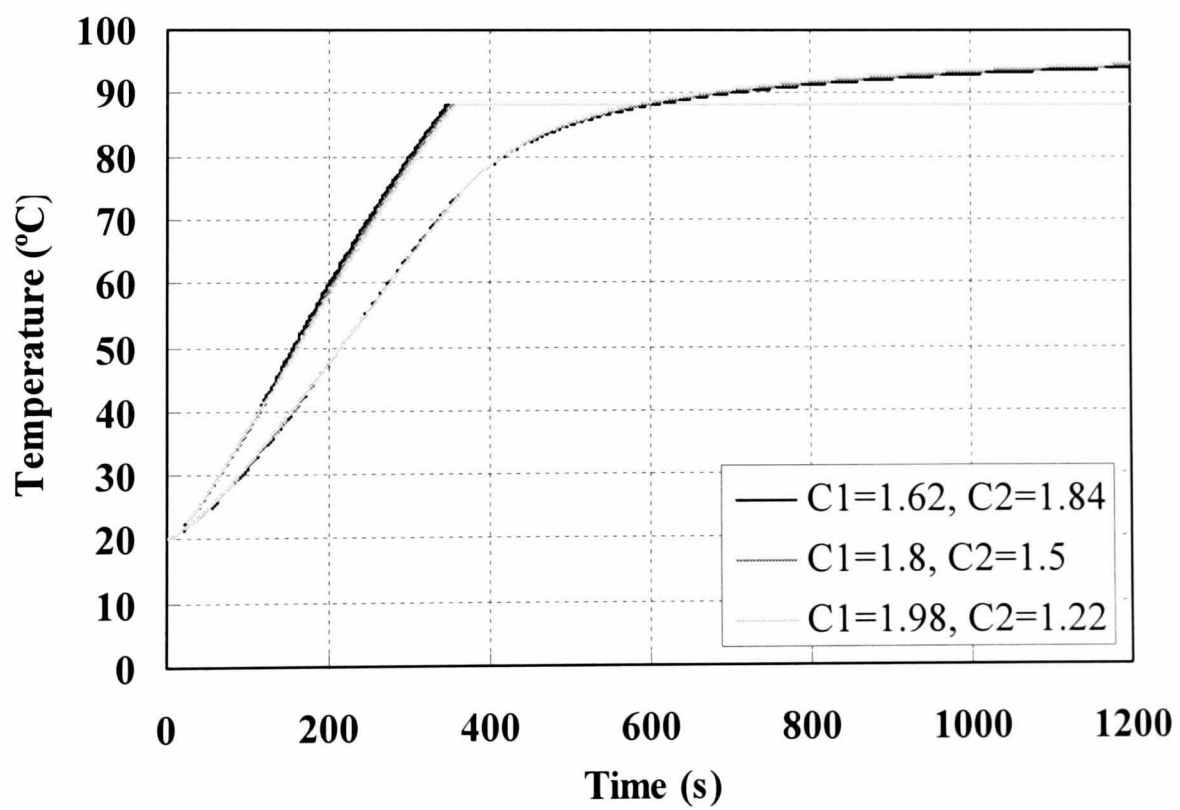


Figure 5.17 Effect of the values of the gas-side heat transfer coefficients, $C1$ and $C2$, on **a)** the heat transfer rate to the coolant and **b)** bulk coolant and oil temperatures at 1000 rpm, 120 Nm.

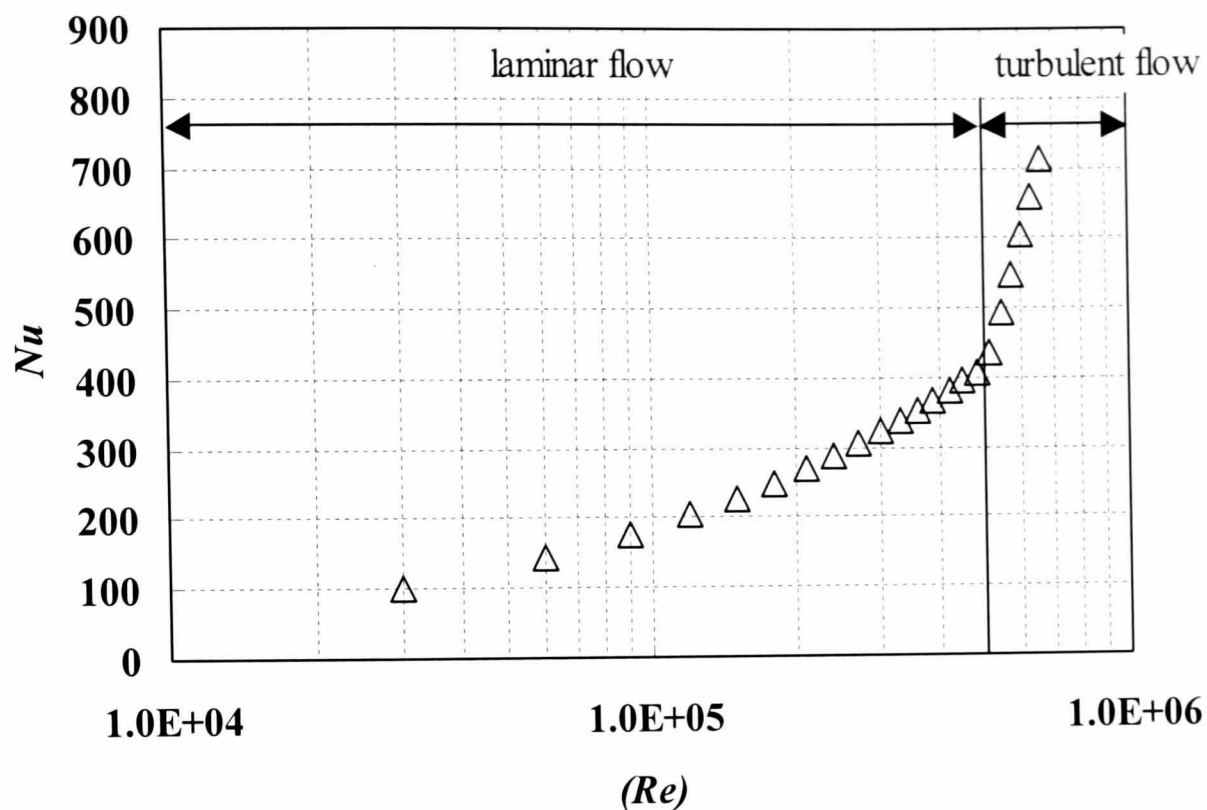


Figure 5.18 Illustration of Nusselt-Reynolds correlations for forced convection over a flat plate using Equations 5.6 and 5.7 for laminar and turbulent flow respectively.

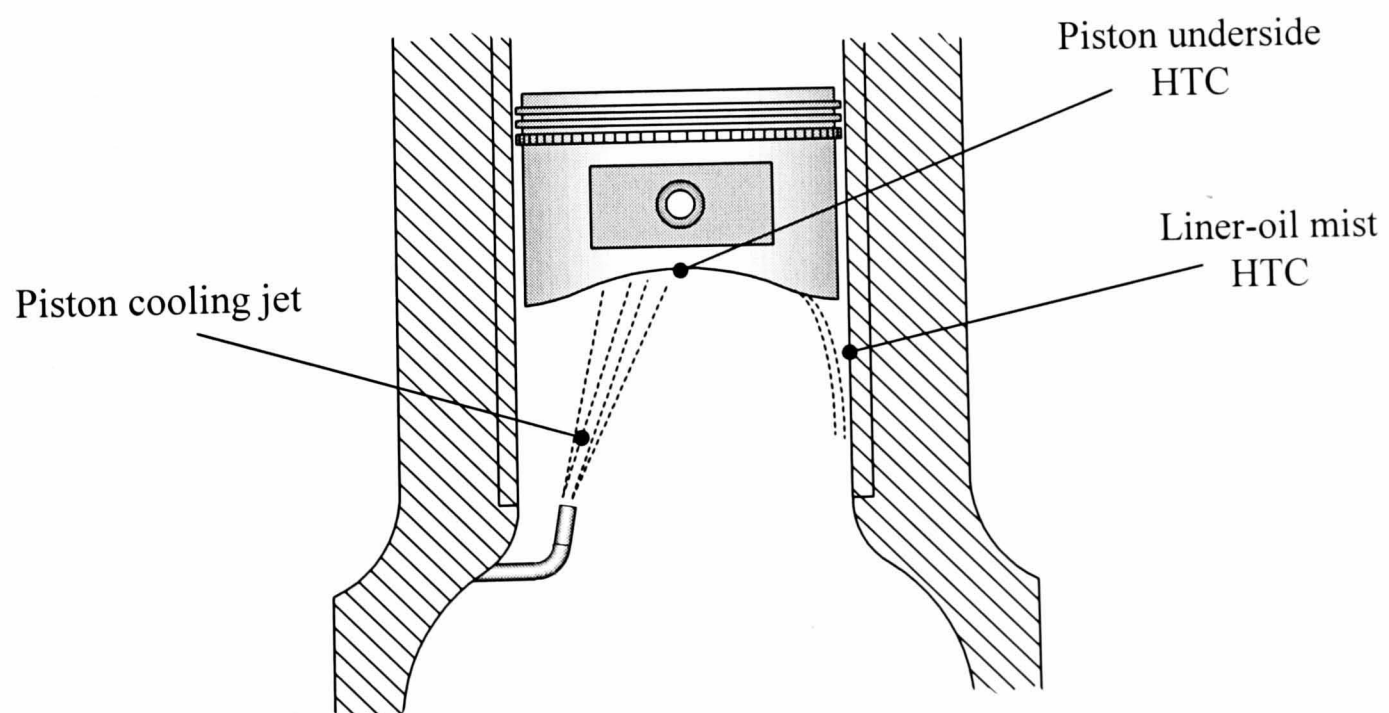
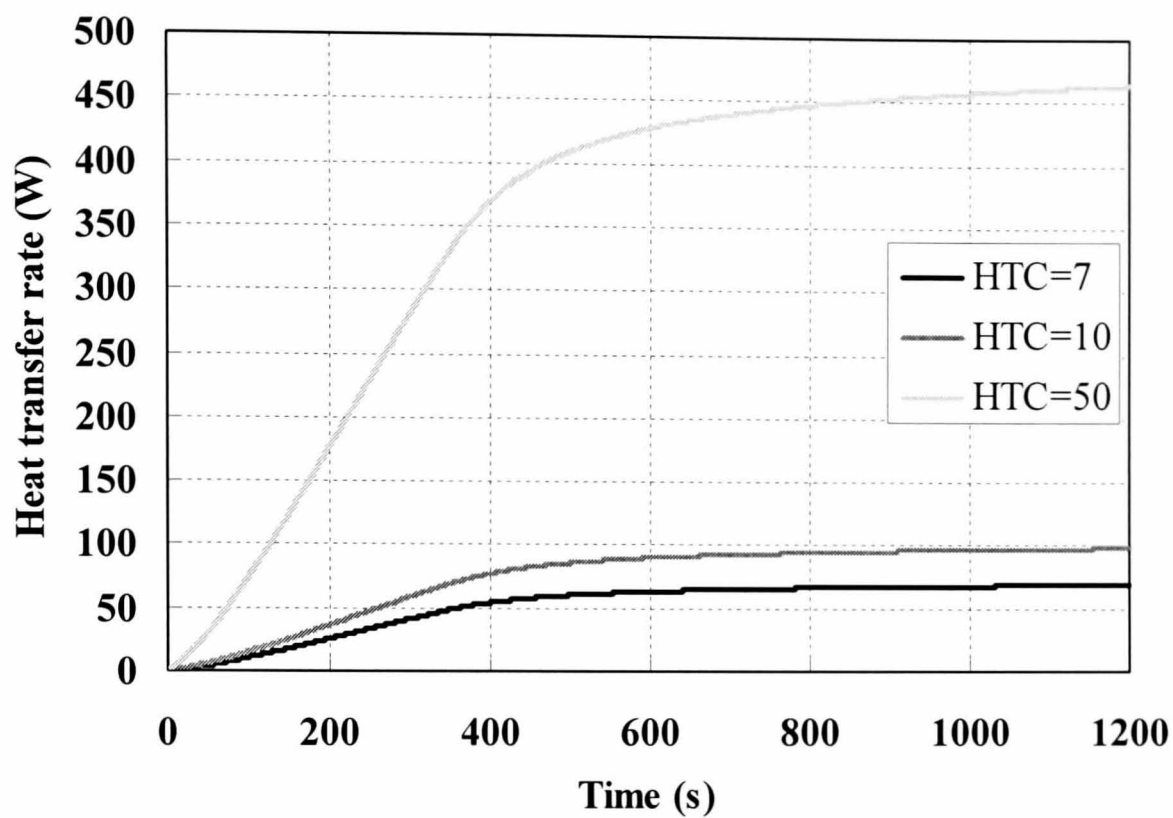


Figure 5.19 The locations for which the oil and piston underside heat transfer coefficients (HTC) are defined.

a)



b)

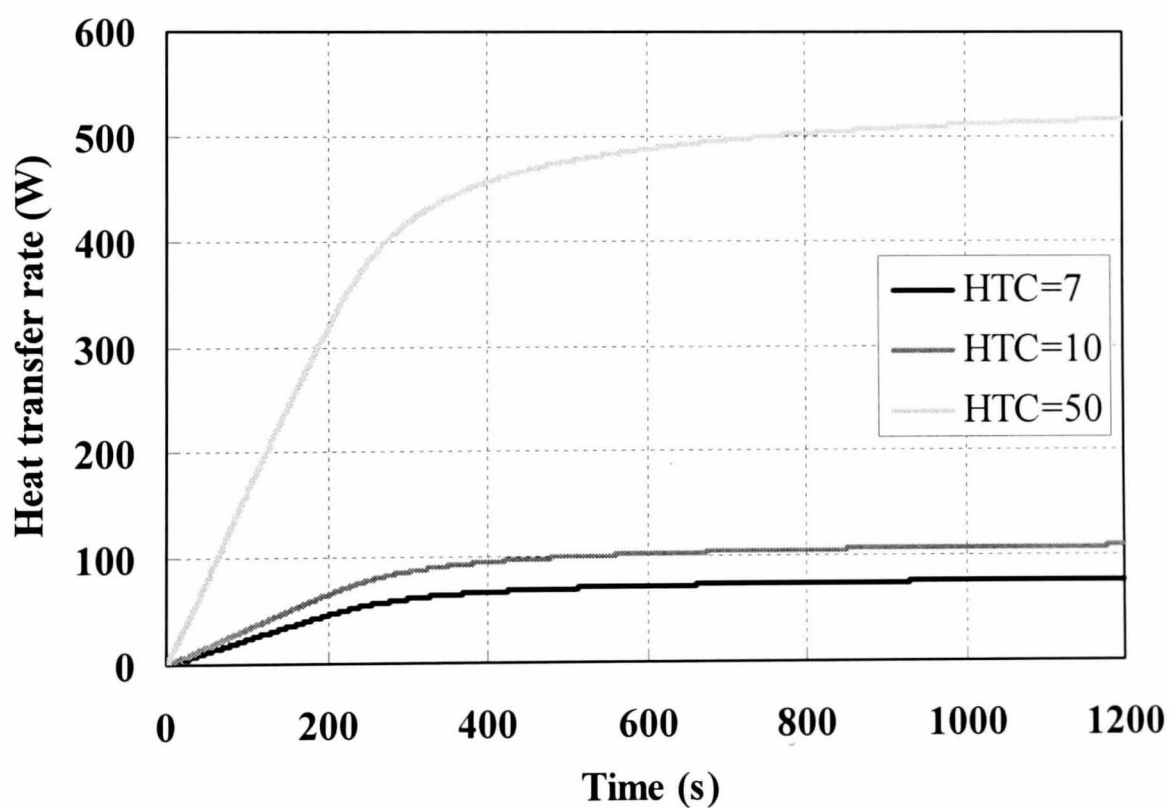


Figure 5.20 Effect of the sump heat transfer coefficient (HTC) in $\text{W/m}^2 \text{K}$ on the heat transfer rate from the oil sump to ambient at a) 1000 rpm, 120 Nm and b) 3000 rpm, 5 Nm.

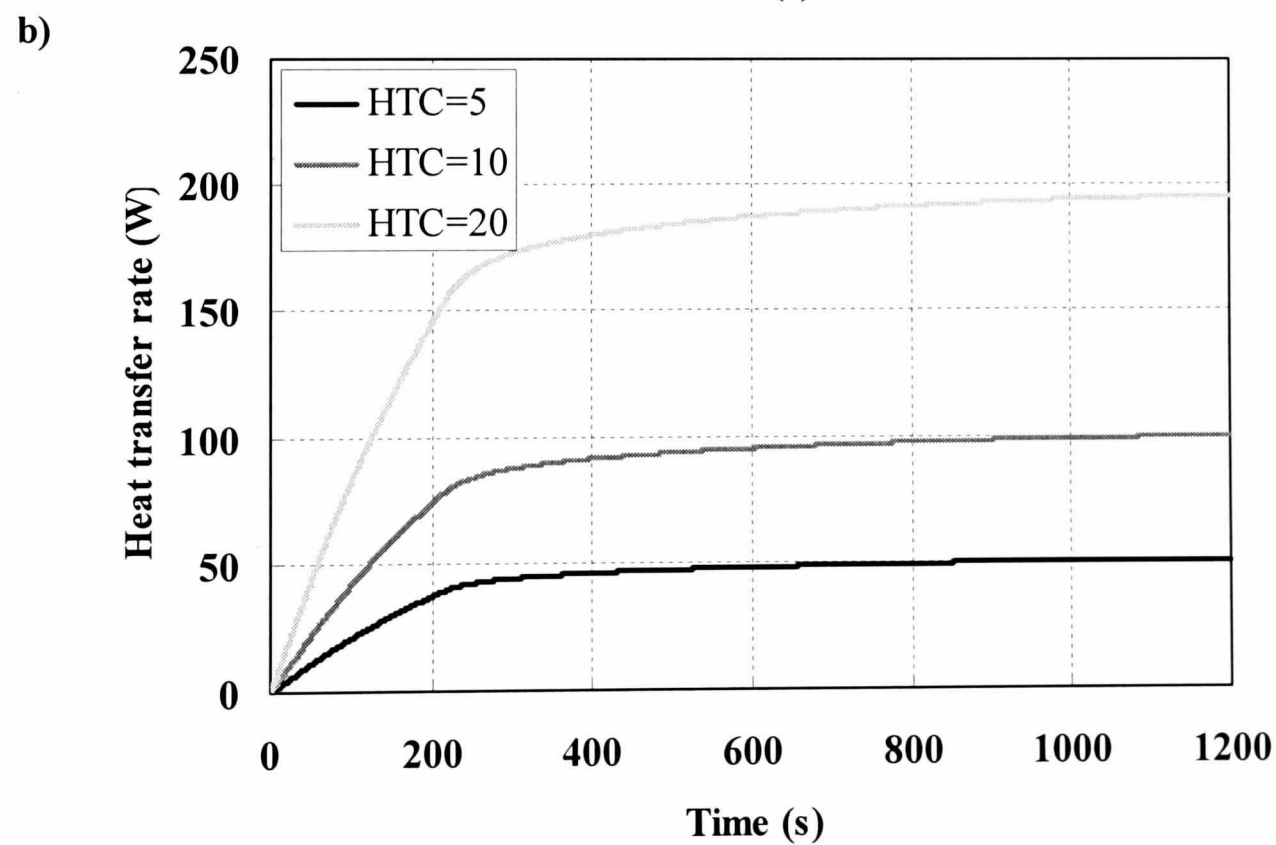
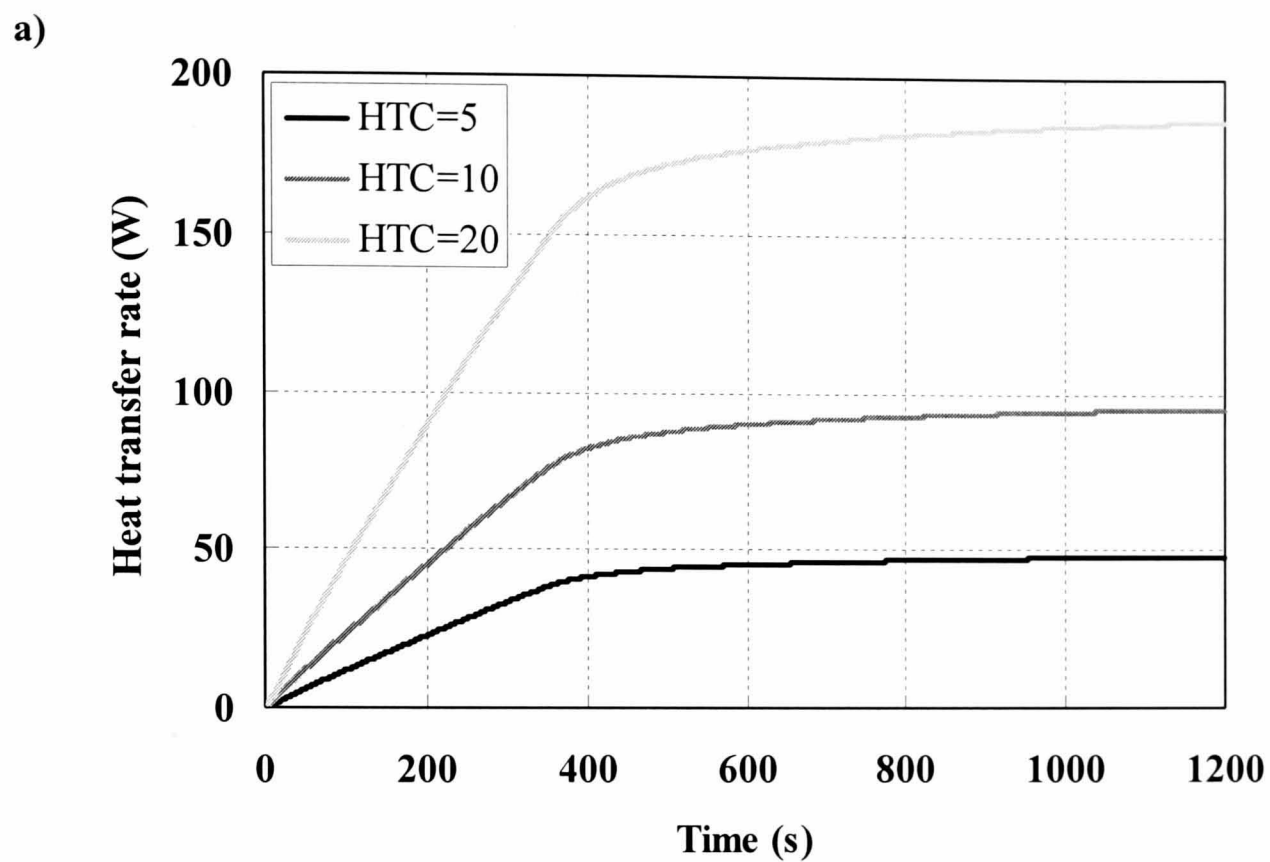


Figure 5.21 Effect of the ambient heat transfer coefficient (HTC) in $\text{W/m}^2 \text{K}$ on the heat transfer rate to ambient at a) 1000 rpm, 120 Nm and b) 3000 rpm, 5 Nm.

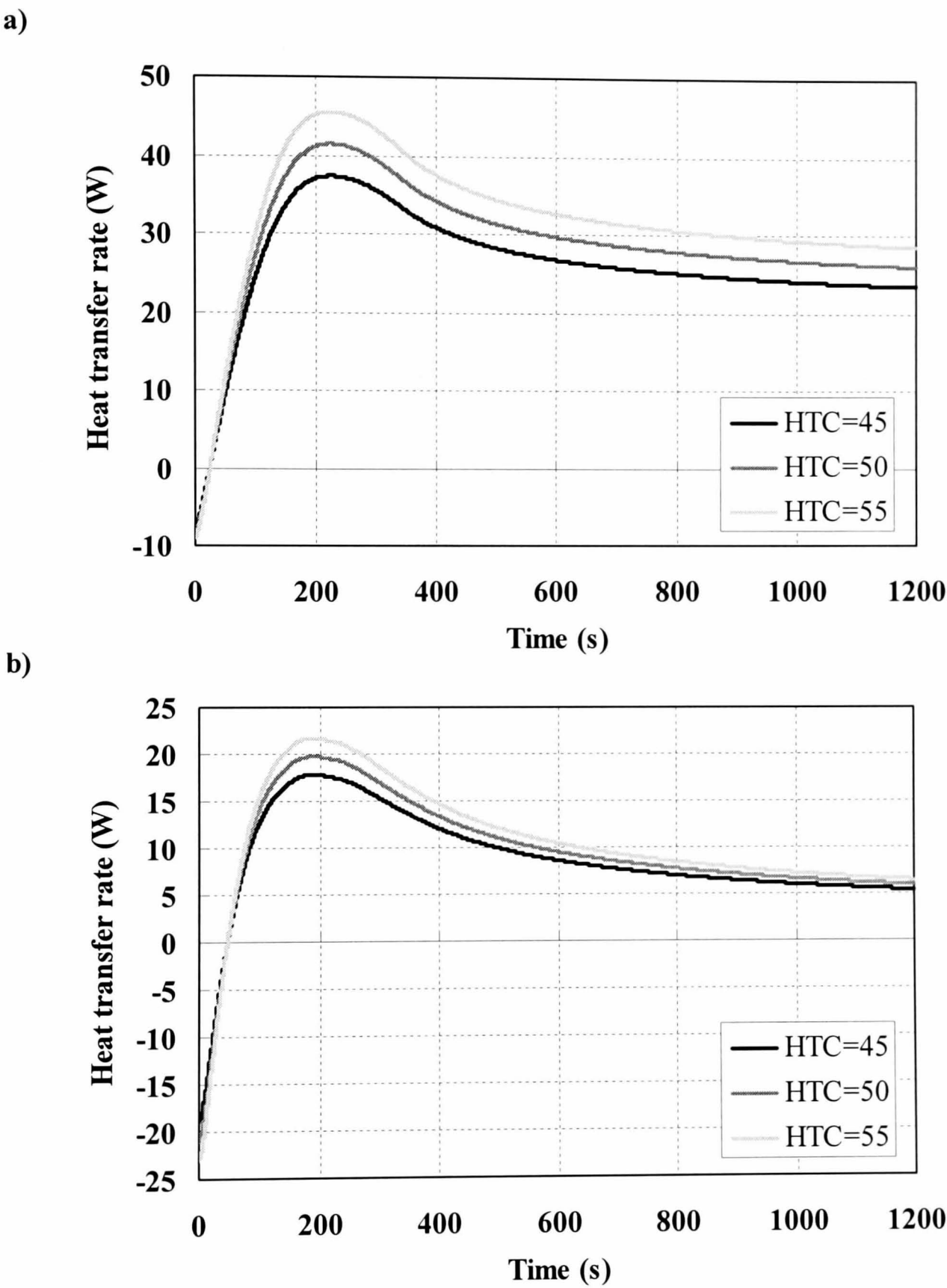


Figure 5.22 Effect of the oil heat transfer coefficient on the heat transfer rate from valve deck to the oil at a) 1000 rpm, 120 Nm and b) 3000 rpm, 5 Nm.

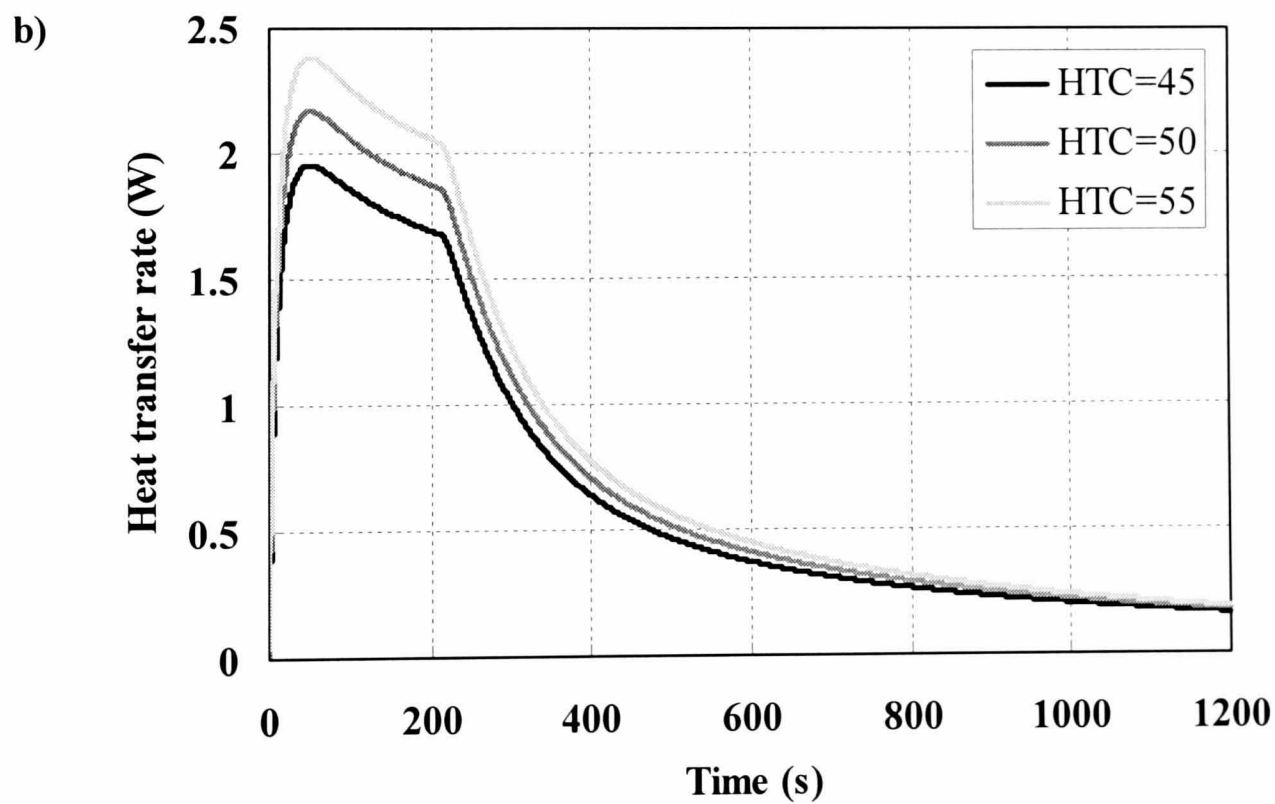
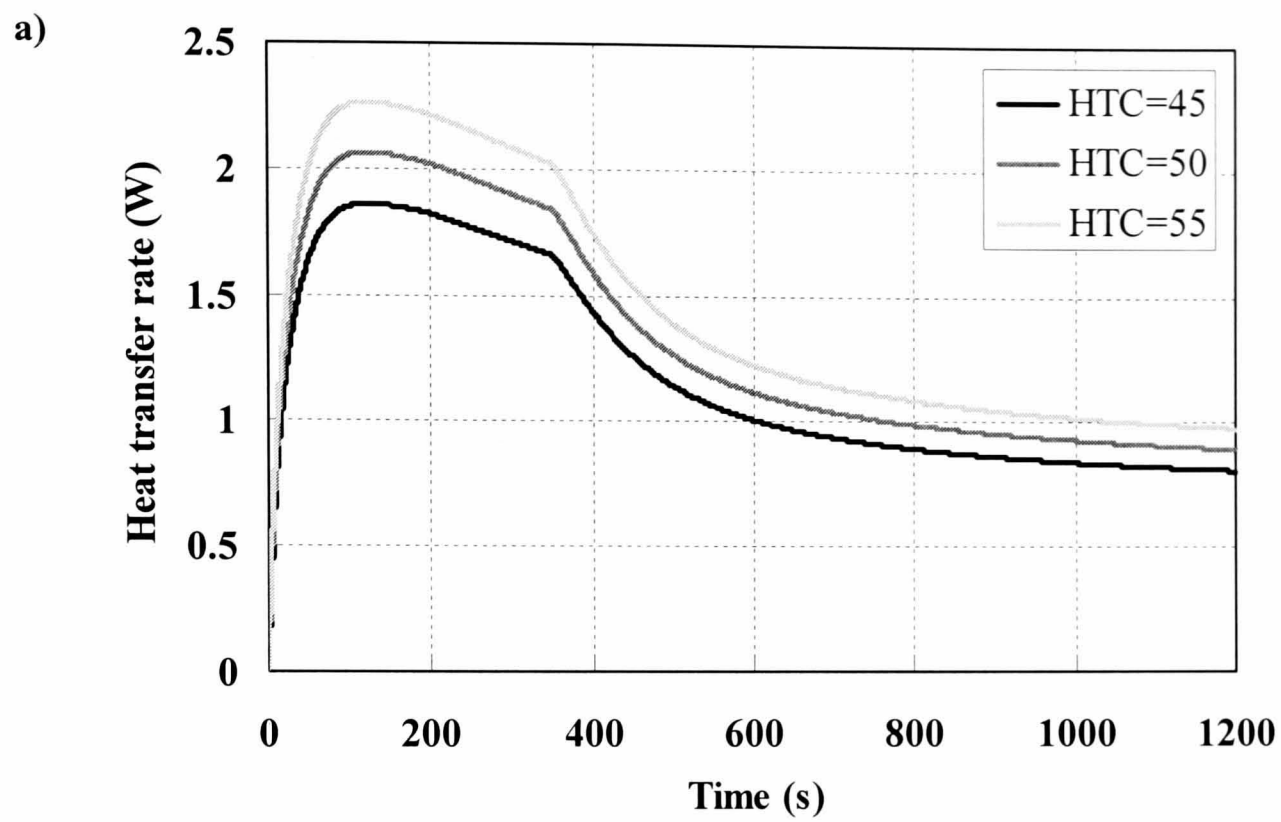
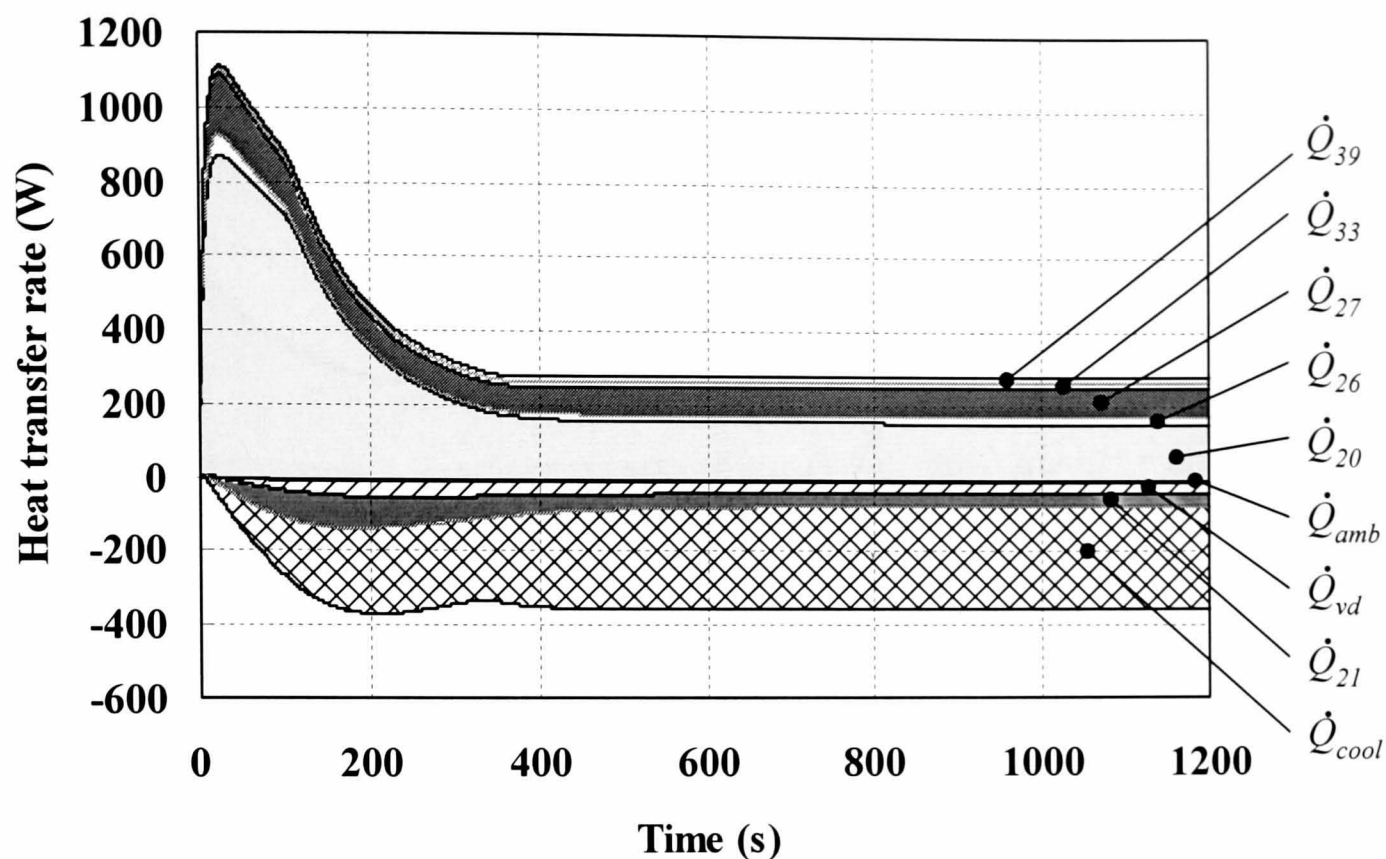
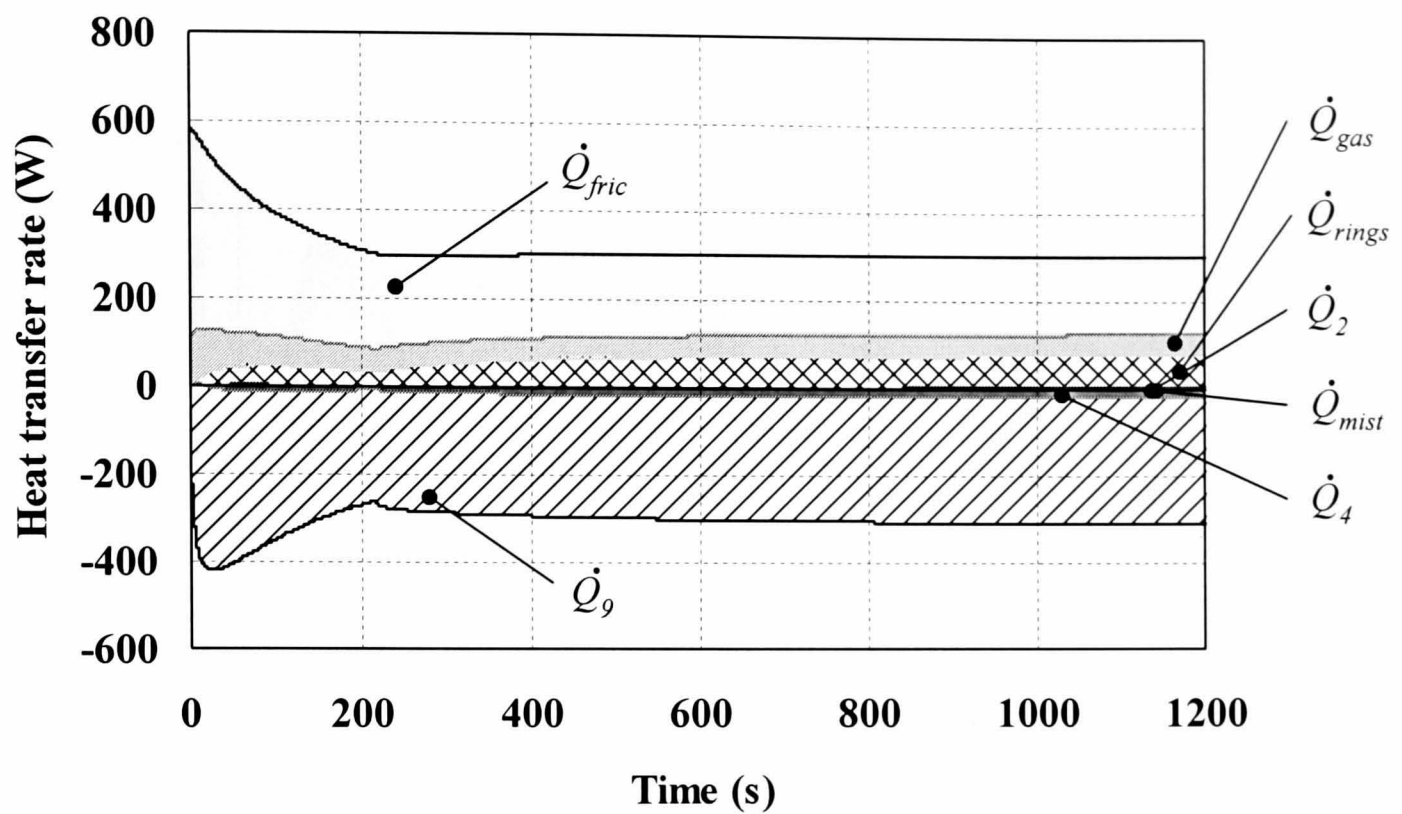


Figure 5.23 Effect of the oil heat transfer coefficient on the heat transfer rate from the liner to the oil mist at **a)** 1000 rpm, 120 Nm and **b)** 3000 rpm, 5 Nm.



\dot{Q}_{39}	Heat transfer rate from the exhaust valve stem (element 39)
\dot{Q}_{33}	Heat transfer rate from the exhaust valve stem (element 33)
\dot{Q}_{27}	Heat transfer rate from the flame deck centre (element 27)
\dot{Q}_{26}	Heat transfer rate from the flame deck exhaust side (element 26)
\dot{Q}_{20}	Heat transfer rate from the exhaust port (element 20)
\dot{Q}_{amb}	Heat transfer rate to ambient from the surface of element 22
\dot{Q}_{vd}	Heat transfer rate from the valve deck (element 22) to the oil
\dot{Q}_{21}	Heat transfer rate to the material in the intake side of the head (excluding the intake port)
\dot{Q}_{cool}	Heat transfer rate to the coolant

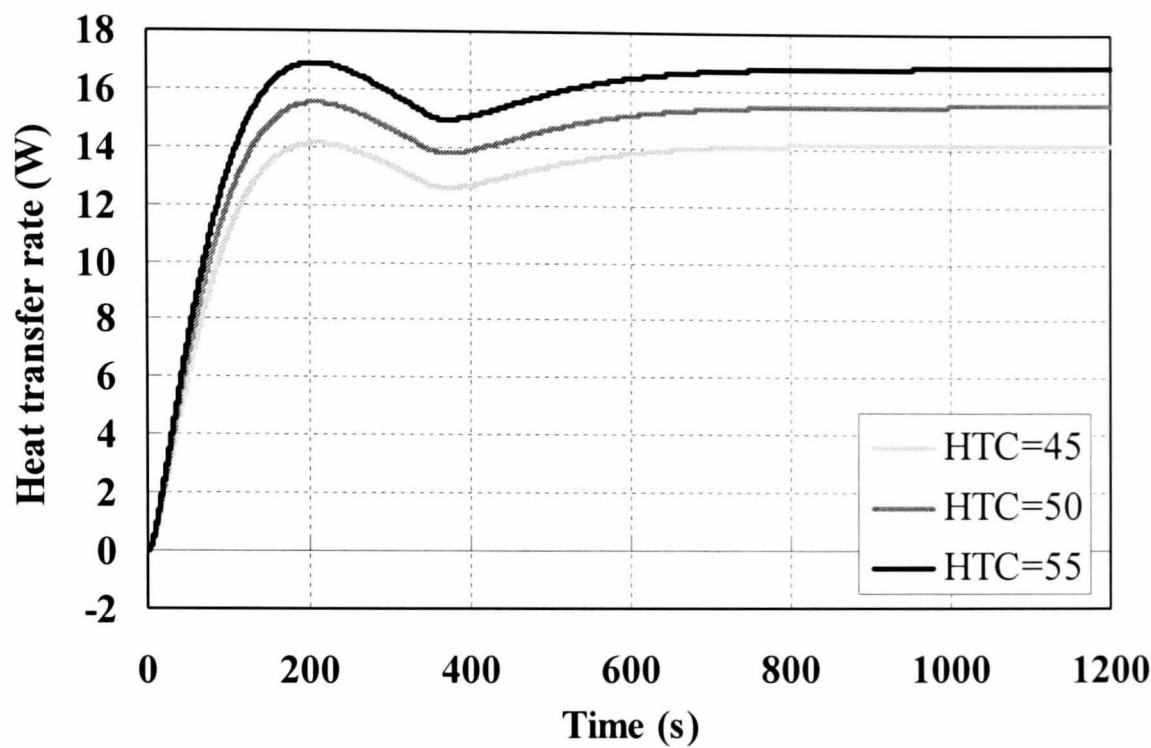
Figure 5.24 Energy balance for the material in the exhaust half of the engine head (element 22) excluding the exhaust port, at 1000 rpm, 120 Nm. The location of element 22 is shown in Figure 3.9.



\dot{Q}_{fric}	Heat transfer rate arising from piston friction
\dot{Q}_{gas}	Heat transfer rate from the combustion gases
\dot{Q}_{rings}	Heat transfer rate from the piston rings
\dot{Q}_2	Heat transfer rate from the liner element above element 3 (element 2)
\dot{Q}_{mist}	Heat transfer rate to the oil mist
\dot{Q}_4	Heat transfer rate to the element below element 3 (element 4)
\dot{Q}_9	Heat transfer rate to the element adjacent to element 3 (element 9)

Figure 5.25 Energy balance for the middle of the liner (element 3) at 3000 rpm, 5 Nm. The location of element 3 is shown in Figure 3.9.

a)



b)

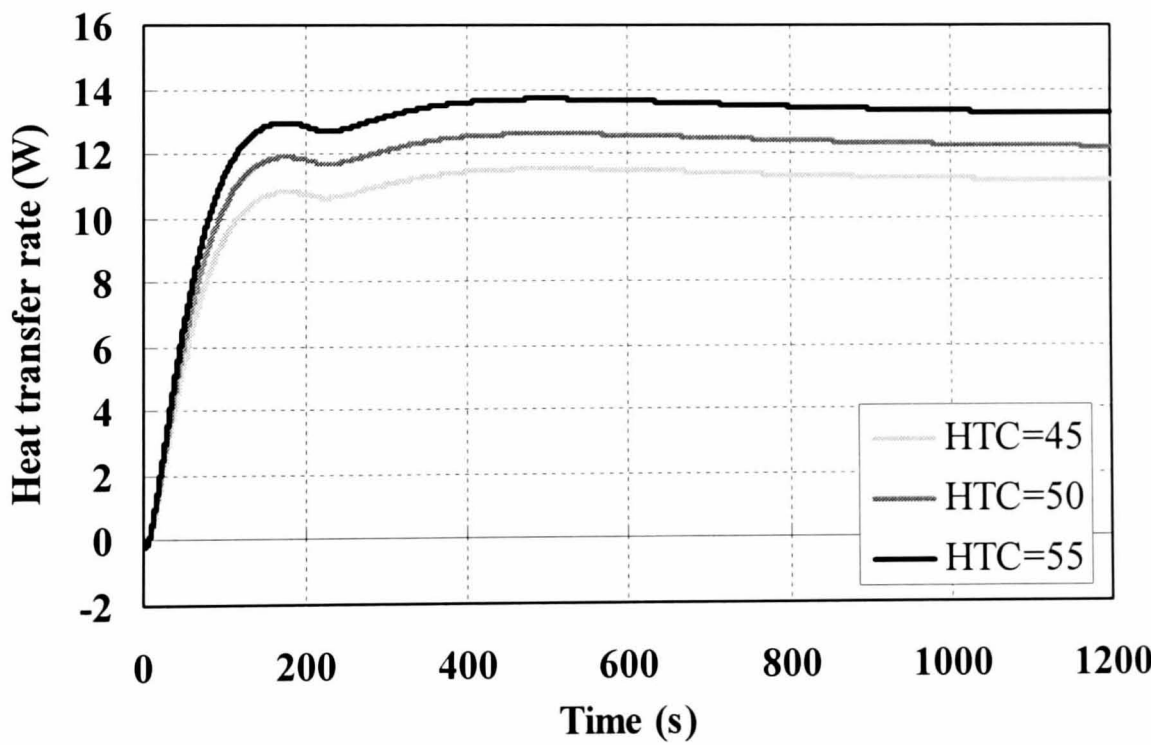
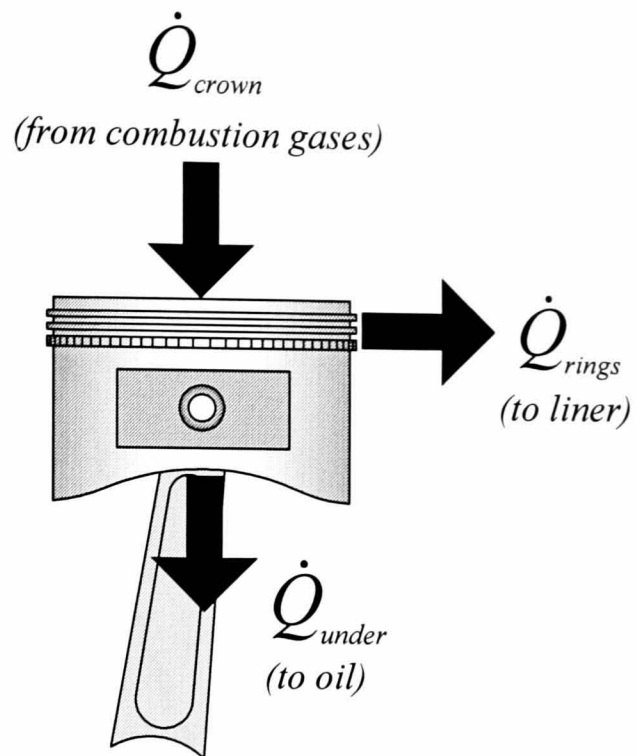


Figure 5.26 Effect of the piston underside heat transfer coefficient on the heat transfer rate from the piston underside to the oil cooling jets at **a)** 1000 rpm, 120 Nm and **b)** 3000 rpm, 5 Nm.



\dot{Q}_{crown} Heat transfer rate from the combustion gases to the piston crown

\dot{Q}_{rings} Heat transfer rate from the piston through the piston rings to the liner

\dot{Q}_{under} Heat transfer rate from the piston underside to the oil mist

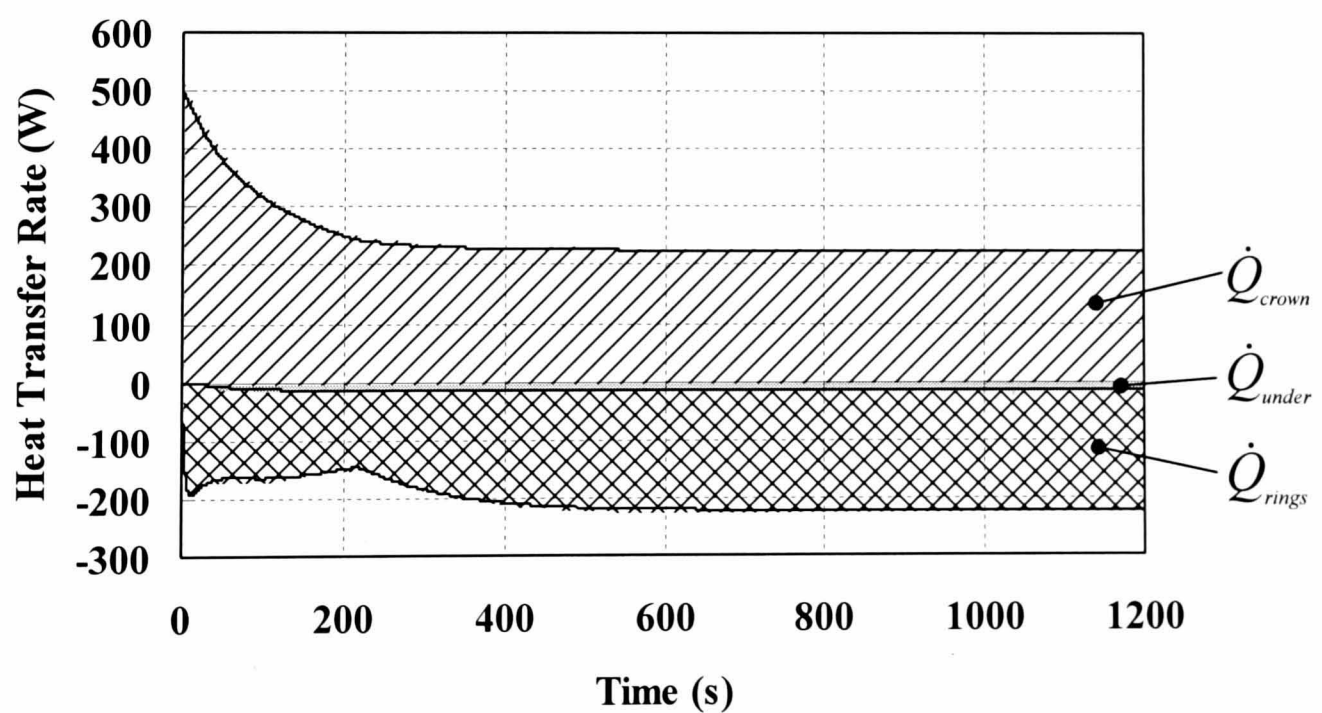


Figure 5.27 Energy balance for the piston at 3000 rpm, 5 Nm.

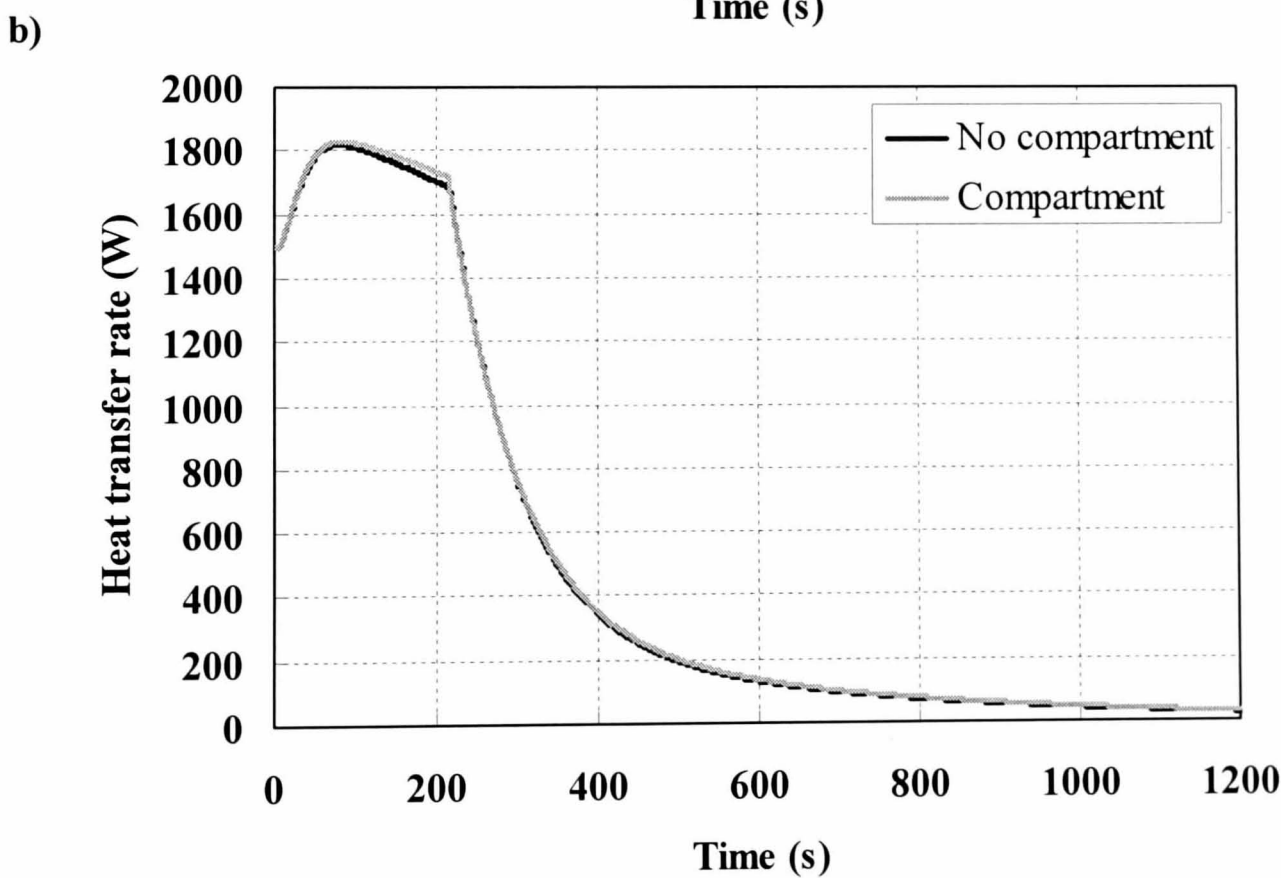
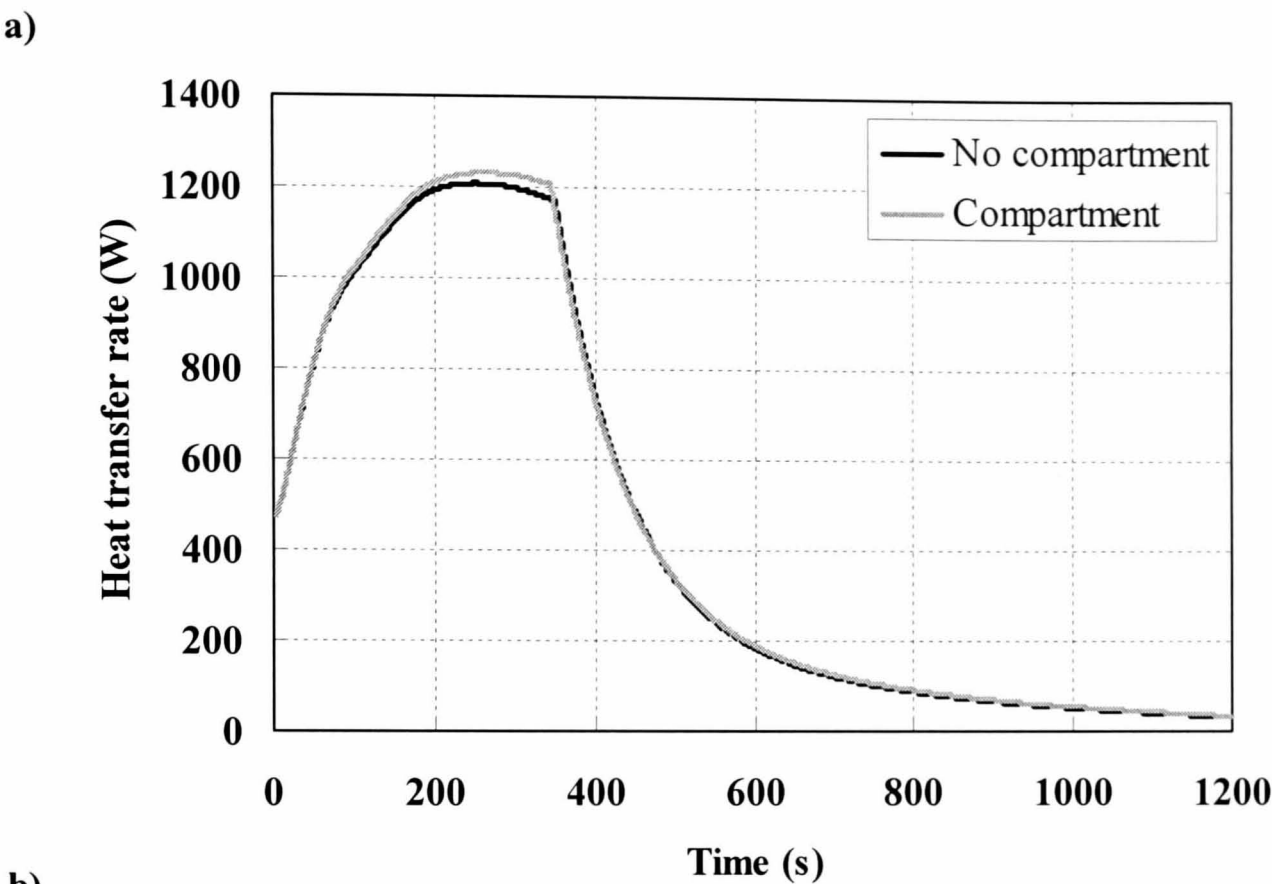
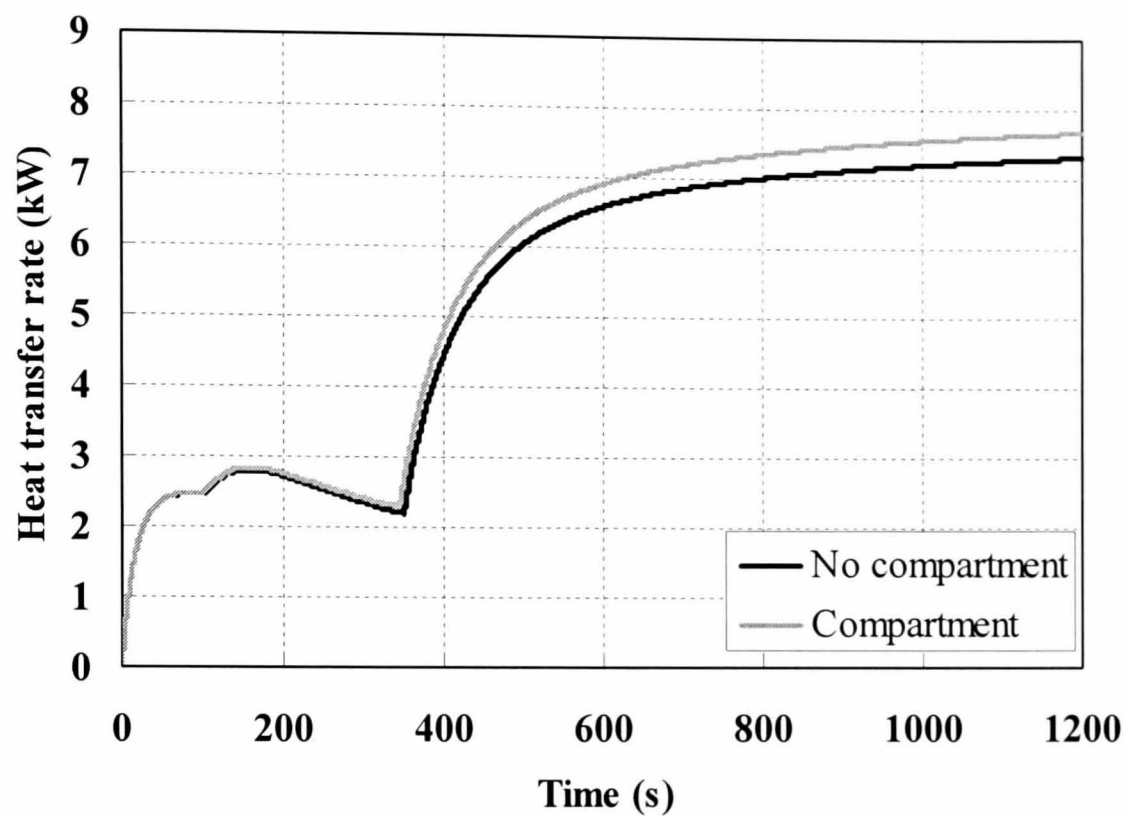


Figure 5.28 Effect of the ambient temperature (simulating with and without an engine compartment) on the net heat transfer rate to the oil, comprising of the heat transferred from the structure, frictional heat retained in the oil and heat transferred to or from the coolant, at **a)** 1000 rpm, 120 Nm and **b)** 3000 rpm, 5 Nm.

a)



b)

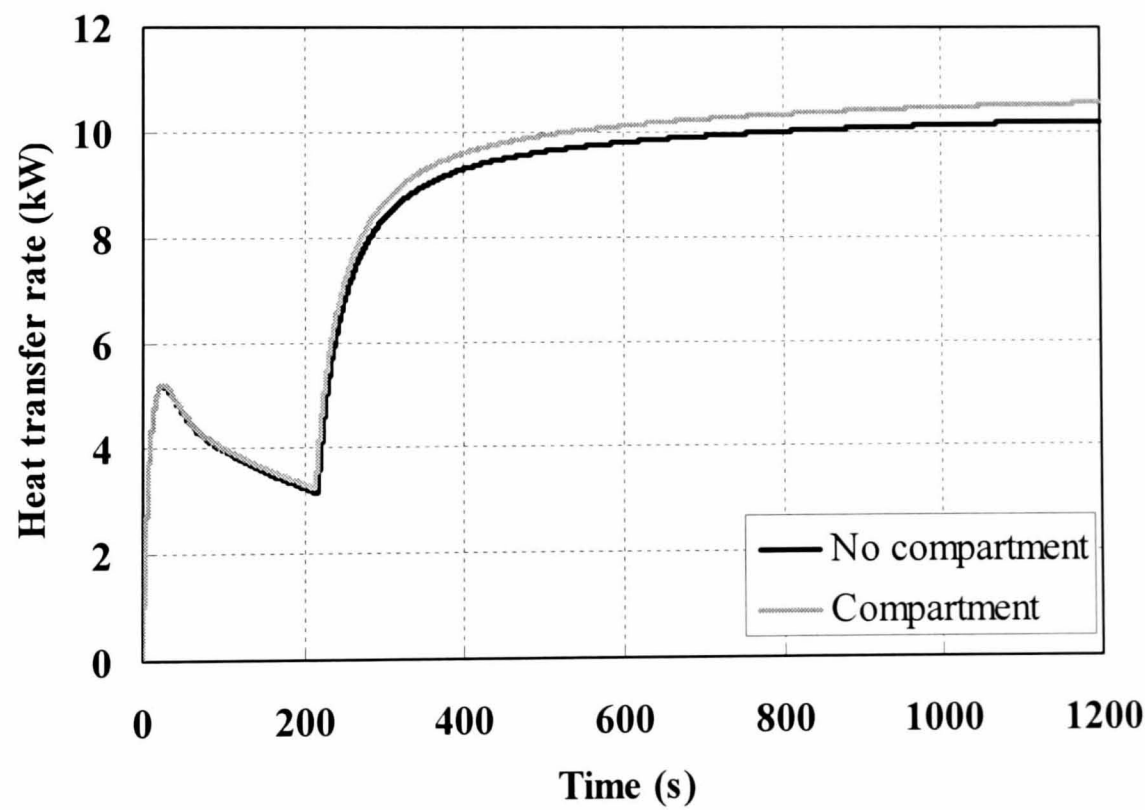
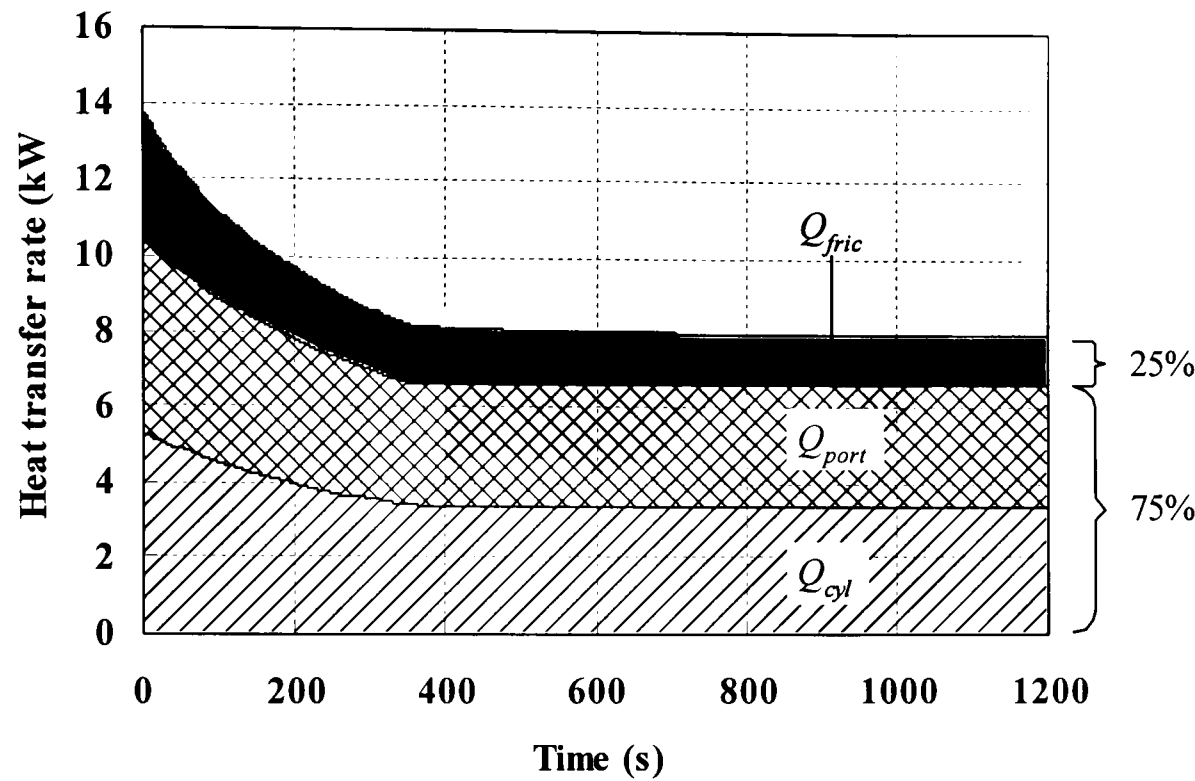


Figure 5.29 Effect of the ambient temperature (simulating with and without an engine compartment) on the heat transfer rate to the coolant at **a)** 1000 rpm, 120 Nm and **b)** 3000 rpm, 5 Nm.

a)



b)

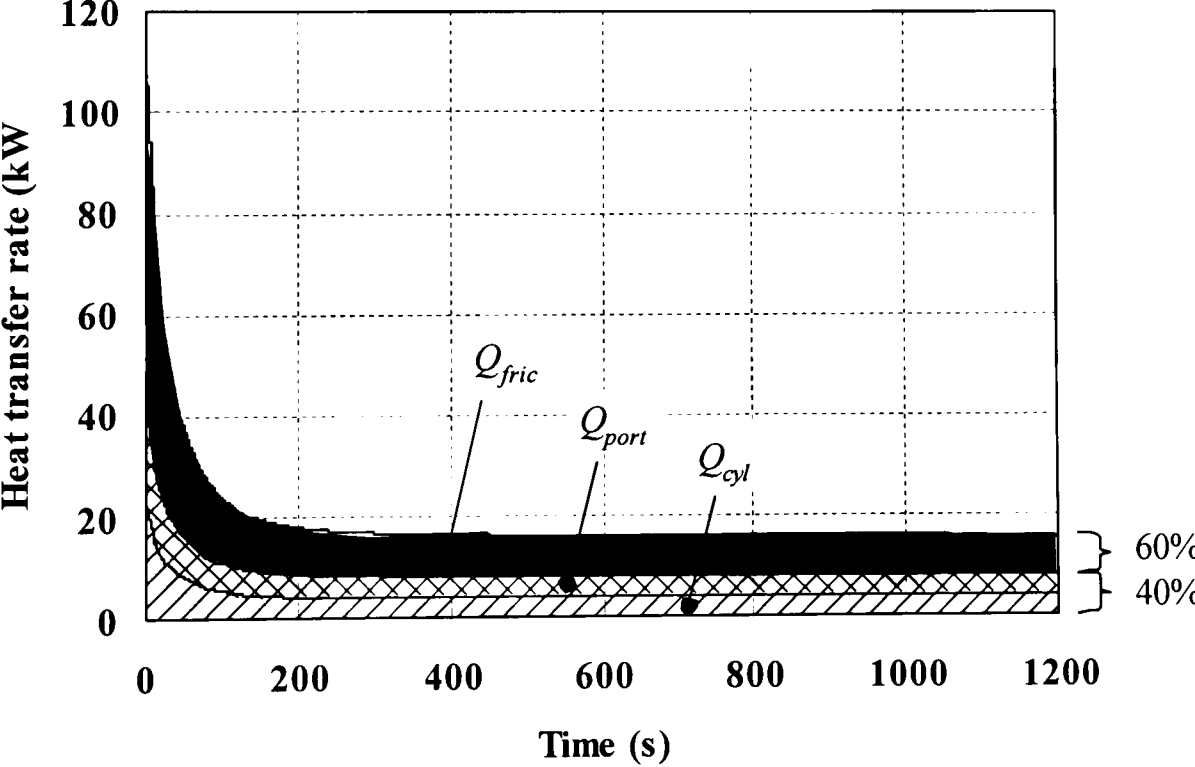


Figure 5.30 a) Heat transferred to the engine structure at 1000 rpm, 120 Nm. Initial and ambient temperatures are 20 °C. Total gas-side heat transfer accounts for 75 % of the steady-state heat transfer. b) Heat transferred to the engine structure at 4500 rpm, 5 Nm. Initial and ambient temperatures are -18 °C. Friction power accounts for 60 % of the steady-state heat transfer.

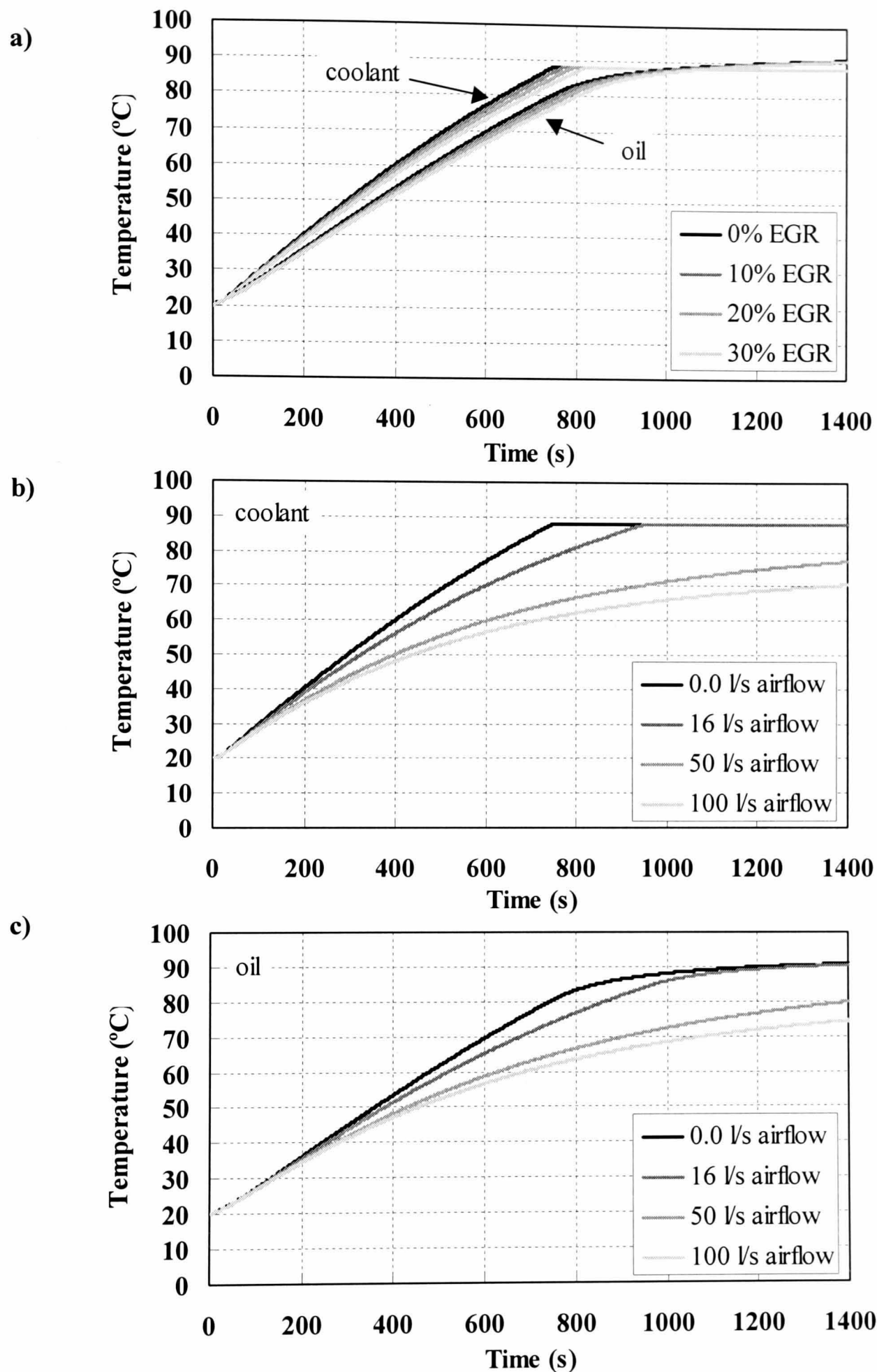
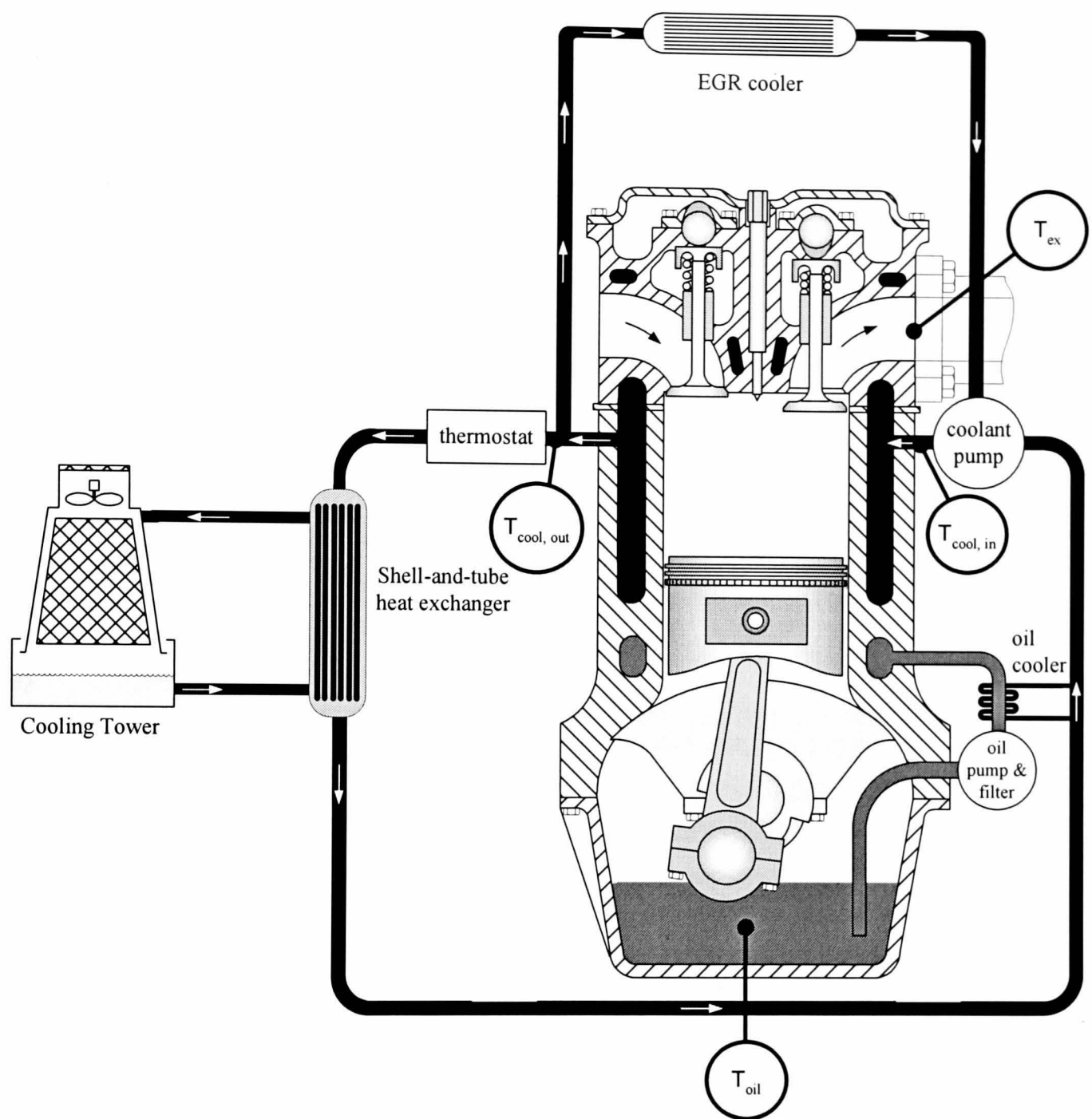


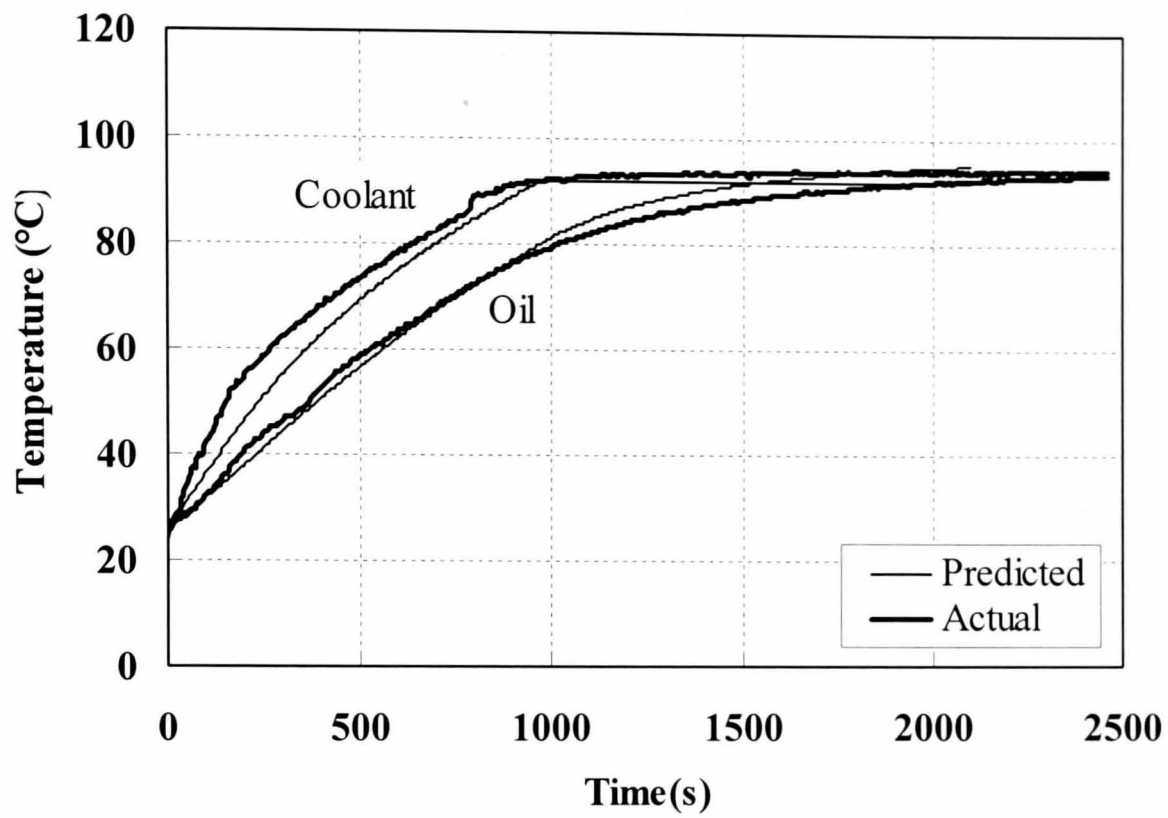
Figure 5.31 a) Effect of increasing EGR on coolant and oil temperatures, b) effect of increasing airflow through heater matrix on coolant temperatures and c) effect of increasing airflow through the heater matrix on oil temperatures at 1000 rpm, 10 Nm.



T_{oil}	Temperature of the oil
$T_{cool, in}$	Temperature of the coolant entering the engine block
$T_{cool, out}$	Temperature of the coolant exiting the engine
T_{ex}	Temperature of the engine-out exhaust gas

Figure 5.32 The preferred location around the engine of thermocouples required for the validation of PROMETS.

a)



b)

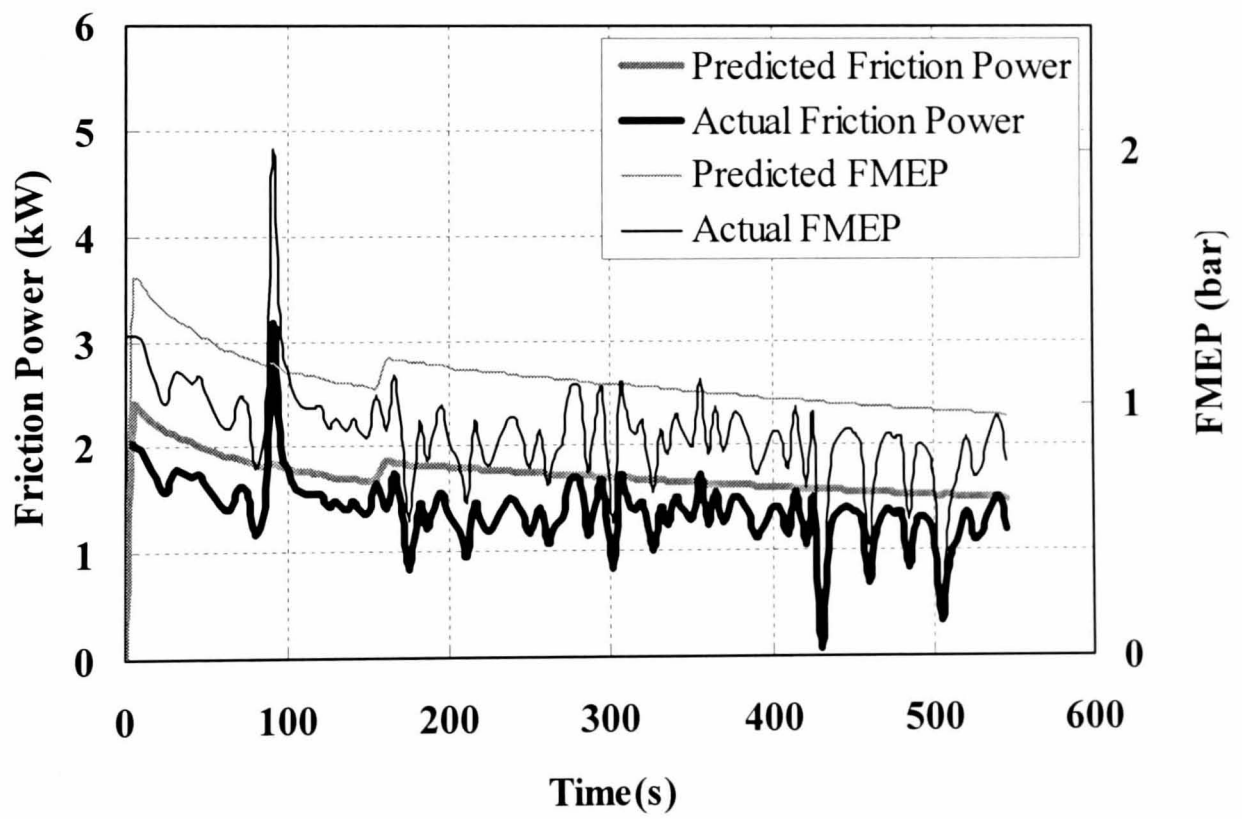
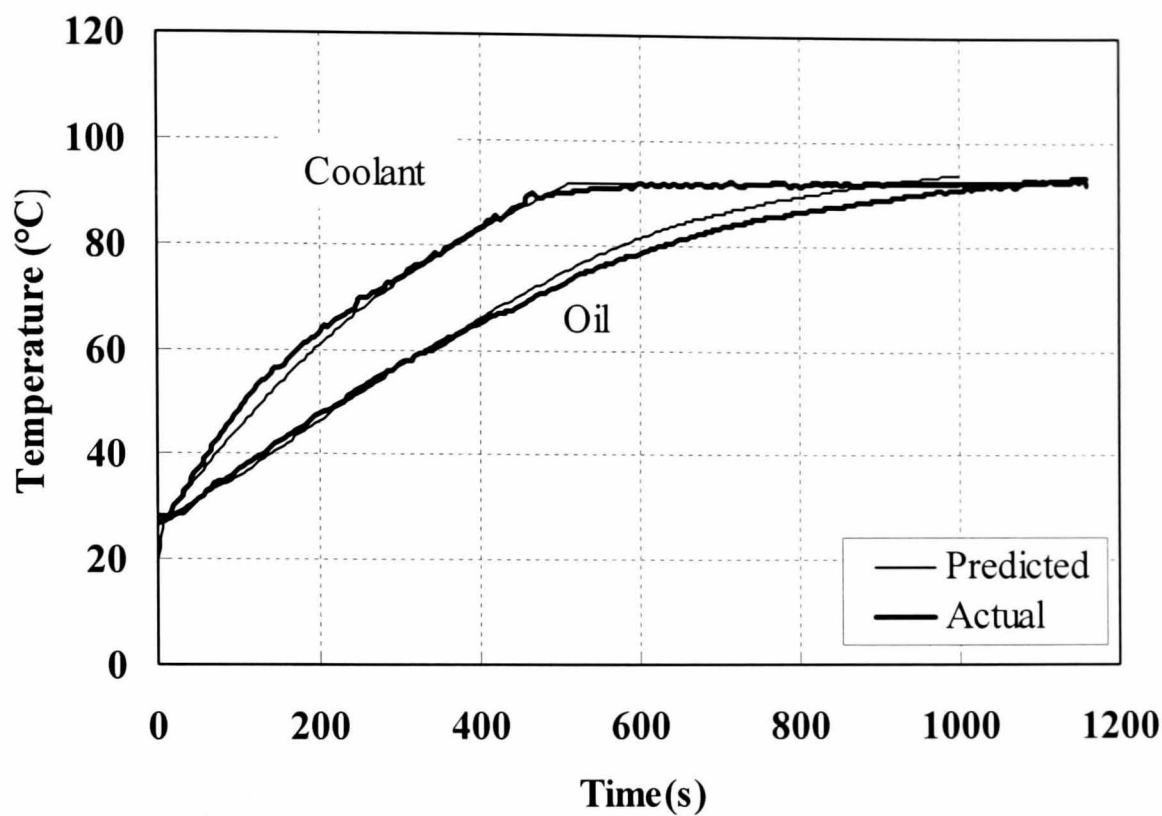


Figure 5.33 Experimental and predicted a) coolant and oil temperatures and b) friction profiles for the 1.9 l Mitsubishi GDi at 1000 rpm, 22 Nm.

a)



b)

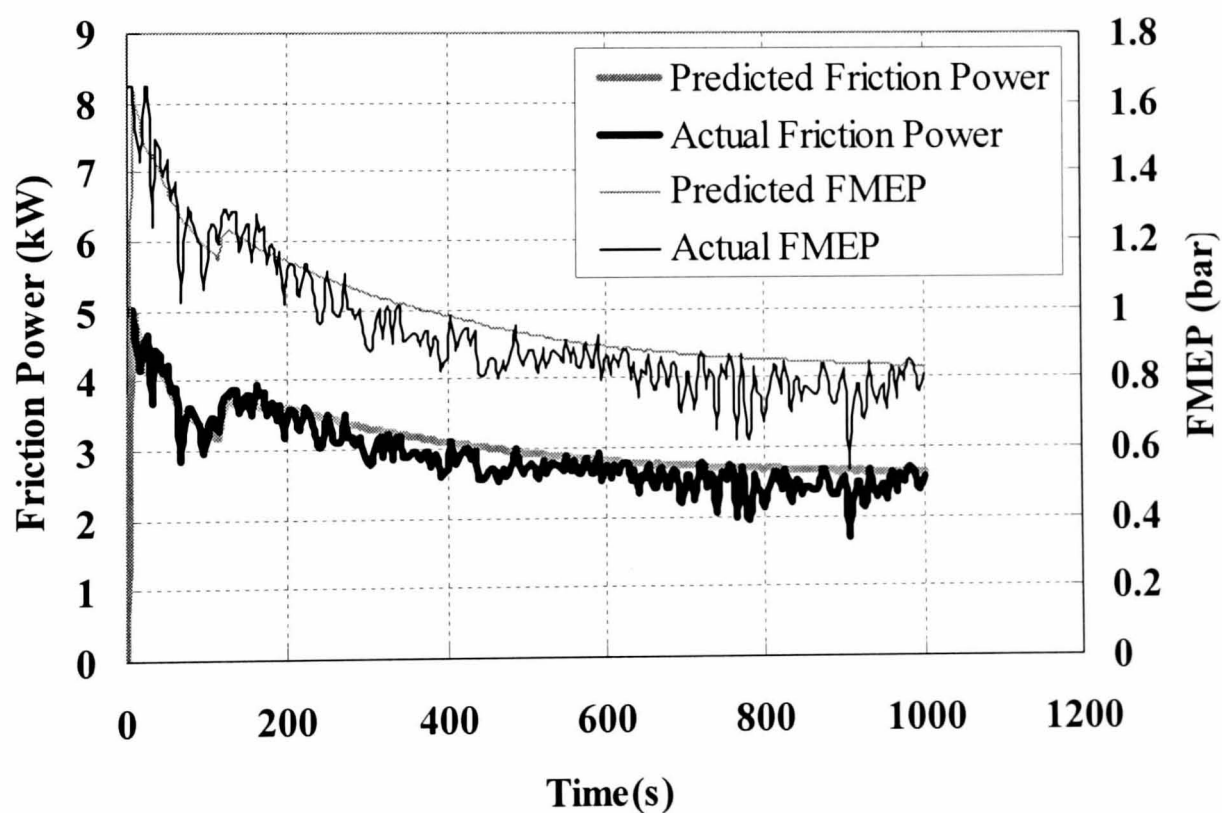
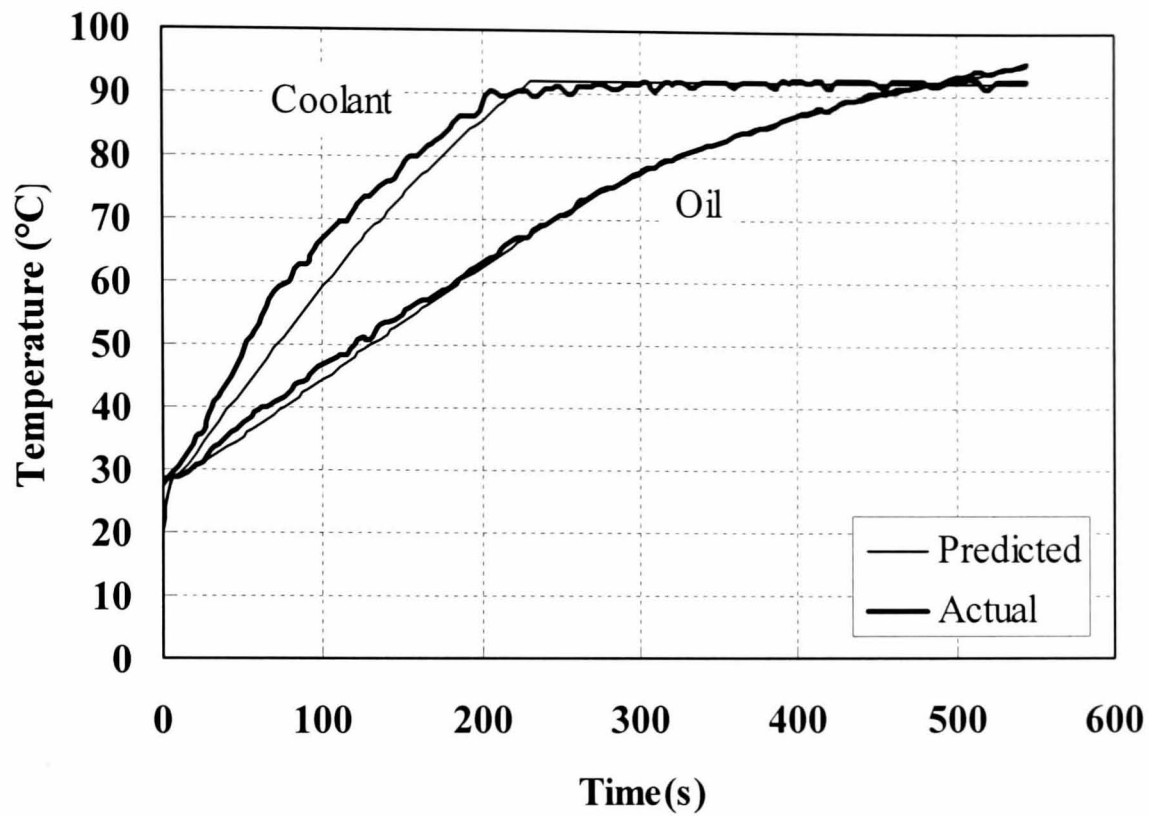


Figure 5.34 Experimental and predicted a) coolant and oil temperatures and b) friction profiles for the 1.9 l Mitsubishi GD_i at 2000 rpm, 0 Nm.

a)



b)

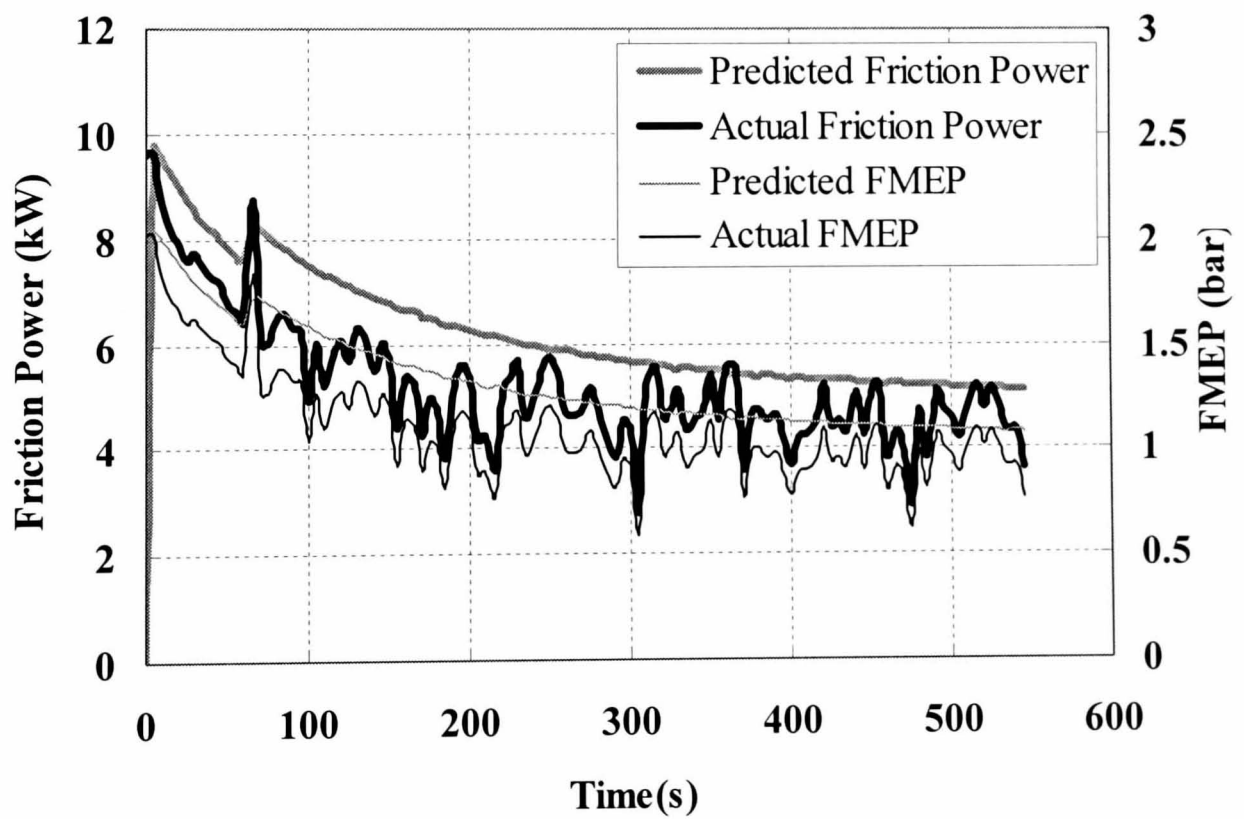
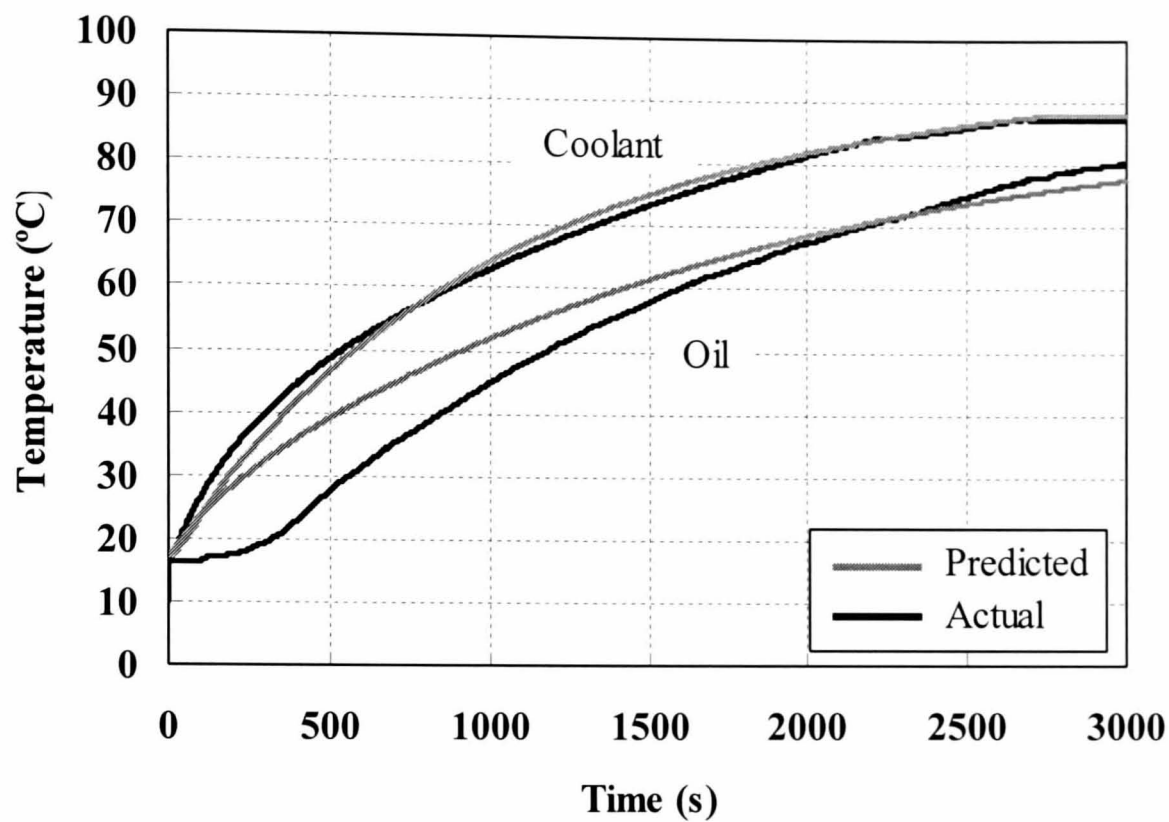


Figure 5.35 Experimental and predicted a) coolant and oil temperatures and b) friction profiles for the 1.9 l Mitsubishi GD_i at 3000 rpm, 38 Nm.

a)



b)

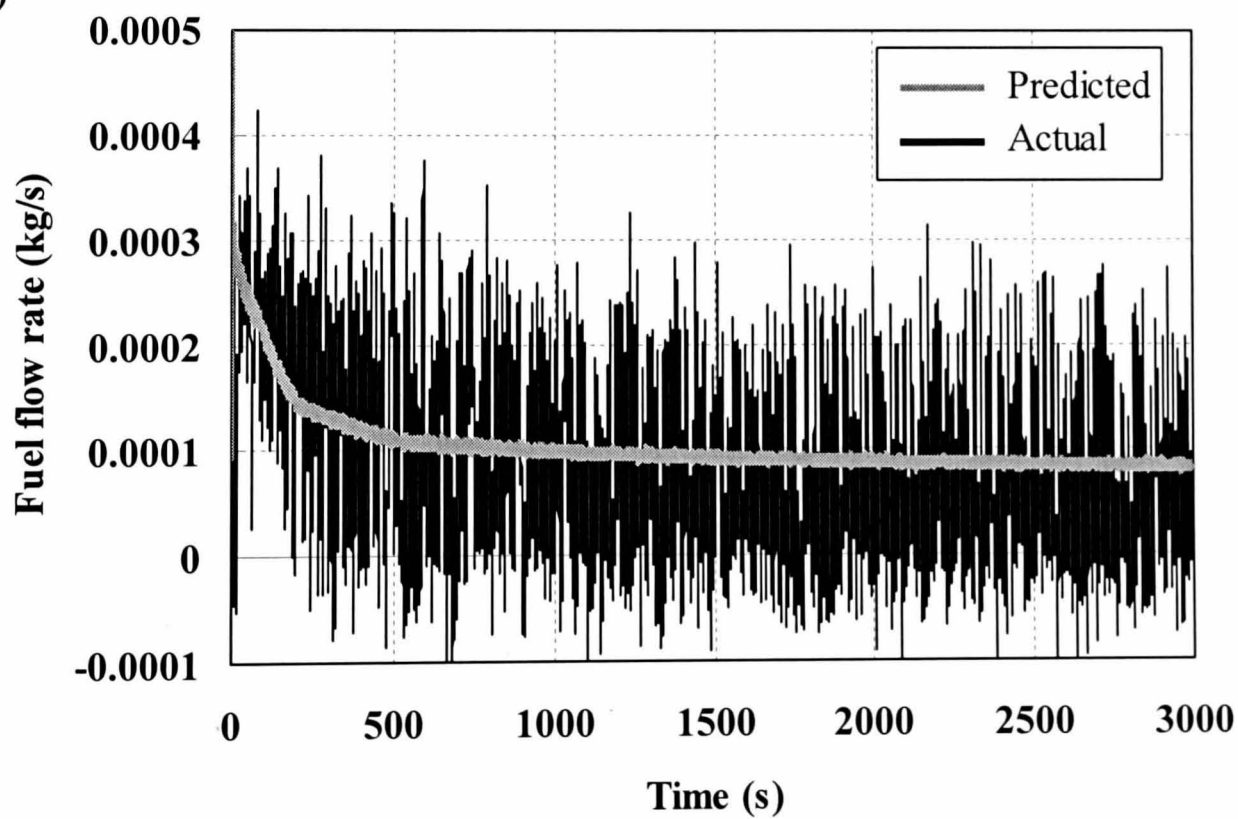
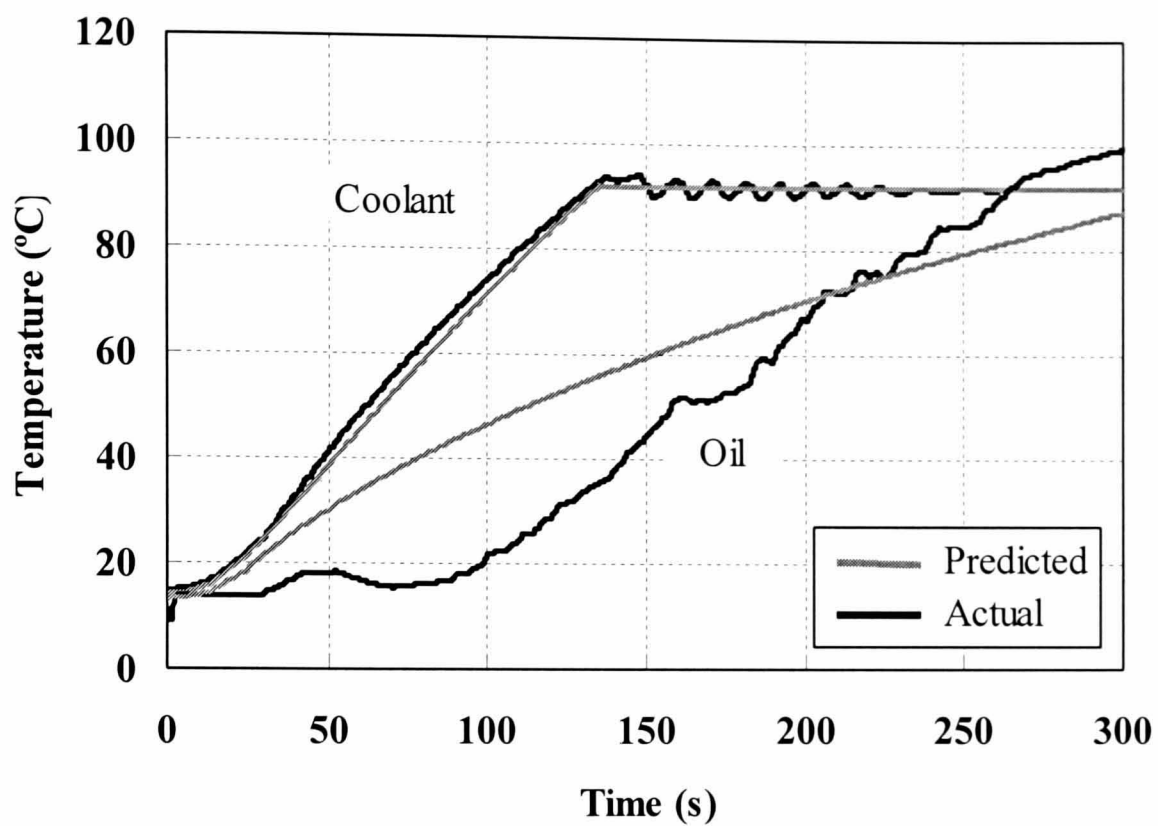


Figure 5.36 Experimental and predicted a) coolant and oil temperatures and b) fuel flow rates for the 2.0 l Puma at idle (1000 rpm, 3 Nm). The fluctuations in the experimental fuel flow rate are due to signal noise.

a)



b)

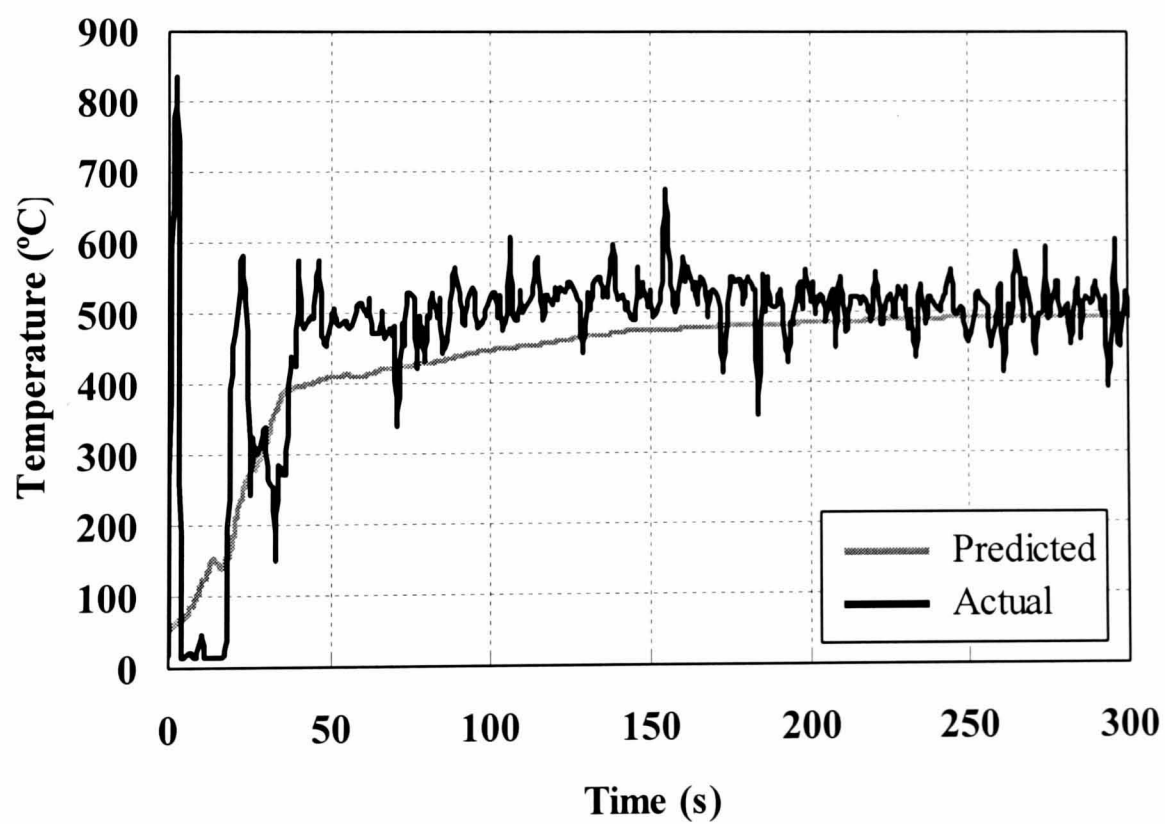


Figure 5.37 Experimental and predicted a) coolant and oil temperatures and b) exhaust gas temperature for the 2.0 l Puma at 3000 rpm, 150 Nm.

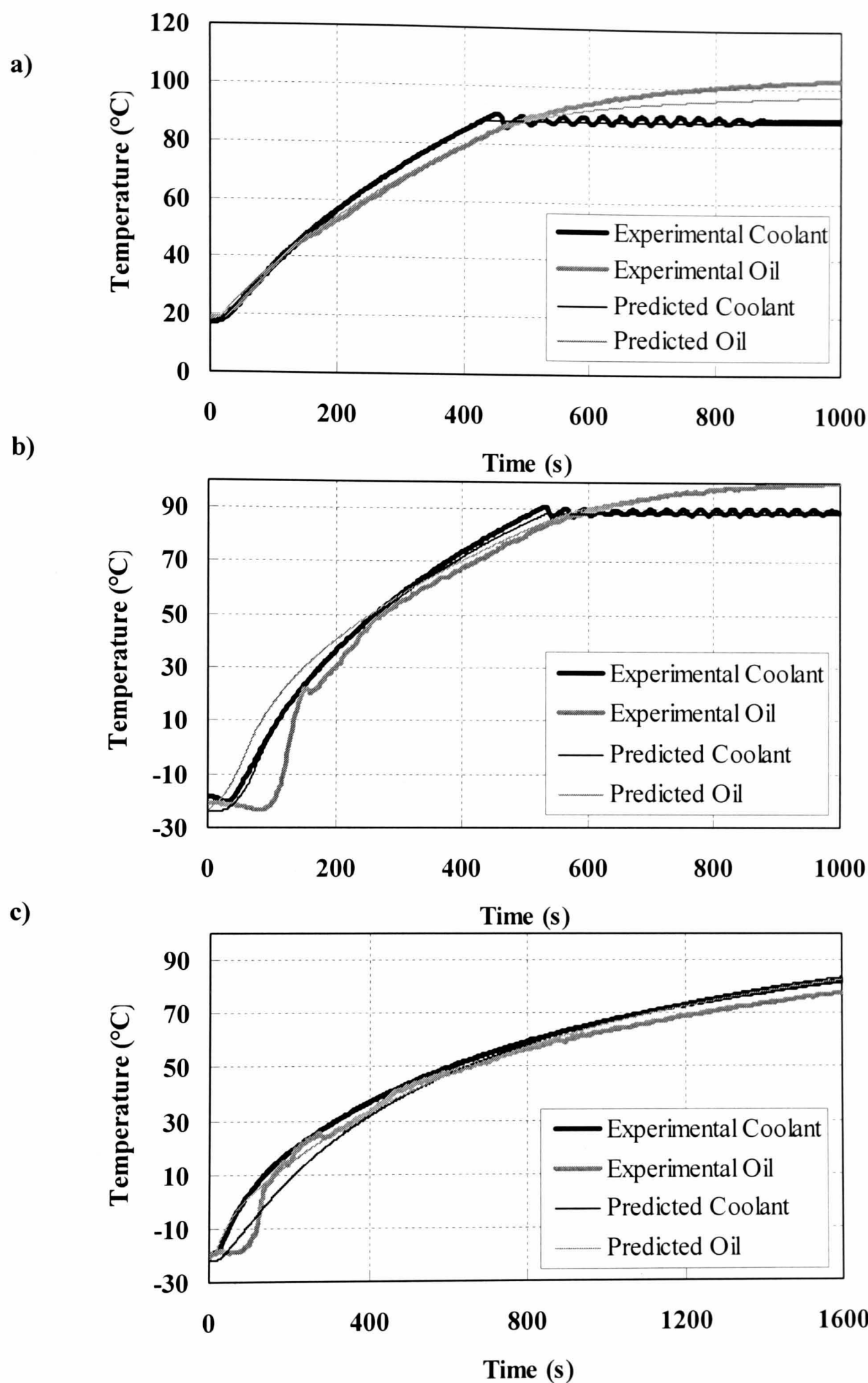


Figure 5.38 Experimental and predicted coolant and oil temperatures for the 1.8l IDI at a) 2340 rpm, 15 Nm, b) 3000 rpm, 5 Nm and c) 1600 rpm, 5 Nm.

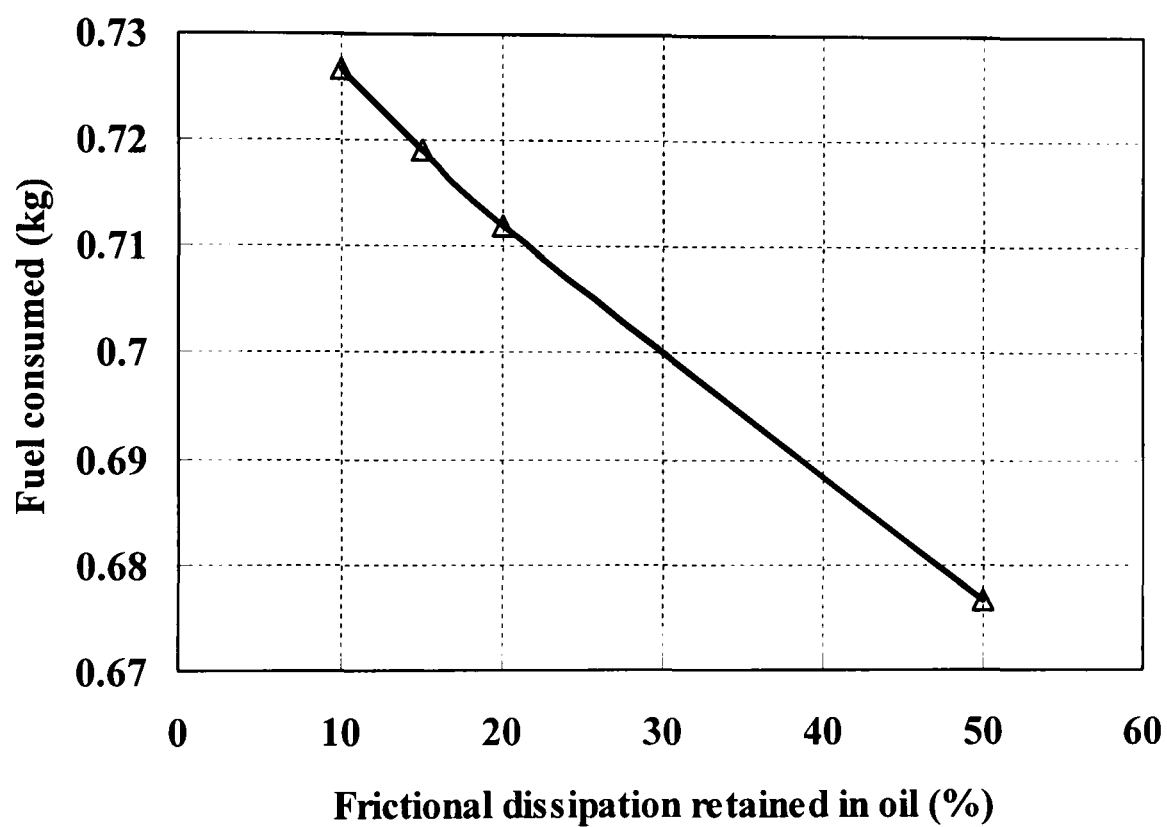


Figure 5.39 Fuel consumed over 1200 seconds at 3000 rpm, 5 Nm for different percentages of friction dissipation retained in the oil. Initial and ambient temperatures are 20 °C.

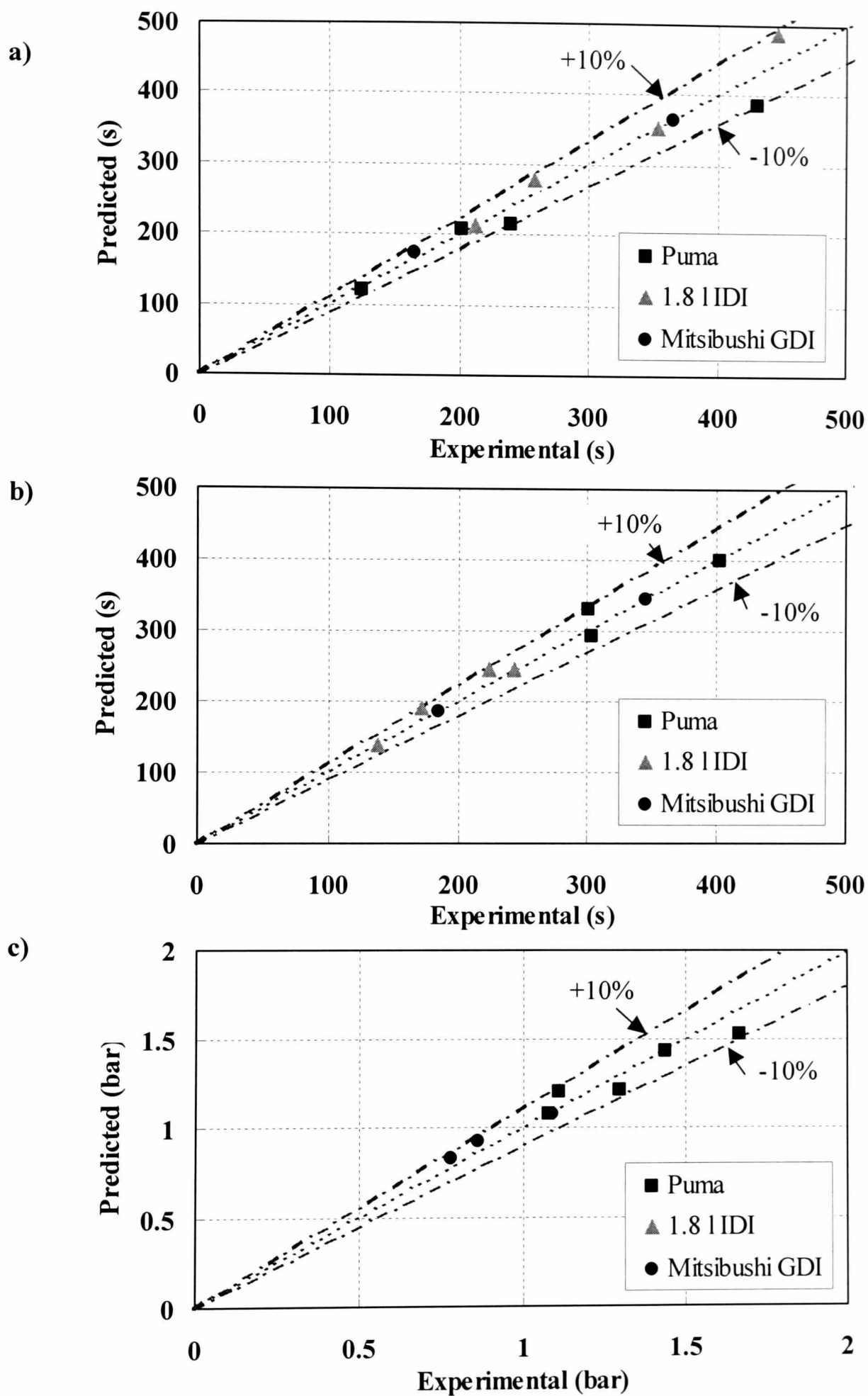
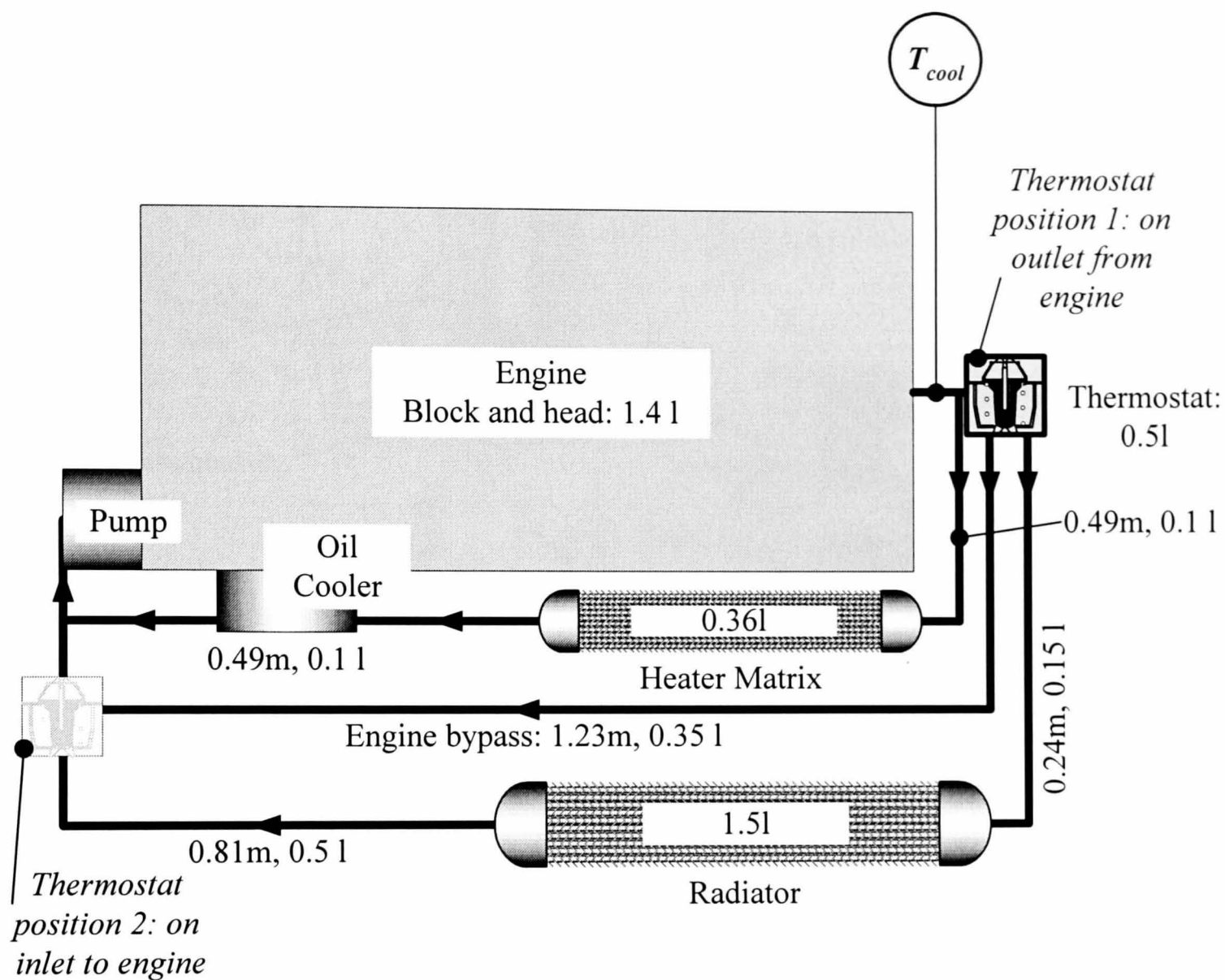


Figure 5.40 Comparisons of experimental and predicted data for **a)** coolant half rise times in seconds, **b)** oil half rise times in seconds and **c)** friction mean effective pressure in bar. Tests were conducted at a variety of speeds and loads (see Figures 5.33 to 5.38).



External circuit pipework: 28 mm ϕ

Inner circuit pipework: 16 mm ϕ

Bypass pipework: 19 mm ϕ

Figure 6.1 Illustration of the cooling circuit layout for the 1.6l Sigma engine. T_{cool} is the point at which coolant temperature measurements are taken.

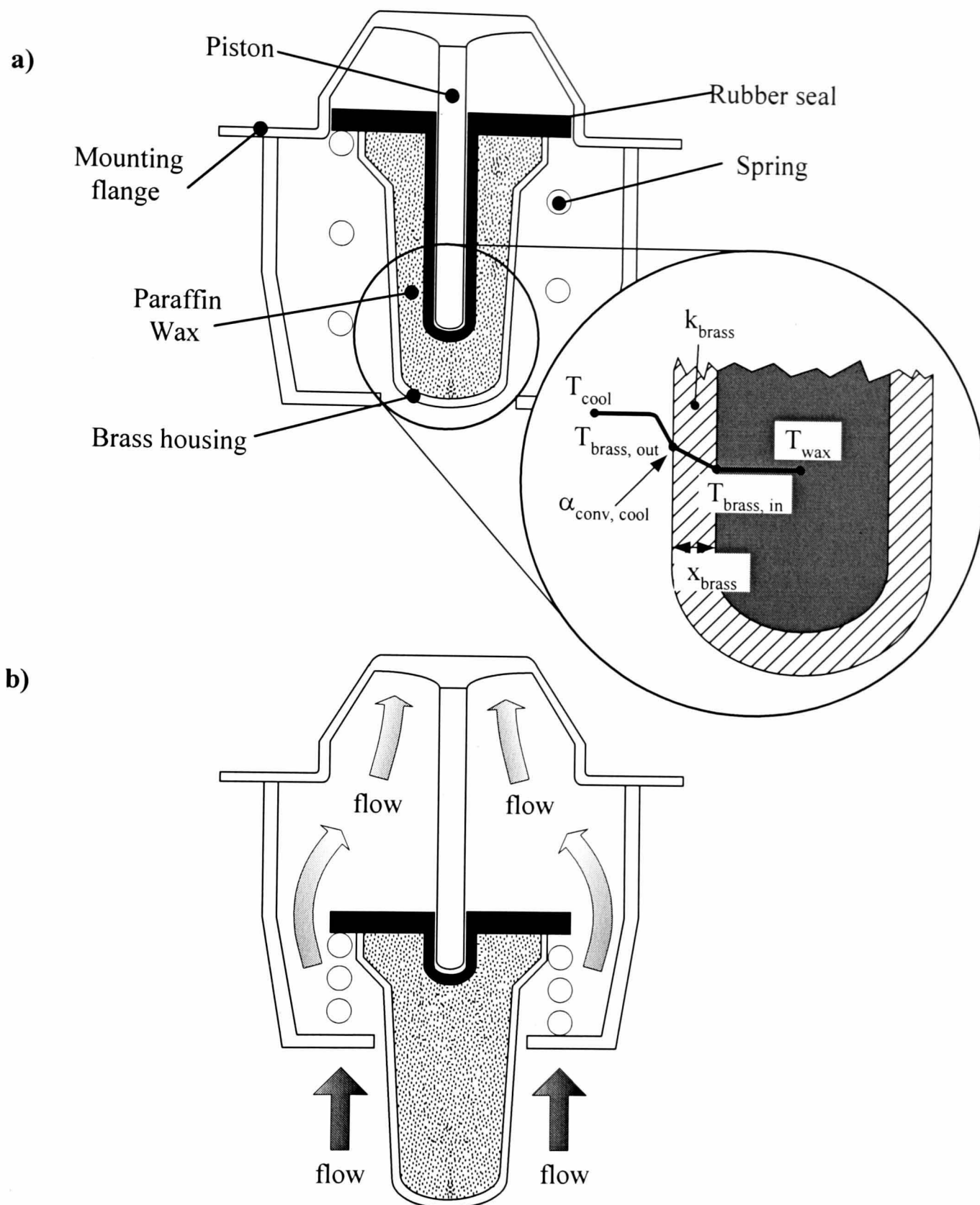


Figure 6.2 a) Closed and b) open positions of a mechanical thermostat. The enlargement illustrates the heat exchange mechanism between the coolant and the wax. α is the convective heat transfer coefficient between the coolant and the brass housing. x_{brass} is the thickness of the brass housing.

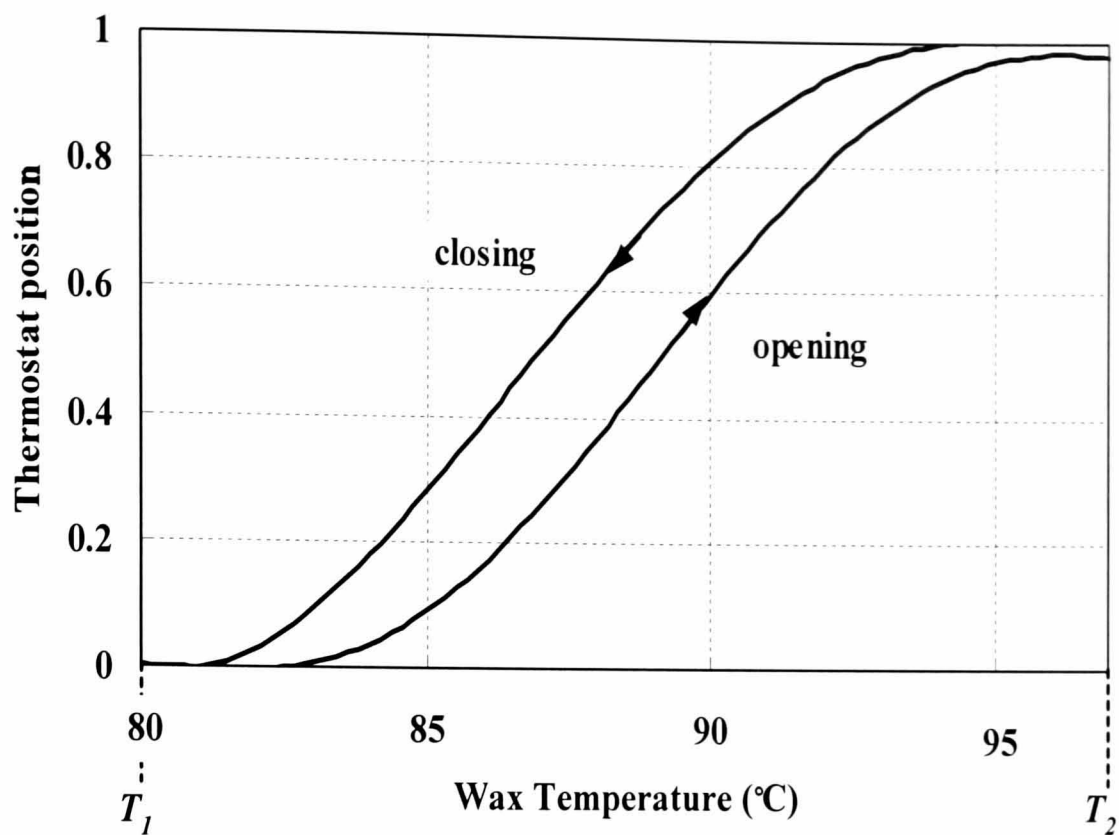


Figure 6.3 Illustration of the variation of thermostat position with temperature. T_1 is the temperature at which the thermostat begins to open. T_2 is the temperature at which the thermostat is fully open. The profile shown is a curve fit to experimental data [6.14].

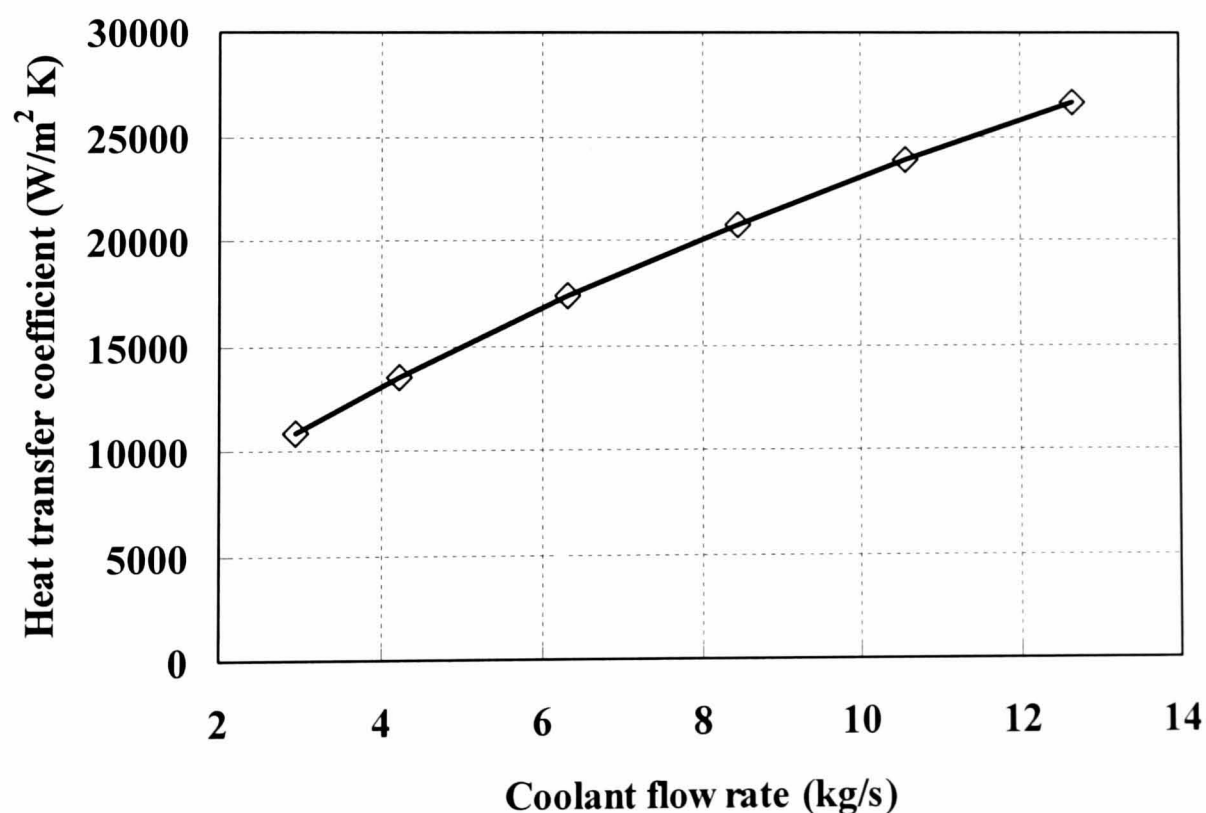


Figure 6.4 Variation of the convective heat transfer coefficient α with coolant flow rate at a coolant temperature of 20°C. The heat transfer coefficient was calculated using Equation 6.5.

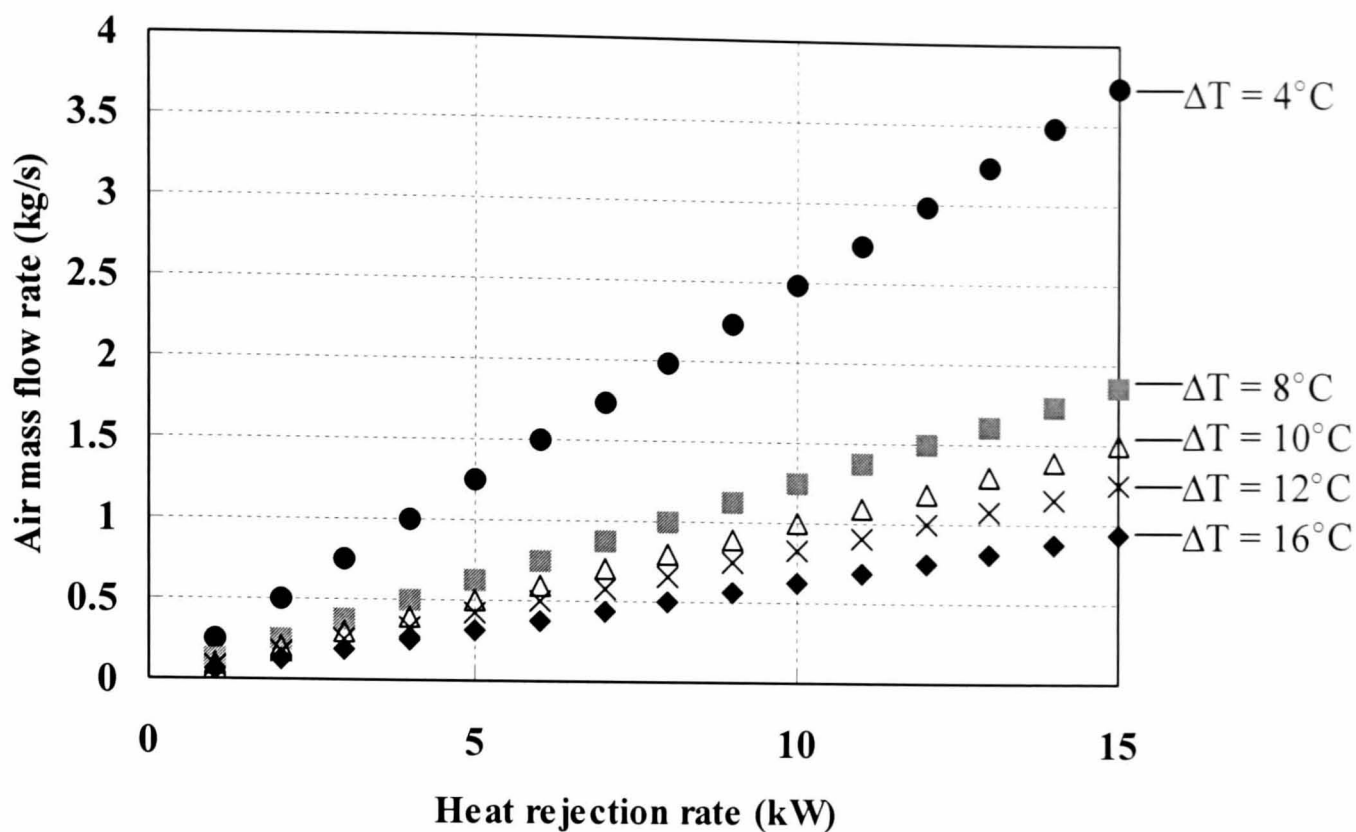


Figure 6.5 Variation of mass air flow rate with required heat rejection for different values of air temperature rise, ΔT , across the radiator.

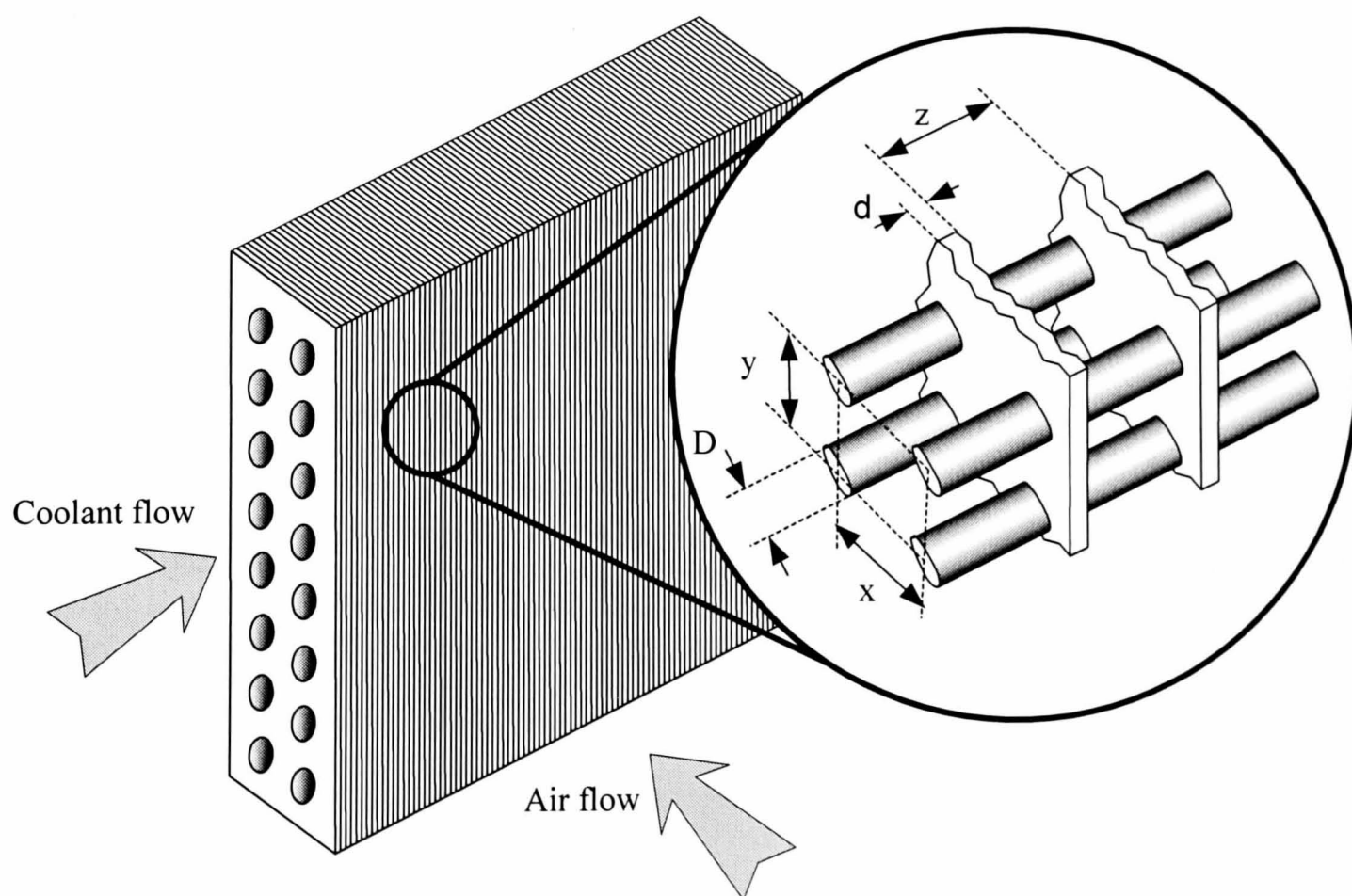
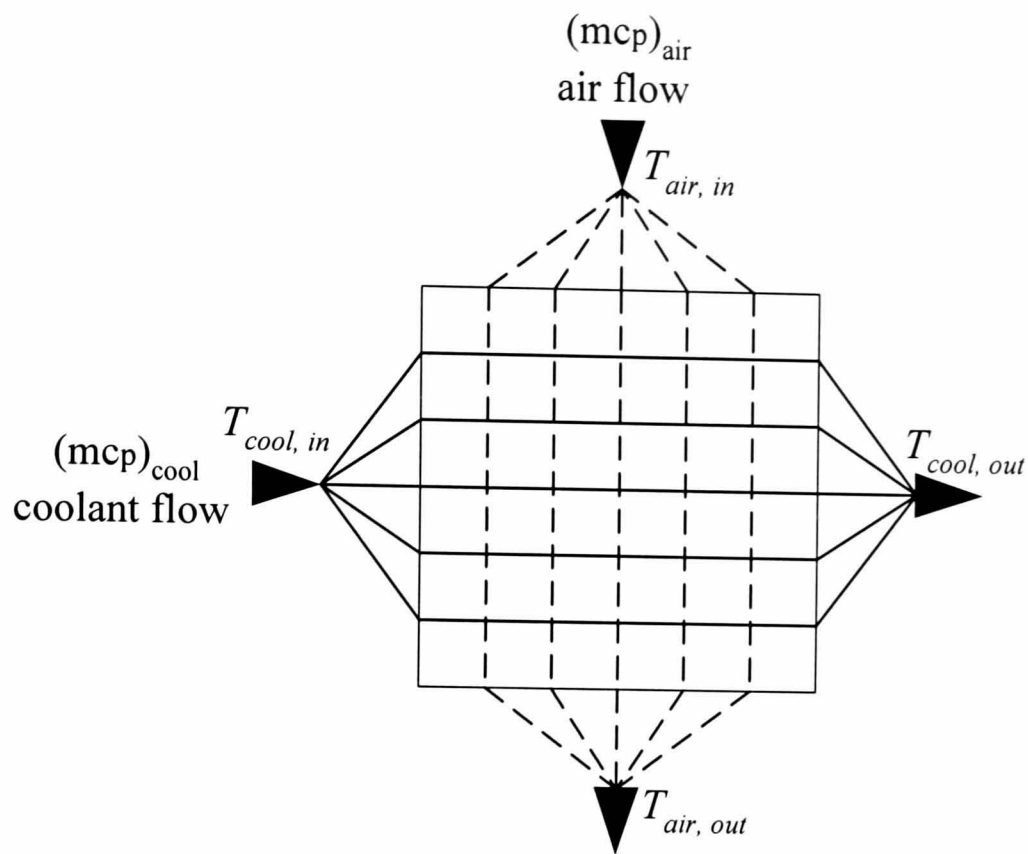


Figure 6.6 Illustration of the basic configuration of a radiator and the dimensions required to determine the values of σ , the ratio of the minimum flow cross sectional area to the frontal area and α , the ratio of the total area available for heat transfer to the volume of the radiator.



$$C = \frac{(mc_p)_{min}}{(mc_p)_{max}}$$

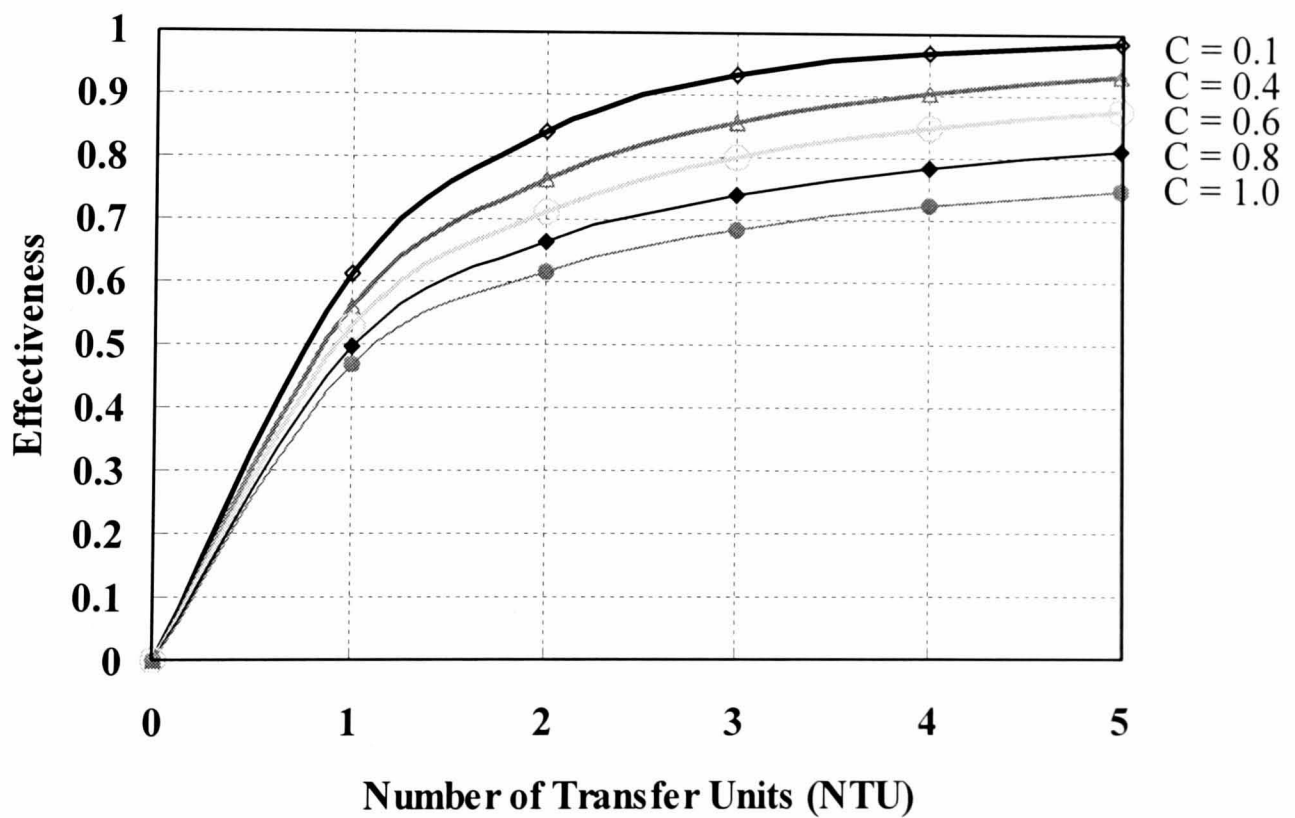


Figure 6.7 The variation of effectiveness with the number of transfer units (NTU) for different capacity rate ratios, C . Effectiveness decreases as the capacity rate ratio increases.

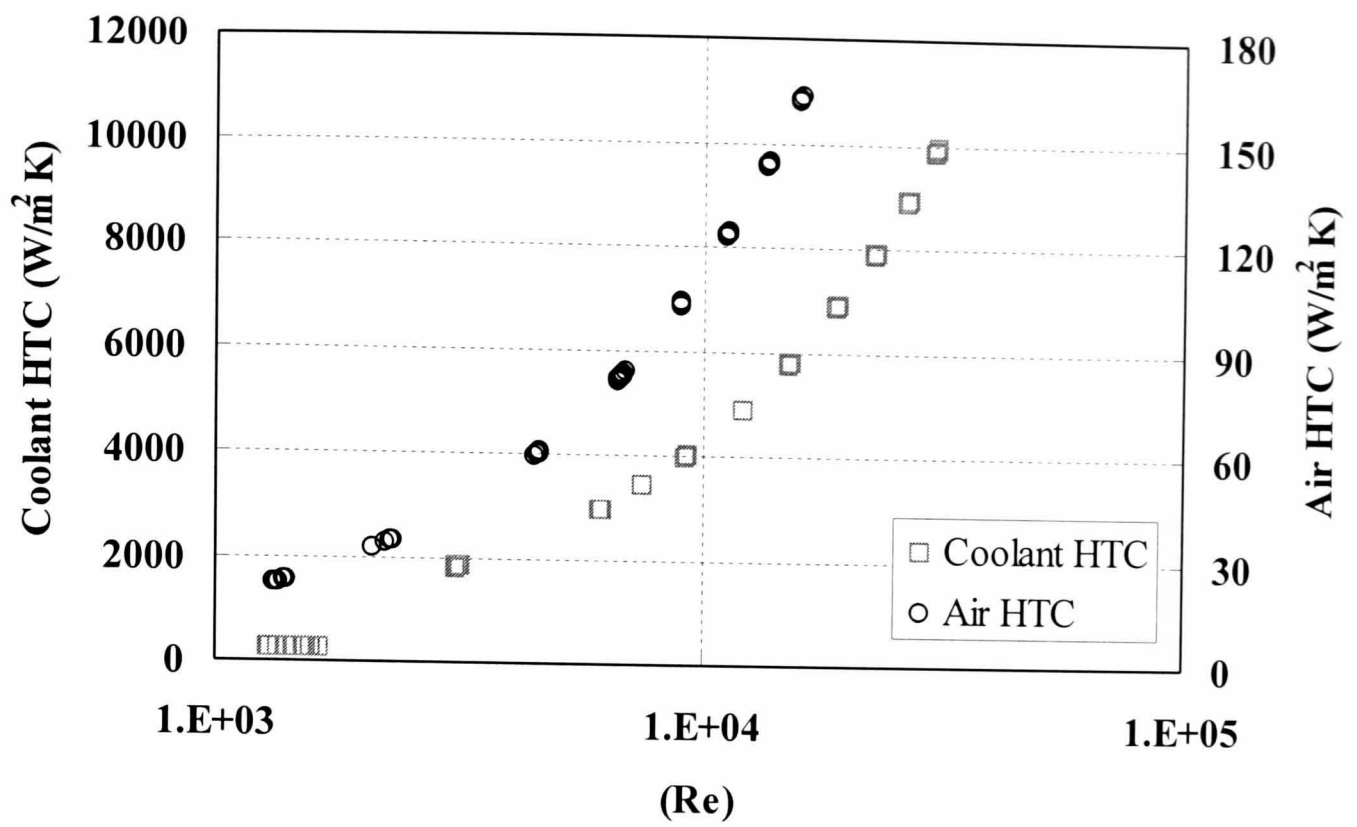


Figure 6.8 Variation of the coolant side and air side heat transfer coefficients (HTC) with Reynolds number.

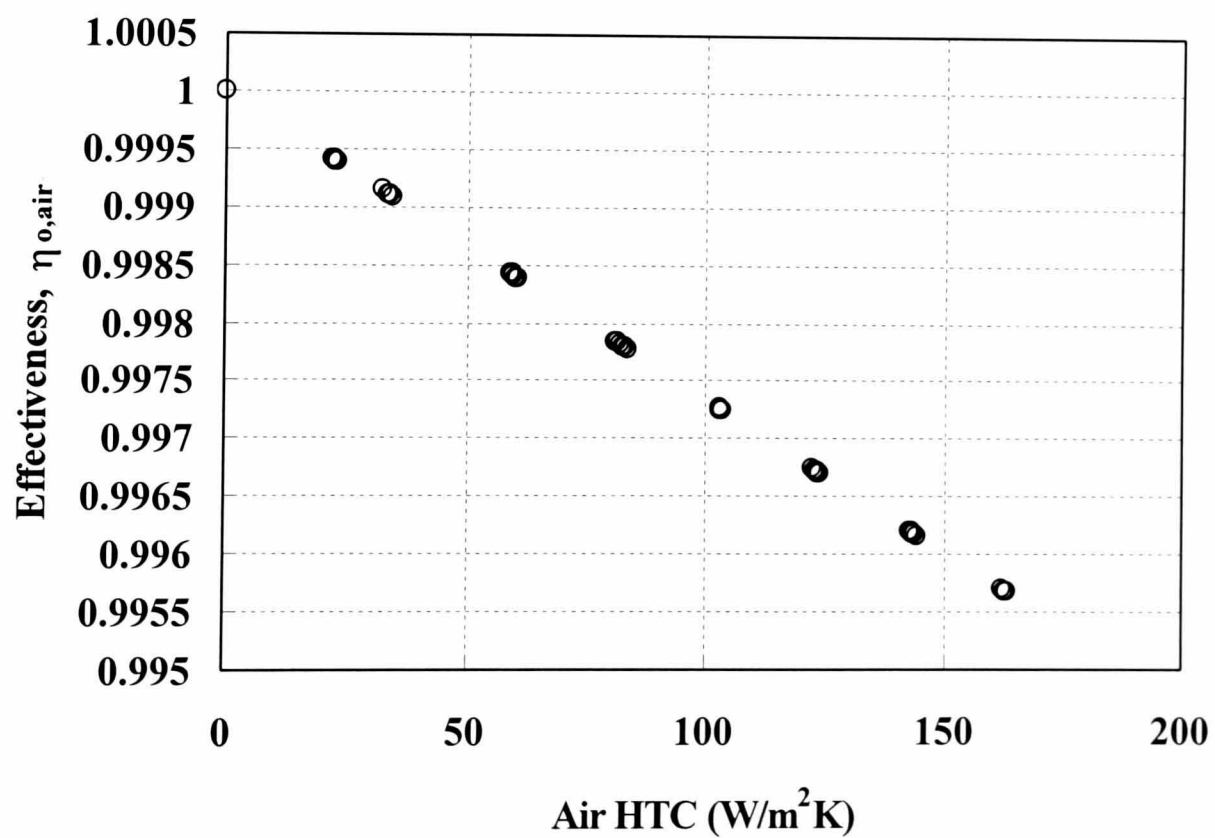


Figure 6.9 Variation of the heat transfer effectiveness of the air side surface with the air side heat transfer coefficient (HTC).

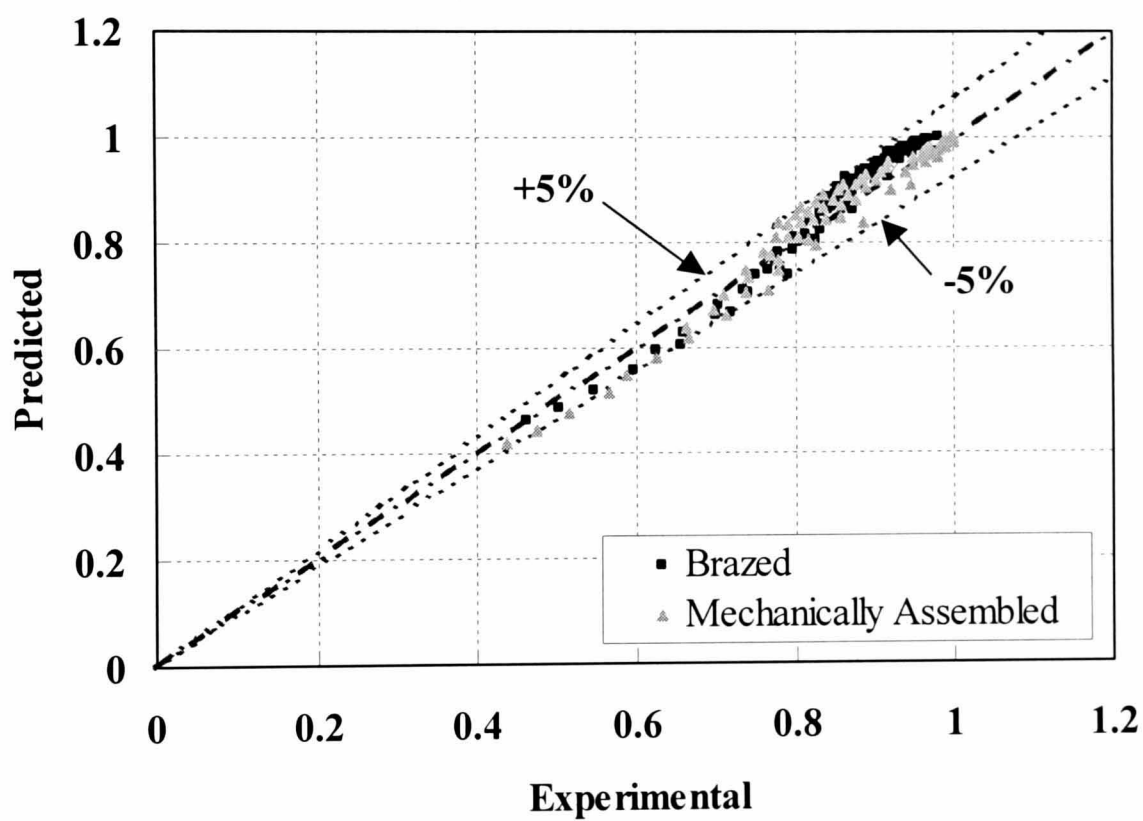
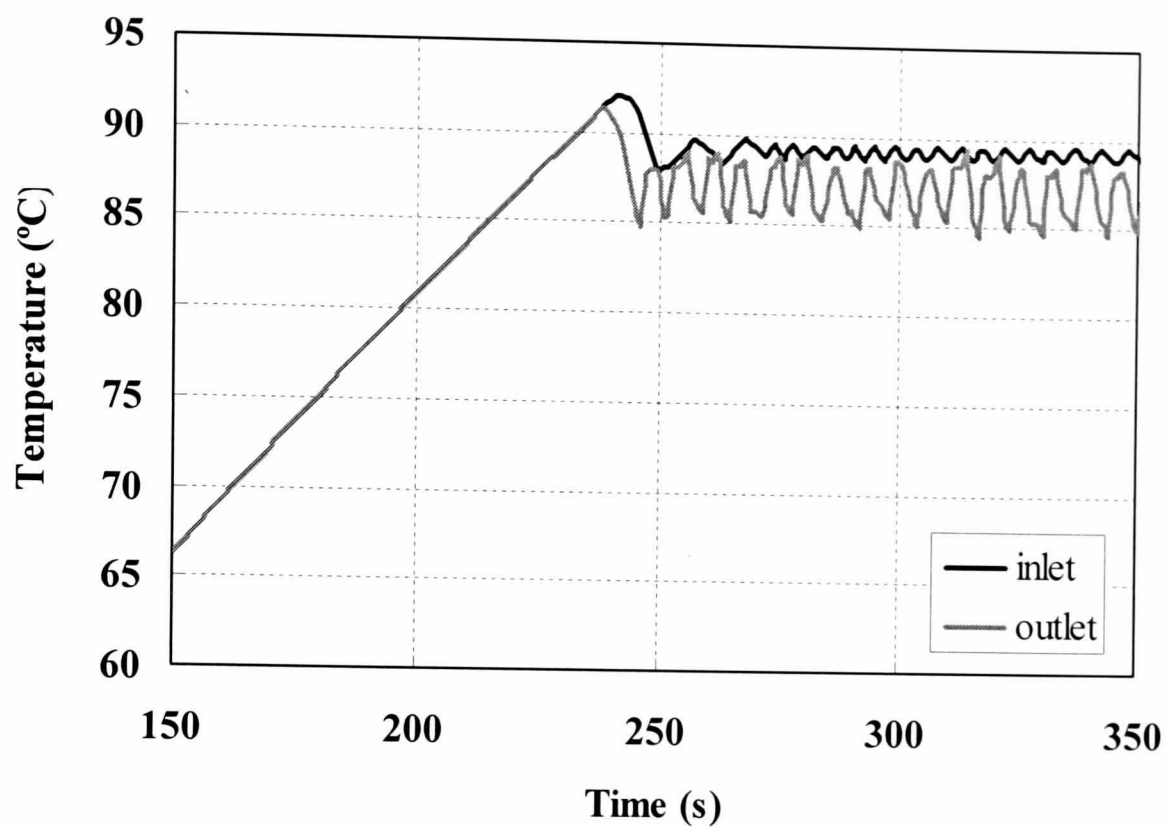


Figure 6.10 Comparison between effectiveness values supplied by Ford Motor Company [6.35] and model predictions for two different cabin heaters, designed for use in the Mondeo/IDI TCi combination.

a)



b)

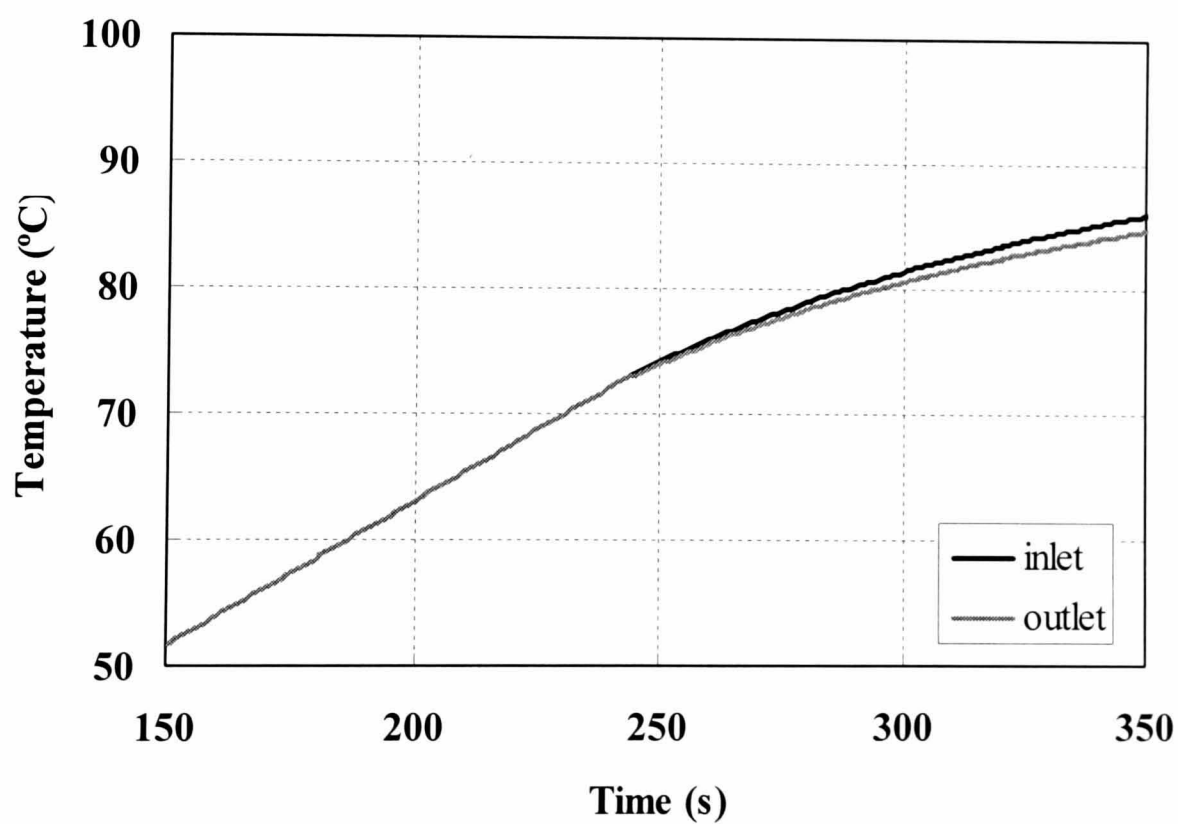


Figure 6.11 Predicted a) coolant and b) oil temperatures for the 1.6l Sigma at 2500 rpm, 20 Nm, showing the difference between the profiles depending upon the position of the thermostat in the external circuit, whether at the inlet to the engine or on the outlet.

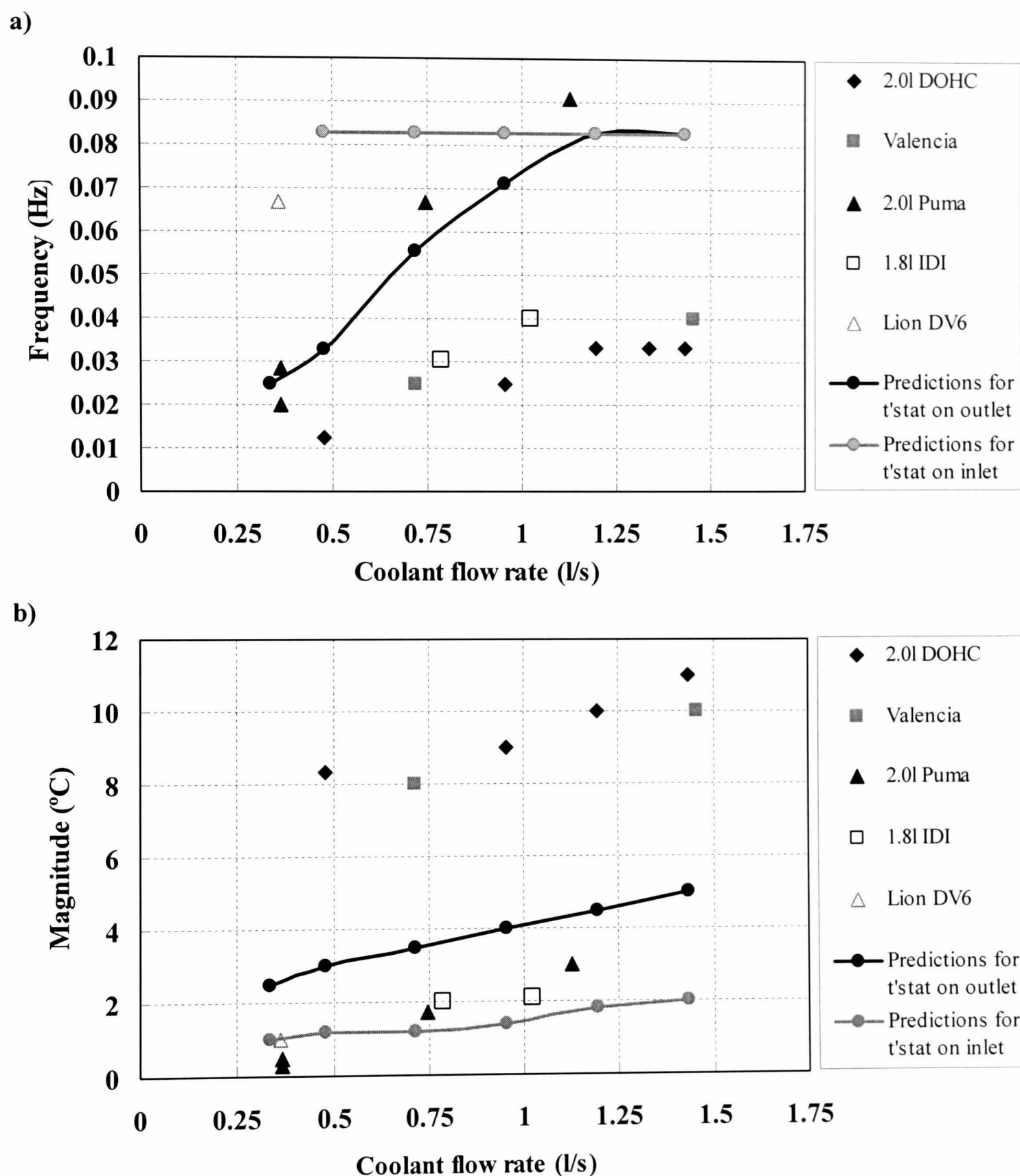


Figure 6.12 Experimental and predicted a) frequency b) magnitude of coolant temperature excursions for various engines. For all engines except the Lion DV6, the thermostat is on the outlet from the engine. Predicted data is for the thermostat (t'stat) for the 1.6l Sigma engine on the inlet to or outlet from the engine.

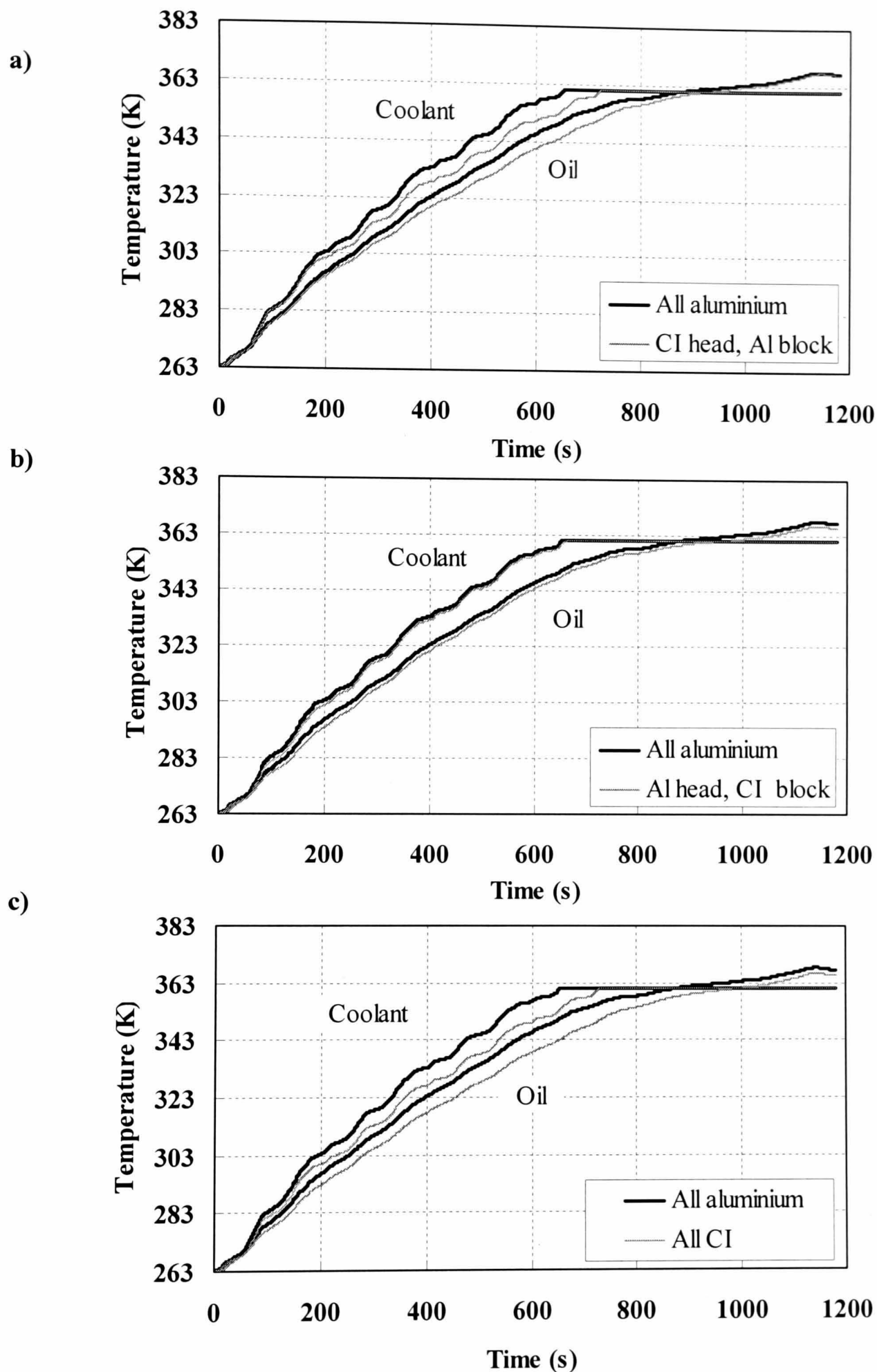
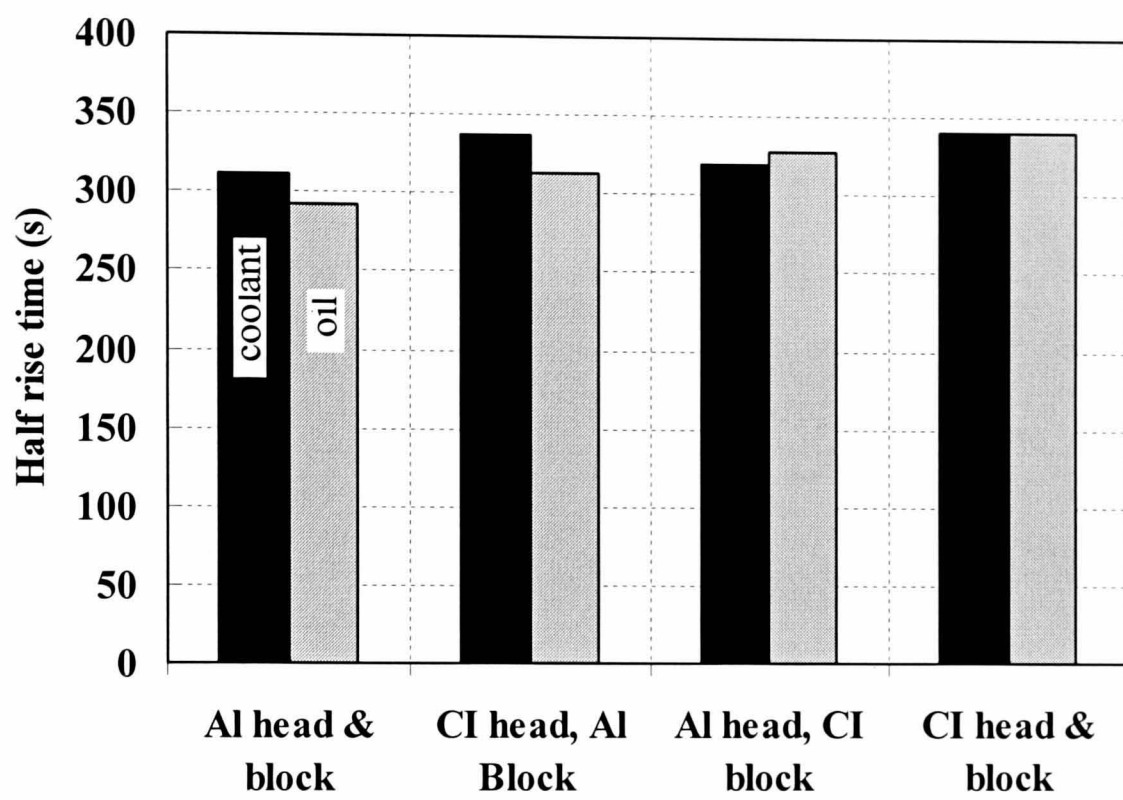


Figure 7.1 The effect of different head and block materials compared to an all aluminium engine (aluminium head and block) on coolant and oil warm-up profiles for the 1.6l Sigma over the NEDC. **a)** Cast iron (CI) head and aluminium (Al) block **b)** Aluminium head and cast iron block **c)** Cast iron head and block

a)



b)

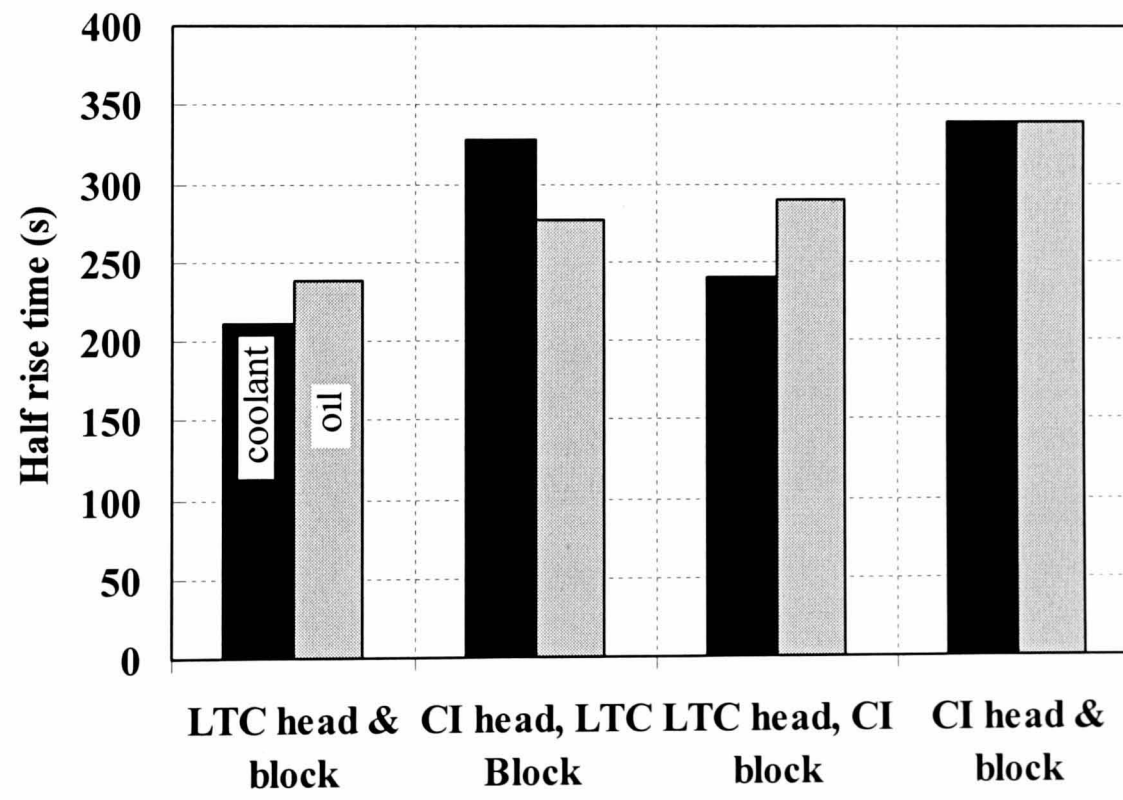


Figure 7.2 The effect of head and block materials on coolant and oil half rise times for a) different combinations of aluminium (Al) and cast iron (CI) components and b) different combinations of a fictitious material with an extremely low thermal capacity (LTC) and cast iron. The half rise times are defined as the time taken for coolant and oil temperatures to rise by 60°C and 40°C respectively.

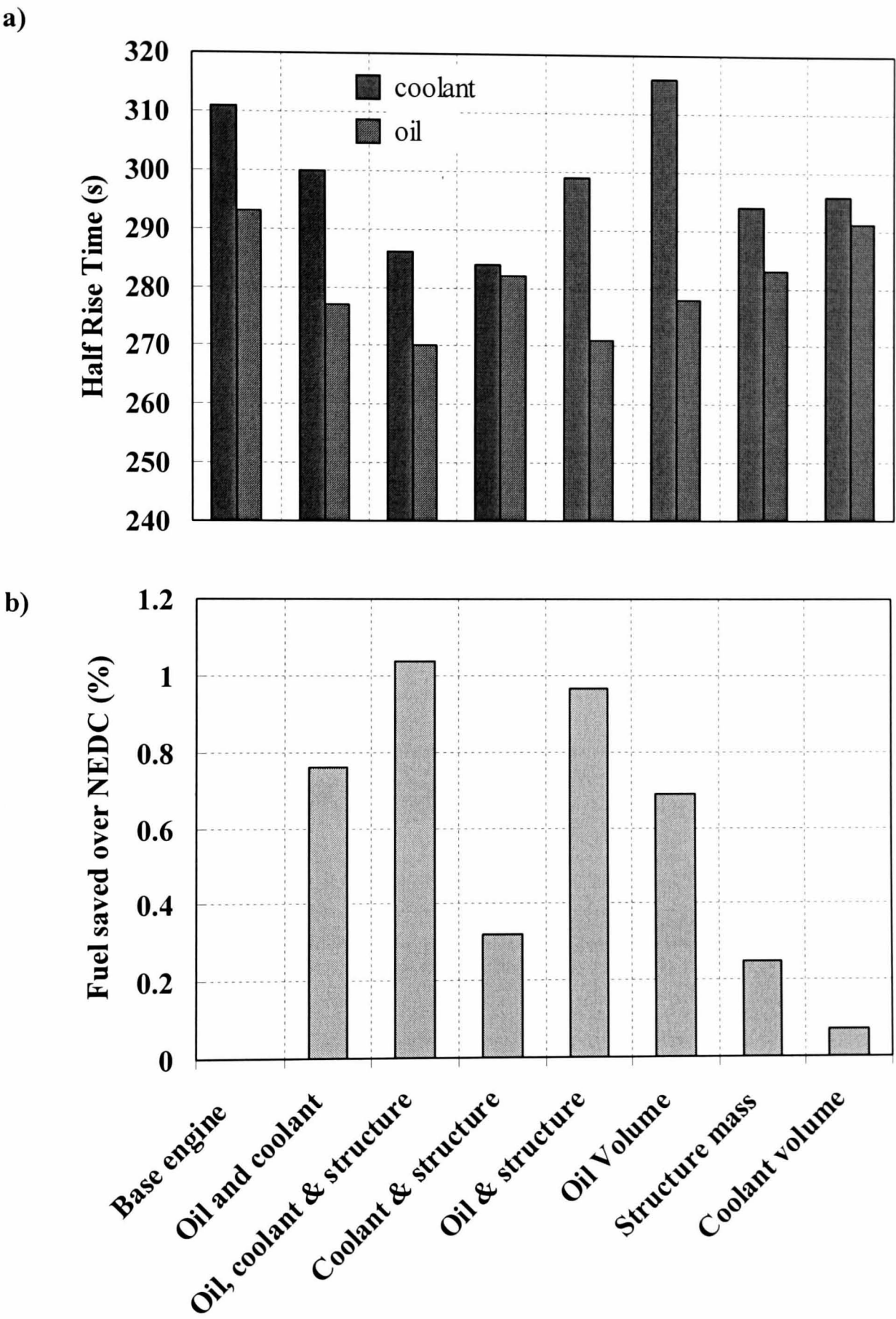


Figure 7.3 The effect of reductions in thermal capacity on a) coolant and oil half rise times and b) the percentage of fuel saved over the NEDC, compared to the base engine.

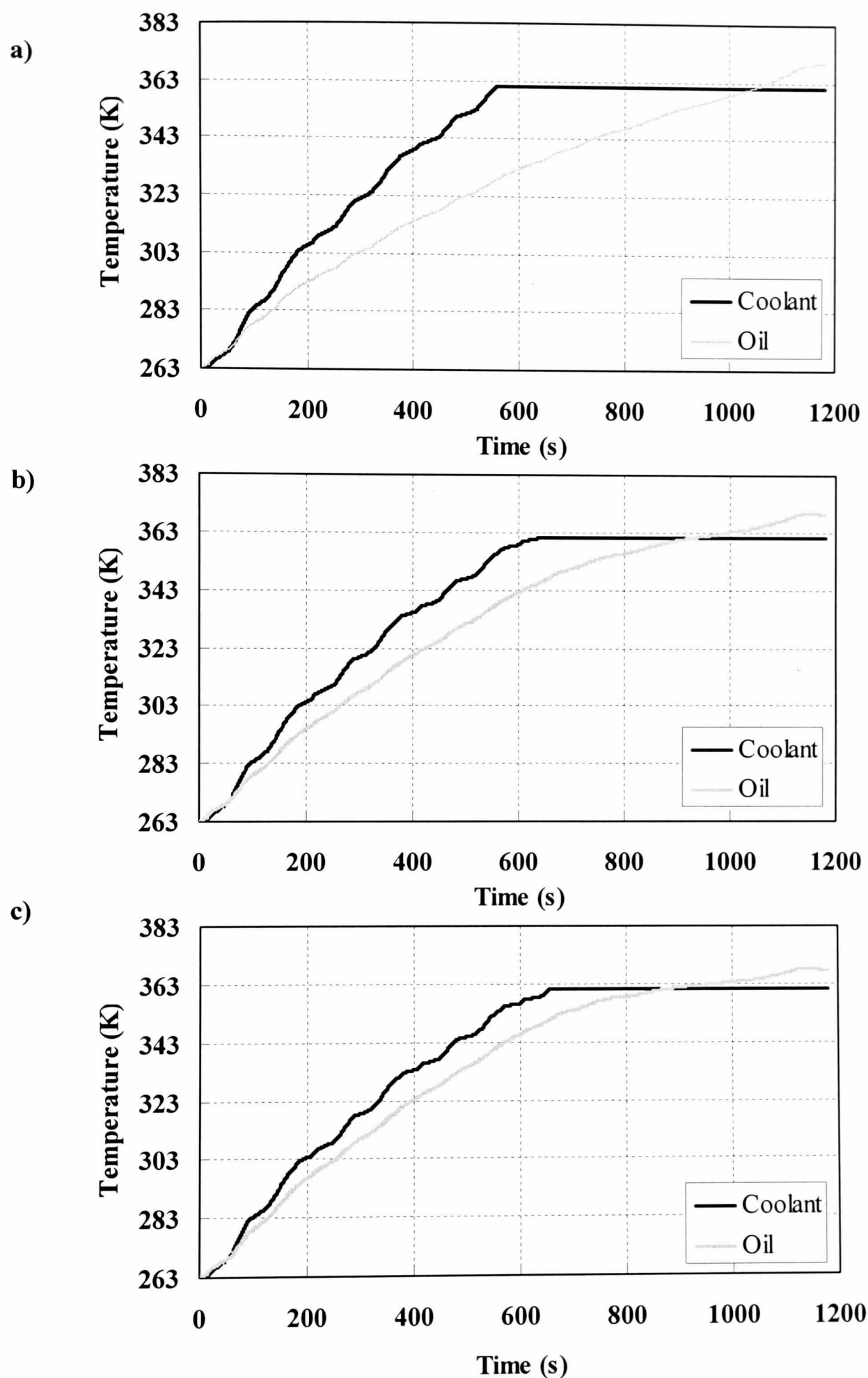


Figure 7.4 Illustration of the effect of oil cooler effectiveness on coolant and oil warm-up profiles for the 1.6l Sigma over the NEDC. **a)** No oil cooler **b)** Oil cooler effectiveness of 0.2 **c)** Oil cooler effectiveness of 0.4

Continued overleaf ...

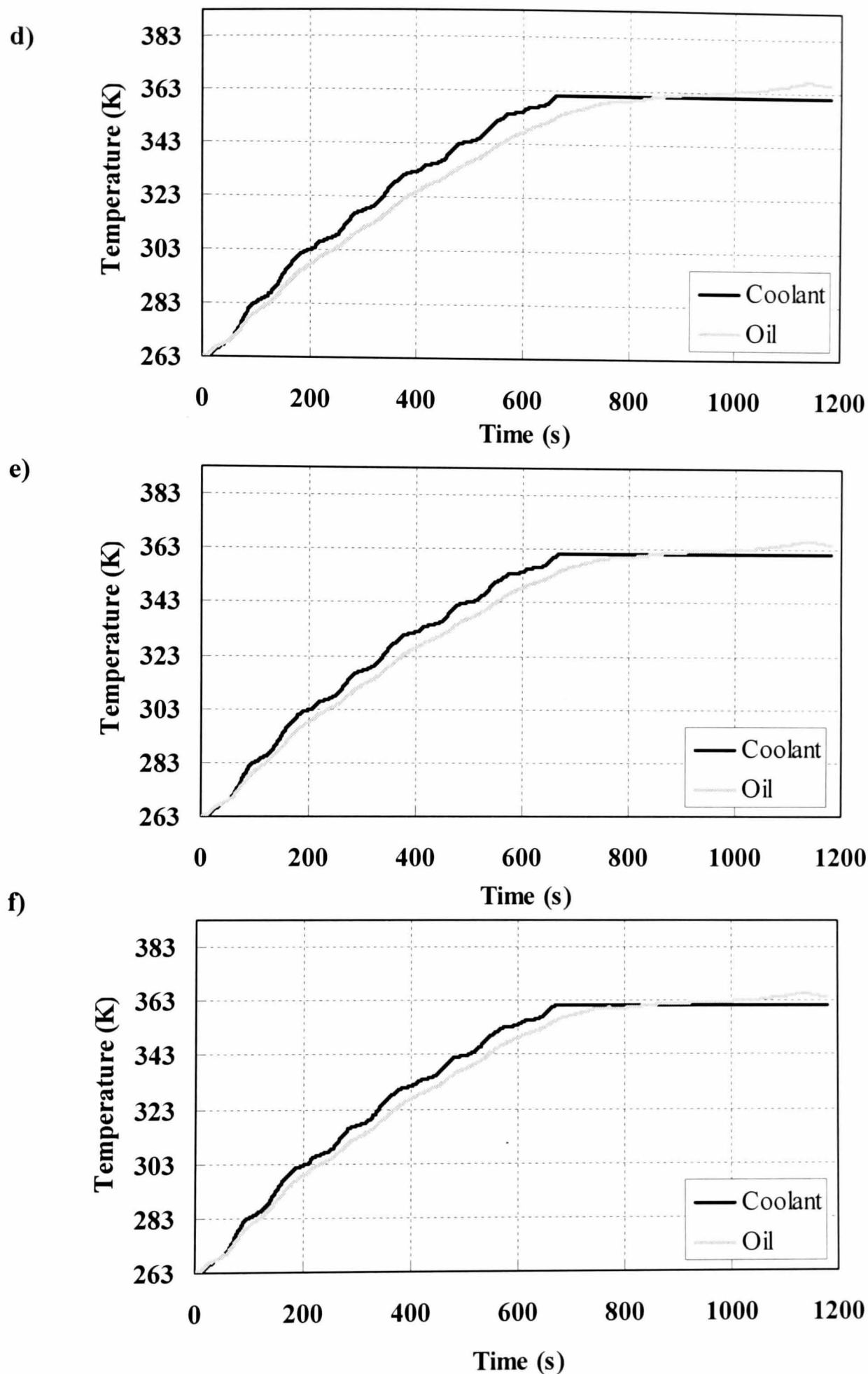


Figure 7.4 Cont. Illustration of the effect of oil cooler effectiveness on coolant and oil warm-up profiles for the 1.6l Sigma over the NEDC. **d)** Oil cooler effectiveness of 0.6 **e)** Oil cooler effectiveness of 0.8 **f)** Oil cooler effectiveness of 1.0

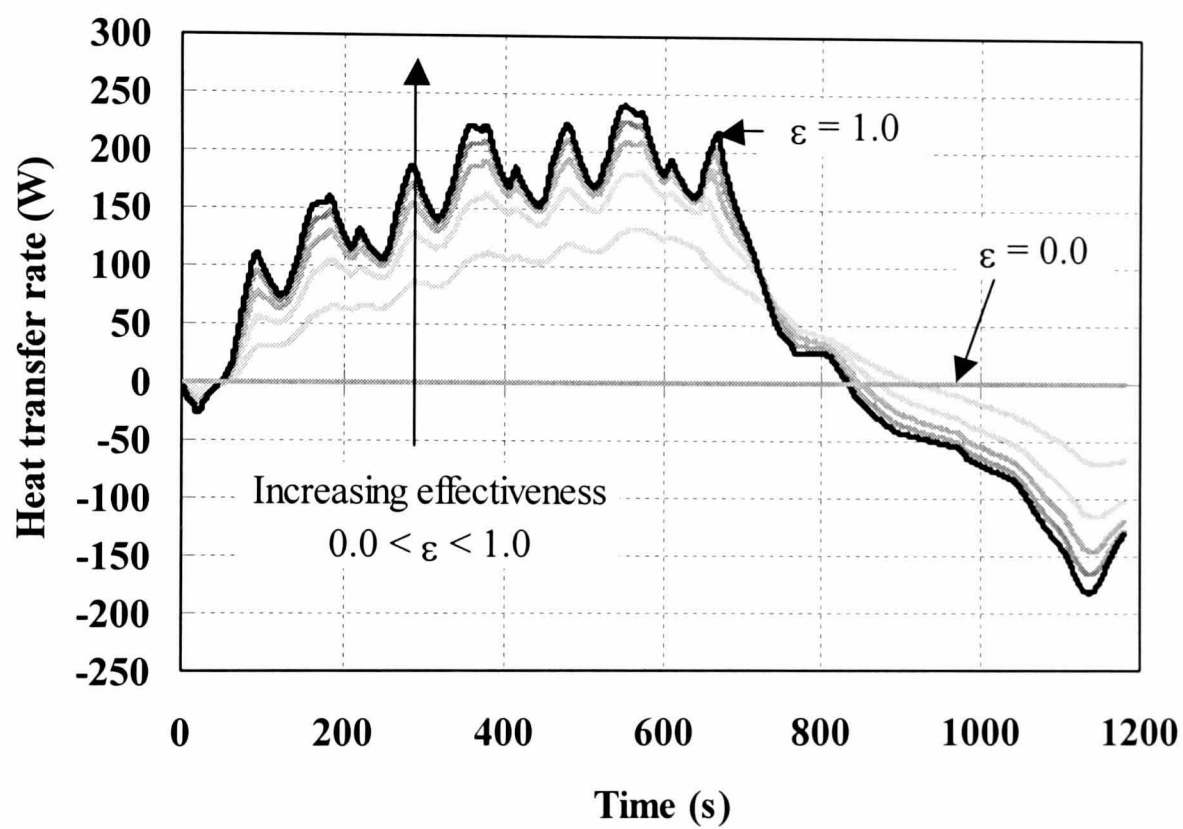


Figure 7.5 The effect of varying the effectiveness of the oil cooler on the heat transfer rate from the coolant to the oil.

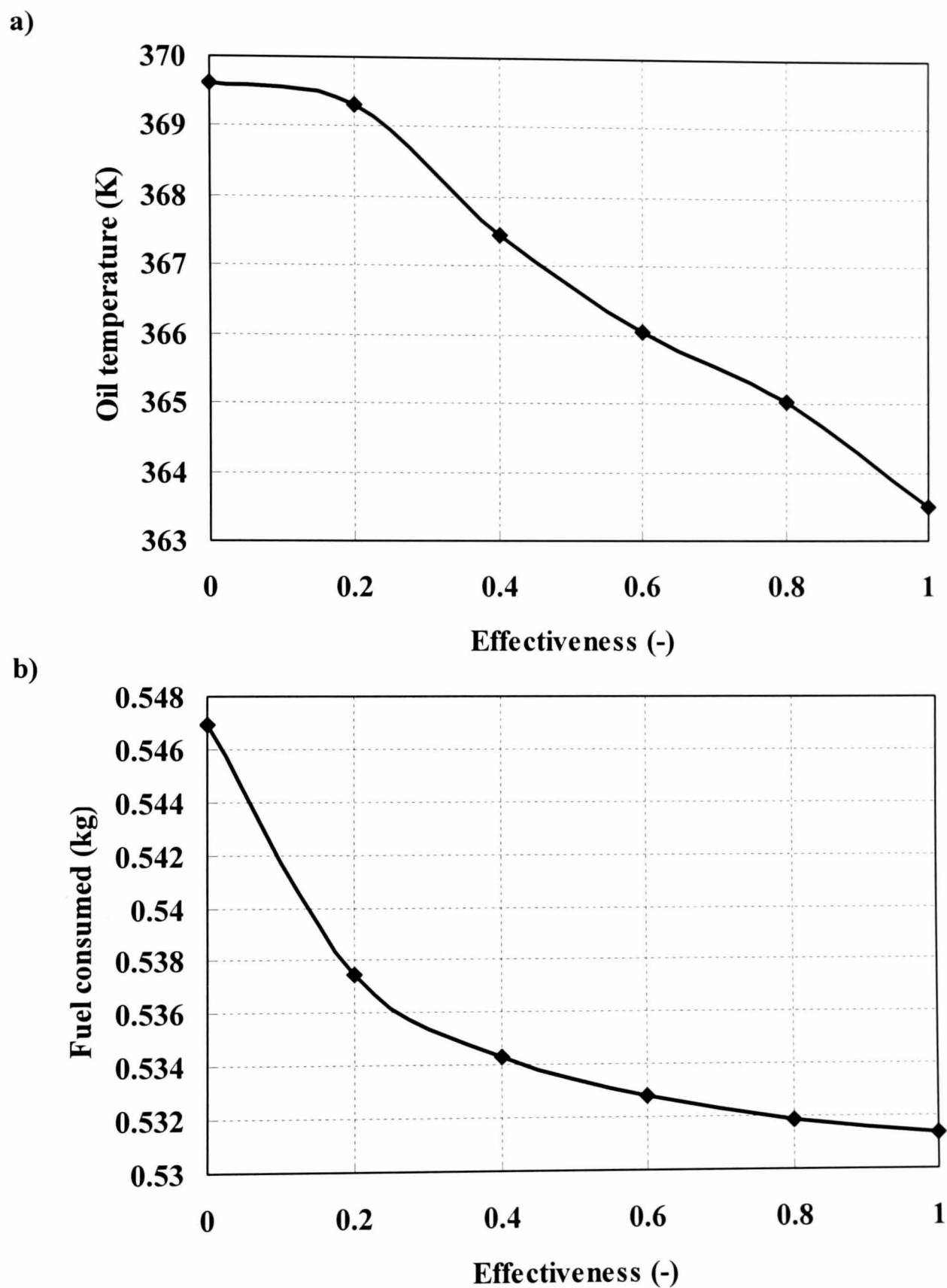


Figure 7.6 The effect of oil cooler effectiveness on **a)** the final oil temperature recorded at the end of the NEDC and **b)** the fuel consumed over the NEDC

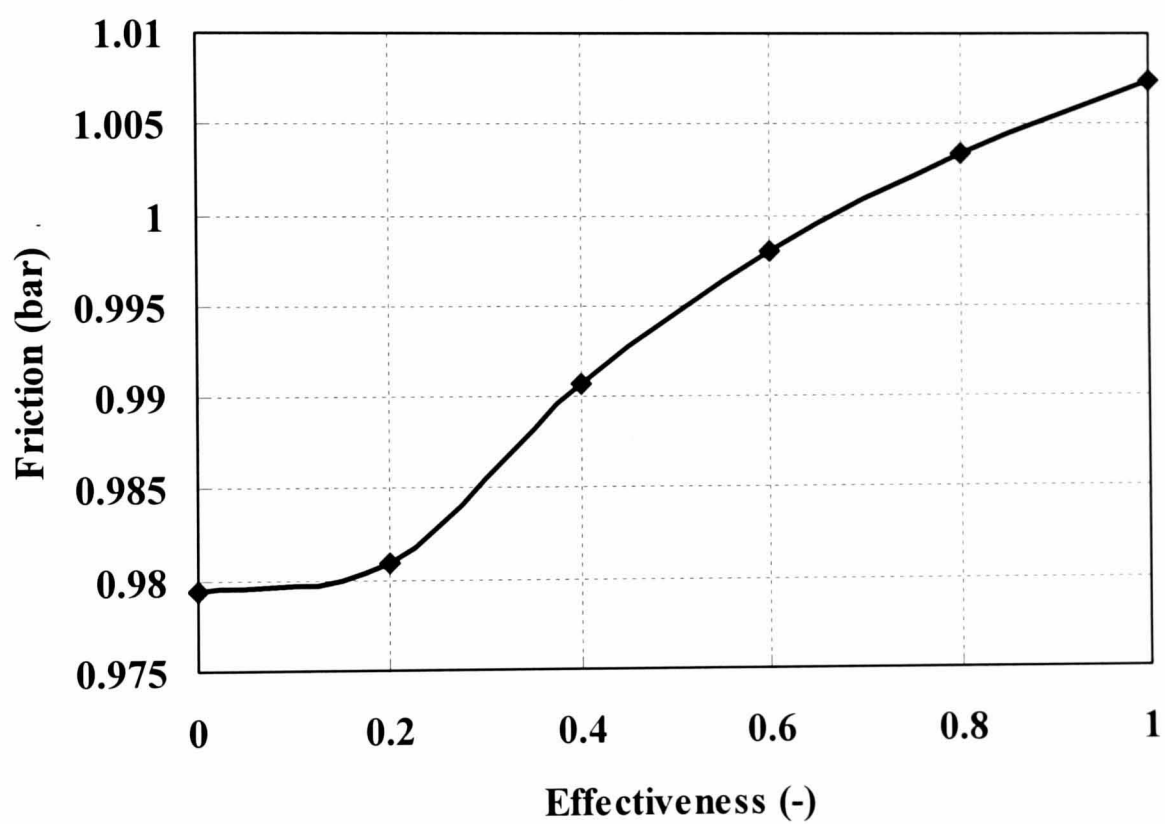


Figure 7.7 Final value of friction at the end of the NEDC for varying oil cooler effectiveness.

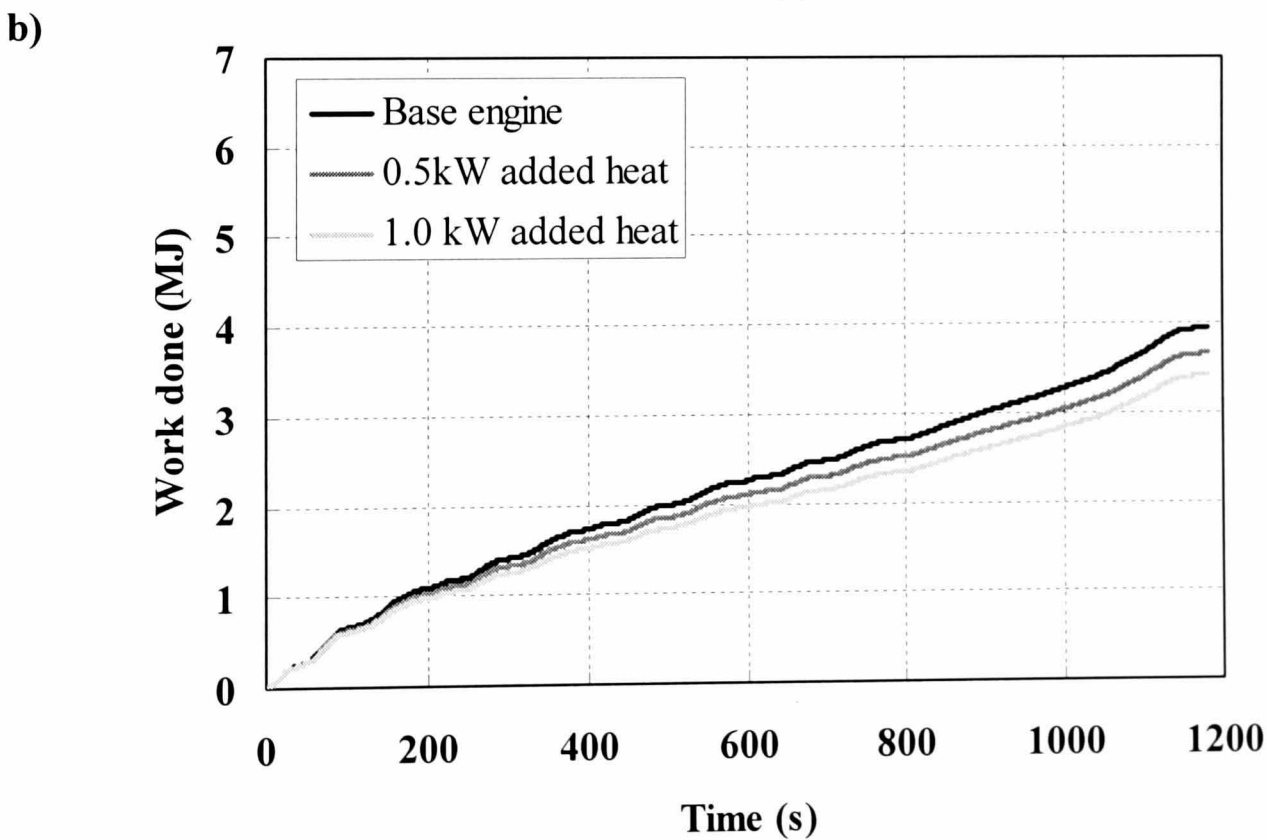
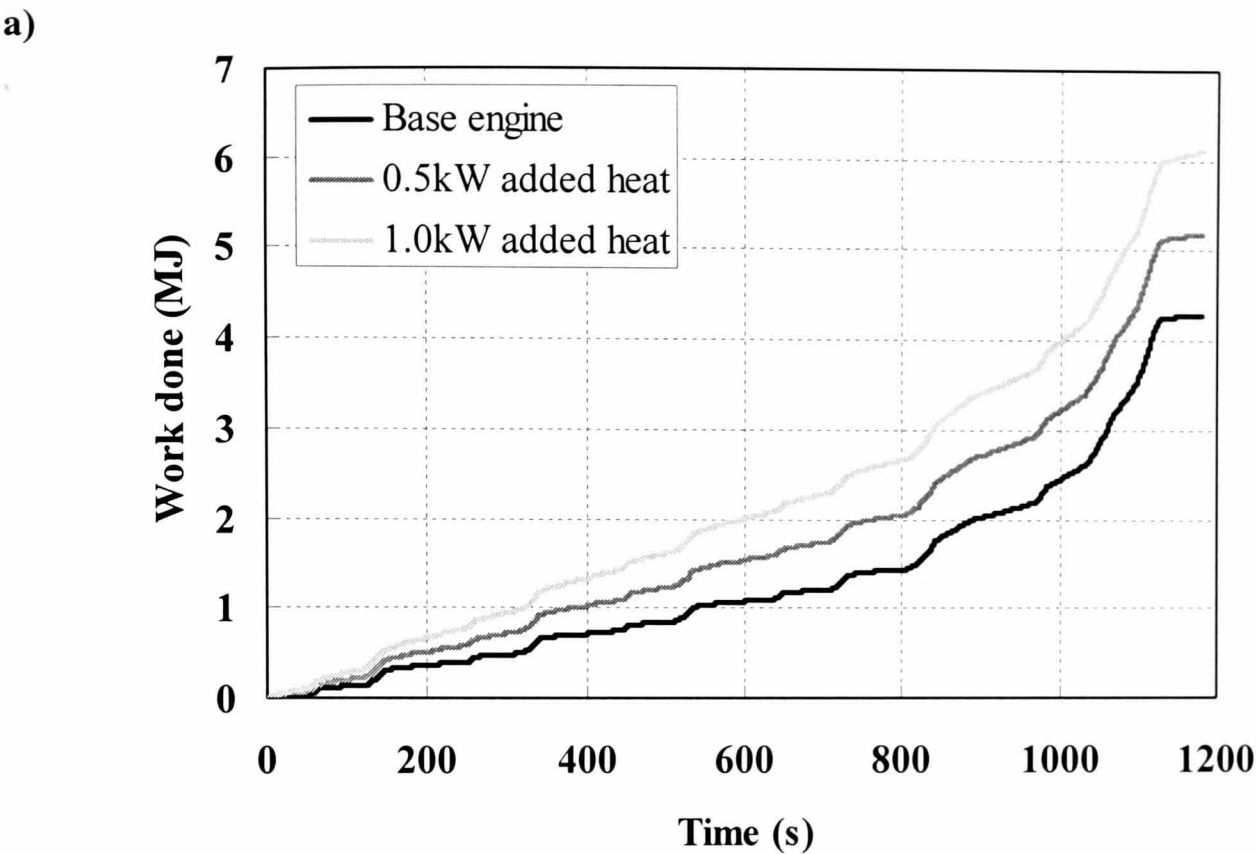


Figure 7.8 The effect of using an oil sump heater driven by the alternator on a) brake work done and b) friction work done. The increase in brake work done for increasing amounts of heat into the sump clearly exceeds the reduction in friction work done over the NEDC.

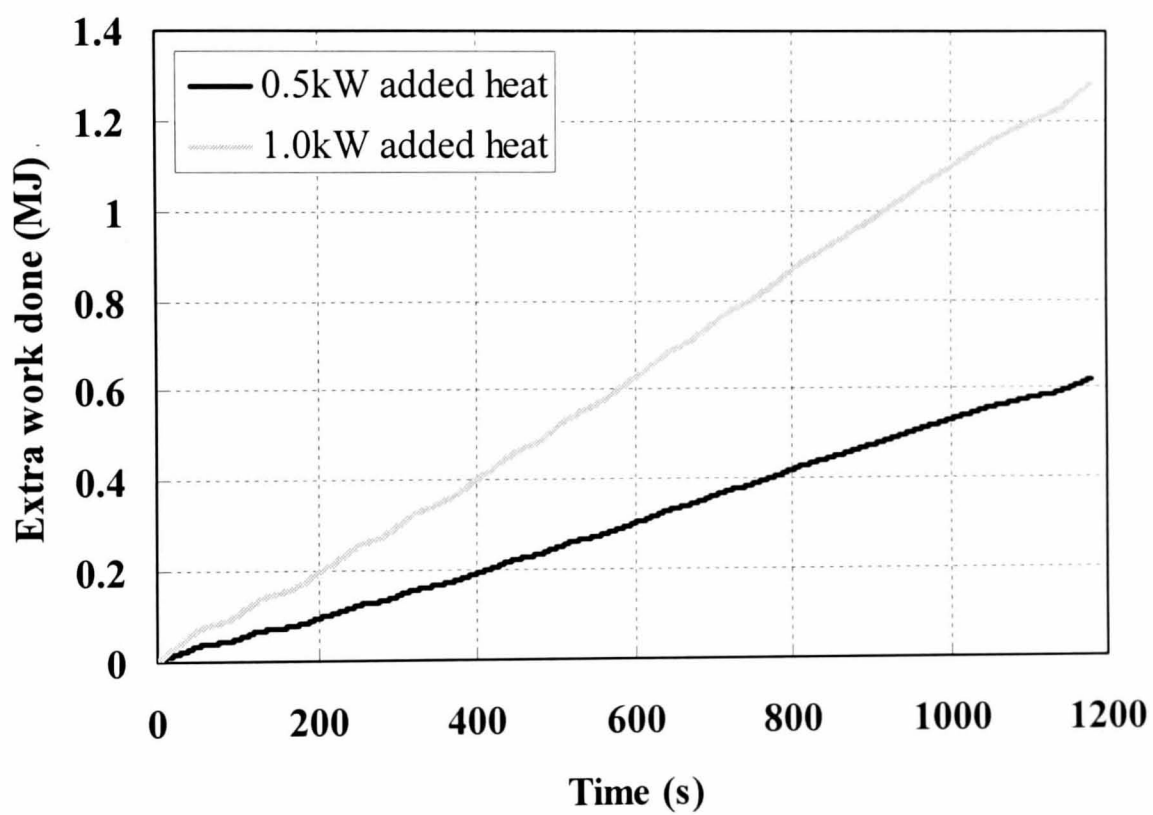


Figure 7.9 The increase in engine indicated work done over the NEDC by using an alternator-driven sump oil heater to add 0.5kW and 1.0kW of heat into the oil

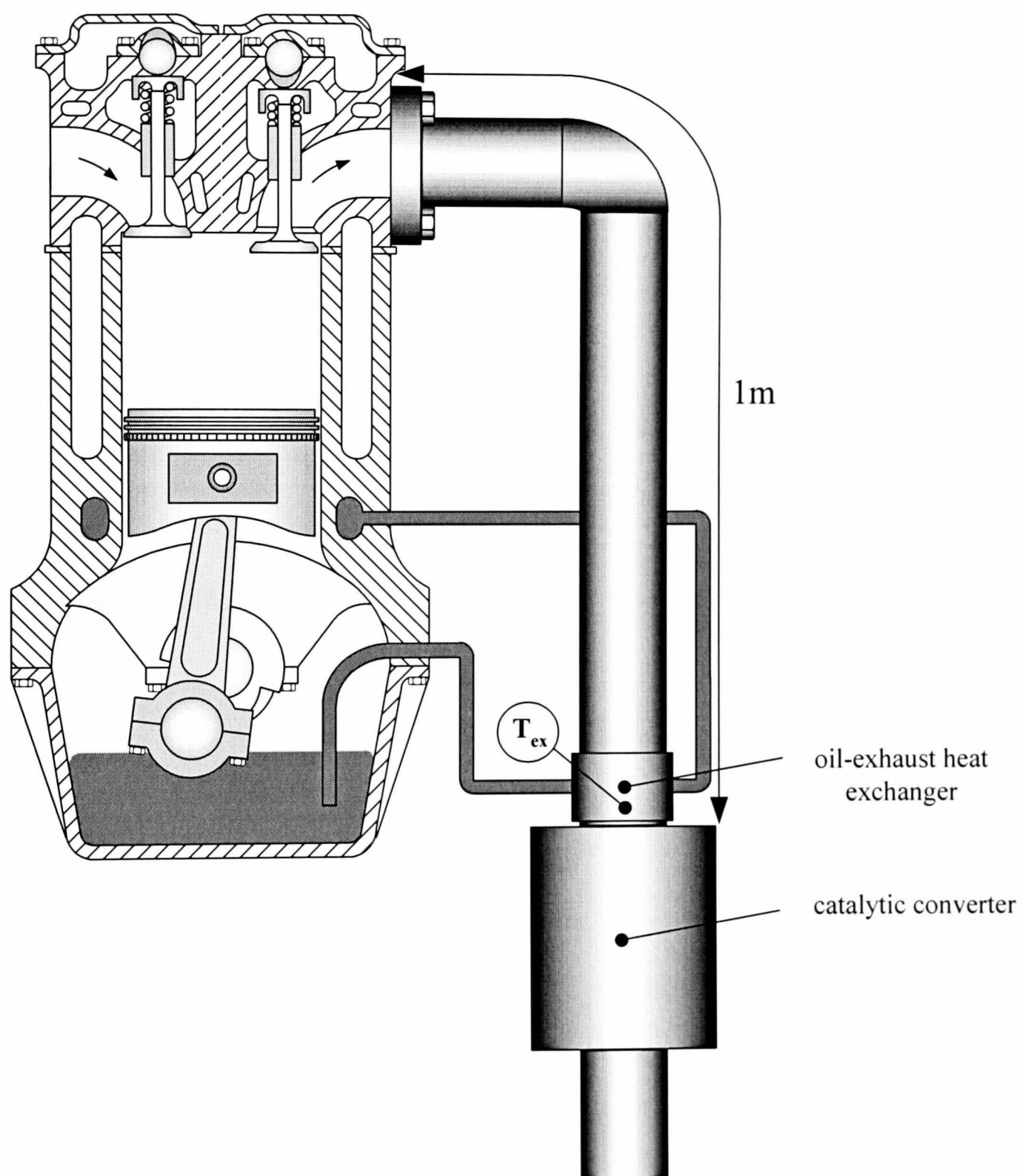
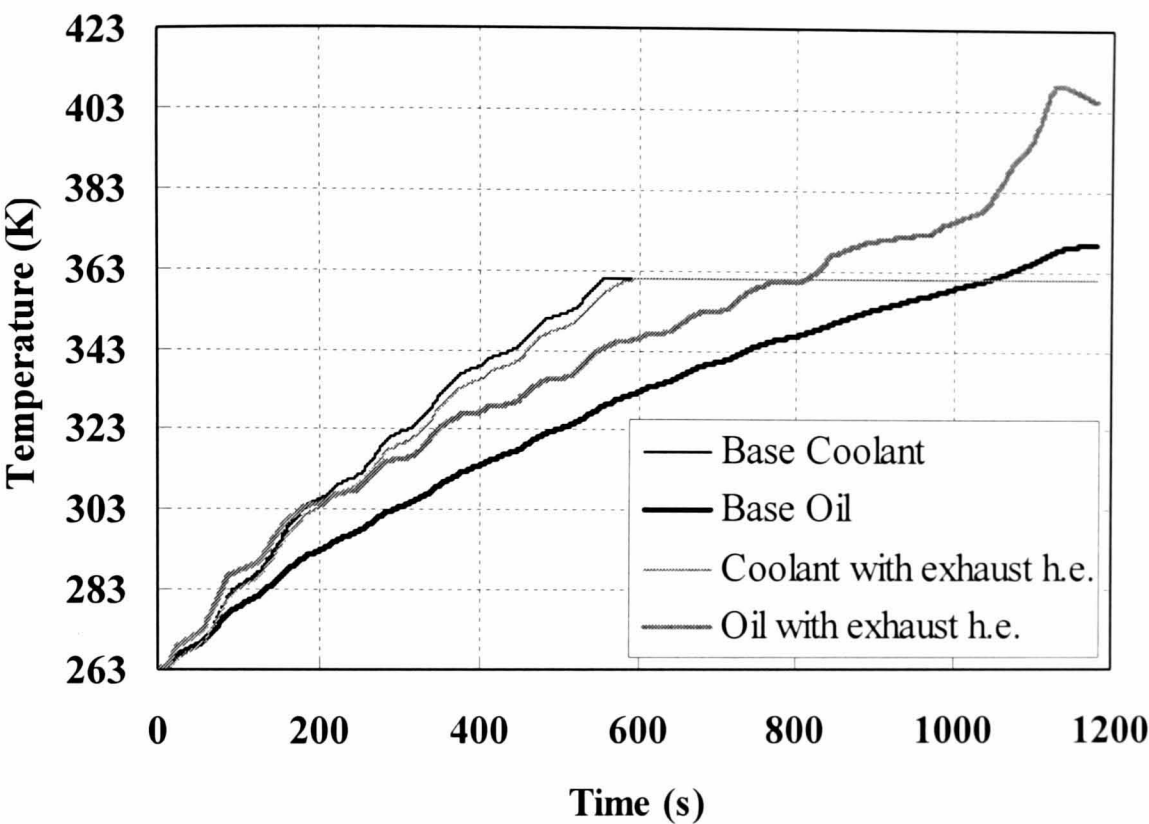


Figure 7.10 Illustration of the position of the measurement of exhaust gas temperature, T_{ex} , 1 metre down the tailpipe, just before the catalytic converter.

a)



b)

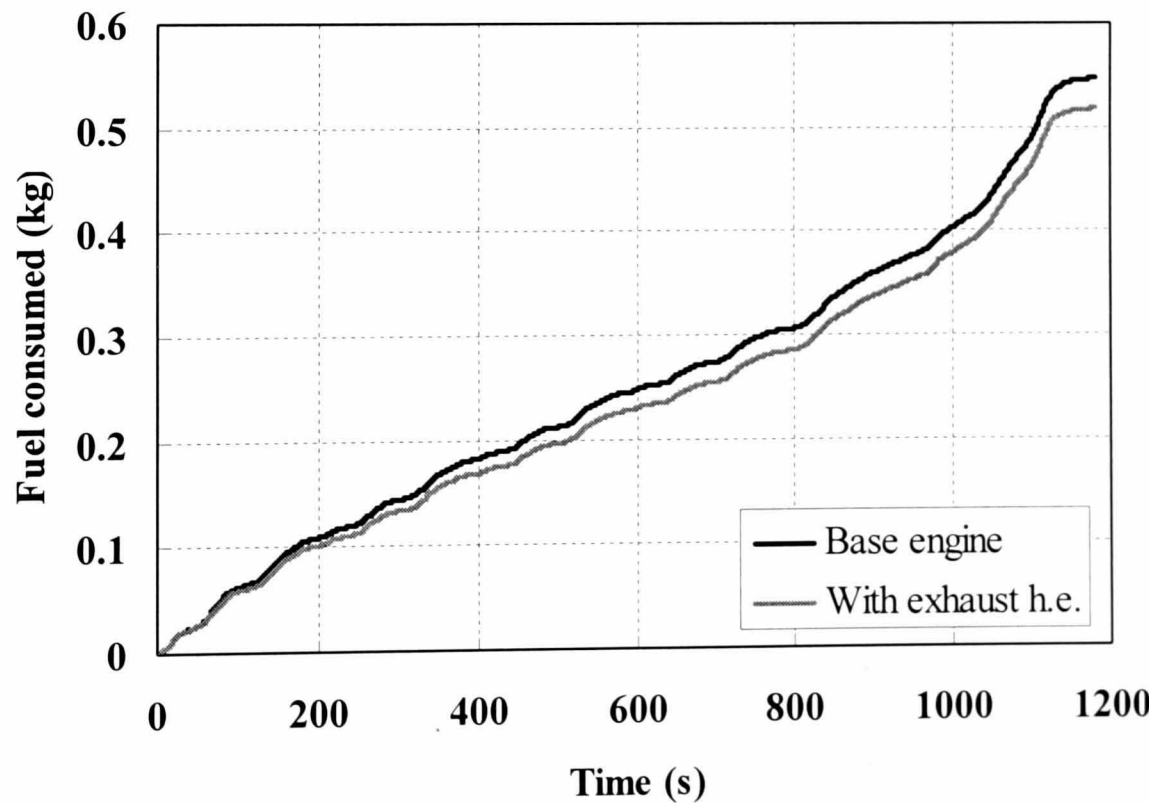
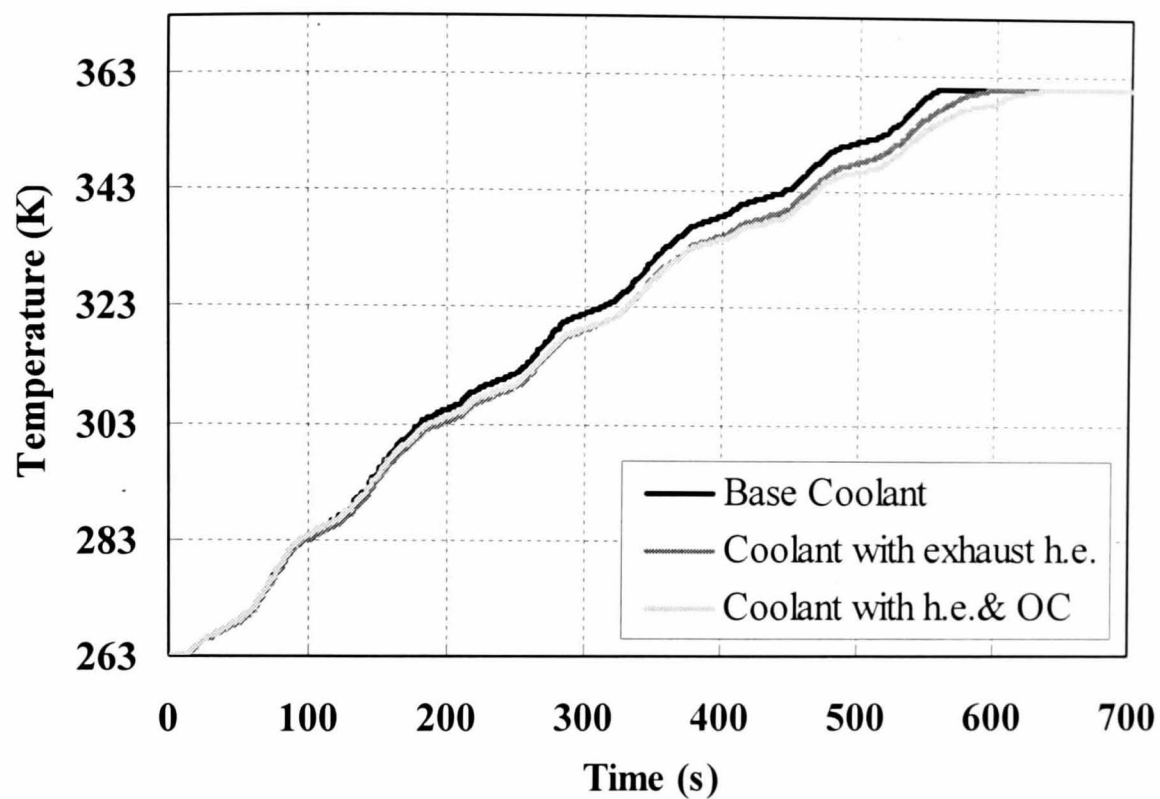


Figure 7.11 The effect of an oil-exhaust heat exchanger, and an oil-exhaust heat exchanger (h.e.) with an oil cooler (OC) on a) coolant temperature and oil temperatures and b) fuel consumed over the NEDC

a)



b)

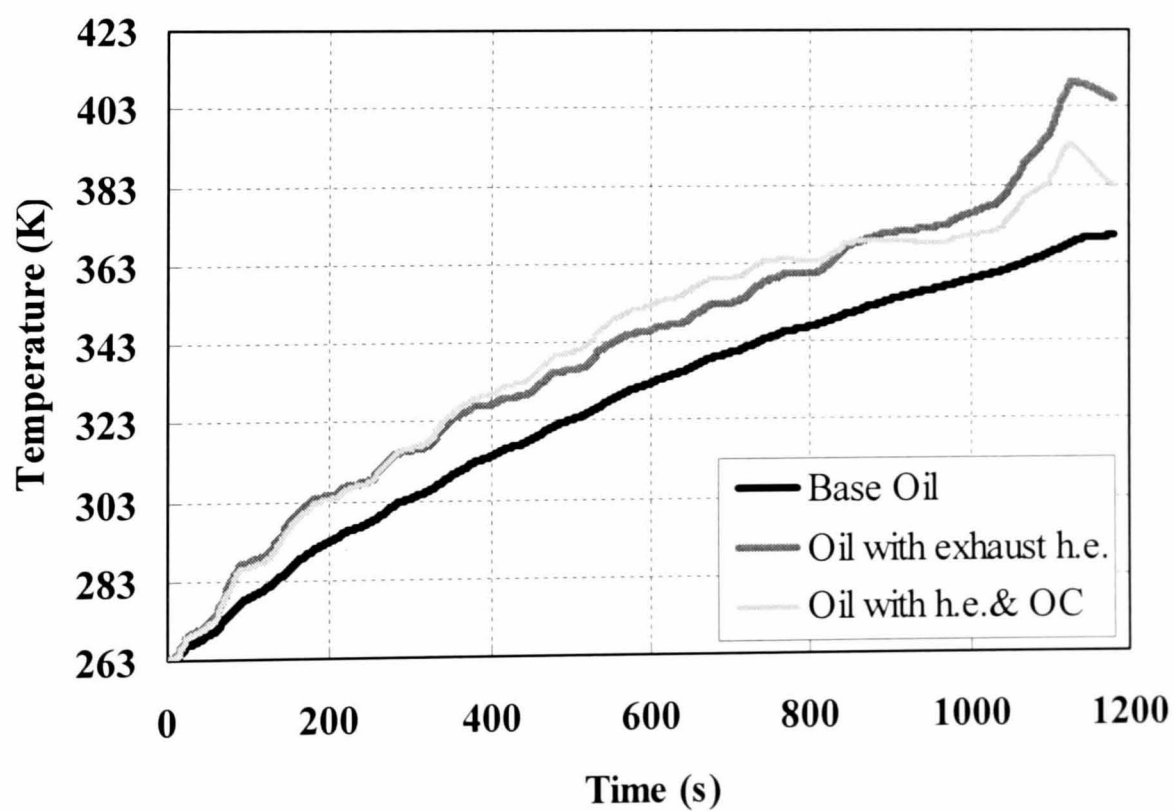


Figure 7.12 The effect of an oil-exhaust heat exchanger, and an oil-exhaust heat exchanger (h.e.) with an oil cooler (OC) on a) coolant temperature and b) oil temperature over the NEDC.

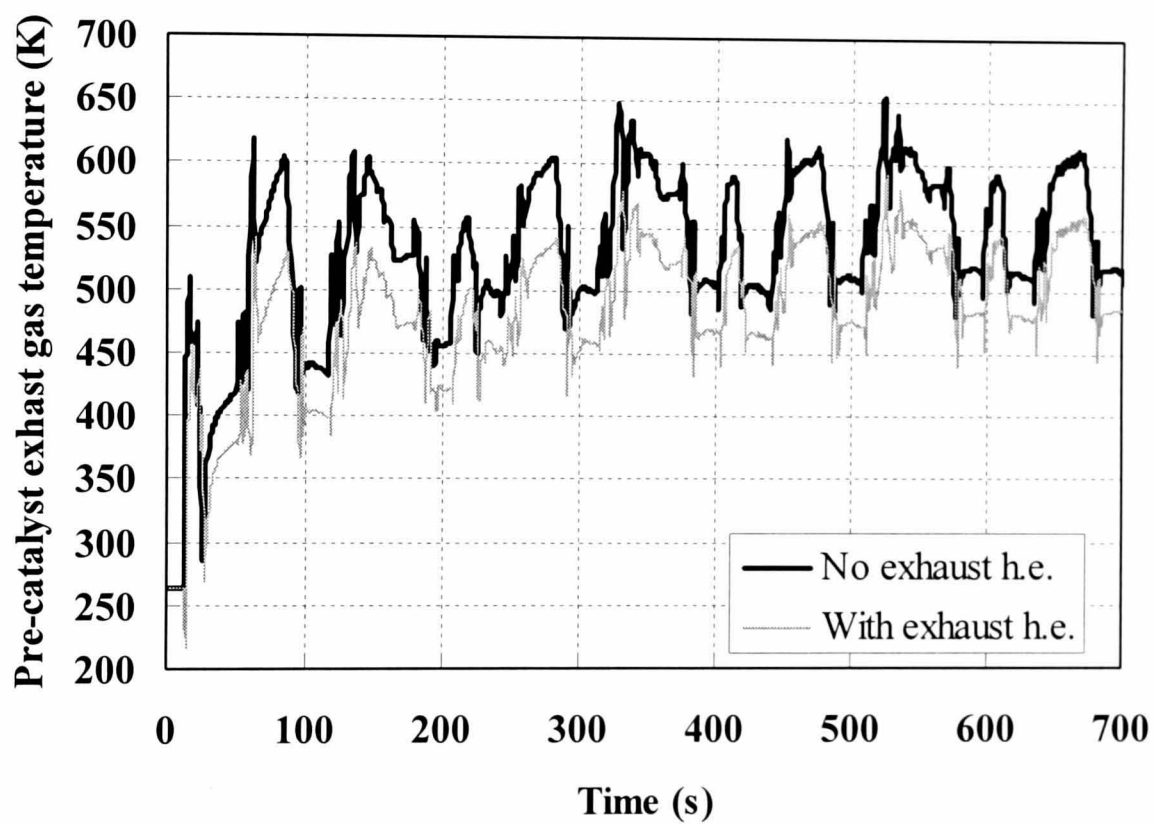


Figure 7.13 Illustration of the pre-catalyst exhaust temperatures with and without an oil-exhaust heat exchanger. The gas temperature is reduced by an average of 47 degrees.

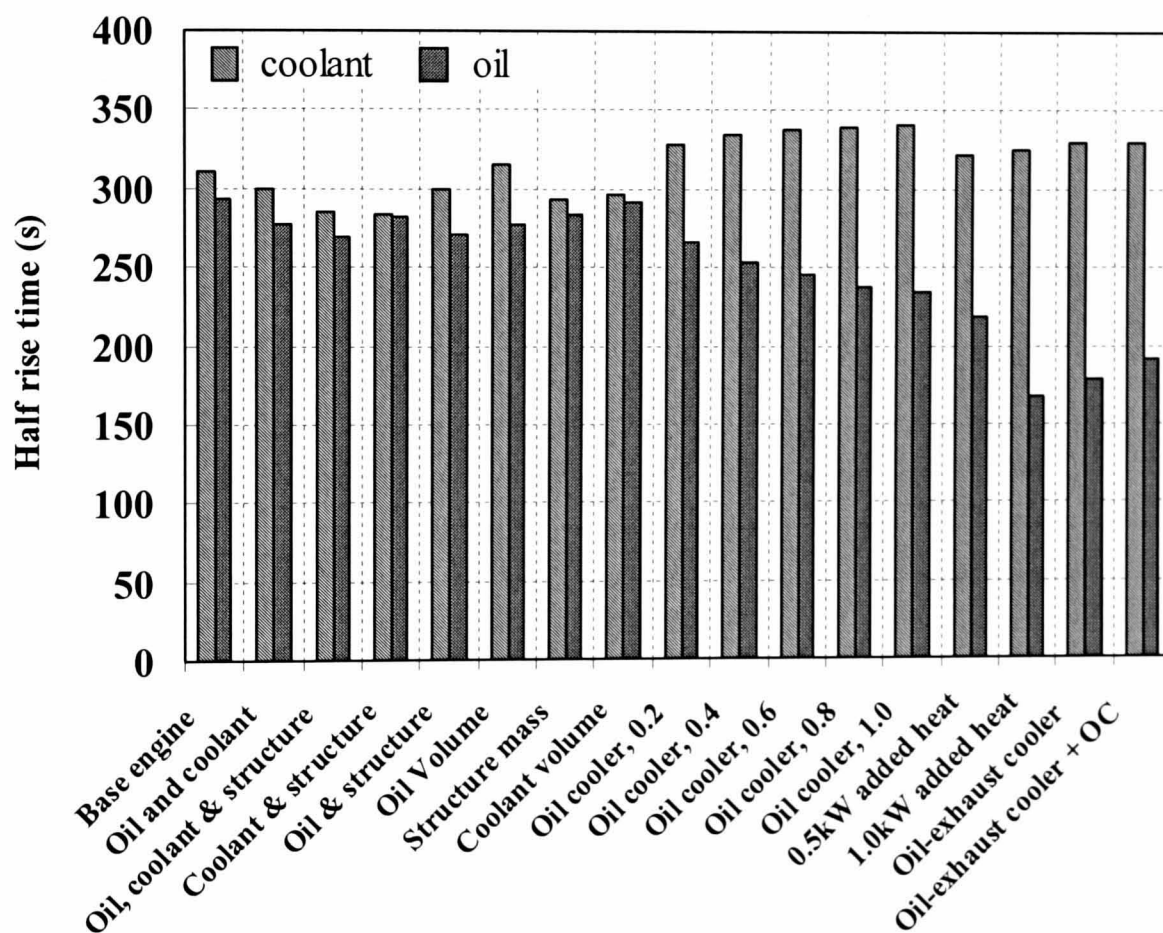


Figure 7.14 Summary of coolant and oil half rise times for all methods investigated. Coolant half rise times are improved most by combined reductions in the coolant volume and structural mass. Oil half rise times are most improved by adding 1kW of heat into the oil sump.

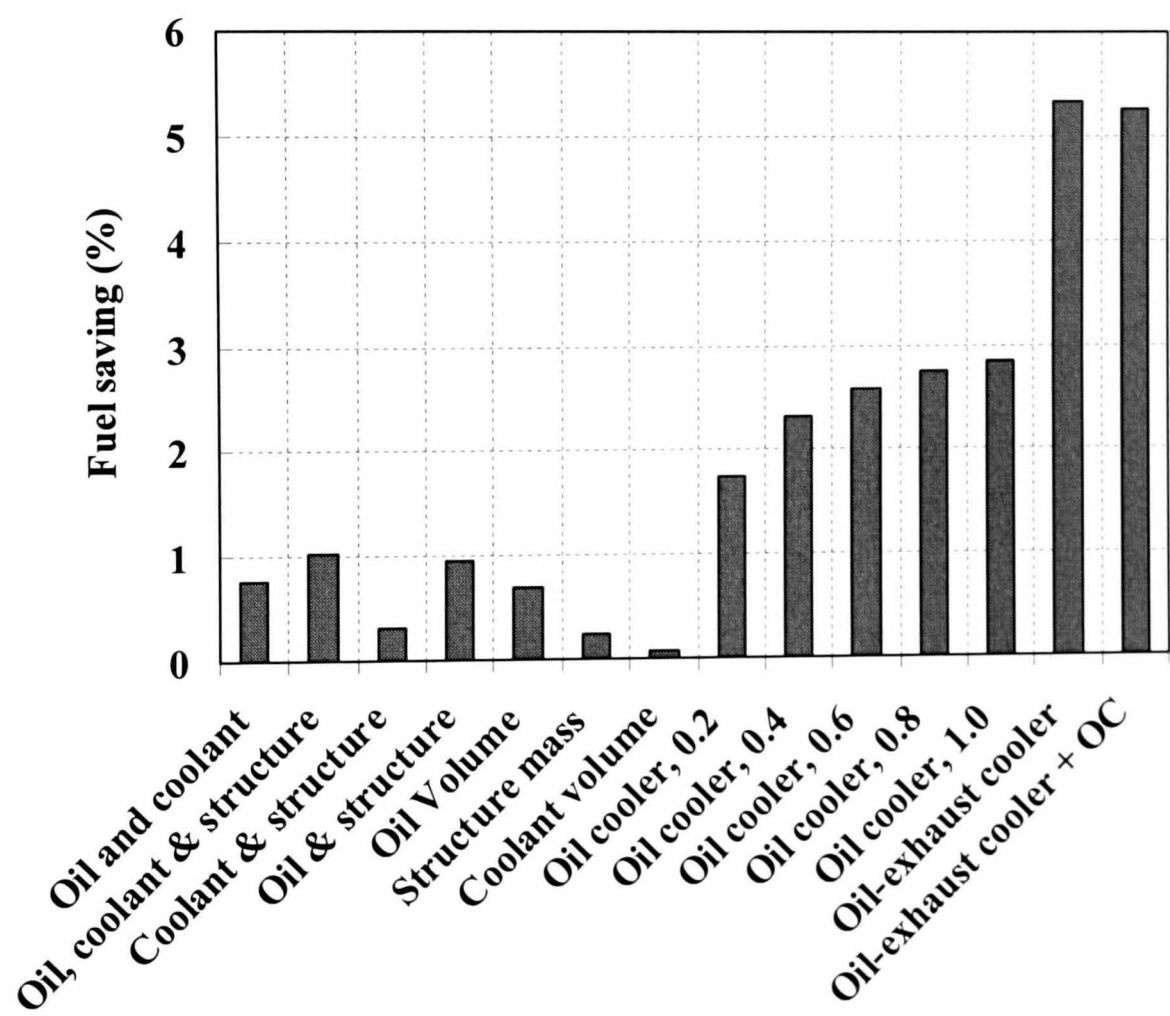


Figure 7.15 Summary of the percentage fuel saved compared to the base engine over the NEDC. The greatest fuel saving is made using an oil-exhaust gas heat exchanger.

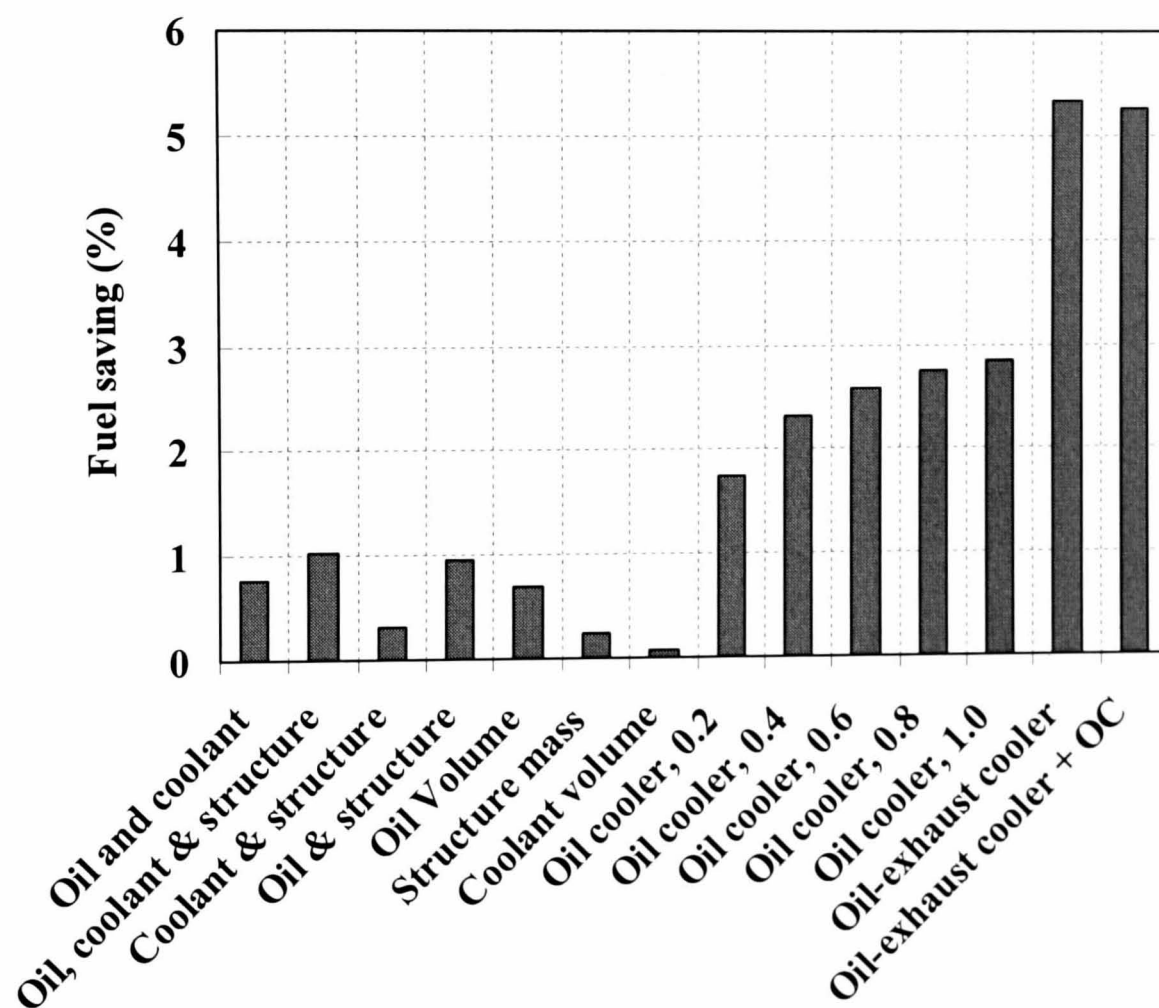


Figure 7.15 Summary of the percentage fuel saved compared to the base engine over the NEDC. The greatest fuel saving is made using an oil-exhaust gas heat exchanger.